THE PHYSICAL REVIEW

A journal of experimental and theoretical physics established by E. L. Nichols in 1893

Published by the American Institute of Physics for the

AMERICAN PHYSICAL SOCIETY

Officers

President

F. W. LOOMIS
University of Illinois
Urbana, Illinois

Vice-President

I. I. RABI
Columbia University
New York, New York

Secretary

K. K. DARROW
Bell Telephone Laboratories
Office:
Columbia University
New York 27, New York

Treasurer

G. B. PEGRAM
Columbia University
New York 27, New York

Local Secretary for the Pacific Coast

J. KAPLAN
University of California at Los Angeles
Los Angeles, California

Managing Editor

JOHN T. TATE
University of Minnesota
Minneapolis, Minnesota

BOARD OF EDITORS

Associate Editors

S. A. GOUDSMIT — W. E. LAMB, JR.
E. M. PURCELL — R. G. HERB
V. F. WEISSKOPF — J. BARDEEN

Manuscripts for publication should be submitted to John T. Tate, University of Minnesota, Minneapolis, Minnesota. The authors' institutions are asked to pay a publication charge of $4 per page which, if honored, entitles them to 100 free reprints. Instructions will be sent with galley proofs.

Proofs and all correspondence concerning papers in the process of publication should be addressed to the Publication Manager, American Institute of Physics, 57 East 55 Street, New York 22, New York.

Subscription Price

United States and Canada $25.00
Elsewhere $27.00

Back Numbers

Yearly back number rate when complete year is available:
Prior to 1949: $30.00
Thereafter: $27.00

Single copies: $2.00 each, prior to July, 1929;
$1.00 each, July, 1929–December, 1941;
$2.00 each, January, 1942–December, 1946;
$1.00 each, January, 1947–December, 1948.

Current issues: $2.50 each.
Current volume, 1949: $30.00.

Subscriptions and orders for back numbers should be addressed to the Business Office, 20 North Queen Street, Lancaster, Pennsylvania, or to the American Institute of Physics, 57 East 55 Street, New York 22, New York.

Notices of address changes of members of the American Physical Society should be addressed to the Treasurer; in the case of other subscribers, to the Publication Manager, American Institute of Physics.

Communications to the Editors: Physics Department, Cornell University, Ithaca, New York.

The Physical Review is published monthly by the American Institute of Physics at 20 North Queen Street, Lancaster, Pennsylvania.

Entered as second-class matter March 6, 1918, at the Post Office at Lancaster, Pennsylvania, under the Act of March 3, 1879.

Acceptance for mailing at special rate of postage provided for in paragraph 4, section 538, P. L. & R., authorized January 29, 1925.

THE
PHYSICAL REVIEW

A journal of experimental and theoretical physics established by E. L. Nichols in 1893

SECOND SERIES, VOL. 76, NO. 11 DECEMBER 1, 1949

Magnetic Analysis of the $C^{12}(d,p)C^{13}$ and $O^{16}(d,p)O^{17}$ Reactions

W. W. BUECHNER, E. N. STRAIT, A. SPERDUTO, AND R. MALM
Laboratory for Nuclear Science and Engineering, Massachusetts Institute of Technology, Cambridge, Massachusetts
(Received July 29, 1949)

The proton groups that result from the deuteron bombardment of C^{12} and O^{16} targets have been analyzed with a high resolution magnetic spectrometer. For the $C^{12}(d,p)C^{13}$, 13* reactions, the Q-values have been measured as 2.729 ± 0.009 and -0.370 ± 0.003 Mev. No evidence has been found for energy levels of lower energy than the one which is thus determined to be at 3.098 ± 0.008. The reaction energies for the two proton groups observed to come from $O^{16}(d,p)O^{17}$ are 1.925 ± 0.008 and 1.049 ± 0.007 Mev, with 0.876 ± 0.009 Mev as the energy of the first excited state in O^{17}.

I. INTRODUCTION

THE various proton groups that result from the deuteron bombardment of C^{12} and O^{16} have been studied in many different ways since the early work of Cockcroft and his collaborators. Knowledge of the energy released from these reactions provides information regarding the masses and the low lying energy levels of the residual nuclei, C^{13} and O^{17}. The energy levels of C^{13} are of particular interest, since their location can be compared with the levels of N^{13} which have been determined by other methods. Such a comparison affords a partial check on certain current ideas regarding the structure of light nuclei.

In the present work, the energies of the protons emitted at 90 degrees to the incident deuteron beam have been determined with a high resolution, 180-degree analyzing magnet. In general, the carbon and oxygen targets were the very thin layers of surface contaminants that experience has shown to be present on nearly all targets operated at red heat in a system evacuated by mercury pumps and provided with liquid-air traps. The presence of such very thin layers is not usually a disadvantage, however, since a precise determination of the energy of the groups that originate in them may make it possible to employ them as convenient secondary energy standards.

II. APPARATUS AND EXPERIMENTAL ARRANGEMENT

The apparatus and the experimental technique are essentially the same as those described[1] in connection with some measurements on the 480-kev level of Li^7. Deuterons from an electrostatic accelerator are analyzed by a 90-degree deflecting magnet, and the resultant atomic beam is directed at a target located between the pole faces of an annular magnet. The particles emitted at right angles to this beam are deflected through 180 degrees by the annular magnet and are detected on nuclear-track plates placed in the focal plane.

In the present experiment, it is essential that the field strength in the annular analyzing magnet be accurately determined over a wide range. For this purpose, the flip-coil flux meter, previously described, has been replaced by a system that has proved very reliable and convenient. A small rectangular coil placed between the pole faces of the magnet is fastened to an arm that is rigidly mounted at the center of the beam of an analytical balance of 0.1 mg sensitivity. The balance is adjusted so that, with no current through the coil and no weight on the balance pan, the system is in equilibrium when the coil is parallel to the lines of force. In use, the coil current required to balance a standard two-gram weight placed on one of the balance pans is used as a measure of the magnetic field. A mirror mounted on the balance arm serves to reflect the image of an incandescent filament onto a scale on the laboratory wall, thus providing a convenient method of determining the balance position.

For the range of field strengths employed in these experiments, the coil current required for balance is between 20 and 50 milliamperes. This current is measured with a type K potentiometer. Careful measure-

[1] Buechner, Strait, Stergiopoulos, and Sperduto, Phys. Rev. 74, 1569 (1948).

TABLE I. Calculation of errors for reaction energy for $C^{12}(d,p)C^{13}$.

Source of error	Magnitude of error
Fundamental constants and $H\rho$ for polonium α-particles	±4.5 kev
Spread of beam at entrance slit	±0.1
Angle of observation (deviation from 90 degrees)	±2.5
Non-uniformity of magnetic field at target and detector	±0.1
Diameter of magnet	±0.6
Homogeneity of field	Negligible
Measurement of field	±6.9
Determination of peak location	±1.7
Net probable error	±9 kev

ments have been made over a wide range of field strengths on the relationship between the coil current and the corresponding balancing weight. This relationship has been found to be accurately linear even for very small field strengths. As in our previous work, this flux meter is calibrated in terms of the magnetic field required to produce a measured deflection of alpha-particles from polonium. A value of 3.3158×10^5 gauss-centimeters for these particles[2] has been used throughout. This flux meter has been in use for approximately one year and has been frequently recalibrated, the individual calibrations being consistent to within 0.1 percent.

The nuclear-track plates used as detectors are exposed at different magnetic field strengths, and thus each records an interval in the energy spectrum of the particles being studied. In order to make possible the accurate determination of the positions on the plates of the peaks observed, the plates are counted in strips 0.1 mm in width. With both the alpha-particles used for calibration and the groups from the reactions, sufficient exposure is given so that there are several hundred tracks in each strip in the region of the peak maximum. Figure 1 is a plot of data obtained in this way for the polonium alpha-particles. The plate from which this curve was obtained was counted with a magnification of 720. Similar curves have been obtained for the various particle groups studied.

Two types of targets have been employed in these experiments. As has been mentioned, experience has shown that a very thin film containing both oxygen and carbon exists upon the surface of all target materials unless extreme precautions are taken. In general, the thickness of these films appears to be less than 5 kilovolts, as determined from the width of the proton peaks that appear as a result of the bombardment. In such cases, this half-width of the proton groups is mainly determined by the width of the slit through which the incident beam is admitted to the target chamber for the annular magnet.

A search for low energy protons from such targets is complicated by the presence of deuterons that have been elastically scattered from the solid material upon which the films have been deposited. To facilitate the counting of the proton tracks in the presence of the heavy background caused by these scattered deuterons, thin aluminum foils have been placed immediately in front of the emulsion surface. These foils are of such a thickness as to stop completely these scattered deuterons. This inconvenience due to the scattering from a solid target may be eliminated by the use of targets of thin carbon- and oxygen-containing organic films, such as Formvar, which are supported by an open-wire framework that is not in the path of the incident beam. With such thin targets, the plates are very free of any background caused by scattering. Such targets tend to disintegrate under prolonged bombardment, however, and frequent replacements are necessary.

The energy of the incident deuteron beam employed in each series of measurements has been determined from measurements of the deflection of elastically scattered deuterons. In this case, it is desirable that the deuterons be scattered from a very thin target. Gold-leaf targets and targets that consist of a thin layer of platinum evaporated onto a copper backing have been used. The latter targets have been very satisfactory and are much more rugged than are the gold-leaf targets. The resolution of the apparatus is sufficient to separate completely the deuterons scattered by the platinum from those scattered by the copper backing. Where the Formvar targets have been employed, the measurements have been carried out

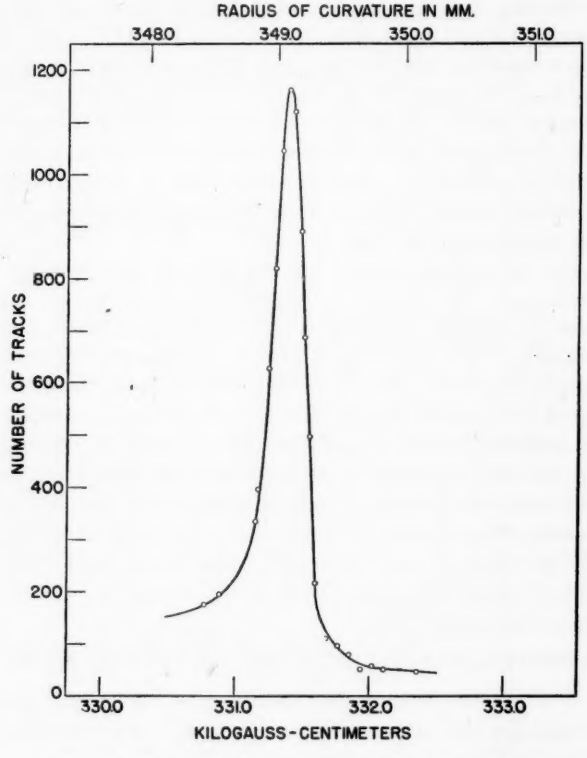

FIG. 1. Alpha-particle group from polonium used for calibration of flux meter.

[2] S. Rosenblum and G. Dupouy, Comptes rendus **194**, 1919 (1932).

from the scattering by the carbon and oxygen in the Formvar. When the measurements are made in this way, there is no uncertainty regarding the effects of surface films of carbon and oxygen. In the case of the other scattering targets, check runs must always be made to insure that these surface films, if they exist, are thin enough so that they do not appreciably affect the energy determination.

The effect of the various possible sources of error in these experiments has been carefully considered. In order to check on the possibility that a gradual accumulation of surface contaminants on the polonium source used for calibration might have occurred during the period of approximately eighteen months that it has been in the vacuum system, fresh sources were prepared at the conclusion of these experiments and were placed in the target position. The calibration constants obtained from the old and new sources agree to within 0.1 percent. The peak shown in Fig. 1 has a half-width of 0.6 mm. Measurements on this and on the other peaks obtained from thicker sources and from sources of greater width agree in indicating that the energy of the group can be taken to be that corresponding to a point on the high energy side of the peak at a height that is one-third the maximum. The measured $H\rho$ of the various groups has been found to be independent of the field strength, and this, together with the sharpness of the peaks, is a confirmation of observations made on the uniformity of the magnetic field in the region of the motion of the particles.

In making the conversion from the observed $H\rho$ values to particle energies, exact mass values have been used,[3] and relativity corrections have been made where required. In making the conversion, an uncertainty arises from the values of the fundamental physical constants that must be employed.[4] In general, errors caused by the uncertainties in the values of these constants and in the value for the $H\rho$ of polonium alpha-particles are approximately the same as the uncertainties due to the various experimental factors involved, such as the energy spread in the beam admitted through the entrance slit onto the target, the uncertainty in the angle of observation with respect to the direction of the incident particles, non-uniformities of the magnetic field at the target and at the photographic plates, the uncertainty in the effective diameter of the path in the magnet from the target to the fiducial mark placed on the photographic plate, the homogeneity of the magnetic field, the determination of the location of the peaks with respect to the fiducial marks on the plates, and the constancy and the evaluation of the magnetic field. All but the last two are systematic errors and thus appear in the same direction in the calculations of the energies of both the incident particles and the emergent ones. Thus, they tend to cancel out when energy differences are being studied, and the energy levels, as measured from the ground state, can be measured with greater accuracy than can the individual Q-values.

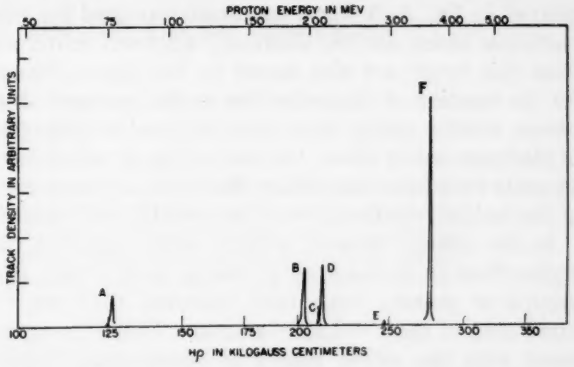

FIG. 2. Proton groups and elastically scattered deuterons from Formvar target. Peaks A and F are protons from $C^{12}(d,p)C^{13}$; C and E are from $O^{16}(d,p)O^{17}$; and B and D are deuterons scattered from carbon and oxygen. The incident deuteron energy was 1.386 Mev.

The largest of the experimental uncertainties arises from the measurement of the magnetic field. Thus far, it has not been feasible to increase the present sensitivity of 0.1 percent for the flux meter because of drifts in the current through the annular magnet. Since an uncertainty in the measurement of the field enters as the square in the energy determination, circuits have been constructed to stabilize the magnet current to allow an increase in the sensitivity of the flux meter. Experience has indicated that this can be increased by a factor of approximately 10. Since the uncertainty in the field measurements enters as a constant percentage in determining both the incident and emergent particle energies, those reactions with high Q-values have a relatively larger error expressed in Mev.

The effect of these various errors has been examined in detail for each reaction. A typical example is that of $C^{12}(d,p)C^{13}$. For this reaction, Table I shows the magnitudes of the various errors that are due to the uncertainties in the quantities listed. In this, as in all the cases herein reported, consideration has been given to the extent to which the systematic errors cancel. The internal consistency of the measurements on the various reactions is considerably better than the calculated errors indicate. In the case of the $C^{12}(d,p)C^{13}$ reaction, for example, the Q-value, as obtained from repeated measurements taken over the range of deuteron energies from 1.0 to 2.0 Mev, agrees to within 2 kev.

III. EXPERIMENTAL RESULTS

In the present experiment, most of the data were taken with the energy of the incident deuterons in the neighborhood of 1.4 Mev. The proton groups observed on a series of twenty-seven plates, taken to cover the range of proton energies from 0.40 to 4.0 Mev, are

[3] K. T. Bainbridge, Preliminary Report No. 1, Nuclear Science Series, National Research Council (1948).

[4] J. W. M. Dumond and E. R. Cohen, Rev. Mod. Phys. **20**, 82 (1948).

plotted in Fig. 2. A Formvar target was used for this particular series, and the elastically scattered deuterons from this target are also shown on the figure. Except for the location of the peaks due to the scattered deuterons, similar results have been obtained with targets of platinum and of silver. For each of the groups shown, separate runs have been taken during which the energy of the incident deuterons was also carefully determined.

In the energy interval studied, which covered the region from 0- to 3.4-Mev excitation in C^{13}, only two groups of protons have been observed that can be attributed to the $C^{12}(d,p)C^{13}$ reaction. This is in agreement with the recent results of Heydenburg, Inglis, Whitehead, and Hafner.[5] Measurements on the energies of these groups yield the values 2.729 ± 0.009 Mev and -0.370 ± 0.003 Mev for the reaction energies. From these data, the value 3.098 ± 0.008 Mev is obtained as the energy of the excited state in C^{13}. This is in good agreement with the corrected values obtained by Heydenburg, Inglis, Whitehead, and Hafner, and it confirms the corrections they applied to the range-energy relation. These values have been used to calculate the mass of C^{13}. Using 12.003856 ± 0.000019 for the mass of C^{12}, we obtain 13.007716 ± 0.000022.

One of the purposes of these experiments was to investigate the possibility of the existence of weak proton groups that might not have been observed in previous experiments of lesser resolution. A particular search was made for a group that would correspond to a level in C^{13} at 0.80 Mev, the existence of which is indicated by the experiments of Merhaut and of Roy[6] on the $B^{10}(\alpha,p)C^{13}$ reaction. No evidence for such a group has been found.

Since N^{13} is known to have a level of 2.34 Mev, and recent work in this Laboratory on the $C^{12}(p,\gamma)N^{13}$ reaction has shown a resonance that indicates an additional level of 3.48 Mev,[7] a search has been made for groups arising from corresponding levels in C^{13}. The resolution of the apparatus and the sharpness of the peaks shown in Fig. 2 indicate the absence of such additional groups. The possibility that, at the bombarding energy of 1.4 Mev, weak groups from carbon might be coincident with the oxygen groups has been eliminated by studying the observed peaks while the incident deuteron energy was varied over the range from 1 Mev to 2 Mev. It is of interest to note that the experiments of Van Patter, to which reference has been made, do not indicate a level in N^{13} that would correspond to the 3.1-Mev level in C^{13}.

The other proton groups shown in Fig. 2 are due to the $O^{16}(d,p)O^{17}$ reaction. Q-values of 1.925 ± 0.008 and 1.049 ± 0.007 Mev are obtained from measurements of these groups. The energy of the excited state in O^{17} is thus found to be 0.876 ± 0.009 Mev. These Q-values are somewhat lower than the corrected values of Heydenburg and Inglis, as reported in reference 5. The mass of O^{17} has been calculated and is found to be 17.004522 ±0.000010.

IV. ACKNOWLEDGMENTS

We are indebted to Dr. John Blatt and to Professor E. P. Wigner for helpful and stimulating discussions and also to Dr. D. M. Van Patter for permission to quote his results. We are particularly grateful to Mr. Wilton Tripp, Miss Cecilia O'Brien, and Mrs. Hester Andrews for their assistance in connection with reading the photographic plates.

This work has been assisted by the Joint Program of the Office of Naval Research and the Atomic Energy Commission.

[5] Heydenburg, Inglis, Whitehead, and Hafner, Phys. Rev. **75**, 1147 (1949).

[6] R. R. Roy, Phys. Rev. **75**, 1775 (1949).

[7] D. M. Van Patter, Phys. Rev. **76**, 1264 (L) (1949).

Magnetic Analysis of $Be^9(d,\alpha)Li^7$ and $Be^9(d,p)Be^{10}$ Reactions

W. W. Buechner and E. N. Strait
Laboratory for Nuclear Science and Engineering, Massachusetts Institute of Technology, Cambridge, Massachusetts
(Received July 29, 1949)

The alpha-particle and proton groups arising from the deuteron bombardment of beryllium targets have been studied with a high resolution magnetic spectrometer. Except for the well-known one at 480 kev, no evidence has been found for energy levels in Li^7 between 3.4 Mev and the ground state. The Q-value for the $Be^9(d,\alpha)Li^7$ reaction has been measured as 7.145 ± 0.024 Mev. Studies of the proton groups indicate that there are no levels in Be^{10} between the ground state and one at 3.375 ± 0.010 Mev. The Q for the $Be^9(d,p)Be^{10}$ reaction has been found to be 4.576 ± 0.012 Mev.

I. INTRODUCTION

WHEN beryllium is bombarded with deuterons, a wide variety of reactions that lead to the emission of gamma-rays, alpha-particles, protons, tritons, and neutrons are observed. Since beryllium consists of a single isotope, the various reactions are readily identified. Studies of the energies of the gamma-radiation and particle groups yield information regarding the masses and energy levels of the residual nuclei produced in the reactions. The alpha-particle groups are associated with the formation of Li^7, which is known to have excited states at 0.480 and 7.38 Mev.[1] The proton groups are associated with the formation of Be^{10}, for which the lowest excited level appears to be at 3.37 Mev. In view of the recent interest in the character of the excited states of Li^7 and because of the success of the mirror-nucleus picture in correlating the ground states of Be^{10} and C^{10} with excited levels in B^{10},[2] the alpha-particles and protons have been studied in some detail with a high resolution magnetic spectrometer. The object of the present experiment was to measure the energies released in the reactions and to investigate the possibility of additional energy levels in Li^7 and Be^{10}. The various reactions that lead to the formation of these two nuclei are shown in Figs. 1 and 2, which are taken from the summary by Lauritsen.[1] The particular reactions that form the basis of our observations are indicated on the figures by the symbol #.

II. APPARATUS AND EXPERIMENTAL ARRANGEMENT

The experimental arrangement was essentially the same as that previously described.[3] Most of the measurements were made on thin targets of beryllium evaporated onto platinum sheets, although thin beryllium-foil targets[4] were also used, particularly for the purpose of checking upon the effects of contaminants. These foils were supplied to us by Professor T. Lauritsen.

As in our previous work, the energies of both the incident and the emergent particles from the reactions were measured in terms of the magnetic field strengths required to bring them onto the photographic plates used as detectors. The sensitivity of the balance-type flux meter has recently been increased by a factor of more than ten so that the principal uncertainty in the energy determination for the particles arises from the uncertainty in the energy of the polonium alpha-particles used for calibration purposes and the uncertainties in the values of the fundamental physical constants that must be employed in calculating the $H\rho$ to energy conversion. Unfortunately in these experiments, there is an additional experimental error that must be considered when the measured particle energies are used for determining the reaction energies. This arises from an uncertainty with regard to the angle of observation with respect to the direction of the incident beam; this angle is essentially 90 degrees. Because of slight spreading of the beam in the target region and other geometrical factors, the angle between the beam and the median plane of the magnet gap is not known to closer than a quarter of a degree. In addition, there is a finite collection angle for the photographic plates, which are 1 centimeter wide placed approximately 100 centimeters from the target. As a result, the value of the reaction energy is uncertain by an amount $\Delta Q=2(M_1,M_2,E_1,E_2)^{\frac{1}{2}}\delta/M_3$, where δ is the uncertainty in angle with respect to the 90-degree position and M_1, M_2, E_1, and E_2 are the masses and energies of the incident and emitted particles, respectively, and M_3 is the mass of the residual nucleus formed in the reaction.[5] This error is particularly important in the reactions of the light nuclei which have a high Q, as is the case here, and is approximately the same as that caused by the other factors mentioned above. The other experimental errors, such as those associated with the readings of the photographic plates, reproducibility of the flux meter, and so forth, are considerably smaller.

III. RESULTS

The various proton and alpha-particle groups that have been observed to result from the deuteron bombardment of beryllium targets are shown in Fig. 3.

[1] T. Lauritsen, Preliminary Report No. 5, National Research Council, Nuclear Science Series (1949).
[2] Scherr, Meuther, and White, Phys. Rev. **75**, 282 (1949).
[3] Buechner, Strait, Sperduto, and Malm, Phys. Rev. **76**, 1543 (1949).
[4] H. Bradner, Rev. Sci. Inst. **19**, 662 (1948).
[5] M. S. Livingston and H. A. Bethe, Rev. Mod. Phys. **9**, 245 (1937), Eq. (770).

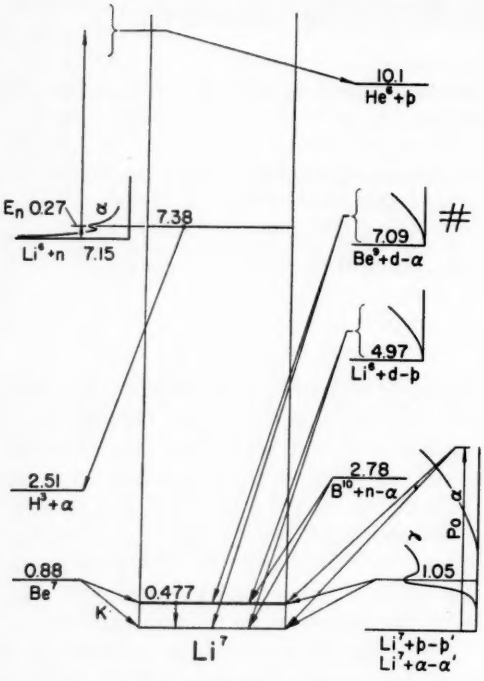

FIG. 1. Energy levels of Li^7.

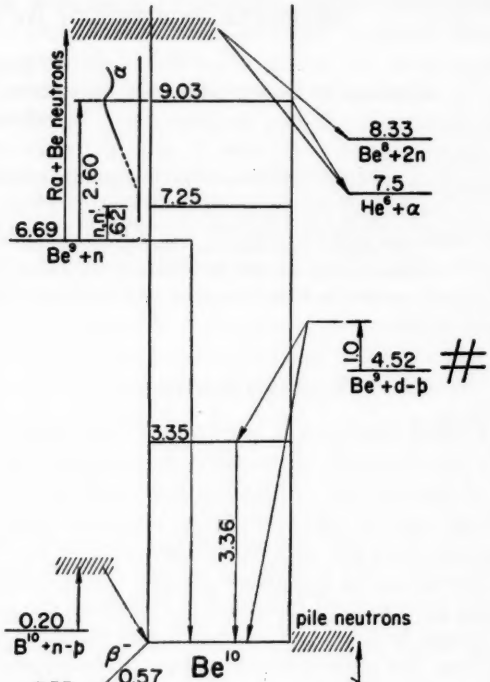

FIG. 2. Energy levels of Be^{10}.

The proton groups due to carbon contamination have not been included, since they are very sharp and are well removed from the groups that are of interest in this experiment. The curves shown in Fig. 1 were obtained with a bombarding energy of 1.396 Mev.

The two alpha-particle groups shown in the figure are from the reaction in which Li^7 is formed. Since, for the same $H\rho$, the range of alpha-particles in the photographic emulsion is less than that for deuterons, it has not been convenient in these experiments to search for alpha-particle groups that have an $H\rho$ of less than approximately 220 kilogauss-centimeters. At this point, a rather heavy background of deuterons that have been elastically scattered from the support for the beryllium targets is encountered. A careful search in the region above this has shown no evidence for additional alpha-particles and indicates that, except for the well-known one at 480 kev, there are no energy levels in Li^7 between the ground state and 3.4 Mev. The possibility that any weak groups might have been obscured at the particular bombarding energy shown in the figure by the groups from carbon and oxygen has been eliminated by studies in which the bombarding energy was varied over the range from 1 to 2 Mev. Also, no evidence of structure in the alpha-particle groups has been found.

Previous work in this Laboratory[6] on the energy difference between the two alpha-particle groups from the $Be^9(d,\alpha)Li^7$ reaction has given 482 ± 0.003 Mev for this energy level in Li^7. In the present experiment, careful studies have been made on the energies of the groups, and these measurements give 7.145 ± 0.024 Mev for the Q-value of the reaction which results in the formation of Li^7 in the ground state. Of the factors that enter into the stated error, 17 kev is due to the geometrical factor discussed previously; 16 kev, to uncertainties in the constants employed; and 5 kev, to other errors of experimental origin. This reaction was also studied by Graves,[7] the energy of the alpha-particles being determined from their range. A value of 7.093 ± 0.022 Mev was obtained from these measurements.

The various proton groups observed have been studied extensively in order to identify those that are

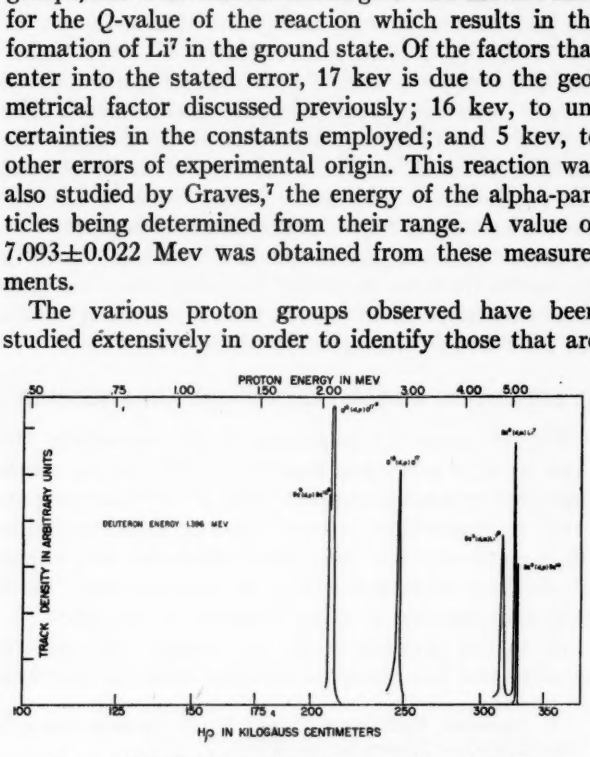

FIG. 3. Alpha-particle and proton groups from beryllium target bombarded with deuterons.

[6] Buechner, Strait, Stergiopoulos, and Sperduto, Phys. Rev. 74, 1569 (1948).

[7] E. R. Graves, Phys. Rev. 57, 855 (1940).

associated with the formation of Be^{10}. As can be seen in Fig. 3, the low energy group from beryllium, at bombarding energies of approximately 1.4 Mev, is nearly in coincidence with a low energy proton group from oxygen contamination. It has not been found possible to prepare beryllium targets that are free of oxygen. In order to separate these groups for purposes of positive identification and accurate energy measurements, the bombarding energy has been varied. Figure 4 shows the appearance of these two groups for a deuteron energy of 1.821 Mev. Check runs of this sort have been made for each of the observed groups to guard against the possibility that, at a particular bombarding energy, two groups of different origins might coincide.

These studies give 4.576 ± 0.012 as the Q for the $Be^9(d,p)Be^{10}$ reaction. Here, the experimental errors are as follows: 10 kev due to the uncertainties in the constants, 6 kev due to geometry, and 2 kev from other experimental sources. The measured Q for the $Be^9(d,p)Be^{10*}$ reaction is 1.201 ± 0.007 Mev. From these values, we obtain 3.375 ± 0.010 Mev for the first excited state in Be^{10} which is observed in this reaction. This is in good agreement with the value of 3.359 ± 0.015 Mev which is determined from measurements on the gamma-rays that accompany the reaction.[8] Using the masses of the proton and deuteron as listed by Bainbridge,[9] the value 1.001675 ± 0.000014 is obtained for the $Be^{10}-Be^9$ mass difference.

The recent success of the idea of mirror nuclei in correlating the ground state of C^{10} and Be^{10} with excited states of B^{10} has indicated that, in such mirror nuclei, the equality of the p–p and n–n forces can be assumed and that the entire energy release of the mirror nuclei can be attributed to Coulomb energy and to the neutron-proton mass difference.[10] A correlation between the excited states of Be^{10} and those of B^{10} might then be expected. The excited states in B^{10} have been measured by Rasmussen, Hornyak, and Lauritsen,[8] who measured the energies of the gamma-rays emitted in the $Be^9(d,n)B^{10}$ reaction. These studies show that energy levels in B^{10} occur at 412, 713, 1424, 2138, and 3580 kev. There is also some evidence for an excited state at 5 Mev.[11] The present work indicates that there are no excited states in Be^{10} between the ground level and 3.37 Mev that are excited at the bombarding energies employed in these experiments.

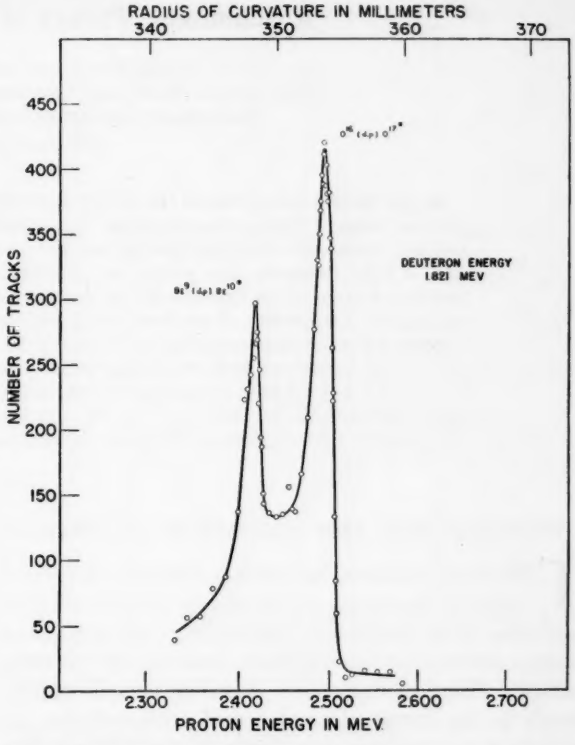

FIG. 4. Low energy proton groups from beryllium and oxygen.

V. ACKNOWLEDGMENTS

We have enjoyed many stimulating discussions with Dr. John Blatt during the course of this work and have had much generous collaboration from the various members of the High Voltage Laboratory, particularly Mr. A. Sperduto and Dr. C. G. Stergis, now at Temple University. We wish also to express our appreciation to Miss C. O'Brien, Mrs. H. Andrews, and Mr. W. A. Tripp for their assistance in the measurements with the photographic plates.

This work was supported by the Joint Program of the ONR and the AEC.

[8] Rasmussen, Hornyak, and Lauritsen, Phys. Rev. **76**, 581 (1949). We are indebted to Professor Lauritsen for supplying these values and the information in reference 11 prior to publication.

[9] K. T. Bainbridge, Preliminary Report No. 1, Nuclear Science Series, National Research Council (1948).

[10] Sherr, Muether, and White, Phys. Rev. **75**, 282 (1949).

[11] Chao, Lauritsen, and Rasmussen, Phys. Rev. **76**, 582 (1949).

A Schematic Theory of Nuclear Cross Sections*

H. FESHBACH AND V. F. WEISSKOPF
Department of Physics and Laboratory for Nuclear Science and Engineering, Massachusetts Institute of Technology Cambridge, Massachusetts

(Received August 8, 1949)

In this paper a description of the energy dependence of nuclear cross sections, especially for neutrons, is given in terms of simple assumptions on the properties of the nuclei. The results are supposed to represent average values over individual fluctuations and resonances. The total cross section, the reaction cross section, and the transport cross section are calculated as functions of the neutron energy. Only two nuclear parameters occur in the expressions; the nuclear radius and the average kinetic energy of a nucleon inside the nucleus. Comparison of the theory with neutron experiments is made. New values of nuclear radii are computed from total cross sections at 14 and 25 Mev. Predictions of the inelastic cross sections at 14 Mev are in good agreement with the measurements. Experiments involving total and transport cross sections between 0.1 and 1.5 Mev are compared with theory and reasonably good agreement is found with most of these. However, for the elements, I, In, Sb, agreement in the context of the theory may be obtained only if the strength of resonance levels for these elements is assumed to be unusually low.

I. INTRODUCTION AND DISCUSSION OF RESULTS

THE cross sections for nuclear reactions are complicated functions of the energy of the incident particles. One observes resonances, maxima, and minima, and no two cross sections show exactly the same features. There seem to exist, however, certain general trends in the energy dependence of cross sections, especially if one averages over the individual fluctuations. It may be worth while, therefore, to try to understand the over-all behavior of nuclear cross sections on the basis of a few very general assumptions.

We are presenting here a schematic theory of nuclear cross sections which is based on an extremely simplified and rough picture of the nuclear structure. In fact, the only information used on the internal structure of the nuclei is the nuclear radius R and the average kinetic energy T of a nucleon within the nucleus.

The results obtained must be considered as a schematic picture of the actual conditions, trimmed of all individual fluctuations and deviations. It is the purpose of this approach to give a first orientation about the magnitude and energy dependence of cross sections without any claims to quantitative validity. On the other hand, the degree in which the predictions are found to be correct may be a measure of the validity of the underlying concepts.

We restrict ourselves to the study of the cross sections averaged over individual fluctuations. Resonances are not reproduced by this theory. If they occur, our theoretical results refer to the average value taken over an energy region containing several resonances. For sufficiently high energies, the resonances or fluctuations in the cross sections as a function of energy become very weak and unimportant. For it is expected that as the energy increases, the resonance levels become broader and finally merge into a continuous curve for the cross section in its dependence on energy. In this region our theoretical predictions should reproduce the actual cross sections without any averaging.

We shall show that the results herein join on continuously to those of an earlier paper[1] (to be designated henceforth as FPW) which apply to the resonance region. Both papers thus have a number of parameters in common. Of particular importance are the nuclear radius R and the wave number K of the incident particle within the nucleus. These are the only two parameters used here to represent the nucleus. Both parameters can only be defined approximately. The wave number K may be estimated by assuming that in the nuclear interior in the neighborhood of the nuclear surface, the dependence of the wave function on the coordinate r of the incident particle is periodic with a wave number corresponding to its kinetic energy within the nucleus. Hence it follows that $K^2=k^2+K_0^2$, where $k^2=2M\epsilon/\hbar^2$, $M=$mass of the incident particle, ϵ its energy outside the nucleus, and K_0 is the wave number K for zero incident energy. K_0 was estimated in FPW using a Fermi-Dirac model for the nucleus by

$$K_0^2=2M/\hbar^2[\epsilon_B+4\pi^2(3A/16\pi V)^{\frac{2}{3}}],$$

where A is the nuclear mass number, V the nuclear volume, and ϵ_B is that part of the binding energy of the added particle which is kinetic. We assume here, in contrast to FPW, that $\epsilon_B\approx 0$, for it is probable that a considerable fraction of the binding energy is potential in virtue of the exchange force between nucleons. For $\epsilon_0=0$, and $R=r_0A^{\frac{1}{3}}$, $r_0=1.5\times10^{-13}$ cm, we find $K_0=1.0\times10^{-13}$ cm^{-1}.

In addition to K_0 and R, the charge on both the incident and target nuclei are important parameters. We shall limit our discussion to neutron-initiated reactions, although formulas of Section II apply more generally. Charged particle reactions have been considered in more detail by J. K. Tyson.[2]

* This work was assisted by the Joint Program of the ONR and AEC.

[1] Feshbach, Peaslee, and Weisskopf, Phys. Rev. **71**, 145 (1947).
[2] J. K. Tyson, Ph.D. thesis, M.I.T. (1948), issued as a Technical Report by the Laboratory of Nuclear Science and Engineer-

The following cross sections are calculated:

(1) *The "total" cross section,* σ_{tot}, which includes all processes that may be initiated by the incident neutrons such as transmutations, elastic, and inelastic scattering, etc. It is this cross section which determines the attenuation of a neutron beam in passing through matter.

(2) *The "reaction" cross section,* σ_r, which we define here, somewhat unconventionally, as the total cross section minus the elastic scattering cross section, $\sigma_r=\sigma_{tot}-\sigma_{el}$. The *elastic cross section,* σ_{el}, includes only those processes in which the quantum state of the target nucleus is left unchanged. Thus the reaction cross section, σ_r, includes all the processes in which the quantum state of the target nucleus is changed; i.e., it includes the processes in which the compound nucleus decays into a different channel than the one by which it was formed. Inelastic scattering, for example, is included in the reaction cross section.

(3) *The transport cross section,* σ_{tr}, which is defined by the integral

$$\sigma_{tr}=\sigma_{tot}-\int \sigma_{el}(\theta)\cos\theta d\Omega, \qquad (1)$$

where $\sigma_{el}(\theta)d\Omega$ is the elastic scattering cross section into the solid angle $d\Omega$ in direction θ. The transport cross section determines the net loss of forward momentum of the incident beam.[a]

All three cross sections will be expressed in units of πR^2, where R is the nuclear radius:

$$\sigma_{tot,\,tr,\,r}=\pi R^2\cdot F_{tot,\,tr,\,r}(x, X). \qquad (2)$$

The three functions, F_{tot}, F_{tr}, F_r, will be shown to depend only on the dimensionless variables $x=kR$, and $X_0=K_0R$, where k is the wave number of the incoming neutron and K_0 is defined above. The following expression is useful for the computation of x:

$$x=0.222R(\epsilon)^{\frac{1}{2}}, \qquad (3)$$

where ϵ is the kinetic energy of the incoming neutron in Mev, and R is expressed in units of 10^{-13} cm.

The result of the calculation of the three functions F_{tot}, F_r, F_{tr} are plotted in Figs. 1 and 2 for different values of X_0 corresponding to different nuclear radii. ($X_0=5$ corresponds to chlorine $X_0=8$ to samarium.) The total cross section approaches $2\pi R^2$ for high energies as is well known. *However, the asymptotic value is reached only for extremely high values of* x. The behavior at higher energies is represented more faithfully by

$$\sigma_{tot}=2\pi(R+\lambda)^2=2\pi R^2(1+1/x)^2$$

which deviates from calculated values by less than 10 percent for $x>4$, as is illustrated by the dotted curve in Fig. 1.

It is interesting to compare σ_{tot} with the cross section σ_0 of an infinitely repulsive (totally reflecting) sphere of radius R. The close agreement of σ_{tot} and σ_0 shows that the value of the total cross section for sufficiently large x is not very sensitive to the choice of the boundary conditions satisfied by the neutron wave at the surface of the nucleus.

The reaction cross section approaches πR^2 at high energies and shows a $1/v$ dependence at low energies.

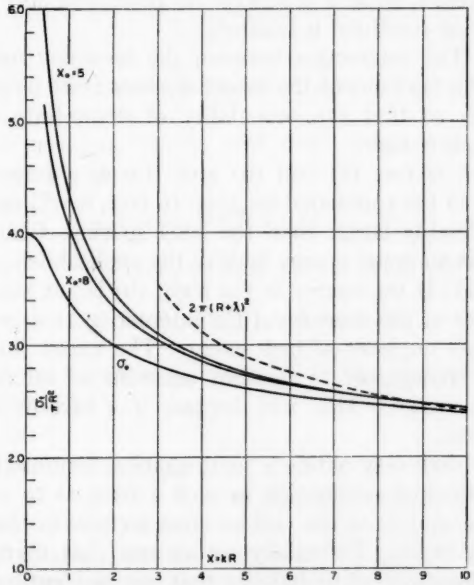

FIG. 1. Total cross sections as a function of $x=kR$, for values of $X_0=5$ and 8. σ_0 is the total cross section for the infinitely repulsive sphere of radius R. The dotted line gives the approximate behavior of all of these curves for high x.

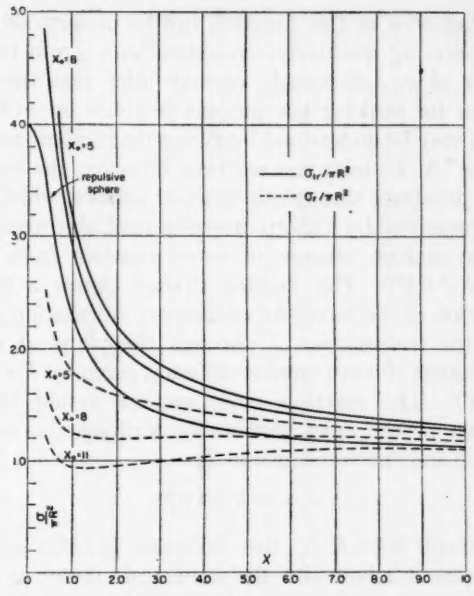

FIG. 2. Reaction and transport cross sections as a function of x for various values of X_0. The full line curves give the transport cross sections including the results for an infinitely repulsive sphere. The broken line curves give the reaction cross sections.

ing, M.I.T. An article by this author will be submitted shortly to Phys. Rev.

[a] It is assumed here that inelastic scattering is spherically symmetric.

The behavior of this function can be understood from the following qualitative considerations. From the behavior of σ_{tot} discussed, we may infer that the cross section for striking the nucleus is given by $\pi(R+\lambda\!\!\!^{-})^2$ which may be understood by giving the incident neutron a "size" $\lambda\!\!\!^{-}$. To initiate a reaction, however, the neutron must penetrate through the nuclear surface, which may be represented by a sharp drop of potential, corresponding to sudden change of wave number from k to $K=(K_0^2+k^2)^{\frac{1}{2}}$. This sudden change causes a partial reflection of the wave. An elementary calculation shows that the transmission T through the plane at which this change of wave number occurs is given by $T=4kK/(k+K)^2$. The reaction cross section should be the product of the cross section for striking the nuclear surface and the transmission T:

$$\sigma_r \approx \pi(R+\lambda\!\!\!^{-})^2 T. \tag{4}$$

For small $k(k \ll R^{-1})$, this becomes $4\pi/kK_0$ and exhibits the $1/v$ law with the same scale factor as given by the precise calculation. In the intermediate energy range, the formula (4) is not a very good approximation to σ_r, because of complications introduced by the contribution of the partial waves with higher values of the angular momentum. It should also be apparent now why σ_{tot} has a $1/v$ dependence for small x, since it is composed of σ_r and σ_{el}, the latter being finite at zero energy.

Among the three sets of curves the strongest dependence on X_0 is found in σ_r. In both σ_{tot} and σ_{tr} the increased penetration for smaller X_0 is offset by a correspondingly lower scattering.

The expressions for σ_{tot} and σ_{tr} should be valid over the entire energy range. At low energies they signify average values over resonances. The expression for the reaction cross section σ_r, however, should be applied only within a limited energy range. It is calculated with the assumption that, once the neutron has penetrated through the nuclear surface, it will not leave the nucleus again by the same channel, i.e., in such a way that the nucleus is left in the same quantum state in which it was before the reaction. Thus, our expression for σ_r should not be applied if the main process induced by the neutron is elastic scattering. Therefore, the curve for σ_r is valid only at high energies (above 2 Mev for all nuclei except the lightest ones), where we expect strong inelastic scattering, and at very low energies if the main process is neutron capture. In the low energy region σ_r should represent the average over resonances. There is, however, a large region, between a few kilovolts and a few million volts, in which σ_r is not represented by our curves.

A critical remark is necessary in regard to the nuclear radius R which enters into the evaluation of the predicted cross sections, since they are proportional to πR^2. The nuclear radius is defined in this theory as the distance of the neutron from the center of the nucleus at which the wave number of the neutron changes from k (the value outside) to K (the value inside). Actually, this occurs gradually over a region of the order $1/K$. We expect therefore that R should be uncertain by this amount, so that R may deviate from the values of any other radius determination by as much as $\pm 1\times 10^{-13}$ cm. Very probably R may vary within these limits for different energies of the incident neutron. The validity of this theory is based upon the smallness of $1/K$ compared to R. Actually $(KR)^{-1}$ is not a very small number, so that the results of the theory must be considered as rough approximations only.

II. CALCULATION OF THE CROSS SECTIONS

The derivation of our results follows different lines in the high energy region and in the low energy region. The upper region is defined by the validity of the following condition:

(a) The energy of the incident neutron must be high enough so that it is energetically possible for the compound nucleus to decay into many channels; for example, the residual nucleus may be left in many different excited states. Thus the high energy region includes energies ϵ which are considerably larger than the first excitation energy of the target nucleus, say $\epsilon > 2$ Mev.

We start with the calculation of the cross sections in the high energy region. The guiding principle employed is akin to the Bohr hypothesis of the compound nucleus. We assume that once the particle has penetrated to within the boundaries of the nucleus, it will not leave it by the same channel in which it entered. This assumption is valid if condition (a) holds and also if the following condition is fulfilled:

(b) The interaction between the incoming neutron and the nucleons of the target nucleus must be strong enough so that the probability of decay into other channels is high.

Both factors (a) and (b) give rise to a large level width in the compound nucleus. In fact, it will make it considerably larger than the level spacing. Condition (b) sets an upper energy limit to the applicability of our method: If the energy is too high, (b) is not satisfied, because of the decrease of the interaction cross section between nucleons of high energy. The nuclei thus become transparent to incident neutrons of sufficiently great energy.[3] This will happen if ϵ exceeds about 70 Mev.

We shall now obtain a mathematical formulation of the principal assumption in such a form as to permit the calculation of the various cross sections in the high energy region. Essentially we assume that there is a vanishingly small probability that any incident particle which enters the nucleus will be re-emitted without any loss of coherence with the initial beam. Thus the target nucleus acts as a "sink" for the incident particles. We express this assumption in the following mathematical form: the wave function ψ for the neutron within the nucleus cannot be given as a function of $\mathbf{r}$ (its dis-

[3] Fernbach, Serber, and Taylor, Phys. Rev. 75, 1352 (1949).

tance to the center of the nucleus) alone; however, its dependence on r may be approximated by a *converging* wave

$$r\psi \sim e^{-iKr},$$

expressing the fact that the entering particle does not return. K is the wave number which corresponds to the average kinetic energy inside the nucleus.[b] This can be expressed by a boundary condition: At the nuclear surface the logarithmic derivative of $r\psi$ equals:

$$f=R[\partial(r\psi)/\partial r/r\psi]_{r=R}=-iKR=-iX. \quad (5)$$

We recall that $K^2=K_0^2+k^2$; $K_0=1.0\times10^{-13}$ cm^{-1} as estimated in FPW. Boundary condition (5) determines the behavior of the wave function outside the nucleus; i.e., the entire nucleus is represented by the parameters X_0 in addition to the nuclear radius R. (An infinitely repulsive sphere corresponds to $\psi=0$ at $r=R$ and therefore $X_0=\infty$.)

We follow FPW in determining the cross sections as determined by boundary condition (5). For the region $r>R$, the wave function $\varphi=r\psi$ for a neutron (the following treatment applies as well to charged incident particles) with an angular momentum l in units of $\hbar$ may be written

$$\varphi=u_l+\eta v_l, \quad (6)$$

where

$$u_l \underset{r\to\infty}{\longrightarrow} e^{-i(kr-l\pi/2)}$$
$$v_l \underset{r\to\infty}{\longrightarrow} e^{+i(kr-l\pi/2)}, \quad (7)$$

u_l and v_l are known functions of x, and form a conjugate complex pair.

The reaction, elastic, and total cross sections for neutrons are then

$$\sigma_r^{(l)}=(\pi/k^2)(2l+1)(1-|\eta|^2) \quad (7a)$$

$$\sigma_{el}^{(l)}=(\pi/k^2)(2l+1)|1+\eta|^2 \quad (7b)$$

$$\sigma_{tot}^{(l)}=(\pi/k^2)(2l+1)2(1+Re\eta). \quad (7c)$$

η_l can be adjusted so that (6) fulfills the boundary condition (5):

$$\eta_l=-\frac{xu_l'+iXu_l}{xv_l'+iXv_l},$$

where u_l and v_l are the values, u_l' and v_l' the derivatives in respect to x, of the functions (7) evaluated at $x=kR$. We define the phases δ and δ' by $v=|v|e^{i\delta}$ and $v'=|v'|e^{i\delta'}$ and use the Wronskian relation $|vv'|\sin(\delta_l'-\delta_l)=1$. We then get[c]

[b] This approach is similar to that of H. Bethe (Phys. Rev. **57**, 1125 (1940)) to describe nuclear absorption.

[c] These two expressions follow directly from formulas (38) and (39) in FPW, if one puts $f=f_0-ih=-iX$ so that $f_0=0$, $h=X$.

TABLE I. Re-evaluation of nuclear radii.

Element	Observed $\sigma_{tot}\times10^{24}$	Energy in Mev	$R\times10^{+13}$ cm	r_0	Reference
Be	0.65	14	2.4	1.17	2
B	1.16	14	3.4	1.54	2
C	1.29	25	3.8	1.65	3
O	1.60	25	4.3	1.71	3
Mg	1.83	14	4.5	1.57	2
Al	1.92	14	4.6	1.53	2
Al	1.85	25	4.6	1.52	3
S	1.58	14	4.1	1.30	2
Cl	1.88	25	4.7	1.44	3
Fe	2.75	14	5.6	1.46	2
Cu	2.50	25	5.5	1.38	3
Zn	3.03	14	5.9	1.48	2
Se	3.35	14	6.3	1.46	2
Ag	3.82	14	6.8	1.44	2
Ag	3.70	25	6.9	1.46	3
Cd	4.25	14	7.2	1.48	2
Sn	4.52	14	7.4	1.52	2
Sb	4.35	14	7.3	1.46	2
Au	4.68	14	7.5	1.33	2
Hg	5.64	14	8.3	1.42	2
Hg	5.25	25	8.4	1.44	3
Pb	5.05	14	7.8	1.32	2
Bi	5.17	14	7.9	1.34	2

$$\sigma_r^{(l)}=\frac{4\pi}{k^2}(2l+1)\frac{xX}{x^2|v_l'|^2+X^2|v_l|^2+2Xx}$$

$$\sigma_{el}^{(l)}=\frac{4\pi}{k^2}(2l+1)\left|\sin\delta_l e^{i\delta_l}+\frac{x/|v_l|^2}{i(x/|v_l|^2+X)+x|v'/v|\cos(\delta_l'-\delta)}\right|^2. \quad (8)$$

The sum of these two expressions can be written in the form:

$$\sigma_{tot}^{(l)}=(4\pi/k^2)(2l+1)\left[\sin\delta_l+\frac{\cos2\delta_l(x/|v_l|^2+X)+\sin2\delta_l(x|v'/v|\cos(\delta_l'-\delta_l))}{x^2|v_l'|^2+X^2|v_l|^2+2Xx}\right]. \quad (9)$$

These cross sections are to be summed over l to obtain σ_r, σ_{el}, and σ_{tot}. Note that the $\sin^2\delta_l$ term in σ_{tot} is just the term which would arise from the scattering by an infinitely repulsive sphere of radius R. No resonances appear in any of these cross sections, as may be expected from the fact that the value of f in (5) is a pure imaginary. The value of $\sigma_r^{(0)}$ is $(4\pi/k^2)Xx/(X+x)^2$ which is just $4\pi/k^2$ times the transmission T discussed in the introduction.

Finally, σ_{tr} the transport cross section is computed. We need to evaluate the integral

$$J=\int \sigma_{el}(\theta)\cos\theta/d\Omega.$$

Writing $\sigma_{el}=|f(\theta)|^2$ and $f(\theta)=(1/k)\sum A_lP_l(\cos\theta)$ where

$$A_l=(2l+1)^{\frac{1}{2}}e^{-2i\delta_l}\left[e^{i\delta_l}\sin\delta_l+\frac{x/|v_l|^2}{x|v_l'/v_l|\cos(\delta_l'-\delta_l)+i(X+x/|v_l|^2)}\right]$$

TABLE II. Reaction cross sections at 14 Mev.

Element	$\sigma_r \times 10^{24}$ cm² Exp.	Theor.	Reference
Al	0.90	1.0	5
Al	1.06		7
Fe	1.43	1.4	5
Fe	1.45		7
Cd	1.89	2.0	7
Au	2.51	2.2	7
Hg	2.47	2.5	5
Bi	2.56	2.3	7
Pb	2.22		5
Pb	2.29	2.3	7a
Pb	2.56		7

then

$$J=(4\pi/k^2)\sum_l (2l)/(4l^2-1)Re(A_l\delta A_{l-1}). \quad (10)$$

The transport cross sections are given by $\sigma_{tot}-J$. The curves in Figs. 1, 2, and 3 were computed from formulas (8), (9), and (10).

We now turn to the calculation of the cross sections in the low energy region. This is the region in which the condition (a) is no longer fulfilled. We no longer can use the simplified boundary condition (5). It is expected that resonances will occur at low energies and it seems natural to fall back upon the more detailed expressions derived in FPW and average them over an energy region containing many resonances.

We will prove two points:

(A) The concepts of FPW join continuously into the ones of the present paper; the calculation of the cross sections in the high energy region is a generalization of the ideas used in FPW.

(B) The cross sections as calculated by FPW, and averaged over many resonances, yield the same expressions (9) and (10) for σ_{tot} and σ_{tr} for the low energy region also.

In order to demonstrate (A), we show that the boundary condition (5) follows from the more complicated boundary condition of FPW if the energy of the incident neutron is high. We compare (5) with the corresponding condition, Eqs. (17a) and (24) of FPW:

$$f(W)=f_0(W+i\Gamma_a/2)=-X\tan\frac{\pi}{D}\left(W+\frac{i\Gamma_a}{2}-E_r\right) \quad (11)$$

where Γ_a was called the absorption width in FPW. In the terminology of the present paper Γ_a should be referred to as the reaction width since it is the partial width corresponding to the processes we have included in the reaction cross section. D is the level distance. Expression (11) becomes $f(W)=-iX$ (Eq. (5)) if[d]

$$\pi\Gamma_a/2D\gg 1. \quad (12)$$

Condition (12) requires that the reaction width be large compared to the level distance D. This is the region in which resonances disappear. Thus the boundary condition of FPW goes over into the one used here when the energy of the incident neutron is sufficiently high so that the width of the levels is larger than the distance between them.

We turn next to point (B). In FPW, the total cross section σ_{tot}, is the sum of σ_{sc} and σ_{abs}. The former σ_{sc}, is identical with the elastic scattering cross section σ_{el} of this paper, the latter, σ_{abs}, is the same as the reaction cross section of this paper. The total cross section averaged over many resonances for a partial wave of angular momentum l can be found by adding $\langle\sigma_{abs}\rangle_{Av}^{(l)}$ as given in FPW by the unnumbered equation on p. 154, preceding Eq. (47), and $\langle\sigma_{sc}\rangle_{Av}^{(l)}$ as given by the unnumbered equation on p. 156 preceding Eq. (49). One obtains

$$\langle\sigma_{tot}^{(l)}\rangle_{Av}=\frac{4\pi}{k^2}(2l+1)\left\{\sin^2\delta_l+\frac{\pi}{2}\frac{\Gamma_{nl}}{D}\cos 2\delta_l\right\}. \quad (13)$$

This goes over into expression (9) derived above for the

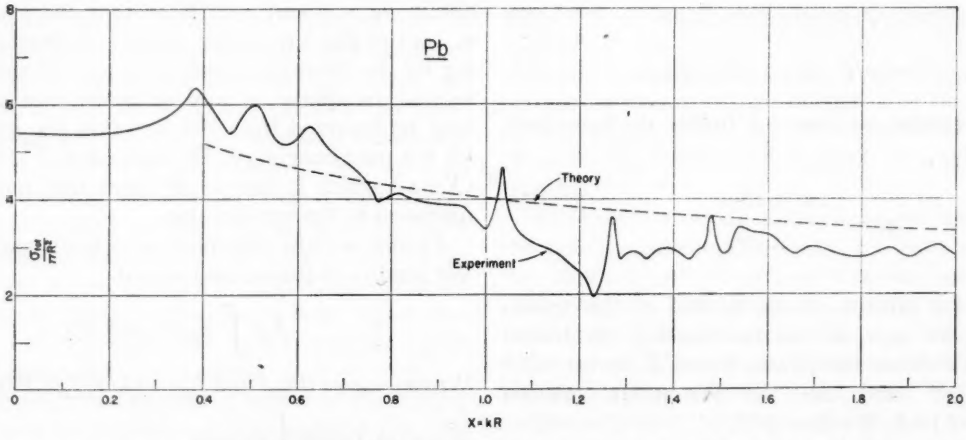

FIG. 3. σ_{tot} for Pb. The full line curve is drawn through the experimental points as given in reference 10. Some fluctuations appearing in this curve are interpreted as resonances, others are within the statistical errors of the measurements. The broken line curve gives the theoretical values for a radius of 7.8×10^{-13} cm.

[d] This has been pointed out first by J. K. Tyson in reference 2.

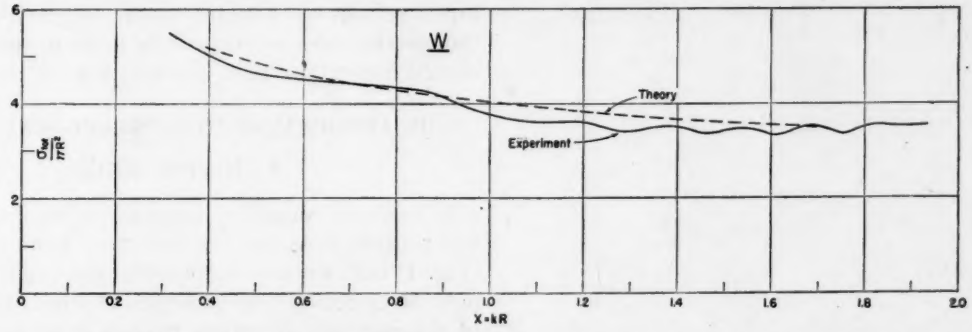

FIG. 4. σ_{tot} for W. The full line curve is drawn through the experimental points of yet unpublished measurements of H. Barschall. We are grateful to the author for giving us his results before publication. The broken line curve gives the theoretical values for a radius of 7.8×10^{-13} cm.

high energy region if $x\ll X$ and if the relation

$$\Gamma_{nl}=\frac{2x}{X}\frac{1}{|v_l|^2}\frac{D}{\pi} \tag{14}$$

is used. Formula (14) was derived in FPW as a qualitative relation between neutron width and level density. It has been found to hold reasonably well in a recent analysis of the experimental data.[4] The condition $x\ll X$ is always fulfilled in the resonance region for there $\Gamma_{nl}\ll D$. Thus we may conclude that the total cross sections given in Fig. 1 hold in the low energy region if the experimental data are averaged over many resonance levels.

The same can be shown to be valid for the transport cross section by employing expression (10) for J. A_l is given by expression (39) in FPW which may be conveniently written as the sum of two terms:

$$A_l=(A_l)_{res}+(A_l)_{pot}$$

$$(A_l)_{res}=(2l+1)^{\frac{1}{2}}e^{-2i\delta_l}\times\frac{x/|v_l|^2}{i(x/|v_l|^2+h)-[f_0-x|v_l'/v_l|\cos(\delta_l'-\delta_l)]}$$

$$(A_l)_{pot}=e^{-i\delta_l}\sin\delta_l.$$

In averaging J over resonances, we make use of the fact that resonances occur at different energies for different l's. Therefore, $Re(A_l^*A_{l-1})$ averaged over a resonance equals

$$\langle Re(A_l^*A_{l-1})\rangle_{Av}=Re\left(\left[(A_l^*)_{pot}(A_{l-1})_{pot}+\frac{1}{\Delta}\int(A_l^*)_{res}(A_{l-1})_{pot}d\epsilon+\frac{1}{\Delta}\int(A_l^*)_{pot}(A_{l-1})_{res}d\epsilon\right]\right),$$

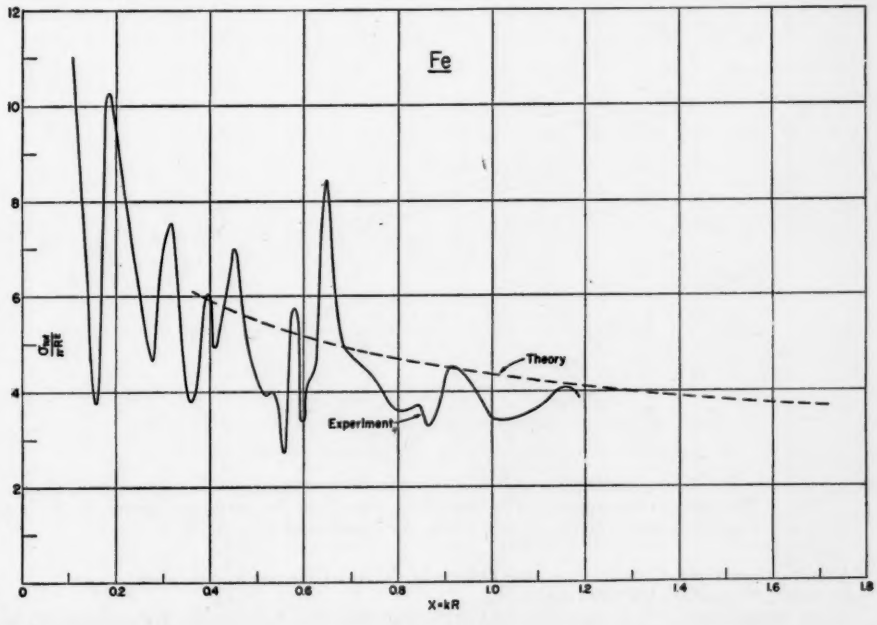

FIG. 5. σ_{tot} for Fe. The full line curve is drawn through the experimental points as given in reference 8. Some fluctuations appearing in this curve are interpreted as resonances, others are within the statistical errors of the measurement. The broken line curve gives the theoretical values for a radius of 4.6×10^{-13} cm.

[4] E. Wigner, Am. J. Phys. 17, 107 (1949).

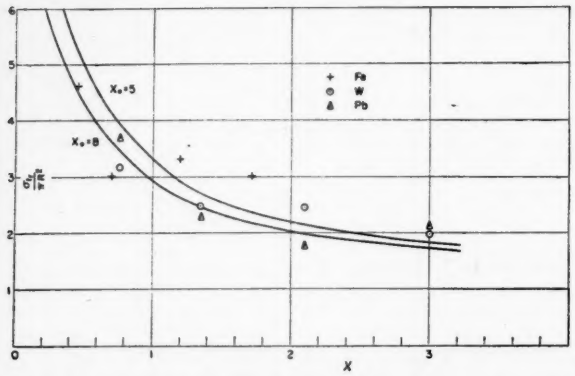

FIG. 6. σ_{tr} for Pb, W, Fe. The full line curves give the theoretical values. The upper curve ($X_0=5$) should be valid for Fe, the lower one ($X_0=8$) for W and Pb.

where the integrals extend over a small energy interval, $\Delta \ll D$, around a characteristic resonance. The result of this calculation is again identical with (10) if we place $x \ll X$ and employ relation (14).

One would not expect the expression (8) for the reaction cross section to hold at the lower energies. Following the derivation, it is clear that σ_r may also be described as the cross section σ_c for the formation of the compound nucleus, since it was calculated by asserting that the neutron is "absorbed" after entering the nucleus. At high energies (and sometimes at very low energies) σ_c and σ_r are identical since the compound nucleus almost always decays into a channel other than the entrance channel. At intermediate energies the compound nucleus will decay with appreciable probability into the entrance channel so that σ_c and σ_r will differ considerably. σ_c will also contain the elastic resonance scattering (which is that decay of the compound nucleus in which the residual nucleus is the target nucleus in its original state). We may expect that the reaction cross section will be lower in the resonance energy region than that shown in Fig. 2.

III. APPLICATION TO EXPERIMENTAL DATA

A. Nuclear Radii

It has been commonly assumed in the evaluation of fast neutron cross sections that $\sigma_{tot}=2\pi R^2$. Our curves (Fig. 1) indicate that this asymptotic value is reached only at extremely high energies at which the concept of a completely absorbing nucleus is no longer applicable. Thus the determination of nuclear radii from the measured cross sections by Amaldi *et al.*,[5] and Sherr[6] must be revised since, at the energies of 14 Mev and 25 Mev, the theoretical values are considerably larger than $2\pi R^2$. Table I gives the result of this re-evaluation on the basis of Fig. 1; the table also includes the value of r_0 required to satisfy the relation

$$R=r_0A^{\frac{1}{3}}.$$

The discrepancy between nuclear radii calculated from 14 and 25 Mev noted in the literature is absent. We should emphasize once more that the value of R determined in this fashion may differ from other evaluations at different energies by as much as 1 or 2×10^{-13} cm.

B. Cross-Section Measurements

A number of neutron cross sections have been measured at an initial neutron energy of 14 Mev which can be interpreted as reaction cross sections. The inelastic scattering cross sections measured by Amaldi *et al.*[5] can be considered as reaction cross sections since inelastic scattering is the principal reaction at that energy. Recently D. D. Phillips and R. W. Davis[7] and also

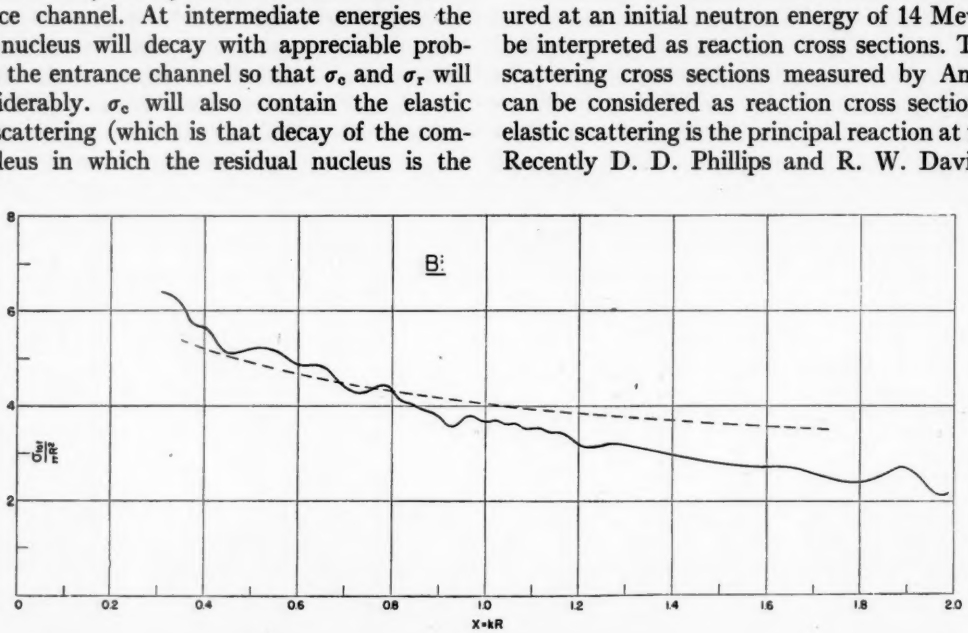

FIG. 7. σ_{tot} for Bi. The full line curve is drawn through the experimental points as given in reference 10. The fluctuations appearing in this curve are within the statistical errors of the measurements. The broken line curve gives the theoretical values for a radius of 7.8×10^{-13} cm.

[5] Amaldi, Bocciarelli, Cacciapuoto, and Trabacchi, Nuovo Cimento 3, 203 (1946).
[6] R. Sherr, Phys. Rev. 68, 240 (1945).
[7] These measurements were made at the Los Alamos Scientific Laboratory. We are grateful to the authors for the communications of these results before publication.

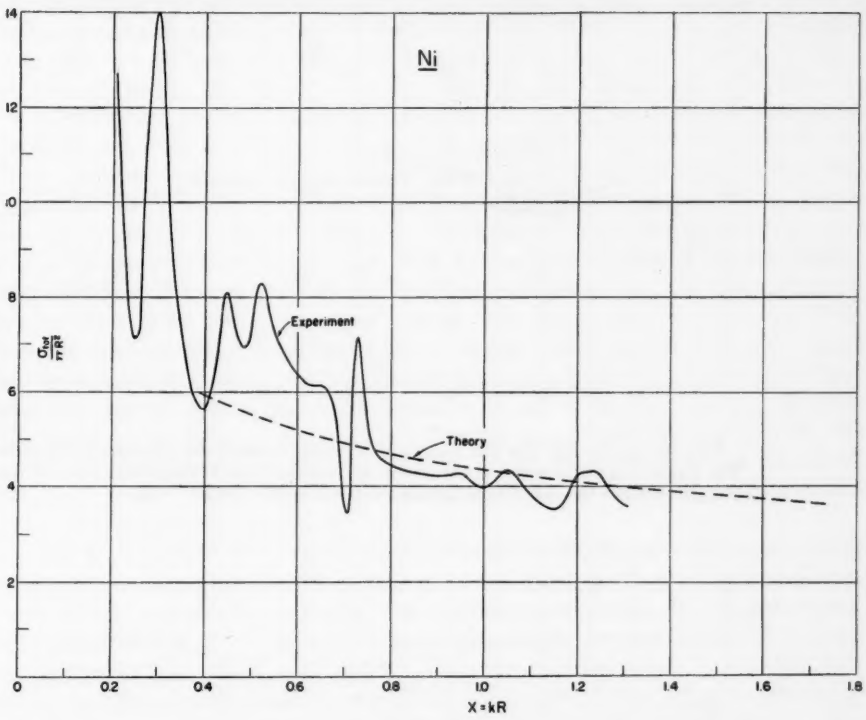

FIG. 8. σ_{tot} for Ni. The full line curve is drawn through the experimental points as given in reference 8. Some fluctuations appearing in this curve are interpreted as resonances, others are within the statistical errors of the measurements. The broken line curve gives the theoretical values for a radius of 4.6×10^{-13} cm.

Gittings *et al.*[7a] have measured the reaction cross section of neutrons at 14 Mev in several elements at determining the cross section for those processes in which the neutron is removed from the beam and is not re-emitted at energies higher than 12 Mev. We do not use the inelastic cross sections given in reference 9 as a measure of the reaction cross section, since they are measured with neutron energies below 3 Mev, where the elastic re-emission of the neutron is not yet negligible. Table II shows the measured values together with the theoretical reaction cross sections calculated with the nuclear radii of Table I. This comparison is a rather sensitive test of the theory, since the reaction cross section is a measure of how many neutrons have penetrated into the nucleus. It checks our basic assumptions, expressed by the boundary condition (5), as to the number of particles which get into the inside of the nucleus and initiate a nuclear reaction. It is also quite sensitive to the value of K_0. The total cross sections are much less sensitive to these assumptions for any change in penetration into the inside of the nucleus is offset by an opposite change in the elastic scattering.

Extensive measurements of total neutron cross sections as functions of the neutron energy have been

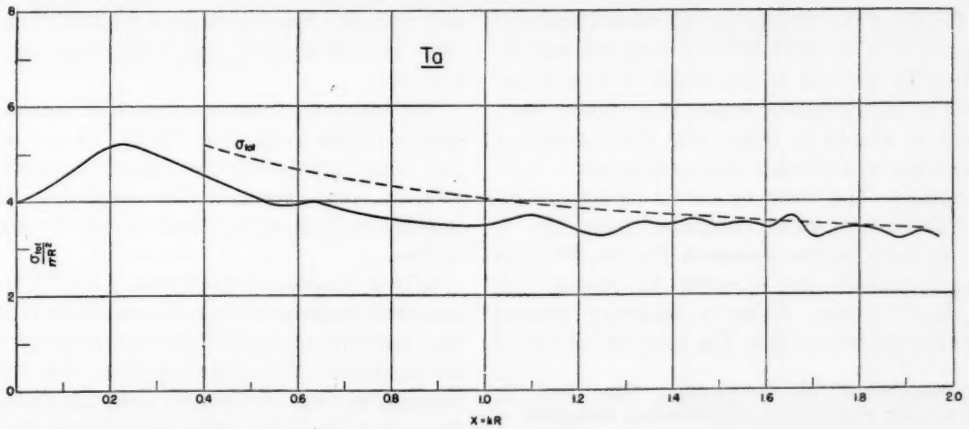

FIG. 9. σ_{tot} for Ta. The full line curve is drawn through the experimental points as given in reference 8a. The fluctuations appearing in this curve are within the statistical errors of the measurements. The broken line curve gives the theoretical values for a radius of 8.5×10^{-13} cm.

[7a] Gittings, Barschall, and Everhart, Phys. Rev. **75**, 1610 (1949).

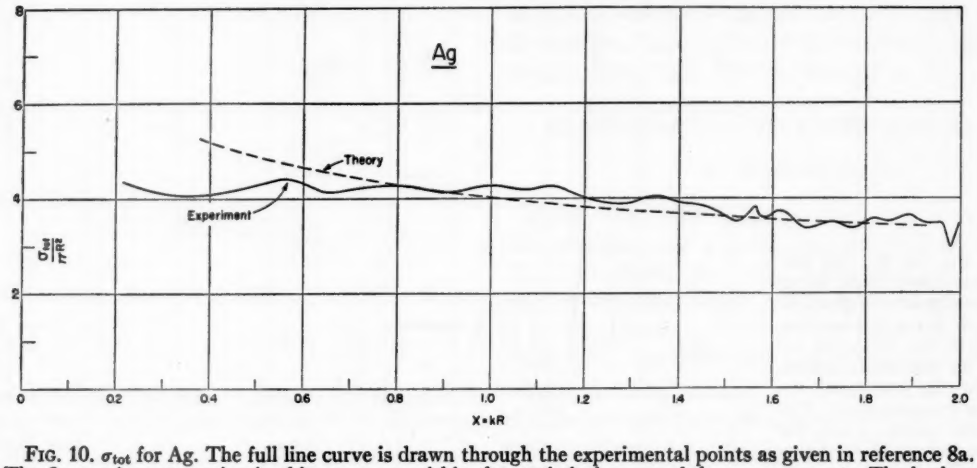

FIG. 10. σ_{tot} for Ag. The full line curve is drawn through the experimental points as given in reference 8a. The fluctuations appearing in this curve are within the statistical errors of the measurements. The broken line curve gives the theoretical values for a radius of 7.5×10^{-13} cm.

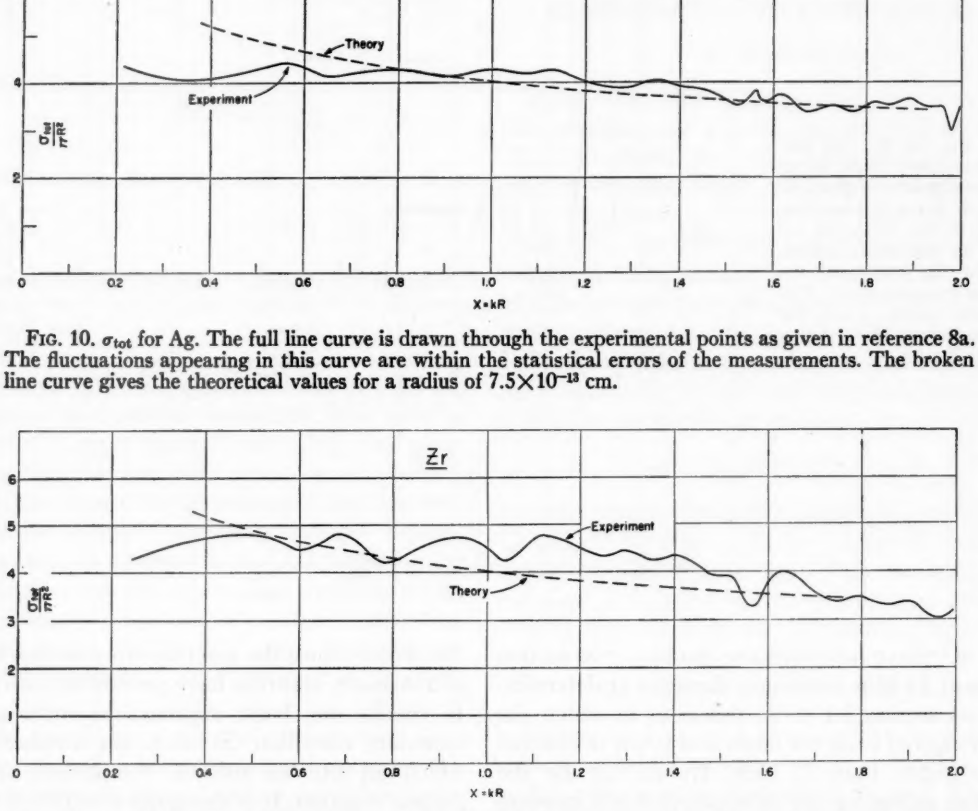

FIG. 11. σ_{tot} for Zr. The full line curve is drawn through the experimental points as given in reference 8a. The fluctuations appearing in this curve are within the statistical errors of the measurements. The broken line curve gives the theoretical values for a radius of 7.8×10^{-13} cm.

made by Barschall *et al.*[8, 8a] on a series of nuclei in the energy region between 50 and 1400 kev. Transport cross sections have been measured at several energies by Barschall *et al.*[9] on a number of elements, especially Fe, W, and Pb. Figures 3–5 show σ_{tot} for these elements. In these figures, and in the following ones, the experimental values are plotted as functions of x and are compared with the theoretical expectation taken from Figs. 1 and 2. It should be noted that the theoretical curve is supposed to represent the average over individual fluctuations. The observed curves lie reasonably close to the theoretical curve computed from Fig. 1. The radius for each of the elements Pb, Bi, W, was taken to be 7.8×10^{-13} cm in order to obtain best agreement. Bi, however, shows a tendency toward lower radii at the higher energies. The value of 7.8×10^{-13} agrees with the radius of Pb as determined by Amaldi *et al.*,[5] which is perhaps fortuitous since the measurements are made in quite different energy regions. The radius taken for Fe, 4.8×10^{-13} cm, does not agree as well with the Amaldi value of 5.4×10^{-13} cm; the difference is within the expected range of fluctuation, however.

The transport cross sections have been measured[8] in a similar energy region for Pb, W, Fe and are plotted in Fig. 6 and compared with theory employing the same radii as were chosen in the calculation of σ_{tot}. It is possible to fit both σ_{tot} and σ_{tr} by the same choice of radius.

It is of interest to note that σ_{tot} for Pb and Bi has the expected theoretical behavior although it is well known that both elements show an exceptionally small $\sigma_{capture}$ for neutrons. This behavior does not contradict our theories in view of the fact that the distance between resonance levels has been found by Barschall[10] for Pb to be large, of the order of 100 kev. This is in contrast to

[8] Barschall, Bockelmann, and Seagondollar, Phys. Rev. **73**, 659 (1948). A number of additional measurements were given to the authors by Barschall prior to publication. We express our appreciation to Dr. Barschall for his communications.

[8a] Bockelmann, Peterson, Adair, and Barschall, Phys. Rev. **76**, 277 (1949).

[9] Barschall, Battat, Bright, Graves, Jorgensen, and Manley, Phys. Rev. **72**, 881 (1947).

[10] Barschall, Bockelman, Peterson, and Adair, Phys. Rev. **76**, 1146 (1949).

most of the other heavy elements investigated so far. In this respect Pb and Bi are similar to light elements such as Fe and Ni. It then follows that the radiation width is much smaller than the neutron width (Eq. (14)), since the neutron width is proportional to the level distance. This has the consequence that neutron re-emission is more probable than neutron capture, leading to low values of σ_{capture}.

We now turn to elements for which only σ_{tot} is measured. Figures 7 to 11 show σ_{tot} for the elements Bi, Ni, Ta, Ag, Zr, between 100 and 1500 kev. We have excluded the region below 100 kev for Ni because it is difficult to average over the strong resonances which occur there. The agreement is fair in Ag, Bi, and Ni, although Bi shows the same tendency toward lower radii at higher energies as Pb. Ta seems to lie below the theoretical curve at low energies. This phenomenon appears more strongly in the following group of elements where it will be discussed. The total cross section for Zr agrees well with theory if a radius of 7.8×10^{-13} is chosen. This value is 1×10^{-13} cm larger than that predicted by $R=1.5\times10^{-13}\ A^{\frac{1}{3}}$ and is still a possible fluctuation of the radius as defined in this theory.

The total cross-section measurements for the elements Sb, I, and In show one common characteristic feature. They are all almost constant in the energy region between 50 and 1400 kev. This behavior is in striking contrast to the elements previously discussed and also to the predictions of our theory. Figures 12, 13, and 14 show that the theoretical curve deviates by almost a factor of 2 if the nuclear radius is chosen so as to fit the high energy end. Only part of this can be explained by assuming variation of nuclear radius with energy. It may be possible to interpret this behavior by assuming an abnormal level distribution such that there is a lack of resonance levels in the low energy region, or that the resonance levels in this region are abnormally weak. We call a level a weak one if its width is much smaller than the relation (14) would predict. The weakness of a level depends therefore upon the level distance. If this is the case, the σ_{tot} is given by σ_0 rather than by σ_{tot} as seen from Eq. (13). We therefore, in Figs. 12–14, have also included the curves for σ_0 which seem to lie closer to the experimental points.

It may be of interest to discuss in this connection the cross section σ_a of radiative capture. This cross section is part of the reaction cross section. It is expected that at very low energies σ_a may approach the full reaction cross section, since the neutron width Γ_n becomes very small (see (13)). Let us call ϵ_0 the energy at which the neutron width is equal to the radiation width Γ_a. For

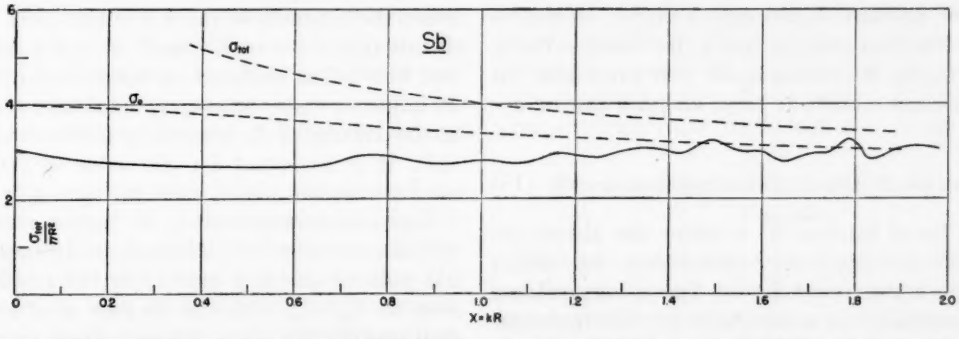

FIG. 12. σ_{tot} for Sb. The full line curve is drawn through the experimental points as given in reference 8a. The fluctuations appearing in this curve are within the statistical errors of the measurements. The broken line curve gives the theoretical values for a radius of 8.5×10^{-13} cm. σ_0 the cross section due to an infinitely repulsive sphere is included.

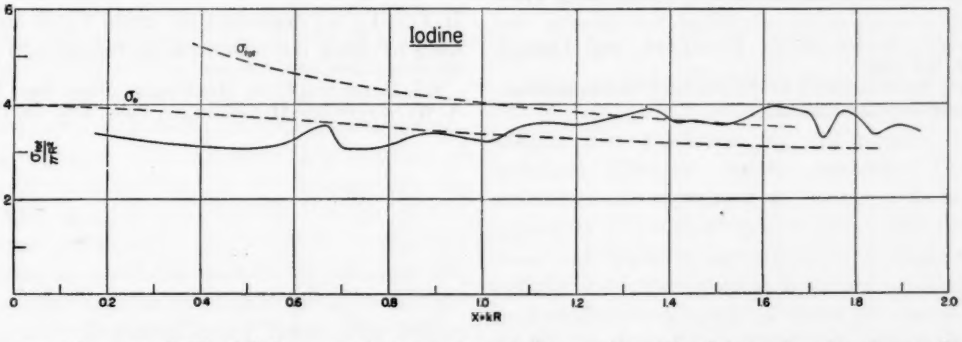

FIG. 13. σ_{tot} for I. The full line curve is drawn through the experimental points as given in reference 8a. The fluctuations appearing in this curve are within the statistical errors of the measurements. The broken line curve gives the theoretical values for a radius of 7.5×10^{-13} cm. σ_0 the cross section due to an infinitely repulsive sphere is included.

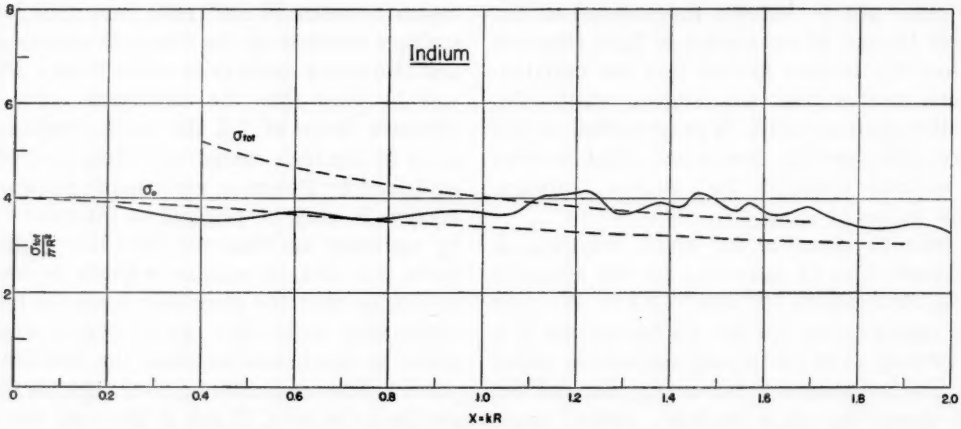

FIG. 14. σ_{tot} for In. The full line curve is drawn through the experimental points as given in reference 8a. The fluctuations appearing in this curve are within the statistical errors of the measurements. The broken line curve gives the theoretical values for a radius of 7.5×10^{-13} cm. σ_0 the cross section due to an infinitely repulsive sphere is included.

energies $\epsilon\ll\epsilon_0$ the re-emission of the neutron is much less likely than the capture, so that we may assume $\sigma_a\cong\sigma_r$, since no other process than capture can occur. In heavier elements ($A>100$) the radiation width Γ_a was found to be of the order of 0.1 ev, and independent of the neutron energy. An approximate average expression for the neutron widths in these nuclei is $\Gamma_n\sim10^{-3}\epsilon^{\frac{1}{2}}$, where ϵ is expressed in ev. This leads to $\epsilon_0\sim10{,}000$ ev, and one should expect that σ_a should be equal to the reaction cross section σ_r for energies below ϵ_0 after averaging over resonances. Our expression for the reaction cross section at these energies can be approximated by

$$\sigma_r\sim4\pi/kK_0\cong500/\epsilon^{\frac{1}{2}} \quad (\epsilon \text{ is expressed in ev}). \quad (15)$$

It would be of interest to measure the absorption cross section averaged over resonances for nuclei $A>100$ in the region below 10^4 ev. The $1/v$ dependence has been established in some nuclei by Lichtenberger *et al.*[11] The value of the constant of the $1/v$ law would be a test of our assumptions concerning Γ_n. Recent measurements by I. H. Dearnley[12] at the G. E. Laboratories have shown some indications that this constant is somewhat smaller than indicated in relation (15). This can be attributed to a number of reasons. A series of "weak" levels, as assumed before to explain the behavior of the total cross section in some elements, would depress the constant in (15). The constant would be decreased also if strong variations of Γ_n occur from level to level. In this case there would be some levels even below ϵ_0 in which $\Gamma_n>\Gamma_r$ and these levels would not lead to capture. Their existence would therefore lower the constant of the $1/v$ law in (15). Some levels of this type have been found[13] in heavy nuclei as W^{186} and Sm^{152}. The existence of these levels, however, has no influence upon the average total cross section as long as the average of Γ_n over many levels remains equal to (14). It is irrelevant for the value of the total cross section whether a level leads to capture or re-emission.

The measurement of σ_a at higher energies ($\epsilon\gg\epsilon_0$) contributes much less information. In fact, as Wigner[4] has pointed out, it is essentially independent of Γ_n as soon as $\Gamma_n\gg\Gamma_r$. This can be seen most simply in the $l=0$ contribution to σ_a whose average over resonances is given by

$$\sigma_a^{(0)}=\frac{2\pi^2}{k^2}\frac{\Gamma_n\Gamma_r}{D(\Gamma_n+\Gamma_r)}.$$

If $\Gamma_n\gg\Gamma_r$, σ_a depends only upon Γ_r/D and cannot be used to check our assumptions regarding Γ_n.

[11] Lichtenberger, Nobles, Monk, Kubitschek, and Dancoff, Phys. Rev. **72**, 164 (1947).

[12] We are very much indebted to Dr. Dearnley for communicating this result prior to publication.

[13] S. Harris and C. O. Muehlhause, Phys. Rev. **76**, 189 (1949); A. W. Sunyar and M. Goldhaber, Phys. Rev. **76**, 189 (1949).

The Uranium 234 Content of Natural Uranium and the Specific Alpha-Activities of the Isotopes

C. A. KIENBERGER
K-25 Laboratory Division, Carbide and Carbon Chemicals Corporation, Oak Ridge, Tennessee
(Received August 1, 1949)

The uranium 234 content of natural uranium was determined, by a combination of alpha-counting and mass spectrometer techniques, to be 0.005481 ± 0.000012 weight percent, the precision being expressed on the basis of 95 percent probability. This corresponds to a half-life of $(2.522 \pm 0.008) \times 10^5$ years. Considering possibilities of bias, these figures are believed to lie within one percent of the true values. In conjunction with this determination, the half-lives of the other natural uranium isotopes were also measured.

PREVIOUS determinations of the weight percent of uranium 234 in natural or "normal" uranium have all involved measurement by the mass spectrometer. Nier first used such an instrument to determine the relative abundance of uranium 238 and uranium 234 in normal uranium.[1] Chamberlain, Williams, and Yuster used two related methods.[2] The first method was identical in principle to Nier's method in that they used the mass spectrometer for a direct measurement of normal uranium. In the second method the specific activity of uranium 234 was determined from the total alpha-activity and relative isotopic abundance of enriched uranium samples, assuming the specific activities of uranium 238 and 235 from the data of others. From their data on the alpha-activity of enriched samples, together with a specific activity figure for uranium 238,[3] it is possible to deduce a value for the content of uranium 234 in natural uranium by computation of the uranium 234 alpha-emission enrichment factor.

By using pure samples of uranium 234 grown from UX_1, Knight, Goldin, P. A. Macklin, and R. L. Macklin of this laboratory have determined the specific activity of uranium 234 from which they calculated, using the specific activity of uranium 238 given in this report, the weight percent of uranium 234 in normal uranium. Their normal abundance figures of 0.005805 ± 0.00008 weight percent is significantly different from that reported in this paper, but the cause of the difference is not yet known.

This report is concerned with a re-determination of the weight percent of uranium 234 in normal uranium by a method similar to the second method used by Chamberlain, Williams, and Yuster, and also an independent re-determination of the specific alpha-activities of the three isotopes. The uranium 234 content of uranium highly enriched in the 234 isotope can be determined with greater accuracy by the use of the mass spectrometer than that achieved in measurements on normal uranium, since the ratio of the uranium 234 to the sum of uranium 235 and 238 in greatly enriched uranium has been increased many times. The alpha-activities of the enriched and normal uranium can then be measured by the use of counting equipment.

EXPERIMENTAL

Apparatus

The counting apparatus consisted of a parallel plate ionization chamber, utilizing electron collection in an atmosphere of nitrogen. The chamber was connected to an amplifier, discriminator, and scaler. The correction for coincident losses on this equipment was of the order of 0.8 percent at 100,000 random counts per minute.

The mass spectrometers used in the present work were of the modified Nier design, as commercially produced by the General Electric Company. The resolution between the ion beams from the 235 and 234 isotopes was such that the height of the valley was less than twenty percent of the height of the 234 voltage peak resulting from ion collection.

Measurement of Alpha-Activity by Alpha-Counting

Uranium samples were prepared for alpha-counting by electroplating a thin film of uranium oxide on an electro-polished nickel disk according to the method described by Cohen and Hull.[4]

The alpha-emissions were counted from films of various weights of uranium 238 and normal uranium, according to a random schedule. The counting rates were corrected for background and expressed as counts per minute per milligram of oxide per one-half solid angle.

Least squares parabolas were placed through each set of data, which permitted the extrapolation to zero weight film thickness for the specific activities of uranium 238 and normal uranium. These specific activities are expressed as oxides with an estimated geometry factor of 50 percent. In order to minimize the bias that might be introduced by a single counter, the specific activities were determined on eight counters.

A correction of 0.4 ± 0.2 count per minute was made on the specific activity of uranium 238 for the 0.05 ± 0.03 p.p.m. of uranium 234 contained in it. All precisions are

[1] A. O. Nier, Phys. Rev. **55**, 150 (1939).
[2] Chamberlain, Williams, and Yuster, Phys. Rev. **70**, 580 (1946).
[3] G. T. Seaborg and I. Perlman, Rev. Mod. Phys. **20**, 637 (1948).
[4] B. Cohen and D. E. Hull, MDDC-387 (October 18, 1946).

TABLE I. Weight percent of uranium 234 in normal.

Sample number	Natural abundance of U^{234}
1	0.005487
2	0.005468
3	0.005487
4	0.005475
5	0.005488
Av.	0.005481±0.000012(±0.2%)

expressed on the basis of 95 percent confidence belts. By placing a visual straight line through a plot of Crawford's back-scattering values against atomic numbers,[5] a correction factor for back-scattering of alpha-particles by the nickel was estimated to be 1.26 ±0.06 percent. Since the counting chamber detects the alpha-particles within an angle of 180°, a counting efficiency value of 50.63 percent was applied to all specific activities. The alpha-disintegration rate of natural uranium metal was then calculated to be 1502±1.5 disintegrations per minute per milligram. The specific activity of uranium 238 was calculated to be 742.7±1.6. Following the assumption of radioactive equilibrium between uranium 238 and 234 in normal uranium, the alpha-activity of uranium 234 in normal was equal to that of uranium 238 in normal, or 737.4 ±1.6 disintegrations per minute per milligram of normal. The remaining 27.2±3.5 disintegrations per minute were assumed to be due wholly to the alpha-activity of uranium 235. The alpha-activity of uranium 235 in normal was then divided by the weight fraction of 235 in normal and a specific activity of 3824±490 disintegrations per minute thus calculated.

Uniform weight films of uranium oxide, prepared from each of four enriched samples and from a fifth sample which was a gravimetric dilution of one of the four, were alpha-counted, and the rates corrected for coincident losses and self absorption in the films. The alpha-counting enrichment factor, A_c, was determined by the formulation of a ratio of the counting rates of enriched uranium to normal uranium as R_c/R_n.

Measurement of the Uranium 234 Content of Uranium Highly Enriched in the 234 Isotope

Using two or more spectrometers, at least forty measurements for uranium 234 and 235 were made of each of the four uranium samples highly enriched in the isotope 234. All weight percents of uranium 234, or e values, were determined to precisions better than one percent.

The Relation of Isotopic Weight Percents and Specific Activities

The following equation relates the alpha-activities of normal and enriched uranium to their isotopic contents:

$$\frac{e}{e_n}=\frac{R_c-R_n^{235}(f/f_n)-R_n^{238}(100-f-e)/(100-f_n-e_n)}{R_n^{234}}, \quad (1)$$

where e=weight percent of uranium 234, f=weight percent of uranium 235, R=alpha-disintegration rate per mg of uranium metal, A_c=relative enrichment in alpha-counting rate over normal or R_c/R_n, subscript c =enriched uranium, subscript n=normal uranium.

Using this expression and the data obtained from measurements on the five enriched samples, the natural abundance of uranium 234 is calculated and summarized in Table I.

TABLE II. Specific activities and half-lives of uranium isotopes.

Isotope	Alpha-activity in normal per mg per min.	Alpha-activity of isotope per mg per min.	Half-life (expressed in years)
U^{234}	737.4±1.6	(1.345±0.004)×10⁷	(2.522±0.008)×10⁵
U^{235}	27.2±3.5	3824±490	(8.8±1.1)×10⁸
U^{238}	737.4±1.6	742.7±1.6	(4.49±0.01)×10⁹
Normal	1502.0±1.5		

DISCUSSION OF RESULTS

The value of 0.005481±0.000012 weight percent of uranium 234 in normal cannot be shown to be significantly different from Nier's value of 0.00574 ±0.00057. Taking into consideration sources of possible bias in spectrometer and counting measurements, it is estimated that the value and the half-life calculated from it are accurate to at least one percent.

The half-life for uranium 234 of (2.522±0.008)×10⁵ years is somewhat less than the (2.69±0.27)×10⁵ value of Nier, and the (2.67±0.04)×10⁵ value of Knight, *et al.*, but is greater than the two values of (2.29±0.14) and (2.35×0.14)×10⁵ years as published by Chamberlain, Williams, and Yuster.[2] Since these values have been calculated using approximately the same alpha-activity, the main discrepancy is then in the weight percent of uranium 234 in normal. The half-life found for uranium 238, given in Table II, is in close agreement with Seaborg's and Perlman's values of 4.498 and 4.51×10⁹ years.[3]

The half-life of uranium 235, given in the preceding table, is not in good agreement with Nier's value of 7.07×10⁸ years[1] but is in good agreement with Clark, Spencer-Palmer, and Woodwards' value of 8.91×10⁸ years as quoted by Seaborg and Perlman.[3]

Since uranium belongs to the actinium series of radio-activity, a comparison in normal uranium of the alpha-activity of the uranium 235 to the alpha-activity of uranium 238 gives the ratio of the actinium series to the uranium series. The value of 3.69±0.48 percent obtained was somewhat lower than that of Nier's value of 4.6 percent but in good agreement with that of

[5] J. A. Crawford, Report AECD 2034 (June 8, 1948).

Clark, Spencer-Palmer, and Woodwards' value of 3.63 percent, obtained with an alpha-ray analyzer. While there are some discrepancies between alpha-activity values, the author feels that since the values determined are dependent on the alpha-activities of both uranium 238 and normal uranium, which are in very close agreement with accepted values,[3,6] the precisions quoted are reasonable.

This document is based on work performed for the Atomic Energy Commission by Carbide and Carbon Chemicals Corporation, at Oak Ridge, Tennessee.

[6] A. F. Kovarik and N. I. Adams, J. App. Phys. **12**, 296 (1941).

PHYSICAL REVIEW VOLUME 76, NUMBER 11 DECEMBER 1, 1949

Comparison of Calculations on Cascade Theory*

HARTLAND S. SNYDER
Brookhaven National Laboratory, Upton, New York
(Received July 25, 1949)

The diffusion equations of the cascade theory of electron showers are solved using improved mathematical methods. The results obtained agree essentially with those obtained earlier by Carlson and Oppenheimer, by Snyder, and by Serber, but do not agree with those obtained by Bhabha and Chakrabarty. Solutions are given corresponding to a single incident electron, a single incident γ-ray, and a $1/E$ spectrum of γ-rays. The total number of particles expected under a given thickness of material are given in tables for various incident energies and each of the above initial conditions. Other tables and formulas are included which enable one to calculate the spectrum of the particles and γ-rays for various initial conditions.

I. INTRODUCTION

SINCE the original papers on the theory of cascade showers by Bhabha and Heitler[1] and by Carlson and Oppenheimer[2] other contributions have been made by Snyder,[3] Landau and Rumer,[4] Serber,[5] Iyengar,[6] and Bhabha and Chakrabarty.[7] The work of Bhabha and Heitler was carried out without including ionization loss and is thus limited to the high energy portion of the spectrum. The calculations of Carlson and Oppenheimer did include ionization loss, but used simplified asymptotic forms for the high energy cross sections. They also replaced the integral equations of cascade theory by a simplifying differential equation. Their solution does not satisfy boundary conditions exactly, but provided the energy of the incident particle is sufficiently large, the error is insignificant. The work of Snyder was an extension of that of Carlson and Oppenheimer, using the same cross sections, but using the integral equations. This solution did not satisfy exact boundary conditions. A difficulty in this work which has been emphasized by Bhabha and Chakrabarty was that a certain function was computed only for integral values of its argument, the non-integral values being obtained by graphical interpolation. Soon after, Landau and Rumer showed that the exact forms for the asymptotic cross sections produced no essential complication. Serber then continued the series of calculations as they were begun by Carlson and Oppenheimer and extended by Snyder, but also with the reservation that the incident energy be large enough so that the errors in the boundary conditions are small. Still later, Iyengar gave a complete solution in which the exact Bethe-Heitler cross sections were used; a solution from which it is not easy to obtain numerical values according to Bhabha and Chakrabarty. At about this same time, Bhabha and Chakrabarty also gave in series forms, an exact solution of the diffusion equations using asymptotic forms for the cross sections.

One of the major difficulties in this work has been to express the solution in such a form that numerical values can be obtained with reasonable ease. This has been particularly true for the total number of particles present at a given thickness and for the energy spectrum of the particles and γ-rays at low energies. Although Bhabha and Chakrabarty have given a series solution which converges even for zero energy, the first two terms in their expansion account for only about seventy-five percent of the total energy dissipated in a shower. On the other hand, the forms of solution as given by Carlson and Oppenheimer, by Snyder and by Serber, give in a single term the total energy dissipated in a shower. The objective of the work being reported in this paper is: (a) to give exact representations for all values of its arguments of the function which had previously been computed only for integral values of its argument, (b) to give a solution of the diffusion equations which satisfies the correct boundary conditions,

* Research carried out at Brookhaven National Laboratory under the auspices of the AEC.
[1] H. J. Bhabha and Heitler, Proc. Roy. Soc. **159**, 432 (1937).
[2] J. F. Carlson and J. R. Oppenheimer, Phys. Rev. **51**, 220 (1937).
[3] H. Snyder, Phys. Rev. **53**, 960 (1938).
[4] L. Landau and Rumer, Proc. Roy. Soc. **166**, 277 (1938).
[5] R. Serber, Phys. Rev. **54**, 317 (1938).
[6] K. S. K. Iyengar, Proc. Ind. Acad. Sci. **A15**, 195 (1942).
[7] H. J. Bhabha and S. K. Chakrabarty, Phys. Rev. **74**, 1352 (1948).

(c) to give formulas and tables by means of which the low energy spectrum of the particles and γ-rays may be computed, (d) to compare the results obtained with those of Bhabha and Chakrabarty.

II. THE DIFFUSION EQUATIONS

The physical basis of the diffusion equations is so well known that we will just reproduce them here. We denote by $P(E, t)$ the number of particles, by $\gamma(E, t)$ the number of quanta each per unit energy at energy E and at depth t. The ionization loss per unit of t we call β. Length t is measured in radiation units

$$\left[4\frac{Z^2N}{137}\left(\frac{e^2}{mc^2}\right)^2 \ln(191Z^{-1/3})\right]^{-1}.$$

The diffusion equations then are

$$\frac{\partial P(E,t)}{\partial t}-\beta\frac{\partial P(E,t)}{\partial E}$$
$$=\lim_{\delta\to 0}\left[\int_{E+\delta}^{\infty} P(E',t)R(E',E'-E)\frac{E'-E}{E'^2}dE'\right.$$
$$\left.-P(E,t)\int_{\delta}^{E} R(E,E')\frac{E'dE'}{E^2}\right]$$
$$+2\int_E^{\infty}\gamma(E',t)R(E,E')\frac{dE'}{E'} \quad (1)$$

$$\frac{\partial\gamma(E,t)}{\partial t}=\int_E^{\infty} P(E',t)R(E',E)\frac{EdE'}{E'^2}$$
$$-\gamma(E,t)\int_0^{E} R(E',E)\frac{dE'}{E}. \quad (2)$$

In these equations we take

$$R(E,E')=\left[1-\frac{4}{3}\frac{E}{E'}+\frac{4}{3}\left(\frac{E}{E'}\right)^2\right]\left[1+\frac{3}{4}\alpha\right]-\frac{3}{4}\alpha \quad (3)$$

$$\alpha=[9\ln 191Z^{-\frac{1}{3}}]^{-1}\simeq\frac{1}{40}. \quad (4)$$

Through the use of Eq. (3) we are limiting outselves to the asymptotic forms for the cross sections. We now look for solutions of (1) and (2) depending on a parameter, y, of the form

$$P_y(E,t)=\frac{1}{2\pi i\beta}$$
$$\times\int_c\left(\frac{\beta}{E}\right)^{y+s+1}K_\mu(y,s)\Gamma(-s)\Gamma(y+s+1)e^{\mu t}ds, \quad (5)$$

$$\gamma_y(E,t)=\frac{1}{2\pi i\beta}$$
$$\times\int_c\left(\frac{\beta}{E}\right)^{y+s+1}L_\mu(y,s)\Gamma(-s)\Gamma(y+s+1)e^{\mu t}ds. \quad (6)$$

The contour of integration for s is taken to be a straight line parallel to the imaginary axis passing to the left of the origin and from $-i\infty-\delta$ to $i\infty-\delta$ with $\delta>0$. Substituting (5) and (6) into (1) and (2) and using (3) we get

$$\frac{1}{2\pi i\beta}\int_c ds\left(\frac{\beta}{E}\right)^{y+s+1}\Gamma(-s)\Gamma(y+s+1)$$
$$\times\left\{[\mu+A(y+s)]K_\mu(y,s)-B(y+s)L_\mu(y,s)\right.$$
$$\left.+(y+s+1)\frac{\beta}{E}K_\mu(y,s)\right\}e^{\mu t}=0, \quad (7)$$

and

$$\frac{1}{2\pi i\beta}\int_c ds\left(\frac{\beta}{E}\right)^{y+s+1}\Gamma(-s)\Gamma(y+s+1)$$
$$\times\{[\mu+D]L_\mu(y,s)-C(y+s)K_\mu(y,s)\}e^{\mu t}=0, \quad (8)$$

in which

$$A(y)=\left(\frac{4}{3}+\alpha\right)\left(\frac{d\ln\Gamma(y+1)}{dy}\right.$$
$$\left.+.5772\cdots-1+\frac{1}{y+1}\right)+\frac{1}{2}-\frac{1}{(y+1)(y+2)}, \quad (9)$$

$$B(y)=2\left(\frac{1}{y+1}-\right)\left(\frac{4}{3}+\alpha\right)\left(\frac{1}{(y+2)(y+3)}\right), \quad (10)$$

$$C(y)=\frac{1}{y+2}+\left(\frac{4}{3}+\alpha\right)\frac{1}{y(y+1)}, \quad (11)$$

$$D=7/9-1/6\alpha. \quad (12)$$

In order that (7) and (8) follow from (1) and (2), the real part of $y+s$ must be positive. Now, both terms in (8), and all except the last term in (7) have the same power of (β/E). If $K_\mu(y,s)$ is an analytic function of s in the strip from $-i\infty$ to $i\infty$ with real part between $-1-\delta$ and $-\delta$, the contour of integration for s may be displaced one unit to the left in the last term of (7). Under these conditions (5) and (6) will be a solution of

(1) and (2) provided

$$[\mu+A(y+s)]K_\mu(y,s)-B(y+s)L_\mu(y,s)=sK_\mu(y,s-1) \quad (13)$$

$$[\mu+D]L_\mu(y,s)-C(y+s)K_\mu(y,s)=0. \quad (14)$$

Eliminating $L_\mu(y,s)$ between Eqs. (13) and (14), we get

$$\{\mu^2+[A(y+s)+D]\mu+A(y+s)D-B(y+s)C(y+s)\}K_\mu(y,s)=s[\mu+D]K_\mu(y,s-1). \quad (15)$$

In order to make the dependence of μ definite, we take it to be a function of y satisfying the equation

$$\mu^2(y)+[A(y)+D]\mu(y)+A(y)D-B(y)C(y)=0. \quad (16)$$

The roots of (16) will now be called $\mu(y)$ and $\nu(y)$ with

$$\begin{aligned}\mu(y)&=-\tfrac{1}{2}[A(y)+D]+\tfrac{1}{2}\{[A(y)-D]^2+4B(y)C(y)\}^{\frac{1}{2}},\\ \nu(y)&=-\tfrac{1}{2}[A(y)+D]-\tfrac{1}{2}\{[A(y)-D]^2+4B(y)C(y)\}^{\frac{1}{2}}.\end{aligned} \quad (17)$$

By eliminating $\mu^2(y)$ between (16) and (15), we get

$$\{[A(y+s)-A(y)][\mu(y)+D]+B(y)C(y)-B(y+s)C(y+s)\}K_\mu(y,s)=s[\mu(y)+D]K_\mu(y,s-1), \quad (18)$$

or, to save writing later,

$$K_\mu(y,s)=g_\mu(y,s-1)K_\mu(y,s-1), \quad (19)$$

with

$$g_\mu(y,s-1)=\frac{s[\mu(y)+D]}{\left([A(y+s)-A(y)][\mu(y)+D]+B(y)C(y)-B(y+s)C(y+s)\right)}. \quad (20)$$

We shall show that a solution of (19) is

$$K_\mu(y,s+z)=K_\mu(y,s)[g_\mu(y,s)]^z\times\prod_{n=0}^{\infty}\left\{\frac{g_\mu(y,s+n)}{g_\mu(y,s+z+n)}\left(\frac{g_\mu(y,s+n+1)}{g_\mu(y,s+n)}\right)^z\right\}. \quad (21)$$

Using the asymptotic form for $A(y)$ it is easy to verify that the infinite product in (21) converges and that $\lim_{N\to\infty}[g_\mu(y,s+N)/g_\mu(y,N)]=1$, conditions which are necessary and sufficient for (21) to be a solution of (19). If (21) is a solution of (19) we should have (setting $s\to 0$, $z\to s$)

$$K_\mu(y,s)=\lim_{N\to\infty}[g_\mu(y,N+1)]^s\times\prod_{n=0}^{N}\frac{g_\mu(y,n)}{g_\mu(y,s+n)}, \quad (22)$$

if we take $K_\mu(y,0)=1$. Substituting (22) into (21) we get

$$\begin{aligned}K_\mu(y,s+z)&=\lim_{N\to\infty}g_\mu(y,N+1)^s\prod_{n=0}^{N}\frac{g_\mu(y,n)}{g_\mu(y,s+n)}\\ &\times\lim_{M\to\infty}g_\mu(y,s+M+1)^z\prod_{m=0}^{M}\frac{g_\mu(y,s+m)}{g_\mu(y,s+z+m)}\\ &=\lim_{N\to\infty}\left(\frac{g_\mu(y,s+N+1)}{g_\mu(y,N+1)}\right)^z g_\mu(y,N+1)^{s+z}\\ &\times\prod_{n=0}^{N}\frac{g_\mu(y,n)}{g_\mu(y,s+z+n)}.\end{aligned} \quad (23)$$

Since $\lim_{N\to\infty}\dfrac{g_\mu(y,s+N+1)}{g_\mu(y,N+1)}=1$ (23) gives

$$K_\mu(y,s+z)=\lim_{N\to\infty}g_\mu(y,N+1)^{s+z}\times\prod_{n=0}^{N}\frac{g_\mu(y,n)}{g_\mu(y,s+z+n)}, \quad (24)$$

which is (22) with s replaced by $s+z$. We thus see that the right-hand side of (21) depends only on $s+z$, as it must, if the left side is to depend only on $s+z$. Since (21) is valid for all values of z, it holds for $z=1$, in which case we get $K_\mu(y,s+1)=g_\mu(y,s)K_\mu(y,s)$ which is (19) with s replaced by $s+1$. Thus we see that (21) is a solution of (19).

The analytic character of $K_\mu(y,s)$ is most readily seen from Eq. (22). From the expression for $g_\mu(y,s)$ as determined from Eq. (20), and the values of $A(y)$, $B(y)$, and $C(y)$, one can see that $g_\mu(y,s)$ is finite and non-vanishing for all finite values of s except for zeros at $s=-y-n$, $n=1,2,3\cdots$. As a consequence of this property and the fact that (21) converges, $K_\mu(y,s)$ is analytic and non-vanishing for all finite values of s except for isolated poles at the points $s=-y-n$ with $n=1,2,3\cdots$. From the fact obtained earlier that real part $(y+s)$ must be greater than zero, we now see that the condition given earlier that the function $K_\mu(y,s)$ must be analytic in s in the strip $-i\infty$ to $i\infty$ with real part of s between $-1-\delta$ and $-\delta$ is in fact satisfied by (21).

The infinite product given by (21) does not converge very rapidly, so it is not very useful for numerical calculations. However, other expressions which con-

verge to the same value, but which converge much more rapidly can be found. The sequence of functions which was used for the numerical calculations is

$$K_\mu(y, s+z)=K_\mu(y, s)\lim_{N\to\infty}[g_\mu(y, s+N-1)]^{\alpha(z)}$$
$$\times[g_\mu(y, s+N)]^{\beta(z)}[g_\mu(y, s+N+1)]^{\gamma(z)}$$
$$\times[g_\mu(y, s+N+2)]^{\delta(z)}\prod_{n=0}^{N}\frac{g_\mu(y, s+n)}{g_\mu(y, s+z+n)} \quad (25)$$

with

$$\alpha(z)=-1/24\, z(z+1)(z-1)(z-2),$$
$$\beta(z)=\ 1/24\, z(z-1)(z-2)(3z+7),$$
$$\gamma(z)=-1/24\, z(z+1)(z+2)(3z-7),$$
$$\delta(z)=\ 1/24\, z(z-1)(z+1)(z+2).$$

The polynomials $\alpha(z)$, $\beta(z)$, $\gamma(z)$, $\delta(z)$ were chosen so that (25) gives exact results for all N if $z=0, \pm1, \pm2$. Also, $\alpha(z)+\beta(z)+\gamma(z)+\delta(z)=z$ which insures that (25) converges for the same values as (21).

However, for a given value of N, the number of terms in the product, and for small z (25) give results better by several significant figures than does (21).

III. THE BOUNDARY VALUE PROBLEM

In Section II we have given two solutions for each value of a certain parameter, y, of the diffusion equations of cascade theory. Our problem in this section will be to combine these solutions in such a manner that the resulting solution will represent either a single charged particle or a single photon of energy E_0, incident on the top of the material. To do this we write

$$P(E, t)=-\frac{1}{(2\pi)^2\beta}\sum_{n=0}^{\infty}\int_D dy\int_C ds$$
$$\times\frac{\Gamma(-s)\Gamma(y+s+n+1)}{\Gamma(y+n+1)[\mu(y+n)-\nu(y+n)]}$$
$$\times\left(\frac{E_0}{\beta}\right)^{y}\left(\frac{\beta}{E}\right)^{y+s+n+1}$$
$$\times\{A_n(y+n)[\mu(y+n)+D]K_\mu(y+n, s)e^{\mu(y+n)t}$$
$$-B_n(y+n)[\nu(y+n)+D]K_\nu(y+n, s)e^{\nu(y+n)t}\}, \quad (26)$$

$$\gamma(E, t)=-\frac{1}{(2\pi)^2\beta}\sum_{n=0}^{\infty}\int_D dy\int_C ds$$
$$\times\frac{\Gamma(-s)\Gamma(y+s+n+1)}{\Gamma(y+n+1)[\mu(y+n)-\nu(y+n)]}$$
$$\times\left(\frac{E_0}{\beta}\right)^{y}\left(\frac{\beta}{E}\right)^{y+s+n+1}C(y+s+n)$$
$$\times\{A_n(y+n)K_\mu(y+n, s)e^{\mu(y+n)t}$$
$$-B_n(y+n)K_\nu(y+n, s)e^{\nu(y+n)t}\}. \quad (27)$$

Equations (26) and (27) are simply linear combinations of (5) and (6), respectively, using both roots of Eq. (16) as given in Eq. (17). The function $K_\nu(y, s)$ is determined by using $\nu(y)$ instead of $\mu(y)$ in (21). In Eq. (27) we have used relation (14) to eliminate $L_\mu(y, s)$ and $L_\nu(y, s)$. Our problem is to determine the functions $A_n(y+n)$ and $B_n(y+n)$ to fit the given boundary conditions. The contour of integration for y is taken to be a straight line from $-i\infty+\epsilon$ to $i\infty+\epsilon$ and with real part of $y+s$ greater than zero.

If we now evaluate the integral over s in $P(E, t)$ in terms of the residues of the integrand at $s=0, 1, 2, \cdots$, we can write the result in the form

$$P(E, t)=\frac{1}{2\pi i\beta}\sum_{N=0}^{\infty}\sum_{k=0}^{N}\int_D dy\Gamma(y+N+1)(-1)^k\left(\frac{E_0}{E}\right)^{y}\left(\frac{\beta}{E}\right)^{N+1}$$
$$\times\frac{\{A_{N-k}(y+N-k)[\mu(y+N-k)+D]K_\mu(y+N-k, k)e^{\mu(y+N-k)t}}{\Gamma(k+1)\Gamma(y+N-k+1)[\mu(y+N-k)-\nu(y+N-k)]}$$
$$-B_{N-k}(y+N-k)[\nu(y+N-k)+D]K_\nu(y+N-k, k)e^{\nu(y+N-k)t}\}. \quad (28)$$

An entirely analogous expression could have been written for $\gamma(E, t)$.

Since the functions $A_n(y+n)$ and $B_n(y+n)$ are not uniquely determined at this point, we subject them to the relationships

$$\sum_{k=0}^{N}\frac{(-1)^k[\mu(y+N-k)-\nu(y+N-k)]^{-1}}{\Gamma(k+1)\Gamma(y+N-k+1)}\{A_{N-k}(y+N-k)[\mu(y+N-k)+D]K_\mu(y+N-k, k)$$
$$-B_{N-k}(y+N-k)[\nu(y+N-k)+D]K_\nu(y+N-k, k)\}=0, \quad (29)$$

$$\sum_{k=0}^{N}\frac{(-1)^k[\mu(y+N-k)-\nu(y+N-k)]^{-1}}{\Gamma(k+1)\Gamma(y+N-k+1)}\{A_{N-k}(y+N-k)K_\mu(y+N-k, k)$$
$$-B_{N-k}(y+N-k, k)K_\nu(y+N-k, k)\}=0, \quad (30)$$

for $N=1, 2, 3, \cdots$. The relations (29) and (30) were chosen so that only the terms with $A_0(y)$ and $B_0(y)$ survive at $t=0$ in (27) and (28). If we use relationships (29) and (30), we find for $t=0$ the values

$$P(E,0)=\frac{1}{2\pi i E_0}\int_D dy\left(\frac{E_0}{E}\right)^{y+1}\times\left\{\frac{A_0(y)[\mu(y)+D]-B_0(y)[\nu(y)+D]}{\mu(y)-\nu(y)}\right\}, \quad (31)$$

$$\gamma(E,0)=\frac{1}{2\pi i E_0}\int_D dy\left(\frac{E_0}{E}\right)^{y+1}\times\left\{\frac{A_0(y)-B_0(y)}{\mu(y)-\nu(y)}\right\}C(y). \quad (32)$$

If the incident radiation is a single charged particle of energy E_0, then from (31) and (32) we obtain

$$A_0(y)=B_0(y)=1. \quad (33)$$

If the incident radiation is a single γ-ray of energy E_0, we obtain

$$A_0\dagger(y)=-\frac{[\nu(y)+D]}{C(y)}, \quad B_0\dagger(y)=-\frac{[\mu(y)+D]}{C(y)}. \quad (34a)$$

If the incident radiation contains no charged particles and has a $1/E$ distribution of γ-rays up to the energy E_0,

$$A_0^*(y)=-\frac{[\nu(y)+D]}{yC(y)}, \quad B_0^*(y)=-\frac{[\mu(y)+D]}{yC(y)}. \quad (34b)$$

Note the fact that we have placed an asterisk on the $A_0(y)$ to indicate these particular boundary conditions. We have also placed a dagger on the $A_0\dagger(y)$ and $B_0\dagger(y)$ to indicate the particular boundary condition as given by (34a). Throughout the remainder of this paper an asterisk or dagger will be placed on various quantities whenever it is necessary to distinguish the initial conditions (34a) or (34b) from (33).

We now give the solution of Eqs. (29) and (30) for $A_N(y+N)$ and $B_N(y+N)$, namely,

$$A_N(y+N)=\sum_{k=1}^{N}\frac{(-1)^{k+1}\Gamma(y+N+1)}{\Gamma(y+N-k+1)[\mu(y+N-k)-\nu(y+N-k)]\Gamma(k+1)}\times\{[\mu(y+N-k)-\nu(y+N)]K_\mu(y+N-k,k)A_{N-k}(y+N-k)-[\nu(y+N-k)-\nu(y+N)]K_\nu(y+N-k,k)B_{N-k}(y+N-k)\}. \quad (35)$$

$$B_N(y+N)=\sum_{k=1}^{N}\frac{(-1)^{k+1}\Gamma(y+N+1)}{\Gamma(y+N-k+1)[\mu(y+N-k)-\nu(y+N-k)]\Gamma(k+1)}\times\{[\mu(y+N-k)-\mu(y+N)]K_\mu(y+N-k,k)A_{N-k}(y+N-k)-[\nu(y+N-k)-\mu(y+N)]K_\nu(y+N-k,k)B_{N-k}(y+N-k)\}. \quad (36)$$

Through the recursion relationships (35) and (36), $A_N(y+N)$ and $B_N(y+N)$ can ultimately be expressed in terms of certain rational functions of y, $\mu(y+N)$, $\nu(y+N)$ through the values of $A_0(y)$ and $B_0(y)$ as given by either (33) or (34).

We note here that if we define

$$f_{N+1}(y+1,t)=\sum_{k=0}^{N}\frac{(-1)^{k+N}\Gamma(y+1)}{\Gamma(k+1)\Gamma(y+N-k+1)[\mu(y+N-k)-\nu(y+N-k)]}\times\{A_{N-k}(y+N-k)[\mu(y+N-k)+D]K_\mu(y+N-k,k)e^{\mu(y+N-k)t}-B_{N-k}(y+N-k)[\nu(y+N-k)+D]K_\nu(y+N-k,k)e^{\nu(y+N-k)t},$$

then we can write (28) in the form

$$P(E,t)=\frac{1}{2\pi i E_0}\int_D dy\left(\frac{E_0}{E}\right)^{y+1}\sum_{N=0}^{\infty}f_N(y+1,t). \quad (37)$$

One can prove, except for notation, if we use $A_0(y)=B_0(y)=1$, that the functions $f_N(y,t)$ are identical with those given by Bhabha and Chakrabarty in their Eqs. (11); thus our solution is, as it must be, identical with their solution.

In order to express the solution in a form which is most useful for obtaining the total number of particles in the shower, and the low energy spectrum of the particles and the γ-rays, we examine the analytic character of the functions $A_N(y)$ and $B_N(y)$. To do this we note that the functions $\mu(y)$ and $\nu(y)$ have branch points at $y=0$ and in the negative half-plane. As one passes around a branch point the functions $\mu(y)$ and $\nu(y)$ interchange. Exactly the same properties are true of the functions $K_\mu(y,s)$ and $K_\nu(y,s)$. This property

TABLE I.

y	$\mu(y)$	$a(y)$	$b(y)$	$H(y)$	$M(y)$	$A_1(y)$	$\alpha(y)$	$\beta(y)$	$A_0^*(y)$	$A_1^*(y)$	$\alpha^*(y)$	$\beta^*(y)$	$f(y)$
0.1	3.7875	2.4997	2.718	0.187	0.100	−0.0019	0.4892	0.4894	3.0711	0.00872	1.0354	0.8103	3.600
0.2	2.2793	1.8904	2.415	0.275	0.200	−0.0099	0.5002	0.4447	2.0975	0.0365	1.0516	0.9388	3.385
0.3	1.5686	1.6239	2.185	0.3295	0.300	−0.021	0.5460	0.3663	1.6800	0.0813	1.0864	0.9487	3.140
0.4	1.1253	1.4614	2.055	0.3645	0.410	−0.041	0.6220	0.2603	1.4424	0.1410	1.1385	0.9096	2.890
0.5	0.8122	1.3458	1.875	0.3830	0.515	−0.054	0.7320	0.1811	1.2900	0.2220	1.2138	0.8616	2.635
0.6	0.5751	1.2548	1.762	0.3940	0.620	−0.061	0.8440	0.0937	1.1859	0.2980	1.2818	0.8225	2.375
0.7	0.3876	1.1785	1.680	0.4005	0.730	−0.063	0.9700	0.0918	1.1128	0.4030	1.3558	0.8684	2.095
0.8	0.2347	1.1110	1.635	0.4021	0.841	−0.052	1.093	0.148	1.0609	0.5153	1.4196	0.9712	1.705
0.9	0.1075	1.0490	1.599	0.4000	0.960	−0.034	1.205	0.250	1.0245	0.6250	1.4681	1.1114	1.530
1.0	0	0.9905	1.562	0.3951	1.074	0	1.304	0.379	1.0000	0.7360	1.4991	1.2687	1.284
1.1	−0.0918	0.9344	1.545	0.3875	1.200	+0.0418	1.390	0.521	0.9848	0.8594	1.5146	1.4261	1.085
1.2	−0.1706	0.8797	1.537	0.3775	1.315	0.087	1.463	0.664	0.9772	0.9870	1.5157	1.5772	0.810
1.3	−0.2390	0.8291	1.520	0.3640	1.435	0.148	1.524	0.796	0.9758	1.123	1.5083	1.6935	0.750
1.4	−0.3001	0.7690	1.500	0.3490	1.550	0.213	1.575	0.916	0.9778	1.272	1.4821	1.7925	0.615
1.5	−0.3500	0.7237	1.475	0.3335	1.670	0.289	1.618	1.024	0.9877	1.430	1.4645	1.8471	0.480
1.6	−0.3952	0.6747	1.445	0.3195	1.790	0.370	1.654	1.121	0.9996	1.590	1.4388	1.8789	0.360
1.7	−0.4346	0.6276	1.420	0.3050	1.910	0.454	1.686	1.208	1.0145	1.759	1.4122	1.8766	0.250
1.8	−0.4692	0.5826	1.375	0.2915	2.035	0.546	1.712	1.279	1.0321	1.950	1.3854	1.8486	0.155
1.9	−0.4996	0.5400	1.335	0.2785	2.150	0.641	1.734	1.342	1.0517	2.140	1.3608	1.8030	0.055
2.0	−0.5262	0.5001	1.276	0.2673	2.272	0.746	1.753	1.389	1.0727	2.333	1.3382	1.7565	−0.034
2.1	−0.5497	0.4625	1.215	0.2555	2.395	0.845	1.770	1.446	1.0962	2.545	1.3185	1.7104	−0.135
2.2	−0.5704	0.4277	1.150	0.2445	2.530	0.950	1.784	1.490	1.1203	2.762	1.3015	1.6455	−0.230
2.3	−0.5887	0.3956	1.090	0.2335	2.655	1.061	1.797	1.522	1.1453	2.984	1.2870	1.5781	−0.310
2.4	−0.6049	0.3659	1.040	0.2240	2.790	1.173	1.808	1.554	1.1710	3.229	1.2752	1.5180	−0.405
2.5	−0.6193	0.3386	0.985	0.2140	2.930	1.286	1.818	1.582	1.1972	3.482	1.2659	1.4592	−0.490
2.6	−0.6322	0.3136	0.935	0.2055	3.060	1.400	1.827	1.609	1.2237	3.740	1.2597	1.4075	−0.565
2.7	−0.6435	0.2908	0.880	0.1975	3.210	1.513	1.835	1.632	1.2506	4.025	1.2551	1.3603	−0.650
2.8	−0.6537	0.2699	0.830	0.1905	3.355	1.633	1.842	1.651	1.2775	4.312	1.2517	1.3154	−0.730
2.9	−0.6628	0.2508	0.780	0.1845	3.510	1.752	1.848	1.666	1.3044	4.601	1.2493	1.2721	−0.805
3.0	−0.6710	0.2335	0.733	0.1799	3.688	1.889	1.854	1.687	1.3307	4.888	1.2501	1.2405	−0.881

also holds true for the $A_0(y)$, and $B_0(y)$, redundantly in case $A_0(y)$ and $B_0(y)$ are given by (33), and also if $A_0(y)$ and $B_0(y)$ are given by (34). By examination of (35) and (36) one can see by an induction argument that the functions $A_n(y)$ and $B_n(y)$ are analytic for real part of y greater than zero, and that they have branch points only where $\mu(y)$ and $\nu(y)$ have branch points, and that if we pass around a branch point the functions $A_N(y)$, and $B_N(y)$ interchange. The analytic property of $A_N(y)$ and $B_N(y)$ for real part of y greater than zero enables us to displace the contour of integration, D,n units to the left in the n^{th} terms of Eqs. (26) and (27). We then obtain

$$P(E,t)=-\frac{1}{(2\pi)^2\beta}\sum_{n=0}^{\infty}\left(\frac{\beta}{E_0}\right)^n\int_D dy\int_C ds \times\frac{\Gamma(-s)\Gamma(y+s+1)}{\Gamma(y+1)[\mu(y)-\nu(y)]}\left(\frac{E_0}{\beta}\right)^{\nu}\left(\frac{\beta}{E}\right)^{\nu+s+1} \times\{A_n(y)[\mu(y)+D]K_\mu(y,s)e^{\mu(y)t} -B_n(y)[\nu(y)+D]K_\nu(y,s)e^{\nu(y)t}\}, \quad (38)$$

$$\gamma(E,t)=-\frac{1}{(2\pi)^2\beta}\sum_{n=0}^{\infty}\left(\frac{\beta}{E_0}\right)^n\int_D dy\int_C ds \times\frac{\Gamma(-s)\Gamma(y+s+1)}{\Gamma(y+1)[\mu(y)-\nu(y)]}\left(\frac{E_0}{\beta}\right)^{\nu}\left(\frac{\beta}{E}\right)^{\nu+s+1}C(y+s) \times\{A_n(y)K_\mu(y,s)e^{\mu(y)t}-B_n(y)K_\nu(y,s)e^{\nu(y)t}\}. \quad (39)$$

It is the first term in the expansion of the solution in the form (38), (39) in powers of β/E_0 that has been used previously by Snyder and Serber, and as one can see from (38) and (39) this is adequate for all values of the energy and thickness provided (β/E_0) is sufficiently small. We observed here for reference that the integrands of (38) and (39) do not have branch points as functions of y and s.

We now write (38) in the form

$$P(E,t)=\sum_{n=0}^{\infty}\left(\frac{\beta}{E_0}\right)^n P_n(E,t),$$

with

$$P_n(E,t)=-\frac{1}{(2\pi)^2\beta}\int_D dy\int_S ds \times\frac{\Gamma(-s)\Gamma(y+s+1)}{\Gamma(y+1)[\mu(y)-\nu(y)]}\left(\frac{E_0}{\beta}\right)^{\nu}\left(\frac{\beta}{E}\right)^{\nu+s+1} \times\{A_n(y)[\mu(y)+D]K_\mu(y,s)e^{\mu(y)t} -B_n(y)[\nu(y)+D]K_\nu(y,s)e^{\nu(y)t}\}. \quad (40)$$

The same type expansion holds for $\gamma(E,t)$. We remark here that the functions $P_n(E,t)$ and $\gamma_n(E,t)$ are themselves solutions of the basic diffusion equations.

IV. LOW ENERGY EXPANSIONS

As has been noted before, the functions $K_\mu(y,s)$ and $K_\nu(y,s)$, $\Gamma(y+s+1)$ and $C(y+s)$ have poles at $s=-y-n$. This makes it convenient for $E<\beta$ to

evaluate the integrals over s as in (38) and (39) in terms of the residues at these poles. We now compute in this manner the total number of particles of energy greater than E,

$$N(E,t)=\sum_{n=0}^{\infty}(\beta/E_0)^n N_n(E,t)$$

with

$$N_n(E,t)=\int_E^{\infty}P_n(E',t)dE'$$

$$=\frac{1}{2\pi i}\int dy\frac{\left(\frac{E_0}{\beta}\right)^y}{\Gamma(y+1)[\mu(y)-\nu(y)]}$$

$$\times\sum_{k=0}^{\infty}\left[\frac{1}{\Gamma(k+1+a(k))}\frac{d^{k+a(k)}}{ds^{k+a(k)}}\left\{\frac{\Gamma(-s)\Gamma(y+s)}{(y+s+k)^{-k-1-a(k)}}\right.\right.$$

$$\times\left(\frac{\beta}{E_0}\right)^{y+s}[A_n(y)[\mu(y)+D]K_\mu(y,s)e^{\mu(y)t}$$

$$\left.\left.-B_n(y)[\nu(y)+D]K_\nu(y,s)e^{\nu(y)t}]\right\}\right]_{s=-y-k}, \quad (41)$$

$$N_n(E,t)=\frac{1}{2\pi i}\int_D dy\left(\frac{E_0}{\beta}\right)^y\left[\frac{A_n(y)[\mu(y)+D]K_\mu(y,-y)e^{\mu(y)t}-B_n(y)[\nu(y)+D]K_\nu(y,-y)e^{\nu(y)t}}{y[\mu(y)-\nu(y)]}\right.$$

$$-\frac{1}{[\mu(y)-\nu(y)]}\left\{A_n(y)[\mu(y)+D]K_\mu(y,-y)\left[\frac{y+s+1}{g_\mu(y,s)}\right]_{s=-y-1}e^{\mu(y)t}\left(\frac{E}{\beta}\right)\left(\ln\frac{\beta}{E}+f(y)\right)\right.$$

$$\left.\left.-B_n(y)[\nu(y)+D]K_\nu(y,-y)\left[\frac{y+s+1}{g_\nu(y,s)}\right]_{s=-y-1}e^{\nu(y)t}\left(\frac{E}{\beta}\right)\left(\ln\frac{\beta}{E}+g(y)\right)\right\}+0\left(\frac{E}{\beta}\right)^2\left\{\ln^3\frac{\beta}{E}+\cdots\right\}\right]. \quad (42)$$

In (42) $f(y)$ and $g(y)$ may be evaluated from (41). The first term in (42) clearly determines the total number of particles. For $t>\frac{1}{2}$ the terms involving $\mu(y)$ are much larger than those involving $\nu(y)$. The terms involving $\mu(y)$ may be evaluated approximately by the saddle point method for $n=0$ in which case we get

$$N_0(E,t)\simeq\frac{e^{\mu(y)t+\epsilon y}}{[\beta(y)+b(y)t]^{\frac{1}{2}}}A_0(y)$$

$$\times\left\{H(y)-M(y)\frac{E}{\beta}\left[\ln\left(\frac{\beta}{E}\right)+f(y)\right]\right.$$

$$\left.+0\left(\frac{E}{\beta}\right)^2\left[\ln^3\frac{\beta}{E}+\cdots\right]\right\}. \quad (43)$$

Here

$$\epsilon=\ln(E_0/\beta),\quad t=(\epsilon y-\alpha(y))/a(y)$$

$$a(y)=-y\frac{d\mu(y)}{dy},\quad b(y)=y^2\frac{d^2\mu(y)}{dy^2}$$

$$H(y)=\frac{[\mu(y)+D]K_\mu(y,-y)}{(2\pi)^{\frac{1}{2}}[\mu(y)-\nu(y)]}$$

$$M(y)=2(4/3+\alpha)DH(y)/[\mu(y)+D].$$

TABLE II. N.

t \ ϵ	2	3	4	5	6	7	8
0.5	2.38						
1	2.32	3.75	4.87	5.68	6.33	6.7	8.5
2	1.760	4.55	8.86	14.46	26.7	33.1	44.3
3	1.170	3.85	10.13	21.17	41.0	68.7	115.8
4	0.729	2.81	9.07	23.6	53.42	106.3	201.5
5		1.94	7.09	22.01	57.33	135.0	287.5
6		1.22	5.23	18.40	54.20	142.1	335.4
7		0.68	3.52	13.97	46.42	135.2	357.5
8		0.48	2.39	9.96	37.25	119.2	346.0
10			0.90	4.72	20.16	75.6	261.3
12			0.31	1.99	9.67	41.1	155.2
14				0.79	4.0	20.2	85.5
16				0.30	1.67	9.1	42.2
18				0.12	0.67	3.9	18.9
20					0.1	1.6	8.0

with

$$a(k)=0 \quad \text{for} \quad k=0,1,$$
$$a(k)=1 \quad \text{for} \quad k=2,$$
$$a(k)=2 \quad \text{for} \quad k=3,4,5\cdots.$$

The general form of the answer is readily discernible from (41) and is

The functions $f(y)$ and $\alpha(y)$, $\beta(y)$ are too complicated to reproduce here. The values of $\mu(y)$, $a(y)$, $b(y)$, $f(y)$, $H(y)$, $M(y)$, $A_1(y)$ and $A_0^*(y)$, $A_1^*(y)$, $\alpha(y)$, $\beta(y)$, $\alpha^*(y)$, $\beta^*(y)$, are given in Table I. Of course, we have $A_0(y)=1$ for an incident electron. Also we have $A_0\dagger(y)=yA_0^*(y)$, $A_1\dagger(y)=(y-1)A_1^*(y)$, $\alpha\dagger(y)=\alpha^*(y)-1$ and $\beta\dagger(y)=\beta^*(y)-1$.

TABLE III. N^*.

t \ ϵ	2	3	4	5	6	7	8
0.5	2.23						
1	2.18	3.96	6.00	8.77	11.67	13.2	30.1
2	1.75	4.29	8.96	15.90	27.16	40.0	65.5
3	1.22	3.66	9.60	21.27	43.67	77.0	131.5
4	0.79	2.71	8.42	22.49	52.8	109.9	213.9
5	0.66	1.92	6.58	20.48	55.6	130.9	291.2
6		1.28	4.99	17.34	51.7	141.0	332.0
7		0.76	3.56	13.01	46.5	129.8	350.5
8		0.51	2.33	10.01	34.67	114.2	328.0
10			1.02	4.81	19.2	70.9	248.8
12			0.36	1.80	9.2	40.6	147.5
14				0.70	4.2	20.9	85.5
16				0.28	1.7	9.7	43.0
18				0.12	0.67	4.2	18.9
20					0.1	1.5	8.0

TABLE IV. $N\dagger$.

t \ ϵ	2	3	4	5	6	7	8
0.5	0.935						
1	1.61	1.88	2.27	3.1	3.2	3.6	8.5
2	1.76	3.59	5.97	8.85	13.33	13.9	24.4
3	1.39	3.86	8.51	16.19	27.2	46.0	71.0
4	0.990	3.34	9.02	20.40	42.5	78.9	140.2
5	0.632	2.49	8.04	21.60	51.2	109.0	218.2
6	0.412	1.75	6.51	19.96	53.5	130.1	285.2
7		1.12	4.85	16.93	49.9	133.9	326.0
8		0.80	3.48	13.20	43.0	126.5	342.1
10		0.29	1.60	7.40	26.5	93.5	291.4
12			0.65	3.28	13.8	54.5	201.2
14				1.32	6.8	29.4	113.5
16				0.52	3.5	13.5	61.2
18				0.19	1.9	5.8	29.9
20					0.5	2.6	9.9

In a manner quite similar to that in which (43) was obtained we obtain, for $\gamma(E, t)$, the value

$$\gamma(E,t)=(4/3+\alpha)\frac{N(0,t)}{E[\mu(y)+D]}+0\left(\frac{E}{\beta}\right)\left[\ln^3\frac{\beta}{E}+\cdots\right] \quad (44)$$

with the saddle point relationship between t and y as given above. If we compare the γ-ray distribution as given by (44) with the γ-ray distribution as given by Carlson and Oppenheimer in their Eq. (34) and the total number of particles as given by their Eq. (36), we see that the relation between the γ-ray distribution and the total number of particles as given by them as compared with (44) differs only by the factor $(4/3+\alpha)$. One can also see that the differentiation of (43) with respect to the energy gives a particle distribution of the same logarithmic form as was found by Carlson and Oppenheimer in their Eq. (34). We find

$$P(E,t)=\frac{2D(4/3+\alpha)N(0,t)}{\beta[\mu(y)+D]}\left\{\ln\frac{\beta}{E}+f(y)-1\right\}+\cdots$$
$$=2D\frac{E}{\beta}\gamma(E,t)\left\{\ln\frac{\beta}{E}+f(y)-1\right\}+\cdots. \quad (45)$$

On the other hand, the answer we find for $P(E, t)$ does not agree with that given by Bhabha and Chakrabarty in their Eq. (37). Of course, if all the terms in their expansion (35) had been used, the results would have to agree. The expansions which we have given here are particularly useful for $E<\beta$, while the expansions given by Bhabha and Chakrabarty are most useful for larger values of the energy. We also note here that if $\beta/E_0>1$, the saddle point that was used to obtain (43) and (44) does not exist. In general, formulas (43) and (44) give the proper dependence of the answer on t only if β/E_0 is small. However, the type of energy dependence is still correctly given for diffusion Eqs. (1) and (2) as in (42), since it depends only on the location and order of the poles in the integrands of Eqs. (5) and (6) and not on the thickness and initial conditions. It is possible to evaluate the integrals over y in (42) in terms of residues of various poles in the left-hand plane. This leads to an expansion in powers of t, which is unfortunately not very useful for numerical calculations unless t is very small.

There is one check which may be made on the expansions which have been given and on the saddle point method of integration: the total initial energy must be absorbed by ionization. This leads to the relation

$$\int_0^\infty N(0,t)dt=E_0/\beta. \quad (46)$$

If we use the value of $N_n(E, t)$ as given by (42) and those of $A_0(y)$ and $B_0(y)$ as given by (33) or (34a) or (34b) for the different initial conditions, one can show that

$$\int_0^\infty N_n(0,t)dt = \begin{cases} 0; & n>0 \\ E_0/\beta; & n=0 \end{cases}$$

$$\int_0^\infty N_n\dagger(0,t)dt = \begin{cases} 0; & n>0 \\ E_0/\beta; & n=0 \end{cases}$$

$$\int_0^\infty N^*(0,t)dt = \begin{cases} 0; & n>1 \\ (E_0/\beta)/(4/3+\alpha); & n=1 \\ E_0/\beta-1/(4/3+\alpha); & n=0. \end{cases} \quad (47)$$

From the small values of $A_1(y)$ as shown in Table I, it is evident that $N_0(E, t)$ will be quite close to $N(E, t)$ even for $\beta/E_0\sim.1$. And, we see from (47) that the higher terms $N_n(E, t)$ and $N_n\dagger(E, t)$ can only change the shape of the $N(E, t)$ and $N\dagger(E, t)$ curves slightly. For $N(E, t)$

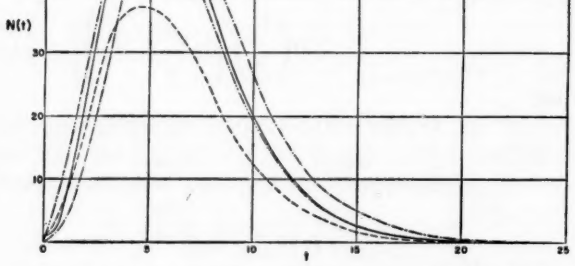

FIG. 1. Graph of $N(t)$ (solid curve, ——), $N^*(t)$ (dash double dot curve, ——··), $N\dagger(t)$ (dash dot curve, —·), $N_{BC}(t)$ (dashed curve — —) for $\epsilon=6$.

this is actually a small decrease in $N(E, t)$ for small t and a small increase in $N(E, t)$ for large t. Thus, in our case, the numerical evaluation of the integrals in (47) essentially gives a gross check on the saddle point method of evaluating $N_0(t)$, $N_0\dagger(t)$, $N_0{}^*(t)$ and $N_1{}^*(t)$. One can also show, using (42), that $N_0(0, 0)=1$ and $N_0\dagger(0, 0)=0$. We also wish to observe at this point that the saddle point method can be used for the approximate evaluation of only $N_0(t)$, $N_0{}^*(t)$, $N_0\dagger(t)$ and $N_1{}^*(t)$. For the other $N_n(t)$, etc., the functions $A_n(y)$ have zeros at $y=1, 2, 3\cdots n$ which zeros prevent the application of the saddle point method.

In Tables II, III, and IV we give the values of $N(t)$, $N^*(t)$ and $N\dagger(t)$, respectively, for $\epsilon=2, 3, 4, 5, 6, 7,$ and 8. These values were calculated using formulas (43). Since the values of t and $N(t)$ are determined parametrically by assigning values of y, these values of t and $N(t)$ were plotted with $N(t)$ as a function of t and the values of $N(t)$ etc., as given in Tables II, III, and IV were obtained by reading the graphs. The values of $N(t)$ and $N\dagger(t)$ were calculated using $N(t)=N_0(t)$ and $N\dagger(t)=N_0\dagger(t)$; however, we used $N^*(t)=N_0{}^*(t)+(\beta/E_0)N_1{}^*(t)$. It is not practical to compute higher terms in the series for $N(t)$, $N\dagger(t)$, and $N^*(t)$ since we cannot use the saddle point method for their computation. In addition, relations (47) insure that the areas under these curves will be correct to the accuracy of the saddle point method.

In Table V we give the values for various ϵ of $\int_0^\infty N(t)dt$, $\int_0^\infty N^*(t)dt$, $\int_0^\infty N\dagger(t)dt$, and $\int_0^\infty N_{BC}(t)dt$ as numerically evaluated by plotting curves for $N(t)$ $N^*(t)$ and $N\dagger(t)$ as determined by using Eqs. (43), and for $N_{BC}(t)$ the values as given by Bhabha and Chakrabarty[7] in their Table III, and then measuring the area under the curves, using a planimeter. These areas should, of course, be equal to E_0/β which is listed in column 2 of this table. It is evident on inspection of this table that the agreement of columns 3, 4, and 5 with column 2 is much better than is that of column 6.

Figure 1 is a graph of $N(t)$, $N^*(t)$, $N\dagger(t)$, and $N_{BC}(t)$ for $\epsilon=6$. It is evident from these curves that the numerical values obtained by Bhabha and Chakrabarty are in error by about 35 percent near the maximum of the shower curve.

I wish here to thank Miss Jean Snover who is primarily responsible for the numerical work and preparation of the graph and the tables.

TABLE V.

ϵ	$e^\epsilon=\frac{E_0}{\beta}$	$\int_0^\infty N dt$	$\int_0^\infty N^* dt$	$\int_0^\infty N\dagger dt$	$\int_0^\infty N_{BC} dt$
2	7.389	7.22	7.52	7.26	5.64
3	20.086	20.4	20.8	20.3	14.29
4	54.598	55.1	55.2	55.5	38.27
5	148.41	149.4	149.2	149.7	102.8
6	403.43	406.4	406.3	407.4	279.8
7	1096.6	1106.8	1111.5	1103.1	736.3
8	2981.0	2997	3001	2998	2001

Note added after completion of manuscript.—The results of this paper have recently been obtained by W. T. Scott,[8] starting with a Laplace transform in t, and Mellin transforms in both E and E_0. The resulting homogeneous difference equation is analogous to Eq. (19) and was solved in a similar way. This approach yields explicit formulas for A_n and B_n, namely:

$$A_n(y)=\frac{\Gamma(y+1)}{\Gamma(y-n+1)}(-1)^n[\mu(y)+D]^n \times\prod_{j=1}^{n}\frac{1}{[\mu(y)-\mu(y-j)][\mu(y)-\nu(y-j)]}$$

$$B_n(y)=\frac{\Gamma(y+1)}{\Gamma(y-n+1)}(-1)^n[\nu(y)+D]^n \times\prod_{j=1}^{n}\frac{1}{[\nu(y)-\nu(y-j)][\nu(y)-\mu(y-j)]}.$$

Furthermore,

$$A_n\dagger(y)=(y-n)A_n{}^*(y)=\frac{B(y-n)}{\mu(y)+D}A_n(y)$$

$$B_n\dagger(y)=(y-n)B_n{}^*(y)=\frac{B(y-n)}{\nu(y)+D}B_n(y).$$

From these explicit expressions for $A_n(y)$ and $B_n(y)$, one can directly verify the statements made earlier in this paper covering the analytic properties of these functions, together with the fact that they satisfy Eqs. (29) and (30).

[8] Privated communication. The method is outlined in W. T. Scott's unpublished thesis (University of Michigan, 1941).

The Scattering of Slow Neutrons by Paramagnetic Crystals

I. W. RUDERMAN
Department of Chemistry and Department of Physics, Columbia University, New York, New York
(Received August 1, 1949)

The paramagnetic scattering of neutrons by anhydrous crystals of manganous fluoride, manganous oxide, and α-ferric oxide was studied, using neutron transmission data obtained with the Columbia slow neutron velocity spectrometer. Details are given of the experimental arrangement, which permits measurements to be made with neutrons having wave-lengths up to 6.4A. The paramagnetic cross section, σ_{pm}, may be separated from the total cross section in regions where there are no interfering crystal diffraction effects. Large values of σ_{pm} were found for the manganous compounds, but no paramagnetic scattering by α-Fe_2O_3 was observed. The results are compared with the theoretical predictions of Halpern and Johnson. The dependence of σ_{pm} on the neutron wave-length was determined, and is compared with a theoretical form factor based on purely elastic scattering.

INTRODUCTION

IN 1936 Bloch[1] pointed out that neutrons should be scattered by ferromagnetic media because of the interaction of the magnetic moment of the neutron with the atomic magnetic field. The latter was described by a dipole distribution around and within the atom that was assumed to be unaffected by the scattering process. Schwinger[2] subsequently extended Bloch's results in a detailed quantum mechanical analysis, emphasis being placed on polarization effects in ferromagnetic substances.

In a comprehensive theoretical treatment of magnetic scattering Halpern and Johnson[3,4] introduced two new concepts: they considered in their analysis changes produced in the scatterer during the scattering process, and they proposed that magnetic scattering of neutrons be studied by means of *paramagnetic* substances. These investigators indicated that under suitable conditions the paramagnetic scattering cross section could be at least as large as, or even several-fold larger than the total nuclear scattering cross section; in such cases the experimental results might be analyzed more quantitatively and directly than ferromagnetic scattering data. The interest in magnetic scattering at that time was primarily for the purpose of gaining information about the magnetic properties of the neutron; indeed, Bloch's original intention was to provide a method for measuring the magnetic moment of the neutron.

Earlier investigators who sought to establish the existence of magnetic scattering by paramagnetic substances were handicapped by the lack of monochromatic neutron sources, meager information about neutron diffraction and scattering processes, and the difficulty of preparing pure anhydrous samples of suitable scatterers. The prior experimental evidence is based on the work of Whitaker, *et al.*[5–8] who studied the scattering of slow neutrons from a Ra-Be source by manganese and iron compounds. They compared the total cross sections obtained in transmission experiments with calculated additive nuclear cross sections, any differences being attributed to paramagnetic scattering. Using an annular ring arrangement they also studied the angular distribution of neutrons scattered in the forward direction. Only small effects were observed, and the results were in general inconclusive.

The study to be described in this paper was undertaken with the twofold objective of establishing definitely the existence of paramagnetic scattering, and seeking to utilize this effect to obtain new information about paramagnetism in solids.

THEORY

Let us consider first the simplest possible case of an isolated paramagnetic ion which scatters neutrons elastically (i.e., the neutron wave-length, λ, remains constant). Under these restricted conditions, Halpern and Johnson[4] give the paramagnetic cross section, σ_{pm}, as

$$\sigma_{pm}=[(8\pi/3)(e^2\gamma/mc^2)^2S(S+1)]F. \quad (1)$$

Here γ is the magnetic moment of the neutron in nuclear magnetons, S is the total electron spin quantum number, and F is the form factor integrated over all scattering angles. When λ is large compared with the size of the ionic magnetic domain, F approaches unity and we can evaluate the maximum value of σ_{pm} to be expected. Thus, for Mn^{++} which has five unpaired $3d$ electrons, we find $\sigma_{pm}=21.2$ barns. This is a large cross section which should be easily measurable.

A form factor for elastic scattering was approximated by Halpern in the following way. The ionic spin distribution in the initial and final states was assumed to be the same, and the spin density was taken proportional to the outer electron charge density. The latter in turn was taken to be spherically symmetrical, and was approximated by a hydrogenic wave function. It

[1] F. Bloch, Phys. Rev. **50**, 259 (1936).
[2] J. S. Schwinger, Phys. Rev. **51**, 544 (1937).
[3] O. Halpern and M. H. Johnson, Jr. Phys. Rev. **51**, 992 (1937); Phys. Rev. **52**, 52 (1937).
[4] O. Halpern and M. H. Johnson, Phys. Rev. **55**, 898 (1939).
[5] M. D. Whitaker, Phys. Rev. **52**, 384 (1937).
[6] Whitaker, Beyer, and Dunning, Phys. Rev. **54**, 771 (1938).
[7] M. D. Whitaker and W. C. Bright, Phys. Rev. **57**, 1076 (1940).
[8] M. D. Whitaker and W. C. Bright, Phys. Rev. **60**, 280 (1941).

was then possible[9] to express F as a function of $\alpha/k = 3\chi/r_0$, where r_0 is the most probable radius of the spin distribution, and $k=1/\chi$. F has been evaluated for various values of α/k, and the results are to be found in a recent communication.[10]

In practical cases, however, we must consider that inelastic scattering is likely to occur because of nuclear spin-electron spin, electron spin-orbit, and electron spin-spin coupling. The nuclear coupling should produce negligible effects, since the energy separations are very small compared with the neutron energy. In ionic crystals of the transition elements the crystalline field often decouples the orbital angular momentum, L, and the spin angular momentum, S, and quenches L. If the decoupling is incomplete, however, energy separations of the spin orientations comparable with kT are likely. A part of the scattering will then be inelastic. The effect of spin-spin coupling is most serious, since the energy changes due to exchange forces are probably large. The deviations of the paramagnetic susceptibility of many iron and manganese compounds from the Curie law are considered to be manifestations of spin-spin coupling. The theoretical treatment of this type of coupling is very complex, since little is known of the details of exchange forces in solids. Van Vleck[11] has extimated that in MnS, which has large spin-spin coupling, the form factor for paramagnetic scattering in the forward direction is reduced by inelastic collisions by about 75 percent and 50 percent for monochromatic liquid air and room temperature neutrons, respectively.

Fortunately, the analysis of paramagnetic scattering data may be simplified by the proper choice of scattering materials. The use of ferric and manganous compounds, in which the paramagnetic ions are in an S state, eliminates the effect of spin-orbit coupling. The effect of spin-spin coupling can then be studied by choosing a series of manganous or ferric compounds of various magnetic dilution. Our choice of compounds was influenced by the following considerations.

Paramagnetic susceptibility measurements made by many investigators[12] show that dilute solutions, or hydrates of paramagnetic substances often obey the simple Curie law, when the corresponding anhydrous crystals themselves do not. Unfortunately, aqueous hydrates and solutions are unsuitable for neutron studies because the large incoherent scattering of hydrogen would mask the paramagnetic scattering. The use of solutions would also introduce the complicating and unknown effect of solvent molecules. Only anhydrous solids were used in this study.

In Fig. 1 the closest distance, d, between Mn^{++} ions in various manganous crystals is plotted against the corresponding values of Δ in the Weiss-Curie law $\chi=C/(T+\Delta)$ for each compound. It is seen that Δ is approximately equal to zero when d is greater than 4A, but that a wide range of Δ-values exist for d smaller than 4A. It is interesting to note that there is no apparent relationship between Δ and d in the region of $d<4$A. Experimental values of Δ were used as a criterion of spin coupling. Those compounds which exhibit large values of Δ in the Weiss-Curie law can be expected to have large coupling, while those compounds which have very small values of Δ are very probably essentially free of coupling.

Our method of studying paramagnetic scattering has already been briefly outlined in a recent preliminary communication.[10] Anhydrous crystals of manganous fluoride, manganous oxide, and α-ferric oxide were chosen for study, thus providing a series of compounds of variable magnetic dilution (see Table I) with which to observe the effects of spin-spin coupling. The Columbia neutron velocity spectrometer was used to obtain transmission data for these compounds for neutron wave-lengths up to 6.4A. In the absence of paramagnetic scattering a microcrystalline sample of, say, MnO would be expected to give a cross section *vs.* time of flight curve which would be a straight $1/v$ line up to the first large diffraction peak. Data on numerous microcrystalline materials[13,14] show that there is no

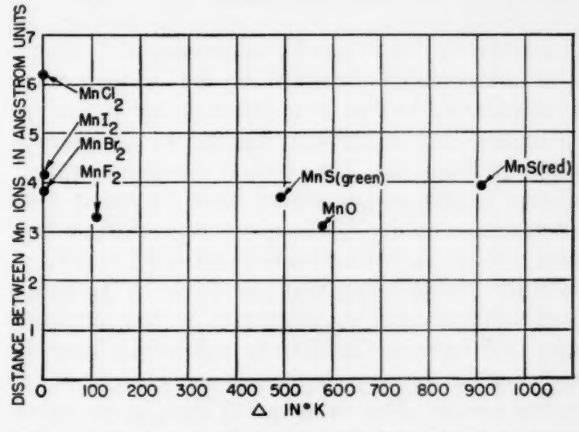

FIG. 1. The closest distance between Mn^{++} ions in several manganous compounds plotted against the corresponding values of Δ in the Weiss-Curie law for each compound. The distances were computed from x-ray data (see reference a of Table I) and the Δ-values were taken from the literature (see reference b of Table I).

[9] The integral form factor is given by Eqs. (7.40)–(7.46) in reference 4. Slight misprints occur in Eqs. (7.42), (7.43), and (7.44); for "h" wherever it appears in these equations "k" should be read.

[10] Ruderman, Havens, Jr., Taylor, and Rainwater, Phys. Rev. **75**, 895 (1949).

[11] J. H. Van Vleck, Phys. Rev. **55**, 924 (1939).

[12] See, for example, J. H. Van Vleck, *The Theory of Electric and Magnetic Susceptibilities* (Oxford University Press, London, 1932); and P. W. Selwood, *Magnetochemistry* (Interscience Publishers, Inc., New York, 1943).

[13] Sources of σ_f were as follows: Mn, this paper; O, Rainwater, Havens, Jr., Dunning, and Wu, Phys. Rev. **73**, 733 (1948); O, Melkonian, Rainwater, Havens, Jr., and Dunning, Phys. Rev. **73**, 1399 (1948); Fe, recent unpublished work in this Laboratory.

[14] See, for example, Havens, Jr., Rabi, and Rainwater, Phys. Rev. **72**, 634 (1947); Havens, Jr., Rainwater, Wu, and Dunning, Phys. Rev. **73**, 963 (1948); and Rainwater, Havens, Jr., Dunning, and Wu, Phys. Rev. **73**, 733 (1948) for curves for lead, calcite, and quartz, respectively.

TABLE I. Some important nuclear and crystallographic properties of the samples. σ_f, σ_{coh}, and σ_b are the free, coherent, and bound scattering cross sections, respectively, expressed in barns per atom for the elements and barns per molecule for the compounds. $(\sigma_b-\sigma_f)$ refers to the difference in σ due only to change in effective reduced mass. $(\sigma_b-\sigma_{coh})$ is the incoherent residual scattering cross section, assuming no lattice vibrations. λ_c is the cut-off wave-length for Bragg reflections for a microcrystalline sample, as computed from x-ray data.

Substance	Crystal class[a]	Unit cell dimensions a_0 in A	c_0 in A, or α in deg.	λ_c, in A	Δ[b]	σ_f[c]	σ_{coh}[d]	$\sigma_b-\sigma_{coh}$	$\sigma_b-\sigma_f$
Mn						1.80	1.35	0.5	0.07
F						3.3	~4	~0	0.4
O						3.7	4.2	0	0.5
Fe						11.4	10.3	1.5	0.4
MnF_2	Tetragonal	4.885	3.295	5.46[e]	113	8.4	~8.7	0.5	0.8
MnO	Cubic	4.40		5.08	548	5.5	5.55	0.5	0.6
α-Fe_2O_3	Rhombohedral	5.414	55°17′	9.14	large[f]	33.9	33.2	2.9	2.2

[a] Crystallographic data for $MnBr_2$, $MnCl_2$, MnI_2, MnF_2, MnO, and α-Fe_2O_3 were taken from R. W. G. Wyckoff, *Crystal Structures* (Interscience Publishers, Inc., New York, 1948). The MnS data were from F. Mehmed and H. Haraldsen, Zeits. f. anorg. allgem. Chemie **235**, 193 (1938).
[b] Δ-values were from the following sources: $MnBr_2$ and MnI_2, de Haas, Schultz, and Koolhaas, Physica **7**, 57 (1940); $MnCl_2$, P. Théodoridès, Comptes Rendus **171**, 948 (1920); MnF_2, H. Bizette and B. Tsaï, Comptes Rendus **209**, 205 (1939); MnO, Bizette, Squire, and Tsaï, Comptes Rendus **207**, 449 (1938), and R. W. Tyler, Phys. Rev. **44**, 776 (1933); MnS, Bhatnagar, Prakash, and Singh, J. Ind. Chem. Soc. **16**, 313 (1939).
[c] See reference 15.
[d] See reference 16.
[e] Although the 110 plane reflects at 6.92A, the structure factor is very small and the reflection is so weak that it may be neglected.
[f] No reliable value of Δ could be found in the literature. Since α-Fe_2O_3 displays incipient ferromagnetism at 300° K, Δ is probably very large.

loss of nuclear scattering cross section until the occurrence of this first discontinuity, which is generally easily discernible. As successive diffraction peaks were passed, the coherent scattering cross section would decrease until the cut-off wave-length for Bragg reflections, λ_c, was reached. At this point all the remaining coherent scattering would disappear and the cross section would consist only of capture and incoherent scattering due to nuclear spin, lattice vibrations, lattice defects, isotope effects, etc. Suppose then that we construct a hypothetical curve consisting of a straight line which coincides with the experimentally determined curve for MnO at high energies (>1 ev), and which has the correct additive capture slope for manganese and oxygen. Let us further assume for simplicity that all the nuclear scattering cross section is retained up to λ_c for this hypothetical curve, but that beyond λ_c all coherent scattering disappears. The residual incoherent scattering cross section was estimated from the recent work of Wollan and Shull[15, 16], who give values of $\sigma_{coh}=4\pi f_0^2$ where f_0 is the true bound nuclear scattering length corrected for thermal vibrations (see Table I). To obtain the effective values of σ_{coh} integrated over-all scattering angles, 0.5 barn was arbitrarily subtracted from the $4\pi f_0^2$ values to account for the loss in coherency due to thermal motion. This value of 0.5 barn is not unreasonable in the light of the work of Latham and Cassels.[17] Figures 8 and 10 show two such hypothetical curves. In those regions where there are no perturbing diffraction effects, that is for λ smaller than that corresponding to the first observable diffraction peak and for $\lambda>\lambda_c$, the difference between the experimental and the hypothetical curve was taken to be σ_{pm}.

The crystal size of the sample is significant. A large single crystal has the advantage of quickly becoming almost transparent with decreasing neutron energy.[14] Approximate values of σ_{pm} (neglecting the small amount of coherent scattering which still remains) can therefore be obtained for a considerable range of λ smaller than λ_c. However, no determinations of σ_{pm} can be made at short wave-lengths (0 to ~3A). For a microcrystalline sample, individual crystals should not be so small (~1μ or less) that appreciable small angle scattering occurs,[18] nor so large that the sample becomes transparent.

EXPERIMENTAL

1. Neutron Spectrometer

The Columbia slow neutron spectrometer has already been described in detail by Rainwater and Havens.[19–21] The spectrometer consists essentially of the 36-in. cyclotron, timing circuits for modulating the arc and operating the detection chain, a slow neutron paraffin "source" slab, collimation and shielding, and BF_3 proportional counters for detection. The details of the collimating system as modified for the experiments described in this paper are given in Fig. 2. The 5-meter source-to-detector distance was used for measurements

[15] The σ_{coh}-values for the elements (corrected for thermal motion) were kindly supplied by Dr. C. G. Shull, and represent his most recent results. These values were taken to be additive in computing σ_{coh} for the compounds.
[16] See for example E. O. Wollan and C. G. Shull, Phys. Rev. **73**, 830 (1948); Shull, Wollan, Morton, and Davidson, Phys. Rev. **73**, 842 (1948).
[17] R. Latham and J. M. Cassels, Nature **161**, 282 (1948); J. M. Cassels and R. Latham, Phys. Rev. **74**, 103 (1948); J. M. Cassels, private communication, September 21, 1948.
[18] Krueger, Meneghetti, Ringo, and Winsberg, Phys. Rev. **75**, 1098 (1949).
[19] J. Rainwater and W. W. Havens, Jr. Phys. Rev. **70**, 136 (1946).
[20] W. W. Havens, Jr., and J. Rainwater, Phys. Rev. **70**, 154 (1946).
[21] Rainwater, Havens, Jr., Wu, and Dunning, Phys. Rev. **71**, 65 (1947).

with neutrons having wave-lengths greater than 3A, and the regular 6-meter collimation for shorter wave-lengths.

Deuterons, produced in the cyclotron chamber by modulating the accelerating potential on the ion source have an energy of 8 Mev when they strike the beryllium target. The fundamental timing for the circuits which control the cyclotron and detector is now provided by a 1-megacycle crystal-controlled oscillator. This provides cyclotron and detector on-times of 2, 4, 8$\cdots$512 or 1024 μsec., and cyclotron repeat times of 1024, 2048$\cdots$16384, or 32768 μsec.

The true resolution function is rather complex, but has always been found to be roughly triangular in shape. The width of the triangular base for all the measurements reported in this paper lies between 2 and 3 times the timing spacing between adjacent experimental points shown on the curves.

A "thin" neutron source, consisting of a 24.2-cm $\times$24.2-cm$\times$3.8-cm paraffin block covered on all sides by $\frac{1}{4}$-in. plywood, was used for neutron wave-lengths up to 1.25A. The back face (away from the collimating system) of the paraffin is mixed with boron carbide for a depth of 0.6 cm to keep out stray slow neutrons. For longer wave-lengths a "thick" source was used in order to obtain greater slow neutron intensity. The thick source is 22.8 cm$\times$22.8 cm$\times$6.5 cm and is covered by $\frac{1}{4}$-in plywood on the faces and $\frac{1}{2}$-in. plywood on the sides; in addition, the back face is covered with a 0.022-in. thick cadmium sheet.

2. Method of Making Transmission Measurements

Transmission measurements were made as follows. The sample was placed in the proper place in one collimated channel, and a "dummy" consisting of an aluminum disk of thickness equal to the total wall thickness of the sample holder was placed in the corresponding position in the second channel. After a definite number of neutron counts from a monitor fission counter placed in the cyclotron enclosure, the counts recorded by the registers for each channel were noted. The sample and dummy were then interchanged in position, and the registers read after another equal number of monitor counts. This constitutes a complete "cycle." Sufficient cycles were run to obtain the desired statistical ac curacy.

The total number of counts for a detection interval taken over all the cycles with the sample in the beam ("in" position), divided by the corresponding total number of counts with the dummy in the beam ("out" position) gives the transmission for this interval. Transmission values obtained in this way for each channel were averaged to give the final value. The cross section, σ, was obtained from the transmission, T, by the relation $T=e^{-n\sigma}$, where n represents the atoms or molecules per cm^2 in the sample. The use of two channels tends to minimize errors due to changes in neutron flux and counter efficiency. To take full advantage of this feature, the number of monitor counts per cycle was kept as low as was compatible with efficient operation and good statistical accuracy.

The background counting rate was determined at least once or twice during each run by substituting 3-in. thick disks of a boron carbide-paraffin mixture for the sample and dummy in each channel. The background counts were in all cases either zero or negligibly small. This test shows that the counters are well-shielded and do not count spuriously, but it gives no indication of the stray neutron effect to be described shortly.

3. Use of "Standard Filters"

Early in this work it was observed that the two channels gave appreciably different transmissions for

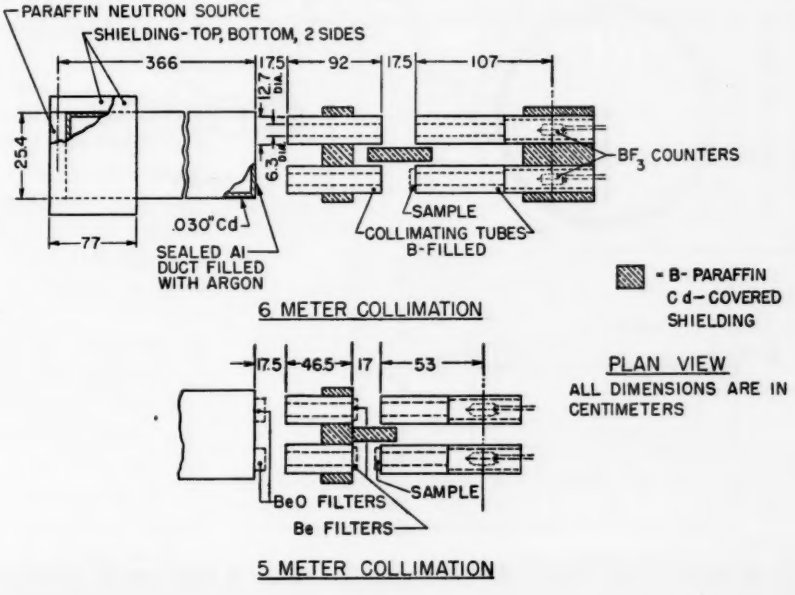

FIG. 2. Details of the collimating system for 5- and 6-meter source-to-detector distances. Not shown for clarity is the additional shielding which surrounds completely the collimating tubes and counters.

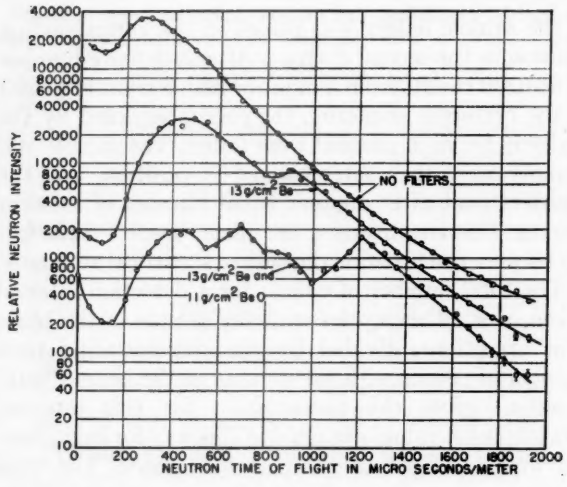

FIG. 3. The effect on the neutron distribution from the source of beryllium and beryllium oxide filters.

the same sample, and that the general reproducibility of results, particularly in the high energy region, over long periods of time was not entirely satisfactory. A rate dependence of the counters was considered to be responsible for this, and "standard filters" whose design and operation are fully described elsewhere,[22] were found to eliminate these discrepancies. These standard filters were used in all our transmission experiments for neutron wave-lengths less than 2.6A.

There are indications that the counter rate dependence has both an instantaneous and a delayed component. The latter arises from the neutron flux which causes pulses in the BF_3 counters and allied circuits during those intervals of time when the source is emitting neutrons but the detection chain is not activated. For $\lambda > 2.6$A standard filters were not used because it was believed that the great reduction in thermal neutron flux resulting from the use of Be and BeO filters (see Fig. 3 and the discussion on stray neutrons which follows) would eliminate the delayed effect, while the normal reduction of slow neutron intensity because of the Maxwellian distribution would markedly diminish the instantaneous effect. The poor neutron intensity at long wave-lengths also discourages the use of any apparatus which reduces this intensity. Recent experiments have shown that standard filters are indeed unnecessary for $\lambda > 2.6$A.

4. Effects and Possible Sources of Stray Neutrons

From preliminary experiments it was found that for neutron wave-lengths greater than 4.4A, the cross section of manganous fluoride ceased to increase with increasing wave-length (as it should do because of the manganese capture slope), but instead flattened off and started to decrease. This effect was interpreted as being due to stray neutrons. It was apparent that the Be filters, which were used for these measurements in order to discriminate against stray neutrons having energies greater than ~0.01 ev, were inadequate. It was decided to examine this difficulty in some detail.

Three main sources of stray neutrons were considered:

(1) Faster thermal neutrons, emitted by the source and reflected from the walls of the cyclotron enclosure, might strike air molecules in the open space inside the enclosure between the source and the collimating tubes (i.e., the space now occupied by the aluminum duct shown in Fig. 2) and be scattered into the neutron beam. These neutrons would reach the detector at the same time as the "regular" group of slow neutrons

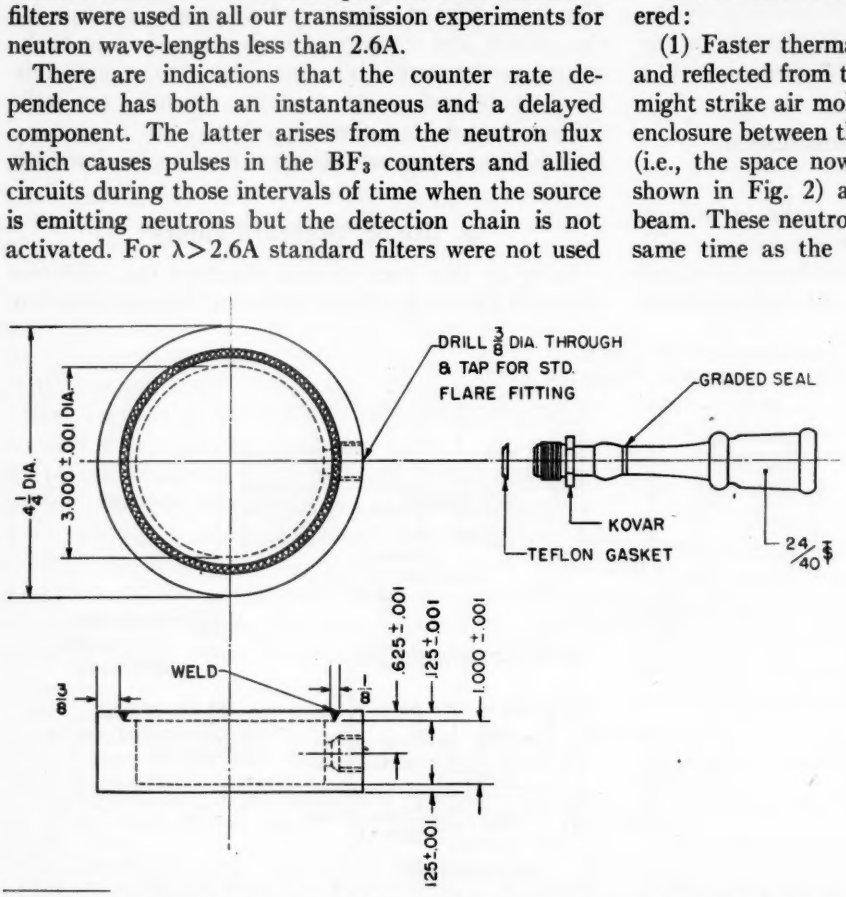

FIG. 4. Details of the aluminum alloy sample holders.

[22] E. Melkonian, Ph.D. thesis, Columbia University, 1949, to be submitted for publication.

which go directly from the source to the detector. Since they would have, in general, a larger straightened out path length, they would have a greater average velocity or energy than that associated with any given timing interval. The *measured* value of the transmission of the sample for a given timing interval would then correspond to a weighted average of the transmission due to the regular group and to these faster in-scattered neutrons. The observed cross section would hence be lower than the true cross section for the given timing.

(2) A small residual neutron production in the vicinity of the arc source, when the latter is supposedly not emitting, would produce a background of neutrons with an essentially Maxwellian distribution. Since the thermal peak is at approximately 1.1A, the weighted contribution of these neutrons would depend upon the transmission of the sample at 1.1A. For manganese and iron compounds, which have a considerable $1/v$ slope, the transmission at 1.1A is much higher than it is at wave-lengths greater than 4.4A. The observed transmission would therefore be higher than it should be, and lower cross sections would be obtained.

(3) The regular group of neutrons reaching the detector in the timing interval t_0 to $t_0+\Delta t_0$ move in a straight line from the source to detector with constant velocity v_0 to $v_0-\Delta v_0$. If small angle inelastic scattering could occur, there would be an additional contribution to the interval t_0 to $t_0+\Delta t_0$ due to neutrons having a velocity $v_1>v_0$ from source to sample and velocity $v_2<v_0$ (after inelastic scattering) from the sample to the detector. In order to reach the detector in the given timing interval, the *time average* value of the velocity must lie in the range v_0 to $v_0-\Delta v_0$. Since the relative number of neutrons $N(v)$ detected in any velocity interval decreases $\sim v^6$ as v is decreased in the low energy range, there will be very many more faster neutrons reaching the sample than neutrons of the given velocity. If any appreciable fraction could be inelastically scattered (as described above) the in count would be considerably increased. However this effect will probably not be serious for a number of reasons.

a. Since the sample-to-detector distance is only one-tenth the source-to-detector distance, the ratio v_0/v_2 must be much larger than the ratio v_1/v_0 (in the energy region of interest) in order to give the proper time average velocity. Since the neutron energy after a collision tends to be restored towards kT, the probability of finding a very low velocity v_2 after collision must be exceedingly small.

b. Properly we should also consider hyperelastic processes where $v_2>v_0$ after collision. This again should be unimportant because $N(v)$ decreases rapidly as v decreases so there are relatively few neutrons with $v_1<v_0$. Both of these processes (a and b) which *add* to the number of neutrons reaching the detector in the given detection interval, will be largely counterbalanced by the loss due to the small angle inelastic scattering of neutrons with velocity v_0 to $v_0-\Delta v_0$ in the source-to-sample region. That is, an inelastic process merely shifts a neutron of given initial velocity from its regular detection interval to a different one, and the losses and gains will tend to balance for any given detection interval.

TABLE II. Source, sample and detector geometry.

	Solid angle (in steradians) subtended at:	By source 5 meters	By source 6 meters	By detector 5 meters	By detector 6 meters
Infinite source	Sample	0.0081	0.0027	0.0069	0.0017
	Detector	0.0023	0.00066		
24.2 cm×	Sample	0.0030	0.0024		
24.2 cm source	Detector	0.0023	0.00066		

c. Since the detector subtends but a small solid angle at the sample, the differential inelastic cross section would have to be quite large to introduce any measurable error. That the total inelastic cross section is small, however, is shown by the work of Weinstock[23] and Latham and Cassels[17] as well as by the small residual cross sections obtained in this Laboratory for various crystalline solids at $\lambda>\lambda_c$.[23a]

In order to reduce any existing background of neutrons scattered into the beam by air molecules, all of

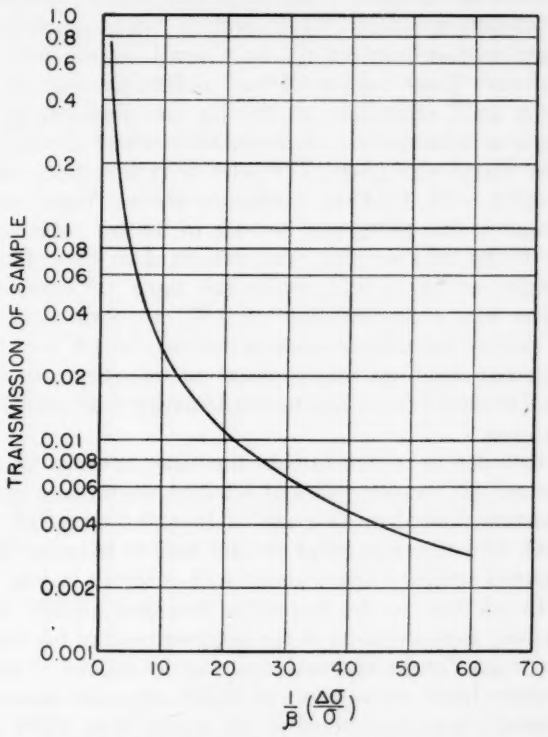

FIG. 5. The relative error in cross section due to small angle scattering into the detector as a function of the transmission of the sample. The total cross section is assumed to be due only to scattering processes, which are spherically symmetrical.

[23] R. Weinstock, Phys. Rev. **65**, 1 (1944).

[23a] P. J. Bendt and I. W. Ruderman, Phys. Rev. **76**, 463 (1949).

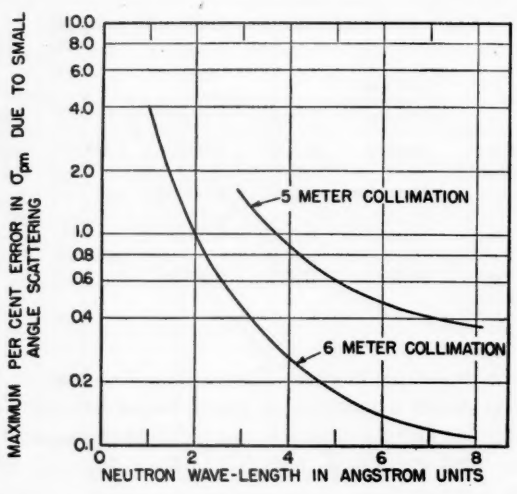

FIG. 6. The maximum percent error in σ_{pm} due to small angle scattering into the detector as a function of neutron wavelength for a typical paramagnetic sample, taking into account non-spherically symmetrical scattering.

the neutron path open to the air in the cyclotron enclosure was replaced by a cadmium-lined, argon-filled duraluminum duct (Fig. 2). The heavier and bulkier construction which an evacuated duct would have entailed mitigated against its use, in spite of its obvious superiority. The duct, constructed in three separate sections for flexibility in handling, was made of 3/32-in. duraluminum sheet. Each section was completely sealed and air-tight except for a small tapped hole at each end. These holes were used to flush the duct with argon until essentially all the air was replaced with argon at atmospheric pressure, after which the holes were sealed with plugs. The sides of each section were covered with 0.030-in. cadmium sheet. Argon was chosen as the filling gas because of its low total and scattering cross sections. Since 366 cm of air has a transmission at 5A of 0.73, while the same thickness of argon has a transmission of 0.97, approximately a 33 percent increase in neutron intensity at 5A is to be expected. Such an improvement in intensity was indeed observed when this new collimating duct was put into use.

In order to reduce further the stray neutron background, all measurements at $\lambda > 2.6$A were made with neutrons filtered by 13 g/cm^2 of Be and 6–11 g/cm^2 of BeO. The effectiveness of Be and BeO in reducing the neutron intensity below about 3.5A is shown in Fig. 3.

In addition to the corrective measures already described, measurements in the neighborhood of 6A were corrected for background neutrons as follows. Using neutron burst repeat times of 32768 μsec., the neutron intensity was determined in the region from 16384 to 32768 μsec. Any neutrons that were counted were considered to be due to background, since the desirable neutron intensity should be immeasureably small in this region. The maximum corrections were of the order of 1 percent, and were significant only when the in count was very small. The background observed in this manner is considered to be due to a (very small) continuous emission of neutrons from the cyclotron, resulting from a weak deuteron production near the ion source when the arc is supposedly turned off.

5. Preparation of Samples

Manganous fluoride: Reagent grade $MnCO_3$ was added to a pure 48 percent HF solution contained in a polyfluorochloroethylene beaker. The precipitate which formed was given time to settle, and the supernatent liquid was decanted. The precipitate was washed several times with pure ethanol, and then dried in air with infra-red lamps. The dry powder was fused in a boron-free graphite crucible at 950°C in an atmosphere of HF. The clear, orange-violet crystalline mass was crushed, and a uniform batch of 0.5-mm crystals was obtained by sieving. The calculated Mn content of MnF_2 is 59.11 percent; found by analysis, 59.03±0.03 percent.

Manganous oxide: Reagent grade $MnSO_4 \cdot 5H_2O$ was dried at 130°, and then heated in air at 1100°C for several days. The brown-black Mn_3O_4 was ground to a fine powder, which was reduced to MnO by heating it at 1100°C in a stream of hydrogen containing a trace of HCl.[24,25] The product was cooled to room temperature in a stream of pure hydrogen, and was thoroughly degassed in a high vacuum system with the aid of infra-red heating (75–130°C). The final product consisted of fine, bright green crystals. The calculated Mn content of MnO is 77.44 percent; found by analysis, 77.42±0.01 percent.

α-Ferric oxide: A large, essentially single, natural crystal of hematite in the shape of a plate 3.65-cm thick was used. The two flat faces of the crystal are very parallel, and are perpendicular to the three-fold axis of symmetry. The calculated Fe content of Fe_2O_3 is 69.94 percent; found by analysis, 69.80±0.08 percent.

Manganese: Electrolytic manganese of 99.9+ percent purity was pulverized, and a uniform quantity of 0.5 to 1-mm particles was obtained by sieving. The sample was dehydrogenated by heating at 400° in vacuum for several hours.

Spectrographic analysis of each of the samples showed the absence of any significant quantity of B, Cd, Co, Cu, Cr, Ni, or Pt.

6. Packing of Samples

The sample holders, shown in Fig. 4, were made of 17ST aluminum alloy. To avoid distortion of the thin, flat walls during welding, both walls were machined $\frac{1}{8}$ in. thicker than desired; after welding the walls were turned down to the proper thickness.

The dry sample was added in small portions to the sample holder through the tapered glass neck, the holder being tapped repeatedly after each addition in order to

[24] R. W. Millar, J. Am. Chem. Soc. **50**, 1875 (1928).
[25] H. S.-C. Deville, Comptes Rendus **53**, 199 (1861).

provide good packing of the sample. When the holder was filled to the top of the Kovar seal, and tapping produced no further change in level, the holder was connected to a high vacuum system. After thorough degasing, the system was filled with dry helium and the holder was sealed off just above the graded seal.

DISCUSSION OF ERRORS

1. Small angle scattering

This error is introduced because some neutrons scattered at small angles are counted by the detector. Moreover, since with the geometry used the sample sees more of the source than does the detector, the in-count neutron flux at the sample is greater than the out-count neutron flux at the detector; the error is consequently magnified. For simplicity, a sample having *no capture* is assumed.

Case I: 6 meter neutron path. Since the neutron source is of such limited size that not all parts of the sample can see the full solid angle of the source permitted by the collimating system, the relative geometry of the source, sample, and detector has been calculated on two bases (Table II). For an infinite source the solid angles subtended at the sample and detector by the source would be defined by the 6.3-cm collimating tube, while for the actual source used these solid angles may be considered to be fixed by the area of the source. As will become apparent shortly, the former basis leads to an upper limit for the error under consideration, and the latter to a minimum error. The true error is somewhere between these limits. It is assumed throughout that the source emits neutrons uniformly over its entire surface; localization of emission at the center of the source would tend to reduce the in-scattering error.

Let the incident neutron flux at the detector in the out position be N. Then the incident flux at the sample position in the in count is, for the case of an infinite source, equal to $(0.0027/0.00066)N=4.1\ N$, of which $3.1N$ cannot be seen by the detector unless it is scattered at very small angles into the detector by the sample. Of the remaining N flux, $(1-T)N$ will be scattered, and a fraction of this will take place at such small angles that it will be seen by the detector. If the scattering is spherically symmetrical, then the total extra in-scattered flux is

$$\frac{(0.0017)}{4\pi}4.1N(1-T)=0.0006N(1-T).$$

The absolute error in T is given by

$$\Delta T=0.0006(1-T)=\beta(1-T),$$

and the relative error in cross section is

$$\Delta\sigma/\sigma=\beta(1-T)/T\ \ln T. \qquad (2)$$

The relative error in cross section thus depends upon the transmission of the sample, and this dependence is shown in Fig. 5. The error increases rapidly for transmissions lower than about 5 percent. It should be noted, however, that an observed transmission of say 14 percent in the case of manganous fluoride corresponds to a transmission of about 61 percent if the manganese capture is corrected for, and only scattering processes are considered. With $T=0.61$ and $\beta=0.0006$ the upper limit for $\Delta\sigma_{pm}/\sigma_{pm}$ is less than 0.1 percent.

The derivation of the in-scattering error given above

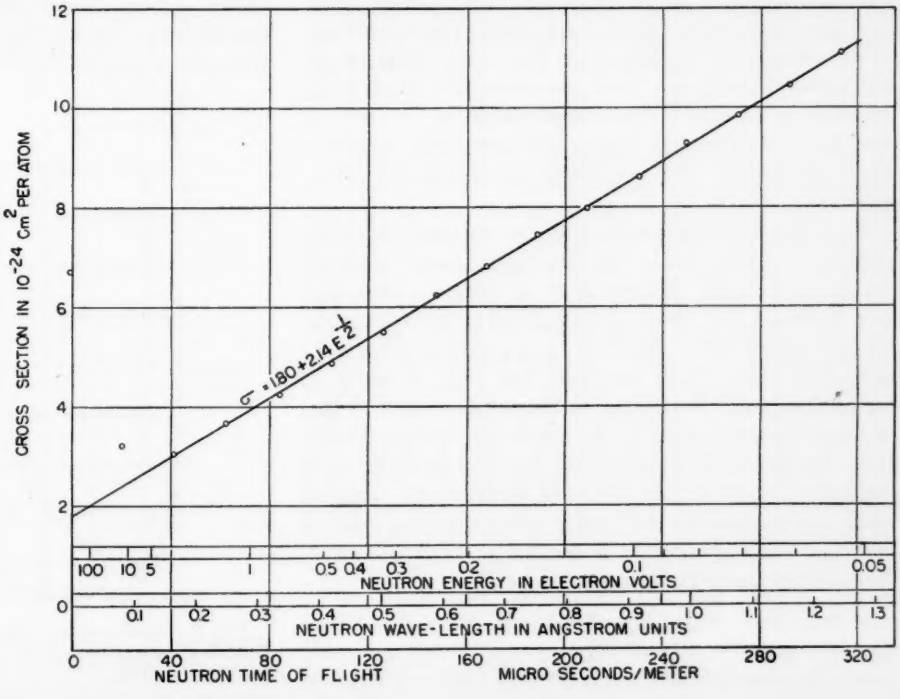
CROSS SECTION IN 10^{-24} Cm^2 PER ATOM
$\sigma = 1.80 + 2.14\,E^{-\frac{1}{2}}$
NEUTRON ENERGY IN ELECTRON VOLTS
NEUTRON WAVE-LENGTH IN ANGSTROM UNITS
NEUTRON TIME OF FLIGHT
MICRO SECONDS/METER

FIG. 7. The observed total cross section of 16.92 g/cm² of manganese as a function of neutron energy. The best $1/v$ line is $\sigma=1.80+2.14E^{-\frac{1}{2}}$.

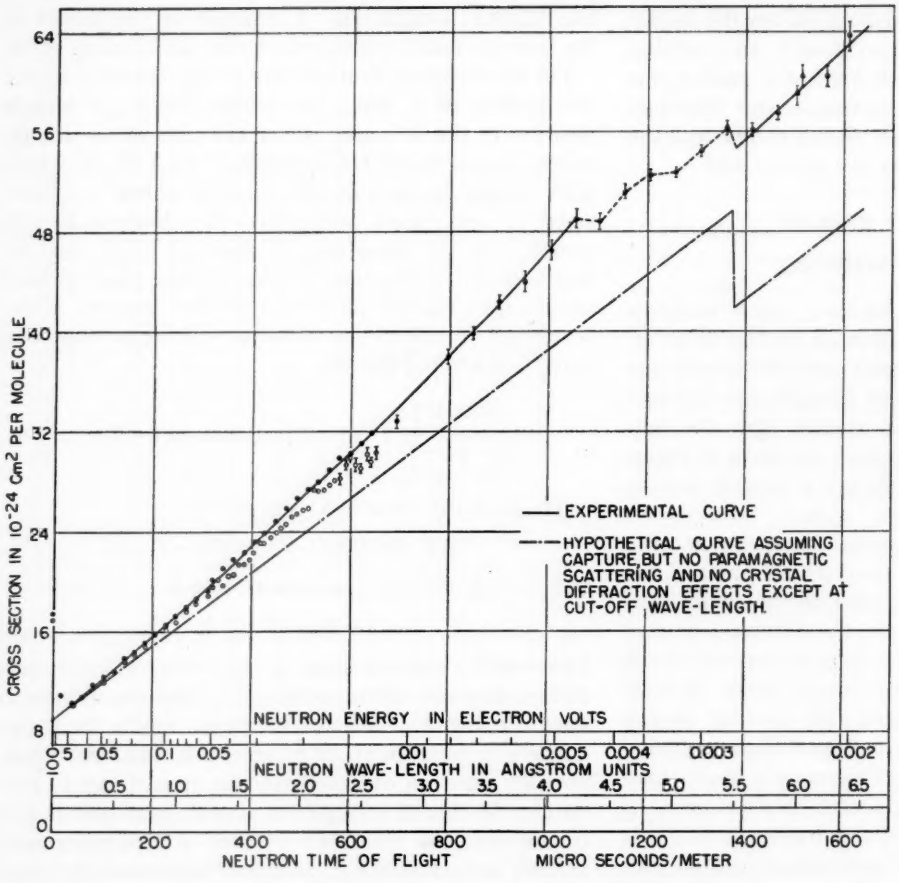
CROSS SECTION IN 10^{-24} Cm^2 PER MOLECULE
EXPERIMENTAL CURVE
HYPOTHETICAL CURVE ASSUMING CAPTURE, BUT NO PARAMAGNETIC SCATTERING AND NO CRYSTAL DIFFRACTION EFFECTS EXCEPT AT CUT-OFF WAVE-LENGTH
NEUTRON ENERGY IN ELECTRON VOLTS
NEUTRON WAVE-LENGTH IN ANGSTROM UNITS
NEUTRON TIME OF FLIGHT
MICRO SECONDS/METER

FIG. 8. The observed slow neutron total cross section of manganese fluoride compared with a hypothetical curve which neglects paramagnetic scattering. ● and ○ points were obtained with and without standard filters, respectively, with 11.13 g/cm² sample; ◒ points indicate 5.63 g/cm² sample.

is, however, over-simplified. Paramagnetic scattering is not spherically symmetrical as was assumed, but is instead under attainable conditions weighted in the forward direction. As a consequence, the error given by Eq. (2) is too low and must be corrected. The magnitude of the correction depends upon the wave-length of the incident neutrons; for short wave-lengths the angular dependence of scattering is large, while in the limit of very long wave-lengths (when the form factor becomes equal to unity) the scattering is spherically symmetrical.

Since the solid angle subtended by the detector at the sample is so very small, the differential form factor for scattering into the detector may be taken to be unity. It is assumed that the scattering is all single scattering, an assumption which leads to an upper limit for the in-scattering error. Since the mean free path of neutrons for paramagnetic scattering in the samples used (5 cm) is approximately equal to the maximum sample dimension, the effect of multiple scattering may be taken to be negligibly small on the basis of Melkonian's detailed analysis[22] of multiple scattering. The corrected relative error in cross section at a particular neutron wave-length may hence be represented by

$$\frac{\Delta\sigma_{pm}}{\sigma_{pm}}=\beta\frac{(1-T)}{T\ln T}\cdot\frac{1}{F} \qquad (3)$$

where F is evaluated at this wave-length. Taking $r_0=0.8$Å as an approximate value, the correction factor $1/F$ has been calculated from the elastic form factor curve[10] for various wave-lengths. The results are summarized by Fig. 6, in which the maximum error, $\Delta\sigma_{pm}/\sigma_{pm}$, given by Eq. (3) (with $\beta=0.0006$ and

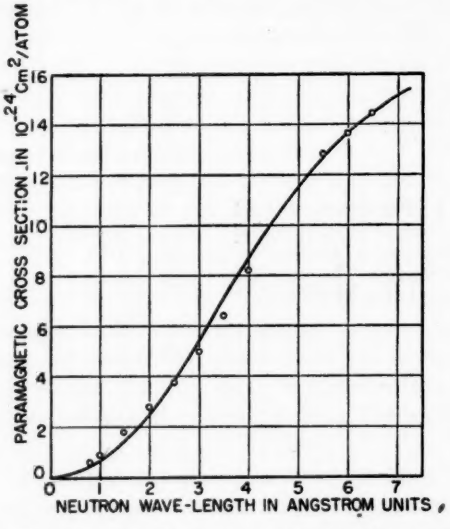

FIG. 9. Experimental values of σ_{pm} for Mn^{++} in manganous fluoride compared with a theoretical curve based on elastic scattering with $r_0=0.64$.

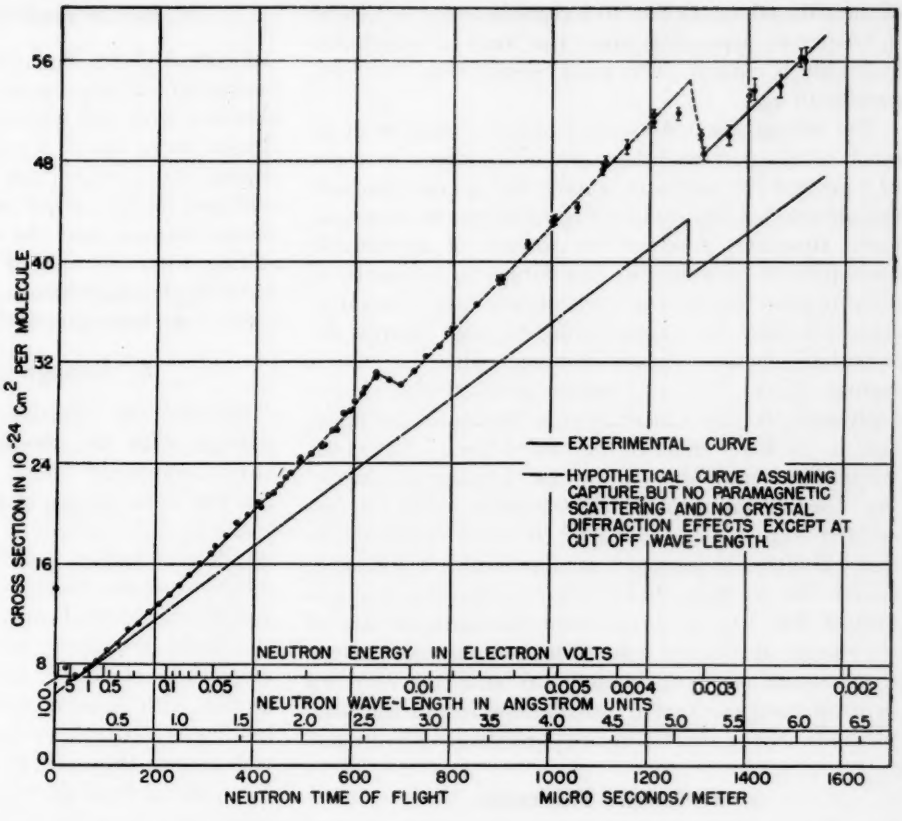
CROSS SECTION IN 10^{-24} Cm^2 PER MOLECULE
56
48
40
32
24
16
8
0
EXPERIMENTAL CURVE
HYPOTHETICAL CURVE ASSUMING CAPTURE, BUT NO PARAMAGNETIC SCATTERING AND NO CRYSTAL DIFFRACTION EFFECTS EXCEPT AT CUT OFF WAVE-LENGTH.
NEUTRON ENERGY IN ELECTRON VOLTS
100 5 1 0.5 0.1 0.05 0.01 0.005 0.004 0.003 0.002
NEUTRON WAVE-LENGTH IN ANGSTROM UNITS
0.5 1.0 1.5 2.0 2.5 3.0 3.5 4.0 4.5 5.0 5.5 6.0 6.5
0 200 400 600 800 1000 1200 1400 1600
NEUTRON TIME OF FLIGHT MICRO SECONDS/METER

FIG. 10. The observed slow neutron total cross section of 7.25 g/cm² of manganous oxide compared with a hypothetical curve which neglects paramagnetic scattering. ◒ points were obtained with standard filters; ● and ○ points indicate 256 and 512 μsec. detection intervals, respectively.

$T=0.65$) is plotted as a function of neutron wave-length.

It should be mentioned at this point that the scattering in general has been tacitly assumed to be perfectly elastic, in the sense that the velocity of the scattered neutrons is the same as that of the incident neutrons. Under this restriction, the BF_3 counters, whose detection efficiency obeys a $1/v$ law, will count scattered and transmitted neutrons with the same efficiency. Moreover, only in the case of elastic scattering may the form factor in the forward direction be taken to be unity, and the use of Halpern's form factor be justified.

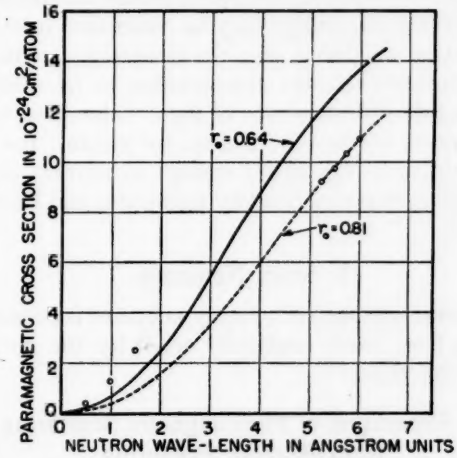

FIG. 11. Experimental values of σ_{pm} for Mn^{++} in manganous oxide compared with two theoretical curves based on elastic scattering.

Case II: 5-meter neutron path. The poorer geometry in this case leads to somewhat greater errors. The maximum total error as a function of λ is given in Fig. 6 (with $\beta=0.002$ and $T=0.65$). No corrections are given for $\lambda<3$A, since the 5-meter collimation was used only for $\lambda>3$A.

2. Sample Purity

Chemical analysis established the major composition of each sample, while spectrographic analysis showed the absence in any significant amount of high cross-section elements as impurities. However, the presence in any of the samples of about 0.1 percent by weight of hydrogen, a quantity difficulty to detect chemically, would introduce a serious error. This powerful effect of hydrogen arises from its very low atomic weight, high scattering cross section, and large reduced mass effect which makes the completely bound cross section four times as large as its free scattering cross section. Moreover, the hydrogen scattering is almost all incoherent and hence does not disappear at the cut-off wave-length for Bragg reflections. A simple calculation shows that the presence of 0.1 percent by weight of hydrogen in the manganous fluoride sample would lead to an error of +1.9 barns in the free scattering cross section of manganous fluoride; at low neutron energies (~0.002 ev) the error would increase because

of the reduced mass effect to a value between +3.4 and +7.6 barns, depending upon the form in which the hydrogen is bound. The error would then be comparable to σ_{pm}.

The manganese analyses indicate the absence of as much as 0.1 percent by weight of hydrogen *as water* (0.9 percent by weight of water), but do not preclude the presence of this quantity of hydrogen in elemental form. However, proof of the absence of appreciable quantities of hydrogen in any form can be obtained directly from the neutron transmission data. The intercept, obtained by extrapolating to high energy the hypothetical curve (where it merges with the experimental curve, i.e., at energies greater than 1 ev) represents the free scattering cross section of the molecule, σ_f, which is equal to the sum of the σ_f of the constituent elements. Thus, in the case of manganous oxide, the observed intercept is 5.6±0.2 barns, while the calculated sum is 5.5±0.1 barns. It may, therefore, be concluded that hydrogen, if at all present in the sample, contributes no more than 0.4 barn at neutron energies greater than 1 ev, with this error increasing because of the change in effective reduced mass of the hydrogen to a maximum of approximately 1.6 barns for very low neutron energies. Similar calculations for all the samples indicate the absence of large quantities of hydrogen.

3. Sample Thickness

The determination of the thickness of a sample in g per cm² involves measurements of the volume and thickness of the sample holder, and the weight of the sample. The errors in weighing and volume determination are negligible, being less than 0.1 percent. The sample holders were machined to tolerances which would give a maximum error of only 0.1 percent in the distance between walls. The accuracy of the machine work was checked by comparing the observed and calculated volumes of several sample holders.

4. Counting

a. *Statistical Accuracy*

The fractional uncertainty in the observed cross section is given by reference 22:

$$\frac{\Delta\sigma}{\sigma}=\frac{(1/N_i+1/N_0)^{\frac{1}{2}}}{\ln T}, \tag{4}$$

where N_i and N_0 represent the number of counts in the sample in and out positions, respectively, for the same number of neutron monitor counts. Whenever possible the sample thickness was adjusted to give a transmission within or close to 0.05 to 0.2, since the statistical error is a fairly constant minimum in this region. The statistical uncertainty is represented by vertical bars through the experimental points on the various cross section curves.

b. *Rate Dependence of Neutron Counters*

Figure 8 shows the cross-section data for manganous fluoride in the neutron wave-length region of 0 to 2.6A, obtained with and without the use of standard filters. Errors up to about 3 percent in the direction of decreased cross section are seen to be introduced when standard filters are not used. The good agreement between channels and the reproducibility of results resulting from the use of standard filters, as well as theoretical considerations, indicate that rate dependence errors have been effectively eliminated.

5. Change in Reduced Mass

Because the effective reduced mass of an atom changes with the binding, the cross section of an atom completely bound in a crystal is larger than the free cross section of this same atom by the factor $[(A+1)/A]^2$, where A is the atomic weight. The magnitude of this effect is shown in Table I, which gives the difference in the bound and free cross section for each sample, neglecting capture, paramagnetic scattering, etc. If the form factor for the binding was known, then corrections could be made for the increase in cross section with neutron wave-length. Unfortunately, the binding is a complicated phenomenon which is not now well known. However, for neutron wave-lengths beyond λ_c all but a small part of the nuclear scattering disappears. Any error due to change in reduced mass is then present only in the small residual incoherent scattering cross section, and is, indeed, only equal to a small part of the latter. It may be concluded then that for wave-lengths smaller than λ_c, errors up to the maximums shown in Table I are incurred, but that beyond λ_c the error due to changed reduced mass is negligible. The errors will tend to make the calculated σ_{pm} larger than its true value.

6. Effect of Resolution Width

The effect of varying neutron intensity and transmission with neutron energy may be considered to change the effective weighting over the resolution function so as to cause the correct transmission to be observed for a slightly different time of flight value. For detection interval widths of 512 μsec. (or greater) the shift was found to be significant enough to warrent correction. The method described by Rainwater and Havens[19] was used.

7. Stray Neutrons

The error introduced by stray neutrons is considered to have been made negligibly small by the methods already described.

8. Separation of Paramagnetic Scattering from Nuclear Scattering

For those wave-lengths below λ_c at which there are no perturbing crystal diffraction effects, the method of

subtracting the hypothetical from the experimental curve is probably accurate to within ±0.5 barn. This probable error is attributed to the uncertainty in the plotting of these curves, and to the possible presence of unresolved diffraction peaks. Beyond the cut-off the approximation of the residual incoherent scattering cross section introduces a further uncertainty in σ_{pm} of $\sim\pm 0.75$ barn.

9. Summary

Since the determinate errors discussed above are generally much smaller than the known indeterminate errors, no corrections other than for background and time of flight shift were applied to the observed results. For $\lambda<\lambda_c$ the maximum error may be taken to be $\sim\pm 0.5$ barn, while beyond λ_c the maximum error is probably $\sim\pm 1.5$ barns.

DISCUSSION OF RESULTS

In order to determine accurately σ_{pm} for MnF_2 and MnO by the method already described, it is necessary to have an accurate value of the capture slope of manganese. A slow neutron transmission study of 16.92 g/cm² of pure manganese was therefore carried out. The results are shown in Fig. 7. The best $1/v$ line is given by the equation

$$\sigma=(1.80\pm 0.05)+(2.14\pm 0.02)E^{-\frac{1}{2}}.$$

This may be compared with the recently published value[24]

$$\sigma=(2.2\pm 0.4)+(2.24\pm 0.05)E^{-\frac{1}{2}}.$$

The new value is considered to be more accurate because of the use of standard filters, and the particular care taken to remove hydrogen from the sample.[26]

Large values of σ_{pm} for manganous fluoride were found at $\lambda>\lambda_c$, as shown in Fig. 8. No analysis of the experimental curve was made between 4 and 5.5A because of the perturbing effect of crystal diffraction peaks. In constructing the hypothetical curve only the capture slope of manganese was taken into account, since the capture of fluorine is very small.[27] The differ-

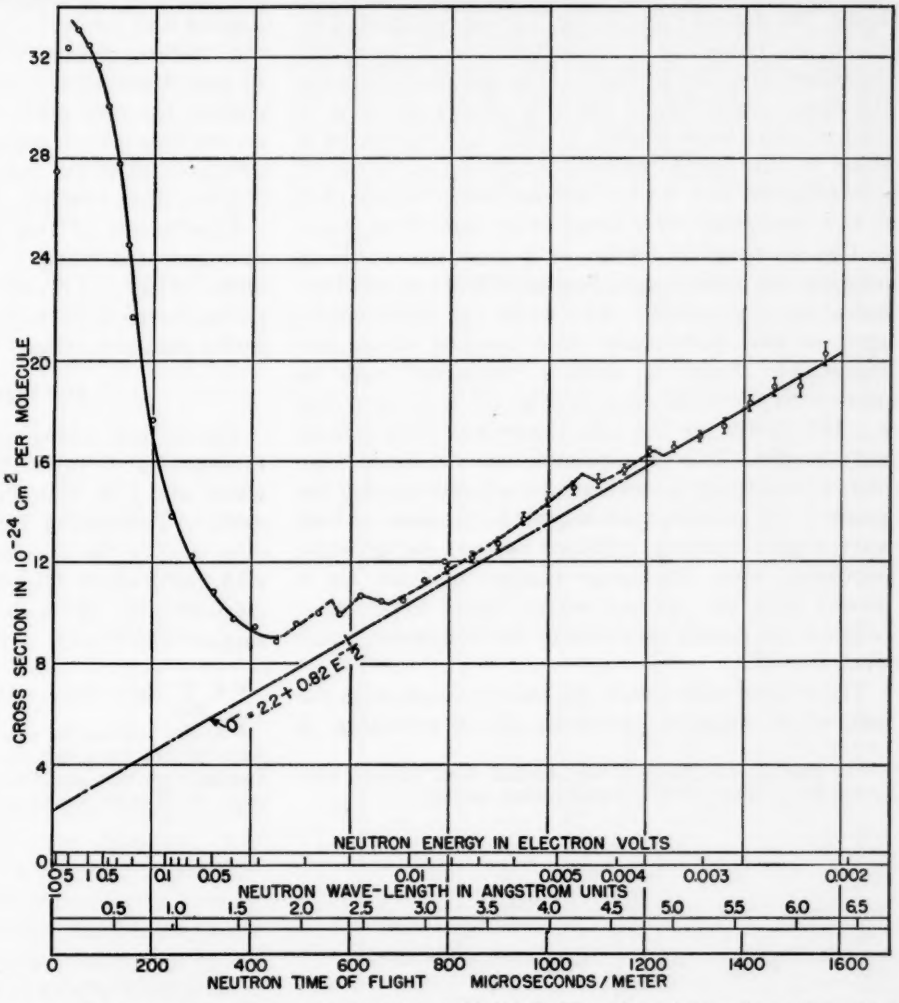

FIG. 12. The observed slow neutron total cross section of 19.30 g/cm² of α-ferric oxide.

[26] Potter, Hayes, and Lukens, Am. Inst. of Mining and Met. Eng., Tech. Pub. No. 1809 (1945). These investigators have shown that considerable quantities of hydrogen are adsorbed or entrapped in electrolytic manganese.

[27] Manley, Haworth, and Luebke, Phys. Rev. **59**, 109 (1941); H. Volz, Zeits. f. Physik **121**, 201 (1943); C. O. Muehlhause and M. Goldhaber, Phys. Rev. **70**, 85 (1946).

ence between the experimental curve and the hypothetical curve beyond λ_c is attributed to paramagnetic scattering.

In Fig. 9 the experimental values of σ_{pm} for MnF_2 are compared with a theoretical curve based on the Halpern-Johnson elastic form factor. The parameter r_0 was taken to be 0.64A to give the best fit. It is perhaps of interest to compare this value of r_0 with the empirical ionic radius of Mn^{++} in crystals as given by Pauling,[28] namely 0.80A. Even though MnF_2 is not expected to have a large degree of spin coupling, since Δ is only 113, the agreement between the experimental points and the theoretical curve is surprisingly good. These results for MnF_2 represent an improvement over the preliminary results already reported[10] in that standard filters and a more accurate manganese capture slope were used.

Similar results for MnO are shown in Figs. 10 and 11. It is to be noted that beyond the cut-off σ_{pm} is considerably less than for MnF_2 at corresponding values of λ. This can be attributed to the large spin coupling in MnO. The dashed curve in Fig. 11 was constructed by taking the parameter r_0 to be 0.81A so as to fit the experimental points beyond λ_c. The agreement between the experimental points and this theoretical curve is poor at short wave-lengths, a result to be expected if there is considerable inelastic scattering in virtue of spin coupling. For, it then becomes rather meaningless to fit a theoretical curve based on an *elastic* form factor to the experimental results. It is more reasonable to compare the experimental results with the same theoretical curve ($r_0=0.64$A) with which the MnF_2 results agree so well, particularly since coupling should not appreciably change r_0. Such a comparison may be made with the solid curve in Fig. 11. It is seen that σ_{pm} falls well below the solid theoretical curve at long wave-lengths. This is explicable on the basis that inelastic scattering causes a greater attenuation of F the longer is the neutron wave-length. In the limit of long wave-lengths inelastic collisions become energetically impossible when the energy change involved, $h\nu$, is greater than the neutron energy, while hyperelastic collisions are greatly restricted by the Boltzmann factor when $h\nu > kT$.

The α-ferric oxide results can best be discussed in the light of the magnetic properties of this substance. A recent careful study by Hayes[29] shows that although the susceptibility values of α-Fe_2O_3 are those of a strongly paramagnetic substance, it displays properties of incipient ferromagnetism. It was found to have a slight residual magnetism and a Curie point (685°C), and to exhibit hysteresis phenomena. A very large degree of spin coupling is hence expected to be present in this compound. Since Fe^{+++} has five unpaired $3d$ electrons, Eq. (1) predicts the same amount of paramagnetic scattering for it as for Mn^{++}. Figure 12 shows the observed dependence of the total cross section on neutron energy for α-Fe_2O_3. The latter was oriented in the collimating system so that the neutron beam was parallel to the three-fold symmetry axis of the crystal.[30] As is typical of large single crystals,[14] the cross section decreases rapidly with increasing neutron wave-length. At 3A almost all the coherent scattering has vanished, and a straight line drawn through the remaining points and extrapolated back to zero wave-length fits the equation $\sigma=2.2+0.82E^{-\frac{1}{2}}$. Recent unpublished measurements in this Laboratory for pure iron give a $1/v$ slope of 0.41 per iron atom. Since a considerable part of the 2.2-barns residual cross section must be attributed to spin, thermal, etc., effects (see Table I), it is concluded that very little, or no paramagnetic scattering occurs. This is not a surprising result for a paramagnetic substance in which spin coupling is so strong that it displays weak ferromagnetism.

Experiments of the kind discussed in this paper, complemented, perhaps, by angular scattering experiments (which can reveal the differential form factor for paramagnetic scattering), offer a new tool for investigating paramagnetism.

ACKNOWLEDGMENT

The author wishes to express his appreciation to Professors T. I. Taylor, W. W. Havens, Jr., L. J. Rainwater, and J. R. Dunning for help and guidance in the work, to Professor O. Halpern for his interest and criticism, and to the members of the Columbia cyclotron staff, particularly Miss M. Levin, for assistance in the measurements. He is also indebted to the AEC for the support which made this research possible.

[28] L. Pauling, *The Nature of the Chemical Bond* (Cornell University Press, Ithaca, 1940), second edition, p. 350.

[29] E. T. Hayes, Bur. of Mines Report of Investigations 3570, June, 1941.

[30] In this position the most widely spaced plane which can reflect, the 111 plane, is perpendicular to the neutron beam. Reflection from this plane then takes place at $\lambda=9.14$A, which is the same cut-off as for a microcrystalline sample.

The Radiations of Tantalum^{182}, Rhenium^{186,188}, and Gold^{199}*

LOUIS A. BEACH, CHARLES L. PEACOCK, AND ROGER G. WILKINSON
Indiana University, Bloomington, Indiana

(Received July 21, 1949)

A survey of the radiations of Ta^{182}, $Re^{186,188}$ and Au^{199} has been made down to energies of the order of 5 kev with a small 180 degree spectrometer.

The disintegration scheme of Ta^{182} is complex. The twenty or more conversion lines found superimposed on the beta-ray spectrum and the numerous peaks found in the photoelectron spectrum are analysed into seventeen gammas in the energy region 80 to 330 kev. In addition, three gamma-rays of energies 1.13, 1.22, and 1.24 Mev are found. The continuous spectrum has an end point at 0.53 Mev.

The radiations of Re^{186} consist of a single beta-ray group of maximum energy 1.07 Mev and two gamma-rays of energies 0.138 and 0.212 Mev. The 0.138 Mev gamma-ray is converted. Coincidence experiments strongly suggest that the mode of decay is one involving the emission of a single beta-ray group, followed by the cascade emission of the two gamma-rays. The disintegration of Re^{188} is more complicated. A single group of beta-rays is found with the end point at 2.10 Mev. Five gamma-rays with energies essentially the same as those reported by Miller and Curtiss are present.

All the radiations of Au^{199} lie below 0.32 Mev. Superimposed on the beta-ray spectrum are eight conversion lines that may be attributed to 4 gamma-rays having energies of 0.024, 0.051, 0.156 and 0.207 Mev. The beta-rays have a maximum energy of 0.32 Mev. A possible decay scheme is suggested.

I. INTRODUCTION

THE disintegration schemes of the heavier unstable isotopes are in many cases complex and the radiation is characterized by the presence of several beta-ray groups and numerous gamma-rays, especially in the low energy region. As a consequence, there generally appears a number of conversion lines superimposed on the beta-ray spectra of these elements with the K, L, and M components so disposed as to make analysis difficult. The radiations of Ta^{182}, $Re^{186,188}$, and Au^{199} which are discussed in this paper are typical examples. Since the low energy region is of particular importance in these cases, most of the previous work has been done with spectrometers using photographic plate detection.[1] This gives a rather accurate determination of the energies of the individual conversion lines but does not give sufficient information about the relative intensities or the photoelectron spectrum to make analysis into corresponding gamma-rays definite. In this work an attempt has been made to determine the energies of the gamma-rays with greater certainty by studying both the photoelectrons and beta-rays with thin window G-M tube detection.

II. APPARATUS

A small 180° spectrometer, previously described, was used for the measurements.[2] The range of the instrument has been extended down to about 5 kev by the use of very thin window G-M tube detection. The windows consist of five to seven layers of zapon film 0.005 mg/cm^2 in thickness supported on a grid. During the filling process the spectrometer chamber and tube are evacuated simultaneously, thus eliminating excessive pressure on the window. The tube is filled from a reservoir containing the proper mixture of argon and alcohol. In the event of slow diffusion of the mixture through the window and consequent threshold change, the counter can be stabilized by leaving it connected to the reservoir. In most of the work the diffusion was negligible during the period of operation. Since several hours were sometimes required for the counter to come

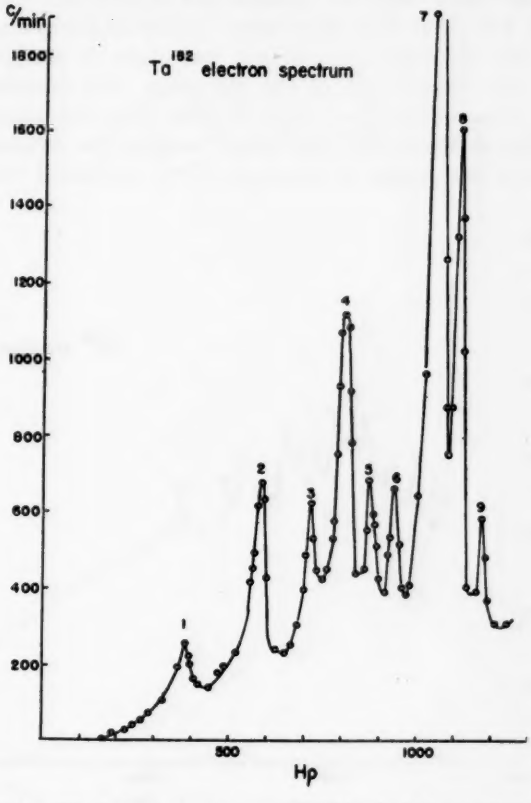

FIG. 1. The beta-ray spectrum of Ta^{182} in the low energy region obtained with a G-M tube detector having a window 0.03 mg/cm^2 thick. See Tables I and III for the energies and identification.

* Assisted by the Joint Program of the ONR and the AEC.

[1] J. M. Cork, Phys. Rev. 72, 581 (1947).

[2] C. L. Peacock and R. G. Wilkinson, Phys. Rev. 74, 297 (1948).

TABLE I. The conversion lines of Ta^{182}.

Line* number	Energy (Mev)	Identification	Line* number	Energy (Mev)	Identification
1	0.0129	K_1	11	0.1395	L_7+M_6
2	0.0286	K_2	12	0.1541	$K_{11}+L_8+M_7$
3	0.0428	K_3	13	0.1595	L_9+M_8
4	0.0527	K_4	14	0.1699	M_9
5	0.0625	K_5	15	0.1795	K_{12}
6	0.0690	K_6+L_1	16	0.1882	$K_{13}+L_{10}$
7	0.0877	K_7+L_2	17	0.1963	$K_{14}+L_{11}+M_{10}$
8	0.0957	$K_8+L_3+M_2$	18	0.2189	$K_{15}+M_{11}$
9	0.1105	$K_9+L_4+M_3$	19	0.2294	$K_{16}+L_{12}$
10	0.1286	$K_{10}+L_6+M_5$	20	0.2539	K_{17}

* The number in this column refers to the legend of Fig. 2.

TABLE II. The photoelectron lines of Ta^{182}.

Line number*	Energy (Mev)	Identification	Line number*	Energy (Mev)	Identification
1	0.0435	K_5	11	0.1760	K_{13}
2	0.0530	K_6	12	0.2055	$K_{15}?+L_{11}$
3	0.0656	L_1	13	0.2370	$K_{17}+L_{13}$
4	0.0698	K_7	14	0.2480	L_{14}
5	0.0840	K_9	15	1.045	K_{18}
6	0.0975	L_3	16	1.131	K_{19}
7	0.1140	$K_{10}+L_5$	17	1.149	K_{20}
8	0.1340	K_{11}	18	1.201	L_{19}
9	0.1550	$K_{12}+L_9$	19	1.234	L_{20}
10	0.1640	K_{13}			

* The number in this column refers to the legend in Fig. 3.

to equilibrium after filling, the data above 60 kev was taken with a conventional counter having a mica window 2 mg/cm² in thickness.

III. TANTALUM[182]

The radiations of Ta^{182} have been studied by several investigators in various energy regions. Cork[1] has surveyed the conversion electrons in the low energy region with a 180° spectrometer using photographic plate detection. Some thirty-four conversion lines are reported which he has attributed to sixteen gamma-rays on the basis of the characteristic differences of the K, L, and M binding energies of tungsten. Rall and Wilkinson[3] have reported gamma-rays of energies 0.15, 0.22, 1.13, and 1.22 Mev from a study of the photoelectron spectrum. No attempt was made to examine the low energy part of the spectrum. The beta-ray end point was found to be 0.53 Mev. The coincidence studies of Mandeville and Scherb[4] suggest the presence of only one group of beta-rays. They concluded that the high energy gamma-rays are not in cascade since no appreciable gamma-gamma coincidences were found.

Sources for the present investigation were prepared from a sample of TaO_2 irradiated by slow neutrons in the Oak Ridge pile. Chemical separations were performed to insure purity, with special attention given to the separation of calcium, iron, and tungsten. Sources were made from Ta_2O_5 precipitated from $K_8Ta_3O_{19}$. For the low energy work, the beta-ray source consisted of less than 0.2 mg/cm² of Ta_2O_5 on a backing of zapon film about 0.003 mg/cm² thick.

Figure 1 shows the beta-ray spectrum obtained with the very thin window G-M tube detector in the region 7–125 kev. The remainder of the beta-ray spectrum was taken with a conventional mica window tube (Fig. 2). In all, twenty conversion lines are found superimposed upon the beta-ray spectrum. Undoubtedly, greater resolution would reveal further L and M components reported by Cork. Line No. 7 is by far the most intense. Assignment of the gamma-ray energies from these data

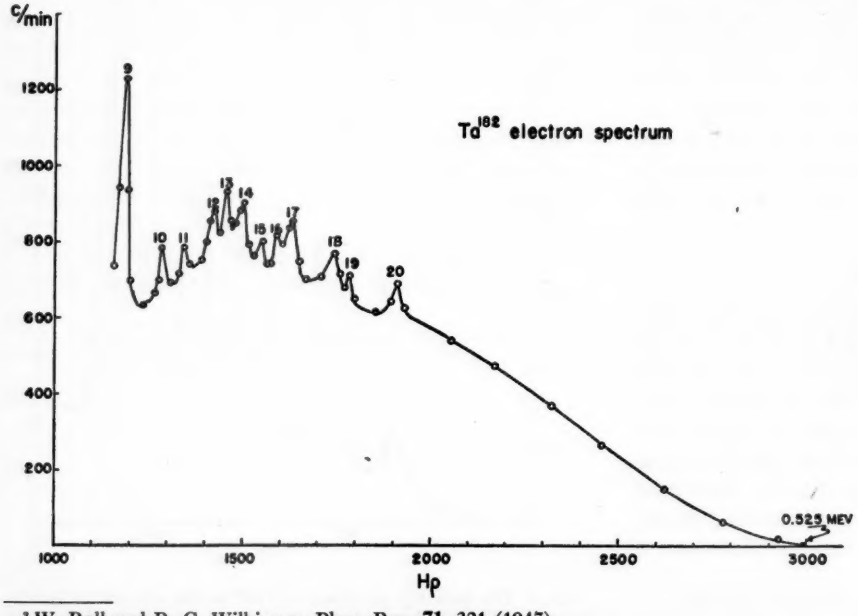

FIG. 2. The higher energy portion of the beta-ray spectrum obtained with a G-M tube detector having a mica window 2 mg/cm² thick. See Tables I and III for the energies and identification.

[3] W. Rall and R. G. Wilkinson, Phys. Rev. **71**, 321 (1947).
[4] C. E. Mandeville and M. V. Scherb, Phys. Rev. **73**, 340 (1948).

alone is difficult and uncertain, since the lines are closely spaced and since it is possible for L and M lines from certain gamma-rays to be masked by stronger K lines of others. Furthermore, it is possible for the L line in some cases to be stronger than the K, so that relative intensities do not furnish a sufficient criterion. Table I summarizes the conversion electron data and gives the most probable gamma-ray assignments consistent with the photoelectron data. Although four significant figures are given for convenience in analysis, no claim for accuracy of the measurements to this extent is made.

In order to make gamma-ray assignments more positive, the photoelectrons ejected from a 30 mg/cm² lead radiator were studied. Figure 3 shows 16 of the 19 lines so obtained, together with the strong Compton electron distribution associated with the high energy gamma-rays. Three lines measured with the thin window counter are not shown. The high energy lines are readily resolved into K and L components due to three gamma-rays at 1.13, 1.22, and 1.24 Mev. Rall and Wilkinson[3] have previously reported only two gamma-rays in this region, the latter two apparently being unresolved. Table II gives the energies of the photoelectron lines and the most probable gamma-ray assignments.

The analysis of all data is given in Table III. In at least four cases no photoelectron lines were found. The K photoelectron lines associated with the first four gamma-rays are too low in energy to be observed. In other cases, e.g., gamma-ray No. 8, the gamma-ray is probably highly converted. The overlapping of several components of the conversion electron data makes it

TABLE III. Analysis and summary of the conversion line and photoelectron line data.

Gamma-ray number*	Gamma-energy (Mev) from conversion in the: K shell	L shell	M shell	Gamma-energy (Mev) from photoelectrons from: K shell	L shell	Average gamma-energy (Mev)
1	0.0822	0.0811	—	—	0.0816	0.0820
2	0.0979	0.0998	0.0985	—	—	0.0980
3	0.1121	0.1078	0.1133	—	0.1135	0.1120
4	0.1220	0.1226	—	—	—	0.1220
5	0.1318	—	0.1314	0.1315	0.1300	0.1317
6	0.1383	0.1407	0.1423	0.1410	—	0.1410
7	0.1570	—	0.1569	0.1578	—	0.1570
8	0.1650	0.1662	0.1623	—	—	0.1650
9	0.1798	0.1716	0.1727	0.1720	0.1710	0.1720
10	0.1979	0.2003	0.1991	0.2020	0.1920	0.1980
11	0.2234	—	0.2217	0.2220	0.2215	0.2220
12	0.2488	0.2415	—	0.2430	—	0.2430
13	0.2575	—	—	0.2520	0.2530	0.2550
14	0.2656	0.2660	—	0.2640	0.2640	0.2640
15	0.2882	—	—	0.2935	—	0.2900?
16	0.2987	—	—	—	—	0.2990?
17	0.3232	—	—	0.3250	—	0.3240
18	—	—	—	1.1330	—	1.1330
19	—	—	—	1.2190	1.2170	1.2190
20	—	—	—	1.2370	1.2500	1.2370

* The number in this column refers to the identification number in column three of Tables I and II.

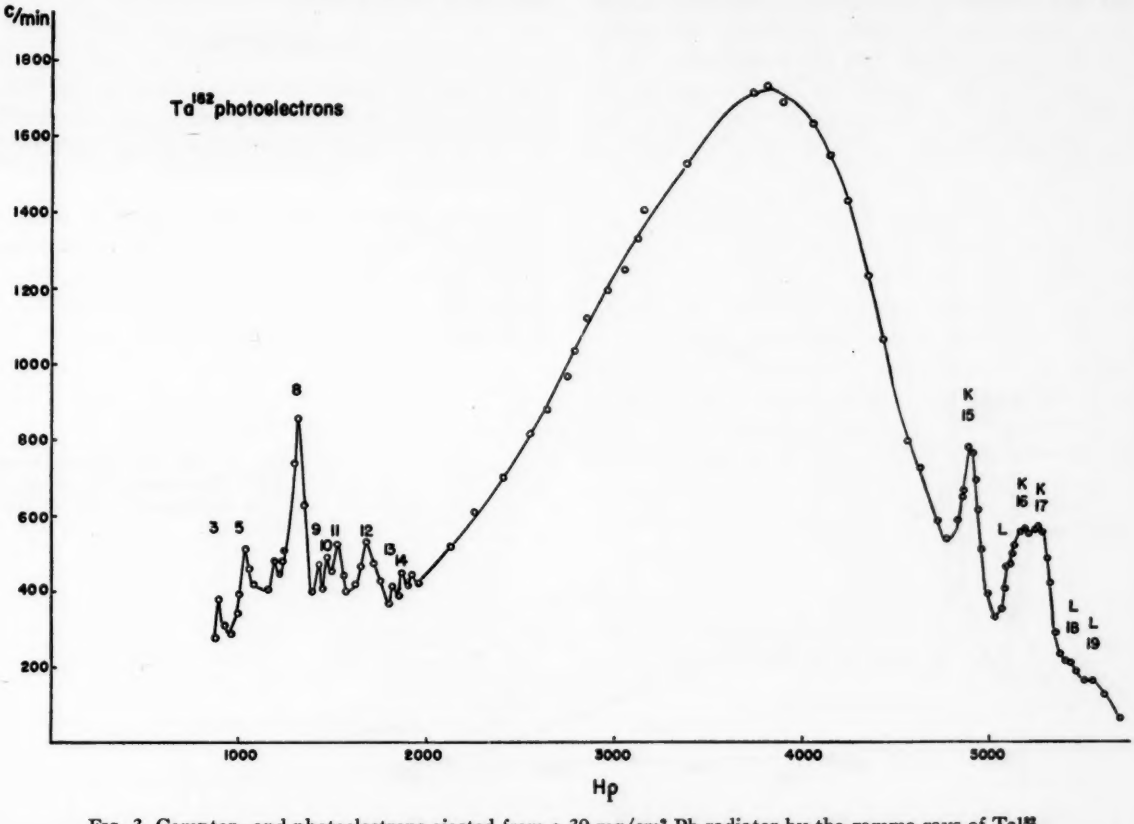

FIG. 3. Compton- and photoelectrons ejected from a 30 mg/cm² Pb radiator by the gamma-rays of Ta^{182}. See Tables II and III for the energies and identification.

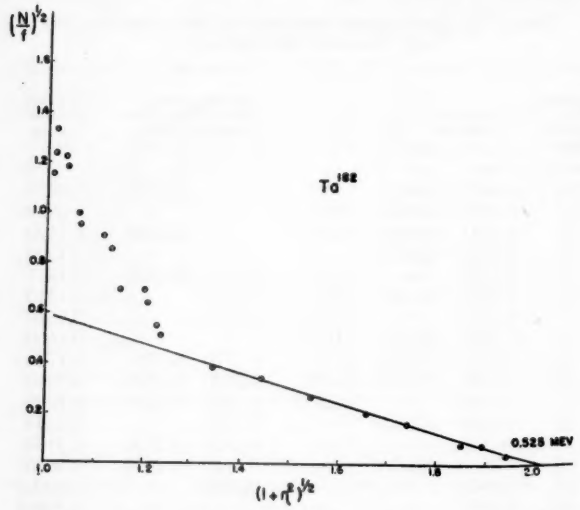

FIG. 4. Fermi plot of the beta-rays of Ta^{182}. The deviation from the straight line at low energy is possibly due to a second group having a maximum energy at about 0.25 Mev.

impossible in some instances to make a definite assignment. For example, the L conversion line of gamma-ray No. 5 is masked by the K line of No. 10. If the identification is correct, gamma-rays Nos. 7, 8, 9, 11, 18, 19, 20 are the most intense. Gamma-ray No. 7, assigned as 0.157 Mev, is the most intense of the low energy group and is highly converted. The corresponding conversion line has been previously reported by Cork[1] as the L line due to a gamma-ray at 0.996. However, the photoelectron spectrum suggests that the assignment as a K line is more probable. Gamma-ray No. 11, assigned as 0.222 Mev, exhibits the strongest photo-peak in the low energy region and is weakly converted. Of all the gamma-rays, those of highest energy are the most intense (Nos. 18, 19, 20) and are about equally strong. Even with the additional information afforded by the photoelectron spectrum, some uncertainty persists in the identification. However, at least seven of the suggested gamma-rays of Table III agree with Cork's assignment.

A Fermi plot of the continuous portion of the beta-ray spectrum is shown in Fig. 4. The graph is a straight line down to 0.15 Mev and yields an end point at 0.525 Mev, in agreement with the previous value given by Rall and Wilkinson.[3] There is some evidence for another group at approximately 0.25 Mev but the presence of the conversion lines does not permit positive identification.

The results of this investigation may be summarized as follows. Ta^{182} decays by the emission of a beta-ray of maximum energy 0.53 Mev and possibly by the emission of another group of beta-rays of approximately 0.25 Mev to excited W^{182}, which returns to the ground state by complex gamma-ray emission. The gamma-rays of highest energy (1.13, 1.22, and 1.24 Mev) are the most intense. Of the fifteen or more low energy gamma-rays (Table III) those of energies 0.157, 0.165, and 0.222 Mev are the most prominent. No attempt at formulating a decay scheme is made. Since the high energy gamma-rays are so close in energy, the coincidence data of Mandeville and Scherb[4] does not eliminate the possibility of cascade emission. This, however, is probably not the case.

IV. RHENIUM[186, 188]

The previous studies of the radiations of the 90-hour Re^{186} have been made by absorption[5] and cloud-chamber[6] methods. A single group of beta-rays with a maxi-

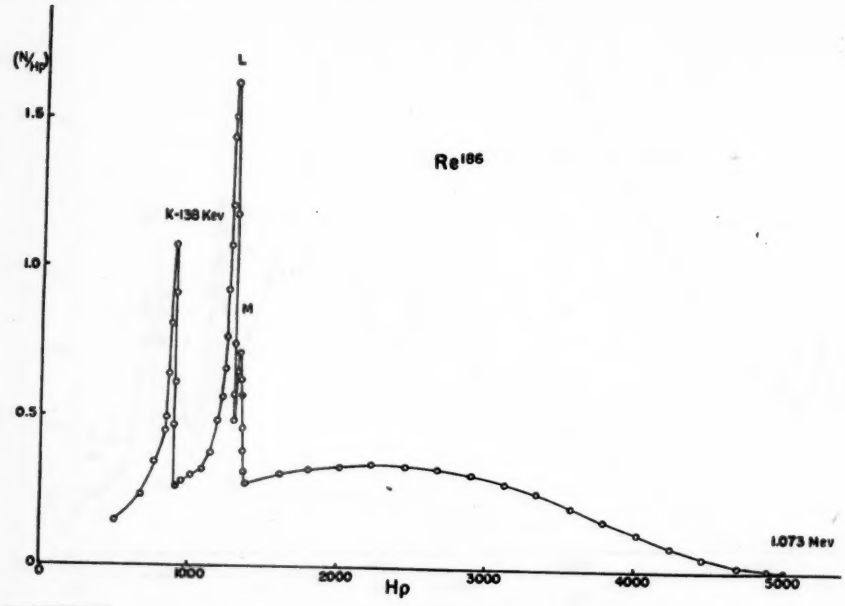

FIG. 5. The beta-ray spectrum of Re^{186}. The value of the energy is for the gamma-ray, not the conversion line.

[5] L. J. Goodman and M. L. Pool, Phys. Rev. **71**, 288 (1947).
[6] K. Sinma and H. Yamasaki, Phys. Rev. **55**, 320 (1939).

mum energy of 1.07 Mev is reported. No gamma-rays have been observed. The 18-hour Re^{188} has been investigated by a number of workers. Only the gamma-rays have been studied by spectrometer methods. By means of a thin lens spectrometer, Miller and Curtiss[7] found five gamma-rays associated with Re^{188}. The coincidence work of Mandeville, Scherb, and Keighton[8] suggests a complex mode of decay involving two groups of beta-rays and the cascade emission of some of the gamma-rays.

The results of the present work were obtained with neutron activated samples from Oak Ridge. High specific activity permitted the use of very thin sources (<0.1 mg/cm^2) for the beta-ray studies. Figure 5 shows the beta-ray spectrum of Re^{186} taken after the Re^{188} had decayed. Three conversion lines are present all of which

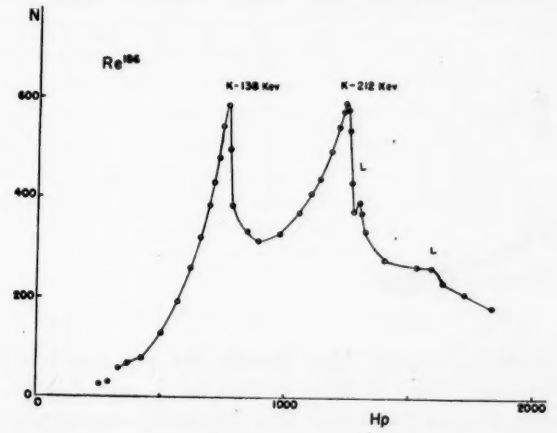

FIG. 6. Photoelectrons ejected from a 32 mg/cm^2 Pb radiator by the gamma-rays of Re^{186}. The values of the energies are for the gamma-rays, not the photoelectron lines.

decay with the 90-hour period. The energies of the conversion lines correspond to the K, L, and M components associated with a single gamma-ray of energy 0.138 Mev. The photoelectron spectrum, measured after most of the 18-hour activity had died away, is shown in

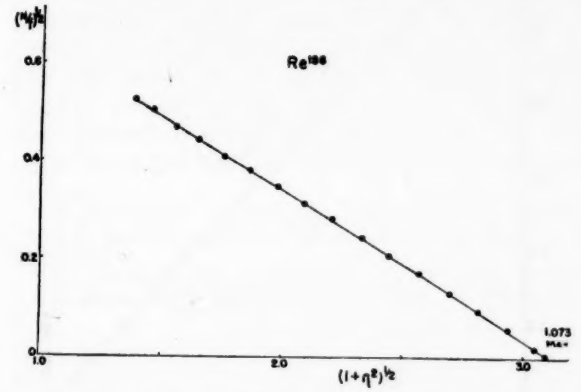

FIG. 7. Fermi plot of the beta-rays of Re^{186}.

TABLE IV. The gamma-rays of Au^{199}.

Conversion line energy (Mev)	Photo-line energy (Mev)	Gamma-ray energy (Mev)
0.0090(L)	—	0.024
0.0360(L) 0.0473(M)	— —	0.051
—	0.054(L)	0.070
0.0735(K) 0.1470(L) 0.1590(M)	0.068(K) — —	0.156
0.1243(K) 0.1970(L)	0.119(K) 0.189(L)	0.207
0.1470(K)	0.143(K)	0.230

Fig. 6. Two lines are present which correspond to gamma-rays having energies 0.138 and 0.212 Mev. If the 0.212-Mev gamma-ray is converted, the conversion must be weak. Unfortunately, the K conversion line would be superimposed on the M line due to the 0.138-Mev gamma-ray so that no definite decision can be made. A conventional Fermi-plot of the continuous spectrum (Fig. 7) shows conclusively that only one group of beta-rays is present with a maximum energy of 1.07 Mev.

The interpretation of these results is made clear by the recent coincidence measurements of Cuffey and Jurney[9] in this laboratory. They find a substantial number of beta-gamma- and gamma-gamma coincidences which are associated with the 90-hour activity. It is therefore natural to assume that the gamma-rays are in cascade and that the decay scheme of Re^{186} (Fig. 8) involves the emission of beta-rays of a single group, which leaves the resulting Os^{186} in an excited state 0.350 Mev above ground. On this assumption, the conversion coefficients of the 0.138-Mev gamma-ray are $\alpha_K=3$ percent, and $\alpha_L=7$ percent. The K to L ratio is found to be 0.40 and suggests a spin change of 2 or 3 for this gamma-ray transition, according to the curves of Hebb and Nelson.[10] The conversion coefficient of the third line shown in Fig. 5 is 1.2 percent and represents the sum of the K conversion of the 0.212-Mev gamma-ray and the M conversion of the 0.138-Mev gamma-ray. Com-

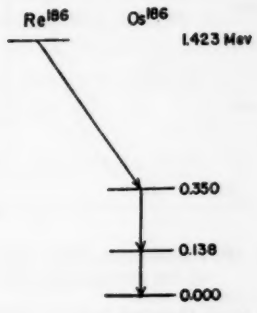

FIG. 8. Probable decay scheme of Re^{186}.

[7] L. C. Miller and L. F. Curtiss, Phys. Rev. **70**, 983 (1946).
[8] Mandeville, Scherb, and Keighton, Phys. Rev. **74**, 888 (1948).
[9] To be published.
[10] M. H. Hebb and E. Nelson, Phys. Rev. **58**, 486 (1940).

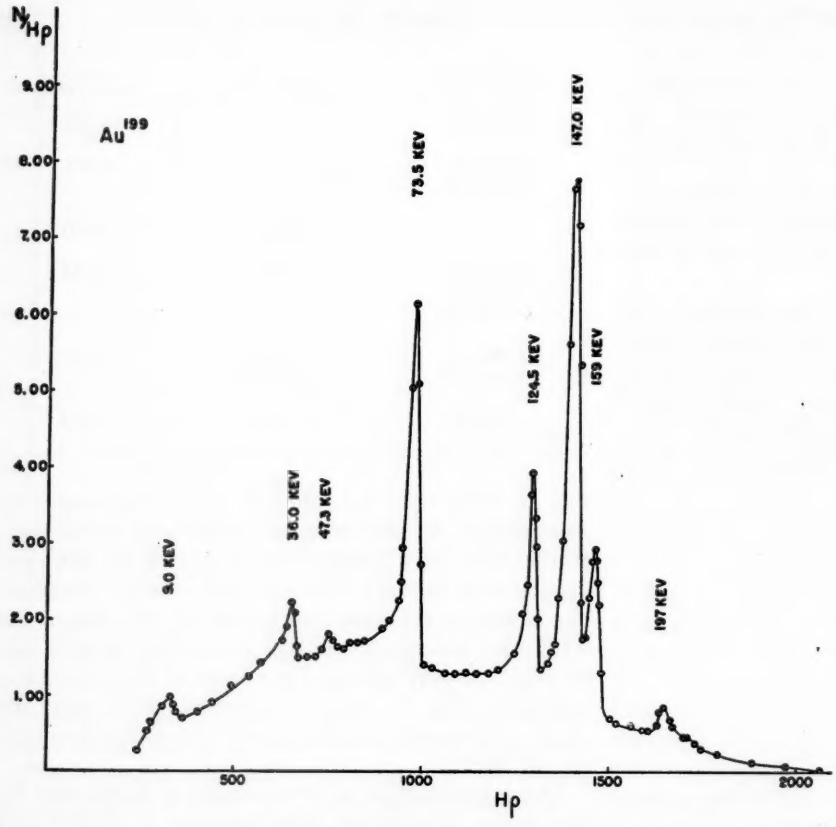

FIG. 9. The beta-ray spectrum of Au^{199}. The energies given are those of the conversion lines, not the associated gamma-rays.

parison of the values with the tables of Rose and his associates[11] shows that both gamma-rays are probably electric dipole radiation. The coincidence work of Cuffey and Jurney further indicates that no metastable state exists in the Os^{186}.

The data obtained for the 18-hour Re^{188} essentially verifies the findings of Miller and Curtiss.[7] Five gamma-rays were found with energies 0.15, 0.48, 0.64, 0.95, and 1.40 Mev. The 0.15-Mev gamma-ray was found to be converted. The 1.40-Mev gamma-ray is probably quite strong in spite of the fact that the corresponding photoelectron line was observed to be weak. The presence of beta-rays in excess of two Mev necessitated the use of a thick copper absorber, hence the geometry for photoelectron production was poor. A strong Compton elec-

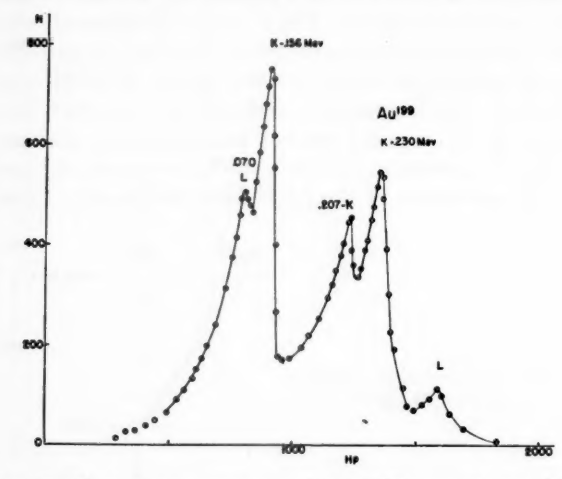

FIG. 10. Photoelectron spectrum of Au^{199}. The energies are those of the gamma-rays, not the photoelectron lines.

[11] Rose, Goertzel, Spinrad, Harr, and Strong, "Tables of *K*-Shell Internal Conversion Coefficients" (privately distributed prior to publication).

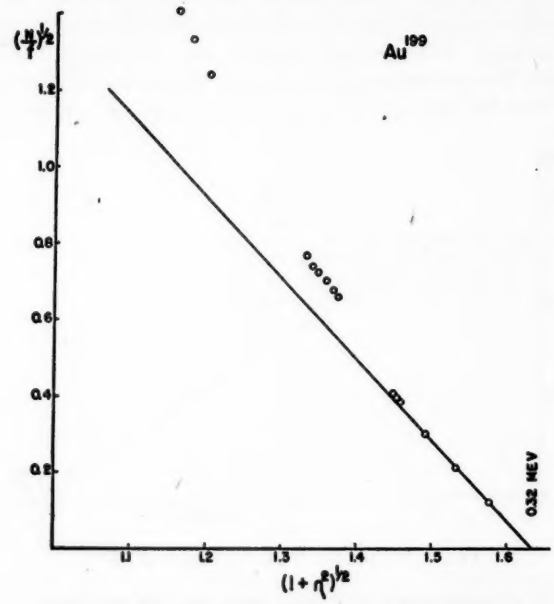

FIG. 11. Fermi plot of the beta-rays of Au^{199}.

tron distribution due to this gamma-ray was obtained owing to the thick copper absorber. A significant result is the fact that only one group of beta-rays was found. Two groups have been previously reported by Beach *et al.*[12] and by Mandeville, Scherb, and Keighton.[8] However, subsequent measurements with cyclotron activated samples led to the conclusion that there is a single group of beta-rays with a maximum energy of 2.10 Mev.

V. GOLD[199]

The radiations of 3.3-day Au^{199} are entirely in the low energy region and therefore have not been previously studied by spectrometer methods. Absorption and coincidence measurements have been made by Krishnan and Nahum,[13] Mandeville, Scherb, and Keighton[14] and by Meem and Maienschein.[15] The latter group finds evidence for one partially converted gamma-ray at 0.18 Mev and a simple beta-ray spectrum with an end point at 0.38 Mev.

The sources used for this study were prepared by separating Au^{199} from its 31-minute parent, Pt^{199}, produced by neutron bombardment at Oak Ridge. Separation was accomplished by repeated ethyl acetate extraction of $AuCl_3$. Subsequent examination of the decay showed that the separation was good. Beta-ray sources were made by evaporating a water solution of $AuCl_3$ on a zapon backing approximately 0.003 mg/cm² thick. Since the specific activity was very high, the sources were less than 0.1 mg/cm² thick. Photoelectron sources were made by depositing the $AuCl_3$ on a 10-mil copper strip to eliminate the beta-rays. The radiator was a lead strip 32 mg/cm² thick.

The complete beta-ray spectrum is shown in Fig. 9. The continuous spectrum is complicated by the presence of eight conversion lines from 9 to 197 kev in energy. The 9-kev line is probably more intense than it appears to be, since it lies in the region of strong counter window cut-off. Figure 10 shows the photoelectron spectrum produced by the gamma-rays. The five lines are readily identified as the K and L components due to four gamma-rays. Table IV shows the analysis of the conversion and photoelectron data. Estimation of the relative intensities of the six gamma-rays is made difficult by the overlapping of several of the components. The photoelectron spectrum shows that the 0.156, 0.207, and 0.230-Mev gamma-rays are the most prominent. Estimates based on Gray's[16] empirical curve suggest that the 0.156 and the 0.207-Mev gamma-rays are about the same intensity, while the 0.230-Mev gamma-ray is about twice as strong as these. However, the conversion electron data shows that the 0.156-Mev radiation is most strongly converted, with the L conversion being at least as strong as the K. The K conversion of the 0.230-Mev gamma-ray, if any, overlaps the L line of the 0.156-Mev gamma-ray. The fact that no L conversion of the 0.230 gamma-ray is detected suggests that conversion in this case is weak. It may be assumed that these three gamma-rays are not in cascade and that they account for 30 percent, 25 percent, and 45 percent of the transitions from the highest excited state of the Hg^{199}. This assumption is in accord with the results of Mandeville, Scherb, and Keighton,[14] since they found no gamma-gamma coincidences.

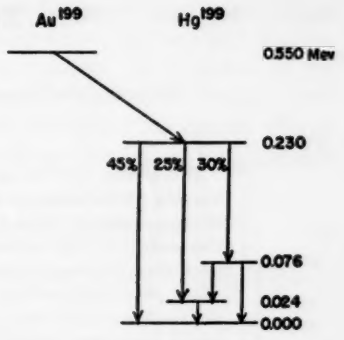

FIG. 12. Possible decay scheme of Au^{199}.

A conventional Fermi plot of the continuous portion of the beta-ray spectrum is shown in Fig. 11. No attempt is made to interpret the curvature since the spectrum lies wholly in the low energy region and is perturbed by the presence of many conversion lines. Probably only one group of beta-rays is present with an end point at 0.32 Mev. This conclusion is substantiated by Mandeville *et al.*[14] and Meem[15] since their $N_{\beta-\gamma}/N_{\beta}$ coincidence curve was a straight line, characteristic of a simple spectrum.

Figure 12 summarizes the results and suggests a possible decay scheme. The mode of decay given is very consistent with the measured energy values, coincidence data, and the relative intensities. One apparent inconsistency appears in connection with the 0.024-Mev gamma-ray which is observed to be weak but which must be assumed to be strong since it follows two of the most dominant gamma-rays. However, it lies too low to be observed as a photo-line and the conversion line is in the region of counter tube cut-off.

[12] Beach, Peacock, and Wilkinson, Phys. Rev. **76**, 187 (1949).
[13] R. S. Krishnan and E. A. Nahum, Proc. Camb. Phil. Soc. **37**, 422 (1941).
[14] Mandeville, Scherb, and Keighton, Phys. Rev. **74**, 601 (1948).
[15] L. Meem and F. Maienschein, Phys. Rev. **76**, 328 (1949).
[16] L. H. Gray, Proc. Camb. Phil. Soc. **27**, 103 (1931).

Electrons in Perturbed Periodic Lattices*

J. C. SLATER
Research Laboratory of Electronics, Massachusetts Institute of Technology, Cambridge, Massachusetts

(Received June 17, 1949)

It is shown that the motion of an electron in a periodic potential, such as is found in a solid, plus a slowly varying perturbative potential, can be derived from the energy in the periodic lattice alone, as a function of momentum or wave number. A Schrödinger equation is set up, in which the Hamiltonian is the sum of this energy in the periodic lattice—the momentum being replaced by a differential operator—and of the perturbative potential energy. The resulting wave function modulates atomic functions to provide a solution of the perturbed problem. This method is applied to give proofs of simple theorems in conduction theory, to discuss the energy levels of impurity atoms in a semiconductor, and to consider excitons; all are problems which have been considered before, but which are treated more straightforwardly by the present method. Applying the method statistically, the combined Poisson's equation and Fermi-Dirac statistics is set up for impurities in metals and semiconductors, and for the theory of rectifying barriers.

I. INTRODUCTION

MANY of the most important problems in the theory of solids concern the motion of electrons in perturbed periodic lattices. Examples of such problems are: the effect of impurities, of the *P*- or *N*-type, in semiconductors; the behavior of rectifying barriers, either between semiconductors and metals, or between *P*- and *N*-type semiconductors; and the behavior of optically excited energy levels in crystals. All these problems have received much discussion in the literature, by methods involving various approximations to the solution of the wave-mechanical problem of the motion of electrons in a perturbed periodic lattice. It is the purpose of this paper to point out that there is a quite general theorem in wave mechanics, regarding the motion of an electron in such a perturbed lattice, which serves to unify the treatment of all these problems. This theorem was essentially discovered by Wannier,[1] and used by him in discussing excited energy levels of crystals. That problem, unfortunately, is one of the most complicated to which the method can be applied, and the theorem has tended to lie buried in Wannier's paper, attracting little attention, without general realization of the important simpler problems to which it is applicable. James[2] has independently arrived at many of the qualitative results of the present paper, but is apparently unaware of the importance of Wannier's theorem, and bases his conclusions on quite different and less powerful methods of discussing the problem, applicable only in the one-dimensional case, though he has carried his approximations one step further than we have. A number of other writers have used similar less powerful methods for special problems.[3]

In the present paper, we shall first state the general theorem, and prove it by a method similar to that used by Wannier for his special problem. We shall then apply it to discussion of the important problems, such as impurity semiconductors and excited energy levels, which result in discrete energy levels. For problems of rectifying barriers and surface states, a statistical approach is more appropriate, and we point out the relation of our theorem to self-consistent field methods, and thence to statistical treatment by the Fermi-Dirac statistics. This leads us to a discussion of rectifying barriers and surface states, not essentially different from that appearing in the literature, but somewhat more general and unified.

II. THE MOTION OF ELECTRONS IN PERTURBED PERIODIC LATTICES

In Appendix I we give a general proof of our theorem; in this section we shall merely state it and discuss its applications. The theorem is one which starts by assuming that the problem of the motion of electrons in a given periodic lattice has been solved, and uses that solution as the starting point for discussion of the problem in which the potential is the sum of the original periodic potential and an additional potential varying only slightly from atom to atom of the periodic potential. We first remind the reader of the nature of the solution of the periodic potential problem.[4] We describe the solution as if we were considering a metal, although the extension to non-metals with more than one atom per cell presents no difficulties. We surround each atom by an appropriate polyhedral cell, the vectors from the origin (located at the nucleus of one of the atoms) to other atoms being denoted by Q_k, so that the potential is unchanged when we make the translation Q_k. Then each solution of the wave equation can be characterized by a vector quantity p, of the dimensions of a momentum, such that the wave function is multiplied by a

* This work has been supported in part by the Signal Corps, the Air Materiel Command, and the ONR.

[1] G. H. Wannier, "Structure of electronic excitation levels in insulating crystals," Phys. Rev. **52**, 191 (1937).

[2] H. M. James, "Electronic states in perturbed periodic systems," unpublished report of Contract No. W-36-039-SC-32020, Department of Physics, Purdue University. The writer is indebted to Professor K. Lark-Horovitz, director of the project, for the privilege of inspecting this report. See also paper in Phys. Rev., this issue.

[3] For instance, S. C. Tibbs, Trans. Faraday Soc. **35**, 1471 (1939), who discussed excited energy levels in NaCl, and S. Peckar, J. Phys. U.S.S.R. **10**, 431 (1946).

[4] We use substantially the notation in J. C. Slater, Rev. Mod. Phys. **6**, 209 (1934).

factor $\exp[(i/\hbar)\mathbf{p}\cdot\mathbf{Q}_k]$ when we make the translation Q_k. Bloch[5] made a well-known approximation to the form of the wave function by starting with functions $u(q-Q_k)$ (where q is the vector position of the point where we are finding the wave function) representing the wave function of an electron at a vector displacement $q-Q_k$ from the nucleus of the kth atom, in the case where that atom alone was present; such a function is generally called an atomic function. He then set up the approximate wave function

$$b(p, q)=\sum_k \{\exp[(i/\hbar)p\cdot Q_k]\}u(q-Q_k), \quad (1)$$

which clearly has the required periodicity property and which, at the same time, behaves in the neighborhood of each atom like an atomic wave function.

This Bloch function $b(p, q)$ suffers from two defects. First, it is not an exact solution of the problem; secondly, the functions $u(q-Q_k)$, for different k's, are not orthogonal to each other, so that in calculating any sort of integrals over the Bloch functions we meet integrals coming from lack of orthogonality. Wannier[1] showed that both difficulties can be overcome by setting up a new set of atomic functions $a(q-Q_k)$ (see Appendix I for their definition), similar to the u's near each atom, but oscillating and falling off in amplitude like the function $(\sin x)/x$ at a distance from the atom. These functions have the properties that they are normalized, are exactly orthogonal to each other, and when they are substituted in an expression like (1) they form an exact solution of the problem of the periodic lattice. Thus the real solution $\psi_0(p, q)$ can be written in the form

$$\psi_0(p, q)=\sum_k 1/N^{\frac{1}{2}}\{\exp[(i/\hbar)p\cdot Q_k]\}a(q-Q_k). \quad (2)$$

The factor $(1/N^{\frac{1}{2}})$, where N is the total number of atoms in the crystal, is introduced so that ψ_0 will be normalized when integrated over the whole volume of the crystal. We notice from (2) that the function $\psi_0(p, q)$ is periodic in p-space, or momentum space: if p is increased by one of the vectors P_j of the reciprocal lattice, defined by the relation $P_j\cdot Q_k=\text{integer}\times h$, the expression on the right side of (2) is unchanged. Then the energy $E_0(p)$, the energy of the level associated with a given p, will likewise be a periodic function of p, being unchanged when p increases by any one of the P_j's. All solutions can then be obtained by allowing p to range over the interior of the central zone in momentum space; it is easily shown that, when p is quantized by the boundary conditions appropriate to a finite crystal with N atoms, there will be N allowed stationary states. For a given p, there will, of course, be an infinite number of energy levels, just as for an isolated atom. The N levels continuously joined together, corresponding to the various allowed p's, form an energy band; we see that there are an infinite number of such bands. Their properties and relations to the theory of metals (where they overlap) and semiconductors or insulators (where gaps in energy remain between them) are well known.

Now we are ready to consider our problem of the perturbed periodic lattice. Let the Hamiltonian function of the unperturbed problem (the kinetic energy plus periodic potential energy) be H_0, so that the ψ_0's satisfy the equation

$$H_0\psi_0(p, q)=E_0(p)\psi_0(p, q). \quad (3)$$

Then we wish to find functions $\psi_n(q)$, n being a quantum number, satisfying

$$H\psi_n(q)=E_n\psi_n(q), \quad (4)$$

where $H=H_0+H_1$, H_1 being the slowly varying function of q. We try to express the ψ_n's in the form:

$$\psi_n(q)=\sum_k \Psi_n(Q_k)a(q-Q_k). \quad (5)$$

That is, we try to find a function $\Psi_n(q)$ which we can use to modulate the atomic functions $a(q-Q_k)$ to get the correct solution of the problem, replacing the exponential function $(1/N^{\frac{1}{2}})\exp[(i/\hbar)p\cdot q]$ which is used in the problem of the unperturbed periodic potential, in the solution (2). Our theorem now states that $\Psi_n(q)$ satisfies the following differential equation, provided H_1 varies slowly with position, so that it does not change its value greatly from one atom to the next:

$$[E_0[-i\hbar(\partial/\partial q)]+H_1(q)]\Psi_n(q)=E_n\Psi_n(q). \quad (6)$$

Here the first term $E_0(-i\hbar\partial/\partial q)$ stands as an abbreviation for the differential operator in which E_0, regarded as a function of the three rectangular components of the vector p, is transformed by replacing p_x by $-i\hbar\partial/\partial x$, p_y by $-i\hbar\partial/\partial y$, etc., as in the ordinary kinetic energy operator in Schrödinger's equation. In (6) we then have a Schrödinger equation for $\Psi_n(q)$, in which the perturbative potential H_1 appears as the potential energy, while the kinetic energy operator is derived from the energy $E_0(p)$ of the unperturbed problem by replacing p by a differential operator. It is this theorem which is proved in Appendix I, and which was applied to the problem of excited energy levels by Wannier.[1] By means of it, we effectively reduce the problem of electrons in periodic lattices and additional perturbing potentials to a problem much like that of free electrons in the perturbing potential (as we shall show in the next section) and hence make the problem of electrons in periodic lattices not much more complicated than free-electron theory.

III. APPLICATIONS OF THE GENERAL THEOREM

The first application which we shall make of our general theorem (6) is to the motion of wave packets of electrons in the perturbed periodic lattice. We can set up such wave packets just as well from the functions Ψ_n, which modulate the atomic functions, as from the functions ψ_n, which take into account the oscillations in the neighborhood of each atom. It is a well-known

[5] F. Bloch, Zeits. f. Physik **52**, 555 (1928).

theorem of quantum mechanics that the center of gravity of a wave packet moves according to the classical Hamiltonian equations. Since (6) is derived from the Hamiltonian $E_0(p)+H_1(q)$, we see that the equations of motion of the packet (writing them in terms of their rectangular components) are:

$$\frac{dx}{dt}=\frac{\partial E_0}{\partial p_x},\quad \frac{dy}{dt}=\frac{\partial E_0}{\partial p_y},\quad \frac{dz}{dt}=\frac{\partial E_0}{\partial p_z}, \tag{7}$$

and

$$\frac{dp_x}{dt}=-\frac{\partial H_1}{\partial x},\quad \frac{dp_y}{dt}=-\frac{\partial H_1}{\partial y}\quad \frac{dp_z}{dt}=-\frac{\partial H_1}{\partial z}. \tag{8}$$

Both these theorems are familiar, but they are ordinarily derived by much more involved methods than are used here.[6] In (7) we see the formula for the velocity of a wave packet in terms of the gradient of the function E_0 in momentum space, and in (8) the statement that the momentum p of a packet is governed by the classical equation of motion in terms of the additional force resulting from the perturbation H_1. These two results are the basis of most of the band theory of electrical conduction in solids, but it has hardly been realized that they form merely the classical Hamiltonian equations of the Hamiltonian of Eq. (6).

Our next example will be the behavior of wave packets near the bottom or top of an energy band, and hence the concept of effective mass. At the bottom of a band, provided the axes are properly oriented, the energy E_0 may be written in the form

$$E_0(p)=E_1+\frac{p_x^2}{2m_x}+\frac{p_y^2}{2m_y}+\frac{p_z^2}{2m_z}. \tag{9}$$

Here m_x, m_y, m_z are three coefficients of the dimensions of masses and E_1 the energy of the bottom of the band. In this case, (7) and (8) become

$$\frac{dx}{dt}=\frac{p_x}{m_x},\quad \frac{dp_x}{dt}=-\frac{\partial H_1}{\partial x},$$
$$m_x\frac{d^2x}{dt^2}=-\frac{\partial H_1}{\partial x}, \tag{10}$$

with similar equations for the y- and z-components, showing that the packet obeys an ordinary equation of motion corresponding to a particle of mass m_x for the x-coordinate, m_y for the y-coordinate, and m_z for the z-coordinate. Similarly, near the top of a band, we have:

$$E_0(p)=E_1-\frac{p_x^2}{2m_x}-\frac{p_y^2}{2m_y}-\frac{p_z^2}{2m_z}, \tag{11}$$

where these m_x's are different from those in (9), but still positive. Hence the equations corresponding to (10) are

$$m_x(d^2x/dt^2)=\partial H_1/\partial x, \text{ etc.}, \tag{12}$$

showing that a packet at the top of a band will be accelerated by an external field in the opposite direction to a particle of positive mass exposed to the perturbative force. It is well known, and we need not repeat the discussion, that this leads a hole in an almost filled band, near the top of that band, to be accelerated as a positively charged particle of electronic charge and mass m_x, m_y, m_z would be.

If we are near the top or bottom of a band, so that one of the approximations (9) or (11) is correct, it is clear that Eq. (6) reduces to a Schrödinger equation of the conventional type, with a quadratic differential operator for the kinetic energy (though, in general, with different coefficients for the x-, y-, and z-derivatives). We can thus solve it by conventional methods, resulting in discrete energy levels as in atomic problems. We shall shortly give examples of this situation. In case the energy is such that these approximations are not appropriate, the problem becomes more complicated, higher derivatives entering the differential equation. In such circumstances, at least in one-dimensional problems, the most appropriate method of solution would presumably be the WKB approximation. This depends on finding the momentum p, which is equal to h/λ, where λ is the wave-length, in terms of position. From the equation $E_0(p)+H_1(q)=E$ we can find p, and hence set up the wave function and quantum condition.

There is a useful graphical method of discussing the solution, in the one-dimensional case (James[2] makes considerable use of this method). This is shown in Fig. 1. In Fig. 1(a), we show a schematic periodic potential, with its energy bands. In Fig. 1(b), we draw the energy bands, pushed upward for each value of x by the amount $H_1(x)$, the potential energy. We also draw a horizontal line of constant energy, E. We now see that the kinetic energy and momentum are determined by the position of E with respect to the energy bands, just as they would be in the absence of H_1. For instance, at point A in Fig. 1(b), the energy E is in the same position with respect to the energy band which the energy E' occupies in Fig. 1(a). Thus, at this point A, in the presence of the potential H_1, the de Broglie wave-length of the function Ψ will be the same as the de Broglie wavelength of the sinusoidal function in Fig. 1(a), corresponding to energy E'. Our graphical representation of Fig. 1(b) thus has many of the characteristics of an energy diagram in classical mechanics, in which potential energy and total energy are plotted as functions

[6] R. Peierls, Zeits. f. Physik **53**, 255 (1929); F. Bloch, Zeits. f. Physik **52**, 555 (1928); A. Sommerfeld and H. Bethe, *Handbuch der Physik* (Verlag. Julius Springer, Berlin, 1933), second edition, vol. XXIV, pp. 374–375, 506–509; H. Jones and C. Zener, Proc. Roy. Soc. **A144**, 101 (1934); C. Zener, Proc. Roy. Soc. **A145**, 523 (1934); L. Brillouin, *Les Electrons dans les Métaux du Point de Vue Ondulatoire* (Hermann and Cie, Paris, 1934); J. C. Slater, Rev. Mod. Phys. **6**, 209, 259–262, Appendix VI (1934); Mott and Jones, *Properties of Metals and Alloys* (Oxford University Press, New York, 1936), p. 92–96; W. V. Houston, Phys. Rev. **57**, 184 (1940); and many other references.

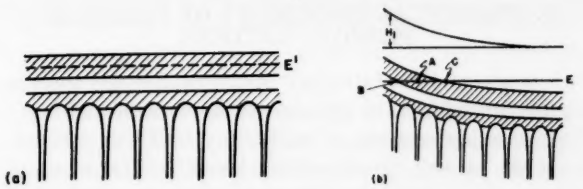

FIG. 1. (a) Periodic potential, with energy bands (shaded). (b) Energy bands and potential pushed upward by amount H_1 (shown in upper curve). Line of constant energy E cuts band, at point A, at same relative height as energy E' in Fig. 1(a). B and C, reversing points of oscillation of particle.

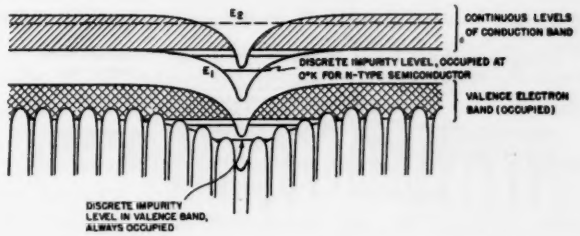
E2
E1
CONTINUOUS LEVELS OF CONDUCTION BAND
DISCRETE IMPURITY LEVEL, OCCUPIED AT 0°K FOR N-TYPE SEMICONDUCTOR
VALENCE ELECTRON BAND (OCCUPIED)
DISCRETE IMPURITY LEVEL IN VALENCE BAND, ALWAYS OCCUPIED

FIG. 2. Continuous and discrete levels surrounding impurity atom in N-type semiconductor. E_1, energy of a discrete level; E_2, energy in continuum.

of x, the difference giving the kinetic energy. When E, in Fig. 1(b), lies outside any of the energy bands, the kinetic energy is negative, the wave-length imaginary, and the wave function is damped off exponentially. When E is inside one of the bands, kinetic energy is positive, and the wave-length real. A classical particle of energy E, moving according to the classical Hamiltonian $E_0(p)+H_1(q)$, would then oscillate between points like B and C, Fig. 1(b), reversing at each point as its kinetic energy and momentum become zero, and a quantized particle will obey a quantum condition. Such a picture, as James has emphasized, allows us to deduce the nature of the stationary states and wave functions in such a problem. If, for instance, the external field represented by H_1 is constant, so that the energy bands are tilted at a constant angle, the electron will oscillate back and forth in coordinate space with a very large amplitude (for a small external field), at the same time having its position in the energy band go from bottom to top and back again, in a way familiar in the theory of electrical conduction.

Let us now consider the application of our theorem to cases actually met in the theory of solids. First we take P- and N-type impurity atoms. The N-type is a little easier to understand, and we deal with it first. It is usually an atom substituted for one of the atoms normally present in the lattice, and containing more valence electrons than the atom which it replaces; for definiteness, we may be considering an atom of P or As in a lattice of Si or Ge. If the atom loses an electron, it has enough remaining electrons to fit properly into the lattice, but it then carries a positive charge, which introduces a Coulomb potential (modified as to its absolute value by the dielectric constant of the material) into the lattice. Thus the energy bands, as modified by this Coulomb potential, will be as shown in Fig. 2. In these bands, we clearly have the possibility of discrete energy levels, of a hydrogen-like sort, at energies such as E_1. Just compensating these levels, which if they were occupied would introduce extra charge near the impurity, we see that with higher energies in the band, such as E_2, the electrons will effectively be repelled like positive charges as they approach too close to the impurity atom, their kinetic energy going to zero and the electrons being turned back at the point where the line at height E_2 emerges from the top of the energy band. Thus these other states will provide less than the normal charge near the impurity, so that, if all the states of a band are occupied, we shall still have just enough charge to account for one electron per atom of each spin in the band. In the N-type semiconductor, these modified levels are all occupied in the lower, or valence-electron band. We still have one electron per impurity atom left over, however, and this at low temperature will go into the lowest discrete level below the upper (or conduction) band, but at slightly higher temperatures will go into one of the conduction levels.

The P-type semiconductor is handled similarly. A P-type impurity atom normally contains one less valence electron than the atom of the lattice, e.g., an atom of Al or B in a lattice of Si or Ge. If we provide such an atom with an extra electron, to make it a negative ion, it has the right number of electrons to fit into the lattice. Then the modified energy bands will be as in Fig. 3, clearly giving discrete levels lying above the bands, with compensating diminished electron density in those wave functions lying at the bottom of the band. In the neutral crystal, there must be one less electron per impurity atom than the number necessary to fill the complete valence-electron band, so that at low temperatures this electron will be missing from the discrete level lying above the band; but at higher temperatures it will often be missing from one of the continuous levels lying in the band, leading therefore to hole conduction.

The case of excited energy levels in crystals, which has often been discussed (see, for instance, Wannier[1]), is more involved, but similar to these cases of impurities. It is, perhaps, easiest to understand in the case where a tightly bound, or x-ray, electron is excited to the conduction band.[7] If an atom of the crystal has lost one of its inner electrons, it acts approximately, so far as its valence electrons are concerned, like an atom with a nuclear charge greater by one unit; the missing electron can act like an additional valence electron. Thus the atom temporarily plays the role of an N-type impurity atom, and will set up discrete energy levels as in Fig. 2. When the corresponding emission spectrum is observed, resulting from an electron in the valence-

[7] The application of the theory to this case, the soft x-ray problem of Skinner and O'Bryan and other writers, is discussed by F. Seitz, *Modern Theory of Solids* (McGraw-Hill Book Company, Inc., New York, 1940) p. 436–438.

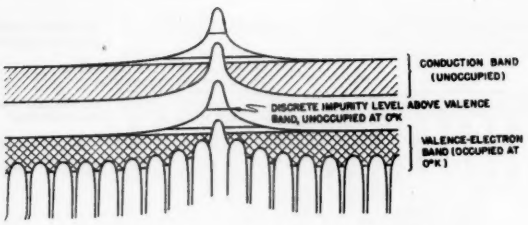
CONDUCTION BAND (UNOCCUPIED)
DISCRETE IMPURITY LEVEL ABOVE VALENCE BAND, UNOCCUPIED AT 0°K
VALENCE-ELECTRON BAND (OCCUPIED AT 0°K)

FIG. 3. Continuous and discrete levels surrounding impurity atom in P-type semiconductor.

electron band falling down into the empty x-ray level, there is the possibility that the electron may come from one of the levels in the continuum of the valence-electron band (the possibility considered by Skinner and O'Bryan, discussed in many references, some given in reference 7), but also the possibility that it may come from one of the discrete levels lying below the valence-electron band, resulting therefore in a longer wave radiation than we should otherwise find. Such tails are observed in the soft x-ray emission spectra, and Seitz suggests this interpretation of them.

The really optical case of excitation, where an electron is removed from the valence-electron band to a conduction band, is more complicated, in that both electron and hole are readily mobile. We may then best describe it essentially as Wannier did in reference 1, and as Frenkel had done earlier.[8] Considering it classically, the electron in the conduction band attracts the hole in the valence-electron band, and, since each has a comparable effective mass, they each execute hydrogen-like orbits about their center of mass, resulting in certain discrete states. These discrete states lie below the continuous states; that is, the electron effectively is at the bottom of the conduction band, like the discrete states in an N-type semiconductor as in Fig. 2, while the positive hole is at the top of the valence electron band, like the discrete states in a P-type semiconductor as in Fig. 3. The electron and hole together form a stable structure, however, which, because of the mobility of both electron and hole, is free to wander through the crystal, forming what has been called an exciton (see reference 8). Being a neutral structure, it carries no current. Less energy is required to set up such an exciton than to raise an electron from the valence-electron band to the conduction band, leaving both electron and hole dissociated from each other and free to move, so that the wave-length for absorption to this exciton level, which does not result in photo-conductivity, is longer than for the limit of photo-conductivity. It is well known that such exciton levels exist, for instance, in the alkali halides.[9]

[8] J. Frenkel, Phys. Rev. **37**, 17 (1931); **37**, 1276 (1931); Physik Zeits. Sowjetunion **9**, 158 (1936).

[9] See, for instance, J. C. Slater and W. Shockley, Phys. Rev. **50**, 705 (1936), in which the theory of the exciton is considered without benefit of Wannier's theorem.

IV. STATISTICAL TREATMENT OF PERTURBED PERIODIC LATTICES

A study of the stationary states of the electrons in the perturbed lattice, such as we have been making in the preceding section, is really only half the problem; we wish, as well, to ask which levels will be occupied, which ones empty. In thermal equilibrium, which is the only case we shall consider, we must then supplement our theory by use of the Fermi-Dirac statistics: the average number of electrons in a state of total energy E, with a given spin, is $1/\{\exp[(E-E_F)/kT]+1\}$, where E_F is the electrochemical potential or Fermi level. From this fact, supplemented by the knowledge of the wave functions Ψ_n, we can find the average charge density at each point of the lattice. It is by no means necessarily true that this charge density will automatically come out zero; hence we have space charge, and from this space charge we can compute an electrostatic potential by Poisson's equation. We can then apply a self-consistent condition, in essentially the sense of Hartree: we can demand that the potential energy of an electron in this potential be the same quantity $H_1(q)$ which is responsible for perturbing the energy bands.

To set up our self-consistent condition, we must first find the net charge density as a function of position arising from our assumed energy bands with the assumed Fermi level. First we shall find this in the case of the unperturbed periodic potential. In this potential, let the number of energy levels per unit volume, in the energy range dE, be $n(E)dE$; this can be found, as is well known, from the volume of momentum space lying between surfaces $E_0(p)=E$ and $E_0(p)=E+dE$, since states are distributed in momentum space with uniform density in the periodic case. In forbidden bands of energy, $n(E)$ is, of course, equal to zero. Let N_0 be the number of electrons per unit volume necessary to render the crystal electrically neutral. Then the excess number of electrons per unit volume, with an arbitrary value of E_F, is

$$N(E_F)=\int_{-\infty}^{\infty} n(E) \times\{\exp[(E-E_F/kT)+1]\}^{-1}dE-N_0. \quad (13)$$

Ordinarily, we determine E_F by the condition that N must be zero, or the lattice uncharged, so that we set $N(E_F)$ in (13) equal to zero. Our present problem, however, is different: we wish to investigate the results of volume charge in the lattice, resulting from N being not zero but, instead, a slowly varying function of position. If we have such a volume charge, then the potential in the lattice will differ from its periodic value by a slowly varying function determined from the volume charge by Poisson's equation. We let H_1 be the potential energy of an electron in this slowly varying potential, as before. Since the charge density is $-Ne$, where e is the magni-

tude of the electronic charge, $\nabla^2 H_1 = -Ne^2/\epsilon$, where ϵ is the permittivity of the material, or the dielectric constant times ϵ_0.

In the presence of the slowly varying electrostatic potential, $n(E)$ will, of course, no longer be given as it was previously. We know from the preceding sections, however, that the effect of H_1 will be to push up the energy bands with respect to their original position by an amount equal to the local value of H_1. It seems reasonable that the number of excess electrons per unit volume will then be given by $N(E_F - H_1) = N(\zeta)$, where the function N is as defined in (13), and where we introduce the abbreviation $\zeta = E_F - H_1$. This is an assumption much like that made in the well-known Thomas-Fermi method of discussing atomic structure, where we assume at every point of space that the statistical distribution of electron energies is what would be found for free electrons moving in a constant potential equal to the local value of the actual potential. It takes no specific account of the discrete energy levels, but merely handles them in a statistical or averaged-out way. Our method differs from the Thomas-Fermi method in three respects: we are handling our kinetic energy by the energy-band method, so that it is given by $E_0(p)$ instead of the usual expression; we are dealing with a modulating function $\Psi_n(q)$, instead of with the actual wave function $\psi(q)$; and we are handling our statistics in a form appropriate to an arbitrary temperature, rather than for the absolute zero of temperature as is done in the ordinary Thomas-Fermi method.

When we make the assumption above, we can write Poisson's equation in the following form:

$$\nabla^2 \zeta = N(\zeta) e^2/\epsilon, \tag{14}$$

where we have used the fact that E_F must be constant over-all space, to satisfy the condition for thermal equilibrium in the Fermi statistics, so that its Laplacian is zero. In Eq. (14), supplemented by Eq. (13) for the function N, we have the general formulation of the problem of setting up the electrostatic potential within a solid in thermal equilibrium. This equation has, of course, been used and solved in special cases by many writers. It has essentially been used by Schottky[10] in an extensive series of papers, and is similarly used by Mott and Gurney, and by Bethe.[11] Fan[12] has carried out careful studies of the contact between metals and between a metal and a semiconductor, which are complete enough so that many of our results will be merely a restatement of some of Fan's conclusions. Quite recently, Markham and Miller[13] have used essentially similar methods in closely related problems. Many other writers are aware of these methods of handling the problem. To give a complete picture, we shall state some of the methods of solving this equation, and some of the applications to well-known cases, as well as some new aspects of the problem.

The nature of the solution depends on the form of the function $N(\zeta)$. In Fig. 4 we show this function for two familiar cases: the metal and the intrinsic semiconductor. In the first case, N increases very rapidly as ζ departs from the value appropriate for no charge, and over a considerable range it can be treated as proportional to $\zeta - \zeta_0$, where ζ_0 is the value associated with no charge. In the semiconductor, however, N increases very slowly with $\zeta - \zeta_0$, behaving approximately as a hyperbolic sine, although when ζ becomes so large, negatively or positively, that the Fermi level penetrates either the lower valence-electron band or the upper conduction band, N begins to get very large, negatively or positively as the case may be. If $N(\zeta)$ can be approximated as $a(\zeta - \zeta_0)$ (where a is a constant) as it can over a considerable range in these two cases, then Eq. (14) takes on the mathematical form of the wave equation, and solutions can be set up by familiar methods. Thus, if we are dealing with a one-dimensional problem, we have solutions $\zeta - \zeta_0 = \exp(\pm x/X)$, where $X = (\epsilon/ae^2)^{\frac{1}{2}}$, and where x is the coordinate in the direction in which the potential is changing. As shown by Fan,[12] this quantity X for a metal is very small—of the order of magnitude of an angstrom unit; on the other hand, for an intrinsic semiconductor it becomes large and in the limit of zero temperature for this case it becomes infinite. For a three-dimensional problem of spherical symmetry, we similarly have $\zeta - \zeta_0 = \exp(\pm r/X)/r$, where r is the distance from the center, and X is as given above.

We can now examine several applications of these simple results. First we consider the metal, and the one-

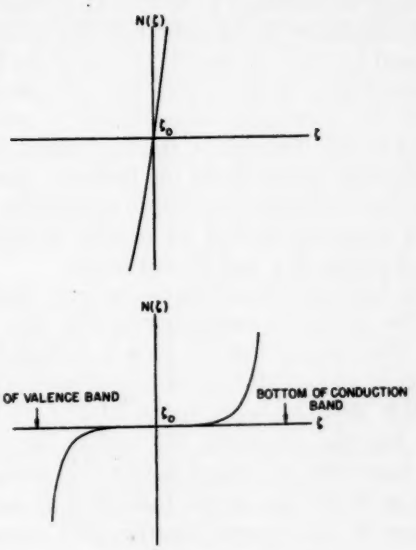

FIG. 4. $N(\zeta)$ as function of ζ. Above, metal; below, intrinsic semiconductor.

[10] W. Schottky, Zeits. f. Physik **118**, 539 (1941); other references quoted in this paper.

[11] N. F. Mott and R. W. Gurney, *Electronic Processes in Ionic Crystals* (Oxford University Press, New York, 1940), Chapter V; H. A. Bethe, M.I.T. Radiation Laboratory Report 43-12 (November 23, 1942).

[12] H. Y. Fan, Phys. Rev. **62**, 388 (1942).

[13] J. J. Markham and P. H. Miller, Jr., Phys. Rev. **75**, 959 (1949).

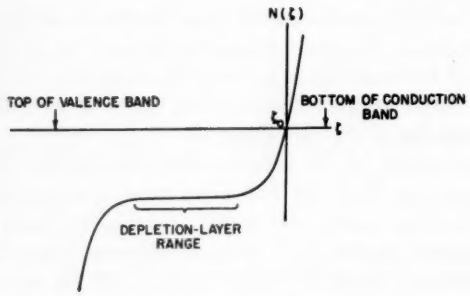

FIG. 5. $N(\zeta)$ *vs.* ζ for N-type semiconductor.

dimensional problem; this is met in investigating the surface charge at the free surface of a metal in an external electric field. Clearly, we can adjust boundary conditions so that the electric field at the surface resulting from the gradient of H_1 has any desired value, and yet the resulting potential will penetrate into the metal only to a distance of the order of a single atomic layer, with the related charge density confined to this same small depth. This allows us, in other words, to assume an arbitrary surface charge on the surface layer of atoms of a metal, of suitable amount to match any external boundary conditions. Similarly, if two metals are close to each other and connected electrically, so that they must bear surface charges enough to produce the difference of potential equal to their difference of work function, these surface charges will be formed according to this same method; and as the metals are brought into contact, the double layer between them is formed from surface charges of the same variety at the surfaces of each. This description of the double layer has been worked out in detail by Fan.[12] Another example relating to the metal comes from the spherically symmetrical problem. If we had an impurity atom in a metal, of the type which we have in a semiconductor, and which we discussed in Section II, it would produce a local singularity in the potential. The solution which we should have to use would then be of the form $\zeta=\zeta_0$ $=$constant $\exp(-r/X)/r$, showing a suitable singularity at $r=0$, but decreasing exponentially to zero in a distance of atomic dimensions. In other words, the conduction electrons would shield the impurity atom so completely that it would not produce appreciable perturbation of potential beyond its nearest neighbor atoms. This, of course, is a well-known result.

In an intrinsic semiconductor, we may consider these same two problems, remembering that here X is very large. This means that in such a material, which is practically an insulator, we can accumulate a practically negligible volume charge in the interior, so that if the whole material (including the surface layers) behaves in the same way, we cannot have a thin surface layer of charge as we can in a metal. Instead, if we have such an insulator in an external electric field normal to the surface, the field penetrates the surface, the normal component of D being continuous as in the usual theory of dielectrics. To account for surface charges which unquestionably can build up on the surface of a dielectric, as, for instance, by bombarding with electrons, which have no chance to leak off, we must introduce surface states, capable of holding extra charge; we postpone discussion of such surface states to the next section. In the interior of an intrinsic semiconductor,we may use the spherical solution of our equation to discuss an impurity atom; and we find, with our large X, that the field is essentially an inverse square field, the effect of the dielectric being seen only in the dielectric constant. Thus we have correctly drawn our perturbed energy bands around impurity atoms, in Figs. 2 and 3, as though the potential varied inversely as the distance from the impurity center, without the type of shielding found in the metal.

V. IMPURITY SEMICONDUCTORS AND RECTIFYING BARRIERS

The method of treatment we have used in the preceding section handles the action of impurity atoms on a microscopic scale, asking how the potential behaves around each impurity atom; Section II handled similarly the energy levels of such impurity atoms on the same microscopic scale. In treating impurity semiconductors, however, it is usually more convenient to treat average behavior over a volume which is small compared to the thickness of a rectifying barrier, but large compared to the distance between impurity atoms; or, alternatively, it is better somehow to average the impurity levels, so that we do not have to consider the fine-grained inhomogeneities arising from the discrete impurity atoms. When we do this, we have a different distribution of energy levels, $n(E)$, for now we include an appropriate number of levels per unit volume arising from the discrete levels in N- or P-type impurity atoms, and hence located just below or just above the continuous bands. Also in computing the net amount of charge per unit volume, we must take account of

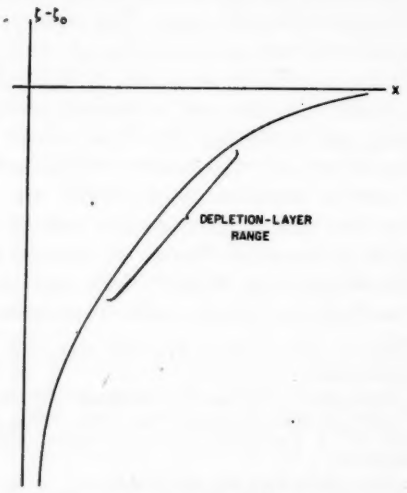

FIG. 6. $\zeta-\zeta_0$ *vs.* x, for N-type semiconductor.

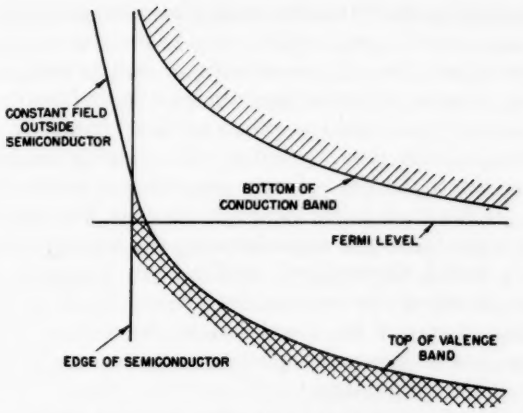

FIG. 7. Energy bands at boundary of N-type semiconductor, large external electric field, but no double layer.

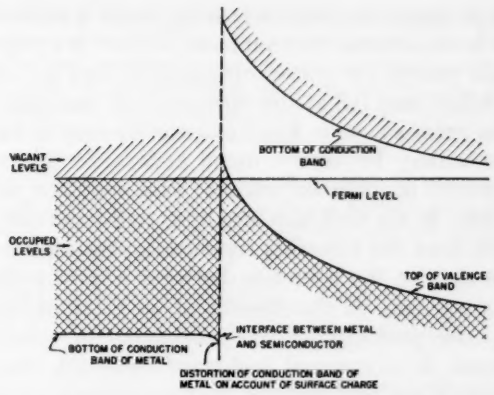
VACANT LEVELS
BOTTOM OF CONDUCTION BAND
FERMI LEVEL
OCCUPIED LEVELS
TOP OF VALENCE BAND
INTERFACE BETWEEN METAL AND SEMICONDUCTOR
BOTTOM OF CONDUCTION BAND OF METAL
DISTORTION OF CONDUCTION BAND OF METAL ON ACCOUNT OF SURFACE CHARGE

FIG. 8. Energy bands at interface between metal and semiconductor, no surface states.

the charge furnished by these impurity ions. When we do this, we may get for $N(\zeta)$ for, say, a material containing N-type impurity atoms uniformly distributed, a curve of the nature shown in Fig. 5.

In Fig. 5, there are shown several distinct regions, with different behavior of $N(\zeta)$ in each. First, for ζ less than ζ_0, there is a long region in which N is negative and approximately constant. This is the range in which the impurity atoms have lost their extra electrons, so that they yield a positive space charge. This is the region in which Schottky's depletion-layer theory is appropriate. As ζ decreases still further, there is a very rapid and large decrease in N; this arises when ζ is so low that it begins to empty the levels in the valence-electron band. In this region, the material would act like a P-type semiconductor, and with still further decrease of ζ it would show metallic properties, whereas in the depletion-layer region there are practically no holes in the lower band, or electrons in the upper band, so that the material acts like an intrinsic semiconductor, or practically as an insulator. Proceeding in the other direction, of increasing ζ, we find that N is zero when $\zeta=\zeta_0$, and beyond that point N starts to increase very rapidly. This is the range where there are enough electrons to start filling the conduction band. Of course, even with $N=0$, there are some electrons in the conduction band, raised by thermal agitation from the donator impurity atoms; but this number very rapidly increases with increase of ζ, so that the material becomes a much better conductor, and soon acquires metallic properties.

With as complicated a function $N(\zeta)$ as is given in Fig. 5, it is clear that the simple approximation used previously (of setting it proportional to $\zeta-\zeta_0$) is inadequate, and we must use the whole form of the function. Even in this case, in the one-dimensional problem, we can integrate Poisson's equation, (14), as is done, for instance, by Mott and Gurney[11] and by Fan.[12] The equation becomes $d^2\zeta/dx^2=f(\zeta)$, where $f(\zeta)$ is a function of ζ. Mathematically, this is similar to a one-dimensional equation of motion in mechanics, $md^2x/dt^2=f(x)$, where $f(x)$ is the force; and, as in the mechanical case, we can integrate by a method entirely equivalent to the energy integral in mechanics. When we do this, carrying out the integrations numerically if $N(\zeta)$ is as complicated as in Fig. 5, we can find the relation between ζ and x. We find that there are solutions approaching ζ_0 asymptotically for large values of x, one for ζ greater than ζ_0, the other for ζ less than ζ_0; all such solutions differ from each other only by uniform translation along the x-axis. In Fig. 6 we show such a solution for the case coming into the problem of a rectifying barrier at the surface of an N-type semiconductor.

There are sections of the curve of Fig. 6 which are associated with the various parts of Fig. 5. As ζ departs only slightly from ζ_0, we are in a linear part of Fig. 5. Here we have the Laplacian of $\zeta-\zeta_0$ equal to a constant times $\zeta-\zeta_0$, so that we can set up an exponential solution for $\zeta-\zeta_0$ as a function of x, just as we did with the metals. We find, however, a much slower exponential variation, extending over much greater distances. Next we have the region where ζ is considerably less than ζ_0, so that we are in the region of the depletion layer. In this region, as we have mentioned earlier, $N(\zeta)$ is practically constant, and our solution agrees exactly with Schottky's,[10] leading to ζ as a quadratic function of x. This parabolic function, of course, fits smoothly to the exponential function which holds as ζ approaches its asymptotic value ζ_0. Finally, when ζ gets so small that electrons of the lower band begin to be removed, ζ begins to decrease very rapidly with change of x. This is because we are now meeting high positive volume charges, arising from the emptying of this lower band, and the electric field can change with position about as rapidly as in a metal (where we have already seen that we can accommodate a large enough charge in a layer of atomic thickness to be equivalent to a surface charge). This happens here as ζ penetrates into the lower band, and the reason for its happening is essentially the large reservoir of charge available, similar to the case of a metal. In the nature of things, however, this surface

layer of charge can only be positive, since it arises from holes in the valence-electron band. If there is a negative surface charge, the curve corresponding to Fig. 6 must rise rather than fall at the surface of the material.

The result shown in Fig. 6 can now be used to discuss the boundary between a metal and an *N*-type semiconductor, or between such a semiconductor and a vacuum. If we used this result straightforwardly, we should draw the following conclusions. We should conclude that at the boundary between a semiconductor and a vacuum, in the absence of an external electric field, the potential in the semiconductor would be constant. If an external field were impressed, then the surface charge to terminate the lines of force would be actually distributed through the whole depth of a depletion layer, instead of being located on the surface, as in a metal. The only exception would come if the field were so strong that the Fermi level dipped down into the valence-electron band at the surface; then any remaining charge required to terminate the lines of force would be located almost exactly at the surface. In other words, the total amount of charge which can be distributed through the interior of the volume in the depletion layer is limited. In such an extremely large field, the energy bands would look as in Fig. 7, and the external field would be indicated by the slope of the curve to the left of the solid. If now the semiconductor were placed in contact with a metal between which the difference of work function was so great as to require on the semiconductor a positive charge, and on the metal a negative charge, great enough to produce a field of the magnitude shown in Fig. 7 in the double layer between the two materials, then we should find the situation shown in Fig. 8. Here the Fermi level would come slightly below the top of the valence-electron band of the semiconductor just at the surface, and the resulting situation would be almost independent of the work function of the metal, provided only that it was different enough from that of the semiconductor to require a large enough double layer.

It is well known that the situation we have just described does not fit the observations, at least in germanium and silicon, two semiconductors which are very well understood as a result of the large amount of work done on them during the war and since at Purdue University, the Bell Telephone Laboratories, the University of Pennsylvania, and elsewhere. Meyerhof[14] in a set of measurements on contact difference of potential between silicon and metals found definite evidence that our simple picture is wrong, and his effect was explained by Bardeen[15] with his theory of surface states. Since then, the group at the Bell Telephone Laboratories has arrived at substantially the following conclusions regarding the surface of germanium, explainable in terms of surface states.[16] At a free surface between germanium and air, there is good evidence that in the absence of an external field there is, nevertheless, a well-formed positively charged depletion layer below the surface, compensated by an equal negative surface charge. In an external electric field, the extra surface charge required to terminate the lines of force appears just on the surface, rather than in the depletion layer in the interior. And when contact is made between the semiconductor and a metal, the required double layer adjusting the Fermi levels of the two to coincidence is made up of a surface charge of the usual sort at the surface of the metal, and a surface charge of opposite sign on the surface of the germanium.

It thus appears that the surface layer of atoms on a germanium crystal must behave differently from the interior and, to explain this, Bardeen introduces the idea of surface states. The action can be described, roughly, as if there were part of a monomolecular layer of metal on the surface of the germanium, whose work function differed from that of a hypothetical germanium which lacked the surface states by something like the amount considered in Fig. 8. This layer of metal would have to acquire enough negative charge to raise its Fermi level—normally far below that of the germanium —up to equality with that of the germanium. Having the large reservoir of electrons characteristic of a metal, it could acquire any other amount of surface charge necessary to compensate for an applied external field, or for a double layer arising when another metal made contact with it. Thus the rectifying barrier would remain something like that of Fig. 8, which is not unlike what is observed (see, for instance, reference 16), independent of the material of the metal making contact.

In this description of the surface, which is substantially that suggested by the group at the Bell Telephone Laboratories, it is not clear whether the surface states arise from real impurities on the surface (either metallic or, at any rate, setting up a distribution of states of the sort characteristic of a metal), or whether they are inherent in the germanium itself. The evidence indicates that the surface states depend on surface conditions, suggesting impurities, and certainly it is very difficult to get the surface really clean. Furthermore, the absence of surface conductivity suggests that the surface states are localized at widely separated spots on the surface, as if they arose from impurities. On the other hand, the photoelectric experiments of Apker, Taft, and Dickey,[17] performed on the cleanest surfaces obtainable, gave evidence of the same sort of situation observed in ordi-

[14] W. E. Meyerhof, Phys. Rev. **71**, 727 (1947).
[15] J. Bardeen, Phys. Rev. **71**, 717 (1947).

[16] W. H. Brattain and W. Shockley, Phys. Rev. **72**, 345 (1947); W. H. Brattain, Phys. Rev. **72**, 345 (1947); J. Bardeen and W. H. Brattain, Phys. Rev. **74**, 230 (1948); W. H. Brattain and J. Bardeen, Phys. Rev. **74**, 231 (1948); W. Shockley and G. L. Pearson, Phys. Rev. **74**, 232 (1948); J. Bardeen and W. H. Brattain, Phys. Rev. **75**, 1208 (1949). The author is indebted to Dr. Bardeen for an opportunity to see this latter paper before its appearance in print.
[17] Apker, Taft, and Dickey, Phys. Rev. **73**, 46 (1948).

nary germanium, suggesting that the situation may be inherent in a clean germanium surface. This is not impossible: the spacing between the surface layer of germanium atoms and the next layer below it may well be different from that between layers in the interior because of the unbalanced forces near the surface; this would bring about a distortion of the energy bands near the surface, quite aside from anything we have considered, which might have the effect of making the surface layer of atoms behave quite differently from the interior. At any rate, it seems to be empirically clear that we must treat the surface layer of such a crystal as a different material from the interior; hence, to apply the arguments of the present theory to the boundary layer, we must consider the interior and the surface separately, and consider the boundary conditions at the interface between them, as well as at the interface between the surface and air or another conductor.

VI. ACKNOWLEDGMENTS

Most of the material described in this paper was prepared for presentation at the M.I.T. Conference on Physical Electronics in April 1949, and at a preliminary session before it, and the writer is indebted to Professor W. B. Nottingham for the stimulus to prepare it, and for valuable discussion. He is also indebted to Professor K. Lark-Horovitz, Professor H. M. James, and Dr. H. Y. Fan, of Purdue University, for valuable comments and much information about the semiconductor program at Purdue; and to Dr. J. Bardeen, Dr. W. H. Brattain, and Dr. W. Shockley, of the Bell Telephone Laboratories, for valuable comments and suggestions.

APPENDIX I

We start with the functions $\psi_0(p, q)$, satisfying Eq. (3). From them we form the functions

$$a(q-Q_k)=N^{-\frac{1}{2}}\Sigma_p \{\exp[(-i/\hbar)p\cdot Q_k]\}\psi_0(p, q), \quad (1A)$$

where the sum is over all the quantum states p. These functions are the normalized atomic functions of Wannier, written in our notation; we refer to reference 1 for their properties. Equation (2) follows at once from (1A) by multiplying by $\exp[(i/\hbar)p'\cdot Q_k]$, summing over k, and using the theorem

$$\Sigma_k \exp[(i/\hbar)(p'-p)\cdot Q_k]=0 \quad \text{if} \quad p'\neq p,$$
$$=N \quad \text{if} \quad p'=p.$$

Now we set up the solution (5) for Eq. (4). In (4) we write $\psi_n(q)$ in the form (5), multiply both sides of the equation by $a^*(q-Q_m)$, and integrate over q, obtaining the equation

$$0=\Sigma_k \int a^*(q-Q_m)(H_0+H_1-E_n)\Psi_n(Q_k)a(q-Q_k)dq. \quad (2A)$$

We remember that H_0 is an operator operating on a function of q, H_1 is a slowly varying function of q, and E_n is a constant. On account of the orthogonality of the a's, proved by Wannier, $\int a^*(q-Q_m)a(q-Q_k)dq=0$ if $m\neq k$, 1 if $m=k$. Thus the term in E_n reduces to $-E_n\Psi_n(Q_m)$. So far as the term in H_1 is concerned, let us assume that H_1 is so slowly varying with q that it can be regarded as approximately constant over the atomic wave function of an atom. Then, again using the orthogonality of the a's, this term reduces to $H_1(Q_m)\Psi_n(Q_m)$. If H_1 varies more rapidly, we can use the deviations from this result as a starting point for a higher order of approximation.

The other term of (2A), the one in H_0, must be handled differently. We rewrite $a^*(q-Q_m)$ and $a(q-Q_k)$, as they appear in (2A), by using (1A), and make use of the fact that the ψ_0's satisfy Eq. (3). Then we have

$$\Sigma_k \int a^*(q-Q_m)H_0\Psi_n(Q_k)a(q-Q_k)dq$$
$$=\sum_{k,p,p'} (1/N)\Psi_n(Q_k)\{\exp[(i/\hbar)(p'\cdot Q_m-p\cdot Q_k)]\}$$
$$\times\int \psi_0^*(p', q)H_0\psi_0(p, q)dq.$$

We use (3), and the orthogonality of the functions ψ_0, for different p's, to show that $\int\psi_0^*(p', q)H_0\psi_0(p, q)dq=E_0(p)\delta(p', p)$. When we substitute this above, we have

$$\Sigma_k \int a^*(q-Q_m)H_0\Psi_n(Q_k)a(q-Q_k)dq$$
$$=\sum_{k,p} (1/N)\Psi_n(Q_k)E_0(p)\exp[(i/\hbar)p\cdot(Q_m-Q_k)]$$
$$=\sum_{s,p} (1/N)\Psi_n(Q_m-Q_s)E_0(p)\exp[(i/\hbar)p\cdot Q_s], \quad (3A)$$

where we have substituted $Q_m-Q_k=Q_s$.

We can now rewrite this expression (3A). We recall that $E_0(p)$ is a periodic function in the p-space, having the periodicity of the reciprocal lattice. Thus it can be written in the form

$$E_0(p)=\sum_{Q_k} A(Q_k)\exp[(-i/\hbar)p\cdot Q_k], \quad (4A)$$

where the Fourier coefficients $A(Q_k)$ are given by

$$A(Q_k)=\Sigma_p (1/N)E_0(p)\exp[(i/\hbar)p\cdot Q_k].$$

Thus the right-hand side of (3A) can be expressed in the form

$$\Sigma_s A(Q_s)\Psi_n(Q_m-Q_s). \quad (5A)$$

Now we expand $\Psi_n(Q_m-Q_s)$ in Taylor's series about the point Q_m. We have

$$\Psi_n(Q_m-Q_s)=\Psi_n(Q_m)-\frac{d}{dq}\Psi_n(Q_m)(Q_s)$$
$$+\frac{1}{2!}\frac{d^2}{dq^2}\Psi_n(Q_m)(Q_s^2)+\cdots$$
$$=\left[\exp\left(-Q_s\frac{d}{dq}\right)\right]\Psi_n(Q_m). \quad (6A)$$

In this expression we have written only the case where q is a scalar quantity, but an exactly analogous form holds if it is a vector, $Q_s(d/dq)$ being replaced by the scalar product $Q_s\cdot\nabla$, where the ∇ operator denotes vector differentiation with respect to the components of the vector q. We now use the result (6A) to modify (5A), and it takes on the form

$$\Sigma_s A(Q_s)[\exp(-Q_s\cdot\nabla)]\Psi_n(Q_m).$$

Comparison with Eq. (4A) shows that this is what we should get if we took $E_0(p)$, replaced p in it by the operator $(\hbar/i)\nabla$, and allowed this to operate on $\Psi_n(Q_m)$. When we combine this with the expressions for the terms in H_1 and E_n in Eq. (2A) which we have already discussed, we see that we are led to Eq. (6), which we wished to prove.

PHYSICAL REVIEW VOLUME 76, NUMBER 11 DECEMBER 1, 1949

Energy Bands and Wave Functions in Periodic Potentials*

HUBERT M. JAMES
Purdue University, Lafayette, Indiana
(Received July 26, 1949)

In preparation for treatment of the one-dimensional wave equation with perturbed periodic potentials, this paper discusses the case of perfectly periodic potentials. Solutions for the entire range of x are constructed by joining together "cell solutions"—solutions defined for a single period of the potential. Several types of cell solution are discussed. The concept of "self-matching cell solutions" leads to a simple demonstration of the band structure of permitted energy levels. The effective momentum of the particle is defined for energies in the forbidden bands, and a parameter $\sigma(E)$ of interest in the treatment of perturbed periodic systems is introduced. Expansions are given for solutions of the wave equation near the band edges, in both the permitted and forbidden bands.

I. INTRODUCTION

THE wave mechanics of particles in perfectly periodic potentials can be regarded as completely understood, at least in principle. Many years before the advent of wave mechanics, Hamel[1] and Haupt[2] discussed, from the mathematician's point of view, an equation essentially identical with the one-dimensional wave equation for a particle of mass m in a periodic potential $W(x)$:

$$-\frac{\hbar^2}{2m}\frac{d^2\psi(x)}{dx^2}+W(x)\psi(x)=E\psi(x). \tag{1.1}$$

They were particularly concerned with the "oscillation theorems" for this equation, relating to the dependence on E of the existence or non-existence of bounded solutions $\psi(x)$. They showed that all solutions are bounded for certain ranges of E (the "permitted energy bands" for electrons in crystals), separated, in general, by ranges of energy for which no solutions are bounded ("forbidden bands"). This wave equation, and the corresponding three-dimensional one, have since been studied by a number of methods suited to various special purposes; it will suffice to mention here the work of Bloch,[3] Brillouin,[4] and Kramers.[5]

The present paper deals only with periodic potentials, but is intended to lay the foundation for a study of the one-dimensional wave equation with perturbed periodic potentials. These perturbations may consists of slowly varying additions to the potential, such as are considered in a succeeding paper, or of radical but localized changes in the potential, which are to be treated in a paper now in preparation. In either case it is useful and illuminating to construct solutions for the whole range of the variable x by fitting together solutions valid for single periods of the unperturbed potential. As applied to periodic potentials this method is well known.[6] It is here discussed from a very general point of view, with the following purposes:

(1) To give a particularly clear and elementary demonstration of the band structure of permitted energy levels.

(2) To discuss the properties of all solutions of the wave equation, including those which do not satisfy the boundary conditions of wave mechanics. Consideration of solutions in the forbidden ranges of energy is required in the treatment of perturbed periodic potentials. Particular attention will be paid to the forms of solutions with energies near the band edges.

(3) To introduce a new parameter, $\sigma(E)$, which, like the effective momentum $p(E)$, depends on and partially characterizes the periodic potential. This parameter plays an important role in the theory of perturbed periodic potentials.

The discussion will also exhibit some of the advantages to be gained from consideration of several alternative sets of solutions of the wave equation for single periods of the potential (cell solutions).

II. SPECIAL TYPES OF CELL SOLUTION

Let $W(x)$ be a periodic function with period a:

$$W(x)=W(x+na), \quad n=\pm1, \pm2, \cdots. \tag{2.1}$$

The range of x will be divided into periods or *cells* of length a, such that in the nth cell

$$na\leq x\leq(n+1)a. \tag{2.2}$$

The potential has then the same form in each cell. It is often convenient to choose the origin of coordinates so that the potential in each cell is symmetrical about the center; this is not always possible, nor is it necessary for application of the methods to be described.

We now fix attention on the zeroth cell, $0\leq x\leq a$, and on a particular value of E. The wave equation is then a linear second-order differential equation with two linearly independent solutions. This section deals with the properties of three special pairs of independent cell solutions.

* This work was supported in part by Signal Corps Contract W36-039-SC-32020 with the Department of Physics at Purdue University. It has been circulated as a Signal Corps report, but appears here in slightly enlarged form, with some changes of notation and sign conventions.

[1] G. Hamel, Math. Ann. **73**, 371 (1912).
[2] O. Haupt, Math. Ann. **76**, 67 (1914); **79**, 278 (1919).
[3] F. Bloch, Zeits. f. Physik **52**, 555 (1928).
[4] L. Brillouin, Comptes Rendus **191**, 198, 292 (1930); J. de physique VII, **1**, 377 (1930).
[5] H. A. Kramers, Physica **2**, 483 (1935).
[6] R. deL. Kronig and W. G. Penney, Proc. Roy. Soc. **130**, 499 (1931).

A. The y Solutions

Let $y_1(E;x)$ and $y_2(E;x)$ be solutions of Eq. (1.1) such that

$$\left.\begin{aligned} y_1(E;0)&=1, \quad y_1'(E;0)=0, \\ y_2(E;0)&=0, \quad y_2'(E;0)=1. \end{aligned}\right\} \tag{2.3}$$

These solutions are always real and can be obtained by numerical integration, if necessary.

We define

$$\left.\begin{aligned} y_1(E;a)&=c_{11}(E), \quad y_2(E;a)=c_{12}(E), \\ y_1'(E;a)&=c_{21}(E), \quad y_2'(E;a)=c_{22}(E), \end{aligned}\right\} \tag{2.4}$$

where the prime denotes the derivative with respect to x. The constancy in x of the Wronskian of y_1 and y_2,

$$W(y_1,y_2)=y_1(E;x)y_2'(E;x)-y_1'(E;x)y_2(E;x) \tag{2.5}$$

(or of any pair of solutions of Eq. (1.1) with the same E) requires that

$$c_{11}(E)c_{22}(E)-c_{12}(E)c_{21}(E)=1. \tag{2.6}$$

Henceforth, the dependence of the y's and c's on E will be understood, but made explicit only on occasion.

One can easily construct from the functions $y_1(x)$ and $y_2(x)$, defined only for the range $0\leq x\leq a$, solutions of the periodic problem for all x. Since the potential has the same form in every cell, $y_1(x-na)$ and $y_2(x-na)$ will be independent solutions in the nth cell. Within each cell an arbitrary solution ψ of the wave equation can be expressed as an appropriate linear combination of the corresponding cell solutions:

$$\psi(x)=a_n y_1(x-na)+b_n y_2(x-na),$$

$$\begin{cases} na\leq x\leq (n+1)a \\ n=0,\ \pm 1,\ \pm 2,\ \cdots. \end{cases} \tag{2.7}$$

Continuity of ψ and its first derivative at the boundary between the nth and $(n+1)$st cells demands that

$$a_{n+1}=c_{11}a_n+c_{12}a_n, \quad b_{n+1}=c_{21}a_n+c_{22}b_n. \tag{2.8}$$

In matrix form this becomes

$$\begin{pmatrix} a_{n+1} \\ b_{n+1} \end{pmatrix}=(c_{ij})\begin{pmatrix} a_n \\ b_n \end{pmatrix}. \tag{2.9}$$

By Eq. (2.6), the matrix (c_{ij}) always has an inverse $(c_{ij})^{-1}$. It follows that

$$\begin{pmatrix} a_n \\ b_n \end{pmatrix}=(c_{ij})^n\begin{pmatrix} a_0 \\ b_0 \end{pmatrix} \tag{2.10}$$

for all n, positive or negative; the constants a_n and b_n characteristic of any given solution are thus easily determined as soon as a_0 and b_0 are given.

It is a matter of elementary matrix algebra to discuss the conditions under which a_n, b_n, and ψ remain bounded as $n, x\to\pm\infty$, and ψ is therefore physically acceptable.

An equivalent but more picturesque discussion of the band structure of energy levels will be given later, using another set of basic cell solutions.

Use of the y cell solutions is particularly advantageous when the problem to be treated is not strictly periodic. If the range of x is divided into cells (which need not even have the same extent), one can define for the mth cell the solutions y_{1m} and y_{2m} satisfying Eq. (2.3) at the left edge of the cell, and can determine the corresponding constants $c_{ij}^{(m)}$. The conditions of continuity at the boundary between the mth and $(m+1)$st cell involve only the constants $c_{ij}^{(m)}$, and the generalization of Eq. (2.10) is (for positive n)

$$\begin{pmatrix} a_n \\ b_n \end{pmatrix}=(c_{ij}^{(n-1)})\cdots(c_{ij}^{(1)})(c_{ij}^{(0)})\begin{pmatrix} a_0 \\ b_0 \end{pmatrix}. \tag{2.11}$$

B. The Solutions g and u

When the cell division can be made in such a way that $W(x)$ is symmetrical about the center of each cell, it is convenient to consider, for each E, another set of real solutions, $g(E;x)$ and $u(E;x)$, such that

$$\left.\begin{aligned} g(E;a/2)&=1, \quad g'(E;a/2)=0, \\ u(E;a/2)&=0, \quad u'(E;a/2)=1. \end{aligned}\right\} \tag{2.12}$$

These solutions need be defined only for the zeroth cell, about the center of which they are symmetric and antisymmetric, respectively.[7] We shall write

$$\left.\begin{aligned} &g(E;0)=g(E;a)=g_0(E); \\ &g'(E;0)=-g'(E;a)=g_0'(E); \\ &u(E;0)=-u(E;a)=u_0(E); \\ &u'(E;0)=u'(E;a)=u_0'(E). \end{aligned}\right\} \tag{2.13}$$

The constancy in x of $W(g;u)$ assures that

$$g_0(E)u_0'(E)-g_0'(E)u_0(E)=1. \tag{2.14}$$

The dependence of these quantities on E will hereafter be indicated only as required.

One can, of course, express the solutions g and u in terms of y_1 and y_2, and conversely. From consideration of magnitudes and slopes at $x=0$, it is obvious that

$$\left.\begin{aligned} g(x)&=g_0y_1(x)+g_0'y_2(x), \\ u(x)&=u_0y_1(x)+u_0'y_2(x). \end{aligned}\right\} \tag{2.15}$$

Solution of these equations, with use of Eq. (2.14), yields

$$\left.\begin{aligned} y_1(x)&=u_0'g(x)-g_0'u(x), \\ y_2(x)&=-u_0g(x)+g_0u(x). \end{aligned}\right\} \tag{2.16}$$

On setting $x=a$ and using Eq. (2.13), one finds

$$\left.\begin{aligned} c_{11}&=u_0'g_0+g_0'u_0=c_{22}, \\ c_{12}&=-2u_0g_0, \\ c_{21}&=-2u_0'g_0'. \end{aligned}\right\} \tag{2.17}$$

[7] These solutions have been employed in the discussion of surface states of crystals by W. Shockley, Phys. Rev. **56**, 317 (1939).

It is thus proved that for symmetric cell potentials $y_1(a)=y_2'(a)$.

The values of the c's are determined by the values of g_0, g_0', u_0, u_0', but the converse is not true; the c's remain unchanged when one replaces the latter quantities by κg_0, $\kappa g_0'$, $\kappa^{-1}u_0$, $\kappa^{-1}u_0'$, respectively. It does, however, follow from Eqs. (2.14) and (2.17) that

$$\frac{g_0'}{g_0}=\frac{1-c_{11}}{c_{12}}=-\frac{c_{21}}{1+c_{11}},\quad \frac{u_0'}{u_0}=\frac{c_{21}}{1-c_{11}}=-\frac{1+c_{11}}{c_{12}}. \tag{2.18}$$

As with the y's, an arbitrary solution of the wave equation with periodic potential can be expressed in terms of the cell solutions $g(x)$ and $u(x)$:

$$\psi(x)=\alpha_n g(x-na)+\beta_n u(x-na),$$

$$\begin{cases} na\leq x\leq (n+1)a, \\ n=0, \pm 1, \pm 2, \cdots. \end{cases} \tag{2.19}$$

Continuity in the magnitude and slope of ψ at $x=na$ requires

$$\left.\begin{aligned} \alpha_n g_0-\beta_n u_0&=\alpha_{n+1}g_0+\beta_{n+1}y_0, \\ -\alpha_n g_0'+\beta_n u_0'&=\alpha_{n+1}g_0'+\beta_{n+1}u_0'. \end{aligned}\right\} \tag{2.20}$$

Solving these equations for α_{n+1} and β_{n+1}, with use of Eq. (2.14), one finds

$$\begin{pmatrix}\alpha_{n+1}\\ \beta_{n+1}\end{pmatrix}=\begin{pmatrix} g_0u_0'+g_0'u_0 & -2u_0u_0' \\ -2g_0g_0' & g_0u_0'+g_0'u_0\end{pmatrix}\begin{pmatrix}\alpha_n\\ \beta_n\end{pmatrix}. \tag{2.21}$$

Like Eq. (2.9), this can (but will not here) be made the basis of a discussion of the band structure of the energy levels.

In the treatment of non-periodic problems g and u are less conveniently used than are y_1 and y_2, since the matrix that transforms the coefficients α_n and β_n into α_{n+1} and β_{n+1} depends on the potential in both cells n and $n+1$.

C. "Self-Matching" Cell Solutions, $f_\pm(x)$

The problem of constructing wave functions for an infinite periodic potential by connecting cell solutions can be made particularly simple by the use of solutions $f(E;x)$, defined for $0\leq x\leq a$, which have the same slope-to-magnitude ratio at the two ends of the cell:

$$\frac{f'(E;0)}{f(E;0)}=\frac{f'(E;a)}{f(E;a)}=\sigma(E). \tag{2.22}$$

To normalize these functions, it will be required that

$$f(E;0)=1. \tag{2.23}$$

In passing from the left end of the cell to the right, the solution will increase in magnitude by the factor

$$\frac{f(E;a)}{f(E;0)}=r(E). \tag{2.24}$$

Such solutions will here be called "self-matching" or, for brevity, f solutions. They derive their importance from the following property: given a *single* self-matching solution in the zeroth cell, one can construct from it a continuous solution of the wave equation through the whole range of x. If $f(x)$ is a cell solution in the zeroth cell, $c_1f(x-a)$ will be a cell solution in the first cell, $c_2f(x-2a)$ a cell solution in the second cell, and so on. All these cell solutions will have the same slope-to-magnitude ratio at the ends of their respective cells. Therefore, if c_1, c_2, $\cdots$ are so chosen that the cell solutions have the same magnitudes at their common cell boundaries, they will have there also the same slopes: they will fit together smoothly to form a continuous solution through the whole range of x. Since each solution changes by a factor r in passing from the left end of the cell to the right end, the magnitudes can be made continuous by choosing $c_n=r^n$, for all n, positive or negative. Thus one obtains from the given cell solution a solution of the wave equation for all x:

$$\psi(E;x)=r^nf(E;x-na)\begin{cases} na<x<(n+1)a \\ n=0, \pm 1, \pm 2, \cdots. \end{cases} \tag{2.25}$$

This solution has the same form in every cell; it changes from cell to cell only by a (possibly complex) multiplying constant.

It is now necessary to investigate the existence of self-matching cell solutions. If one exists, it must be expressible as a linear combination of the special solutions y_1 and y_2 already discussed, which always exist:

$$f(x)=ay_1(x)+by_2(x). \tag{2.26}$$

From Eqs. (2.3) and (2.23) it follows that $a=1$; Eq. (2.22) then requires

$$\sigma=b=(c_{21}+bc_{22})/(c_{11}+bc_{12}). \tag{2.27}$$

Solving for b, with use of Eq. (2.6), one finds two values:

$$\sigma_\pm=\frac{c_{22}-c_{11}\mp\{(c_{11}-c_{22})^2+4c_{12}c_{21}\}^{\frac{1}{2}}}{2c_{12}} =\frac{c_{22}-c_{11}\mp\{(c_{11}+c_{22})^2-4\}^{\frac{1}{2}}}{2c_{12}}. \tag{2.28}$$

Thus, the only self-matching solutions are

$$f_\pm(E;x)=y_1(E;x)+\sigma_\pm y_2(E;x). \tag{2.29}$$

If σ_+ and σ_- are distinct, there are exactly two self-matching solutions. If $\sigma_+=\sigma_-$, there is only one such solution; this will occur when $c_{11}+c_{22}=\pm 2$.

The values of r for $f_\pm(E;x)$,

$$r_\pm(E)=\frac{c_{11}+c_{22}\mp\{(c_{11}+c_{22})^2-4\}^{\frac{1}{2}}}{2}, \tag{2.30}$$

can be written as

$$r_\pm(E)=(1\mp\rho^{\frac{1}{2}})/(1\pm\rho^{\frac{1}{2}}), \tag{2.31}$$

where

$$\rho=(c_{11}+c_{22}-2)/(c_{11}+c_{22}+2). \tag{2.32}$$

The definition of $f_\pm(E;x)$ will be made complete by the convention that

$$\left.\begin{aligned}\rho^{\frac{1}{2}}&=|\rho^{\frac{1}{2}}| \quad \text{if } \rho\geqslant 0,\\ \rho^{\frac{1}{2}}&=-i|\rho^{\frac{1}{2}}| \quad \text{if } \rho<0,\end{aligned}\right\} \tag{2.33}$$

with a similar definition of $\{(c_{11}+c_{22})^2-4\}^{\frac{1}{2}}$ in Eq. (2.28).

It is important to note that

$$r_+r_-=1. \tag{2.34}$$

If the cell potential is symmetrical, one can also express any self-matching solution in terms of $g(x)$ and $u(x)$:

$$f(x)=\alpha g(x)+\beta u(x). \tag{2.35}$$

For symmetrical cell potentials one has, by Eqs. (2.17) and (2.18),

$$\rho(E)=(c_{11}-1)/(c_{11}+1)=g_0'u_0/g_0u_0'. \tag{2.36}$$

Equation (2.22) demands

$$(\beta/\alpha)^2=(g_0g_0')/(u_0u_0')=(g_0/u_0)^2\rho. \tag{2.37}$$

The self-matching solutions then become

$$f_\pm(E;x)=\frac{1}{1\pm\rho^{\frac{1}{2}}}\left\{\frac{g(E;x)}{g_0}\pm\rho^{\frac{1}{2}}\frac{u(E;x)}{u_0}\right\}, \tag{2.38}$$

with

$$\sigma_\pm(E)=\pm\left(\frac{g_0'u_0'}{g_0u_0}\right)^{\frac{1}{2}}=\pm\frac{u_0'}{u_0}\rho^{\frac{1}{2}}. \tag{2.39}$$

The relation

$$\sigma_-=-\sigma_+ \tag{2.40}$$

is valid in general only for symmetrical cell potentials.

III. GENERAL SOLUTIONS OF THE PERIODIC WAVE EQUATION: BAND STRUCTURE OF THE PERMITTED ENERGY LEVELS

The self-matching cell solutions provide the basis for a particularly simple discussion of the properties of the general solution of the periodic wave equation. In Section II it has been shown that from any self-matching solution one can construct a corresponding ψ which changes only by a multiplying factor r from cell to cell. For each E we have then the solutions:

$$\psi_\pm(x)=r_\pm{}^n f_\pm(x-na), \quad \begin{cases} na<x<(n+1)a,\\ n=0,\pm1,\pm2,\cdots.\end{cases} \tag{3.1}$$

(The dependence of $f_\pm$ and $\psi_\pm$ on the parameter E is to be understood.) If f_+ and f_- are not identical, ψ_+ and ψ_- are independent solutions of a second-order differential equation: the general solution is accordingly expressible as

$$\psi(x)=C_+\psi_+(x)+C_-\psi_-(x). \tag{3.2}$$

The character of the general solution, and in particular its boundedness or non-boundedness, depends in any case on the value of ρ, which in turn depends on E. We shall here consider the characteristics of the ψ's as they depend on ρ, deferring for the moment a discussion of the occurrence of the various values of ρ.

Case 1: $\rho>0$

In this case $\rho^{\frac{1}{2}}$, $r_\pm$, β/α, $f_\pm$, and $\psi_\pm$ are all real. If $0<\rho<1$, $r_->1$. Then ψ_- increases in magnitude from cell to cell with increasing n; it may oscillate within each cell, but with an amplitude that increases exponentially as n, $x\to+\infty$. As $x\to-\infty$, $\psi_-\to0$ exponentially. On the other hand, since $0<r_+<1$, $\psi_+\to0$ exponentially as $x\to+\infty$, but increases exponentially as n, $x\to-\infty$. The general solution of the wave equation is thus unbounded as $x\to\infty$ unless $C_-=0$, and is unbounded as $x\to-\infty$ unless $C_+=0$; there is no physically acceptable solution of the wave equation.

If $\rho>1$, $r_-<-1$. The functions ψ_+ and ψ_- change sign from cell to cell, but it remains true that ψ_+ and ψ_- show exponential increases in amplitude as $x\to-\infty$ or $x\to+\infty$, respectively. Again there is no physically acceptable solution of the wave equation.

Case 2: $\rho<0$

In this case $\rho^{\frac{1}{2}}$ is imaginary, β/α is imaginary, and $f_\pm$ and $\psi_\pm$ are complex. Since $1+\rho^{\frac{1}{2}}$ and $1-\rho^{\frac{1}{2}}$ are complex conjugates, their ratio has modulus 1:

$$r_\pm=e^{\pm i\theta}. \tag{3.3}$$

Thus, ψ_+ and ψ_- change phase from cell to cell, but do not increase in magnitude: both are bounded as $x\to\pm\infty$. The same is true of the general solution ψ, for all values of C_+ and C_-; every solution of the wave equation is physically acceptable.

Case 3: $\rho=0$

If $\rho=0$, $c_{11}+c_{22}=2$, then $\sigma_+=\sigma_-$ [by Eq. (2.28)] and there is only one self-matching solution, with $r=1$. The corresponding ψ repeats itself exactly from cell to cell; it is periodic with period a, and is physically acceptable. (A normalization different from that of Eq. (2.23) may be necessary if σ becomes infinite as $\rho\to0$; see Section V.)

An independent solution can be constructed as follows. As $\rho\to0$, ψ_+ and ψ_- approach the common periodic form mentioned in the preceding paragraph. An independent solution for every $\rho\neq0$ is given by $\psi_+(x)$

$-\psi_-(x)$. By Eqs. (3.1) and (2.29) we have

$$\psi_+(x)-\psi_-(x)=(r_+{}^n-r_-{}^n)y_1(x-na)+(\sigma_+r_+{}^n-\sigma_-r_-{}^n)y_2(x-na), \quad [na<x<(n+1)a]. \tag{3.4}$$

As $\rho\to 0$, this sequence of solution approaches zero everywhere, proportionally to $\sigma_+-\sigma_-$, as is evident from inspection of its form in the zeroth cell. Thus there is a solution of the form $(\psi_+-\psi_-)/(\sigma_+-\sigma_-)$ for each ρ, and this sequence approaches a non-zero limit, itself a solution of the wave equation, as $\rho\to 0$. A simple calculation with Eqs. (2.28), (2.31), (2.32) shows that

$$\psi_0(x)=\lim_{\rho\to 0}\left\{\frac{\psi_+(x)-\psi_-(x)}{\sigma_+-\sigma_-}\right\} =nc_{12}y_1(x-na)+\left[1+\frac{n}{2}(c_{22}-c_{11})\right]y_2(x-na), \quad [na<x<(n+1)a], \tag{3.5}$$

is the desired independent solution for $\rho=0$. This increases in magnitude linearly as n, $x\to\pm\infty$.

The general solution of the wave equation in this case is expressible as

$$\psi(x)=C_0\psi_0(x)+C_+\psi_+(x). \tag{3.6}$$

It will be bounded only if $C_0=0$. Thus when $\rho=0$ there is (aside from an arbitrary multiplying constant) only one physically acceptable solution of the wave equation, approached by both ψ_+ and ψ_-.

Case 4: $\rho=\infty$

If $\rho=\infty$, $c_{11}+c_{22}=-2$, $\sigma_+=\sigma_-$, and there is only one self-matching solution, with $r=-1$. The corresponding ψ, approached by both ψ_+ and ψ_- as $\rho\to\infty$, changes from cell to cell only by a change in sign; it is periodic with period $2a$, and is physically acceptable.

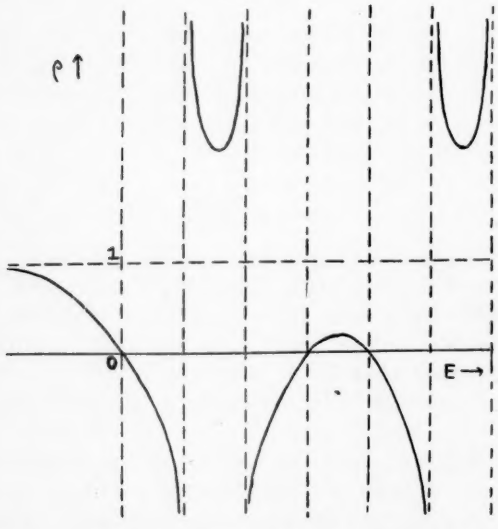

FIG. 1. Qualitative character of $\rho(E)$ for any periodic problem.

An independent solution can be constructed as in Case 3. One finds here

$$\psi_0(x)=\lim_{\rho\to 0}\left\{\frac{\psi_+(x)-\psi_-(x)}{\sigma_+-\sigma_-}\right\} =(-1)^{n+1}nc_{12}y_1(x-na)+(-1)^n\left[1-\frac{n}{2}(c_{22}-c_{11})\right]y_2(x-na), \quad [na\leq x\leq(n+1)a]. \tag{3.7}$$

This special solution also increases linearly in amplitude as x, $n\to\pm\infty$; so does the general solution (Eq. 3.6)) of the wave equation, unless $C_0=0$. Thus for $\rho=\infty$ there is only one independent physically acceptable solution of the wave equation, approached by both ψ_+ and ψ_-.

In summary, all solutions of the wave equation are physically acceptable for E such that $\rho<0$; no solutions are acceptable for E such that $\rho>0$; and there is just one independent physically acceptable solution for E such that $\rho=0, \pm\infty$.

To complete the proof of the band structure of the permitted energies in periodic potentials, it is only necessary to prove that ρ is positive for some ranges of E, negative for others. A discussion of this problem for the general case can be based on the work of Kramers.[8] Here it will suffice to consider the simpler case of symmetrical cell potentials, for which

$$\rho(E)=g_0'u_0/g_0u_0'.$$

The behavior of g_0, g_0', u_0, u_0' as functions of E follows from the most familiar properties of the solutions of the one-dimensional wave equation. The solutions $g(x)$ and $u(x)$ are convex to the x axis where $W(x)>E$, and concave (oscillatory) where $W(x)<E$. For very low E (certainly for $E<W_{\min}$) the regions of convexity are dominant, and one must have $g_0, u_0'>0$, $g_0', u_0<0$. As E increases, $g(x)$ and $u(x)$ become oscillatory, and then oscillate with decreasing wave-length; with increasing E, maxima and zeros appear alternately at $x=0$ and move monotonely to increasing x. It follows that g_0, g_0', u_0, u_0' oscillate between positive and negative values. It is easily seen that, as E increases, g_0' is the first of these quantities to vanish, and that its zeros thereafter alternate with zeros of g_0; similarly, u_0' vanishes before u_0, and these zeros alternate thereafter.

From the relation $g_0u_0'-g_0'u_0\equiv 1$ it follows that con-

[8] See reference 6. If one chooses Kramers' ϕ_1, and ϕ_2 as the y_1 and y_2 of this paper, his α_{11} and α_{22} become identical with the c_{11} and c_{22} defined here. Kramers shows that $\alpha_{11}+\alpha_{22}$, or $c_{11}+c_{22}$, is an oscillatory function of E, crossing the range from -2 to $+2$ (corresponding to $\rho>0$) and from time to time assuming values greater than 2 or less than $-2(\rho<0)$. It follows easily that ρ varies as illustrated in Fig. 1.

secutive zeros of g_0u_0' cannot be separated by a single zero of $g_0'u_0$, or conversely; if this were to occur, g_0u_0' and $-g_0'u_0$ would necessarily both be negative in some range of E, which is impossible. From this, and the facts mentioned in the preceding paragraph, it follows that the quantities under consideration vanish in the following order:

$$g_0',\ (g_0,\ u_0'),\ (g_0',\ u_0),\ (g_0,\ u_0'),\ (g_0',\ u_0)\cdots.$$

The order (within a parenthesis) of the zeros of g_0 and u_0' or of g_0' and u_0 is not fixed, but varies with the character of the potential considered; indeed these zeros may coincide.

The nature of the function $\rho(E)$ is determined sufficiently by consideration of the sequence of its zeros and infinities, together with the fact that it cannot assume the value 1, since $g_0'/g_0=u_0'/u_0$ would imply $g(x)\equiv u(x)$. The preceding paragraphs show that, for low E, $\rho>0$. As E increases, ρ goes through zero with g_0', and thereafter has alternate infinities and zeros in pairs. Its behavior must therefore be that shown in Fig. 1. Positive values of ρ, forbidden bands of E, occur below the first zero of g_0', and thereafter between consecutive zeros of g_0 and u_0', and of g_0' and u_0. If these zeros should happen to coincide, the forbidden band in question will disappear. The constant potential is a very special periodic potential for which all forbidden bands except the lowest disappear in this way.

IV. SPECIAL SOLUTIONS OF THE PERIODIC WAVE EQUATION; EFFECTIVE MOMENTUM

We now define the quantity

$$p(E)=(\hbar/ia)\ \ln r_+(E), \tag{4.1}$$

to be identified as the effective momentum associated with the energy E. In a permitted band, for which $r_+=e^{i\theta}$ [Eq. (3.3)],

$$p=(\hbar/a)\theta \tag{4.2}$$

is a real quantity. In a forbidden band, where r_+ is real, $p(E)$ must be imaginary or complex. In any case,

$$r_\pm{}^n=\exp\left(\pm\frac{i}{\hbar}pna\right). \tag{4.3}$$

The solutions $\psi_\pm$ of the wave equation, as defined by Eq. (3.1), can now be expressed as

$$\psi_\pm(x)=\exp[\pm(i/\hbar)px]$$
$$\times\{\exp[\mp(i/\hbar)p(x-na)]f_\pm(x-na)\},$$
$$\begin{cases} na<x<(n+1)a, \\ n=0,\ \pm1,\ \pm2\cdots. \end{cases} \tag{4.4}$$

Defining

$$P_\pm(E;\ x)=\exp[\mp(i/\hbar)p(E)(x-na)]f_\pm(E,\ x-na),$$
$$\begin{cases} na<x<(n+1)a, \\ n=0,\ \pm1,\ \pm2\cdots, \end{cases} \tag{4.5}$$

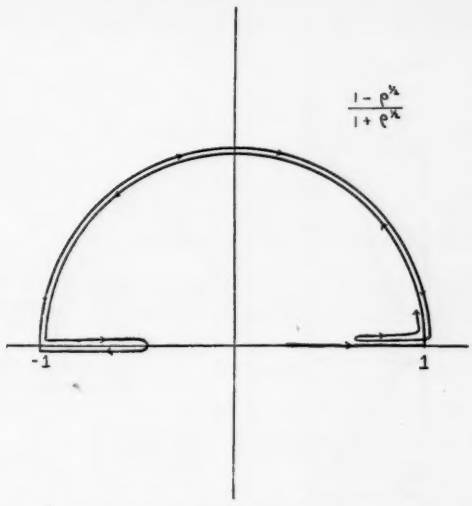

FIG. 2. Path in the complex plane of the point $(1-\rho^{\frac{1}{2}})/(1+\rho^{\frac{1}{2}})$ as E increases.

we can write these solutions as

$$\psi_\pm(E;\ x)=\exp\left[\frac{i}{\hbar}p(E)x\right]P_\pm(E;\ x). \tag{4.6}$$

It is obvious that P_+ and P_- are periodic in x with period a: these solutions of the periodic wave equation are thus of the familiar form discovered by Floquet. The role of $p(E)$ in these solutions is sufficient to identify this quantity as the effective momentum of crystal theory, here extended by the assignment of complex values for energies in the forbidden bands.

The logarithm in Eq. (4.1) is multiple-valued, with values differing by multiples of $2\pi i$; thus $p(E)$ is defined only to multiples of $2\pi\hbar/a=h/a$. Use of the convention expressed in Eq. (2.33), and of the principal value of the logarithm, limits p in the permitted bands to the positive values assumed by the "reduced momentum." Figure 2 sketches the path traversed in the complex plane by the point $(1-\rho^{\frac{1}{2}})/(1+\rho^{\frac{1}{2}})$, as E increases; Fig. 3 shows the corresponding values of the real part p_r and imaginary part p_i of p. If one takes $\rho^{\frac{1}{2}}=\pm i|\rho^{\frac{1}{2}}|$, with alternating $-$ and $+$ signs in the consecutive permitted bands, one assures for p the behavior sketched in Fig. 4. Here p takes on the values of the total effective momentum in the permitted bands, and reduces to the true momentum when the periodic potential becomes constant.

With these conventions, ψ_+ and ψ_- have in the permitted band the character of complex waves progressing to the right and left, respectively, multiplied by appropriate periodic functions. In the forbidden bands, on the other hand, they are real exponentials, attenuating to the right or left, respectively, multiplied by functions with period a or $2a$, depending on the value of p_r.

Let p denote the quantity defined in Fig. 3. We now

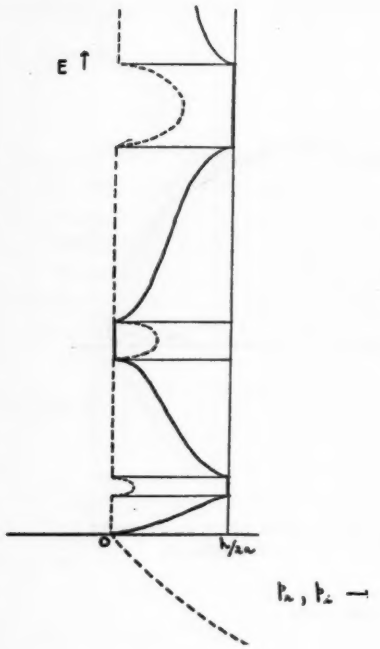

FIG. 3. Dependence on E of the real part p_r (solid line) and imaginary part p_i (dashed line) of the reduced effective momentum.

define

$$\left.\begin{aligned} &p_d=p, \text{ if } 0\leq p\leq h/4a, \\ &p_d=p-(h/2a), \text{ if } (h/4a)<p\leq h/2a. \end{aligned}\right\} \quad (4.7)$$

This may be expressed also as

$$p_d=p-p_e, \quad (4.8)$$

where p is defined as in Fig. 3 *or* Fig. 4, and p_e is its value at the nearest band edge. The behavior of p_d is indicated in Fig. 5; it is pure real in the permitted bands, and pure imaginary in the forbidden bands.

In terms of p_d, one can write

$$\psi_\pm(E;x)=\exp\left(\pm\frac{i}{\hbar}p_d x\right)P_{d\pm}(E;x), \quad (4.9)$$

where

$$P_{d\pm}(E;x)=\exp\left(\pm\frac{i}{\hbar}p_e x\right)P_\pm(E;x) \quad (4.10)$$

is periodic with period a or $2a$, according as p_e is 0 or $h/2a$. At every band edge P_{d+} and P_{d-} approach a common form, that of the physically acceptable solution at that band edge.

V. SOLUTIONS FOR ENERGIES NEAR A BAND EDGE

The following discussion of the problem for energies near a band edge will deal mainly with symmetric cell potentials.

A band edge occurs whenever ρ vanishes or becomes infinite. In the first case one has (Eqs. (4.1); (2.31))

$$p(E)\cong(2hi/a)\rho^{\frac{1}{2}}, \quad (\rho \text{ small}), \quad (5.1)$$

and in the second

$$p(E)\cong(h/2a)+(2hi/a)\rho^{-\frac{1}{2}} \quad (\rho \text{ very large}). \quad (5.2)$$

Then

$$\left.\begin{aligned} &p_d^2\cong-(4\hbar^2/a^2)\rho, \quad (\rho \text{ small}), \\ &p_d^2\cong-(4\hbar^2/a^2)1/\rho, \quad (\rho \text{ large}). \end{aligned}\right\} \quad (5.3)$$

The quantity p_d^2 is positive in a permitted band, but negative in a forbidden band.

A band edge occurs when any one of the quantities g_0, g_0', u_0, u_0' vanishes. Sufficiently near this band edge one can treat the vanishing quantity as linear in E, and can neglect the dependence on E of the three non-vanishing quantities, replacing them by corresponding values at the band edge: g_e, g_e', u_e, u_e'. That is, one can treat ρ and ρ^{-1}, and hence p_d^2, as linear functions of E in this region, writing

$$E-E_e=(p_d^2/2m^*). \quad (5.4)$$

The constant of proportionality m^* will vary from one band edge to the other. It is, of course, the effective mass of the particle at the band edge, and is positive for the lower edge of a permitted band, negative for the upper edge.

Solutions of the wave equation near the band edges can be approximated as follows.

The solutions $g(E;x)$ and $u(E;x)$ (like $y_1(x)$ and $y_2(x)$) can be expanded in powers of $E-E_0$ about any value of E_0. We shall here carry out such an expansion about the band-edge energy E_e. The periodic wave equation can be written as

$$\frac{d^2\psi(x)}{dx^2}+\frac{2m}{\hbar^2}[E_e-W(x)]\psi(x)=-\frac{2m}{\hbar^2}(E-E_e)\psi(x). \quad (5.5)$$

As independent solutions of the homogeneous equation

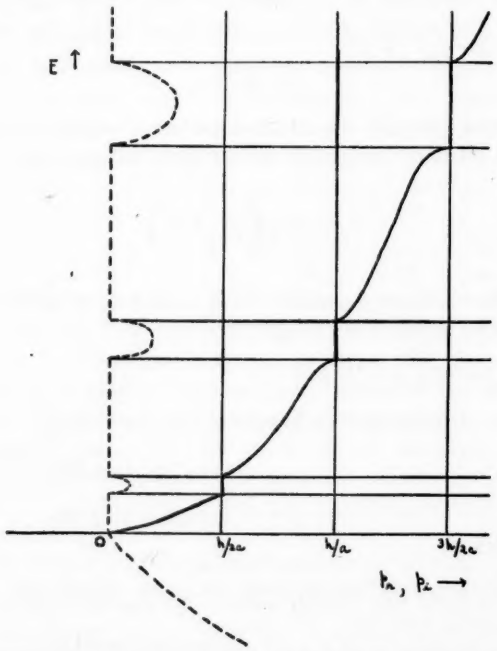

FIG. 4. Dependence on E of the real part p_r (solid line) and imaginary part p_i (dashed line) of the total effective momentum.

we have $g(E_e;x)=g_e(x)$ and $u(E_e;x)=u_e(x)$, such that

$$g_e(x)u_e'(x)-g_e'(x)u_e(x)\equiv 1. \tag{5.6}$$

If one replaces the quantity on the right by an arbitrary function $\phi(x)$, the inhomogeneous equation has as its general solution.

$$\psi=Ag_e(x)+Bu_e(x)-g_e(x)\int_{a/2}^{x}\phi(x)u_e(x)dx + u_e(x)\int_{a/2}^{x}\phi(x)g_e(x)dx. \tag{5.7}$$

Let

$$\xi=(2m/\hbar^2)(E-E_e). \tag{5.8}$$

Replacing $\phi(x)$ by $-\xi g(x)$ and choosing the constants A and B so that ψ satisfies the defining conditions for $g(x)$, one finds

$$g(x)=g_e(x)+\xi\left\{g_e(x)\left\{\int_{a/2}^{x}g(x)u_e(x)dx - u_e(x)\int_{a/2}^{x}g(x)g_e(x)dx\right\}\right. . \tag{5.9}$$

Similarly,

$$u(x)=u_e(x)+\xi\left\{g_e(x)\int_{a/2}^{x}u(x)u_e(x)dx - u_e(x)\int_{a/2}^{x}u(x)g_e(x)dx\right\}. \tag{5.10}$$

Let

$$\left.\begin{aligned} g(x)&=g_e(x)+\sum_{\tau=1}\xi^\tau g_\tau(x),\\ u(x)&=u_e(x)+\sum_{\tau=1}\xi^\tau u_\tau(x).\end{aligned}\right\} \tag{5.11}$$

Substituting these expansions into Eqs. (5.9) and (5.10), and equating coefficients of equal powers of ξ, one finds

$$g_{\tau+1}(x)=g_e(x)\int_{a/2}^{x}g_\tau(x)u_e(x)dx - u_e(x)\int_{a/2}^{x}g_\tau(x)g_e(x)dx, \tag{5.12}$$

$$u_{\tau+1}(x)=g_e(x)\int_{a/2}^{x}u_\tau(x)u_e(x)dx - u_e(x)\int_{a/2}^{x}u_\tau(x)g_e(x)dx. \tag{5.13}$$

By repeated quadratures one can thus carry the series expansions as far as is desired.[9]

[9] The same general method has been used by L. Brillouin, Quart. App. Math. 6, 167 (1948).

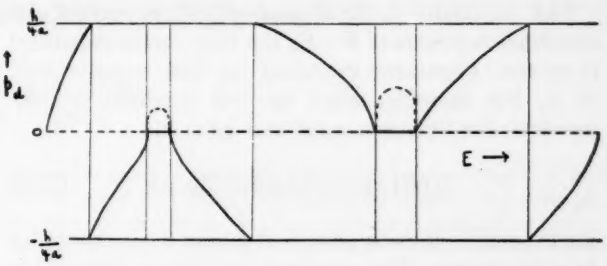

FIG. 5. Dependence on E of the real part (solid line) and imaginary part (dashed line) of the effective momentum p_d.

Let

$$I_{gg}=\int_0^{a/2}g_e(x)g_e(x)dx, \tag{5.14}$$

and let I_{gu} and I_{uu} be similarly defined. Then one finds easily

$$\left.\begin{aligned} g_0&=g_e+\xi[-I_{gu}g_e+I_{gg}u_e]+\cdots,\\ g_0'&=g_e'+\xi[-I_{gu}g_e'+I_{gg}u_e']+\cdots,\\ u_0&=u_e+\xi[-I_{uu}g_e+I_{gu}u_e]+\cdots,\\ u_0'&=u_e'+\xi[-I_{uu}g_e'+I_{gu}u_e']+\cdots.\end{aligned}\right\} \tag{5.15}$$

Use of these relations with Eqs. (5.3), (5.4), and (5.6) leads to expressions for m^* that depend on which of the four quantities vanishes at the band edge:

$$\left.\begin{aligned} m^*&=\pm(2/a)^2u_eu_e'I_{gg}, &&\begin{cases}+ \text{ if } g_e=0\\ - \text{ if } g_e'=0\end{cases}\\ m^*&=\pm(2/a)^2g_eg_e'I_{uu}. &&\begin{cases}+ \text{ if } u_e=0\\ - \text{ if } u_e'=0\end{cases}\end{aligned}\right\} \tag{5.16}$$

In the same way one can show that

$$\left.\begin{aligned} y_1(x)&=y_{1e}(x)+\sum_{\tau=1}\xi^\tau y_{1\tau}(x),\\ y_2(x)&=y_{2e}(x)+\sum_{\tau=1}\xi^\tau y_{2\tau}(x),\end{aligned}\right\} \tag{5.17}$$

where

$$y_{1,\tau+1}(x)=y_{1e}(x)\int_0^{x}y_{1\tau}(x)y_{2e}(x)dx - y_{2e}(x)\int_0^{x}y_{1\tau}(x)y_{1e}(x)dx, \tag{5.18}$$

$$y_{1,\tau+1}(x)=y_{1e}(x)\int_0^{x}y_{2\tau}(x)y_{2e}(x)dx - y_{2e}(x)\int_0^{x}y_{2\tau}(x)y_{1e}(x)dx.$$

The functions $f_\pm(E;x)$ and $P_\pm(E;x)$ cannot be expanded in powers of $E-E_e$, but they can be expanded in powers, sometimes including the first negative one, of p_d. For example, when the cell potential is symmetrical, the functions $y_1(x)$ and $y_2(x)$ in

$$f_\pm(E;x)=y_1(x)\pm\sigma_+(E)y_2(x) \tag{5.19}$$

are expansible in even powers of p_d, but σ_+ is expansible in odd powers. The required expansions depend on whether it is g_0, g_0', u_0, or u_0' that vanishes at the edge in question. We note here only the leading terms in the expansions for σ_+:

$$\left.\begin{aligned}
&g_e=0 \quad \sigma_+=+\frac{2ih}{a}\frac{u_e'}{u_e}p_d^{-1}+O(p_d),\\
&g_e'=0 \quad \sigma_+=-\frac{ia}{2h}\frac{u_e'}{u_e}p_d+O(p_d^3),\\
&u_e=0 \quad \sigma_+=\frac{2ih}{a}\frac{g_e'}{g_e}p_d^{-1}+O(p_d),\\
&u_e'=0 \quad \sigma_+=-\frac{ia}{2h}\frac{g_e'}{g_e}p_d+O(p_d^3).
\end{aligned}\right\} \tag{5.20}$$

Expansions for $f_\pm$ and $P_\pm$ will be given only for the case of a band edge with $g_e'=0$, where these functions remain finite:

$$f_\pm(x)=\frac{g_e(x)}{g_e}\pm\frac{iap_d}{2h}\left\{\frac{g_e(x)}{g_e}-\frac{u_e(x)}{u_e}\right\}+\cdots, \tag{5.21}$$

$$P_\pm(x)=\frac{g_e(x)}{g_e}\pm\frac{ip_d}{\hbar}\left\{\left(\frac{a}{2}-x\right)\frac{g_e(x)}{g_e}-\frac{a}{2}\frac{u_e(x)}{u_e}\right\}+\cdots. \tag{5.22}$$

In both expansions the third term is independent of the subscript sign.

In treating the perturbed-periodic wave equation one needs to know the behavior of $\{P_{d+}(E;x)+P_{d-}(E;x)\}/2$ and $\{P_{d+}(E;x)-P_{d-}(E;x)\}/2\sigma(E)$ near the band edges. By Eq. (4.5), (4.10) and (5.19), one has

$$P_{d\pm}(E;x)=\exp\left(\mp\frac{i}{\hbar}p_dx\right)[y_1(x)\pm\sigma_+y_2(x)], \qquad (0<x<a). \tag{5.23}$$

Then

$$\begin{aligned}
\frac{P_{d+}(E;x)+P_{d-}(E;x)}{2}&=\cos\left\{\frac{p_dx}{\hbar}\right\}y_1(x)\\
&\quad -i\sigma_+\sin\left\{\frac{p_dx}{\hbar}\right\}y_2(x),\\
\frac{P_{d+}(E;x)-P_{d-}(E;x)}{2\sigma_+}&=-\frac{i}{\sigma_+}\sin\left\{\frac{p_dx}{\hbar}\right\}y_1(x)\\
&\quad +\cos\left\{\frac{p_dx}{\hbar}\right\}y_2(x).
\end{aligned} \tag{5.24}$$

Expanding the quantities on the right in powers of p_d, with use of Eq. (5.20), one obtains

$$\left.\begin{aligned}
&\frac{P_{d+}(E;x)+P_{d-}(E;x)}{2}\\
&\quad=\left[y_{1e}(x)-\frac{i}{\hbar}(p_d\sigma_+)_e x y_{2e}(x)\right]+O(p_d^2), \qquad (0<x<a)\\
&\frac{P_{d+}(E;x)-P_{d-}(E;x)}{2\sigma_+}\\
&\quad=\left[-\frac{i}{\hbar}\left(\frac{p_d}{\sigma_+}\right)_e x y_{1e}(x)+y_{2e}(x)\right]+O(p_d^2),
\end{aligned}\right\} \tag{5.25}$$

where

$$\left.\begin{aligned}
(p_d\sigma_+)_e&=\frac{2ih}{a}\frac{u_e'}{u_e} \quad \text{if} \quad g_e=0,\\
&=0 \quad \text{if} \quad g_e'=0,\\
&=\frac{2ih}{a}\frac{g_e'}{g_e} \quad \text{if} \quad u_e=0,\\
&=0 \quad \text{if} \quad u_e'=0,
\end{aligned}\right\} \tag{5.26}$$

and

$$\left.\begin{aligned}
\left(\frac{p_d}{\sigma_+}\right)_e&=0 \quad \text{if} \quad g_e=0,\\
&=\frac{2ih}{a}\frac{u_e}{u_e'} \quad \text{if} \quad g_e'=0,\\
&=0 \quad \text{if} \quad u_e=0,\\
&=\frac{2ih}{a}\frac{g_e}{g_e'} \quad \text{if} \quad u_e'=0.
\end{aligned}\right\} \tag{5.27}$$

Similar expansions exist for $\{\psi_+(E;x)+\psi_-(E;x)\}/2$ and $\{\psi_+(E;x)-\psi_-(E;x)\}/2\sigma$; the leading terms are identical with those given in Eq. (5.25).

Electronic States in Perturbed Periodic Systems*

HUBERT M. JAMES
Purdue University, Lafayette, Indiana
(Received July 26, 1949)

The occurrence in perturbed periodic systems, such as impure crystals, of localized states with discrete energies is discussed from both qualitative and quantitative points of view. Semiclassical considerations, modified in the usual way by wave concepts, make it clear that impurities will give rise to impurity states above or below corresponding permitted bands of energy, according as the ionic charge of the impurity is less than or greater than that of the ion it replaces. Localized states at crystal interfaces and free surfaces can be discussed in the same way. Consideration of the behavior of wave packets leads to formulation of the effective-mass wave equation of Peckar. Complete solutions of the perturbed-periodic wave equation are then constructed by joining together solutions valid for a single period of the unperturbed potential. When the perturbation is slowly varying (though not necessarily small in its total effect) this approach leads to an analytic solution of the problem involving errors of the order of the ratio of the change in the perturbation potential across a single cell to the total kinetic energy of the particle. The effective-mass equation appears in connection with an approximate form of this solution, but the relation of its solution $\varphi(x)$ to the correct wave function $\psi(x)$ is more complex than has previously been realized. To construct $\psi(x)$ in any small region one should resolve $\varphi(x)$ locally into the sum of two exponentials $C\exp\{\pm(i/\hbar)p_d x\}$, multiply each by the appropriate periodic function, and add the results. A quadradically integrable $\varphi(x)$ corresponds to a quadratically integrable $\psi(x)$ with the same energy; thus stationary-state energies determined by solving the effective-mass wave equation are found to be surprisingly reliable.

I. INTRODUCTION

ELECTRONIC states of crystals can be treated only approximately in wave mechanics, by a forced separation of variables. In many cases, however, one can with good approximation treat each electron as moving in a static potential field $W(x, y, z)$ due to the other electrons, and to all other charges in the system. If the crystal is ideally perfect and infinite, W is periodic throughout all space. The behavior of an electron with energy E is then described by a solution ψ of the wave equation

$$-(\hbar^2/2m)\nabla^2\psi+W(x, y, z)\psi=E\psi.$$

This equation, and its one-dimensional analog,

$$-(\hbar^2/2m)[d^2\psi(x)/dx^2]+W(x)\psi(x)=E\psi(x), \quad (1.1)$$

have been extensively studied.[1]

Recent work on the solid state has directed increasing interest to the behavior of electrons in imperfect crystals. Electrons in real crystals move in potential fields which deviate from perfect periodicity for many reasons: imperfections in the crystal, missing or foreign atoms in the lattice, and in any case, termination of the crystal at free surfaces. These deviations from periodicity, if not too extensive, do not greatly disturb the band structure of the permitted energy values. Experiment and theory have, however, made it clear that they may give rise to electronic states with energies outside the permitted bands—states in which the electron cannot move freely through the crystal, but is restricted to a limited range near the surface or crystal cell where the periodicity is disturbed.

The existence of localized surface states in crystals was first suggested by Tamm,[2] on the basis of study of a special one-dimensional model. The latest and most instructive work of this type is that of Shockley,[3] who discussed the solutions of the one-dimensional wave equation for a potential that is perfectly periodic in a finite range of x, representing the crystal, and rapidly approaches a constant value outside (Fig. 1(b)). In such a case one might write the wave equation as

$$\left.\begin{aligned}-\hbar^2/2m(d^2\psi/dx^2)+W(x)\psi=E\psi, \quad 0<x<L,\\ -\hbar^2/2m(d^2\psi/dx^2)+V(x)\psi=E\psi, \quad x<0,\ x>L,\end{aligned}\right\} \quad (1.2)$$

where $W(x)$ is the periodic potential of the crystal, and $V(x)$ a prescribed non-periodic function. An alternative approach to the physical problem is that of Goodwin,[4] who used the perturbation method in treating a finite chain of identical atoms. Both methods indicate the existence of surface states, but closer investigation of their nature is required.

A quite different type of deviation from periodicity occurs where there is a foreign atom in a crystal lattice. The potential is profoundly modified in the crystal cell that contains this atom. In addition, if the net charge in this cell (due to all charges except the electron under consideration) is different from that in other cells, then the periodicity of the potential through the whole crystal is modified by the Coulomb potential of the excess charge. The corresponding one-dimensional wave equation is

$$-\hbar^2/2m(d^2\psi/dx^2)+[W(x)+V(x)]\psi=E\psi, \quad (1.3)$$

where $W(x)$ is again the periodic potential. A similar modification of a periodic potential may arise from

* This work was supported in part by Signal Corps Contract W36-039-SC-32020 with the Department of Physics at Purdue University. It has been circulated in a Signal Corps report in which the more mathematical parts have a somewhat less general form.

[1] References to the earlier literature are given in the preceding paper (H. M. James, Phys. Rev. **76**, 1602 (1949)), which establishes the notation and many of the basic methods and results to be used in the present one. Familiarity of the reader with this paper will be assumed, and it will hereafter be referred to as (I).

[2] I. Tamm, Physik Zeits. Sowjetunion **1**, 733 (1932).

[3] W. Shockley, Phys. Rev. **56**, 317 (1939).

[4] E. T. Goodwin, Proc. Camb. Phil. Soc. **35**, 205 (1939).

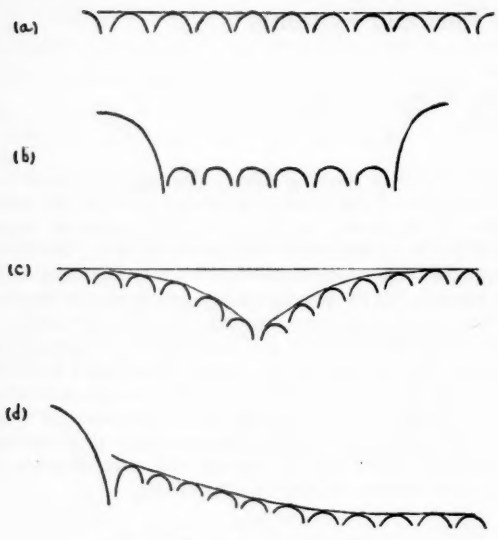

FIG. 1. Modified periodic potentials.

charges outside a crystal, or on its surface. Figure 1(c) represents the total potential energy of an electron in the presence of a foreign ion with excess positive charge. Figure 1(d) represents the potential energy of an electron near the surface of a crystal that has a negative surface charge and a corresponding positive Schottky layer, where the negative charge density falls below that existing in the interior of the crystal.

The present paper falls into two parts. The first is concerned with qualitative considerations that make clear the existence and nature of localized surface and impurity states in imperfect crystals. The second presents a quantitative attack on the solution of Eq. (1.3), for the special case of slowly varying (but not necessarily small) perturbations $V(x)$. The method here employed is based on the construction of solutions of the wave equation valid for all x by joining together solutions valid for a single period of the unperturbed periodic potential.[5] The same basic idea is suitable also for the treatment of random and abrupt changes in the potential, such as arise in very impure crystals and disordered alloys; such problems will be treated in a paper now in preparation.

II. QUALITATIVE CONSIDERATIONS

A. Semiclassical Discussion

A semiclassical discussion of the behavior of particles in perturbed periodic potentials can be based on the consideration of wave packets.

In a perfectly periodic potential there exist, for every energy E except the band-edge energies, two independent stationary-state solutions of the general wave equation, of the form

$$\psi_{\pm}(E;x)\exp[-(i/\hbar)Et)] = P_{\pm}(E;x)\exp[i/\hbar(\pm px-Et)]. \quad (2.1)$$

Here $P_{\pm}(E;x)$ are functions periodic with the period a of the potential, and p is a parameter, the effective momentum, which depends on E. As defined in (I), Fig. 4, p is real and positive in permitted bands of E, and complex in forbidden bands. When attention is to be restricted to permitted bands, one can treat $\pm p$ as a real parameter p ranging from $-\infty$ to $+\infty$, and can write the above solutions as

$$\psi(p;x)\exp[-(i/\hbar)Et] = P(p;x)\exp[i/\hbar(px-Et)], \quad (2.2)$$

there being one such solution for every value of p. The most general physically acceptable wave function is then expressible as

$$\Psi(x,t)=\int_{-\infty}^{+\infty} a(p)P(p;x)\exp[i/\hbar(px-Et)]dp, \quad (2.3)$$

E being a single-valued function of p. If $a(p)$ is very small except in a limited range about a mean value p_0, Ψ may be a wave packet describing a particle with well defined (but not exactly defined) position and effective momentum. In the small range about p_0 in which the integrand is appreciable, one may represent $px-Et$ by the first two terms of a Taylor's expansion in powers of $(p-p_0)$, to obtain

$$\Psi(x,t)=\exp[i/\hbar(p_0x-E_0t)]\int_{-\infty}^{+\infty} dpa(p)P(p;x) \times\exp\{i/\hbar(p-p_0)[x-(dE/dp)_{p_0}t]\}. \quad (2.4)$$

This has the form of a progressive wave with energy E_0, momentum p_0, modulated by a function of x and t given by the integral. If t is increased by $\Delta t=na/(dE/dp)_{p_0}$ and x by $\Delta x=na$, then both $P(p;x)$ and the exponential are unchanged, and the integral has the same value as before: after the interval Δt the form of the wave packet is unchanged except for an increase Δx in all coordinates. The wave packet thus moves as a unit with velocity

$$v=(dE/dp)_{p=p_0}, \quad (2.5)$$

undergoing (in this approximation) only changes in form periodic with period a/v.

Equation (2.5) for v is valid both for free particles and for particles in crystals; in crystals, however, p is a quite different function of E, and v depends on E in a quite different way. If the periodic variation in the potential is small, p will approximate closely to the classical momentum for constant potential, and one can write

$$E=p^2/2m, \quad (2.6)$$

except for energies near the band edges. Where this is

[5] In the case of perfectly periodic potentials this method has been used by R. de L. Kronig and W. G. Penney, Proc. Roy. Soc. **130**, 499 (1931), for the special case of square-well potentials. It is discussed at length, for more general types of potential, in reference 1. It has been employed by Shockley (reference 3) in the discussion of Eq. (1.2).

valid the velocity $v=p/m$ of the wave packet is that of a classical particle with the same energy, momentum, and mass. Near any band edge one has, however, in any case,

$$E-E_e=(p-p_e)^2/2m^*, \tag{2.7}$$

m^* being the effective mass of the particle at the band edge. The velocity of the wave packet,

$$v=(p-p_e)/m^*, \tag{2.8}$$

is then that of a "classical" particle with kinetic energy $E-E_e$, momentum $p-p_e$, mass m^*. Near the bottom of a permitted band $E-E_e$ and m^* are positive, but near the top $E-E_0$ and m^* are negative.

The significance of a negative effective mass becomes particularly clear when one considers a particle moving in a periodic potential, but subject to an additional constant force F. This problem was treated, very early in the development of wave mechanics, by Bloch,[6] who showed that the mean momentum of a wave packet changes with time in the classical way,

$$dp_0/dt=F, \tag{2.9}$$

except near the band edges. It has been shown by Jones and Zener,[7] Zener,[8] and Houston[9] that as the momentum and energy of the packet reach those of a band edge it is split by a partial Bragg reflection; the particle which it represents may have its momentum changed abruptly (reversed in sign in the one-dimensional case) or it may continue to increase, with a corresponding jump in energy to the next permitted band. The probability of reflection is very great, unless the forbidden band is narrow. Attention is called particularly to the work of Zener, who has computed the probability of transmission using ideas closely related to those of the present paper.

The motion of such a packet subject to a constant force to the right is illustrated in Fig. 2. Let its initial

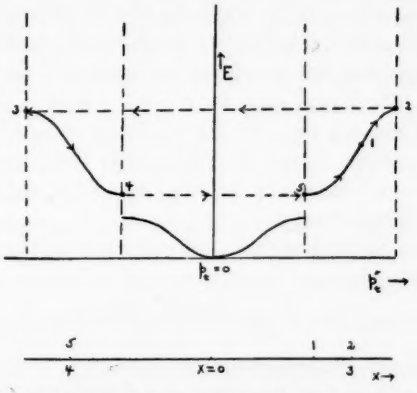

FIG. 2. Motion of a particle in a periodic potential, subject to an additional constant force to the right.

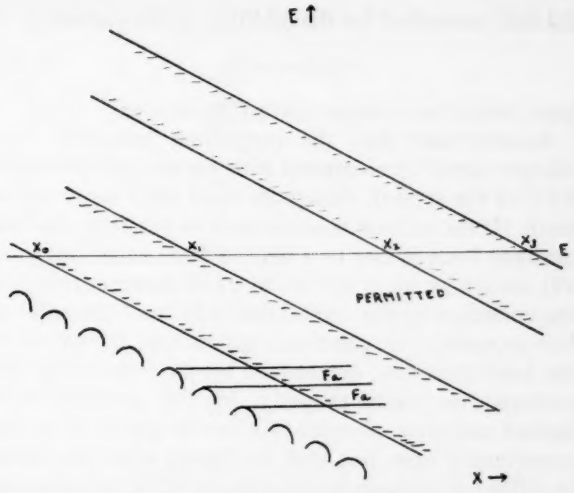

FIG. 3. Potential and band edges in a periodic potential perturbed by an additional constant force to the right.

energy be near the top of the second permitted band, and its momentum p_0 positive. Its position on the E, p diagram and in space are indicated in Fig. 2. by the numeral 1. As p_0 increases at a constant rate the energy of the packet will increase, but $|p_0-p_e|$ and v will *decrease*. Thus a force to the right produces an acceleration to the left: the ratio of these quantities, the effective mass, is negative. As the energy of the electron reaches the top of the permitted band the packet comes to a stop (points 2 in Fig. 2) and reverses its direction of motion. This reversal of p brings the momentum to point 3. As the packet moves to the left it loses energy; its velocity increases until, in the middle of the band, it may approach the classical value for a free electron. As the energy approaches the bottom of the band the velocity again decreases and the electron begins to move like a particle of positive effective mass m^*; it comes to a stop at the bottom of the band (point 4). It now undergoes a change in its direction of motion, through Bragg reflection of its momentum to point 5, and its energy increases as it moves to the right until its original position and energy are regained. Since the total change of momentum in the cycle is h/a, the period of the oscillation will be

$$\tau=h/Fa. \tag{2.10}$$

It may be noted that for a cell diameter of 4A and an applied field of 1000 volts/cm the period of oscillation of an electron in a crystal would be about 10^{-10} sec., in the microwave region. However, since the distance traversed in such oscillations would be of the order of 10^{-3} cm, much greater than the mean free path in most real crystals, it may be difficult to observe them in nature.

Instead of treating this motion as one of variable energy in a periodic potential field, one can treat it as a motion with constant total energy in a periodic poten-

[6] F. Bloch, Zeits. f. Physik **52**, 555 (1928).
[7] H. Jones and C. Zener, Proc. Roy. Soc. **144**, 101 (1934).
[8] C. Zener, Proc. Roy. Soc. **145**, 523 (1934).
[9] W. V. Houston, Phys. Rev. **57**, 184 (1940).

tial field perturbed by the addition of the potential

$$V(x)=-Fx, \tag{2.11}$$

from which the constant force F is derived.

Assume now that the perturbing potential $V(x)$ changes slowly as compared with the periodic potential $W(x)$ of the crystal, though its total effect need not be small. (If the particle is an electron in a crystal, and the constant force is due to a field of 1000 volts/cm, $V(x)$ will change by some 10^{-5} ev in a cell diameter, whereas the variations in the crystal field will be of the order of 1 ev or more.) One can then suppose that the nature of the band structure, determined by the form of the cell potential (or, more properly, by the potential in a limited sequence of cells) will be the same as in the unperturbed case, but that the bands will everywhere be shifted up or down by the amount of the perturbation energy $V(x)$ in that region. This is a suitable basis for qualitative thinking about such problems (see reference 8). As an illustration of this situation, Fig. 3 greatly exaggerates the dimensions of the cell and the change in potential across a cell. A particle with energy E will be in a permitted band between x_1 and x_2, in forbidden bands between x_0 and x_1, or x_2 and x_3. The oscillation of the wave packet described above is an oscillation between x_1 and x_2, with speed at any point corresponding to its position in the band at that point. Reflection occurs with high probability when the packet is about to enter a forbidden band, but there is a small probability of transmission to the next permitted band (splitting of the packet).

The generalization to slowly varying but non-linear perturbations $V(x)$ is immediate. Figure 4(a) shows a periodic potential modified by a perturbation $V(x)$ downward, say the change in potential energy of an electron in a crystal due to a local excess of positive charge. A band edge of energy E_e in the *unperturbed* crystal will then lie at energy $E_e+V(x)$. If a wave packet has an energy everywhere so near the band edge that Eq. (2.7) applies, one will expect it to move at any x like a particle of mass m^*, kinetic energy $E-E_e-V(x)$, and potential energy $E_e+V(x)$. For the energy illustrated it would then oscillate between the turning points x_1 and x_2 where the energy of the particle equals the energy of the band edge.

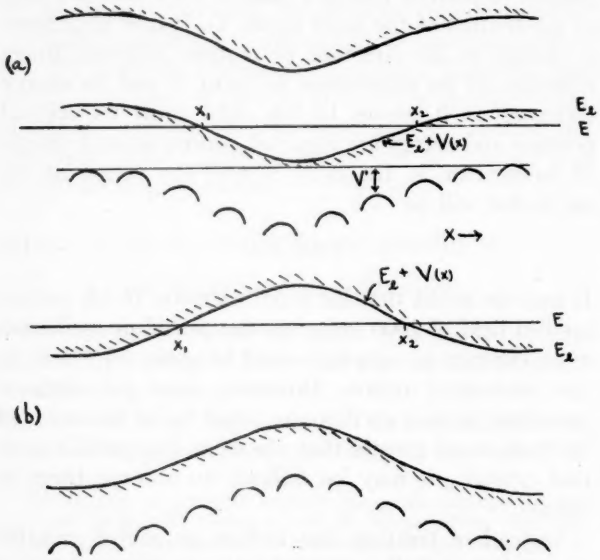

FIG. 4. Stable oscillations of a wave packet in a perturbed periodic potential.

Similar stable oscillations of a packet can occur when the particle is subject to a local *repulsive* force, if its energy lies as shown in Fig. 4(b). Its oscillation will be that of a particle of negative mass m^* in a region of negative kinetic energy $E-E_e-V(x)$, or, in more familiar terms, that of a particle of positive mass $|m^*|$, positive kinetic energy $E_e+V(x)-E$. It cannot pass outside the range $x_1\leq x\leq x_2$, for there its energy would lie in a forbidden band.

It will be noted that the energy of these stable oscillations lies outside the permitted band for the unperturbed crystal—below if the potential is perturbed downward, above if it is perturbed upward.

B. Discussion in Terms of Waves

In essence, the preceding section applies to the discussion of perturbed periodic systems a particle picture derived from the wave-mechanical treatment of perfectly periodic systems. It is useful for some purposes, and is commonly applied in discussions of rectification at crystal surfaces. The validity of the method is limited, however, for it leaves out of account characteristic wave phenomena that appear in imperfectly periodic systems: quantization of energy, the penetration of barriers, and reflections due to potential changes. For purposes of qualitative argument, these deficiencies can be corrected by use of the following wave ideas:

1. Let $\psi_+(E;x)$ and $\psi_-(E,x)$, as defined by Eq. (2.1) and discussed at length in reference 1, be wave functions for the unperturbed periodic potential. If $V(x)$ is slowly varying, then, in any small region there $V(x)\cong V_0$ and the potential is effectively periodic, the wave equation has good approximate solutions of the form $\psi_+(E-V_0;x)$ and $\psi_-(E-V_0;x)$. In a permitted region these are periodic functions modulated by progressive waves; in a forbidden region they are periodic functions exponentially attenuated to the right and to the left, respectively.

2. In a limited region one can express any solution approximately as

$$\psi=A\psi_+(E-V(x);x)+B\psi_-(E-V(x);x), \tag{2.12}$$

where A and B are constants.

3. In any region, however long, where the perturbing potential is constant, Eq. (2.12) will give an exact solution.

4. Where $V(x)$ is slowly varying one will have slow variations in the form of ψ_+ and ψ_-, and the appropriate values of A and B for exact representation of a given ψ

will also change slowly with x:

$$\psi = A(x)\psi_+(E-V(x);x)+B(x)\psi_-(E-V(x);x). \quad (2.13)$$

It must, however, be remarked that the problem of extending solutions of the form of Eq. (2.13) from a permitted to a forbidden region is completely parallel to the problem of connecting W.B.K. solutions for non-periodic problems across a classical turning point.

Let us now return to the problem of Fig. 4(a), assuming that $V(x)=0$ outside a finite range of x. If ψ is to be bounded as $x\to\infty$, and thus be physically acceptable, it is essential that $B(x)=0$ in the region of large positive x. For any given E this can be satisfied by only one independent solution of the wave equation. If ψ is to be bounded as $x\to-\infty$, it is also essential that $A(x)=0$ in the region of large negative x. This condition also can be satisfied by only one independent solution for a given E. In general these conditions will be inconsistent, but for special values of E one can expect to find a ψ that satisfies both conditions simultaneously. Thus one concludes that for discrete energies in the forbidden band there may exist wave functions that are physically acceptable. These are exponentially attenuated away from the perturbation in the lattice, and represent particles remaining indefinitely in the neighborhood of the perturbation. One may say that the particle is trapped in a region where its energy is permitted, because it is perfectly reflected by the surrounding unperturbed part of the crystal where its energy is in the forbidden band.

By the same argument one sees that in the situation of Fig. 4(b) there will be discrete permitted energies above the permitted band of the unperturbed crystal.

The system of Fig. 3 exhibits the analog of ordinary weak quantization. For certain narrow bands of energy there will exist stationary-state solutions of the wave equation for which $B(x)$ vanishes near x_3 and $A(x)$ vanishes near x_0. Such solutions will be oscillatory in the central permitted region, strongly attenuated in the forbidden region on either side, and very small in the permitted regions beyond. Particles known to be in the central permitted region will have one of these weakly quantized energies with very high probability. In the course of time, however, they may penetrate the barriers formed by the forbidden bands and appear in nearby permitted regions.

The spacing of the weakly quantized states is easily determined. It is obvious that if $\psi(x)$ is a solution of the wave equation of this system for energy E, then $\psi(x-na)$ is a solution for energy $E-nFa$, where n is any integer. The spacing of the weakly quantized states is thus $\Delta E=Fa$ and the frequencies emitted in transitions between them will be

$$\nu = n(Fa/h), \quad (2.14)$$

as one must expect also from Eq. (2.10).

Figure 5 represents the potential near the surface of a crystal, with the potential periodic inside the crystal

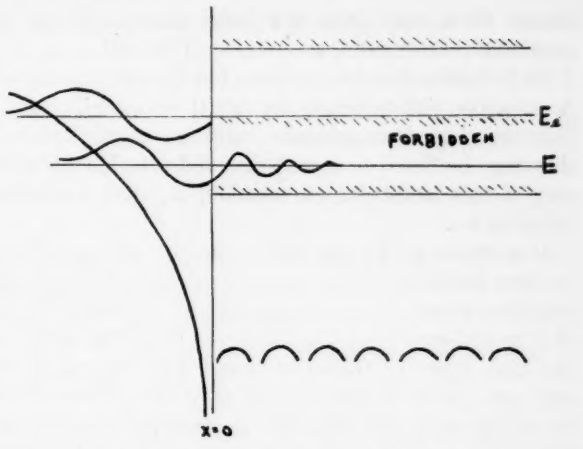

FIG. 5. Quantization of the energy of "end states" of a terminated periodic potential.

($x>0$) and having the form of an image force potential outside. Part of the band structure for the periodic potential is sketched. Consider first the solutions for the band-edge energy E_e. A solution well-behaved for negative x will have exponential character in the non-classical region to the left, will oscillate in the classical region near the crystal, and will reach $x=0$ with definite slope-to-magnitude ratio. On the other hand, for $x>0$ there will exist only one (see reference 1) physically acceptable, periodic solution, say with zero slope at the edge of the first cell, $x=0$. (Symmetric cell potentials are assumed; then the well-behaved solution has at the cell boundary either zero slope or zero magnitude.) These two functions cannot in general be fitted together to form a continuous physically acceptable solution. As E is lowered, however, the acceptable solution for negative x will reach $x=0$ with smaller slope-to-magnitude ratio, whereas the well-behaved solution for $x>0$ will have a greater and greater value for this ratio. For some E these values will become equal, and there will exist a continuous quadratically integrable solution of the wave equation, exponentially attenuated as $x\to\pm\infty$. This represents a discrete energy state in which an electron is trapped near the surface of the crystal; it cannot move away from the crystal because of the image force, and it cannot go far into the crystal, being perfectly reflected because its energy is in the forbidden band of the crystal. Such surface states can occur only for energies in the forbidden bands of crystals; they may be above or below nearby permitted bands.

It would be incorrect to infer that localized electronic states of energy E can arise only when E is a permitted energy in a region surrounded by other regions where E is forbidden or less than the potential energy. Figure 6(a) illustrates the termination of a periodic potential by an abrupt potential jump. For energy E the entire region $x<0$ is a non-classical one, and for $x>0$, E is a "forbidden" energy. Nevertheless, if E is properly

chosen there may exist a ψ large near $x=0$ but exponentially attenuated as $x\to\pm\infty$. This will occur only if the forbidden band in question has the right character. A solution well-behaved for $x<0$ necessarily has a positive slope-to-magnitude ratio at $x=0$, and can therefore be fitted to a well-behaved solution for $x>0$ only if this well-behaved solution, ψ_+, has a positive value of σ_+.

It is shown in (I), Eq. (2.39), that σ_+ will be positive in some forbidden regions, where u_0'/u_0 is positive, and negative where u_0'/u_0 is negative; all forbidden bands of a crystal may have one character, or all the other, or the two types of forbidden band may alternate. At any rate, these localized states may arise in any band for which σ_+ is positive. The electron is then trapped, but not in a region where it is to be expected by either classical ideas or by those derived from consideration of infinite crystals. Shockley's conclusions (reference 3) concerning the location of surface states in forbidden bands apply to states of this type, but not to those considered in the second preceding paragraph.

Figure 6(b) illustrates another situation of this sort, as where crystals of two different types meet. There can then exist quadratically integrable ψ's for discrete energies E in the forbidden band for both crystals—provided the forbidden band to the right is one of positive u_0'/u_0 and the band to the left is one of negative u_0'/u_0, or conversely. In such cases it is possible to fit together smoothly at $x=0$ a solution for $x>0$ attenuated to the right and a solution for $x<0$ attenuated to the left. Thus one can have localized electronic states existing at ideal crystal interfaces, with

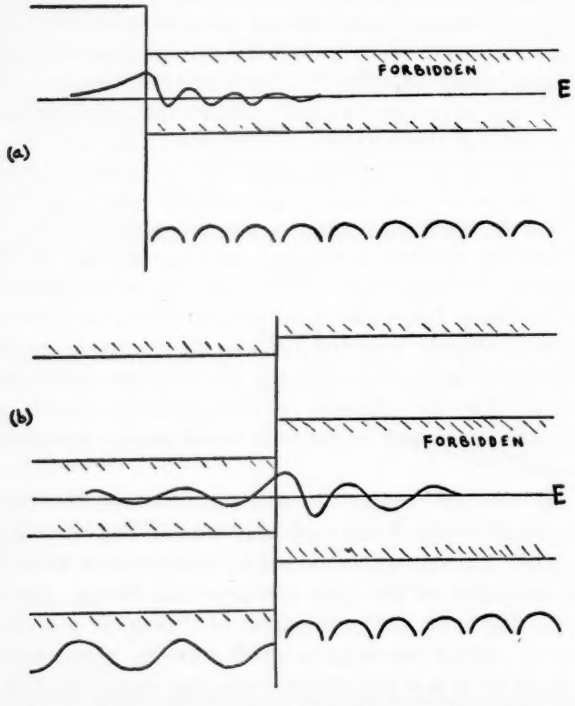

FIG. 6. Occurrence of localized states in forbidden bands.

energies in the forbidden band for both types of crystal. The existence of such states is easily understood, however, since the potential deviates strongly from periodicity in the region where the two types of potential meet; for an electron in this region the forbidden bands of the individual crystals have no absolute significance.

III. THE REDUCED-MASS WAVE EQUATION

We now turn to the problem of treating in detail the wave equation for a perturbed periodic potential. In preparation for a more systematic attack, an intuitive approach to the problem will first be described, with attention restricted to cases in which the energy E of the particle is everywhere near the energy $E_e+V(x)$ of a band edge of the perturbed system, as in Fig. 4.

Let p_t denote the effective total momentum of the particle, as defined in (I), Fig. 4; let p_{te} be the value of p_t at the band edge, and let

$$p_d=p_t-p_{te}. \tag{3.1}$$

The local value of p_d will then satisfy the relation (see Eq. (2.7))

$$E-E_e-V(x)=p_d^2/2m^*. \tag{3.2}$$

In the semiclassical approximation, the motion of the particle will be that of a classical particle with mass m^*, energy E, potential energy $E_e+V(x)$. We have seen that this approximation has the defects to be expected when particle ideas are applied but wave ideas are more appropriate. It is therefore natural to guess that a more satisfactory description of the behavior of the particle would be given by a wave function Φ that satisfies the general wave equation for a particle of mass m^* and potential energy $E_e+V(x)$:

$$-(\hbar^2/2m^*)(\partial^2\Phi/\partial x^2)+\{E_e+V(x)\}\Phi =-(\hbar/i)(\partial\Phi/\partial t). \tag{3.3}$$

We shall be particularly interested in the solutions with definite energy E. These have space factors $\phi(x)$ which satisfy a corresponding stationary-state equation:

$$-(\hbar^2/2m^*)(d^2\phi/dx^2)+\{E_e+V(x)\}\phi=E\phi. \tag{3.4}$$

These equations will be called the "effective-mass equations."

The relation between the solutions Φ and ϕ of the effective-mass equations and the solutions Ψ and ψ of the ordinary wave equations for the same system is particularly clear when $V=0$. Equation (3.4) then has the solutions

$$\phi_\pm=\exp\{\pm(i/\hbar)[2m^*(E-E_e)]^{\frac{1}{2}}x\} =\exp[\pm(i/\hbar)p_dx], \tag{3.5}$$

and Eq. (1.3) the corresponding solutions [see (I), Section IV]

$$\psi_\pm=\exp[\pm(i/\hbar)p_dx]P_{d\pm}(E;x). \tag{3.6}$$

Here the ϕ's appear in the ψ's as factors modulating periodic functions. Further, Eq. (3.3) has been so constructed that it will have wave packet solutions

behaving like the wave packet solutions of

$$-(\hbar^2/2m)(\partial^2\Psi/\partial x^2)+\{W(x)+V(x)\}\Psi = -(\hbar/i)(\partial\Psi/\partial t) \quad (3.7)$$

wherever the ideas of the semiclassical discussion are valid. The similarity of Ψ and Φ extends, however, only to the envelopes or modulating functions of the wave packets; the local wave-length of the packet Φ will be h/p_d, whereas that of Ψ will be h/p_t. In general, then, the most that one can expect is that the solutions of the reduced-mass equation shall play the role of modulating factors in the true wave functions. They will then give an incomplete, but perhaps very useful, representation of the electronic state. In particular, if

$$\psi(x)=\phi(x)P(x), \quad (3.8)$$

where $P(x)$ is not necessarily periodic but has the same integral in the square over every cell, then $\phi^*\phi(x)$ will give the relative probability of finding the particle in the several cells.

The relation between ψ and ϕ is, in general, more complex than that of Eq. (3.8). One can, however, make some progress by guessing as to the form of this relation, and testing the validity of the resulting ψ as a solution of the correct wave equation. This has, in effect, been the procedure of Tibbs[10] and of Peckar.[11] Their guesses will be described briefly.

It has been assumed that the energy E is everywhere close to the energy of the band edge. One might then try as a solution

$$\psi_T(x)=\phi(x)P(E_e;x), \quad (3.9)$$

where $P(E_e;x)$ is the uniquely defined periodic solution of the unperturbed wave equation having the energy of the band edge:

$$-\frac{\hbar^2}{2m}\frac{d^2P(E_e;x)}{dx^2}+W(x)P(E_e;x)=E_eP(E_e;x). \quad (3.10)$$

If one ignores the difference between the real and effective masses of the particle, writing

$$-(\hbar^2/2m)(d^2\phi/dx^2)+\{E_e+V(x)\}\phi=E\phi, \quad (3.11)$$

then Eq. (3.9) defines the approximate solution used by Tibbs. If this were an exact solution of Eq. (1.3) one would have (substituting Eq. (3.9) into Eq. (1.3) and rearranging terms),

$$\phi(x)\left[-\frac{\hbar^2}{2m}\frac{d^2P(E_e;x)}{dx^2}+(W(x)-E_e)P(E_e;x)\right] +P(E_e;x)\left[-\frac{\hbar^2}{2m}\frac{d^2\phi}{dx^2}+(E_e+V(x)-E)\phi\right] =\frac{\hbar^2}{m}\frac{d\phi}{dx}\frac{dP(E_e;x)}{dx}. \quad (3.12)$$

By Eqs. (3.10) and (3.11) the terms on the left vanish identically; Ψ_T would be an exact solution of the wave equation if the quantity on the right also vanished.

One can estimate the magnitude of this term as follows: If the periodic potential were constant, Eq. (3.10) would have solutions

$$P(E_e;x)=C\exp\{\pm[i/\hbar]p_{te}x\}. \quad (3.13)$$

If V is locally constant, solutions of Eq. (3.11) may assume the form

$$\phi(x)=C\exp\{\pm[i/\hbar]p_dx\}. \quad (3.14)$$

Thus, to orders of magnitude only, one has

$$\frac{dP(E_e;x)}{dx}\approx\frac{p_{te}}{\hbar}P(E_e;x), \quad (3.15)$$

$$d\phi/dx\approx(p_d/\hbar)\phi. \quad (3.16)$$

The error term in Eq. (3.12) is thus of the order of $(p_{te}p_d/m)\psi$. The kinetic and potential energy terms in Eq. (1.3) are, however, of the order of $(p_{te}^2/2m)\psi$. Thus the relative error in ψ_T (or, more precisely, in $d^2\psi_T/dx^2$) is of the order of $2p_d/p_{te}$.

A more sophisticated guess as to the relation of ϕ to ψ has been made by Peckar. With the unperturbed periodic potential each modulating function $\exp(i(p_d/\hbar)x)$ is associated with a different periodic function $P(p_d;x)$. If a solution of Eq. (3.4) is expressible as a sum of such functions,

$$\phi(x)=\sum_{p_d}c(p_d)\exp[i(p_d/\hbar)x] \quad (3.17)$$

then one may guess that in ψ each of these exponentials will appear with the same coefficient, but multiplied by its appropriate periodic function:

$$\psi_P(x)=\sum_{p_d}c(p_d)\exp[(i/\hbar)p_dx]P_d(p_d;x). \quad (3.18)$$

This is the solution proposed by Peckar, reduced to the one-dimensional case. If one assumes that the sum contains only terms with p_d so small that $P_d(p_d;x)$ can be replaced by $P(E_e;x)$, then this solution becomes

$$\psi_M(x)=\phi(x)P(E_e;x), \quad (3.19)$$

identical with Tibbs' except for the use of the reduced mass in the calculation of $\phi(x)$. This is the only solution that Peckar examines in detail. He shows that the errors in this solution are of relative order p_{dm}^3/p_{te}^3, where p_{dm} is the largest value of p_d appearing in an important way in the Fourier expansion of $\phi(x)$, Eq. (3.17). Thus the use of the reduced mass in computing $\phi(x)$ will greatly improve the accuracy of the solution $\psi_T(x)$, at least in cases where p_{dm} is not too large. It will appear later that Eq. (3.18) defines a still more accurate solution. Unfortunately, the mathematical and practical difficulties in the use of such expansions are excessive.

[10] S. R. Tibbs, Trans. Faraday Soc. **35**, 1471 (1939).

[11] S. Peckar, J. Phys. U.S.S.R. **10**, 431 (1946). The author is indebted to Dr. K. Lark-Horovitz for calling his attention to this paper.

IV. CONSTRUCTION OF COMPLETE SOLUTION BY JOINING CELL SOLUTIONS

We now apply to the treatment of the perturbed periodic wave equation the method, developed in (I), of constructing a complete solution of the wave equation by joining cell solutions. This leads to an analytic solution closely allied to that of Eq. (3.18), but of more convenient form, and to other solutions that are still more accurate and more generally applicable.

A. Definitions

We shall assume that the potential consists of two parts, a periodic potential $W(x)$, which for simplicity we shall take to be symmetric about the center of each cell, and a slowly varying potential $V(x)$, which can on occasion be treated as constant within any single cell.

Since the total potential varies from cell to cell, the special cell solutions of the wave equation, as discussed in (I), will differ from cell to cell. For the nth cell, $na\leq x\leq(n+1)a$, we define the y solutions of the wave equation $y_{1n}(E;x)$ and $y_{2n}(E;x)$, such that

$$\left.\begin{aligned} y_{1n}(E;na)&=1, \quad y_{1n}'(E;na)=0,\\ y_{2n}(E;na)&=0; \quad y_{2n}'(E;na)=1. \end{aligned}\right\} \tag{4.1}$$

We define also the self-matching solutions

$$f_{n\pm}(E;x)=y_{1n}(E;x)\pm\sigma_{n+}y_{2n}(E;x) \tag{4.2}$$

such that

$$\frac{f_{n\pm}'(E;na)}{f_{n\pm}(E;na)}=\frac{f_{n\pm}'(E,(n+1)a)}{f_{n\pm}(E,(n+1)a)}. \tag{4.3}$$

Since the perturbing potential within each cell can be treated as constant, we can define the solutions $g_n(E;x)$ and $u_n(E;x)$, symmetric and antisymmetric, respectively, about the center of the nth cell. For each cell we define the quantities $c_{ij}^{(n)}$, g_{0n}, g_{0n}', u_{0n}, u_{0n}', ρ_n, $r_{n\pm}$, σ_{n+}, p_n, and p_{dn}, all of which depend on the energy and satisfy, for each n, the relations given in (I). In particular, we note that

$$\rho_n=\frac{g_{0n}'u_{0n}}{g_{0n}u_{0n}'}, \tag{4.4}$$

$$\sigma_n=\sigma_{n+}=\left(\frac{g_{0n}'u_{0n}'}{g_{0n}u_{0n}}\right)^{\frac{1}{2}}, \tag{4.5}$$

$$r_{n\pm}=\frac{1\mp\rho_n^{\frac{1}{2}}}{1\pm\rho_n^{\frac{1}{2}}}=\exp[\pm(i/\hbar)p_na]. \tag{4.6}$$

The subscript $+$ is here dropped in the case of σ, as having no further value, since $\sigma_{n-}=-\sigma_{n+}$ will not appear; p or p_n will denote the reduced momentum of (I), Fig. 3. Finally, we define the functions $P_{n\pm}(E;x)$, periodic with period a, which have in the nth cell the form

$$P_{n\pm}(E;x)=\exp[\mp(i/\hbar)p_n(x-na)]f_{n\pm}(x), \quad [na\leq x\leq(n+1)a]. \tag{4.7}$$

In the above notation all quantities appear to depend on two parameters, E and n; in fact, however, they depend on a single parameter. If the perturbing potential in the nth cell is treated as constant, equal to V_n, then the special functions defined above are solutions of

$$-\hbar^2/2m(d^2\psi/dx^2)+W(x)\psi=(E-V_n)\psi. \tag{4.8}$$

Since $W(x)$ is the same in every cell, the forms of the cell solutions, and the values of the constants derived from them, depend only on $E-V_n$. Let the solutions of the unperturbed problem in the zeroth cell be $y_1(E;x)\cdots$, the periodic functions $P_\pm(E;x)$, the associated constants $\rho(E)$, $p(E)$, and so on. Then all the quantities defined in the preceding paragraph are given by relations of the form

$$y_{1n}(E;x)=y_1(E-V_n;x-na), \quad [na\leq x\leq(n+1)a], \tag{4.9}$$

$$P_{n\pm}(E;x)=P_\pm(E-V_n;x), \tag{4.10}$$

(by the periodicity of $P_\pm$), and

$$p_n=p(E-V_n). \tag{4.11}$$

In a detailed calculation all quantities could thus be determined with reasonable ease, even by numerical integration, for any special form of $W(x)$.

It is now a simple matter to define the numbers and functions considered above as continuously variable with x. We shall write

$$p(x)=p(E-V(x)), \quad \sigma(x)=\sigma(E-V(x)), \tag{4.12}$$

thus defining continuous functions which take on at the center of the nth cell the values p_n and σ_n, respectively. Treatment of p and σ as functions of $E-V(x)$ corresponds to the assumption, made in the preceding qualitative discussion, that the perturbation everywhere displaces the band edges by an amount $V(x)$. Similarly,

$$P_\pm(x)=P_\pm(E-V(x);x) \tag{4.13}$$

will be functions which change form slowly from cell to cell, taking on the value $+1$ at the left edge of each cell, and within that cell approximating very closely to the periodic functions $P_{n\pm}(E;x)$ defined for that cell. As in (I), Eq. (4.10), we also define the functions

$$\left.\begin{aligned} P_{d\pm}(x)&=P_\pm(x), \qquad \text{where} \quad 0\leq p\leq h/4a,\\ P_{d\pm}(x)&=\exp(\pm i\pi x/a)P_\pm(x),\\ &\qquad \text{where } h/4a<p\leq h/2a. \end{aligned}\right\} \tag{4.14}$$

At every band edge P_{d+} and P_{d-} approach a common form, the form of the periodic solution at that band edge, which is periodic with period a or $2a$, according as p is there 0 or $h/2a$.

Since p changes slowly, one can write

$$r_{n\pm}=\exp\left\{\pm[i/\hbar]\int_{na}^{(n+1)a}p\,dx\right\}. \tag{4.15}$$

One can also write

$$r_{n\pm}{}^2=\exp\left\{\pm[2i/\hbar]\int_{na}^{(n+1)a}p_d dx\right\}, \quad (4.16)$$

since a change of the integrand by $-h/2a$ does not affect the value of this quantity.

B. The Connection Formulas

An arbitrary wave function ψ can be expressed within the nth cell as a linear combination of any pair of independent cell solutions. A particularly useful expression of this type is

$$\psi=A_n y_{1n}(x)+B_n y_{2n}(x), \quad \begin{cases} na\leq x\leq(n+1)a, \\ n=0,\ \pm1,\ \pm2\cdots, \end{cases} \quad (4.17)$$

because the coefficients A_n and B_n give direct and useful measures of the magnitude of the wave function. By the definition of the y cell solutions they are, respectively, the magnitude and slope of ψ at the left edge of the nth cell. Together, they give a fairly precise measure of the local amplitude of ψ: if ψ can be treated as locally sinusoidal with wave-length $\lambda=h/p_t$ [p_t being the total effective momentum of Fig. 4, (I)], then one has

$$y_1(x)=\cos(2\pi x/\lambda),\quad y_2(x)=(\lambda/2\pi)\sin(2\pi x/\lambda), \quad (4.18)$$

and

$$\psi_{\max}{}^2=A_n{}^2+(\lambda/2\pi)^2B_n{}^2. \quad (4.19)$$

These virtues are not shared by the coefficients appearing in other such expressions for ψ. For instance, the coefficients α_n and β_n in the alternative expressions

$$\left.\begin{aligned} &\psi=\alpha_n f_{n+}(x)+\beta_n f_{n-}(x), \\ &\psi=\alpha_n\exp[(i/\hbar)p_n(x-na)]P_{n+}(x) \\ &\qquad+\beta_n\exp[-(i/\hbar)p_n(x-na)]P_{n-}(x); \end{aligned}\right\} \quad (4.20)$$

are not always satisfactory measures of the magnitude of ψ because the functions $f_{n\pm}$, $P_{n\pm}$ may change strongly in amplitude, tending to become infinite at band edges where σ becomes infinite.

Continuity of ψ and its first derivation at $x=(n+1)a$ requires

$$\left.\begin{aligned} A_{n+1}&=c_{11}{}^{(n)}A_n+c_{12}{}^{(n)}B_n, \\ B_{n+1}&=c_{21}{}^{(n)}A_n+c_{22}{}^{(n)}B_n. \end{aligned}\right\} \quad (4.21)$$

By Eq. (2.17) of (I), these relations can be expressed as

$$\begin{aligned} A_{n+1}&=\{u_{0n}{}'g_{0n}+g_{0n}{}'u_{0n}\}A_n-\{2u_{0n}g_{0n}\}B_n, \\ B_{n+1}&=-\{2u_{0n}{}'g_{0n}{}'\}A_n+\{u_{0n}{}'g_{0n}+g_{0n}{}'u_{0n}\}B_n; \end{aligned} \quad (4.22)$$

on further use of Eqs. (2.14), (2.36), and (2.39) of (I), they become

$$\begin{aligned} A_{n+1}&=\frac{1}{2}(r_{n+}+r_{n-})A_n+\frac{1}{2\sigma_n}(r_{n+}-r_{n-})B_n, \\ B_{n+1}&=\frac{\sigma_n}{2}(r_{n+}-r_{n-})A_n+\frac{1}{2}(r_{n+}+r_{n-})B_n. \end{aligned} \quad (4.23)$$

It is evident from Eqs. (4.21) and (4.22) that the coefficients in these relations all remain finite, even at band edges where σ_n may vanish or become infinite.

Although these connection formulas are of simple structure, they do not define a particularly simple behavior of the coefficients A_n and B_n; even when $V(x)$ is constant, and one can write $\sigma_n=\sigma$, $r_{n\pm}=r_\pm$, one has as the solution of Eq. (4.23)

$$\left.\begin{aligned} A_n&=\frac{1}{2}(r_+{}^n+r_-{}^n)A_0+\frac{1}{2\sigma}(r_+{}^n-r_-{}^n)B_0, \\ B_n&=\frac{\sigma}{2}(r_+{}^n-r_-{}^n)A_0+\frac{1}{2}(r_+{}^n+r_-{}^n)B_0. \end{aligned}\right\}$$

$$(n=0,\ \pm1\cdots). \quad (4.24)$$

In studying the variation of A_n, B_n, and ψ with n and x it is therefore convenient to shift attention for the moment to parameters that are constant when $V(x)$ is constant and change only slowly as $V(x)$ changes slowly.

In (I) the functions $f_\pm(x)$ have been so defined that when V is constant the coefficients α_n and β_n of Eq. (4.20) change from cell to cell by factors r_+ and r_-, respectively. Thus, if one writes

$$\psi(x)=C_n{}^+\left\{\prod_{\tau=0}^{n-1}r_{\tau+}\right\}f_{n+}(x)+C_n{}^-\left\{\prod_{\tau=0}^{n-1}r_{\tau-}\right\}f_{n-}(x), \quad (4.25)$$

$$(na\leq x\leq(n+1)a),$$

one can be sure that the coefficients $C_n{}^\pm$ will be constant throughout any region where $V(x)$ is constant.[12] One might also expect that they will vary slowly wherever $V(x)$ varies slowly. This is not the case, however, in the neighborhood of band edges where σ, f_{n+}, and f_{n-} become infinite.

This difficulty can be avoided in the following way. Let such a band edge occur in the zeroth cell: $\sigma_0=\infty$. Since, by Eq. (4.2),

$$\left.\begin{aligned} \frac{1}{2}\{f_{n+}(x)+f_{n-}(x)\}&=y_{1n}(x), \\ \frac{1}{2\sigma_n}\{f_{n+}(x)-f_{n-}(x)\}&=y_{2n}(x), \end{aligned}\right\} \quad (4.26)$$

the functions

$$F_{n+}(x)=\frac{1}{2}\left[\left\{\prod_{\tau=0}^{n-1}r_{\tau+}\right\}f_{n+}(x)+\left\{\prod_{\tau=0}^{n-1}r_{\tau-}\right\}f_{n-}(x)\right], \quad (4.27a)$$

$$na<x<(n+1)a,$$

[12] This notation does not express well the situation for $n\leq0$, but the generalization is obvious.

$$F_{n-}(x)=\frac{1}{2\sigma_n}\left[\left\{\prod_{\tau=0}^{n-1} r_{\tau+}\right\}f_{n+}(x) - \left\{\prod_{\tau=0}^{n-1} r_{\tau-}\right\}f_{n-}(x)\right], \quad (4.27b)$$

do not tend to become infinite as $n\to 0$ and the band edge is approached. If, then, one writes Eq. (4.25) as

$$\psi(x)=D_n^+F_{n+}(x)+D_n^-F_{n-}(x), \quad na<x<(n+1)a, \quad (4.28)$$

where

$$D_n^+=C_{n+}+C_{n-}, \quad D_n^-=\sigma_n(C_{n+}-C_{n-}), \quad (4.29)$$

one can expect D_n^+ and D_n^- to vary slowly when $V(x)$ varies slowly, even at the band edge. Comparison of Eqs. (4.17) and (4.28), with use of Eqs. (4.26) and (4.27), shows that

$$\left.\begin{aligned} A_n&=\frac{1}{2}\left\{\prod_{\tau=0}^{n-1} r_{\tau+}+\prod_{\tau=0}^{n-1} r_{\tau-}\right\}D_n^+ \\ &\quad+\frac{1}{2\sigma_n}\left\{\prod_{\tau=0}^{n-1} r_{\tau+}-\prod_{\tau=0}^{n-1} r_{\tau-}\right\}D_n^-, \\ B_n&=\frac{\sigma_n}{2}\left\{\prod_{\tau=0}^{n-1} r_{\tau+}-\prod_{\tau=0}^{n-1} r_{\tau-}\right\}D_n^+ \\ &\quad+\frac{1}{2}\left\{\prod_{\tau=0}^{n-1} r_{\tau-}+\prod_{\tau=0}^{n-1} r_{\tau-}\right\}D_n^-, \end{aligned}\right\} \quad (4.30)$$

where D_n^+ and D_n^- can be expected to vary slowly so long as $V(x)$ varies slowly. This result is an obvious generalization of Eq. (4.24) to the case of variable potential, except in that it is essential to treat as the zeroth cell any cell wherein $\sigma=\infty$.

Substitution of Eqs. (4.30) into Eqs. (4.23) yields the connection formulas for the D's. By Eq. (4.16), one has

$$\prod_{\tau=0}^{n} r_{\tau\pm}{}^2=\exp\left\{\pm\frac{2i}{\hbar}\int_0^{(n+1)a} p_d dx\right\}. \quad (4.31)$$

The connection formulas can then be written as

$$D_{n+1}^+-D_n^+=\frac{\sigma_{n+1}-\sigma_n}{2\sigma_{n+1}}\left[\cos\left\{\frac{2}{\hbar}\int_0^{(n+1)a} p_d dx\right\}-1\right]D_n^+ + \frac{i}{2}\frac{(\sigma_{n+1}-\sigma_n)}{\sigma_{n+1}\sigma_n}\sin\left\{\frac{2}{\hbar}\int_0^{(n+1)a} p_d dx\right\}D_n^-, \quad (4.32)$$

$$D_{n+1}^--D_n^-=-\frac{i}{2}(\sigma_{n+1}-\sigma_n)\sin\left\{\frac{2}{\hbar}\int_0^{(n+1)a} p_d dx\right\}D_n^+ - \frac{\sigma_{n+1}-\sigma_n}{2\sigma_n}\left[\cos\left\{\frac{2}{\hbar}\int_0^{(n+1)a} p_d dx\right\}-1\right]D_n^-. \quad (4.33)$$

It is evident that the coefficients on the right are small, and the variation of the D's is relatively slow, except possibly near the band edge, $n=0$, where σ may vanish or become infinite. It is easily verified that they remain small even at the band edge.

C. Replacement of the Connection Formulas by Differential Equations

We shall now replace the difference equations that define the numbers $D_n^\pm$ by differential equations defining continuous functions $D_+(x)$ and $D_-(x)$ such that

$$D_n^\pm=D_\pm([n+\tfrac{1}{2}]a) \quad (4.34)$$

with good approximation, for not-too-long ranges of integration. Since $D^+(x)$ and $D^-(x)$ vary slowly, we can write

$$D_{n+1}^\pm-D_n^\pm\cong a\frac{dD_\pm}{dx}\bigg|_{x=(n+1)a}. \quad (4.35)$$

We write also

$$\frac{\sigma_{n+1}-\sigma_n}{\sigma_{n+1}}\cong a\frac{d}{dx}(\ln\sigma)\bigg|_{x=(n+1)a}; \quad (4.36)$$

factors multiplying this expression vanish at the band edges, where the approximation may not be good. Finally we treat the upper limit in the integrals of Eqs. (4.32) and (4.33) as continuously variable.[13] We thus obtain the differential equations

$$\left.\begin{aligned} \frac{dD_+}{dx}&=\frac{1}{2}\frac{d}{dx}(\ln\sigma)\left[\cos\left\{\frac{2}{\hbar}\int_0^x p_d dx-1\right\}D_+ - \frac{i}{2}\frac{d}{dx}\left(\frac{1}{\sigma}\right)\sin\left\{\frac{2}{\hbar}\int_0^x p_d dx\right\}D_-, \right. \\ \frac{dD_-}{dx}&=-\frac{1}{2}\frac{d\sigma}{dx}\sin\left\{\frac{2}{\hbar}\int_0^x p_d dx\right\}D_+ \\ &\quad-\frac{1}{2}\frac{d}{dx}(\ln\sigma)\left[\cos\left\{\frac{2}{\hbar}\int_0^x p_d dx\right\}-1\right]D_-. \end{aligned}\right\} \quad (4.37)$$

This cumbersome relation can immediately be replaced by a much simpler one.

We define functions $A(x)$ and $B(x)$ by the relations

$$\left.\begin{aligned} A(x)&=D_+(x)\cos\left\{\frac{1}{\hbar}\int_0^x p_d dx\right\} \\ &\quad+\frac{i}{\sigma(x)}D_-(x)\sin\left\{\frac{1}{\hbar}\int_0^x p_d dx\right\}, \\ B(x)&=i\sigma(x)D_+(x)\sin\left\{\frac{1}{\hbar}\int_0^x p_d dx\right\} \\ &\quad+D_-(x)\cos\left\{\frac{1}{\hbar}\int_0^x p_d dx\right\}. \end{aligned}\right\} \quad (4.38)$$

[13] In the interior of a pass band the integrals change rapidly with n, and this step can be justified only because these terms are negligible.

These relations are the continuous analogs of Eqs. (4.30). If n is even,

$$\exp\left\{\pm\frac{i}{\hbar}\int_0^{na} p_d dx\right\}=\exp\left\{\pm\frac{i}{\hbar}\int_0^{na} p dx\right\}=\prod_{r=1}^{n-1} r_{r\pm}; \quad (4.39)$$

if n is odd, the exponentials are identical if $p_d=p$, but differ in sign if $p_d=p-(h/2a)$. Thus one has in any case

$$\left.\begin{aligned} A_n&=A(na),\\ B_n&=B(na),\end{aligned}\right\}(n \text{ even}). \quad (4.40)$$

(The small change of $D_\pm(x)$ in the distance $a/2$ has been ignored.) If n is odd, changes in sign may be required in Eqs. (4.40), but this is a matter of little interest, since the magnitude of ψ is sufficiently indicated by the values for even n.

When Eq. (4.38) is substituted into Eq. (4.37), extensive cancelation of terms occurs, and one obtains simple equations for $A(x)$ and $B(x)$:

$$\frac{dA}{dx}=-\frac{i}{\hbar}\frac{p_d(x)}{\sigma(x)}B, \quad (4.41a)$$

$$\frac{dB}{dx}=-\frac{i}{\hbar}p_d(x)\sigma(x)A. \quad (4.41b)$$

The coefficients $p_d(x)/\sigma(x)$ and $p_d(x)\sigma(x)$ are everywhere finite; their values at the various types of band edge are given in (I), Eqs. (5.26) and (5.27).

From Eqs. (4.29), (4.38) it follows that if

$$\left.\begin{aligned} C_+(x)&=\frac{1}{2}\left\{D_+(x)+\frac{D_-(x)}{\sigma(x)}\right\}\\ &=\frac{1}{2}\left\{A(x)+\frac{B(x)}{\sigma(x)}\right\}\exp\left\{-\frac{i}{\hbar}\int_0^x p_d dx\right\},\\ C_-(x)&=\frac{1}{2}\left\{D_+(x)-\frac{D_-(x)}{\sigma(x)}\right\}\\ &=\frac{1}{2}\left\{A(x)-\frac{B(x)}{\sigma(x)}\right\}\exp\left\{+\frac{i}{\hbar}\int_0^x p_d dx\right\},\end{aligned}\right\} \quad (4.42)$$

then

$$C_{n\pm}=C_\pm([n+\tfrac{1}{2}]a). \quad (4.43)$$

D. Continuous Representations of ψ

Using the functions just defined, one can now replace the cell-by-cell representation of ψ by a continuous one. By Eqs. (4.7), (4.14), and (4.15), one can write

$$\left\{\prod_{r=0}^{n-1} r_{r\pm}\right\}f_{n\pm}(x)=\exp\left\{\pm\frac{i}{\hbar}\int_0^x p dx\right\}P_{n+}(x) \quad [na<x<(n+1)a] \quad (4.44)$$

$$=\exp\left\{\pm\frac{i}{\hbar}\int_0^x p_d dx\right\}P_{dn+}(x).$$

These cell functions are approximated within every cell by the continuous functions (see Eqs. (4.10), (4.13))

$$\psi_\pm(x)=\exp\left\{\pm\frac{i}{\hbar}\int_0^x p dx\right\}P_\pm(E-V(x);x)$$

$$=\exp\left\{\pm\frac{i}{\hbar}\int_0^x p_d dx\right\}P_{d\pm}(E-V(x);x). \quad (4.45)$$

Similarly, the functions $F_{n\pm}(x)$ are approximated closely in every cell by

$$\left.\begin{aligned} F_+(x)&=[\psi_+(x)+\psi_-(x)]/2,\\ F_-(x)&=[\psi_+(x)-\psi_-(x)]/2\sigma(x).\end{aligned}\right\} \quad (4.46)$$

Since D_n^+ and D_n^- are closely approximated in every cell by $D_+(x)$ and $D_-(x)$, one can replace the cell-by-cell representation of ψ in Eq. (4.28) by a closely equivalent continuous representation:

$$\psi(x)=D_+(x)F_+(x)+D_-(x)F_-(x). \quad (4.47)$$

By use of Eqs. (4.42), (4.44), and (4.46) this can also be written as

$$\psi(x)=C_+(x)\psi_+(x)+C_-(x)\psi_-(x), \quad (4.48)$$

or

$$\psi(x)=A(x)\left[\frac{P_{d+}(E-V(x);x)+P_{d-}(E-V(x);x)}{2}\right]$$

$$+B(x)\left[\frac{P_{d+}(E-V(x);x)-P_{d-}(E-V(x);x)}{2\sigma(x)}\right]. \quad (4.49)$$

Of these representations the last is the most convenient. It has been shown that the functions $A(x)$ and $B(x)$ by themselves give a good indication of the amplitude of ψ. Unlike ψ_+ and ψ_-, the quantities in brackets are everywhere finite; the forms which they assume when $E-V(x)=E_e$ are given in (I), Section V.

E. Generalization of the Effective-Mass Equation

We shall now derive and interpret the effective-mass equation, as it appears in the treatment of problems such as are illustrated in Fig. 4.

We assume that the energy E to be considered lies everywhere closer (in p) to one band edge than to any other, thus avoiding the possibility that p_d will be discontinuous at any point. The quantities $p_d(x)/\sigma(x)$ and $p_d(x)\sigma(x)$ which appear in Eq. (4.41) will then be continuous everywhere, and, as follows immediately from (I), Eq. (5.20), both will have zero derivative at the band edge. One of these quantities will also vanish at the band edge [see (I), Eqs. (5.26), (5.27)]. We shall assume that this quantity is $p_d(x)\sigma(x)$ (i.e., that g_e' or $u_e'=0$); when $p_d(x)/\sigma(x)$ vanishes the roles of $A(x)$ and $B(x)$ are simply interchanged.

By Eq. (4.41a),

$$\frac{d^2A}{dx^2}=-\frac{i}{\hbar}\frac{p_d(x)}{\sigma(x)}\frac{dB}{dx}+\frac{i}{\hbar}B\frac{d}{dx}\left(\frac{p(x)}{\sigma(x)}\right). \quad (4.50)$$

The last term will vanish at the band edge and be small everywhere, if $V(x)$ varies slowly. We therefore neglect it. Using (4.42b), we obtain

$$(d^2A/dx^2)+(p_d^2(x)/\hbar^2)A=0. \quad (4.51)$$

If E is everywhere so close to $E_e+V(x)$ that Eq. (3.2) is valid, Eq. (4.51) becomes identical with the effective mass equation, Eq. (3.4), and one can write

$$A(x)=\phi(x) \quad (4.52)$$

and, by Eq. (4.41a),

$$B(x)=-\frac{\hbar}{i}\frac{\sigma(x)}{p_d(x)}\frac{d\phi}{dx}. \quad (4.53)$$

Then, by Eq. (4.49), one has

$$\psi(x)=\phi(x)Q(x)+(d\phi/dx)R(x) \quad (4.54)$$

where

$$Q(x)=[P_{d+}(E-V(x);x)+P_{d-}(E-V(x);x)]/2, \quad (4.55)$$

$$R(x)=\frac{\hbar}{ip_d}\frac{P_{d+}(E-V(x);x)-P_{d-}(E-V(x);x)}{2}. \quad (4.56)$$

We have thus shown the applicability of the effective-mass equation to problems in which there is a well defined effective mass, but have arrived at a new and more precise interpretation of its solution $\phi(x)$.

At the same time, Eq. (4.51) defines a solution of the perturbed periodic problem that is not limited by the assumption that the energy E is everywhere so close to the band edge that Eq. (3.2) applies. For any periodic, unperturbed potential one can in principle determine the function $p_d^2(E)$. In treating a given perturbed problem, for a particular energy E, one can determine

$$p_d^2(x)=p_d^2(E-V(x)), \quad (4.57)$$

and can define a function $V_{\text{eff}}(x)$ by the relation

$$E-E_e-V_{\text{eff}}(x)=p_d^2(x)/2m^*, \quad (4.58)$$

where m^* is the effective mass at the neighboring band edge. Equation (4.51) then becomes

$$-\frac{\hbar^2}{2m^*}\frac{d^2A(x)}{dx^2}+\{E_e+V_{\text{eff}}(x)\}A(x)=EA(x). \quad (4.59)$$

$A(x)$ is thus a solution of a one-dimensional wave equation involving an effective perturbation energy $V_{\text{eff}}(x)$ that is in general different from $V(x)$; in particular, it may depend on the E considered, as well as on $V(x)$. Since p_d^2 increases more rapidly than $E-E_e$ [(I), Fig. 4], one sees easily that the effective potential $V_{\text{eff}}(x)$ tends to be larger than the real perturbing potential. In this more general case, Eq. (4.54) is replaced by

$$\psi(x)=A(x)Q(x)+(dA/dx)R(x). \quad (4.60)$$

In principle, ψ can be determined still more accurately by integrating Eqs. (4.41), without neglect of the last term in Eq. (4.50). These solutions will not be discussed here.

F. Significance of the New Solutions

The structure of the wave function given in Eq. (4.60), and of its less accurate counterpart Eq. (4.54), becomes clearest when it is written as

$$\psi(x)=\frac{1}{2}\left\{A(x)+\frac{\hbar}{ip_d}\frac{dA}{dx}\right\}P_{d+}(x)+\frac{1}{2}\left\{A(x)-\frac{\hbar}{ip_d}\frac{dA}{dx}\right\}P_{d-}(x). \quad (4.61)$$

(Note, however, that in this expression the two quantities on the right become infinite at the band edge.) In any very small region one can regard $p_d(x)$ as constant and can write $A(x)$, a solution of Eq. (4.51), as

$$A(x)=C_1\exp\{[i/\hbar]p_dx\}+C_2\exp\{-[i/\hbar]p_dx\}, \quad (4.62)$$

a linear combination of special exponential solutions; thus,

$$\tfrac{1}{2}\{A(x)+[\hbar/ip_d]dA/dx\}=C_1\exp\{[i/\hbar]p_dx\} \quad (4.63a)$$

and

$$\tfrac{1}{2}\{A(x)-[\hbar/ip_d]dA/dx\}=C_2\exp\{-[i/\hbar]p_dx\} \quad (4.63b)$$

are the locally determined exponential components of $A(x)$. In each small neighborhood $\psi(x)$ can then be formed from $\phi(x)$ or $A(x)$ by resolving that function locally into real or complex exponentials of the form $\exp\{\pm[i/\hbar]p_dx\}$, multiplying each exponential by the appropriate periodic function $P_{d+}(x)$ or $P_{d-}(x)$, and adding the results.

It will now be shown that the $\psi(x)$ of Eq. (4.54), constructed from $\phi(x)$, is essentially the solution $\psi_P(x)$ [Eq. (3.18)] proposed but not discussed by Peckar. This solution is not precisely defined unless one specifies the normalization of the functions $P_d(p_d;x)$. For simplicity, we shall here assume that the band edge is one at which the periodic functions defined in this paper remain finite; specifically, one where $g_e'=0$. From Eq. (5.22) of (I) and Eqs. (4.55) and (4.56) of this paper, it follows that

$$P_d(p_d;x)=Q_e(x)+(ip_d/\hbar)R_e(x)+O(p_d^2), \quad (4.64)$$

$Q_e(x)$ and $R_e(x)$ being the forms assumed by $Q(x)$ and $R(x)$ at the band edge. Neglecting second-order terms

in p_d, one can then write

$$\psi_P(x)=\{\sum_{p_d} c(p_d)\exp[(i/\hbar)p_d x]\}Q_e(x)$$
$$+\{\sum c(p_d)(ip_d/\hbar)\exp[(i/\hbar)p_d x]\}R_e(x). \quad (4.65)$$

The first of the sums on the right is just the initial expansion of $\phi(x)$, and the second is $d\phi/dx$ if (as assumed by Peckar) one can operate on the expansion term by term. Thus,

$$\psi_P(x)=\phi(x)Q_e(x)+(d\phi/dx)R_e(x), \quad (4.66)$$

which agrees with Eq. (4.54) to within terms in p_d^2.

The less accurate approximation actually discussed by Peckar, ψ_M, in which $\phi(x)$ appears merely as an amplitude modulating a periodic function, is obtained by neglecting the last term in Eq. (4.66). From Eq. (5.22) of (I) it follows that

$$\left.\begin{aligned} Q_e(x)&=g_e(x)/g_e,\\ R_e(x)&=[(a/2)-x]g_e(x)/g_e-(a/2)u_e(x)/u_e;\end{aligned}\right\}(0<x<a)$$

$R_e(x)$ differs in magnitude from $Q_e(x)$ by a factor of the order of a. The term neglected by Peckar is thus of order $a(d\phi/dx)/\phi=\Delta\phi/\phi$ compared to the term retained, $\Delta\phi$ being the change in ϕ across a cell. This ratio will be small if E is near a band edge, but it is not a direct measure of the local errors in ψ_M as a solution of the wave equation; the magnitude of these has been indicated previously.

G. Accuracy of the New Solutions

The accuracy of the solutions derived here can be tested by substituting them into the perturbed-periodic wave equation, and observing the magnitude of the non-vanishing terms. For this purpose it is convenient to make more explicit the dependence on x of the terms in Eq. (4.60):

$$\psi(x)=Q(E-V(x);x)A(x)+R(E-V(x);x)A'(x). \quad (4.67)$$

We shall distinguish the derivatives of $Q(E-V(x);x)$ with respect to x in the first and second arguments by $'Q$ and Q', respectively; a similar notation will be used with R. Then

$$[dQ(E-V(x);x)]/dx='Q+Q'. \quad (4.68)$$

Considered as functions of $E-V(x)$ or p_d, Q and R can be expanded in powers of $p_d^2a^2/4\hbar^2$, with the multiplying functions of x having the same order of magnitude. Thus near a band edge $'Q$ is a small quantity of the order of

$$\frac{dV}{dx}\frac{d}{dE}\left(\frac{p_d^2a^2}{4\hbar^2}\right)Q=\frac{m^*}{2}\frac{a^2}{\hbar^2}\frac{dV}{dx}Q, \quad (4.69)$$

whereas Q' is much larger, of the order of $(p_t/\hbar)Q$ [Eq. (3.15)]. R and its derivatives are smaller than Q and its corresponding derivatives by a factor of the order of a, as has been shown in the case of $Q_e(x)$ and $R_e(x)$ at the end of the preceding section.

Now the functions

$$f_\pm(x)=\exp[\pm(i/\hbar)p_d x]P_{d\pm}(E;x) \quad (4.70)$$

are exact solutions of

$$f''=-(2m/\hbar^2)(E-W(x)-V)f \quad (4.71)$$

for constant V and p_d. It follows easily that, under the same conditions,

$$P_{d\pm}''(E;x)\pm\frac{2ip_d}{\hbar}P_{d\pm}'(E;x)$$
$$=-\frac{2m}{\hbar^2}\left\{E-W(x)-V-\frac{p_d^2}{2m}\right\}P_{d\pm}(E;x) \quad (4.72)$$

and that

$$Q''(E-V;x)=2\frac{p_d^2}{\hbar^2}R'(E-V;x)$$
$$-\frac{2m}{\hbar^2}\left\{E-W(x)-V-\frac{p_d^2}{2m}\right\}Q(E-V;x), \quad (4.73)$$

$$R''(E-V;x)=-2Q'(E-V;x)$$
$$-\frac{2m}{\hbar^2}\left\{E-W(x)-V-\frac{p_d^2}{2m}\right\}R(E-V;x). \quad (4.74)$$

Equations (4.73) and (4.74) remain true, in the notation introduced above Eq. (4.68), even when one treats V as a parameter varying with x. When p_d varies with x one has

$$A''=-\frac{p_d^2(x)}{\hbar^2}A \quad (4.75)$$

and

$$A'''=-\frac{1}{\hbar^2}\frac{dp_d^2}{dx}A-\frac{p_d^2(x)}{\hbar^2}A'. \quad (4.76)$$

On substituting Eq. (4.67) into the perturbed-periodic wave equation, and using Eqs. (4.73) to (4.76), one finds, after extensive cancellation of terms,

$$\psi''-\frac{2m}{\hbar^2}\{W(x)+V(x)-E\}\psi$$
$$=-\frac{1}{\hbar^2}\frac{dp_d^2}{dx}AR+2A('Q')+2A'('Q)+A(''Q)$$
$$-\frac{2p_d^2}{\hbar^2}A('R)+2A'('R')+A'(''R). \quad (4.77)$$

The local error in the solution is measured by the terms on the right. Of these, all but the first vanish if one neglects the slow variation of Q and R with varying V, in taking derivatives. As compared with the in-

dividual terms on the right, this term is of relative magnitude:

$$\frac{1}{\hbar^2}\frac{dp_d^2}{dx}AR\Big/\frac{2m}{\hbar^2}\{W(x)+V(x)-E\}AQ$$

$$\sim\frac{m^*}{m}\left(\frac{a(dV/dx)}{W+V-E}\right), \quad (4.78)$$

since

$$R/Q\sim a, \quad (4.79)$$

near a band edge, where the effective mass is defined. The first of the remaining terms is the largest of these, and can be shown to be of the same order of magnitude as the term just considered. It thus appears that Eq. (4.67) gives a solution for which the error terms in the wave equation are small, in about the ratio of the change in perturbation energy across a single cell to the true value of the local kinetic energy. For a slowly varying perturbation the solution is locally very accurate indeed; the long-range effect of accumulated local errors cannot be discussed here.

Perhaps the most interesting qualitative result of this analysis is the confidence it gives in the use of the effective-mass wave equation for the calculation of stationary-state energies, when $V(x)$ varies slowly. To each quadratically integrable solution ϕ of this equation there corresponds a quadratically integrable ψ *with the same energy*, providing a good approximate solution of the perturbed-periodic equation. The error in the energy E as an approximation to a stationary-state energy corresponds to the small error in this ψ, and not to the roughness in the arguments usually employed in arriving at the effective-mass equation.

PHYSICAL REVIEW VOLUME 76, NUMBER 11 DECEMBER 1, 1949

The Radiation Spectra of Barium^{140} and Lanthanum^{140}

LOUIS A. BEACH,* CHARLES L. PEACOCK,** AND ROGER G. WILKINSON
Indiana University, Bloomington, Indiana

(Received August 3, 1949)

The radiations of Ba^{140} and La^{140} have been measured with a small 180° spectrometer. For the case of Ba^{140} three gamma-rays are present, all of which are converted, with energies 0.16, 0.31, and 0.54 Mev. The beta-ray spectrum shows the presence of two groups with maximum energies of 0.48 (40 percent) and 1.022 (60 percent) Mev.

The radiations of La^{140} are complex. Six gamma-rays of energies 0.093?, 0.335, 0.49, 0.82, 1.60, and 2.5 Mev are present, the first three being internally converted. The beta-ray spectrum is resolved into three groups with end points at 1.32 (70 percent), 1.67 (20 percent), and 2.26 (10 percent) Mev. Decay schemes for these isotopes are suggested.

I. INTRODUCTION

THE radiations of 12.8-day Ba^{140} and its daughter, 40-hour La^{140}, have been re-investigated with the aim of formulating the mode of decay of these elements. These isotopes have been studied by numerous workers[1–7] and their results tend toward consistency insofar as energy values are concerned. However, previous investigations have been fragmentary and no integrated survey has been reported.

The present work was carried out with a small 180° spectrometer and very thin window G-M tube detection. Equilibrium samples of Ba^{140} and La^{140} obtained from Oak Ridge were used. Beta-ray sources were of the order of 0.1 mg/cm² in thickness. Photoelectron spectra were obtained with a lead radiator 30 mg/cm² thick. The procedure consisted of measuring the beta-ray and photoelectron spectra initially with equilibrium sources, and finally with chemically isolated sources of Ba^{140} and La^{140}.

II. EQUILIBRIUM MEASUREMENTS

The composite radiations were first measured by using sources in which the constituents were in equilibrium. Since the gamma-radiation of La^{140} is complex and the half-life relatively short, equilibrium photoelectron measurements furnish more reliable values of the energies. Subsequent runs with separated sources were, of course, necessary to identify the gamma-rays with the correct isotope.

Figure 1 shows the equilibrium photoelectron spectrum. The K and L photoelectron peaks associated with five gamma-rays are superimposed on a pronounced Compton-electron distribution. The photoelectron lines may be resolved into gamma-rays of energies 0.335,

* Now at Cornell University, Ithaca, New York.
** Now at Tulane University, New Orleans, Louisiana.

[1] W. Rall and R. G. Wilkinson, Phys. Rev. **71**, 321 (1947).
[2] D. W. Engelkemeir, Plutonium Project Report CC-1959 (Ausust 1944).
[3] H. J. Born and W. Seelmann-Eggebert, Naturwiss. **31**, 201 (1943).
[4] V. A. Nedzel and M. B. Sampson, Plutonium Project Report CP-2160 (September 1944).
[5] R. K. Osborne and W. C. Peacock, Phys. Rev. **69**, 679 (1946).
[6] L. C. Miller and L. F. Curtiss, Phys. Rev. **70**, 983 (1946).
[7] A. Wattenberg, Phys. Rev. **71**, 497 (1947).

0.49, 0.54, 0.82, and 1.60 Mev. The dominant Compton-electron curve is primarily caused by the 1.60-Mev gamma-ray. The Compton-electron spectrum persists beyond 1.60 Mev and finally comes to zero in the region of 2.5 Mev. No marked evidence of a photoelectron line associated with this energy could be found. The use of a thorium radiator and much stronger sources did not add appreciably to the information obtained with the lead radiator. Evidently, a gamma-ray of about 2.5 Mev is present which is so low in intensity that the corresponding photoelectron peak cannot be reliably located in the presence of the background due to the numerous strong gamma-rays.

The combined beta-ray spectrum exhibits a number of conversion lines which can be identified as the K and L components of gamma-rays of energies 0.16, 0.335, 0.49, and 0.54 Mev. The shape of the continuous spectrum is complex and was resolved by a Fermi analysis into five groups of beta-rays with end points at 0.47, 0.98, 1.32, 1.68, and 2.19 Mev. While the accuracy of these values is subject to question because of the number of successive subtractions, the analysis nevertheless serves as a check on the values obtained with separated sources.

III. BARIUM^{140}

Lanthanum-free barium was prepared by adding NH_4OH to a solution of the chlorides of Ba and La. Repeated precipitation of the $La(OH)_3$ in this way assured a clean separation. The Ba was then precipitated as the carbonate by adding NH_4OH and finally converted to the chloride by adding HCl. Since very little Ba carrier was added, the specific activity of the source material was high. Measurements were taken as soon after the separation as possible to avoid the effect of the growth of the La.

Figure 2 shows the continuous spectrum of Ba^{140}. Three conversion lines appear which are associated with gamma-rays of energies 0.160, 0.306, and 0.540 Mev. Subsequent measurements taken during the growth of the La indicated that these gamma-rays should be attributed to Ba^{140}, since the intensities of the conversion lines did not increase. In addition, as growth proceeded, conversion lines corresponding to the 0.335- and 0.49-Mev gamma-rays found in the equilibrium run became evident. As equilibrium was approached, the conversion line due to the 0.306-Mev gamma-ray of the Ba was masked by the stronger line of the 0.335-Mev gamma-ray from the La.

A Fermi analysis of the continuous spectrum is shown in Fig. 3. Two groups of beta-rays are found with end points at 0.48 and 1.022 Mev. These values are in good agreement with two of those found in the equilibrium spectrum.

IV. LANTHANUM^{140}

Barium-free lanthanum, prepared by the chemical procedure outlined above, was used to complete the study of these radiations. All of the gamma-rays found in the equilibrium photoelectron spectrum, with the exception of the 0.54-Mev gamma-ray, are due to La^{140}. Figure 4 shows the beta-ray spectrum. All parts

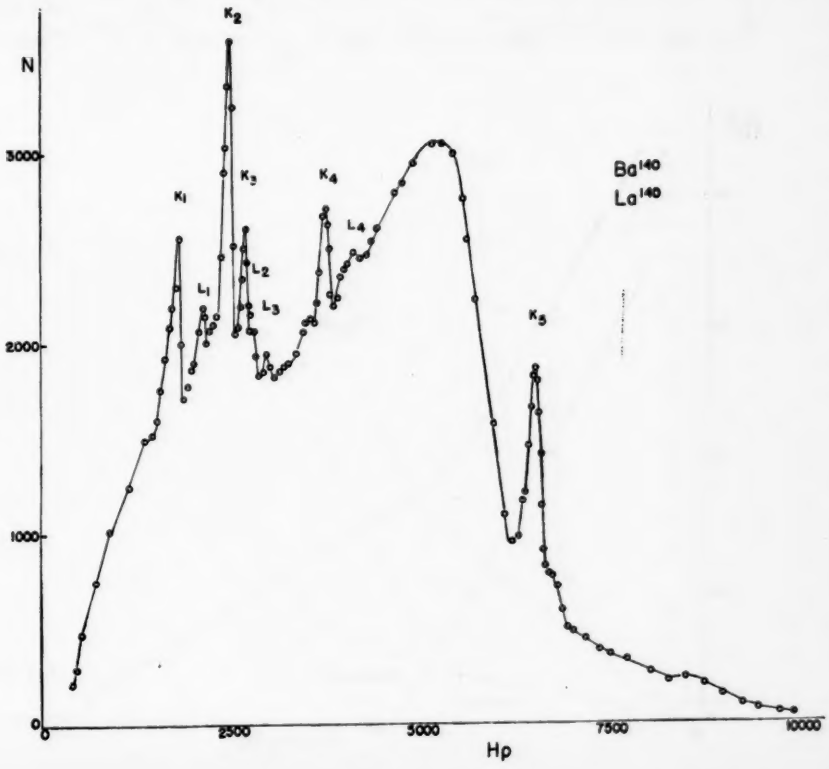

FIG. 1. Photoelectrons ejected from a Pb radiator 30 mg/cm² thick by the gamma-rays of Ba^{140} and La^{140} in equilibrium. The energy values are given in Table I.

of the spectrum decayed with the characteristic 40-hour half-life. No evidence of residual Ba^{140} or other impurity could be detected. In addition to conversion lines corresponding to gamma-rays at 0.335 and 0.49 Mev, observed previously in the growth from Ba^{140}, there appear three lines in the low energy region. The lowest line is most probably the Auger line associated with the conversion of the gamma-rays. The remaining two lines are weak and their identification uncertain. As K and L components they would correspond to a gamma-ray of energy 0.093 Mev. A gamma-ray of this energy could not be observed in the photoelectron spectrum.

A Fermi plot of the beta-ray spectrum (Fig. 5) yields three groups of beta-rays with end points at 1.32, 1.67, and 2.26 Mev. These values are in good agreement with three of the five groups found in the equilibrium spectrum.

V. RESULTS

These experiments make it clear that the disintegration of Ba^{140} involves the emission of two groups of beta-rays with maximum energies of 0.48 and 1.022 Mev, and three gamma-rays having energies 0.160, 0.306, and 0.540 Mev. The higher energy beta-group comprises 60 percent of the transitions. The 0.54-Mev

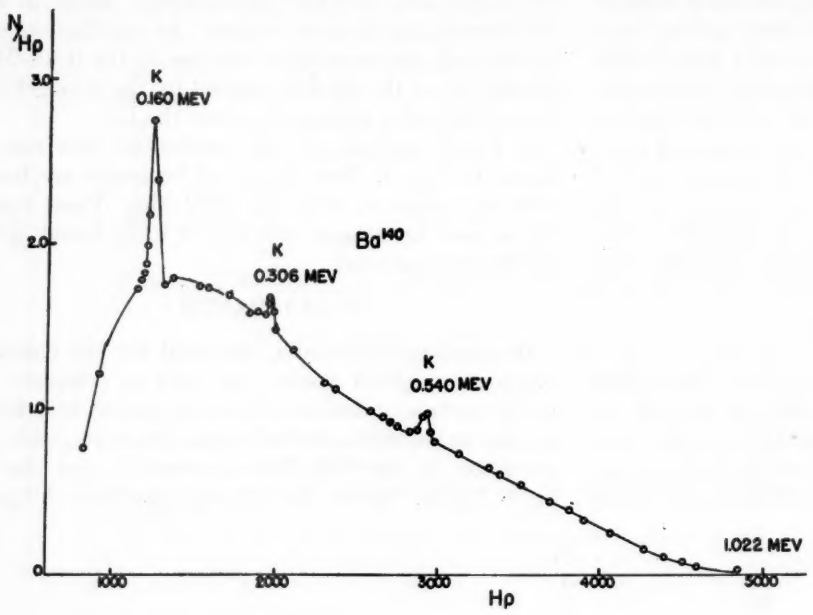

FIG. 2. Beta-ray spectrum of Ba^{140}. The energies given are those of the gamma-rays, not the conversion lines.

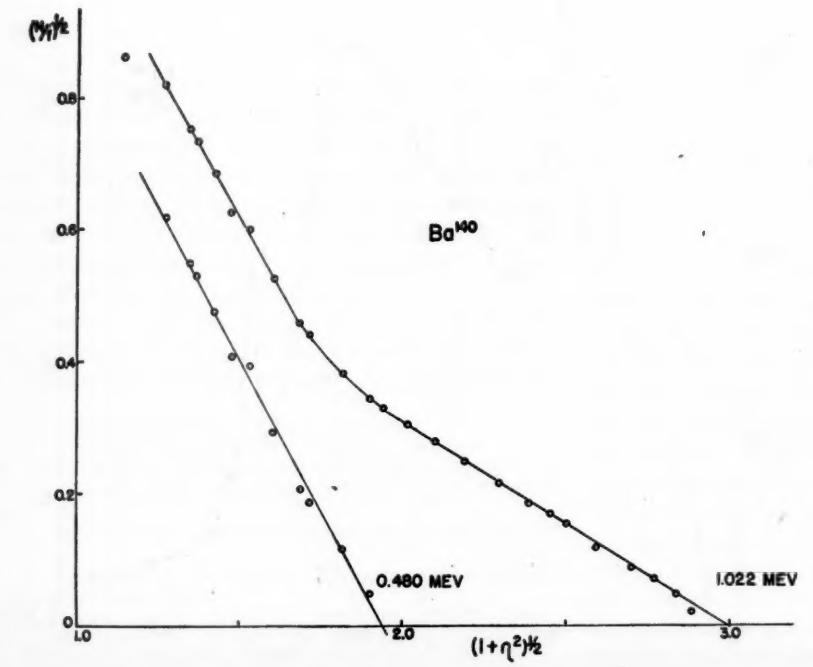

FIG. 3. Conventional Fermi plot of the beta-ray spectrum of Ba^{140}.

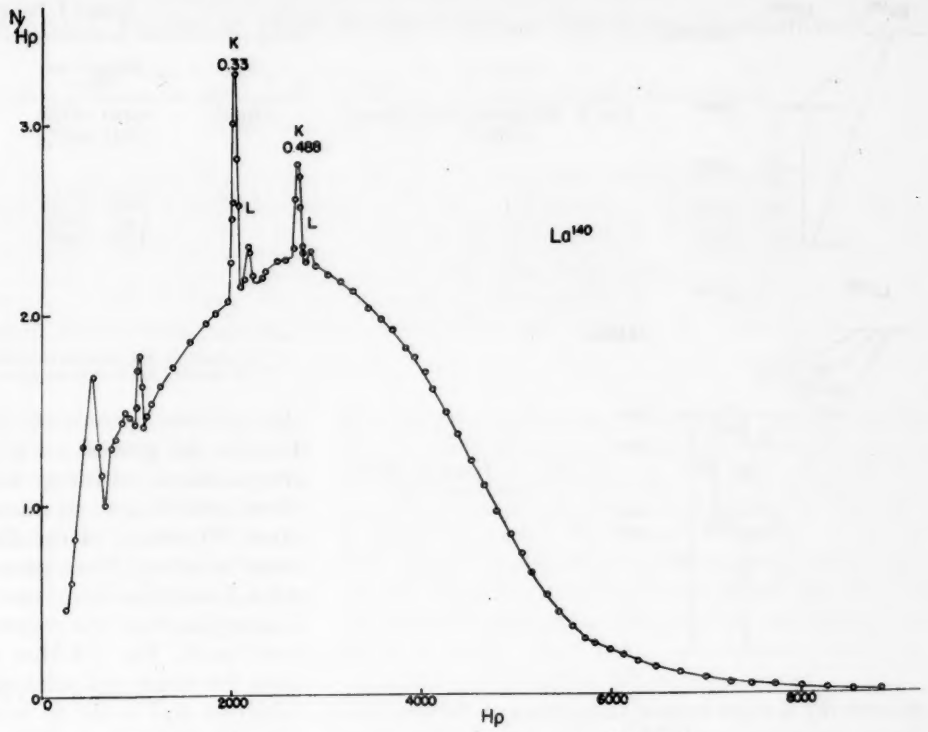

FIG. 4. Beta-ray spectrum of La^{140}. The energies given are those of the gamma-rays, not the conversion lines.

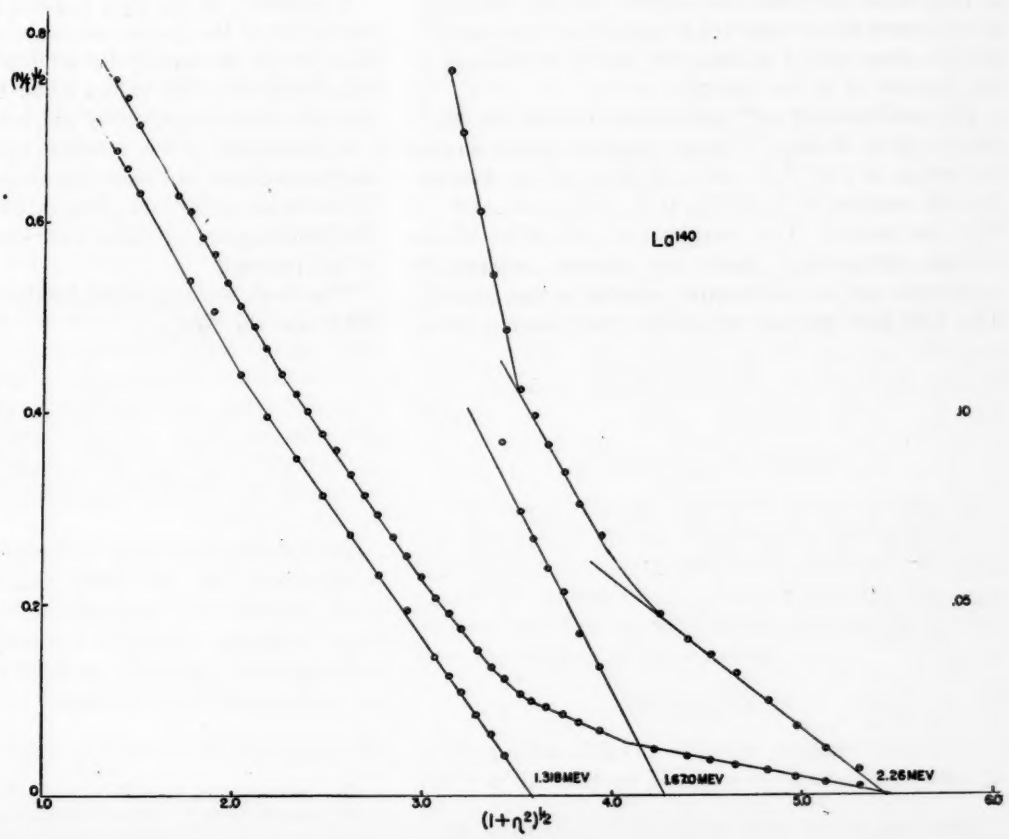

FIG. 5. Conventional Fermi plot of the beta-ray spectrum of La^{140}.

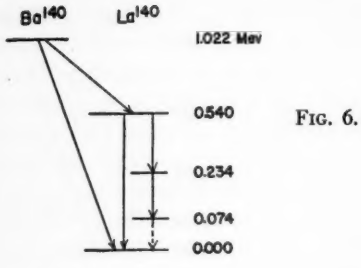

FIG. 6. Proposed decay sheme of Ba^{140}.

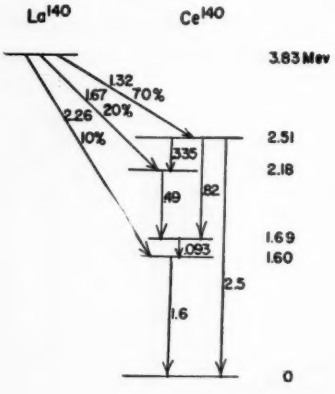

FIG. 7. Tentative decay scheme of La^{140}.

gamma-ray is more intense than either of the other two and is, therefore, probably not in cascade with them. Coincidence experiments done in this laboratory to verify this were inconclusive because of the masking effect of the La^{140}. A tentative decay scheme is given in Fig. 6. To complete the scheme, it would be necessary to prove the existence of a weak 70-kev gamma-ray. In this case, such a gamma-ray would be difficult to find because of its low energy.

The radiations of La^{140} are summarized in the decay scheme given in Fig. 7. Three beta-ray groups having end points at 1.32, 1.67, and 2.26 Mev and six gamma-rays of energies 0.093, 0.335, 0.49, 0.82, 1.60, and 2.5 Mev are present. The energies and intensities of the various components make the scheme remarkably consistent and no alternative scheme seems possible. The 1.60-Mev gamma-ray is the most intense, while

TABLE I. Summary of data.

	Beta-energy (Mev)	Gamma-energy (Mev)*	Gamma-ray No.**
Ba^{140}	0.480 (40%)	0.160 (IC)	
	1.022 (60%)	0.306 (IC)	
		0.540 (IC)	3
La^{140}	1.32 (70%)	0.093? (IC)	
	1.67 (20%)	0.335 (IC)	1
	2.26 (10%)	0.490 (IC)	2
		0.820	4
		1.600	5
		2.50	

* (IC) signifies that internal conversion of the gamma-ray was observed.
** The number in this column refers to the legend of Fig. 1.

the 2.5-Mev gamma-ray is probably the weakest. Perhaps the grestest uncertainty is the assignment of the gamma-ray of energy 0.093 Mev. If this is to follow three gamma-rays, as shown, it must be present in about 90 percent of the disintegrations and therefore must be strong. Since the assignment is based on two weak conversion lines, one is led to the questionable assumption that the conversion of the gamma-ray is very small. The 2.5-Mev gamma-ray was estimated from the visual end point of the Compton-electron distribution and is not as accurately determined as the rest. However, the value obtained is consistent with the decay scheme suggested in Fig. 7 and the value which Wattenberg[7] has obtained by quite different means $(D-\gamma-n)$.

A summary of the data is given in Table I. Relative intensities of the gamma-rays are not given since estimates must necessarily be arbitrary for such complex disintegrations. The values given by Rall and Wilkinson[1] and Miller and Curtiss[6] are, however, thought to be a fair measure of the relative intensities. Conversion coefficients have not been calculated since this requires a knowledge of the branching ratios of the gamma-rays. The results given in Table I are thought to be accurate to one percent.

This work was supported by the Joint Program of the ONR and the AEC.

Limits for the Diffusion Theory of High Frequency Gas Discharge Breakdown*

SANBORN C. BROWN AND A. D. MACDONALD**
Research Laboratory of Electronics, Massachusetts Institute of Technology, Cambridge, Massachusetts
(Received August 5, 1949)

A study is made of the limits within which diffusion phenomena control the breakdown of a high frequency discharge. The discussion is based on proper variables for dimensional analysis, using the parameters $p\Lambda$, $p\lambda$ and $E\Lambda$, where p is the pressure, Λ the characteristic diffusion length, λ the wave-length of the excitation, and E the breakdown electric field. The limits of applicability of the diffusion theory are found to be a uniform field limit, a mean free path limit, and an oscillation amplitude limit. Within these limits, a single function for the effective breakdown voltage, $E\Lambda$, and the energy per mean free path, E/p, correlated the breakdown voltages for all published data tested, covering a wave-length range from 10 cm to 17,000 cm.

THE breakdown mechanism for a high frequency a.c. gas discharge is much simpler than that for the corresponding d.c. breakdown. It is for this reason that relatively simple exact theories may be written for breakdown at the high frequencies. It is important to determine over how wide a range in frequency and pressure these discharge theories are applicable, and such a study for the case of hydrogen is the subject of this paper.

I. DIMENSIONAL ANALYSIS

If a gas contained in a vessel is placed in an alternating electric field, for a certain value of the electric field, the gas will break down into an electrical discharge. This breakdown field can be expressed as

$$E_b = E(u_i, \Lambda, \lambda, p),$$

where E is the electric field intensity; u_i is the ionization potential; Λ is a parameter describing the vessel; λ is the wave-length of the exciting field; and p is the pressure. The field E is measured in volts per cm, and u_i is measured in volts. The term Λ has the units of length, and its appearance in explicit calculations also involves various known dimensionless ratios to describe the shape of the vessel. It is customary to measure pressure in millimeters of mercury, and the mean free path, which is inversely proportional to pressure, is measured in centimeters. A relation between pressure and mean free path is obtained by introducing a quantity, P_c, which is the number of collisions per mean free path at 1 mm Hg pressure. Thus, P_c, which is called the probability of collision, may be regarded as having the units of reciprocal length, even though this is not its true dimension.

Treating the breakdown problem dimensionally, there are five variables with but two fundamental dimensions, volts and centimeters. This leads to three independent dimensionless variables between which there is a functional relation.[1] It is often convenient in physical problems to introduce variables which are not dimensionless but are nevertheless proper variables for dimensional analysis because the completely dimensionless variables contain one or more physically invariant quantities which need not be carried along in a practical discussion. There are a number of sets of such proper variables in a gas discharge problem which may be transformed into one another and their relative convenience depends on the purpose for which they are to be used.

One very useful set of proper variables is

$$E\Lambda,\ p\Lambda,\ p\lambda. \tag{1}$$

The advantage of these variables lies in the fact that p, Λ, and λ are the experimentally independent parameters which determine the dependent variable E, the observed breakdown field. These are the same variables which give the Paschen law in d.c. breakdown, since in d.c., $p\lambda$ has no meaning; $E\Lambda$ is analogous to voltage and $p\Lambda$ to the parallel plate pd.

Another set of proper variables which we shall use is obtained by dividing the first variable in (1) by the second and so obtaining

$$E\Lambda,\ E/p,\ p\lambda. \tag{2}$$

This set has the particular advantage, in a discussion of breakdown phenomena, that we may define[2] an ionization coefficient $\zeta = 1/E^2\Lambda^2$ which is a function of E/p and $p\lambda$. In many ways, ζ is equivalent to the Townsend first coefficient $\eta(\text{volt}^{-1})$ which is a function of E/p alone.

II. DIFFUSION THEORY

The simplest breakdown condition to calculate is for the high frequency case in which the ionization rate is balanced by the loss of electrons by diffusion. The simplicity lies in the absence of complicating secondary phenomena. This breakdown criterion may be derived from the solution of the equation

$$\nabla^2\psi + (\nu/D)\psi = 0, \tag{3}$$

where $\psi = Dn$. D is the diffusion coefficient for electrons and n is the electron density, and the product must be

* This work has been supported in part by the Signal Corps, the Air Materiel Command, and ONR.
** Now at Dalhousie University, Halifax, Nova Scotia.
[1] P. W. Bridgman, *Dimensional Analysis* (Yale University Press, New Haven, Connecticut, 1922), Chapter 4.

[2] M. A. Herlin and S. C. Brown, Phys. Rev. 74, 291 (1948).

equal to zero on the boundary. The quantity ν is the net production rate per electron. For the case of infinite parallel plates with a uniform field, the solution to Eq. (3) is

$$\psi = A \sin(z/\Lambda), \tag{4}$$

where z is the distance from one plate to an arbitrary point in the cavity, and A is a constant. The length parameter Λ used in the above dimensional analysis is called the characteristic diffusion length, and can be calculated exactly for a few common shapes of discharge tube. For example, with a cylinder of radius R and length L,

$$1/\Lambda = [(\pi/L)^2 + (2.405/R)^2]^{\frac{1}{2}}. \tag{5}$$

When the sideways diffusion to the walls is negligible, the parallel plate case results, namely $\Lambda = L/\pi$, while only the last term of Eq. (5) is important for very long cylindrical tubes.

Certain basic assumptions are made in the calculations of breakdown as a balance between the ionization rate and the loss of electrons by diffusion. We examine here the limits which the assumptions place on the application of the theory to various experimental conditions. These can be discussed in terms of the proper independent variables of Eq. (1), $p\Lambda$ and $p\lambda$. One can plot on the $p\Lambda - p\lambda$ plane the conditions for all breakdown data for a single gas and derive limits in these variables which will define the applicability of the diffusion theory.

III. UNIFORM FIELD LIMIT

The solution of Eq. (3) in the form given in Eq. (4) assumes a uniform field between infinite parallel plates. At low frequencies, the experimental measurements of breakdown are always taken in vessels whose dimensions are small compared to a wave-length of the exciting power. For this case, the uniform field assumption may be very good. At very high frequencies, there exists a limit to the size of the discharge tube consistent with the uniform field assumption of the diffusion theory.

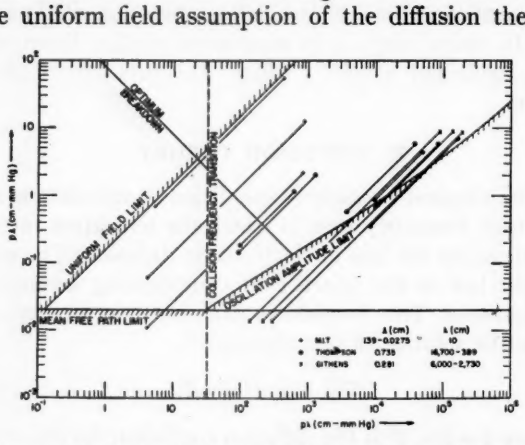

FIG. 1. A plot of the limits of the diffusion theory for breakdown of high frequencies in terms of variables derived from dimensional analysis. The extent of experimental data is represented by 45° lines.

This can be written in terms of the size of vessel allowable to sustain a single loop of a standing wave of the electric field. The relation between the parallel plate separation, the wave-length, and the diffusion length given in Eq. (5) may be written as

$$\lambda/2 = \pi\Lambda. \tag{6}$$

For parallel plates where the separation is small, so that sideways diffusion can be neglected, $\lambda/2 = L$. In general, however, we must use both terms in Eq. (5). Thus one arrives at a limit which may be written in terms of $p\lambda$ and $p\Lambda$ as:

$$p\lambda = 2\pi(p\Lambda). \tag{7}$$

This limiting line is plotted in Fig. 1 and designated as the Uniform Field Limit.

IV. MEAN FREE PATH LIMIT

The diffusion theory will not apply where the electron mean free path becomes comparable to the tube size. In the limiting case, this can be expressed as the mean free path, l, being equal to Λ. The probability of collision, P_c, is equal to $1/pl$. To plot this condition in Fig. 1, we may write

$$p\Lambda = 1/P_c. \tag{8}$$

The value of P_c is not a constant, but depends upon the electron energy. Assuming that the average electron has an energy equal to one-third of the ionization potential, the average electron energy would be 5.1 volts for hydrogen. Using Brode's[3] measured value for the probability of collision in hydrogen for the average electron, $P_c = 49$ (cm−mm Hg)$^{-1}$. With this value, we obtain the horizontal line in Fig. 1 marked Mean Free Path Limit.

V. COLLISION FREQUENCY TRANSITION

Within the limits of experimental conditions in which diffusion theory adequately explains the breakdown behavior, several different phenomena may occur. One of the phenomenological changes which is important is the transition from many collisions per oscillation of the electron to many oscillations per collision. This can be written as the condition that $\nu_c = \omega$, where ν_c, the collision frequency, is the ratio of the average velocity v to the mean free path, and ω is the radian frequency of the applied field. From Brode's data, we can obtain a relation, $\nu_c = 5.93 \times 10^9 p$. Putting this in terms of the proper variables, we obtain

$$p\lambda = 32. \tag{9}$$

This relation is plotted in Fig. 1 as the dotted line marked as the Collision Frequency Transition.

On the low pressure side of this transition, the oscillatory velocity of the electron lags the applied field by nearly 90°, and little energy is transferred from the ap-

[3] R. B. Brode, Rev. Mod. Phys. 5, 257 (1933).

plied field to the electron. As the pressure increases, the increasing frequency of interruption of electron oscillation decreases the lag, and the resulting in-phase component of the velocity represents an increasing absorption of energy. This may be taken into account by introducing an effective field[4] for energy transfer, defined by the relation

$$E_e^2 = E^2 \frac{\nu_c^2}{\nu_c^2 + \omega^2}, \tag{10}$$

where E is the r.m.s. value of the applied alternating field and ω is the radian frequency. E_e is therefore the effective field which would produce the same energy transfer as a steady field.

VI. OPTIMUM BREAKDOWN

The most striking characteristic of the effects of changing pressure on the breakdown field intensity is the fact that at high pressure the field decreases with decreasing pressure, and at low pressure the field increases with decreasing pressure. In discussing this effect, let us start with high pressure. Here the power which goes into the electron from the electric field is dissipated in elastic collisions between the electrons and the gas molecules. The region corresponds to the lowest values of E/p measured experimentally. The data on either the Townsend first ionization coefficient or the a.c. ionization coefficient[5] show that here E/p is a constant equal in hydrogen to 10 r.m.s. volts/cm/mm Hg. Thus for a discharge in which nearly all the loss goes into non-ionizing collisions, the field and pressure are related by the equation

$$E = 10p. \tag{11}$$

In the low pressure region, the electrons make many oscillations per collision and the breakdown field may be determined by equating the number of collisions to ionize to the number of collisions to diffuse out of the tube. The change in energy of an electron on collision is $\Delta u = (m/2e)\langle(\Delta v^2)\rangle_{Av}$ where $\langle\Delta v^2\rangle_{Av}$ is the average value of the square of the change in velocity on collision. Since

$$\langle\Delta v^2\rangle_{Av} = (E_e e/m)^2 \langle t_c^2\rangle_{Av},$$

where E_e is the effective value of the field, and the mean squared collision time $\langle t_c^2\rangle_{Av}$ is given by $2l^2/v^2$ from kinetic theory, we may write for the change in energy on collision

$$u = \frac{E_e^2 e}{m}\frac{l^2}{v^2} = \frac{E_e^2 e}{m}\frac{1}{\nu_c^2}.$$

An electron can reach ionization energy in n collisions when

$$n\Delta u = u_i.$$

[4] H. Margenau, Phys. Rev. **69**, 508 (1946).

[5] See, for example, Fig. 4 of A. D. MacDonald and S. C. Brown, Phys. Rev. **76**, 1634 (1949).

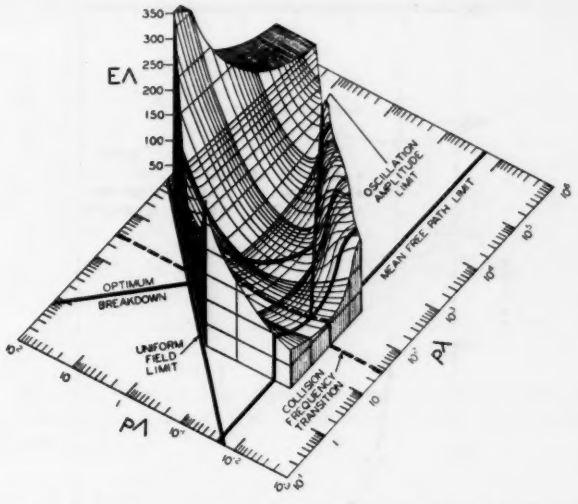

FIG. 2. A surface constructed from the experimental determinations indicated in Fig. 1, correlating the breakdown voltage measurements in terms of variables derived from dimensional analysis.

The number of collisions to diffuse out of a tube of size Λ is calculated from kinetic theory[6] to be $(\frac{3}{2})(\Lambda^2/l^2)$ and hence

$$\frac{u_i \nu_c^2}{E_e^2/m} = \frac{3}{2}\frac{\Lambda^2}{l^2}.$$

Substituting in this equation the value of the effective field from Eq. (10) and rearranging terms, the resulting expression for E becomes

$$E = \frac{2\pi c}{\Lambda\lambda P_c p}\left(\frac{2}{3}\frac{u_i}{e/m}\right)^{\frac{1}{2}}. \tag{12}$$

For hydrogen, this equation reduces to

$$E = 785/p\Lambda\lambda. \tag{13}$$

Equation (11) gives the relation between field and pressure at high pressure and Eq. (13) the relation at low pressure. Eliminating the field between these two equations will allow us to calculate the pressure at which breakdown will occur most easily. In terms of the variables of Fig. 1, this leads to the equation

$$p\lambda = 78.5/p\Lambda. \tag{14}$$

This relation is plotted in Fig. 1 as the line marked as the Optimum Breakdown.

VII. OSCILLATION AMPLITUDE LIMIT

When the amplitude of the electron oscillation in the electric field is sufficiently high, the electrons can travel completely across the tube and collide with the walls on every half cycle. The presence of the gas complicates

[6] E. H. Kennard, *Kinetic Theory of Gases* (McGraw-Hill Book Company, Inc., New York, 1938), p. 273.

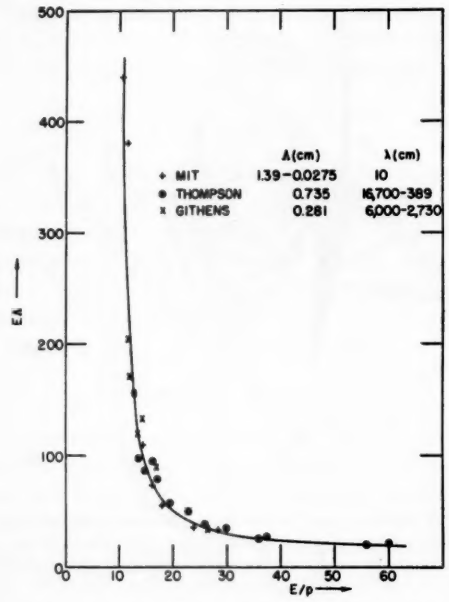

FIG. 3. Effective breakdown voltages as a function of E/p calculated from breakdown measurements of numerous workers (see references 8, 10, and 11).

the problem somewhat, but Gill and Donaldson[7] showed that this phenomenon accounts for abrupt changes in the breakdown behavior.

The electric field may be written in the form

$$E=E_p \sin\omega t,$$

where E_p is the peak value. Under the action of the field, an electron is accelerated an amount Ee/m for the time between collisions t_c to attain a velocity given by

$$v=at_c=(eE/m)1/\nu_c, \tag{15}$$

where ν_c is the collision frequency. Putting in the sinusoidal variation of the field with time,

$$v=(eE_p/m)(1/\nu_c)\sin\omega t,$$
$$x=(eE_p/m\omega\nu_c)\cos\omega t.$$

The limiting case on the diffusion mechanism in which all of the electrons will hit the walls would be calculated by setting the oscillation amplitude equal to one-half of the electrode separation. In order to take account of the greater density of electrons at the center due to the sinusoidal spatial distribution, the distance the electrons must travel is multiplied by the average value of the sine function. Thus, the oscillation amplitude becomes equal to

$$(eE_p/m\omega\nu_c)=L/\pi. \tag{16}$$

Substituting λ in terms of ω, v/l in place of ν_c, and $1/pP_c$ for l, we obtain

$$p\lambda=\left(\frac{2mc}{e}vP_c\right)\frac{pL}{(E_p/p)}. \tag{17}$$

[7] E. W. B. Gill and R. H. Donaldson, Phil. Mag. **12**, 719 (1931).

Examination of Brode's data for the probability of elastic collision of an electron with hydrogen shows that over most of the energy range, the hyperbolic form of the curve gives $vP_c=5.96\times10^9$ (sec.—mm Hg)$^{-1}$. Putting this numerical value in Eq. (17), and using the parallel plate relation that $L=\pi\Lambda$, Eq. (17) reduces to

$$p\lambda=2\pi\times10^5\left(\frac{p\Lambda}{E_p/p}\right). \tag{18}$$

This equation can be solved numerically where experimental values of the breakdown field are available. Experiments of this sort have been carried out for parallel plate geometry using hydrogen gas, and numerical values for Eq. (18) can therefore be determined. This calculation yields the oscillation amplitude limit of Fig. 1.

VIII. CORRELATION OF DATA OF VARIOUS WORKERS

Many experimenters have studied the breakdown of a gas discharge at various frequencies and in various different geometrical arrangements. Most workers have obtained breakdown data for hydrogen and several have included in their reports sufficient detail to enable the parameters p, λ, and Λ to be determined. Since the data were determined by measuring breakdown voltage in a given size container at a given applied frequency at various pressures, a single run plots as a line at 45° in Fig. 1. In this figure, the range of data in $p\lambda$ and $p\Lambda$ taken by several observers is indicated by such lines. Many of the breakdown curves which have been obtained have complicated shapes and it is difficult to visualize a correlation in a two-dimensional plot between different workers. On the other hand, if we make a three-dimensional plot in which the horizontal axes are the $p\lambda$, $p\Lambda$ parameters of Fig. 1 and the vertical axis the effective breakdown voltage $E\Lambda$, all available data may be represented on a single surface. This is done in Fig. 2. Breakdown voltage data between parallel plates for hydrogen for the experimental conditions of $p\lambda$ and $p\Lambda$ (shown in Fig. 1) were used to construct this surface. The data covers a wave-length range from 17,000

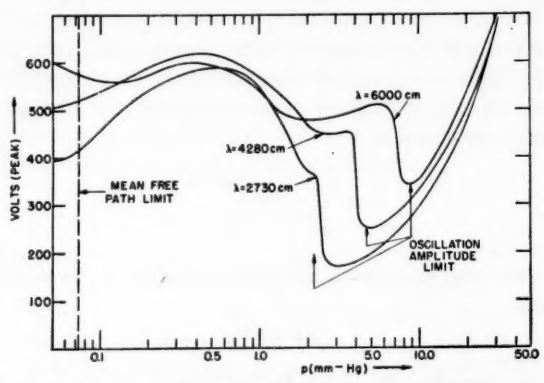

FIG. 4. Breakdown measurements in hydrogen by Githens (reference 8) showing calculated and observed transition points.

cm to 10 cm and a range in Λ from 1.4 cm to 0.0275 cm and the surface extends only as far as experimental data exist from which to construct it. One can see that in the diffusion theory regions, the curves are smooth and well behaved, as one would expect if a single theory were applicable. In crossing over the oscillation amplitude limit, the breakdown curves appear to be much more complicated due to the effects of secondary electrons produced by the collision of the electrons with the walls or electrodes of the discharge vessel.

Sufficient data are available to check the generality of the breakdown theory at high pressure where the electrons make many collisions per oscillation. In the region where the diffusion theory is valid, one should observe the same value of the effective breakdown voltage $E\Lambda$ at a given value of the energy per mean free path E/p, independent of the frequency at which the measurements are made. Figure 3 shows this to be the case since a single curve is determined, within the limits of experimental accuracy, for breakdown in hydrogen using data taken by various observers over a wide range of wave-length and discharge tube size.

IX. DISCUSSION

The general agreement of the shape of the experimental curves with the limits shown in Fig. 1 is illustrated by the position of these limits on the three-dimensional projection of Fig. 2. To illustrate this agreement in a more quantitative fashion, sets of curves by different workers are shown in Figs. 4 and 5. Figure 4 shows data taken with a given electrode spacing, hence fixed Λ, for different wave-lengths.[8] The calculated positions of the oscillation amplitude limit for the given frequencies are shown by the appropriately marked arrows. The portions of the curves to the right of these arrows lie in the region where electron diffusion controls, and it is from these parts of the curves that the data in Fig. 3 were taken. The complicated shape of the curves to the left of the oscillation amplitude limit involves the production of secondary electrons at the electrodes or walls of the container. Such curves have been reported by numerous observers.[8–10] Well-defined changes in the data can be recognized where the data cross the mean free path limit.

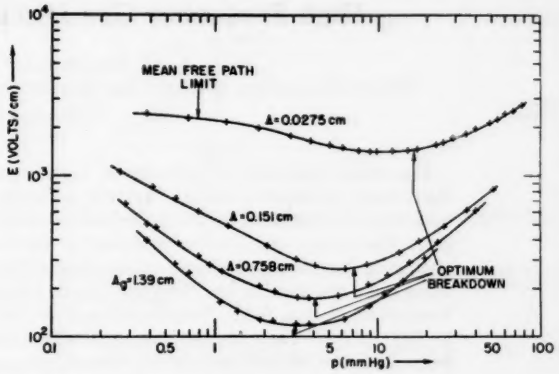

FIG. 5. Breakdown measurements in hydrogen (see reference 5) at 10 cm wave-length showing calculated and observed transition points.

Experiments carried out at microwave frequencies[11] allow one to explore the transition through the optimum breakdown condition. Figure 5 shows a series of runs for breakdown field as a function of pressure taken at a constant frequency for different values of Λ. When Λ is high, corresponding to large plate separation, the curves cross only one controlling transition, that from many collisions per oscillation to many oscillations per collision where the shape of the curve is given by expression (1). When the value of Λ is very small, on decreasing pressure, the data first cross the optimum breakdown condition and then the mean free path limit. The values of Λ shown in Fig. 5 are the geometrical values calculated from Eq. (5), since it is these values which are used in computing $p\Lambda - p\lambda$ values for inclusion in Fig. 1. In calculating the $E\Lambda$ values in Figs. 2 and 3, a correction must be applied for those cases where the height is so great that the cavity cannot be considered a parallel plate system. The two largest cavities of Fig. 5 required this correction which was carried out in accordance with the non-uniform field theory given in a recent paper by Herlin and Brown.[12]

[8] S. Githens, Phys. Rev. **57**, 822 (1940).
[9] C. Gutton and H. Gutton, Comptes Rendus **186**, 303 (1928).
[10] J. Thompson, Phil. Mag. **23**, 1 (1937).
[11] See reference 5.
[12] M. A. Herlin and S. C. Brown, Phys. Rev. **74**, 1650 (1948).

High Frequency Gas Discharge Breakdown in Hydrogen*

A. D. MacDonald** and Sanborn C. Brown
Research Laboratory of Electronics, Massachusetts Institute of Technology, Cambridge, Massachusetts

(Received August 5, 1949)

Electrical breakdown of hydrogen at high frequencies has been treated theoretically on the basis of the Boltzmann transport equation. Inelastic collisions are taken into account as a loss term in the Boltzmann equation and measured values of the ionization efficiency are used in the integral determining the ionization rate. The energy distribution function for electrons may be expressed in terms of the confluent hypergeometric function and simple exponentials. The ionization rate and diffusion coefficient are calculated using these distribution functions and kinetic theory and are combined with the diffusion equation to predict breakdown electric fields. These predicted electric fields are compared with experimental values measured at 3000 mc/sec. They are also compared with older measurements by other workers at frequencies ranging from 3 mc/sec. to 100 mc/sec. The breakdown equation calculated from kinetic theory and using no gas discharge data other than the collision cross-section measurements and involving no adjustable constants predicts breakdown electric fields well within the limits of accuracy determined by these cross sections over a large range of pressure, container size and frequency of applied field.

THE theory, based on a solution of the Boltzmann transport equation for electrons, which was used in predicting breakdown in helium,[1] has been applied to molecular hydrogen. The method follows closely that used in reference 1, but some of the simplifications used in treating helium are not permissible in the case of hydrogen. The second-order differential equation derived from the Boltzmann equation is solved for the electron distribution function. The ionization rate and diffusion coefficient are calculated using standard kinetic theory formulas. The breakdown condition is that the number of electrons produced by ionization equal the number diffusing to the walls of the container. This breakdown condition is combined with a solution of the diffusion equation, the ionization rate, and diffusion coefficient to obtain an equation which predicts breakdown electric fields.

I. THE BOLTZMANN EQUATION

The phase space continuity equation for electrons is[1,2]

$$C=\partial f/\partial t+\mathbf{v}\cdot\nabla f+\mathbf{a}\cdot\nabla_v f, \tag{1}$$

where f is the electron energy distribution function; C is the net rate at which electrons appear in an element in phase space and is calculated in terms of f by determining energy changes due to collision; $\mathbf{v}$ is the velocity, $\mathbf{a}$ the acceleration, t the time, and ∇_v the gradient operator in velocity space.

The distribution function may be expanded in spherical harmonics in velocity,

$$f=f_0+\frac{\mathbf{v}\cdot\mathbf{f}_1}{v}+\cdots. \tag{2}$$

The spherically symmetric term f_0 is predominant because collisions tend to disorder any directional motion of the electrons. The series is rapidly convergent and we shall consider only those cases where the first two terms represent a good approximation to the distribution function. The limits of theory discussed in the previous paper indicate those values of the experimental parameters for which this approximation is valid.

The term C arising from collisions may also be expanded in spherical harmonics, since it may be represented in terms of integrals over the distribution function. The r.m.s. value of the electric field is given by E, and an energy variable $u=mv^2/2e$ is introduced; m is the mass and e the charge of an electron.

On substitution of these terms and separation of vector and scalar parts, Eq. (1) becomes

$$C_0=\frac{\partial f_0}{\partial t}-\frac{v}{3u}\frac{\partial}{\partial u}(u\mathbf{E}\cdot\mathbf{f}_1)+\frac{v}{3}\nabla\cdot\mathbf{f}_1 \tag{3}$$

and

$$\mathbf{C}_1=\frac{\partial\mathbf{f}_1}{\partial t}+v\nabla f_0-v\mathbf{E}\frac{\partial\mathbf{f}_0}{\partial u}. \tag{4}$$

Elastic collisions are accounted for in the manner of Morse, Allis, and Lamar,[3] who considered collisions as instantaneous processes and found equivalent energy loss terms by conserving momentum and energy and averaging over space at each collision. It is shown in reference 3 that these terms are

$$C_{0el}=\frac{2m}{M}\frac{v}{u}\frac{d}{du}\left(\frac{u^2 f_0}{l}\right) \tag{5}$$

and

$$\mathbf{C}_{1el}=-\frac{v}{l}\mathbf{f}_1, \tag{6}$$

where l is the electronic mean free path and M is the

* This work has been supported in part by the Signal Corps, the Air Materiel Command, and ONR.

** Now at Dalhousie University, Halifax, Nova Scotia.

[1] A. D. MacDonald and S. C. Brown, Phys. Rev. 75, 411 (1949).

[2] S. Chapman and T. G. Cowling, *The Mathematical Theory of Non-Uniform Gases* (Cambridge University Press, London, 1939), Chapter 3; H. Margenau, Phys. Rev. 69, 508 (1946); 73, 303 (1948); Morse, Allis, and Lamar, Phys. Rev. 48, 412 (1935).

[3] Morse, Allis, and Lamar, Phys. Rev. 48, 412 (1935).

mass of the molecule. The remainder of the C_0 term results from inelastic collisions and may be represented by $-h_x(v/l)f_0-h_i(v/l)f_0$, where h_x and h_i are efficiencies of excitation and ionization, respectively. Inelastic collisions have no angular dependence and therefore do not enter the higher order terms in the distribution function.

Each term in the distribution function may be expanded in a Fourier series in time

$$f_n=f_n^0+f_n^1e^{j\omega t}+\cdots, \tag{7}$$

where ω is the radian frequency of the applied electric field. The electric field is represented by $\sqrt{2}Ee^{j\omega t}$ and in the expansion of Ef_n, we must replace the exponential notation by its real part before taking the product, so that

$$\sqrt{2}Ef_n=2Ef_n^0e^{j\omega t}+Ef_n^1(1+2e^{2j\omega t})+\cdots. \tag{8}$$

Combining the results of Eqs. (5), (6), and (8) with Eqs. (3) and (4) and equating terms in like exponents of t, we have

$$-(h_x+h_i)\nu_c f_0^0=\frac{v}{3}\nabla\cdot\mathbf{f}_1^0-\frac{v\mathbf{E}}{3u}\cdot\frac{\partial}{\partial u}(u\mathbf{f}_1^1)$$

$$-2\frac{mv}{Mu}\frac{\partial}{\partial u}\left(\frac{u^2f_0^0}{l}\right), \tag{9}$$

$$\nu_c\mathbf{f}_1^0=-v\nabla f_0^0, \tag{10}$$

$$(\nu_c+j\omega)\mathbf{f}_1^1=v\mathbf{E}\frac{\partial}{\partial u}f_0^0. \tag{11}$$

In these equations, v/l has been replaced by ν_c and the terms in f_0^1 have been dropped. The f_0^1 term represents the first harmonic of the spherically symmetric part of the distribution function and cannot be generated physically unless there is either a d.c. field or the amplitude of oscillation of the electric field is sufficient to sweep out electrons from the container each half cycle.

Equations (10) and (11) may be substituted in Eq. (9) to derive an equation for f_0^0. From this point on, we shall drop the subscripts and superscripts on f and understand by f the zero-order term f_0^0. We use the diffusion equation to replace $\nabla^2f_0^0$ by $-1/\Lambda^2f_0^0$, where Λ is the characteristic diffusion length, depending only on the geometry of the discharge container.[4] Thus,

$$-\nu_c(h_x+h_i)f+\frac{2m}{M}\frac{v}{u}\frac{\partial}{\partial u}\left(\frac{u^2f}{l}\right)$$

$$=\frac{lv}{3\Lambda^2}f-\frac{v}{3u}\frac{d}{du}\left\{lu\frac{df}{du}\frac{E^2}{(1+\omega^2/\nu_c^2)}\right\}, \tag{12}$$

[4] M. A. Herlin and S. C. Brown, Phys. Rev. 74, 291 (1948).

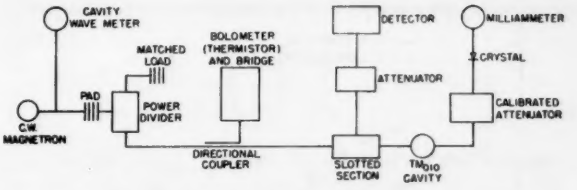

FIG. 1. Block diagram of experimental microwave apparatus.

where we take only the real part in the last of these terms, as f is real.

II. COLLISION CROSS SECTION

In Eq. (12), we must now specify l, h_x, and h_i. As was the case in helium, the collision frequency for elastic collisions in hydrogen is constant in energy[1,5] to a very good approximation. Using Brode's data, we obtain the value of $\nu_c=5.93\times10^9p(\text{sec.}^{-1})$ (p in mm of Hg).

The excitation and ionization efficiencies for hydrogen have been measured by Ramien.[6] A linear approximation to his data gives

$$h_x+h_i=h_{1x}(u-u_x)=9.0\times10^{-3}(u-8.9), \quad u\gtrsim8.9 \text{ volts}.$$

The fact that some energy goes into excitation below the dissociation level is explained by Ramien on the basis of wave mechanics.

The ionization efficiency h_i is approximated by

$$h_i=h_{1x}(u-u_i)=9.4\times10^{-3}(u-16.2), \quad u\gtrsim16.2 \text{ volts}.$$

These efficiencies are to be substituted in Eq. (12) from which the distribution function is determined. Below the lowest excitation level, the term in h_x+h_i is zero and the distribution function is similar to that found for helium.[1] Above this level, the differential equation for the distribution function is different and the solution must be matched in magnitude and slope to the previously determined one.

III. THE DISTRIBUTION FUNCTIONS

We let

$$\mu=\frac{3m}{M}\frac{m}{e}\Lambda^2\nu_c^2,$$

$$\beta=\frac{(E\Lambda)^2}{\omega^2/\nu_c^2+1},$$

and then Eq. (12) becomes

$$u\frac{d^2f}{du^2}+\left(\frac{3}{2}+\frac{\mu u}{\beta}\right)\frac{df}{du}$$

$$+f\left[\frac{3}{2}\frac{\mu}{\beta}-\frac{u}{\beta}-\frac{1}{2}\frac{M}{m}\frac{\mu}{\beta}(h_x+h_i)\right]=0. \tag{13}$$

[5] R. B. Brode, Rev. Mod. Phys. 5, 257 (1933).
[6] H. Ramien, Zeits. f. Physik 70, 353 (1931).

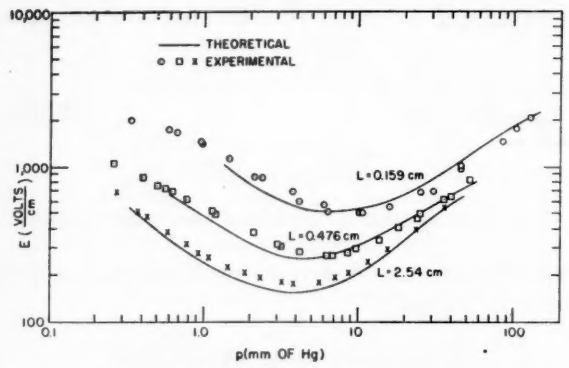

FIG. 2. Comparison of experimental electric fields with those theoretically predicted from Eq. (29) (3000 mc/sec.).

For convenience, we introduce a dimensionless independent variable

$$w=\frac{\mu}{\beta}\left(1+\frac{4\beta}{\mu^2}\right)^{\frac{1}{2}}u=\frac{\mu}{\beta}bu.$$

Equation (13) becomes

$$\frac{d^2f}{dw^2}+\left(\frac{1}{b}+\frac{3}{2w}\right)\frac{df}{dw}+f\left[\frac{3}{2bw}-\frac{\beta}{\mu^2b^2}-\frac{M}{2m}\frac{h_x}{wb}\right]=0. \quad (14)$$

When $u<8.9$ volts, we transform the dependent variable

$$f=g\exp\left[-\frac{1}{2}\left(\frac{1}{b}+1\right)w\right],$$

and the differential equation becomes

$$w\frac{d^2g}{dw^2}+\frac{dg}{dw}\left(\frac{3}{2}-w\right)-\alpha g=0, \quad (15)$$

where

$$\alpha=\tfrac{3}{4}[1-(1/b)].$$

Equation (15) is the differential equation for the confluent hypergeometric function; therefore, we may write the two independent solutions

$$g_1=M(\alpha;\tfrac{3}{2};w)\ g_2=w^{-\frac{1}{2}}M(\alpha-\tfrac{1}{2};\tfrac{1}{2};w). \quad (16)$$

Hereafter, for brevity, we shall use the notation

$$M(\alpha;\tfrac{3}{2};w)=M_1(w)$$
$$w^{-\frac{1}{2}}M(\alpha-\tfrac{1}{2};\tfrac{1}{2};w)=M_2(w).$$

Tables of the confluent hypergeometric function are available.[7]

For u greater than 8.9 volts, we transform Eq. (14) to the reduced form by letting

$$f=y\left\{\exp\left[-\frac{1}{2}\int\left(\frac{1}{b}+\frac{3}{2w}\right)dw\right]\right\}. \quad (17)$$

Then

$$(d^2y/dw^2)+I(w)y=0, \quad (18)$$

where

$$I(w)=\frac{3}{16w^2}+\frac{1}{w}\left[\frac{Mh_{1x}\beta w_x}{2m\mu b^2}+\frac{3}{4b}\right]$$
$$-\frac{\beta}{\mu^2b^2}-\frac{Mh_{1x}\beta}{2m\mu b^2}-\frac{1}{4b^2}. \quad (19)$$

When w is that corresponding to a few tenths of a volt more than 8.9, the first term in Eq. (19) becomes negligible and we may write

$$I=-(A^2w-B/w), \quad (20)$$

where

$$A^2=\frac{h_{1x}\beta M}{2m\mu b^2}+\frac{1}{4},$$

$$B=\frac{1}{b}\left(\frac{h_{1x}M\beta w_x}{2m\mu b}+\frac{3}{4}\right),$$

and in the case of hydrogen, these are numerically,

$$A^2=1.03(E/p)^2[1/(b^2[(31.8/p\lambda)^2+1])]+\tfrac{1}{4},$$

$$B=146/b,$$

and λ is the free-space wave-length of the electric field in cm.

Equation (18) may be written

$$\frac{d^2y}{dw^2}-\frac{A^2w-B}{w}y=0,$$

whose solution is

$$y=e^{-Aw}w^{B/2A}\left[1+\frac{a_1}{w}+\frac{a_2}{w}+\cdots\right]. \quad (21)$$

The series converges rapidly for all values of w which are necessary, and in most cases, a_2 is completely negligible. q_1 and a_2 are given in terms of A and B;

$$a_1=[1-(B/2A)]B/4A^2$$

and

$$a_2=\frac{a_1}{4A}\left[\frac{B}{A}\left(\frac{3}{2}+\frac{B}{4A}\right)-2\right].$$

We shall drop the term in a_2 at this point; although the nature of the final result for the ionization coefficient will indicate how this term affects the answer.

Combining Eq. (21) with Eq. (17), we have

$$f=e^{-wS}w^T[1+(a_1/w)], \quad (22)$$

where $S=A+(1/2b)$ and $T=(B/2A)-3/4$. The solution in Eq. (22) is valid for u a few tenths of a volt above the lowest excitation level, so we extrapolate the

[7] A. D. MacDonald, J. Math. Phys. 28 (October, 1949); "Properties of the confluent hypergeometric function," Technical Report No. 84, Research Laboratory of Electronics, M.I.T., Cambridge, Massachusetts.

solution in Eq. (16) to $u=9.5$ volts and use Eq. (22) for $u>9.5$ volts.

We are now in a position to write down the distribution function

$$f=[M_1(w)+CM_2(w)]\exp[-w(1-\tfrac{2}{3}\alpha)] \qquad u<9.5 \text{ volts}$$
$$=Rw^T\left(1+\frac{a_1}{w}\right)\exp(-wS) \qquad u>9.5 \text{ volts}, \tag{23}$$

where the constants R and C are to be determined by the boundary conditions that the distribution function be continuous in value and slope when $u=9.5$ volts.

If we let

$$\frac{1}{\Phi}=\frac{T}{w_p}-\frac{a_1}{w_p^2(1+a_1/w_p)}-S, \tag{24}$$

these conditions give

$$C=\frac{M_1(w_p)-\Phi[M_1'(w_p)-(1-\tfrac{2}{3}\alpha)M_1(w_p)]}{\Phi[M_2'(w_p)-M_2(w_p)(1-\tfrac{2}{3}\alpha)]-M_2(w_p)} \tag{25}$$

and

$$R=\frac{\exp[-w_p(1-\tfrac{2}{3}\alpha)][M_1(w_p)+CM_2(w_p)]}{e^{-w_pS}w_p^T[1+(a_1/w_p)]}, \tag{26}$$

where w_p is w corresponding to $u=9.5$ volts, and M' denotes differentiation with respect to w.

IV. THE BREAKDOWN CONDITION

We next compute the ionization rate $n\nu$ by the use of formula (16) of reference 1

$$n\nu=-8\pi(e^2/m^2)\int_{u_i}^{\infty}(u/v)\nu_c h_i f du$$
$$=-16\pi(e/2m)^{3/2}(\beta/\mu b)^{5/2}\nu_c R 9.4\ 10^{-3}$$
$$\times\int_{w_i}^{\infty}e^{-wS}[w^V+(D-w_i)w^{V-1}-w_iDw^{V-2}]dw. \tag{27}$$

Evaluation of this integral gives

$$\frac{V!}{S^{V+1}}\left\{1-I(V,Z_i)+\left(\frac{Sa_1-Z_i}{V}\right)[1-I(V-1,Z_i)]-\frac{Sa_1Z_i}{V(V-1)}[1-I(V-2,Z_i)]\right\},$$

where $Z_i=Sw_i$, $V=T+\frac{3}{2}$, $I(x,p)=[\Gamma_x(p+1)/\Gamma(p+1)]$, and $\Gamma_x(p+1)$ is the incomplete Γ-function. Extensive tables of the I functions are available.[8]

[8] K. Pearson, *Tables of Incomplete Γ Function* (His Majesty's Stationers, London, 1922).

The diffusion coefficient, D, is determined from the equation

$$nD=\frac{2\pi}{3\nu_c}\left(\frac{2e}{m}\right)^{5/2}\int_0^{\infty}fu^{3/2}du.$$

After substitution of the distribution function from Eq. (23), the expression for nD becomes

$$nD=\frac{2\pi}{3\nu_c}\left(\frac{2e\beta}{m\mu b}\right)^{5/2}\left\{\int_0^{w_p}w^{3/2}\exp[-w(1-\tfrac{2}{3}\alpha)]\times[M_1(w)+CM_2(w)]dw+R\int_{w_p}^{\infty}w^Ve^{-wS}\left(1+\frac{a_1}{w}\right)dw\right\}. \tag{28}$$

The confluent hypergeometric functions in the first part of the integral in Eq. (28) have been integrated[7] and those in the second integral result in incomplete Γ-functions. The total integral yields

$$\frac{3}{2\alpha}\frac{w_p^{3/2}}{(1-\tfrac{2}{3}\alpha)}\exp[-w_p(1-\tfrac{2}{3}\alpha)]\times\left\{[M_1'(w_p)-\tfrac{2}{3}\alpha M_1(w_p)]+C\left[M_2'(w_p)-\tfrac{2}{3}\alpha M_2(w_p)+\frac{1}{2w_p^{3/2}}\right]\right\}+\frac{RV!}{S^{V+1}}\left\{1-I(V,Z_p)+\frac{Sa_1}{V}[1-I(V-1,Z_p)]\right\}.$$

The high frequency ionization coefficient[4] ζ is then given by

$$\zeta=\frac{\nu}{DE^2}=\frac{1}{\Lambda^2E^2}\left[\frac{282(p\Lambda)^2J}{K+FG}\right] \tag{29}$$

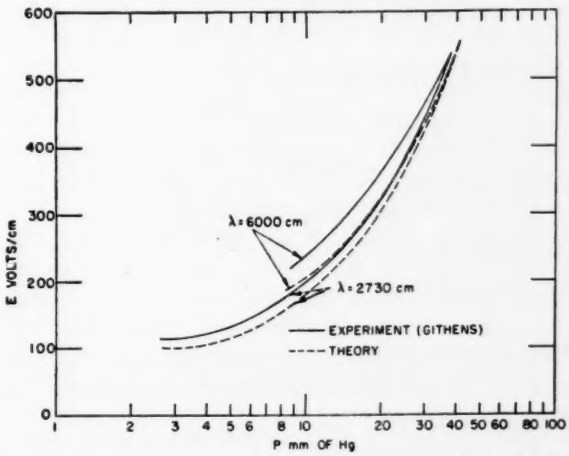

FIG. 3. Comparison of theory of this paper with experiments of Githens (1940) at frequencies of 5 mc/sec. and 11 mc/sec.

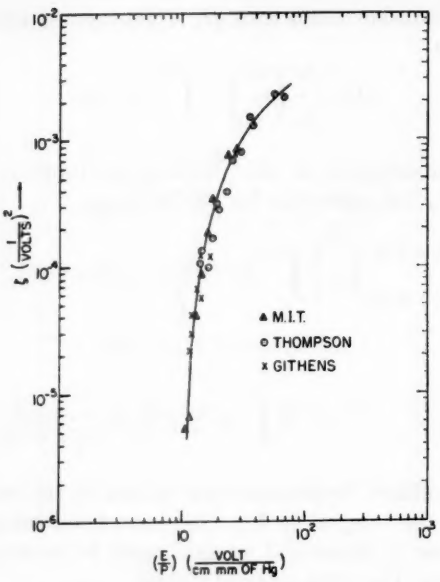

FIG. 4. Experimental ζ-curves of Thompson (1937), Githens (1941) and the present work. The data cover a frequency range of 5 to 3000 mc/sec. and a range of diffusion length from $\Lambda=0.0505$ cm to $\Lambda=0.50$ cm.

where

$$K=1-I(V,Z_p)+\frac{Sa_1}{V}[1-I(V-1,Z_p)]$$

$$J=1-I(V,Z_i)+\frac{Sa_1}{V}[1-I(V-1,Z_i)]$$
$$-\frac{Z_i}{V}\left\{1-I(V-1,Z_i)+\frac{Sa_1}{V-1}[1-I(V-2,Z_i)]\right\}$$

$$F=\frac{3S^{V+1}\exp[-(1-\frac{2}{3}\alpha)w_p]}{2\alpha R(1-\frac{2}{3}\alpha)V!}$$

$$G=w_p{}^{3/2}\left\{M_1'(w_p)-\tfrac{2}{3}\alpha M_1(w_p)\right.$$
$$\left.+C[M_2'(w_p)-\tfrac{2}{3}\alpha M_2(w_p)]\right\}+\frac{C}{2}\exp[w_p(1-\tfrac{2}{3}\alpha)]$$

$$w=\frac{16.2bu[1+(31.8/p\lambda)^2]}{(E/p)^2}\qquad Z=Sw$$

$$b=\left\{1+(E/p)^2\frac{1.52(10^{-2})}{(p\Lambda)^2[1+(31.8/p\lambda)^2]}\right\}^{\frac{1}{2}}$$

$$\alpha=0.75(b-1/b)$$

$$S=A+(1/2b)$$

$$A^2=1.03(E/p)^2\frac{1}{b^2[(31.8/p\lambda)^2+1]}+\frac{1}{4}$$

$$V=\tfrac{1}{2}[(146/Ab)+3]$$

$$a_1=[1-(B/2A)]B/4A^2$$

$$B=146/b$$

and Φ, C and R are defined in Eqs. (24)–(26). The breakdown condition is that $\zeta=1/\Lambda^2E^2$, so that we obtain the breakdown equation by setting ζ computed from Eq. (29) equal to $1/\Lambda^2E^2$. This produces a transcendental equation which is very difficult to solve and which is done in practice by successive approximations.

V. EXPERIMENTAL RESULTS

Breakdown electric fields have been measured at microwave frequencies using the experimental apparatus shown in Fig. 1. The details of the experiment are similar to those of the helium breakdown measurements.[1] Microwave power with a free-space wavelength of approximately 10 cm generated by a $c-w$ magnetron is coupled to a microwave resonant cavity through coaxial transmission lines. A known fraction of the power delivered is measured by a bolometer. The power absorbed by the cavity is combined with the cavity Q and the known field configuration to determine the electric field by standard methods.[9,10] The cavities in which breakdown takes place are made of oxygen-free high conductivity copper and connected through Kovar to an all-glass vacuum system. The vacuum system holds at a pressure of better than 10^{-7} mm of Hg for a period of about two hours with the pumps turned off. A single series of breakdown measurements takes about this time. The pressure is measured by an ionization gauge. Air Reduction Company spectroscopically pure hydrogen was used. Measurements were made in cylindrical cavities having heights of 0.1586, 0.476, and 2.54 cm. The experimental data are presented in Fig. 2, which gives breakdown electric field as a function of pressure. On Fig. 2 are also drawn theoretical curves of E computed from Eq. (29).

The theory of breakdown derived in this paper is not restricted to microwave frequencies but applies to any high frequency discharge in which electrons are produced by field ionization and lost by diffusion to the walls of the container. Theoretical electric fields have been computed for electric field wave-lengths of 6000 cm and 2730 cm. On Fig. 3, these are compared with the experimental data obtained by Githens in 1940.[11] Figure 4 presents ionization coefficients experimentally obtained by Githens,[11] and Thompson,[12] as well as the experimental data of this paper.

VI. DISCUSSION

Breakdown electric fields at high frequencies have been derived theoretically on the basis of kinetic theory, the only experimental data used being collision cross

[9] S. C. Brown, *et al.*, "Methods of measuring the properties of ionized gases at microwave frequencies," Technical Report No. 66, Research Laboratory of Electronics, M.I.T., Cambridge, Massachusetts.

[10] C. G. Montgomery, *Microwave Techniques* (McGraw-Hill Book Company, Inc., New York, 1948).

[11] S. Githens, Phys. Rev. **57**, 822 (1940).

[12] J. Thompson, Phil. Mag. **23**, 1 (1937).

sections. The elastic collision cross section for hydrogen used in this theory is probably correct within 10 percent. Calculations of the theory indicated that this will not introduce more than 2 or 3 percent error in electric fields. The excitation and ionization efficiencies are very difficult to measure and the experimental error in the best measurements in hydrogen may be as high as 20 percent. These introduce an error of approximately 14 percent in the theoretical electric fields. These effects combine to give a possible error of 16 percent in theoretical fields and indicate a need for more precise collision cross-section measurements. The maximum error in the experimental electric fields in the 10-cm wavelength region is 5 percent and in pressure is 1 percent. The derivation of the equation for the distribution function implicitly assumed that each electron dropped back to zero energy after an inelastic collision. Since excitation takes place over a certain range of energy, this is not exactly correct, but the error which it introduces is small.

Equation (29), calculated from kinetic theory and using no gas discharge data other than collision cross-section measurements and involving no adjustable constants, predicts breakdown electric fields well within the limits of accuracy over a large range of pressure, container size and frequency.

PHYSICAL REVIEW VOLUME 76, NUMBER 11 DECEMBER 1, 1949

Interference Effects in Gamma-Gamma Angular Correlations

DANIEL S. LING, JR.*
University of Michigan, Ann, Arbor, Michigan, and University of Kansas, Lawrence, Kansas

AND

DAVID L. FALKOFF†
University of Michigan, Ann Arbor, Michigan, and University of Notre Dame, South Bend, Indiana

(Received August 19, 1949)

The theory of the directional correlation of successive nuclear gamma-rays is extended to include transitions in which mixtures of multipoles are present. For such cases interference effects can radically modify the angular correlation from what is predicted in the usual theory assuming pure multipole transitions. Correlation functions are tabulated for all possible cascade emissions in which one of the transitions is a mixture of magnetic dipole and electric quadrupole and the other either dipole or quadrupole. It is shown that the experimental data on Sr^{88} which had previously seemed anomalous can be consistently interpreted with the mixture theory developed here, but the agreement with the observed angular correlation in Pd^{106} is not possible if the highest gamma-multipole order is assumed to be quadrupole.

I. INTRODUCTION

THE theory of the directional correlation of successive nuclear γ-rays has been treated in detail by Hamilton[1] and Goertzel.[2] Hamilton has given the basic quantum mechanical theory and has put the results of his calculations in a form which can be compared with experiment whenever the multipole orders of the radiation are dipole or quadrupole. (The distinction between the electric or magnetic character of the multipole radiation can be made in an angular correlation experiment only if the polarization of one or both of the γ-rays is specified.)[3,4] The conditions which must be fulfilled in order that Hamilton's theory and tables can be validly applied are:

(1) That the natural line width of the intermediate nuclear state be much larger than the hyperfine splitting of that state, and

(2) that the respective γ-transitions each correspond to pure multipole radiation.

Goertzel has extended the theory to the case when (1) is not satisfied due to the presence of internal atomic fields or an externally applied magnetic field. However, he still retains assumption (2).

In view of the absence of any detailed knowledge of the wave functions and hence charge and current distributions for nuclear states, assumption (2) proves to be particularly convenient for angular correlation calculations since it can then be shown that the correlation function $W(\theta)$ is independent of the intensities of the respective γ-rays. In fact, it is then possible (as is done in reference 1) to tabulate $W(\theta)$ wholly in terms of "rotational information" such as the spins of the nuclear states involved and the known angular distributions of the energy radiated for the given multipole orders of the γ-rays. However, comparison of theory with experiment[5-7] shows good agreement in several cases, but poor agreement in others, notably for Pd^{106} and Sr^{88}. In these experiments condition (1) is satisfied

* Now at the University of Kansas, Lawrence, Kansas.
† Now at the University of Notre Dame, South Bend, Indiana.
[1] D. R. Hamilton, Phys. Rev. **58**, 122 (1940).
[2] G. Goertzel, Phys. Rev. **70**, 897 (1946).
[3] D. L. Falkoff, Phys. Rev. **73**, 518 (1948).
[4] D. R. Hamilton, Phys. Rev. **74**, 782 (1948).
[5] E. L. Brady and M. Deutsch, Phys. Rev. **72**, 870 (1947); **74**, 1541 (1948).
[6] M. Deutsch and F. Metzger, Phys. Rev. **74**, 1542 (1948).
[7] M. Wiedenbeck, private communication.

TABLE I. Multipole vector potentials in the gauge $\varphi=0$. The multipole order corresponding to given L is 2^L. There are $2L+1$ linearly independent "submultipoles" (L, M), $M=-L, -(L-1), \cdots, L-1, L$ for each electric or magnetic 2^L pole. All potentials are normalized to $1/\pi^2\hbar k$ quanta/sec.

Magnetic multipoles, $A_m(L, M)$

$$A_z=\frac{M}{(L(L+1))^{\frac{1}{2}}}R_L(kr)Y_L{}^M(\theta, \varphi)e^{-ickt}$$

$$A_x\pm iA_y=-\left(\frac{(L\mp M)(L\pm M+1)}{L(L+1)}\right)^{\frac{1}{2}}R_L(kr)Y_L{}^{M\pm1}(\theta, \varphi)e^{-ickt}$$

Electric multipoles, $A_e(L, M)$

$$A_z=-\left\{\left(\frac{L(L+M+1)(L-M+1)}{(L+1)(2L+1)(2L+3)}\right)^{\frac{1}{2}}R_{L+1}(kr)Y_{L+1}{}^M(\theta, \varphi)-\left(\frac{(L+1)(L-M)(L+M)}{L(2L-1)(2L+1)}\right)^{\frac{1}{2}}R_{L-1}(kr)Y_{L-1}{}^M(\theta, \varphi)\right\}e^{-ickt}$$

$$A_x\pm iA_y=\mp\left\{\left(\frac{L(L\pm M+1)(L\pm M+2)}{(L+1)(2L+1)(2L+3)}\right)^{\frac{1}{2}}R_{L+1}(kr)Y_{L+1}{}^{M\pm1}(\theta, \varphi)-\left(\frac{(L+1)(L\mp M-1)(L\mp M)}{L(2L+1)(2L-1)}\right)^{\frac{1}{2}}R_{L-1}(kr)Y_{L-1}{}^{M\pm1}(\theta, \varphi)\right\}e^{-ickt}$$

with $R_L(kr)=\frac{i}{(kr)^{\frac{1}{2}}}H_{L+\frac{1}{2}}{}^{(1)}(kr)\to(-i)^L\left(\frac{2}{\pi}\right)^{\frac{1}{2}}\frac{e^{ikr}}{kr}$ for $kr\gg1$.

as was tested by observing no change in the angular correlation with strong applied magnetic field. One is therefore led to examine the modifications in the theory which result when assumption (2) is not valid.

The assumption of pure multipole transitions, while convenient, is otherwise quite arbitrary, for although the angular momentum and parity selection rules do limit the possible multipole radiations between two quantum states, the simultaneous occurrence of two or more multipole radiations is often consistent with these selection rules. As an example of such a mixed transition, magnetic dipole and electric quadrupole radiation are both possible between states differing by $0, \pm1$ units of angular momentum and having the same parity. Moreover, in the case of nuclear γ-rays, unlike atomic optical spectra, electric dipole radiation is often wholly absent on account of the symmetry of the nuclear charge distribution, and higher multipole radiations such as electric quadrupole and magnetic dipole can occur with comparable intensities.[8–12] In this paper we shall treat the theory of the directional correlation of successive nuclear γ-rays when one of the transitions is mixed. In particular, the tables of reference 1 will be extended to include all possible $W(\theta)$ for the case where one of the transitions is a mixture of electric quadrupole and magnetic dipole radiation, and the other is either dipole or quadrupole. It will then be shown that the experimental data[5] on Sr^{88} which had previously seemed anomalous, can be consistently interpreted with the theory developed here.

II. ON MIXED TRANSITIONS

On first consideration, it might be thought that the correlation function for successive nuclear γ-emissions in which the first transition was a mixture of magnetic dipole and electric quadrupole, say, with respective intensities $|\alpha|^2$ and $|\beta|^2$, and the second γ-ray any pure 2^L-pole, should be simply the weighted sum $|\alpha|^2W(\theta)_{D-L}+|\beta|^2W(\theta)_{Q-L}$ where $W(\theta)_{D-L}$ is the correlation function for a dipole-2^L-pole cascade emission and $W(\theta)_{Q-L}$ that for successive quadrupole and 2^L-pole γ-rays. However, in general this is not the case: Interference contributions arise from the mixing of the electric quadrupole and magnetic dipole fields. Such interference effects have in fact been observed[13] for a single transition in the Zeeman effect for forbidden lines in the atomic spectra of PbI, and the necessary theory given by Gerjouy.[14] In this section we give a resume of the theory of the interference due to mixtures of multipoles in a single transition which will at the same time serve to introduce the necessary notions and notations for treating angular correlations with mixtures in Section III.

(A) Angular Distributions for Multipole Fields

Consider first the classical electromagnetic problem of finding the angular distribution, i.e., magnitude of the Poynting vector as a function of angle, for the various multipole radiation fields. In general, for any electromagnetic field with vector potential $\mathbf{A}e^{-ickt}$ one obtains for the magnitude of the Poynting vector at large distances from all sources of the field in terms of the asymptotic form of $\mathbf{A}$:

$$\mathbf{n}\cdot\mathbf{S}=\frac{ck^2}{8\pi}[\mathbf{A}\cdot\mathbf{A}^*-(\mathbf{n}\cdot\mathbf{A})(\mathbf{n}\cdot\mathbf{A}^*)] \quad (1)$$

where $\mathbf{n}$ is a unit vector in the direction $\mathbf{S}$. For the electric and magnetic multipoles, the well-known[15] spherical

[8] H. A. Bethe, Rev. Mod. Phys. **9**, 222 (1937).
[9] Hulme, Mott, Oppenheimer, and Taylor, Proc. Roy. Soc. **A155**, 315 (1936).
[10] A. C. Helmholtz, Phys. Rev. **60**, 415 (1941).
[11] M. H. Hebb and E. Nelson, Phys. Rev. **58**, 486 (1940).
[12] E. Segrè and A. C. Helmholtz, Rev. Mod. Phys. **21**, 271 (1949).
[13] F. A. Jenkins and S. Mrozowski, Phys. Rev. **60**, 225 (1941).
[14] E. Gerjouy, Phys. Rev. **60**, 233 (1941). See also Shortley, Aller, Baker, and Menzel, Astrophys. J. **93**, 178 (1941).
[15] W. Heitler, Proc. Camb. Phil. Soc. **32**, 112 (1936); W. W. Hansen, Phys. Rev. **47**, 139 (1935); H. A. Kramers, Physica **10**, 261 (1943); G. Goertzel, see reference 2; O. Laporte, Am. J. Phys. **16**, 206 (1948).

eigenwave solutions of Maxwell's equations, $\mathbf{A}_e(L, M)$ and $\mathbf{A}_m(L, M)$ respectively, are listed in Table I. Inserting these in (1), one obtains for both electric and magnetic (LM) pole:

$$\mathbf{n}\cdot\mathbf{S}_L{}^M=\frac{c}{2\pi r^2}\frac{1}{L(L+1)}[2M^2|Y_L{}^M|^2 +(L-M)(L+M+1)|Y_L{}^{M+1}|^2 +(L+M)(L-M+1)|Y_L{}^{M-1}|^2]. \quad (2)$$

It is convenient for later references to define the angular distribution associated with an (LM) pole by:

$$F_L{}^M(\theta)=\frac{8\pi^3r^2}{c}\mathbf{n}\cdot\mathbf{S}_L{}^M. \quad (3)$$

It is then evident that $F_L{}^M(\theta)$ is a polynomial of degree L in $\cos^2\theta$ satisfying:

$$F_L{}^M(\theta)=F_L{}^{-M}(\theta), \quad (3a)$$

$$\int F_L{}^M(\theta)d\Omega=8\pi, \text{ independent of } M, \quad (3b)$$

$$\sum_{M=-L}^{L} F_L{}^M(\theta), \quad \text{independent of } \theta, \quad (3c)$$

and

$$F_L{}^M(0)=0 \quad \text{unless } M=\pm 1. \quad (3d)$$

In particular (3) yields for electric or magnetic dipole radiation:

$$F_1{}^0(\theta)=3(1-\cos^2\theta),\quad F_1{}^{\pm 1}(\theta)=3/2(1+\cos^2\theta), \quad (4)$$

and for electric or magnetic quadrupole:

$$F_2{}^0(\theta)=(5/2)(6\cos^2\theta-6\cos^4\theta)$$
$$F_2{}^{\pm 1}(\theta)=(5/2)(1-3\cos^2\theta+4\cos^4\theta) \quad (5)$$
$$F_2{}^{\pm 2}(\theta)=(5/2)(1-\cos^4\theta).$$

Consider now the radiation field from a charge distribution which gives rise to two multipole fields, say $\mathbf{A}(L, M)$ and $\mathbf{A}(L', M')$, with respective complex amplitudes α and β. Inserting $\mathbf{A}=\alpha\mathbf{A}(L, M)+\beta\mathbf{A}(L', M')$ in (1), the resultant angular distribution is found to be:

$$\mathbf{n}\cdot\mathbf{S}=|\alpha|^2\mathbf{n}\cdot\mathbf{S}_L{}^M+|\beta|^2\mathbf{n}\cdot\mathbf{S}_{L'}{}^{M'} +[\alpha\beta^*\mathbf{n}\cdot\mathbf{S}_{LL'}{}^{MM'}+c.c.] \quad (6)$$

where $\mathbf{n}\cdot\mathbf{S}_{LL'}{}^{MM'}$ is the interference term due to the mixing of the two multipoles:

$$\mathbf{n}\cdot\mathbf{S}_{LL'}{}^{MM'}=(ck^2/8\pi)\mathbf{A}(L, M)\cdot\mathbf{A}^*(L', M'). \quad (7)$$

Without recourse to the explicit functional form of the $\mathbf{A}(L, M)$ in Table I, it is possible to state that

$$\int \mathbf{n}\cdot\mathbf{S}_{LL'}{}^{MM'}d\Omega=0, \quad (8)$$

if $L\neq L'$ or $M\neq M'$ or also if $L=L'$ but one multipole is electric, the other magnetic. The physical interpretation of this is that the interference in the radiation pattern is just a redistribution of the energy radiated; the total energy radiated is still the same, namely, the sum of that from each multipole individually. The proof of (8) follows from the fact that the $\mathbf{A}(L, M)$ transform irreducibly under the three-dimensional rotation group[16] and the group theoretic theorem[17] that two functions transforming according to different irreducible representations of a group are orthogonal.

For the case of most interest in nuclear transitions, a mixture of an (L, M) electric 2^L pole and $(L-1, M)$ magnetic 2^{L-1} pole (the M's must be the same because of the magnetic quantum number selection rule), (7) and (3) yield for the interference contribution to the angular distribution:

$$F_{L,\,L-1}{}^M(\theta)=-4\pi\left(\frac{(2L+1)}{(2L-1)}\frac{(L+M)(L-M)}{L^2(L^2-1)}\right)^{\frac{1}{2}} \times[2M|Y_{L-1}{}^M|^2+(L-M-1)|Y_{L-1}{}^{M+1}|^2 -(L+M-1)|Y_{L-1}{}^{M-1}|^2]. \quad (9)$$

This interference term is a polynomial of degree $(L-1)$ in $\cos^2\theta$ having the properties:

$$\int F_{L,\,L-1}{}^M(\theta)d\Omega=0, \quad (9a)$$

$$F_{L,\,L-1}{}^M(\theta)=-F_{L,\,L-1}{}^{-M}(\theta), \quad (9b)$$

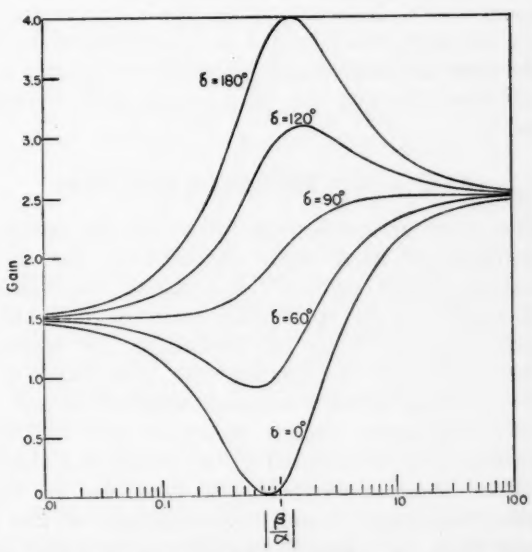

FIG. 1. Gain in the forward ($\theta=0$) direction for a classical mixture of magnetic dipole and electric quadrupole radiation as a function of the mixture amplitude ratio $|\beta/\alpha|$ and phase difference, δ.

[16] See H. A. Kramers, reference 15, and G. Goertzel, reference 2. Also H. C. Brinkman, Zur Quantenmechanik der Multipolstrahlung, 1932.

[17] See E. Wigner, Gruppentheorie (1931), p. 124.

whence

$$F_{L,\,L-1}{}^{0}(\theta)\equiv 0, \tag{9c}$$

and

$$\sum_{M=-(L-1)}^{L-1} F_{L,\,L-1}{}^{M}(\theta)=0. \tag{9d}$$

In particular for a mixture of electric quadrupole and magnetic dipole, the only non-zero interference angular distributions will be:

$$F_{2,1}{}^{\pm 1}(\theta)=\pm(15^{\frac{1}{2}}/2)(3\cos^2\theta-1) \tag{10}$$

and the total angular distributions (6) for such a mixture, with $M=\pm 1$ take the form:

$$\begin{aligned} F^{\pm 1}(\theta)=3/2|\alpha|^2(1+\cos^2\theta) \\ +5/2|\beta|^2(1-3\cos^2\theta+4\cos^4\theta) \\ \pm R(\alpha\beta^*)(15)^{\frac{1}{2}}(3\cos^2\theta-1) \end{aligned} \tag{11}$$

where α and β are the amplitudes of the magnetic dipole and electric quadrupole fields respectively.

To show the effect of the interference term in this purely classical angular distribution, we have plotted in Fig. 1 the gain in the $\theta=0$ direction as a function of the magnitude $|\beta/\alpha|$ and phase $\delta=\arg\beta/\alpha$ of the mixture amplitude ratio for the angular distribution (11) with $M=-1$. (We define the *gain*[18] in a given direction as the ratio of the intensity in that direction to the average intensity over all directions). It is evident from Fig. 1 that interference can radically change the directional pattern for the radiating system from what one would have for pure dipole, pure quadrupole, or for an arbitrarily weighted mixture with no interference: $\delta=90°$. Indeed for pure dipole or quadrupole fields, the gain would be 3/2 or 5/2 respectively, but when these are superposed with different phases and amplitudes, the gain can vary continuously between 0 and 4.

(B) Quantum Mechanical Intensities

The quantum mechanical intensities for radiative transitions are most easily obtained by the correspondence theory method[19] of replacing the classical field amplitudes by appropriate quantum mechanical matrix elements. Thus the probability for emission of an (LM) pole γ-quantum with direction $\mathbf{k}(\theta,\varphi)$ in a transition between magnetic sublevels m and m' of two degenerate nuclear states denoted by their quantum numbers σJm and $\sigma'J'm'$ (where σ, σ' denote all other quantum numbers than those for the total angular momentum J and its z-component m) can be gotten from the classical formula (1) provided one takes as the vector potential:

$$(\sigma Jm|LM|\sigma'J'm')\mathbf{A}(L,M) \tag{12}$$

where $(\sigma Jm|LM|\sigma'J'm')$ is the matrix element for the transition. This matrix element can always be written in the form:[20]

$$(\sigma Jm|LM|\sigma'J'm')=(\sigma J|L|\sigma'J')(Jm|LM|J'm'). \tag{13}$$

The matrix element $(Jm|LM|J'm')\equiv(JLJ'm'|JLmM)$ is the (real) transformation coefficient[21] for the vector addition of angular momenta: $\mathbf{J}+\mathbf{L}=\mathbf{J}'$, $m+M=m'$, and depends only on the quantum numbers J, J', L, m, $m'M$. The matrix element $(\sigma J|L|\sigma'J')$ is independent of m and m' and hence the same for each component of a line. In general it will depend on the explicit form of the unknown nuclear wave functions.

From (12) and (1) one gets that the intensity of the radiation in the direction θ for an (LM) pole γ-emission between states σJm and $\sigma'J'm'$ is proportional to:

$$|(\sigma J|L|\sigma'J')|^2(Jm|LM|J'm')^2F_L{}^M(\varphi), \tag{14}$$

so that the relative intensities of the components of the line which differ in initial and final sublevels m and m' are determined by:

$$(Jm|LM|J'm')^2F_L{}^M(\vartheta). \tag{15}$$

On account of the degeneracy of the initial and final states, it is necessary to sum (14) over all initial and final magnetic sublevels, m and m', consistent with the selection rule $m'=m+M$, to get the total intensity in the direction θ. Using the group theoretic relation:[22]

$$\sum_m (Jm|LM|J'm')(Jm|L'M|J'm')=\frac{2J'+1}{2L+1}\delta_{LL'}, \tag{16}$$

and (3c), one verifies that the intensity in any direction due to the sum of all components of the line is independent of θ. Another isotropy requirement, following from (14), (16), and (3a) is that the probability for a transition terminating in any sublevel m' of the final state is the same for each m' provided one averages over-all directions of emission of the γ-ray. If, however, one does not average over θ but rather specifies the direction of emission, then even though the initial sublevels m are assumed equally populated, the final sublevels m' will *not* in general have equal probabilities to be occupied.

Consider now a transition between the same two degenerate states with emission of a mixture of $2^L(L,M)$

[18] See J. C. Slater, *Microwave Transmission* (McGraw-Hill Book Company, Inc., New York, 1942), p. 215. We depart from conventional usage in evaluating the gain for $\theta=0$ even though this is not in general the direction of maximum intensity when mixtures are involved. However, this is more convenient for the angular correlation application.

[19] E. U. Condon and G. H. Shortley, *Theory of Atomic Spectra* (Cambridge University Press, London, 1935), Ch. IV.

[20] See C. Eckart, Rev. Mod. Phys. 2, 305 (1930). Also E. Wigner, reference 17, p. 264.

[21] See Condon and Shortley, reference 19, pp. 73–78, or Wigner, reference 17, p. 206.

[22] This theorem has been used by H. B. Casimir, Archives du Musée Teyler, Series III, VIII, 274 (1936), to show that the total probability for internal conversion in a field which is a superposition of two multipole fields is the sum of the probabilities due to each separately. For a formal proof of (16) see G. Breit and B. T. Darling, Phys. Rev. 71, 405 (1947).

TABLE II. Q and R for dipole-mixture correlation.

$\Delta J=1$	$\Delta j=1$	$Q=13J\|\alpha\|^2+(5/21)(55J-6)\|\beta\|^2+(2/3)(15J(J+2))^{\frac{1}{2}}Re(\alpha\beta^*)$
		$R=J\|\alpha\|^2+(5/7)(J+6)\|\beta\|^2-2(15J(J+2))^{\frac{1}{2}}\mathrm{Re}(\alpha\beta^*)$
	$\Delta j=0$	$Q=J(14J+13)\|\alpha\|^2+(5/21)(58J^2+67J-6)\|\beta\|^2-(2/3)(15J(J+2))^{\frac{1}{2}}(2J-1)Re(\alpha\beta^*)$
		$R=-J(2J-1)\|\alpha\|^2-(5/7)(J+6)(2J-1)\|\beta\|^2+2(15J(J+2))^{\frac{1}{2}}(2J-1)Re(\alpha\beta^*)$
	$\Delta j=-1$	$Q=(26J^2+67J+40)\|\alpha\|^2+(5/21)(110J^2+269J+174)\|\beta\|^2+(2/3)(15J(J+2))^{\frac{1}{2}}(2J-1)Re(\alpha\beta^*)$
		$R=J(2J-1)\|\alpha\|^2+(5/7)(J+6)(2J-1)\|\beta\|^2-2(15J(J+2))^{\frac{1}{2}}(2J-1)Re(\alpha\beta^*)$
$\Delta J=0$	$\Delta j=1$	$Q=(2J-1)(14J+1)\|\alpha\|^2+(5/7)(36J^2-20J+5)\|\beta\|^2-2(5(2J-1)(2J+3))^{\frac{1}{2}}Re(\alpha\beta^*)$
		$R=-(2J-1)(2J+3)\|\alpha\|^2+(5/7)(2J+5)(2J-3)\|\beta\|^2+6(5(2J-1)(2J+3))^{\frac{1}{2}}Re(\alpha\beta^*)$
	$\Delta j=0$	$Q=(12J^2+12J+1)\|\alpha\|^2+(5/7)(20J^2+20J-5)\|\beta\|^2+2(5(2J-1)(2J+3))^{\frac{1}{2}}Re(\alpha\beta^*)$
		$R=(2J-1)(2J+3)\|\alpha\|^2-(5/7)(2J-3)(2J+5)\|\beta\|^2-6(5(2J-1)(2J+3))^{\frac{1}{2}}Re(\alpha\beta^*)$
	$\Delta j=-1$	$Q=(2J+3)(14J+13)\|\alpha\|^2+(5/7)(36J^2+92J+61)\|\beta\|^2-2(5(2J-1)(2J+3))^{\frac{1}{2}}Re(\alpha\beta^*)$
		$R=-(2J-1)(2J+3)\|\alpha\|^2+(5/7)(2J-3)(2J+5)\|\beta\|^2+6(5(2J-1)(2J+3))^{\frac{1}{2}}Re(\alpha\beta^*)$
$\Delta J=-1$	$\Delta j=1$	$Q=(26J^2-15J-1)\|\alpha\|^2+(5/21)(110J^2-49J+15)\|\beta\|^2-(2/3)(15(J^2-1))^{\frac{1}{2}}(2J+3)Re(\alpha\beta^*)$
		$R=(J+1)(2J+3)\|\alpha\|^2+(5/7)(2J+3)(J-5)\|\beta\|^2+2(15(J^2-1))^{\frac{1}{2}}(2J+3)Re(\alpha\beta^*)$
	$\Delta j=0$	$Q=(J+1)(14J+1)\|\alpha\|^2+(5/21)(58J^2+49J-15)\|\beta\|^2+(2/3)(15(J^2-1))^{\frac{1}{2}}(2J+3)Re(\alpha\beta^*)$
		$R=-(J+1)(2J+3)\|\alpha\|^2-(5/7)(2J+3)(J-5)\|\beta\|^2-2(15(J^2-1))^{\frac{1}{2}}(2J+3)Re(\alpha\beta^*)$
	$\Delta j=-1$	$Q=13(J+1)\|\alpha\|^2+(5/21)(55J+61)\|\beta\|^2-(2/3)(15(J^2-1))^{\frac{1}{2}}Re(\alpha\beta^*)$
		$R=(J+1)\|\alpha\|^2+(5/7)(J-5)\|\beta\|^2+2(15(J^2-1))^{\frac{1}{2}}Re(\alpha\beta^*)$

electric multipole and $2^{L-1}(L-1, M)$ magnetic multipole radiation. The appropriate vector potential is now:

$$\mathbf{A}=(\sigma J|L|\sigma' J')(Jm|LM|J'm')\mathbf{A}_e(L, M)+(\sigma J|L-1|\sigma' J')(Jm|L-1, M|J'm')\mathbf{A}_m(L-1, M).$$

Denoting the unknown nuclear matrix elements $(\sigma J|L|\sigma' J')$ and $(\sigma J|L-1|\sigma' J')$ by α and β respectively,[23] the quantum mechanical analogue of (6) for the intensity of the component $m\to m'=m+M$ in the direction θ is of the same form as the classical expression (6):

$$\mathbf{n}\cdot\mathbf{S}_{m\to m'}=|\alpha|^2(Jm|LM|J'm')^2F_L{}^M(\theta)+|\beta|^2(Jm|L-1, M|J'm')^2F_{L-1}{}^M(\theta)+(\alpha\beta^*+\alpha^*\beta)(Jm|LM|J'm')\times(Jm|L-1, M|J'm')F_{L, L-1}{}^M(\theta), \quad (17)$$

where $F_L{}^M(\theta)$ and $F_{L, L-1}{}^M(\theta)$ are given by (3) and (9), respectively. Hence, here too the interference term will vanish when averaged over θ. But in addition, even for specified θ, the mixture contribution will vanish when summed over all initial and final sublevels, m and m', in virtue of (16)! How then is the interference observable?

If one considers only those transitions $m\to m'$ characterized by fixed $M=m'-m$, then the interference term need not vanish. When a strong magnetic field is present so that those components with different M differ in frequency, as in the atomic Zeeman effect, the interference contributions to the angular intensities are detectable as reported in references 13 and 14.

Interference effects are also detectable in angular correlations. In this case the individual components of a line are distinguished not by their frequencies, which are all the same, but by different statistical weights.

[23] Strictly speaking, α and β are not the usual multipole matrix elements but are implicitly defined by Eq. (17). Summing over-all initial and final degenerate sublevels m and m', and over-all directions of emission, one gets for the total intensity of the line (using (3b), (9a) and (16)): $8\pi(2J'+1)[|\alpha|^2+|\beta|^2]$. Hence $|\alpha|^2$ and $|\beta|^2$ determine the absolute intensities of the two multipole radiations and must, except for a common proportionality factor, be the same as the Einstein coefficients for spontaneous emission for the respective multipoles. One may, therefore, interpret α and β as phenomenologically renormalized matrix elements whose absolute value squared are the respective Einstein probabilities. The phases of α and β are defined to be the same as those of the associated nuclear matrix elements. Experimentally one can take $|\alpha|^2$ and $|\beta|^2$ as the number of quanta emitted by the respective multipoles; actually only their ratio is needed here.

TABLE III. Q, R, and S for quadrupole-mixture correlation.

$\Delta J=1$	$\Delta j=2$	$Q=87J\lvert\alpha\rvert^2+5(17J+2)\lvert\beta\rvert^2-6(15J(J+2))^{\frac{1}{2}}R(\alpha\beta^*)$
		$R=-9J\lvert\alpha\rvert^2+5(J-2)\lvert\beta\rvert^2+18(15J(J+2))^{\frac{1}{2}}R(\alpha\beta^*)$
		$S=-(20/3)(2J+5)\lvert\beta\rvert^2$
	$\Delta j=1$	$Q=(3/2)J(55J+61)\lvert\alpha\rvert^2+(5/2)(35J^2+35J+6)\lvert\beta\rvert^2+3(15J(J+2))^{\frac{1}{2}}(J-5)R(\alpha\beta^*)$
		$R=(9/2)J(J-5)\lvert\alpha\rvert^2-(5/2)(17J^2+17J-30)\lvert\beta\rvert^2-9(15J(J+2))^{\frac{1}{2}}(J-5)R(\alpha\beta^*)$
		$S=(40/3)(2J-3)(2J+5)\lvert\beta\rvert^2$
	$\Delta j=0$	$Q=3J(36J^3+92J+61)\lvert\alpha\rvert^2+5(20J^3+52J^2+41J+6)\lvert\beta\rvert^2+2(15J(J+2))^{\frac{1}{2}}(2J-3)(2J+5)R(\alpha\beta^*)$
		$R=3J(2J-3)(2J+5)\lvert\alpha\rvert^2+5(2J-3)(2J+5)(5J-2)\lvert\beta\rvert^2-6(15J(J+2))^{\frac{1}{2}}(2J-3)(2J+5)R(\alpha\beta^*)$
		$S=-(80/3)(2J-3)(2J+5)(J-1)\lvert\beta\rvert^2$
	$\Delta j=-1$	$Q=(3/2)(J+2)(110J^2+269J+174)\lvert\alpha\rvert^2+(5/2)(70J^4+289J^3+374J^2+188J+24)\lvert\beta\rvert^2$ $+3(15J(J+2))^{\frac{1}{2}}(J+2)(2J-1)(J+6)R(\alpha\beta^*)$
		$R=(9/2)J(J+2)(J+6)(2J-1)\lvert\alpha\rvert^2-(5/2)(2J-1)(17J^3-18J^2-164J-24)\lvert\beta\rvert^2$ $-9(15J(J+2))^{\frac{1}{2}}(J+2)(2J-1)(J+6)R(\alpha\beta^*)$
		$S=(40/3)(J-1)(2J-3)(2J+5)(2J-1)\lvert\beta\rvert^2$
	$\Delta j=-2$	$Q=(3/2)(J+2)(58J^2+139J+84)\lvert\alpha\rvert^2+(5/2)(34J^3+159J^2+224J+96)\lvert\beta\rvert^2-3(15J$ $(J+2))^{\frac{1}{2}}(J+2)(2J-1)R\alpha(\beta^*)$
		$R=-(9/2)J(J+2)(2J-1)\lvert\alpha\rvert^2+(5/2)(2J-1)(J^2-16J-12)\lvert\beta\rvert^2+9(15J(+2))^{\frac{1}{2}}(J+2)(2J-1)R(\alpha\beta^*)$
		$S=-(10/3)(J-1)(2J-1)(2J-3)\lvert\beta\rvert^2$
$\Delta J=0$	$\Delta j=2$	$Q=(3/2)(2J-1)(26J-3)\lvert\alpha\rvert^2+(15/2)(2J-1)(6J+1)\lvert\beta\rvert^2+9(5(2J-1)(2J+3))^{\frac{1}{2}}R(\alpha\beta^*)$
		$R=(9/2)(2J-1)(2J+3)\lvert\alpha\rvert^2-(15/2)(2J+1)(2J+5)\lvert\beta\rvert^2-27(5(2J-1)(2J+3))^{\frac{1}{2}}R(\alpha\beta^*)$
		$S=10(J+2)(2J+5)\lvert\beta\rvert^2$
	$\Delta j=1$	$Q=(3/2)(2J-1)(58J^2+49J-15)\lvert\alpha\rvert^2+(15/2)(20J^3+8J^2-3J+3)\lvert\beta\rvert^2$ $-9(5(2J-1)(2J+3))^{\frac{1}{2}}(J-5)R(\alpha\beta^*)$
		$R=-(9/2)(2J-1)(2J+3)(J-5)\lvert\alpha\rvert^2+(15/2)(2J-3)(2J+5)(5J+7)\lvert\beta\rvert^2$ $+27(5(2J-1)(2J+3))^{\frac{1}{2}}(J-5)R(\alpha\beta^*)$
		$S=-40(J+2)(2J-3)(2J+5)\lvert\beta\rvert^2$
	$\Delta j=0$	$Q=15(2J-1)(2J+3)(4J^2+4J-1)\lvert\alpha\rvert^2+15(2J-1)(2J+3)(4J^2+4J-1)\lvert\beta\rvert^2$ $-6(5(2J-1)(2J+3))^{\frac{1}{2}}(2J-3)(2J+5)R(\alpha\beta^*)$
		$R=-3(2J-1)(2J+3)(2J-3)(2J+5)\lvert\alpha\rvert^2-15(2J-3)(2J+5)(4J^2+4J-7)\lvert\beta\rvert^2$ $+18(5(2J-1)(2J+3))^{\frac{1}{2}}(2J-3)(2J+5)R(\alpha\beta^*)$
		$S=80(2J-3)(2J+5)(J-1)(J+2)\lvert\beta\rvert^2$
	$\Delta j=-1$	$Q=(3/2)(2J+3)(58J^2+67J-6)\lvert\alpha\rvert^2+(15/2)(20J^3+52J^2+41J+6)\lvert\beta\rvert^2$ $-9(5(2J-1)(2J+3))^{\frac{1}{2}}(J+6)R(\alpha\beta^*)$
		$R=-(9/2)(2J+3)(2J-1)(J+6)\lvert\alpha\rvert^2+(15/2)(2J-3)(2J+5)(5J-2)\lvert\beta\rvert^2$ $+27(5(2J-1)(2J+3))^{\frac{1}{2}}(J+6)R(\alpha\beta^*)$
		$S=-40(2J-3)(2J+5)(J-1)\lvert\beta\rvert^2$
	$\Delta j=-2$	$Q=(3/2)(2J+3)(26J+29)\lvert\alpha\rvert^2+(15/2)(2J+3)(6J+5)\lvert\beta\rvert^2+9(5(2J-1)(2J+3))^{\frac{1}{2}}R(\alpha\beta^*)$
		$R=(9/2)(2J+3)(2J-1)\lvert\alpha\rvert^2-(15/2)(2J-3)(2J+1)\lvert\beta\rvert^2-27(5(2J-1)(2J+3))^{\frac{1}{2}}R(\alpha\beta^*)$
		$S=10(J-1)(2J-3)\lvert\beta\rvert^2$

Namely, if, say, the second transition is mixed, then by specifying the direction of emission of the first quantum, the end states for this first transition which are the initial sublevels for the second transition are unequally populated. Hence, Eq. (16) is no longer applicable, each m for the initial sublevels of the mixed transition being weighted differently, and the interference cross terms in (17) need not vanish when aver-

TABLE III.—*Continued.*

$\Delta J=-1$	$\Delta j=2$	$Q=(3/2)(J-1)(58J^2-23J+3)\|\alpha\|^2+(5/2)(34J^3-57J^2+8J+3)\|\beta\|^2+3(15(J^2-1))^{\frac{1}{2}}(J-1)(2J+3)R(\alpha\beta^*)$
		$R=-(9/2)(J-1)(2J+3)(J+1)\|\alpha\|^2+(5/2)(2J+3)(J^2+18J+5)\|\beta\|^2$ $-9(15(J^2-1))^{\frac{1}{2}}(J-1)(2J+3)R(\alpha\beta)^*$
		$S=-(10/3)(2J+3)(J+2)(2J+5)\|\beta\|^2$
	$\Delta j=1$	$Q=(3/2)(J+1)(J-1)(110J^2-49J+15)\|\alpha\|^2+(5/2)(70J^4-9J^3-73J^2-27J-9)\|\beta\|^2$ $-3(15(J^2-1))^{\frac{1}{2}}(2J+3)(J-5)(J-1)R(\alpha\beta^*)$
		$R=(9/2)(J+1)(J-1)(2J+3)(J-5)\|\alpha\|^2-(5/2)(2J+3)(17J^3+69J^2-77J-105)\|\beta\|^2$ $+9(15(J^2-1))^{\frac{1}{2}}(2J+3)(J-5)(J-1)R(\alpha\beta^*)$
		$S=(40/3)(2J+3)(2J-3)(2J+5)(J+2)\|\beta\|^2$
	$\Delta j=0$	$Q=3(J+1)(36J^2-20J+5)\|\alpha\|^2+5(20J^3+8J^2-3J+3)\|\beta\|^2-2(15(J^2-1))^{\frac{1}{2}}(2J-3)(2J+5)R(\alpha\beta^*)$
		$R=3(J+1)(2J-3)(2J+5)\|\alpha\|^2+5(2J-3)(2J+5)(5J+7)\|\beta\|^2+6(15(J^2-1))^{\frac{1}{2}}(2J-3)(2J+5)R(\alpha\beta^*)$
		$S=-(80/3)(J+2)(2J-3)(2J+5)\|\beta\|^2$
	$\Delta j=-1$	$Q=(3/2)(J+1)(55J-6)\|\alpha\|^2+(5/2)(35J^2+35J+6)\|\beta\|^2-3(15(J^2-1))^{\frac{1}{2}}(J+6)R(\alpha\beta^*)$
		$R=(9/2)(J+1)(J+6)\|\alpha\|^2-(5/2)(17J^2+17J-30)\|\beta\|^2+9(15(J^2-1))^{\frac{1}{2}}(J+6)R(\alpha\beta^*)$
		$S=(40/3)(2J-3)(2J+5)\|\beta\|^2$
	$\Delta j=-2$	$Q=87(J+1)\|\alpha\|^2+5(17J+15)\|\beta\|^2+6(15(J^2-1))^{\frac{1}{2}}R(\alpha\beta^*)$
		$R=-9(J+1)\|\alpha\|^2+5(J+3)\|\beta\|^2-18(15(J^2-1))^{\frac{1}{2}}R(\alpha\beta^*)$
		$S=-(20/3)(2J-3)\|\beta\|^2$

aged over all initial and final states (see Eqs. (18a) or (18b)).

III. ANGULAR CORRELATION WITH MIXTURES

A rigorous quantum mechanical derivation of the angular correlation function $W(\theta)$ requires a second-order time dependent perturbation calculation beginning with an initial system of excited nucleus plus quantised radiation field. Hamilton[1] has given such a derivation in a form sufficiently general to apply to mixed transitions as well. If the successive nuclear states involved have spins J'', J and J' with z-components m'', m and m', and if the first emission is a pure $2^{L'}$ multipole and the second a mixture of 2^L electric and 2^{L-1} magnetic multipoles, then the angular correlation function $W(\theta)$ for the relative probability that the second γ-ray be emitted at an angle θ with respect to the first γ-ray may be written in either of the equivalent forms:

$$W(\theta)=\sum_{m',m,m''}[(J''m''|L'M'|Jm)^2F_{L'}{}^{M'}(0)]\times\mathbf{n}\cdot\mathbf{S}_{mm'}(\theta) \quad (18a)$$

$$W(\theta)=\sum_{m',m,m''}[(J''m''|L'M'|Jm)^2F_{L'}{}^{M'}(\theta)]\times[\mathbf{n}\cdot\mathbf{S}_{mm'}(0)] \quad (18b)$$

according as the direction of emission of the first or second γ-ray is taken as the z-axis, $\theta=0$. Here $\mathbf{n}\cdot\mathbf{S}_{mm'}(\theta)$ is the relative probability for the γ-ray in the second mixed transition to be emitted in the direction θ in the component $m\rightarrow m'$ as given by (17). On expanding (18a or b), $W(\theta)$ takes the form:

$$W(\theta)=|\alpha|^2W_{L',L}(\theta)+|\beta|^2W_{L',L-1}(\theta)+2R(\alpha\beta^*)W_I(\theta) \quad (19)$$

where $W_{L'L}(\theta)$ is the angular correlation due to successive $2^{L'}$ and 2^L multipoles (and similarly for $W_{L'L-1}$) while $W_I(\theta)$, the coefficient of $\alpha\beta^*+\alpha^*\beta=2R(\alpha\beta^*)$ is the interference contribution due to the mixed multipoles in the second transition.

The explicit evaluation of $W(\theta)$ thus requires knowing $|\alpha|^2$, $|\beta|^2$, $R(\alpha\beta^*)$, $F_L{}^M(\theta)$, $F_{L'L-1}{}^M(\theta)$ and the matrix elements $(Jm|LM|J'm')$. When both transitions are pure multipoles, either α or β is zero, say β. Then it is not necessary to know α since $W(\theta)$ is a relative probability and the common factor $|\alpha|^2$ can be dropped. For the mixture case both α and β are non-zero. On dividing (19) by $|\alpha|^2$, only the ratio β/α enters in $W(\theta)$. Since this ratio is a complex number in general, one has to specify both its modulus and argument. Physically this means that both the *relative intensities* of the mixed multipoles and the *relative phases*[24] of their matrix elements must be given. The angular distributions $F_L{}^M(\theta)$ and $F_{L,L-1}{}^M(\theta)$ are given in a form easy to evaluate for any L by Eqs. (3)

[24] For the atomic Zeeman effect considered in reference 14, α and β are simply matrix elements involving radial wave functions and hence both real. For the nuclear case α and β could be evaluated theoretically if one chose some particular model for the nucleus, such as liquid drop.

and (9). General formulas for the normalized transformation coefficients are available[25] but these have been tabulated[26] only for $L=1$ and 2.[27] Hence the correlation functions have been worked out in detail[1] only for dipole and quadrupole γ-rays, and accordingly, we have confined our explicit evaluation of mixture correlations to the cases when the pure multipole transition is either dipole or quadrupole and the mixture multipoles are electric quadrupole and magnetic dipole.

It should be noted, that although for L or $L'=1$ or 2, the $W_{L'L}(\theta)$ must be equivalent to those obtained by Hamilton, it is not correct to insert Hamilton's results directly into (18), for his correlation functions are not properly normalized when mixtures are taken into account. This is shown in the Appendix. Except for this normalization, the actual procedure used in obtaining the $W_{L'L}(\theta)$ completely parallels the method outlined by Hamilton. The interference contribution (19) can be reduced, using (3a, d) and (10), to the form:

$$W_I(\theta)=(15^{\frac{1}{2}}/2)(3\cos^2\theta-1)\cdot$$
$$\sum_{m=-J}^{J}\{[(J''m-1|L',1|Jm)^2+(J''m+1|L',-1|Jm)^2]$$
$$\times[(Jm|1,1|J'm+1)(Jm|2,1|J'm+1)$$
$$-(Jm|1,-1|J'm-1)(Jm|2,-1|J'm-1)]\}.$$

The evaluation of the indicated sums of products of *normalized* transformation coefficients presents the only new computational task for the preparation of Tables II and III which are for dipole—(mixture) and quadrupole—(mixture) correlations, respectively. The notation of Hamilton is used throughout. Successive nuclear states have spins $J-\Delta j$, J, and $J+\Delta J$. The correlation function has the form:

$$W(\theta)=1+R/Q\cos^2\theta+S/Q\cos^4\theta.$$

Factors common to Q, R, and S are dropped in these tables. When $\alpha=0$ or $\beta=0$, each entry in the tables reduce to the corresponding entry in Hamilton's tables for pure multipole transitions which provided a check on our calculation. The same tables may be used to obtain the correlation functions when the first transition is mixed and the second pure dipole or quadrupole. This is illustrated in the following discussion.

IV. DISCUSSION AND APPLICATION TO EXPERIMENT

We now apply the preceding theory to the experimental $\gamma-\gamma$ angular correlations is Sr^{88} and Pd^{106} which were measured by Deutsch[5] and which are not in satisfactory agreement with the theory as given by Hamilton.

[25] See reference 17, p. 206.
[26] See reference 19, pp. 76, 77.
[27] A table for $L=3$ has been prepared but not yet published by one of us (D. L. F.).

The measured correlation function for Sr^{88} can be adequately represented by $W(\varphi)=1+R/Q\cos^2\theta$ with $R/Q=W(\pi)-W(\pi/2)=-0.08$. From Hamilton's tables, this value of R/Q can be obtained only if the spins of the ground, intermediate and initial states are, respectively, 2, 2, 2, or 3, 2, 2, or 2, 2, 3. However, Sr^{88} being an even-even nucleus, its ground state would be expected to have spin 0. In fact, Peacock,[28] on the basis of internal conversion measurements proposes a disintegration scheme for Sr^{88} in which the spins of ground, intermediate, and initial states are respectively 0, 1, 2. Which this choice of spins if both transitions are dipole theory gives $R/Q=+0.077$, while if the first transition is quadrupole, the second dipole, $R/Q=+0.429$. These are the only possible combinations of pure dipole and quadrupole radiations consistent with Peacock's assignment of nuclear spins and the observed $\cos^2\theta$ dependence of $W(\theta)$, and neither of these R/Q values agrees with experiment. One is, therefore, led to examine the possibility that one of the transitions may be mixed.

Since quadrupole radiation is forbidden for the second (1→0) transition, it must be pure (electric or magnetic) dipole and we take the first (2→1) transition as the mixture of magnetic dipole and electric quadrupole radiation. Tables II and III are prepared for the case when the first transition is pure and the second mixed. However, on account of the Hermiticity of all matrix elements in $W(\theta)$, the correlation function must be the same for any direct process as its inverse. Hence the angular correlation for the proposed decay scheme in which the first γ-transition is mixed, the second pure with $\Delta j=\Delta J=-1$, $J=1$ is the same as that tabulated for the case when the first transition is pure, the second mixed with $\Delta j=\Delta J=+1$, $J=1$. From Table II, one has from the $\Delta j=\Delta J=1$ entry after division by $|\alpha|^2$:

$$R/Q=\frac{1+5|\beta/\alpha|^2-13.4R(\beta/\alpha)}{13+11.7|\beta/\alpha|^2+4.46R(\beta/\alpha)}.$$

This function, R/Q is plotted in Fig. 2 for various values of the magnitude and phase δ of the mixture amplitude ratio β/α. The intersection of these curves with the line $R/Q=-0.08$ gives the locus of values of β/α which yield agreement with experiment. It is seen that for any $0\leq\delta\leq58°$, there are two admissible values of β/α. For example for $\delta=0$, i.e., β/α real, the suitable values of β/α are 0.18 and 2.0 corresponding to a quadrupole to dipole intensity ratio of 0.032 or 4.0 respectively. The arbitrariness in the choice of the relative phases and magnitudes of α and β which can satisfactorily explain the observed $\gamma-\gamma$ angular correlation could be removed if the same mixed γ-transition also gave rise to internal conversion electrons. Then the same α and β would enter in the internal-conversion—

[28] W. C. Peacock, unpublished, quoted by Deutsch, reference 5.

γ-angular correlation and afford a consistency check on the assignment of the complex parameter β/α.

It is instructive to consider in more detail the influence of the interference term on the angular correlation as shown in Fig. 2. The curve for $\delta=90°$ gives the values which R/Q would have if there were no interference present; in this case R and Q for the correlation with mixed transition are simply the weighted average of the expressions for pure transitions. It is clear from the figure that the correlation can be radically affected both in magnitude and sign by even a small mixture ratio. Roughly, the relative change in the angular correlation due to interference is of the same order of magnitude as the ratio of the multipole amplitudes, rather than their intensities, in the mixed transition, for the ratio of the interference term to the intensity of the dominant multipole will be of order $|\alpha\beta|/|\alpha|^2 \sim|\beta/\alpha|$ if $|\alpha|^2\geq|\beta|^2$. Although Fig. 2 is drawn for the special choice of nuclear quantum numbers in the proposed decay scheme for Sr^{88}, it is evident from its similarity with Fig. 1 that one may expect the same general behavior due to interference whatever the particular nuclear states involved. Indeed one might say that although the existence of an angular correlation is itself purely a quantum mechanical effect, the interference effects in the angular correlation have a purely classical origin in the interference contributions occurring in the classical angular distribution (6) or (11) due to a mixture of multipoles. In fact, the summands $\mathbf{n}\cdot\mathbf{S}_{mm'}(0)$ for $m'=m\pm1$ occurring in the correlation function (18b) are to within a proportionality factor (if one absorbs the transformation coefficients into the definition of α and β) just the gain in the $\theta=0$ direction, as defined in Section IIA and plotted in Fig. 1, for the angular distribution (17) resulting from the $m-m'$ component of the mixed transition.

Consider now the case of Pd^{106}. We have shown elsewhere[29] that if one assumes the highest multipole radiation present is quadrupole and the ground state of this even-even nucleus has spin 0, then the measured[5,7] correlation function forces the spin of the intermediate state to be 2 and that of the initial state, 1, 2, or 3. The most general set of transitions consistent with these requirements is one in which the first transition is a dipole—quadrupole mixture and the second is pure quadrupole radiation. We now show that even the use of mixtures cannot explain the experimental $\gamma-\gamma$-angular correlation, and therefore one of the γ-rays in the Pd^{106} transitions must be at least octupole.

The observed $W(\theta)$ has the form $W(\theta)=1+R/Q\cos^2\theta+S/Q\cos^4\theta$ with $R/Q=-1.66$ and $S/Q=2.16$. If the initial nuclear spin is 1, then $\Delta j=1$, $\Delta J=-2$, $J=2$. Since the order of the mixed and pure transition is the reverse of that for which the tables are calculated, one must use the $\Delta j=2$, $\Delta J=-1$ entry in Table III with $J=2$ which gives:

$$R/Q=\frac{-94.5+787.5|\beta/\alpha|^2-423R(\beta/\alpha)}{283.5+157.5|\beta/\alpha|^2+141R(\beta/\alpha)},$$
$$S/Q=\frac{-840|\beta/\alpha|^2}{283.5+157.5|\beta/\alpha|^2+141R(\beta/\alpha)}. \tag{20}$$

Equating these to the observed values one obtains two simultaneous linear equations for the two real unknowns $|\beta/\alpha|^2$ and $R(\beta/\alpha)$. These have a unique solution, but it is not physically admissible since one gets $|\beta/\alpha|^2=-0.425$ while it should always be non-negative. (More directly, in this particular case, one can easily see that no matter what value of β/α is used in S/Q in Eq. (20), S/Q will always be negative, in contrast to the experimental value of $+2.16$.) This disagreement is well outside the experimental error. Similar inconsistencies occur if one assumes the initial state to have spin 2 or 3. Thus the observed angular correlation in Pd^{106} cannot be explained either with or without mixtures when the highest γ-multipole order is assumed to be quadrupole.

This negative result shows also that the presence of two additional parameters in mixture angular correlations is by no means a guarantee that a suitable mixture can be found to explain any correlation which eludes the pure multipole tables. On the contrary, a fit may not be possible at all, as with Pd^{106}, or only for restricted values of β/α, as for Sr^{88}. The essential differ-

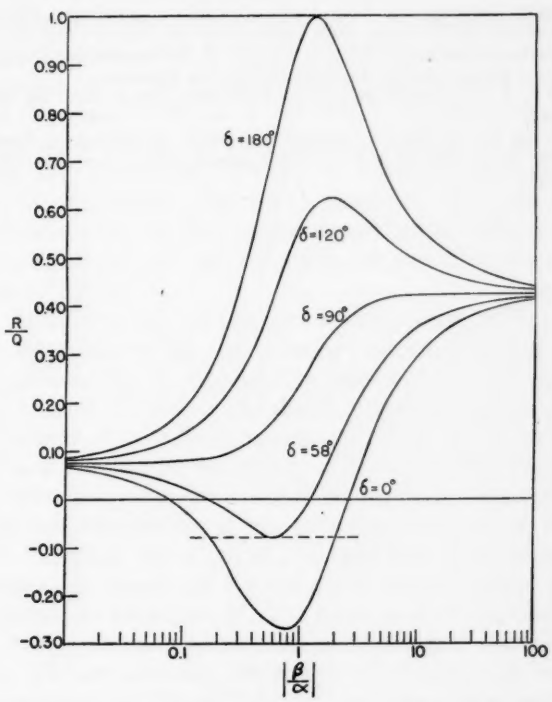

FIG. 2. R/Q as a function of $|\beta/\alpha|$ and δ for a mixture-dipole angular correlation with $\Delta j=\Delta J=-1$, $J=1$. The dotted line represents the experimental value -0.08 for Sr^{88}.

[29] D. S. Ling, Jr. and D. L. Falkoff, Phys. Rev. 76, 431 (1949).

ence between these two cases is that for Sr^{88} the observed correlation requires that the non-mixed transition be pure dipole. Hence only one number, R/Q, need be given to determine $W(\theta)$. Any point of intersection of the line $R/Q=-0.08$ with the curves of Fig. 2 yields admissible values for $|\beta/\alpha|$ and $\delta=\arg\beta/\alpha$. However, for Pd^{106}, the observed correlation having a $\cos^4\theta$ as well as $\cos^2\theta$ dependence requires the specification of two constants, R/Q and S/Q. For such correlations, as shown above, there is no reason to expect that the solution of the resulting simultaneous equations should be physically admissible. If, however, a consistent solution exists it will also be unique.

We conclude with a remark on mixtures in other nuclear processes. Evidence for mixtures of multipole radiation in internal conversion has often been cited.[9-12] As remarked by Casmir[22] interference effects from such mixtures would not ordinarily be detectable in a single transition. However, they would be detectable in internal conversion—internal conversion or internal conversion—γ-angular correlations.[30] Mixtures of matrix elements also arise quite naturally in the theory of forbidden β-decay[31] and interference effects of the type discussed here will, therefore, also occur in the $\beta-\gamma$-angular correlations. The theory of the $\beta-\gamma$-correlation has been treated by one of us[32] and will be discussed elsewhere.

The authors would like to express their appreciation to Professor G. E. Uhlenbeck for suggesting this investigation and for the many invaluable discussions with him concerning this and other aspects of angular correlation theory. Professor Hamilton of Princeton University generously made available to us unpublished computations of his, which greatly facilitated the preparation of the tables. This work was begun while one of the authors (D. L. F.) held a National Research Council Predoctoral Fellowship and the other (D. S. L.) a Rackham Predoctoral Fellowship at the University of Michigan. The preparation for publication was supported in part by the Joint Program of the AEC and ONR at the University of Notre Dame.

APPENDIX

We indicate why it is not correct to merely substitute Hamilton's tabulated correlation functions for $W_{LL'}(\theta)$, $L, L'=1$ or 2, in Eq. (19). For a dipole—(magnetic) dipole correlation, $W(\theta)$ has the form: (*a*) $W_{11}(\theta)=Q_{11}+R_{11}\cos^2\theta$. Since this is a relative probability, it can equally well be written as (*b*) $W_{11}(\theta)=1+R_{11}/Q_{11}\cos^2\theta$ which is the form tabulated by Hamilton. Similarly a dipole—(electric) quadrupole correlation could be written as either: (*a'*) $W_{12}(\theta)=Q_{12}+R_{12}\cos^2\theta$ or (*b'*) $W_{12}(\theta)=1+R_{12}/Q_{12}\cos^2\theta$. When the second transition is mixed, and if for simplicity we assume that $R(\alpha\beta^*)=0$ so that the interference term vanishes, then (19) yields for the correlation with mixtures:

$$W(\theta)=|\alpha|^2W_{11}(\theta)+|\beta|^2W_{12}(\theta)$$
$$=[|\alpha|^2Q_{11}+|\beta|^2Q_{12}]+[|\alpha|^2R_{11}+|\beta|^2R_{12}]\cos^2\theta$$

which is the weighted average of $W_{11}(\theta)$ and $W_{12}(\theta)$ when taken in the form (*a*) and (*a'*). This can now be written in the form:

$$W(\varphi)=1+R'/Q\cos^2\theta$$

with

$$R/Q=\frac{|\alpha|^2R_{11}+|\beta|^2R_{12}}{|\alpha|^2Q_{11}+|\beta|^2Q_{12}}$$

which is correct but clearly not the same as one would get by substituting the forms (*b*) and (*b'*) of reference 1 into (19). The argument is the same when interference is taken into account, only one get additional terms with coefficients $R(\alpha\beta^*)$ in R and Q.

Another respect in which the calculation of correlations for mixtures differs from that for pure multipoles is the necessity to retain the normalizing factors in the transformation coefficients Only those factors common to both multipoles can be dropped.

---

[30] The theory of angular correlations involving internal conversion electrons has been treated by D. S. Ling, Jr., thesis, University of Michigan, April 1948, and D. S. Ling, Jr. and G. E. Uhlenbeck, (to be published). See also V. B. Berestetski, J. Exp. Theor. Phys. U.S.S.R. **18**, 1057 (1948), (*In Russian*).

[31] E. J. Konopinski and G. E. Uhlenbeck, Phys. Rev. **60**, 308 (1941).

[32] See D. L. Falkoff, thesis, University of Michigan, April, 1948; D. L. Falkoff and G. E. Uhlenbeck, Phys. Rev. **73**, 649A (1948).

Radioactive Y^{84}, Y^{88}, and Zr^{87}

B. E. ROBERTSON,* W. E. SCOTT,* AND M. L. POOL
Ohio State University, Columbus, Ohio

(Received August 24, 1949)

A 3.7-hour activity, assigned to Y^{84}, has been obtained by bombardment of Sr^{84} with 10-Mev deuterons. Characteristic radiations are 2.0-Mev positrons, x-rays, and gamma-rays. A 2.0-hour activity, assigned to Zr^{87}, has been obtained by bombarding natural strontium and Sr^{84} with 20-Mev alpha-particles. Characteristic radiations are 2.0-Mev positrons, x-rays, and gamma-rays. Bombardments of $Sr^{87}+d$, $Y+n'$, and $Rb+\alpha$ are in agreement with the assignment of a 105-day activity to Y^{88} but show no evidence of a 2.0-hour positron activity previously assigned to Y^{88}.

I. 3.7-HOUR Y^{84}

WITH electromagnetically enriched isotopes of strontium now available, activities in the strontium, yttrium, and zirconium region have been investigated.

Bombardment of enriched** $Sr^{84}O$ with 10-Mev deuterons yielded a 3.7±0.1-hour positron activity which was followed through ten half-lives on a calibrated spectrometer counter.[1] The $Sr^{84}O$ was enriched to 27.7 percent strontium 84 as compared with the 0.56 percent strontium 84 found in natural strontium. The 3.7-hour activity was also produced by bombardment of $Sr^{84}O$ with 5-Mev protons. The 3.7-hour activity was not brought out by deuterons on $Sr^{86}O$ or $Sr^{87}SO_4$, which contained 0.3 percent and 0.2 percent strontium 84 respectively. To confirm the chemical identity of the 3.7-hour activity, normal SrO was bombarded with deuterons and an yttrium fraction extracted. The 3.7-hour activity was then observed in the yttrium fraction. Its abundance relative to that produced by $Sr^{84}O+d$ was in close agreement with the relative percentages of strontium 84 in SrO and $Sr^{84}O$. Total activity and x-ray activity as measured on a Wulf electrometer are shown in Fig. 1 for $Sr^{84}O+d$. The well-known 55-day and 65-day activities of Sr^{89} and Sr^{85} and the 14-hour, 3.3-day activities of the isomer Sr^{87} may also be seen.[2] Presence of the 3.7-hour x-ray activity indicates that *K*-capture decay is associated with this activity. A 3.7-hour gamma-decay was also noted. By aluminum-absorption measurements taken during the 3.7-hour activity the energy of the positrons was found to be 2.0±0.1 Mev.

To eliminate the possibility that the 3.7-hour positron activity could be the 3.92-hour scandium 43 activity and the 3.9-hour scandium 44 activity produced by deuterons on a possible calcium impurity in the enriched strontium 84, one-milligram samples of normal CaO and $Sr^{84}O$ were bombarded simultaneously on a manually rotated target. Initial intensities of the 3.9-hour scandium activities from deuterons on calcium and of the 3.7-hour activity from deuterons on strontium 84 were 6600 counts per minute and 100,000 counts per minute respectively. Energies of the scandium positrons as measured on the spectrometer counter were in agreement with the reported energies of 1.13 and 1.3 Mev as opposed to the much higher energy of 2.0 Mev determined for the 3.7-hour yttrium positron.

On the basis of these data the 3.7-hour activity is assigned to yttrium. Since the daughter products from an Y^{85} activity were not observed and inasmuch as the yield from p,n reactions on strontium 86 and 87 is found to be approximately six times that of p,γ reactions on the same isotopes, the abundance of the 3.7-hour activity from protons on strontium 84 indicates that placement at Y^{84} is preferable to placement at Y^{85}.

II. 2.0-HOUR Zr^{87}

A bombardment of normal SrO with 20-Mev alpha-particles revealed a 2.0±0.1-hour positron activity present in the zirconium fraction. To determine which of the stable isotopes of strontium contribute to the formation of the 2.0-hour positron activity, a simultaneous alpha-bombardment of enriched $Sr^{84}O$ and $Sr^{86}O$ was made. The $Sr^{84}O$ contained 27.7 percent strontium 84 and 29.9 percent strontium 86. The $Sr^{86}O$ contained 0.3 percent strontium 84 and 69.9 percent strontium 86.

The decay of the positron activity from $Sr^{84}O+\alpha$, as measured on the spectrometer counter, consisted of a 2.0-hour decay through five half-lives and a longer activity of 3.25-days. The decay of the $Sr^{86}+\alpha$-sample consisted of the 3.25-day positron activity of zirconium 89 and the yttrium 91 activity of 57-days.[2] No 2.0-hour activity was observed in the $Sr^{86}O+\alpha$-decay. From the percent composition of the strontium in each of the two samples, one is led to conclude that the 2.0-hour activity is caused by the strontium 84 and should be assigned to zirconium 87. The reaction is $Sr^{84}(\alpha,n)Zr^{87}$.

From aluminum-absorption measurements taken in the 2.0-hour activity, the energy of the positron was determined as 2.0±0.1 Mev. A lead-absorption measurement taken in the 2.0-hour activity showed the existence of two gamma-rays of nearly equal intensity.

* Captain, U. S. Air Forces, research done under auspices U.S.A.F., Institute of Technology, Wright Field, Dayton, Ohio.

** Supplied by the Y-12 Plant, Carbide and Carbon Chemicals Corporation, through the Isotope Division, AEC, Oak Ridge, Tennessee.

[1] L. L. Woodward and D. A. McCown, Rev. Sci. Inst. **19**, 823 (1948).

[2] G. T. Seaborg and I. Perlman, Rev. Mod. Phys. **20**, 585 (1948).

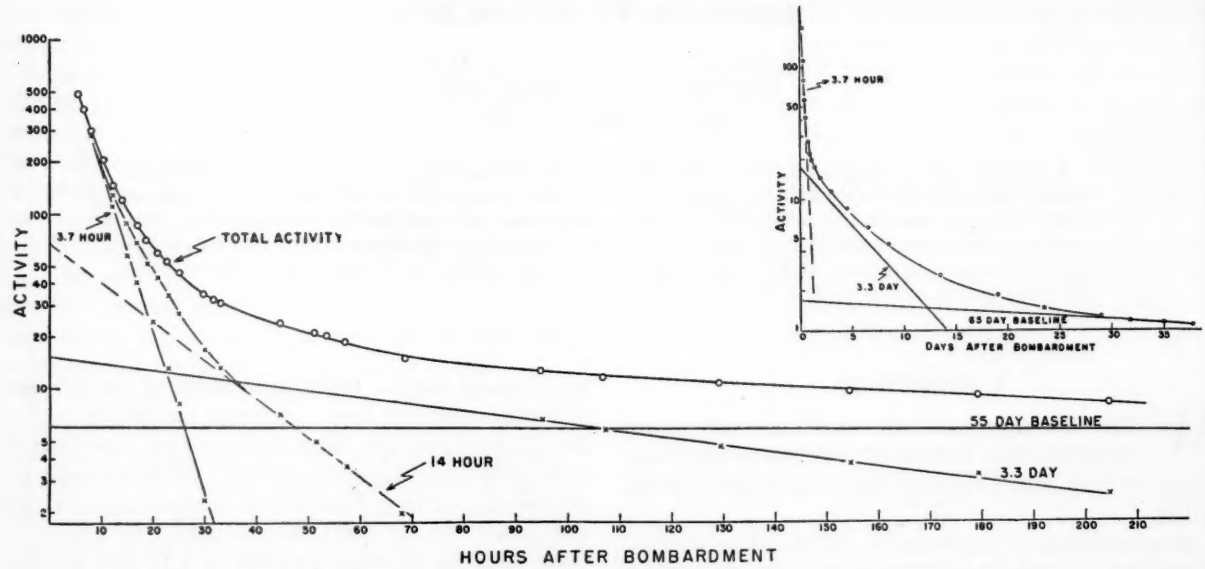

FIG. 1. Decay of $Sr^{84}O+d$. The 55-day activity corresponds to Sr^{89} from $Sr^{88}(d,p)Sr^{89}$. Inset: Decay of electromagnetic radiation as measured on Wulf electrometer equipped with magnet above chamber to deflect charged radiation. The 65-day activity corresponds to Sr^{85} from $Sr^{84}(d,p)Sr^{85}$.

Their energies correspond to 0.35 ± 0.05 Mev and 0.65 ± 0.05 Mev. Both are associated with the 2.0-hour activity. By aluminum-absorption measurements, x-rays, indicating decay by K-capture, were found associated with the 2.0-hour activity.

III. 2.0-HOUR Y^{88} REMOVED

In previous work on yttrium a 2.0-hour activity decaying by positron emission was reported as resulting from deuteron bombardment of strontium,[3-5] and fast neutron bombardment of yttrium.[3] The activity was assigned to yttrium 88. Later this positron activity was reported in the yttrium fraction from a bombardment of strontium with protons.[3] The determinations of the energy of the positrons varied from 1.2 Mev according to cloud-chamber observations to 1.65 Mev by aluminum-absorption measurements.

A 105-day activity of yttrium characterized by K-capture decay has been assigned to yttrium 88.[6] Its formation by a fast neutron bombardment of yttrium has been reported. Recent mass spectrographic analysis indicates that yttrium 88 is the correct mass assignment for this activity.[7]

A bombardment of Hilger Y_2O_3 with fast neutrons from $Li+d$ was made in order to study these reported activities of yttrium 88. The resultant decay of the yttrium fraction gave periods of 2.7-days and 105-days but no 2.0-hour activity. The only particle radiation observed was negative in sign. The 2.7-day activity is in agreement with that of the well-known yttrium 90 activity.

Bombardment of normal SrO with deuterons did not yield a 2.0-hour activity. With enriched strontium no 2.0-hour activity was noted for $Sr^{87}SO_4+d$ or for $Sr^{86}O+d$. To further determine the activities associated with yttrium 88, a bombardment of Hilger RbCl with alpha-particles was made. In the decay of the yttrium fraction no 2.0-hour activity was observed. The 2.7-day activity of yttrium 90 and the 105-day activity of yttrium 88 were both observed, however.

It is concluded that the 2.0-hour positron activity previously observed is not an activity of yttrium 88 which is found to exhibit a 105-day activity.

IV. ACKNOWLEDGMENTS

Grateful acknowledgment is made for the support received from the Ohio State Development Fund and the Graduate School.

[3] D. W. Stewart, Phys. Rev. **56**, 629 (1939).
[4] L. A. Dubridge and J. Marshall, Phys. Rev. **58**, 7 (1940).
[5] R. T. Overman, MDDC 354, AEC.
[6] A. C. Helmholz, Phys. Rev. **62**, 301 (1942).
[7] R. J. Hayden, Phys. Rev. **74**, 652 (1948).

Absolute Voltage Determination of Two Nuclear Resonances below 0.4 Mev

A. H. MORRISH
Institute for Nuclear Studies, University of Chicago, Chicago, Illinois
(Received August 19, 1949)

An absolute voltage determination was made of the $F^{19}(p\alpha', \gamma)$ and the $B^{11}(p,\alpha)$ and $B^{11}(p,\gamma)$ resonances. A calibrated electrostatic analyzer was used to measure the proton beam energy from a Crockroft-Walton linear accelerator. The values obtained were 0.3404±0.0004 Mev and 0.1628±0.0002 Mev, respectively. An approximate estimate of the half-width appears to give 2.0±1.0 kv for the fluorine and 4.5±1.5 kv for the boron resonance.

INTRODUCTION

A NUMBER of absolute voltage measurements have been made of the $Li(p,\gamma)$ resonance,[1,2] and recently[3] absolute determinations of three resonances were made in a precise experiment. Shoupp, Jennings, and Jones[4] have made an absolute determination of the $Li(p,n)$ threshold using a radiofrequency ion speed gauge. Up to now, no highly precise absolute determination has been made below 0.4 Mev. In this work the $F(p\alpha',\gamma)$ and the $B(p,\alpha)$ and the $B(p,\gamma)$ resonances have been measured with the aid of a 90° electrostatic analyzer, calibrated with an electron gun. The advantage in using the analyzer derives from the fact that the voltage is scaled down by a factor, in this case about 15, and the resulting voltage accurately determined with the aid of a stack of wire-wound resistors.

The intense fluorine resonance has the advantage of a much narrower half-width as compared to the Li resonance at approximately 440 kv, and should find considerable use as a calibration point in the future. The gamma-resonance in boron is relatively weak, and perhaps not too well suited as a calibration point. However the alpha-resonance, at the same voltage, is readily detected with an ion chamber.

EXPERIMENTAL TECHNIQUE

A linear accelerator of the Cockcroft-Walton type ("kevatron"), with up to 0.4 million volts range, was used to accelerate hydrogen ions from a low voltage arc.[5] The ionic beam was magnetically analyzed, and either H^+ or H_2^+ ions were selected to impinge on the target. The targets were perforated with a slot along the horizontal axis (except for the pressed amorphous boron ones). Most of the beam hit the target, initiating the desired nuclear reaction. The gamma-rays were detected with a Geiger-Müller counter, the active volume of which was approximately 13 cm from the target. Part of the beam, however, passed through the slot, and entered an electrostatic analyzer. These ions were then collected in a Faraday cage when suitable potentials were applied to the cylindrical plates of the analyzer. In this way the beam energy could be determined to a high degree of precision. The target slots were beveled sharply in order to prevent possible errors in the measurement of the beam due to scattering. A schematic diagram of the experimental arrangement employed for the gamma-resonances is shown in Fig. 1. In the case of the boron alpha-resonance, an ion chamber replaced the G-M tube, and the target was placed at approximately 45° to the proton beam and to the ion chamber. In the case of the pressed boron target, the beam energy was measured by sliding the target up out of the ion beam by means of a shaft working through a Wilson seal. The G-M counter was 5 cm in diameter and 10 cm long, enclosed in a lead shield. The counter was filled with argon at 10 cm pressure, and ethyl acetate was used as the quenching agent. The ion chamber was a wide angle type, 1.43 cm in diameter, 1.71 cm deep, with its window 5.40 cm from the target center, and filled with argon at atmospheric pressure. The window used was a film of mica, 2.6 mg/cm², and a film of aluminum, 3.44 mg/cm² in thickness; the combination stopped all alphas of range less than 3.9 cm of air.

The pulses from the G-M tube and the ion chamber were recorded by a conventional scaling circuit. The ions collected in the Faraday cage were recorded by observing the deflection of a sensitive galvanometer. Since the ions so collected had an energy distribution (see Fig. 2), it was found inconvenient to read the beam energy this way at every point during the study of a resonance. A resistor of approximately 6.6×10^9 ohms was used to drain a small current from the kevatron, which was read on a good milliammeter[6] with a 0.03-ma range scale. When the milliammeter reading for the resonance peak had been obtained from a gamma- or alpha-profile, the kevatron voltage was immediately reset to reproduce this current drain, and the protons bent around the analyzer to establish their energy on the absolute scale. This, of course, also gave an absolute value for the resistance of the 10^9 ohm stack at the time and conditions of the experiment; but this

[1] Hafstad, Heydenburg, and Tuve, Phys. Rev. **50**, 504 (1936); Parkinson, Herb, Bernet, and McKibben, Phys. Rev. **53**, 642 (1938); A. O. Hanson and D. L. Benedict, Phys. Rev. **65**, 33 (1944).
[2] R. Tangen, Kgl. Norske. Vid. Sels. Skrifter, NRI (1946).
[3] Herb, Snowdon, and Sala, Phys. Rev. **75**, 246 (1949).
[4] Shoupp, Jennings, and Jones, O.N.R. report GR-151.
[5] S. K. Allison, Rev. Sci. Inst. **19**, 291 (1948).
[6] Weston Model 622.

value was not used in computing the resonance voltage. Each time a resonance curve was taken the determination of the absolute energy of the hydrogen ion beam at the critical point in the resonance was repeated. The value of the resistance, also found at this time, was used in plotting the off-resonance points to establish the shape of the profile. The consistency of various runs shows that the 10^9 ohm resistor did not vary appreciably in the short time interval required to run a resonance. The resistor did, however, show measureable day to day variations.

THE ELECTROSTATIC ANALYZER

Since the details of the construction and calibration of the electrostatic analyzer are published elsewhere,[7] only a brief summary is included here. The instrument is of the cylindrical type, with an average radius of 15 cm, spacing 0.5 cm, and deflecting angle of 90°. The deflecting potential may be as high as 50 kilovolts, and therefore protons up to 0.75 Mev can be focused. Movable entrance and exit slits are incorporated. A set of calibration constants has been determined, so that given the coordinate of the centers of these slits, and the potentials applied to the deflecting plates, the energy of the focused ion beam can be calculated to within 0.25 percent.

The instrument was calibrated using an electron gun as a source. Electrons in the range 6 to 10 kilovolts were used, and precautions were taken to avoid errors due to stray magnetic fields. The deflector voltages for the calibration were obtained from stacks of B batteries, and measured with a potentiometer and two volt boxes.

The accelerating voltage for the electron gun was supplied by a 540-cycle, high voltage half-wave rectifier. The source of the 540-cycle current was a 5 hp synchronous motor—a.c. generator. The d.c. field of the generator was supplied by a storage battery. A 50-megohm stack of wirewound (Taylor) resistors, of 0.1 percent precision, was used for the accelerating voltage measurement. This stack was calibrated against another 50-megohm stack of Taylor resistors in order to detect any appreciable temperature effect. The two were found to be the same to within one part in a thousand. The resulting current drain was measured with a milliammeter. This meter was calibrated frequently with a potentiometer arrangement, and the

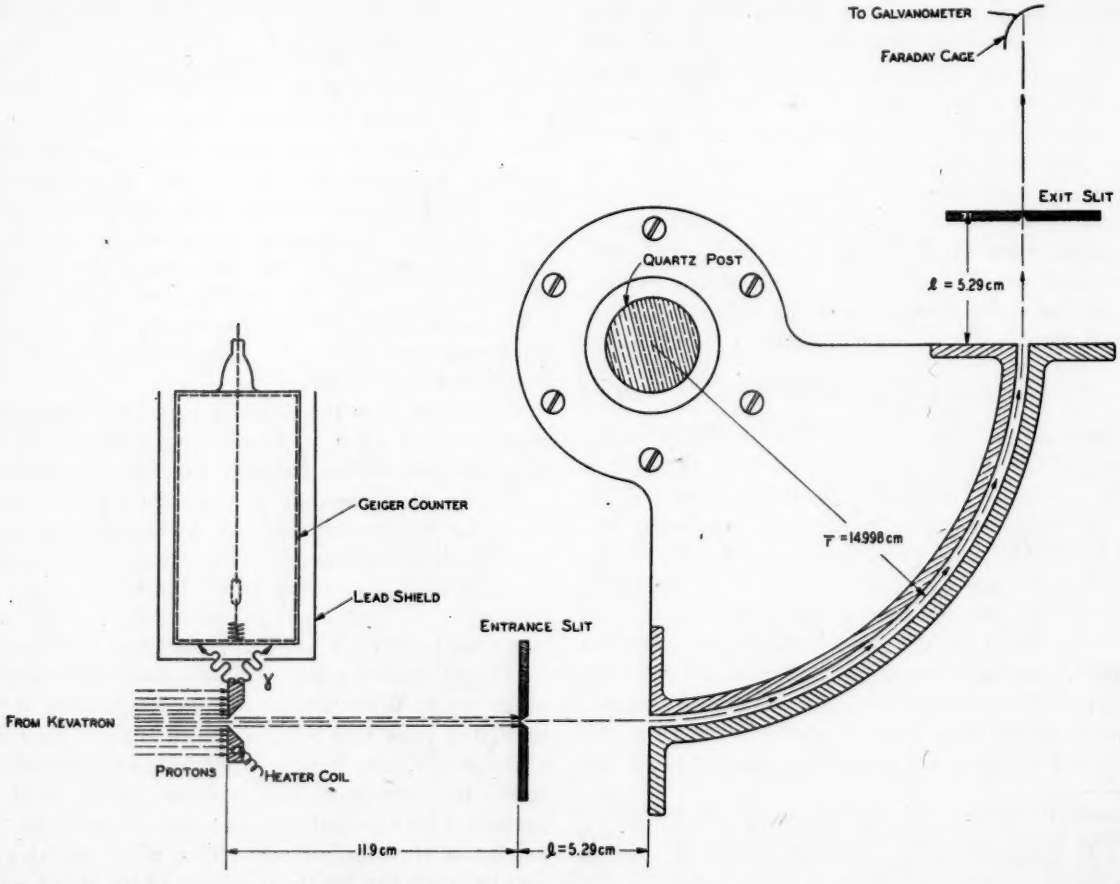

FIG. 1. Schematic diagram of the experimental arrangement for measuring gamma-ray resonances. For the boron alpha-resonance, the G-M counter was replaced by an ion chamber, and the target was at 45° to the proton beam and the chamber.

[7] Allison, Frankel, Hall, Montague, Morrish, and Warshaw, Rev. Sci. Inst., 20, 735 (1949).

standard cell used in this calibration was checked against another standard cell. The drain was about 200 microamperes, and the 540-cycle ripple was suppressed to less than 0.1 percent with a 0.05-microfarad filtering condenser. An electron profile obtained with the instrument, with a certain slit width, could then be used as a measure of the resolving power of the instrument, and later proton profiles from the kevatron were corrected for this effect using the electron curves.

The analyzer constant k, defined as $W_0/\{-(V_2-V_1)\}$, where W_0 is the kinetic energy of the ion, and V_1 and V_2 the deflecting potentials, is given in Table I, with the slits in the positions shown in Fig. 1. Inner charge means that the outer deflecting plate is at ground potential, and all the voltage is applied to the inner cylinder. Outer charge refers to the opposite case, and symmetric charge means that equal voltages, of opposite sign, were applied to the deflecting plates. The constant has been corrected for electron relativistic effects. (At 10 kv this is about 1 percent).

The geometry of the entrance and exist apertures of the deflecting channel is such that the stray field may be calculated analytically. This has been done for the case in which the deflecting plates are symmetrically charged. The predictions have been compared with experiments. Agreement with the calculations is demonstrated within the accuracy of the experiments, which is about 0.3 percent.

VOLTAGE REGULATION AND RIPPLE

The analyzer deflector voltages for the proton beam were obtained from the 540-cycle high voltage half-wave rectifier discussed in the section on the electrostatic analyzer as the electron accelerating voltage.

A Sola constant voltage transformer[8] was installed in the primary of the kevatron circuit. It is estimated that the kevatron voltage was maintained to about one part in 500 or 600 as read by the milliammeter in series with the 6.6×10^9 ohm resistor.

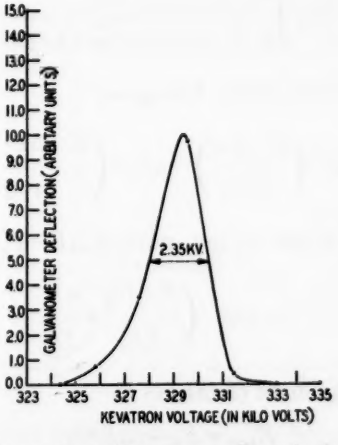

FIG. 2. H_2^+ energy profile as seen through the electrostatic analyzer with slits 1 mm wide. The indicated half-width has to be corrected for the resolving power of the analyzer itself.

[8] Model 30M818, Sola Electric Company, Chicago, Illinois.

TABLE I. Values of the analyzer constant k.

	Arrangement	k
A	Symmetric charge	15.31±0.02
B	Inner charge	14.81±0.02
C	Outer charge	15.81±0.02

A proton profile taken with the electrostatic analyzer is a measure of the inhomogeneity of the beam energy. The inhomogeneity is caused entirely by the voltage ripple in the kevatron, the probe of the arc contributing a negligible (6 volts) amount. A rough calculation of the ripple using the profile of Fig. 2 and others (not illustrated), together with plausible assumptions, may be made in the following way. The electron profiles, discussed in the analyzer section, give a value of 30 volts full width at half maximum at 9430 volts beam energy, using slits 1 mm wide. Taking this as the limit of resolution of the instrument, a value is calculated for the instrumental half-width at 341 kilovolts, the voltage at which the H_2^+ profile was taken, assuming that dE/E is constant. Assuming the profiles are approximately Gaussian, and using the equation $W_{\text{proton}}=(W^2_{\text{obs}}-W^2_{\text{electron}})^{\frac{1}{2}}$, where W_{proton} is the true proton half-width, W_{obs} is the observed proton half-width, and W_{electron} is the electron or instrumental half-width, we obtain the value 2.1 kv for the true half-width of the H_2^+ profile. If the ripple were sinusoidal, and the analyzer presented a narrow energy "window"[9] to the beam, a profile of two peaks should be observed, since the voltage is at the extreme of the sine curve for the longest time in a cycle. A very wide "window," ($\Delta E>2A$), would give a flat topped profile. The limiting case of $\Delta E=2A$ gives one sharp peak, and corresponds most closely with the observed profiles, as illustrated in Fig. 2. A more triangular shaped ripple, which is what one has with a Cockcroft-Walton, gives a curve in fairly good agreement with the observed ones. For this curve the half-width is clearly $2A$, and therefore the 2.1 kilovolts obtained as above may be taken as the value of the total voltage fluctuation due to ripple, to an accuracy of probably 10 to 20 percent.

An analysis of the circuit, making simplifying assumptions concerning the actions of the electronic valves, gives the ripple as 270 volts per 100 microamperes drain. The value 2.1 kilovolts corresponds to a drain of about 800 microamperes, a not too unreasonable figure since the beam and resistor drain are about 400 microamperes, leaving the other 400 to be accounted for by leakage down the supports, the glass accelerator tube, etc.

The proton profiles obtained on different days were all sharply peaked, and of roughly the same half-width,

[9] That is, if the analyzer transmitted particles of energy distribution $\Delta E\ll A$, where A is the amplitude of the ripple.

TABLE II. Values of the resonance obtained from a number of targets.

Target	E (kv)	ΔE (kv)	E_R (kv)	Γ (kv)
PbF_2	340.4	thick	340.4	3.0
PbF_2	340.4	thick	340.4	3.5
PbF_2	340.6	0.57	340.3	4.0
PbF_2	340.8	1.26	340.2	4.2
PbF_2	340.7	0.45	340.5	3.7
PbF_2	340.5	0.52	340.3	3.7
CaF_2	340.4	thick	340.4	3.1
CaF_2	340.6	thick	340.6	3.3
CaF_2	340.5	0.70	340.2	2.4
CaF_2	340.7	0.52	340.5	3.5
CaF_2	340.7	1.40	340.0	3.9
			Average E_R 340.4 kv	

so it is believed the value 2.1 kilovolts may be taken as the ripple in all the experimental work reported in this paper.

TARGET TECHNIQUE

For the fluorine gamma-resonance, targets of CaF_2 and PbF_2 were used. These are non-hygroscopic fluorides which evaporate, in vacuum, at temperatures of the order of 1000°C, apparently without decomposition. Both thick and thin targets of these salts were prepared by vacuum evaporation.

The thin boron targets were prepared by evaporating either amorphous boron or B_2O_3 in vacuum, on steel slotted targets. The B_2O_3 targets had a short life under bombardment, however, and the boron targets were found to be the most satisfactory. The thick targets were made by pressing amorphous boron into a steel cap.

Considerable time was spent in the installation of a new pumping system on the kevatron, to eliminate oil deposits on the targets. A large liquid air trap incorporating two right-angle bends, was placed between the pumps and the acceleration tube. An auxiliary pumping system on the electrostatic analyzer had a trap, cooled with solid CO_2, in an analogous position. Vanes between the traps and the kevatron or deflector were only opened during a run, when the traps were cold. The high consistency of the results leads to the conclusion that the oil problem had been solved, since it is hardly likely that a constant thickness of oil film would be deposited on all targets.

THIN TARGET CORRECTIONS

The point of inflexion of the forward slope of a thick target yield curve gives the value of the resonance. However, for a thin target the peak of the resonance curve is shifted higher with increased target thickness. This thickness may be obtained with the aid of the equation:

$$A(\Delta E)=\int Y dE=\Delta E Y_{\max}(\infty), \tag{1}$$

where A is the area under the excitation curve for a target whose thickness corresponds to a loss of energy ΔE, and $Y_{\max}(\infty)$ is the maximum yield of a corresponding thick target curve. It has been shown[10] that this result is independent of the homogeneity of the beam, and the exact shape of the yield curve.

For a target of thickness Δx, corresponding to loss of energy ΔE, we may say

$$\begin{aligned} Y&=k\int_0^{\Delta x}\sigma(E)dx \\ &=k\int_E^{E-\Delta E}\sigma(E)(\partial x/\partial E)dE, \end{aligned} \tag{2}$$

where $\sigma(E)$ is the cross section for disintegration, and k a constant. The assumption is made the $\partial x/\partial E$ is constant over the resonance, valid if the resonance is sharp. The expression (2) neglects, however, the inhomogeneity of the beam energy, and taking this into account gives

$$Y=k'\int_{E-e}^{E+e}\int_E^{E-\Delta E}\sigma(E)f(E-E')dEdE',$$

where $f(E-E')$ is a function determined by the ripple of the kevatron, and represents that fraction of ions between E' and $E'+dE'$ in energy, and e is the amplitude of the ripple. The function $f(E-E')$ was not known.

The Breit-Wigner resonance equation[11]

$$\sigma=\frac{K}{(E-E_R)^2+(\Gamma/2)^2}$$

is used, neglecting the wave-length and penetration factor. Substitution for σ, and neglecting constants and the inhomogeneity of the beam, gives

$$Y\sim\int_E^{E-\Delta E}\frac{dE}{(E-E_R)^2+(\Gamma/2)^2},$$

Γ being the half-width. This gives

$$Y=\tan^{-1}\left(\frac{E-E_R}{\Gamma/2}\right)-\tan^{-1}\left(\frac{E-\Delta E-E_R}{\Gamma/2}\right). \tag{3}$$

For a thick target we get, putting $\Delta E=E$,

$$Y=\tan^{-1}\left(\frac{E-E_R}{\Gamma/2}+\frac{\pi}{2}\right). \tag{4}$$

Now the maximum of (3) lies at

$$E_{\max}=E_R+(\Delta E/2), \tag{5}$$

and at this value $Y_{\max}(\Delta E)=2\tan^{-1}(E/\Gamma)$. For a

[10] Bernet, Herb, and Parkinson, Phys. Rev. 54, 398 (1938).
[11] G. Breit and E. Wigner, Phys. Rev. 49, 519 (1936).

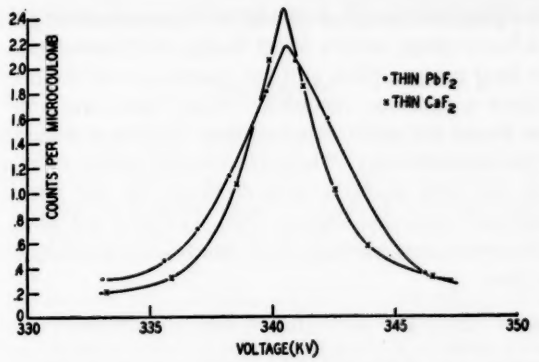

FIG. 3. The fluorine resonance for two thin targets. The resonance value had to be corrected for finite target thickness.

thick target we get $Y_{max}(\infty)=\pi$. Therefore:

$$\frac{Y_{max}(\Delta E)}{Y_{max}(\infty)}=\frac{2\tan^{-1}(E/\Gamma)}{\pi}. \quad (6)$$

Also, if the half-width of the experimental curve is Γ', then

$$\Gamma=(\Gamma'^2-\Delta E^2)^{\frac{1}{2}}. \quad (7)$$

Graphs of Eqs. (6) and (7) may be found in the literature.[12]

In this work, the target corrections applied were obtained from (1) and (5). Values of ΔE obtained from (6) and (7) would have lowered E_R by approximately 3 or 4 tenths of a kilovolt from the values obtained with (1) for the fluorine resonance. This is undoubtedly due to the measured half-width's dependence on the voltage ripple. The results so obtained were in good agreement with the thick target resonance values, as will be seen later.

However, the value of Γ, the width at half maximum, is given as obtained from (6) and (7), and gives an indication of the resonance width, at least in the case of the boron curves, since the half-width was much larger than the ripple. The half-width obtained for fluorine, however, was just slightly wider than the width of the beam energy inhomogeneity, and the values of Γ obtained are not nearly as reliable. Half-widths were also obtained by differentiating the forward slope of the thick yield curves, and were somewhat smaller than the half-widths obtained from the thin targets. The differentiated curves should be corrected for beam energy inhomogeneity, but this was not possible in this work. However, it is believed that an estimate of the half-width to within 1 to 2 kilovolts may be made with the data.

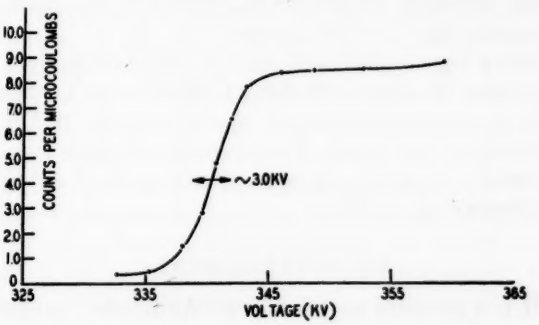

FIG. 4. A thick fluorine yield curve. The line with arrow is a measure of the half-width of the resonance, and should be corrected for the kevatron 2.1-kv ripple.

[12] Fowler, Lauritsen, and Lauritsen, Rev. Mod. Phys. **20**, 236 (1948).

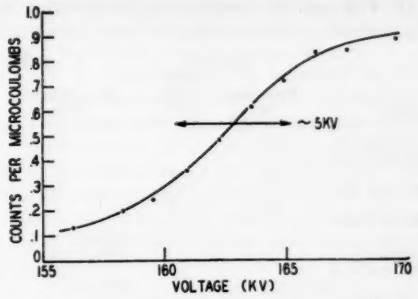

FIG. 5. Thick boron gamma-curve. The half-width, uncorrected for ripple is indicated.

THE FLUORINE RESONANCE

The fluorine gamma-rays were observed first by McMillan.[13] It has been shown[14] that a short range group of alpha-particles occur at the same resonance as the gamma-yield curve, with a range corresponding to the energy available. The reaction, then, is

$$F^{19}+H^1\rightarrow Ne^{20*}\rightarrow O^{16*}+He^4+1.8\text{ Mev}$$
$$O^{16*}\rightarrow O^{16}+h\nu.$$

Values of the resonance obtained by various workers is found in Table IV and discussed in a later section.

The H^+ beam was used in this work, and no difficulty was experienced in obtaining 15 to 25 microamperes of beam on the target. Typical experimental curves obtained are shown in Figs. 3 and 4. Table II lists the values of the resonance obtained from a number of targets. The average is seen to be 340.4 kv. Each determination is believed to be good to 0.25 percent, and the internal consistency good to 0.1 percent.

TABLE III. Complete summary of the data.

Target	Product observed	E (kv)	ΔE (kv)	E_R (kv)	Γ (kv)
Boron	Gamma	162.8	thick	162.8	5
Boron	Gamma	162.8	thick	162.8	5
Boron	Alpha	162.8	thick	162.8	5
Boron	Alpha	163.1	0.60	162.8	5.5
B_2O_3	Alpha	166.1	6.5	162.9	
			Average E_R	162.8 kv	

[13] E. McMillan, Phys. Rev. **46**, 325 (1934).

[14] McLean, Becker, Fowler, and Lauritsen, Phys. Rev. **55**, 796 (1939); W. E. Burcham and C. L. Smith, Nature, **143**, 795 (1939); Dee, Curran, and Strothers, Nature, **143**, 759 (1939); W. E. Burcham and S. Devons, Proc. Roy. Soc. London (A) **173**, 555 (1939).

TABLE IV. Values of the resonances given by other authors.

Authors	Fluorine Resonance (kv)	Fluorine Half-width (kv)	Boron Resonance (kv)	Boron Half-width (kv)
Hafstad and Tuve[a]	320			
Hafstad, Heydenburg, and Tube[b]	328	<4		
Bernet, Herb, and Parkinson[c]	334	8		
Williams, Wells, Tate, and Hill[d]			180(α)	
Bothe and Gentner[e]			180($\alpha+\gamma$)	
Haxby, Allen, and Williams[f]			160(α)	
Waldmann, Waddel, Callihan, and Schneider			165±4($\alpha+\gamma$)	<6
Bowersox[g]			172±5(α)	
McLean, Young, Whitson Plain, and Ellet[h]			160±5(α)	
v. Ubisch[i]			165(α)	
Jacobs and McLean[j]			158±3(α)	
Marvin[k]			162±1(α)	<11
Tangen[l]	339±2	1.5±0.5	162±1(γ)	5.3±1
Fowler, Lauritsen, and Lauritsen[m]	338	4±1		
Fowler and C. C. Lauritsen[n]	340±2	3.2		

[a] L. R. Hafstad and M. A. Tuve, Phys. Rev. **48**, 306 (1935).
[b] See reference 1.
[c] See reference 10.
[d] See reference 15.
[e] See reference 16.
[f] Haxby, Allen, and Williams, Phys. Rev. **55**, 140 (1939).
[g] R. B. Bowersox, Phys. Rev. **55**, 323 (1939).
[h] See reference 18.
[i] See reference 19.
[j] Jacobs and McLean, Proc. Iowa Acad. Sci. **48**, 304 (1941).
[k] J. F. Marvin, Phys. Rev. **68**, 228 (1945).
[l] See reference 2.
[m] See reference 12.
[n] W. A. Fowler and C. C. Lauritsen, Phys. Rev. **76**, 314 (1949).

Since the half-width is probably narrower than any of the values shown in the table, due to the ripple of 2.1 kv, a value of about 2 kv for this resonance width would seem to be a good estimate.

THE BORON RESONANCE

A number of reactions are possible when boron is bombarded with protons. The reactions are usually taken to be [2,15–19]

$$B^{11}+H^1\rightarrow C^{12*}\rightarrow Be^{8*}+He^4\rightarrow 3He^4$$
$$B^{11}+H^1\rightarrow C^{12**}\rightarrow C^{12}+h\nu$$
$$B^{11}+H^1\rightarrow C^{12***}\rightarrow Be^{8}+He^4\rightarrow 3He^4.$$

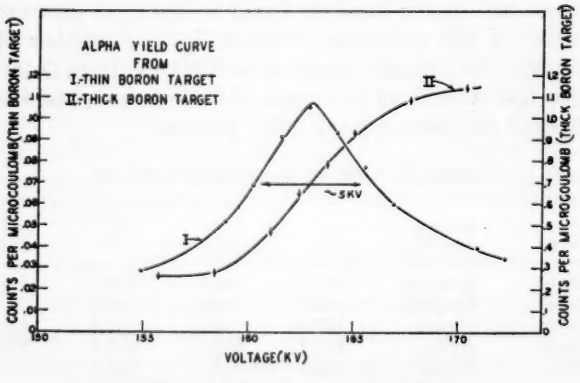

FIG. 6. Thick and thin boron alpha-yield curves.

The alphas are found to consist of a homogeneous group of 4.5-cm range, and a short range continuous group. The long range alphas and the gammas were found[16,17] to have a common resonance. Also, some workers[18,19] have found the short range alphas to have a resonance at this same energy. They are usually taken to result from the first reaction above. Work on the gamma-spectrum[20] revealed lines at 16.6, 11.8 and 4.3 Mev. It is, however, possible that weak lines could be due to the reaction

$$B^{11}+H^1\rightarrow C^{12}\rightarrow Be^{8*}+He^4\rightarrow 3He^4+h\nu$$

at resonance. The 16.6 Mev line was measured at an energy above resonance, and, as pointed out by Tangen,[2] it is not certain that the line actually occurs in the resonance radiation. The origin of all the alpha-particles is not certain yet.

In this work a beam of H_2^+ ions were used, and about 20 microamperes were obtained on the target. Lead shielding $\frac{1}{8}$-inch thick was placed between the G-M counter and the target. A typical gamma-ray curve is shown in Fig. 5, and thick and thin alpha-curves are shown in Fig. 6. A complete summary of the data is given in Table III. It is seen that the average value of the resonance for both the gammas and the alphas is 162.8 kv. The accuracy is probably as good as in the fluorine case. The half-width would seem to be about 4.5 kv, within 1.5 kv.

DISCUSSION

Table IV lists values of the resonances obtained by other workers. Bernet, Herb, and Parkinson obtained their value using a rotating disc voltmeter. Tangen's result of 339±2 kv for fluorine is based on a direct determination of the Li resonance at 440 kv, using a calibrated high resistance stack. He obtains, on weighing his results with other writers, the value 340 kv. Fowler and Lauritsen's value was obtained by using Herb, Snowdon, and Sala's recently determined value for the 873.5 kv fluorine resonance. The half-widths reported by various authors is higher than the estimated value obtained in this work, with the exception of Tangen's result, which is lower.

The previous work on boron is also summarized in the table. Waldman, Waddel, Callihan, and Schneider used a resistance calibrated against a stack of Taylor resistors in their work. The most recent value was obtained by Tangen in the same manner as he determined the fluorine resonance.

ACKNOWLEDGMENTS

It is a pleasure to thank S. K. Allison for extending the facilities of his laboratory to the author for this investigation, and for his interest, suggestions, and assistance. Also, I wish to thank J. H. Montague for

[15] Williams, Wells, Tate, and Hill, Phys. Rev. **51**, 434 (1937).
[16] W. Bothe and W. Gentner, Zeits. f. Physik **104**, 685 (1937).
[17] Waldmann, Waddel, Callihan, and Schneider, Phys. Rev. **54**, 1017 (1938).
[18] McLean, Young, Whitson, Plain, and Ellet, Phys. Rev. **57**, 1083 (1940).
[19] H. v. Ubisch, K.N.V.S. Forh. XV, 71 (1942).
[20] Fowler, Gaerttner, and Lauritsen, Phys. Rev. **53**, 628 (1939).

discussions and assistance, and D. S. Bushnell, who aided in the collection of much of the data.

APPENDIX

Tangen[2] believes his accuracy of the Li(p,γ) resonance to be 0.5 percent, but believes his voltage scale has a much higher relative accuracy. The linearity of his voltmeter scale was tested with protons and diatomic ions, and he got excellent correspondence with two reactions below 450 kev. As noted previously, he obtained 339 kev for the F$(p\,\alpha',\gamma)$ and 162 for the B(p,γ) resonances.

The author's value of boron was found at 162.8±0.2 kev and assuming a linear scale, we get 340.7 kev for the fluorine resonance when Tangen's value of 339 kev is used. The value actually obtained was 340.4±0.4 kev, adding weight to the belief that Tangen's resistor was truly ohmic in character. A linear extrapolation from the fluorine value, using Tangen's result of 440 kev for the lithium resonance, gives 441.8 kev. A linear extrapolation from the boron value gives 442.2 kev, and the average of the two is 442.0 kev. This is in good agreement with the value 441.4±0.5 kev obtained by Fowler and Lauritsen,[21] and the value 442.4 kev obtained by Hudspeth and Swann,[21] both obtained using the F$(p\,\alpha',\gamma)$ resonance at 873.5 kev as recently determined by Herb, Snowdon, and Sala[3] in an absolute measurement.

Recently, N. P. Heydenburg has informed me he has made absolute determinations using a new, carefully calibrated resistor in his high resistance voltmeter. He obtained for $B^{11}(p,\gamma)$ 161.7 ±0.2 kev; for F$(p\,\alpha',\gamma)$ 339.7±0.2 kev; and for $Li^{7}(p,\gamma)$ 440.8 ±0.5 kev. These values are 1.1 and 0.7 kev lower than the ones made in this laboratory, and 1.2 kev lower than the estimate for lithium. If an average of these values is taken, one obtains the following table, in which extra weight has been given to Heydenburg's $Li^{7}(p,\gamma)$ value:

	kev
$B^{11}(p,\gamma)$	162.2
F$(p\,\alpha',\gamma)$	340.0
$Li^{7}(p,\gamma)$	441.2
F$(p\,\alpha',\gamma)$	873.5

These values are quite close on a percentage basis with the results from each laboratory, and one has some confidence they are good to ±0.5 kev, a fairly satisfactory situation.

[21] E. L. Hudspeth and C. P. Swann, Phys. Rev. 75, 1272 (1949).

PHYSICAL REVIEW VOLUME 76, NUMBER 11 DECEMBER 1, 1949

The Application of the Tomonaga-Schwinger Theory to the Interaction of Nucleons with Neutral Scalar and Vector Mesons

P. T. MATTHEWS
Clare College, Cambridge University, Cambridge, England

(Received June 28, 1949)

The Tomonaga-Schwinger theory is applied to the interaction of neutral scalar and vector mesons with nucleons. The Hamiltonians are derived in the interaction representation and virtual effects are transformed away. The meson and nucleon self-energies are calculated. It is shown that they are invariant and, like the electron self-energy, can be transformed away by formal renormalizations of the meson and nucleon masses. All effects are independent of the direction of the general space-like surface in spite of the occurrence in the Hamiltonian of terms explicitly dependent on this direction.

INTRODUCTION

THE generalized Schrödinger equation in the interaction representation was first given by Tomonaga[1] for a Hamiltonian which commuted with itself at all points on a general space-like surface. When this condition was not immediately satisfied, it was found necessary to add certain terms explicitly dependent on the normal to the space-like surface and then to verify that this new Hamiltonian led to an integrable equation and that the generalized equation reduced to the ordinary formalism for a special choice of the general surface. By this method the Hamiltonians have been obtained by Myamoto[2] for the cases to be considered here, namely, the interaction of nucleons with scalar or vector mesons. It has been shown by the present author[3] that the generalized Schödinger equation in the interaction representation can be derived by a development of the work of Weiss.[4] The Hamiltonians of this equation for the nucleon-meson interactions are here deduced by an application of this theory.

The equations so obtained are then transformed by the methods which Schwinger[5] used for the interaction of the electron with the electrodynamic field. Besides real effects, the transformed Hamiltonians contain terms which give rise to infinite self-energies of both types of particle. These are evaluated and it is shown that they can be transformed away, leaving an equation in terms of field variables which satisfy the free field equations of the separate meson and nucleon fields with renormalized masses. Thus the observed free particle is taken to be the "bare" particle plus the vacuum effects.

The main difference between the electromagnetic case dealt with by Schwinger and those dealt with here is that now interactions which contain derivatives of the

[1] S. Tomonaga, Prog. Theor. Phys. 1, 27 (1946); Koba, Tati, and Tomonaga, Prog. Theor. Phys. 2, 101, 198 (1947); S. Kanesawa and S. Tomonaga, Prog. Theor. Phys. 3, 1, 101 (1948).
[2] Y. Myamoto, Prog. Theor. Phys. 3, 124 (1948).
[3] P. T. Matthews, Phys. Rev. 75, 1270 (1949). See also T. S. Chang, Phys. Rev. 75, 967 (1949).
[4] P. Weiss, Proc. Roy. Soc. A 169, 102 (1938).
[5] J. Schwinger, Phys. Rev. 74, 1492 (1948); 75, 615 (1949).

field variables are being considered. Consequently, even the transformed Hamiltonian contains terms which depend explicitly on the direction of the general space-like surface. The most important result of the present paper is that the transformed Hamiltonian contains a further implicit dependence on the surface direction which to the second order in the coupling constants exactly cancels the explicit term. It follows that all self-energies and cross sections predicted by the theory are independent of the surface direction and are thus relativistically invariant. It will be shown elsewhere that this independence of the surface direction can be proved up to any order for any effect.

The integrals in the self-energy calculations are not regular which has given rise to the different values for the photon self-energy obtained by Schwinger[5] and Wentzel.[6] To resolve this difficulty Pauli[7] has suggested a regularizing procedure. The effect of "regularizing" meson self-energies is discussed.

Only neutral meson fields will be considered. The introduction of charge will not affect the first-order self-energies calculated in this paper since for a proton only the positive, and for a neutron only the negative mesons will be significant.

I. THE SCHRÖDINGER EQUATION IN THE INTERACTION REPRESENTATION

Let x_μ be a general point in space-time, the Greek suffix taking the values from 1 to 4, ($x_4=ix_0$). $\sigma(x)$ is a general space-like surface through x_μ and n_μ is the normal to the surface at the point x_μ, pointing to the future, ($n_0>0$, $n_\mu{}^2=-1$). Consider the field whose Lagrangian is $\mathfrak{L}(\varphi^\alpha, \varphi_\mu{}^\alpha)$ where $\varphi_\mu{}^\alpha=\partial\varphi^\alpha/\partial x_\mu$. The energy-momentum tensor is defined in the usual way,

$$U_{\mu\nu}=\mathfrak{L}\delta_{\mu\nu}-(\partial\mathfrak{L}/\partial\varphi_\mu{}^\alpha)\varphi_\mu{}^\alpha. \tag{1.1}$$

Then it has been shown[3] that the canonical conjugate of φ^α can be defined as

$$\pi_\alpha=-(\partial\mathfrak{L}/\partial\varphi_\mu{}^\alpha)n_\mu, \tag{1.2}$$

and the commutation relations for points with space-like separation for Bose statistics are

$$[\varphi^\alpha(x), \pi_\beta(x')]=0 \quad \text{if} \quad (x-x')^2>0, \tag{1.3}$$

$$\int[\varphi^\alpha(x), \pi_\beta(x')]d\sigma'=i\hbar c\delta_{\alpha\beta}, \tag{1.4}$$

and for Fermi statistics are

$$\{\varphi^\alpha(x), \pi_\beta(x')\}=0 \quad \text{if} \quad (x-x')^2>0, \tag{1.5}$$

$$\int\{\varphi^\alpha(x), \pi_\beta(x')\}d\sigma'=i\hbar c\delta_{\alpha\beta}. \tag{1.6}$$

Further, if two fields interact, the Schrödinger equation in the interaction representation is

$$i\hbar c\delta\Psi/\delta\sigma=\mathfrak{IC}_{\text{int}}(\phi, \psi)\Psi, \tag{1.7}$$

where φ and ψ are the field variables of the two interacting fields, $\mathfrak{IC}_{\text{int}}$ is the interaction terms of the Hamiltonian defined

$$\mathfrak{IC}=U_{\mu\nu}n_\mu n_\nu \tag{1.8}$$

$$=-\mathfrak{L}-(n_\mu\partial\mathfrak{L}/\partial\varphi_\mu{}^\alpha)(n_\nu\varphi_\nu{}^\alpha), \tag{1.9}$$

and ϕ and ψ satisfy the equations of motion of their respective free fields. Thus,

$$\phi=R^{-1}\varphi_s R, \tag{1.10}$$

where

$$i\hbar c\delta R/\delta\sigma=\mathfrak{IC}_{\text{free}}(\varphi_s)R. \tag{1.11}$$

φ_s is the Schrödinger variable and $\mathfrak{IC}_{\text{free}}$ is the Hamiltonian of the free field. The commutation relations of ϕ and ψ are given by (1.2)–(1.6) applied to the Lagrangians of their free fields. Also define the energy-momentum vector on the surface as

$$P_\nu=-(1/c)\int U_{\mu\nu}(x')n_\mu' d\sigma', \tag{1.12}$$

then

$$(i/\hbar)[\varphi^\alpha(x), P_\mu]=(\partial\varphi^\alpha/\partial x_\mu). \tag{1.13}$$

To apply this general theory to the interaction of neutral scalar mesons with nucleons we will use the notation of Schwinger[5] which will not be defined here. The meson potential is $\varphi(x)$ while $\psi_\alpha(x)$ denotes the four-component Dirac spinor of the nucleon field. The differential $\partial\phi/\partial x_\mu$ is written $\varphi_\mu(x)$. Also

$$\kappa_0=m_0c/\hbar, \tag{1.14}$$

and

$$\kappa=mc/\hbar, \tag{1.15}$$

where m_0 and m are the mechanical proper masses of the nucleon and the meson, respectively.

The Lagrangian of the free nucleon field is

$$\mathfrak{L}_N=-\tfrac{1}{2}\hbar c\bar{\psi}(\gamma_\mu\partial/\partial x_\mu+\kappa_0)\psi -\tfrac{1}{2}\hbar c\psi(\gamma_\mu{}^T\partial/\partial x_\mu-\kappa_0)\bar{\psi}. \tag{1.16}$$

The Lagrangian of the free scalar meson field is

$$\mathfrak{L}_S=-\tfrac{1}{2}\{(\varphi_\mu{}^2)+\kappa^2\varphi^2\}. \tag{1.17}$$

The equations of motion of the free fields are

$$(\gamma_\mu\partial/\partial x_\mu+\kappa_0)\psi=0; \tag{1.18}$$

$$(\gamma_\mu{}^T\partial/\partial x_\mu-\kappa_0)\bar{\psi}=0, \tag{1.19}$$

and

$$(\Box^2-\kappa^2)\varphi=0. \tag{1.20}$$

The Lagrangian of the interacting fields is

$$\mathfrak{L}=\mathfrak{L}_N+\mathfrak{L}_S+\mathfrak{L}_{\text{int}}, \tag{1.21}$$

where

$$\mathfrak{L}_{\text{int}}=-(1/c)\omega\varphi-(1/c\kappa)j_\mu\varphi_\mu. \tag{1.22}$$

[6] G. Wentzel, Phys. Rev. 74, 1070 (1948).

[7] W. Pauli, Rouse Ball Lecture, Cambridge University, March, 1949. The "regularizing" process was defined and applied to the derivation of the photon self-energy.

ω and j_μ are covariant expressions in the nucleon variables defined by

$$\omega=\tfrac{1}{2}fc(\bar{\psi}\psi-\psi\bar{\psi}), \tag{1.23}$$

$$j_\mu=\tfrac{1}{2}igc(\bar{\psi}\gamma_\mu\psi-\psi\gamma_\mu{}^T\bar{\psi}). \tag{1.24}$$

The strengths of the interactions are determined by the constants f and g (having the dimensions of charge). Following Pais[8] we will consistently use f for an interaction which does not contain differentials of the field variables and g for one which does. We will speak in this sense of f-interactions and g-interactions.

The coefficients in the definitions of ω and j_μ have been chosen so that ω and $j_i=(-ij_4, j_1, j_2, j_3)$ are Hermitian. It is this condition which gives rise to the factor i in the coefficient for j_μ and ultimately leads to the opposite sign for the nucleon self-energy due to the f-interaction in the scalar and vector meson cases. This is the basis of the Pais f-field theory.[8]

To evaluate $\mathcal{H}_{\text{int}}$ we do not need to consider the Hamiltonian of the free nucleon field because the interactions do not contain the derivatives of the nucleon variables and the canonical conjugates of the nucleon field variables are not altered by the interaction. By (1.17), (1.22), and (1.2) the canonical conjugate of ϕ when there is interaction is

$$\pi=(\varphi_\mu+(1/c\kappa)j_\mu)n_\mu. \tag{1.25}$$

Thus by (9) omitting the free nucleon field

$$\mathcal{H}=\tfrac{1}{2}(\varphi_\mu{}^2+\kappa^2\varphi^2)+(1/c)\omega\varphi+(1/c\kappa)j_\mu\varphi_\mu +(\varphi_\mu+(1/c\kappa)j_\mu)\varphi_\rho n_\mu n_\rho. \tag{1.26}$$

Since n_μ is time-like the tangential part of $\varphi_\mu{}^2$ is

$$\varphi_\mu{}^2+(n_\mu\varphi_\mu)(n_\nu\varphi_\nu). \tag{1.27}$$

This is obvious in the special case when the surface is $x_4=$ const. since the components of n_μ are then $(0, 0, 0, i)$. The normal derivative must be formally eliminated from (1.26) in favor of the canonical conjugate by (1.25). Thus

$$\begin{aligned}\mathcal{H}=\tfrac{1}{2}\{&\varphi_\mu{}^2+(n_\mu\varphi_\mu)(n_\nu\varphi_\nu)\\ &-(\pi-(1/c\kappa)j_\mu n_\mu)(\pi-(1/c\kappa)j_\nu n_\nu)+\kappa^2\varphi^2\}\\ &+(1/c)\omega\varphi+(1/c\kappa)\{j_\mu\varphi_\mu+(j_\mu n_\mu)(\varphi_\nu n_\nu)\\ &-(j_\mu n_\mu)(\pi-(1/c\kappa)j_\nu n_\nu)\}+\pi(\pi-(1/c\kappa)j_\nu n_\nu).\end{aligned} \tag{1.28}$$

Thus

$$\mathcal{H}=\mathcal{H}_{\text{free}}+\mathcal{H}_{\text{int}}, \tag{1.29}$$

where

$$\mathcal{H}_{\text{free}}=\tfrac{1}{2}\{\varphi_\mu{}^2+(n_\mu\varphi_\mu)(n_\nu\varphi_\nu)+\pi^2+\kappa^2\varphi^2\}, \tag{1.30}$$

and

$$\mathcal{H}_{\text{int}}=(1/c)\omega\varphi+(1/c\kappa)\{j_\mu\varphi_\mu+(j_\mu n_\mu)(\varphi_\mu n_\mu-\pi)\} +(1/2c^2\kappa^2)(j_\nu n_\nu)^2. \tag{1.31}$$

[8] A. Pais, Kon. Ned. Akad. v. Wet. Verh. D1 **19**, 1 (1947).

But in the interaction representation the field variables satisfy the free-field equations and thus by (1.2) and (1.17)

$$\pi=\varphi_\mu n_\mu, \tag{1.32}$$

and in the interaction representation

$$\mathcal{H}_{\text{int}}=(1/c)\omega\varphi+(1/c\kappa)j_\mu\varphi_\mu+(1/2c^2\kappa^2)(j_\nu n_\nu)^2, \tag{1.33}$$

which is in agreement with the result of Myamoto.[2]

By (1.2) and (1.16) the canonical conjugates of ψ_α and $\bar{\psi}_\alpha$ are

$$\pi_\alpha=\tfrac{1}{2}\hbar c(\bar{\psi}\gamma_\mu)_\alpha n_\mu, \quad \bar{\pi}_\alpha=\tfrac{1}{2}\hbar c(\gamma_\mu\psi)_\alpha n_\mu. \tag{1.34}$$

By (1.5) and (1.6) the commutation relations are

$$i\int\{\psi_\alpha(x), (\bar{\psi}(x')\gamma_\mu)_\beta\}d\sigma'=\delta_{\alpha\beta}, \tag{1.35}$$

$$i\int\{(\gamma_\mu\psi(x'))_\alpha, \bar{\psi}_\beta(x)\}d\sigma_\mu{}'=\delta_{\alpha\beta}, \tag{1.36}$$

where

$$d\sigma_\mu{}'=-n_\mu d\sigma', \tag{1.37}$$

and

$$\begin{aligned}\{\psi_\alpha(x), \psi_\beta(x')\}&=\{\bar{\psi}_\alpha(x), \bar{\psi}_\beta(x')\}\\ &=\{\psi_\alpha(x), \bar{\psi}_\beta(x')\}=0 \quad \text{if} \quad (x-x')^2>0.\end{aligned} \tag{1.38}$$

Also

$$\int[\varphi(x), \varphi_\mu(x')]d\sigma_\mu{}'=-i\hbar c, \tag{1.39}$$

$$[\varphi(x), \varphi(x')]=0 \quad \text{if} \quad (x-x')^2>0. \tag{1.40}$$

In addition the commutation relations between the meson and nucleon field variables are

$$[\varphi(x), \psi(x')]=[\varphi(x), \bar{\psi}(x')]=0. \tag{1.41}$$

The above relations apply only to points with space-like separation. To obtain the general commutation relations for points with any separation introduce the function $\Delta(x)$ such that

$$(\Box^2-\kappa^2)\Delta(x)=0, \quad \Delta(x)=0 \quad \text{if} \quad x_\mu{}^2>0, \tag{1.42}$$

and

$$\int(\partial\Delta(x)/\partial x_\mu)d\sigma_\mu=1. \tag{1.43}$$

It then follows by the same argument as that given by Schwinger[5] in the electron-photon case that

$$[\varphi(x), \varphi(x')]=i\hbar c\Delta(x-x'). \tag{1.44}$$

$$\begin{aligned}\{\psi_\alpha(x), \bar{\psi}_\beta(x')&=-i(\gamma_\mu\partial/\partial x_\mu-\kappa_0)_{\alpha\beta}\Delta_0(x-x')\\ &=-iS_{\alpha\beta}(x-x').\end{aligned} \tag{1.45}$$

$\Delta_0(x)$ is the same expression as $\Delta(x)$ with κ replaced by κ_0. By (1.5) and (1.33) the Schrödinger equation in the

interaction representation is

$$i\hbar c\delta\Psi/\delta\sigma=\{(1/c)\omega\varphi+(1/c\kappa)j_\mu\varphi_\mu +(1/2c^2\kappa^2)(j_\nu n_\nu)^2\}\Psi. \quad (1.46)$$

We now consider the case in which the scalar meson field is replaced by a vector meson field $\varphi_\mu(x)$. Denote the differential $\partial\varphi_\mu(x)/\partial x_\nu$ by $\varphi_{\mu\nu}(x)$. The free field satisfies the equation

$$(\Box^2-\kappa^2)\varphi_\mu(x)=0, \quad (1.47)$$

and in classical theory the relation

$$\varphi_{\mu\mu}(x)=0, \quad (1.48)$$

which ensures that the energy is positive definite. If the Lagrangian of the free field is taken to be

$$\mathfrak{L}=-\tfrac{1}{2}\{\tfrac{1}{2}(\varphi_{\mu\nu}-\varphi_{\nu\mu})^2+\kappa^2\varphi_\mu^2\}, \quad (1.49)$$

then the variation of $\mathfrak{L}$ gives the equation of motion

$$(\partial/\partial x_\nu)(\varphi_{\mu\nu}-\varphi_{\nu\mu})=\kappa^2\varphi_\mu. \quad (1.50)$$

Differentiating gives Eq. (1.48) and substituting back into (1.50) yields Eq. (1.47). It is thus not necessary to introduce (1.48) as a special condition. However the appearance of the differentials of the field variables in the Lagrangian in antisymmetrical combinations leads directly to the equation

$$\pi_\mu n_\mu=0. \quad (1.51)$$

This equation is inconsistent with the commutation relations defined by (1.3), as can immediately be seen by taking the surface to be the plane $x_4=$const.

The immediate generalization of the scalar meson theory is to take the Lagrangian

$$\mathfrak{L}=-\tfrac{1}{2}\{\varphi_{\mu\nu}^2+\kappa^2\varphi_\mu^2\}, \quad (1.52)$$

with Eq. (1.48) as a supplementary condition on the wave function

$$\varphi_{\mu\mu}\Psi=0. \quad (1.53)$$

The application of the general theory to (1.52) would lead to the quantization of φ_μ as independent scalars and the general commutation relations

$$[\varphi_\mu(x),\ \varphi_\nu(x')]=i\hbar c\delta_{\mu\nu}\Delta(x-x'). \quad (1.54)$$

Thus by (1.54) and (1.47)

$$[\varphi_{\mu\mu}(x),\ \varphi_{\nu\nu}(x')]=i\hbar c\kappa^2\Delta(x-x'), \quad (1.55)$$

which is inconsistent with (1.53) since it is required of a supplementary condition that it commutes with itself at different space-time points.

Both these difficulties are avoided if a form of the theory given by Stueckelberg[9] is adopted. Two subsidiary fields are introduced, a vector field $A_\mu(x)$ and a scalar field $B(x)$ both satisfying Eq. (1.47). Write $\partial A_\mu(x)/\partial x_\nu$ as $A_{\mu\nu}(x)$ and $\partial B(x)/\partial x_\nu$ as $B_\nu(x)$. Define

$$\varphi_\mu=A_\mu+(1/\kappa)B_\mu, \quad (1.56)$$

and postulate the subsidiary condition in classical theory

$$A_{\mu\mu}+\kappa B=0. \quad (1.57)$$

The Lagrangian of the free field is

$$\mathfrak{L}_\nu=-\tfrac{1}{2}\{A_{\mu\nu}^2+\kappa^2A_\mu^2+B_\nu^2+\kappa^2B^2\}, \quad (1.58)$$

from which the correct equations of motion for A_μ and B follow directly. By (1.56) and (1.57) it can be shown that φ_μ so defined satisfies the required Eqs. (1.47) and (1.48).

If the meson field is interacting with a nucleon field the additional terms in the Lagrangian are

$$\mathfrak{L}_{\text{int}}=-(1/c)j_\mu(A_\mu+(1/\kappa)B_\mu) -(1/2c\kappa)m_{\mu\nu}(A_{\nu\mu}-A_{\mu\nu}), \quad (1.59)$$

where j_μ is defined by (24) with f replaced by g and

$$m_{\mu\nu}=\tfrac{1}{2}igc(\bar\psi\gamma_\mu\gamma_\nu\psi-\psi\gamma_\mu{}^T\gamma_\nu{}^T\bar\psi). \quad (1.60)$$

The Lagrangian of the free nucleon field is given by (1.16) and again need not be considered in the calculation of $\mathfrak{IC}_{\text{int}}$.

By a calculation similar to that given in the scalar case it can easily be shown that the Hamiltonian in the interaction representation is

$$\begin{aligned}\mathfrak{IC}_{\text{int}}&=(1/c)j_\mu(A_\mu+(1/\kappa)B_\mu)+(1/2c\kappa)m_{\mu\nu}(A_{\nu\mu}-A_{\mu\nu}) +(1/2c^2\kappa^2)\{(n_\mu j_\mu)^2+(n_\mu m_{\mu\nu})^2\}\\ &=(1/c)j_\mu\varphi_\mu+(1/2c\kappa)m_{\mu\nu}(\varphi_{\nu\mu}-\varphi_{\mu\nu}) +(1/2c^2\kappa^2)\{(n_\mu j_\mu)^2+(n_\mu m_{\mu\nu})^2\}. \quad (1.61)\end{aligned}$$

The general commutation relations follow as before

$$[B(x),\ B(x')]=i\hbar c\Delta(x-x'), \quad (1.62)$$

$$[A_\mu(x),\ A_\nu(x')]=i\hbar c\delta_{\mu\nu}\Delta(x-x'). \quad (1.63)$$

Equation (1.56) is replaced in quantum theory by a supplementary condition which in the interaction representation can be written

$$(A_{\mu\mu}+\kappa B)\Psi=\Omega\Psi=0. \quad (1.64)$$

Using the commutation relations (1.62) and (1.63) it can be shown that

$$(\Box^2-\kappa^2)\Omega=0, \quad (1.65)$$

$$[i\hbar c\delta/\delta\sigma(x')-\mathfrak{IC}(x'),\ \Omega(x)]=0. \quad (1.66)$$

and

$$[\Omega(x),\ \Omega(x')]=0. \quad (1.67)$$

These relations show that the supplementary condition is consistent with the field equations, the equation of motion and the commutation relations. From (1.56) and the commutation relations (1.62) and (1.63) the commutation relations for $\varphi_\mu(x)$ are

$$\begin{aligned}&[\varphi_\mu(x),\ \varphi_\nu(x')]\\ &\quad=i\hbar c(\delta_{\mu\nu}-(1/\kappa^2)\partial^2/\partial x_\mu\partial x_\nu)\Delta(x-x')\\ &\quad=i\hbar cT_{\mu\nu}(x-x'). \quad (1.68)\end{aligned}$$

By (1.61) the Schrödinger equation in the interaction

[9] E. C. G. Stueckelberg, Helv. Phys. Acta **11**, 225 (1938).

representation is

$$i\hbar c\delta\Psi/\delta\sigma=[(1/c)j_\nu\varphi_\nu+(1/2c\kappa)m_{\mu\nu}(\varphi_{\nu\mu}-\varphi_{\mu\nu})+(1/2c^2\kappa^2)\{(n_\mu j_\mu)^2+(n_\mu m_{\mu\nu})^2\}]\Psi. \quad (1.69)$$

II. THE VACUUM

To apply Schwinger's methods to the meson-nucleon interactions it is necessary to split the field variables into parts which can be interpreted as annihilation and creation operators and to define the vacuum. It will then be convenient to calculate the expectation values of certain expressions which appear in the later work and to develop explicitly the singular function $\Delta(x)$ and the associated functions $\Delta^{(1)}(x)$ and $\bar{\Delta}(x)$ which will be introduced below. Where this work is the same as that of Schwinger only the results will be quoted.

The scalar meson field can be split into positive and negative frequency parts

$$\varphi(x)=\varphi^{(+)}(x)+\varphi^{(-)}(x). \quad (2.1)$$

Schwinger[5] has shown that this can be done in an invariant manner. Define

$$\varphi^{(1)}(x)=i[\varphi^{(+)}(x)-\varphi^{(-)}(x)]. \quad (2.2)$$

It follows that

$$[\varphi^{(+)}(x),\ \varphi(x')]=i\hbar c\Delta^{(+)}(x-x'), \quad (2.3)$$

$$[\varphi^{(-)}(x),\ \varphi(x')]=i\hbar c\Delta^{(-)}(x-x'), \quad (2.4)$$

$$[\varphi^{(1)}(x),\ \varphi(x')]=i\hbar c\Delta^{(1)}(x-x'), \quad (2.5)$$

where $\Delta^{(+)}(x)$, $\Delta^{(-)}(x)$, and $\Delta^{(1)}(x)$ satisfy the same relations (2.1) and (2.2) as $\varphi^{(+)}(x)$, $\varphi^{(-)}(x)$, and $\varphi^{(1)}(x)$. Then

$$\Delta^{(1)}(x)=\Delta^{(1)}(-x),\quad \Delta(x)=-\Delta(-x). \quad (2.6)$$

$$(\Box^2-\kappa^2)\Delta^{(+)}(x)=(\Box^2-\kappa^2)\Delta^{(-)}(x)=(\Box^2-\kappa^2)\Delta^{(1)}(x)=0. \quad (2.7)$$

The wave function $\Psi(\sigma)$ on any particular surface σ specifies a state of the free field on that surface. The vacuum state must be defined to be that for which the eigenvalue of the energy in any frame is a minimum. Now by (1.12) and (1.13)

$$\varphi^{(+)}(x)P_\nu-P_\nu\varphi^{(+)}(x)=-i\hbar\partial\varphi^{(+)}(x)/\partial x_\nu. \quad (2.8)$$

Applying (2.8) to a Fourier component of $\varphi^{(+)}(x)$ give by

$$\varphi^{(+)}(x)=\int_{-k_\lambda n_\lambda>0}\varphi(k)\delta(k_\lambda{}^2+\kappa^2)\exp[ik_\mu x_\mu]d^4k,\qquad (d^4k=dk_0dk_1dk_2dk_3), \quad (2.9)$$

it follows that

$$\varphi^{(+)}(k)\mathrm{w}-\mathrm{w}\varphi^{(+)}(k)=\hbar\mathrm{w}\varphi^{(+)}(k), \quad (2.10)$$

where $\mathrm{w}=-n_\nu P_\nu c$ and $\mathrm{w}=-n_\nu k_\nu c$ are expressions for the energy and frequency in the arbitrary frame specified by the time-like vector n_μ. Since $-n_\nu k_\nu>0$ by (2.9), ω is positive. Operating with (2.10) on the vacuum state Ψ_0

$$\mathrm{w}\varphi^{(+)}(k)\Psi_0=(\mathrm{w}_0-\hbar\mathrm{w})\varphi^{(+)}(k)\Psi_0. \quad (2.11)$$

Thus $\varphi^{(+)}(k)\Psi_0$ is the state with one less meson in the k energy level and if Ψ_0 is the vacuum

$$\varphi^{(+)}(k)\Psi_0=0. \quad (2.12)$$

This equation is valid for all $\varphi^{(+)}(k)$ and thus

$$\varphi^{(+)}(x)\Psi_0=0. \quad (2.13)$$

In general $\Psi(\sigma)$ specifies occupation numbers of mesons in the various free meson energy states on the surface σ. $\varphi^{(+)}(x)$ and $\varphi^{(-)}(x)$ are annihilation and creation operators, respectively. With this definition the vacuum expectation value of the anticommutator is

$$\langle\{\varphi(x),\ \varphi(x')\}\rangle_0=\hbar c\Delta^{(1)}(x-x'). \quad (2.14)$$

A similar treatment of the free meson field yields the definition of the vacuum

$$\psi^{(+)}(x)\Psi_0=0. \quad (2.15)$$

And the expectation value of the commutator in the vacuum is

$$\langle[\psi_\alpha(x),\ \bar{\psi}_\beta(x')]\rangle_0=-S_{\alpha\beta}{}^{(1)}(x-x'). \quad (2.16)$$

The above theory can immediately be extended to the vector meson field. In place of (2.3)–(2.5) we have

$$[\varphi_\mu{}^{(+)}(x),\ \varphi_\nu(x')]=i\hbar cT_{\mu\nu}{}^{(+)}(x-x'), \quad (2.17)$$

$$[\varphi_\mu{}^{(-)}(x),\ \varphi_\nu(x')]=i\hbar cT_{\mu\nu}{}^{(-)}(x-x'), \quad (2.18)$$

$$[\varphi_\mu{}^{(1)}(x),\ \varphi_\nu(x')]=i\hbar cT_{\mu\nu}{}^{(1)}(x-x'), \quad (2.19)$$

where

$$T_{\mu\nu}{}^{(+)}(x-x')=\{\delta_{\mu\nu}-(1/\kappa^2)(\partial^2/\partial x_\mu\partial x_\nu)\}\Delta^{(+)}(x-x'), \quad (2.20)$$

and similar equations hold for $T_{\mu\nu}{}^{(-)}(x-x')$ and $T_{\mu\nu}{}^{(1)}(x-x')$. The vacuum is defined by

$$\varphi_\mu{}^{(+)}(x)\Psi_0=0. \quad (2.21)$$

Difficulties of the false vacuum do not arise as in the electromagnetic case because the supplementary condition does not exclude longitudinal mesons when $\kappa\neq0$. The vacuum expectation value of the anticommutator is

$$\langle\{\varphi_\mu(x),\ \varphi_\nu(x')\}\rangle_0=\hbar cT_{\mu\nu}{}^{(1)}(x-x'). \quad (2.22)$$

We proceed to develop the expectation values of various expressions in the invariants ω, j_μ, and $m_{\mu\nu}$. It follows from the definitions that

$$\omega(x)=-\tfrac{1}{2}ifc[\psi_\alpha(x),\ \bar{\psi}_\beta(x)](-i\delta_{\beta\alpha})=M^{(0)}(x), \quad (2.23)$$

$$j_\mu(x)=-\tfrac{1}{2}ifc[\psi_\alpha(x),\ \bar{\psi}_\beta(x)](\gamma_\mu)_{\beta\alpha}=M^{(1)}(x), \quad (2.24)$$

and

$$m_{\mu\nu}(x)=-\tfrac{1}{2}igc[\psi_\alpha(x),\ \bar{\psi}_\beta(x)](\gamma_\mu\gamma_\nu)_{\beta\alpha}=M^{(2)}(x). \quad (2.25)$$

Let r, s be suffixes which take the values 0, 1, 2 and define $L^r(\gamma)$ by

$$(L^{(0)})_{\alpha\beta}=-i\delta_{\alpha\beta}, \tag{2.26}$$

$$(L^{(1)})_{\alpha\beta}=(\gamma_\mu)_{\alpha\beta}, \tag{2.27}$$

$$(L^{(2)})_{\alpha\beta}=(\gamma_\mu\gamma_\nu)_{\alpha\beta}, \tag{2.28}$$

so that

$$M^{(r)}(x)=-\tfrac{1}{2}igc[\psi_\alpha(x),\bar\psi_\beta(x)](L^r)_{\beta\alpha}. \tag{2.29}$$

Note that in (2.29) g must be replaced by f if $M^{(r)}$ occurs as a factor in an f-interaction. It then follows after some manipulation of the operators that

$$[M^{(r)}(x), M^{(s)}(x')]$$
$$=\tfrac{1}{2}ig^2c^2([\bar\psi_\beta(x),\psi_\alpha(x')](L^rS(x-x')L^s)_{\beta\alpha}$$
$$-[\bar\psi_\beta(x'),\psi_\alpha(x)](L^sS(x'-x)L^r)_{\beta\alpha}), \tag{2.30}$$
$$=\tfrac{1}{2}ig^2c^2([\psi(x),\bar\psi(x')L^sS(x'-x)L^r]$$
$$-[L^rS(x-x')L^s\psi(x'),\bar\psi(x)]). \tag{2.31}$$

This is a general formula for any commutator of the invariants ω, j_μ, and $m_{\mu\nu}$. By (2.16) and (2.30),

$$\langle[M^{(r)}(x), M^{(s)}(x)]\rangle_0$$
$$=\tfrac{1}{2}ig^2c^2(\mathrm{Tr}[S^{(1)}(x'-x)L^rS(x-x')L^s]$$
$$-\mathrm{Tr}[S^{(1)}(x-x')L^sS(x'-x)L^r]), \tag{2.32}$$

where $\mathrm{Tr}[\cdots]$ denotes the trace. Introduce the notation

$$\xi=x-x', \tag{2.33}$$

and

$$(\partial/\partial\xi_\mu)\Delta_0(\xi)=\Delta_{0\mu}(\xi). \tag{2.34}$$

By evaluating the traces it follows from (2.32) that

$$\langle[\omega(x),\omega(x')]\rangle_0$$
$$=4if^2c^2[\Delta_{0\lambda}{}^{(1)}(\xi)\Delta_{0\lambda}(\xi)-\kappa_0{}^2\Delta_0{}^{(1)}(\xi)\Delta_0(\xi)], \tag{2.35}$$

$$\langle[j_\mu(x), j_\nu(x')]\rangle_0$$
$$=-4ig^2c^2[\Delta_{0\mu}{}^{(1)}(\xi)\Delta_{0\nu}(\xi)+\Delta_{0\nu}{}^{(1)}(\xi)\Delta_{0\mu}(\xi)$$
$$-\delta_{\mu\nu}(\Delta_{0\lambda}{}^{(1)}(\xi)\Delta_{0\lambda}(\xi)+\kappa_0{}^2\Delta_0{}^{(1)}(\xi)\Delta_0(\xi)), \tag{2.36}$$

$$\langle[m_{\mu\nu}(x), m_{\pi\rho}(x')]\rangle_0$$
$$=-4ig^2c^2[\delta_{\rho\nu}(\Delta_{0\pi}{}^{(1)}(\xi)\Delta_{0\mu}(\xi)+\Delta_{0\mu}{}^{(1)}(\xi)\Delta_{0\pi}(\xi))$$
$$+\delta_{\pi\mu}(\Delta_{0\rho}{}^{(1)}(\xi)\Delta_{0\nu}(\xi)+\Delta_{0\nu}{}^{(1)}(\xi)\Delta_{0\rho}(\xi))$$
$$-\delta_{\rho\mu}(\Delta_{0\pi}{}^{(1)}(\xi)\Delta_{0\nu}(\xi)+\Delta_{0\nu}{}^{(1)}(\xi)\Delta_{0\pi}(\xi))$$
$$-\delta_{\pi\nu}(\Delta_{0\rho}{}^{(1)}(\xi)\Delta_{0\mu}(\xi)+\Delta_{0\mu}{}^{(1)}(\xi)\Delta_{0\rho}(\xi))$$
$$+(\delta_{\rho\mu}\delta_{\pi\nu}-\delta_{\pi\mu}\delta_{\rho\nu})(\Delta_{0\lambda}{}^{(1)}(\xi)\Delta_{0\lambda}(\xi)$$
$$-\kappa_0{}^2\Delta_0{}^{(1)}(\xi)\Delta_0(\xi))], \tag{2.37}$$

$$\langle[j_\mu(x),\omega(x')]\rangle_0=0, \tag{2.38}$$

$$\langle[j_\mu(x), m_{\pi\rho}(x')]\rangle_0=4ifgc^2(\delta_{\rho\nu}\delta_{\pi\mu}-\delta_{\pi\nu}\delta_{\rho\mu})$$
$$\times(\Delta_0{}^{(1)}(\xi)\Delta_{0\nu}(\xi)+\Delta_{0\nu}{}^{(1)}(\xi)\Delta_0(\xi)). \tag{2.39}$$

To select out the one nucleon part from an operator of the type $\{M^{(r)}(x), M^{(s)}(x)\}$ the spinors ψ_α must be split into annihilation and creation operators. It is convenient to consider the nucleons in positive energy states to be carrying a charge e. Then the antinucleons, corresponding to the positrons in electron hole theory, will carry a charge $-e$. The charge-current vector is

$$j_\mu'(x)=-\tfrac{1}{2}iec(\bar\psi\gamma_\mu\psi-\psi\gamma_\mu{}^T\bar\psi). \tag{2.40}$$

The total charge on the surface σ is the integral of the normal component

$$Q=-\frac{1}{c}\int j_\mu(x)n_\mu d\sigma$$
$$=-\tfrac{1}{2}ie\int(\bar\psi(x)\gamma_\mu\psi(x)-\psi(x)\gamma_\mu{}^T\bar\psi(x))d\sigma_\mu. \tag{2.41}$$

Hence

$$[\psi(x), Q]=-e\psi(x). \tag{2.42}$$

When applied to an eigenstate of the total charge,

$$Q\psi(x)\Psi(Q')=(Q'+e)\psi(x)\Psi(Q'). \tag{2.43}$$

Thus ψ has the effect of increasing the total charge. Therefore, ψ either creates a nucleon or annihilates an anti-nucleon. Similarly $\bar\psi$ either creates an anti-nucleon or annihilates a nucleon.

Now in the expression

$$\{M^{(r)}(x), M^{(s)}(x')\}=-\tfrac{1}{4}g^2c^2(L^r)_{\alpha\beta}(L^s)_{\gamma\delta}$$
$$\times\{[\bar\psi_\alpha(x),\psi_\beta(x')],[\bar\psi_\gamma(x'),\psi_\delta(x')]\}, \tag{2.44}$$

the terms in ψ and $\bar\psi$ are the same as those in $\{j_\mu(x), j_\nu(x')\}$ which has been evaluated by Schwinger.[5] The selection of the one-particle part of the operator can be taken over unchanged and leads to the general result

$$\{M^r(x), M^s(x')\}=\tfrac{1}{2}g^2c^2\{[\bar\psi(x), L^rS^{(1)}(x-x')L^s\psi(x')]$$
$$+[\bar\psi(x')L^sS^{(1)}(x'-x)L^r,\psi(x)]\}. \tag{2.45}$$

The one-particle part of any anticommutator of the invariants ω, j_μ, and $m_{\mu\nu}$ can be obtained from (2.45) by substituting for L^r from the definitions (2.26)–2.28).

We next consider the singular functions $\Delta(x)$ and $\Delta^{(1)}(x)$. First consider the function which for a scalar variable a is defined,

$$\epsilon(a)=a/|a|. \tag{2.46}$$

For a vector variable,

$$\epsilon(x)=x_0/|x_0|. \tag{2.47}$$

If σ and σ' are any two space-like surfaces through x

and x', respectively, define

$$\epsilon(\sigma, \sigma')=\pm 1, \tag{2.48}$$

according to whether σ' lies before or after σ. Then $\epsilon(\sigma, \sigma')$ can be replaced by $\epsilon(x-x')$ in an integral over x' if the integrand is zero outside the light cone of x. By considering the integral

$$\int_\alpha^\beta f(a)(d\epsilon(a)/da)da$$

in the two cases when the origin does occur and does not occur in the domain of integration, it can easily be shown that

$$d\epsilon(a)/da=2\delta(a), \tag{2.49}$$

and hence

$$\partial\epsilon(x)/\partial x_4=-2i\delta(x_0),\ \partial\epsilon(x)/\partial x_p=0,\ p=1, 2, 3. \tag{2.50}$$

Define

$$\bar{\Delta}(x)=-\tfrac{1}{2}\Delta(x)\epsilon(x). \tag{2.51}$$

Then

$$\begin{aligned}\Box^2\bar{\Delta}(x)&=-\tfrac{1}{2}\epsilon(x)\Box^2\Delta(x)-(\partial\Delta(x)/\partial x_\mu)(\partial\epsilon(x)/\partial x_\mu)\\&\qquad-\tfrac{1}{2}\Delta(x)\Box^2\epsilon(x),\\&=-\tfrac{1}{2}\epsilon(x)\Box^2\Delta(x)+2i\delta(x_0)(\partial\Delta(x)/\partial x_4)\\&\qquad+i\Delta(x)(\partial\delta(x_0)/\partial x_4),\\&=-\tfrac{1}{2}\kappa^2\epsilon(x)\Delta(x)+i\delta(x_0)(\partial\Delta(x)/\partial x_4),\end{aligned} \tag{2.52}$$

where the last term has been integrated by parts. By (1.43) in the "natural" coordinate system (with time axis in the direction n_μ),

$$(\partial\Delta(x)/\partial x_4)=i\delta(x_1)\delta(x_2)\delta(x_3). \tag{2.53}$$

Thus

$$(\Box^2-\kappa^2)\bar{\Delta}(x)=-i\delta_4(x). \tag{2.54}$$

Now

$$\delta_4(x)=\left(\frac{1}{2\pi}\right)^4\int_{-\infty}^{\infty}\exp[ik_\mu x_\mu]d^4k. \tag{2.55}$$

Therefore

$$\bar{\Delta}(x)=\left(\frac{1}{2\pi}\right)^4 P\int_{-\infty}^{\infty}\exp[ik_\mu x_\mu]/(k_\mu{}^2+\kappa^2)d^4k, \tag{2.56}$$

where the principal value is taken at $k_\mu{}^2+\kappa^2=0$. Performing the integration over

$$\Delta(x)=-\left(\frac{1}{2\pi}\right)^3\times\int_{-\infty}^{\infty}\frac{\exp[i(\mathbf{k}\cdot\mathbf{x})]\sin[x_0(\mathbf{k}^2+\kappa^2)^{\frac{1}{2}}]}{(\mathbf{k}^2+\kappa^2)^{\frac{1}{2}}}d^3k. \tag{2.57}$$

Hence

$$\Delta(x)=-i\left(\frac{1}{2\pi}\right)^3\times\int_{-\infty}^{\infty}\epsilon(k)\exp(ik_\mu x_\mu)\delta(k_\beta{}^2+k^2)d^4k, \tag{2.58}$$

and

$$\Delta^{(1)}(x)=\left(\frac{1}{2\pi}\right)^3\int_{-\infty}^{\infty}\exp(ik_\mu x_\mu)\delta(k_\mu{}^2+\kappa^2)d^4k. \tag{2.59}$$

It follows from (2.57) that $\Delta(x)=0$ if $x_0=0$. It is then easy to prove that

$$(\partial\bar{\Delta}(x)/\partial x_\mu)=-\tfrac{1}{2}\epsilon(x)(\partial\Delta(x)/\partial x_\mu). \tag{2.60}$$

III. THE SCHWINGER TRANSFORMATION

It follows from the above development of the field variables that the Hamiltonian in the interaction representation contains terms of the first order in the coupling constants which have matrix elements for the absorption or emission of mesons by free nucleons. These processes cannot occur with conservation of energy and momentum which suggests that they should be removed by a transformation. Following Schwinger,[5] make the unitary transformation

$$\Psi(\sigma)\rightarrow e^{iS(\sigma)}\Psi(\sigma), \tag{3.1}$$

where

$$S(\sigma)=(1/2\hbar c^2)\int_{-\infty}^{\infty}\{\omega(x')\varphi(x')+(1/\kappa)j_\mu(x')\varphi_\mu(x')\}\epsilon(\sigma, \sigma')d\omega'. \tag{3.2}$$

This leads to an equation of motion for the new $\Psi(\sigma)$ from which all first-order transitions have been eliminated.

$$\begin{aligned}ihc\delta\Psi(\sigma)/\delta\sigma(x)&=\Big\{(i/4hc^3)\int_{-\infty}^{\infty}[\omega(x')\varphi(x')\\&\quad+(1/\kappa)j_\mu(x')\varphi_\mu(x'), \omega(x)\varphi(x)\\&\quad+(1/\kappa)j_\nu(x)\varphi_\nu(x)]\epsilon(\sigma, \sigma')d\omega'\\&\quad+(1/2c^2\kappa^2)(j_\mu(x)n_\mu)^2\Big\}\Psi(\sigma),\end{aligned} \tag{3.3}$$

$$=\{\mathfrak{IC}_1{}^s(x)+\mathfrak{IC}_2{}^s(x)+\mathfrak{IC}_3{}^s(x)+\mathfrak{IC}_4{}^s(x)\}\Psi(\sigma), \tag{3.4}$$

where

$$\mathfrak{IC}_1{}^s(x)=(-i/4hc^3)\int_{-\infty}^{\infty}[\omega(x)\varphi(x), \omega(x')\varphi(x')]\times\epsilon(\sigma, \sigma')d\omega', \tag{3.5}$$

$$\mathcal{H}_2^s(x)=(-i/4\hbar c^3\kappa^2)\int_{-\infty}^{\infty}[j_\mu(x)\varphi_\mu(x),\, j_\nu(x')\varphi_\nu(x')]\times\epsilon(\sigma,\sigma')d\omega', \quad (3.6)$$

$$\mathcal{H}_3^s(x)=(-i/4\hbar c^3\kappa)\int_{-\infty}^{\infty}([j_\mu(x)\varphi_\mu(x),\, \omega(x')\varphi(x')] - [j_\mu(x')\varphi_\mu(x'),\, \omega(x)\varphi(x)])\epsilon(\sigma,\sigma')d\omega', \quad (3.7)$$

and

$$\mathcal{H}_4^s(x)=\left(\frac{1}{2c^2\kappa^2}\right)(j_\mu(x)n_\mu)^2. \quad (3.8)$$

Consider the terms arising from $\mathcal{H}_2^s(x)$.

$$\begin{aligned}\mathcal{H}_2^s(x)&=(-i/8\hbar c^3\kappa^2)\int([j_\mu(x),\, j_\nu(x')]\{\varphi_\mu(x),\, \varphi_\nu(x')\}\\&\quad+\{j_\mu(x),\, j_\nu(x')\}[\varphi_\mu(x),\, \varphi_\nu(x')])\epsilon(\sigma,\sigma')d\omega',\\&=(-i/8\hbar c^3\kappa^2)\int([j_\mu(x),\, j_\nu(x')]([\varphi_\mu(x),\, \varphi_\nu(x')\}\\&\quad-\langle\{\varphi_\mu(x),\, \varphi_\nu(x')\}\rangle)\\&\quad+\hbar c[j_\mu(x),\, j_\nu(x')](\partial^2/\partial x_\mu\partial x_\nu')\Delta^{(1)}(x-x')\\&\quad+i\hbar c\{j_\mu(x),\, {}_\mu\nu(x')\}(\partial^2/\partial x_\mu\partial x_\nu')\Delta(x-x'))\\&\qquad\times\epsilon(\sigma,\sigma')d\omega', \quad (3.9)\end{aligned}$$

$$\begin{aligned}&=(-i/8\hbar c^3\kappa^2)\int(([j_\mu(x),j_\nu(x')]\\&\quad-\langle[j_\mu(x),\, j_\nu(x')]\rangle_0)(\{\varphi_\mu(x),\, \varphi_\nu(x')\}\\&\quad-\langle\{\varphi_\mu(x),\, \varphi_\nu(x')\}\rangle_0)\\&\quad+\hbar c[j_\mu(x),j_\nu(x')](\partial^2/\partial x_\mu\partial x_\nu')\Delta^{(1)}(x-x')\\&\quad+i\hbar c\{j_\mu(x),\, j_\nu(x')\}(\partial^2/\partial x_\mu\partial x_\nu')\Delta(x-x')\\&\quad+\langle[j_\mu(x),\, j_\nu(x')]\rangle_0(\{\varphi_\mu(x),\, \varphi_\nu(x')\}\\&\qquad-\langle\{\varphi_\mu(x),\, \varphi_\nu(x')\}\rangle_0))\epsilon(\sigma,\sigma')d\omega', \quad (3.10)\end{aligned}$$

where (1.44) and (2.14) have been used. The first three lines of (3.10) which will be denoted by $\mathcal{H}_{2,1}^s(x)$ are zero unless some of both types of particle are present and have matrix elements for real effects of meson scattering. The next two lines, $\mathcal{H}_{22}^s(x)$, are non-zero when no mesons are present and give part of the nucleon g self-energy and part of the g-interaction Yukawa potential. The last two lines, $\mathcal{H}_{23}^s(x)$, are non-zero when no nucleons are present and account for the meson f self-energy. The other parts of the Hamiltonian $\mathcal{H}_1^s(x)$ and $\mathcal{H}_3^s(x)$ can be split up in the same way and the notation introduced above can obviously be extended. Thus, for example, the scalar meson f self-energy will arise from the last two lines of $\mathcal{H}_1^s(x)$ to be denoted by $\mathcal{H}_{13}^s(x)$.

There is an additional contribution to the nucleon g self-energy and Yukawa potential from $\mathcal{H}_4^s(x)$. It will be shown how this combines with $\mathcal{H}_{22}^s(x)$.

$$\begin{aligned}\mathcal{H}_{22}^s(x)&=(i/8c^2\kappa^2)\int([j_\mu(x),\, j_\nu(x')]\\&\quad\times(\partial^2/\partial x_\mu\partial x_\nu)\Delta^{(1)}(x-x')+i\{j_\mu(x),\, j_\nu(x')\}\\&\quad\times(\partial^2/\partial x_\mu\partial x_\nu)\Delta(x-x'))\epsilon(x-x')d\omega'. \quad (3.11)\end{aligned}$$

$\epsilon(\sigma,\sigma')$ has been replaced by $\epsilon(x-x')$ since the integrand is zero outside the light cone. In the second term the ϵ factor can be taken under the differential and the additional terms subtracted explicitly. These can be evaluated in the "natural" frame by (2.50) and (2.53) and it follows that

$$\begin{aligned}&-\tfrac{1}{2}\{j_\mu(x),\, j_\nu(x')\}\epsilon(x-x')(\partial^2/\partial x_\mu\partial x_\nu)\Delta(x-x')\\&\quad=\{j_\mu(x),\, j_\nu(x')\}(\partial^2/\partial x_\mu\partial x_\nu)\bar{\Delta}(x-x')\\&\qquad-2(j_\mu(x)n_\mu)(j_\nu(x')n_\nu')\delta_4(x-x'). \quad (3.12)\end{aligned}$$

The second term on the right-hand side is just that required to cancel $\mathcal{H}_4^s(x)$. Thus

$$\begin{aligned}\mathcal{H}_{22}^s(x)+\mathcal{H}_4^s(x)&=(i/8c^2\kappa^2)\int[j_\mu(x),\, j_\nu(x')]\\&\quad\times(\partial^2/\partial x_\mu\partial x_\nu)\Delta^{(1)}(x-x')\cdot\epsilon(x-x')d\omega'\\&\quad+(1/4c^2\kappa^2)\int\{j_\mu(x),\, j_\nu(x')\}\\&\quad\times(\partial^2/\partial x_\mu\partial x_\nu)\bar{\Delta}(x-x')d\omega'. \quad (3.13)\end{aligned}$$

By (2.45) the anticommutator in the second term is a function of $S^{(1)}(x-x')$. By (2.31) the commutator in the first term is a function of $S(x-x')$ which by (2.51) and (2.60) combines with $\epsilon(x-x')$ to give a function of $\bar{\Delta}(x-x')$. Thus the whole integrand can be expressed in terms of $\bar{\Delta}(x-x')$ and $\Delta^{(1)}(x-x')$ and the integral is an invariant independent of the particular choice of n_μ. This is the extremely satisfactory result discussed in the introduction. It will now be shown that there are two similar effects in the vector case.

The reader is reminded that in the above treatment of the scalar meson interaction a suffix μ or ν attached to the field variable $\varphi(x)$ denotes differentiation. In the vector meson case only the second suffix ν in $\varphi_{\mu\nu}(x)$ or $A_{\mu\nu}(x)$ denotes differentiation. To avoid confusion, in any equation in which this notation is used a suffix s (scalar) or v (vector) will also occur to distinguish the two cases.

A transformation similar to (3.1) on the wave equation for the vector interaction (1.69) leads to

$$i\hbar c\delta\Psi/\delta\sigma(x)=\{\mathcal{H}_1^v(x)+\mathcal{H}_2^v(x)+\mathcal{H}_3^v(x)+\mathcal{H}_4^v(x)\}\Psi(\sigma), \quad (3.14)$$

where

$$\mathcal{H}_1^v(x)=(-i/4\hbar c^3)\int[j_\mu(x)\varphi_\mu(x),j_\nu(x')\varphi_\nu(x')]\times\epsilon(\sigma\cdot\sigma')d\omega', \quad (3.15)$$

$$\mathcal{H}_2^v(x)=(-i/16\kappa^2\hbar c^3)\times\int[m_{\mu\nu}(x)(\varphi_{\nu\mu}(x)-\varphi_{\mu\nu}(x)),\, m_{\pi\rho}(x')\times(\varphi_{\rho\pi}(x')-\varphi_{\pi\rho}(x'))]\epsilon(\sigma,\sigma')d\omega', \quad (3.16)$$

$$\mathcal{H}_3^v(x)=(-i/8\kappa\hbar c^3)\times\int([m_{\mu\nu}(x)(\varphi_{\nu\mu}(x)-\varphi_{\mu\nu}(x)),\, j_\rho(x')\varphi_\rho(x')]-[m_{\mu\nu}(x')(\varphi_{\nu\mu}(x')-\varphi_{\mu\nu}(x')),\, j_\rho(x)\varphi_\rho(x)])\times\epsilon(\sigma,\sigma')d\omega', \quad (3.17)$$

$$\mathcal{H}_4^v(x)=(1/2c^2\kappa^2)\{(j_\mu(x)n_\mu)^2+(m_{\mu\nu}(x)n_\mu)^2\}. \quad (3.18)$$

The various parts of the Hamiltonian can be split up as above. Consider $\mathcal{H}_{12}^v(x)$ obtained from $\mathcal{H}_1^v(x)$ as $\mathcal{H}_{22}^s(x)$ was from $\mathcal{H}_2^s(x)$.

$$\mathcal{H}_{12}^v(x)=(-i/8c^2)\int([j_\mu(x),\, j_\nu(x')]T_{\mu\nu}^{(1)}(x-x')+i\{j_\mu(x),\, j_\nu(x')\}T_{\mu\nu}(x-x'))\epsilon(\sigma,\sigma')d\omega', \quad (3.19)$$

$$=(-i/8c^2)\int([j_\mu(x),\, j_\nu(x')]\Delta^{(1)}(x-x')+i\{j_\mu(x),\, j_\nu(x')\}\Delta(x-x'))\epsilon(x-x')d\omega'+(i/8c^2)\int([j_\mu(x),\, j_\nu(x')]\times(\partial^2/\partial x_\mu\partial x_\nu)\Delta^{(1)}(x-x')+i\{j_\mu(x),\, j_\nu(x')\}\times(\partial^2/\partial x_\mu\partial x_\nu)\Delta(x-x'))\epsilon(x-x')d\omega'. \quad (3.20)$$

The second term of (3.20) can be expressed in terms of $\bar{\Delta}(x-x')$. The third and fourth terms are identical with $\mathcal{H}_{22}^s(x)$ and combine with the first term, $\mathcal{H}_{41}^v(x)$, of $\mathcal{H}_4^v(x)$. Thus

$$\mathcal{H}_{12}^v(x)+\mathcal{H}_{41}^v(x)=(-i/8c^2)\int[j_\mu(x),\, j_\mu(x')]\times\Delta^{(1)}(x-x')\epsilon(x-x')d\omega'-(1/4c^2)\times\int\{j_\mu(x),\, j_\mu(x')\}\bar{\Delta}(x-x')d\omega'+(i/8c^2\kappa^2)\int[j_\mu(x),\, j_\nu(x')]\times(\partial^2/\partial x_\mu\partial x_\nu)\Delta^{(1)}(x-x')\cdot\epsilon(x-x')d\omega'+(1/4c^2)\int\{j_\mu(x),\, j_\nu(x')\}\times(\partial^2/\partial x_\mu\partial x_\nu)\bar{\Delta}(x-x')d\omega'. \quad (3.21)$$

Virtual meson effects in the g-interaction in the vector meson case can be expressed in terms of the subsidiary field $A_\mu(x)$. Thus

$$m_{\mu\nu}(x)(\varphi_{\nu\mu}(x)-\varphi_{\mu\nu}(x))=m_{\mu\nu}(x)(A_{\nu\mu}(x)-A_{\mu\nu}(x))=2m_{\mu\nu}(x)A_{\nu\mu}(x). \quad (3.22)$$

Hence

$$\mathcal{H}_{22}^v(x)=(-i/8\hbar c^3\kappa^2)\int([m_{\mu\nu}(x),\, m_{\pi\rho}(x')]\times\langle\{A_{\nu\mu}(x),\, A_{\rho\pi}(x')\}\rangle_0+i\{m_{\mu\nu}(x),\, m_{\pi\rho}(x')\}\times[A_{\nu\mu}(x),\, A_{\rho\pi}(x')])\epsilon(\sigma,\sigma')d\omega'$$

$$=(i/8c^2\kappa^2)\int([m_{\mu\nu}(x),\, m_{\pi\nu}(x')](\partial^2/\partial x_\mu\partial x_\pi)\times\Delta^{(1)}(x-x')+i\{m_{\mu\nu}(x),\, m_{\pi\nu}(x')\}\times(\partial^2/\partial x_\mu\partial x_\pi)\Delta(x-x'))\epsilon(x-x')d\omega'. \quad (3.23)$$

The final term combines with the second term, $\mathcal{H}_{42}^v(x)$, of $\mathcal{H}_4^v(x)$ to give an integral of the required form

$$\mathcal{H}_{22}^v(x)+\mathcal{H}_{42}^v(x)=(i/8c^2\kappa^2)\int[m_{\mu\nu}(x),\, m_{\pi\nu}(x')]\times(\partial^2/\partial x_\mu\partial x_\pi)\Delta^{(1)}(x-x')\cdot\epsilon(x-x')d\omega+(1/4c^2\kappa^2)\int\{m_{\mu\nu}(x),\, m_{\pi\nu}(x')\}(\partial^2/\partial x_\mu\partial x_\pi)\times\bar{\Delta}(x-x')d\omega'. \quad (3.24)$$

IV. THE MESON SELF-ENERGIES

The f self-energy of the scalar meson is determined by

$$\mathcal{H}_{13}^s(x)=(-i/8\hbar c^3)\int\langle[\omega(x),\, \omega(x')]\rangle_0\times\{\varphi(x),\, \varphi(x')\}_1\epsilon(\sigma,\sigma')d\omega', \quad (4.1)$$

$$=\{\varphi(x),\, \eta(x)\}_1, \quad (4.2)$$

where

$$\eta(x)=(-i/8\hbar c^3)\int\langle[\omega(x),\, \omega(x')]\rangle_0\times\epsilon(x-x')\varphi(x')d\omega'. \quad (4.3)$$

It must be shown that $\eta(x)$ is a multiple of $\varphi(x)$. By (2.35) and (2.51)

$$\eta(x)=(-f^2/\hbar c)\int\{\Delta_{0\lambda}^{(1)}(x-x')\bar{\Delta}_{0\lambda}(x-x')-\kappa_0^2\Delta_0^{(1)}(x-x')\bar{\Delta}_0(x-x')\}\varphi(x')d\omega', \quad (4.4)$$

$$=(-f^2/\hbar c)\int \mathrm{K}(x-x')\varphi(x')d\omega', \tag{4.5}$$

$$=(-f^2/\hbar c)(1/2\pi)^4\int\int \mathrm{K}(k) \times\exp[ik_\mu\cdot x_\mu-x_\mu']\varphi(x')d\omega' d^4k, \tag{4.6}$$

where

$$\mathrm{K}(x)=(1/2\pi)^4\int K(k)\exp[ik_\mu x_\mu]d^4k. \tag{4.7}$$

If $\eta(x)$ is evaluated for a particular Fourier component $\varphi(p)\exp[ip_\mu x_\mu]$ of $\varphi(x)$ then with ξ defined, by (2.33),

$$\eta(x)=(-f^2/\hbar c)(1/2\pi)^4\int\int \mathrm{K}(k)\exp[ik_\mu\xi_\mu]\varphi(p) \times\exp[ip_\mu\cdot x_\mu-\xi_\mu]d\omega_\xi d^4k,$$
$$=(-f^2/\hbar c)\varphi(p)\exp[ip_\mu x_\mu] \times\int \mathrm{K}(k)\delta_4(k_\mu-p_\mu)d^4k,$$
$$=(-f^2/\hbar c)\varphi(x)\mathrm{K}(p). \tag{4.8}$$

Since $\varphi(p)\exp[ip_\mu x_\mu]$ is a Fourier component of $\varphi(x)$, by (1.20),

$$p_\mu{}^2=-\kappa^2. \tag{4.9}$$

Now

$$\mathrm{K}(x)=\Delta_{0\lambda}{}^{(1)}(x)\bar{\Delta}_{0\lambda}(x)-\kappa_0{}^2\Delta_0{}^{(1)}(x)\bar{\Delta}_0(x). \tag{4.10}$$

And by (2.56) and (2.59)

$$\Delta_0{}^{(1)}(x)=\left(\frac{1}{2\pi}\right)^3\int \exp[iq_\nu x_\nu]\delta(q_\nu{}^2+\kappa_0{}^2)d^4q, \tag{4.11}$$

$$\bar{\Delta}_0(x)=\left(\frac{1}{2\pi}\right)^4 P\int\frac{\exp[i(p_\mu-q_\mu\cdot x_\mu)]}{(p_\lambda-q_\lambda)^2+\kappa_0{}^2}d^4p. \tag{4.12}$$

Thus

$$\mathrm{K}(x)=\left(\frac{1}{2\pi}\right)^7\int\frac{\exp[ip_\mu x_\mu]}{(p_\lambda-q_\lambda)^2+\kappa_0{}^2}\delta(q_\lambda{}^2+\kappa_0{}^2) \times[-q_\lambda(p_\lambda-q_\lambda)-\kappa_0{}^2]d^4pd^4q, \tag{4.13}$$

and

$$\mathrm{K}(p)=\left(\frac{1}{2\pi}\right)^3\int\frac{\delta(q_\lambda{}^2+\kappa_0{}^2)}{(p_\lambda-q_\lambda)^2+\kappa_0{}^2} \times[-q_\lambda(p_\lambda-q_\lambda)-\kappa_0{}^2]d^4q. \tag{4.14}$$

Now

$$\delta(q_\lambda{}^2+\kappa_0{}^2)=(1/2\pi)\int_{-\infty}^{\infty}\exp[i(q_\lambda{}^2+\kappa_0{}^2)a]da, \tag{4.15}$$

and

$$(1/(p_\lambda-q_\lambda)^2+\kappa_0{}^2) =-\tfrac{1}{2}i\int_{-\infty}^{\infty}\exp[ib\{(p_\lambda-q_\lambda)^2+\kappa_0{}^2\}]\epsilon(b)db. \tag{4.16}$$

Substituting in (4.14),

$$\mathrm{K}(p)=\left(\frac{1}{2\pi}\right)^4\frac{i}{2}\int d^4q\int da\int db\exp[ia(q_\lambda{}^2+\kappa_0{}^2) +ib\{(p_\lambda-q_\lambda)^2+\kappa_0{}^2\}]\epsilon(b)[q_\lambda(p_\lambda-q_\lambda)+\kappa_0{}^2]. \tag{4.17}$$

Define

$$q_\nu=Q_\nu+(b/a+b)p_\nu. \tag{4.18}$$

Then

$$\mathrm{K}(p)=\left(\frac{1}{2\pi}\right)^4\frac{i}{2}\int d^4Q\int da\int db \times\exp\left[i(a+b)Q_\lambda{}^2+i\frac{ab}{a+b}p_\lambda{}^2+i(a+b)\kappa_0{}^2\right] \times\epsilon(b)\left[\frac{ab}{(a+b)^2}p_\lambda{}^2+Q_\lambda p_\lambda\frac{a-b}{a+b}-Q_\lambda{}^2+\kappa_0{}^2\right]. \tag{4.19}$$

Now

$$\begin{aligned}
&\int_{-\infty}^{\infty}\exp[iaQ_\lambda{}^2]d^4Q=(i\pi^2/a^2)\epsilon(a),\\
&\int_{-\infty}^{\infty}Q_\mu\exp[iaQ_\lambda{}^2]d^4Q=0,\\
&\int_{-\infty}^{\infty}Q_\mu Q_\nu\exp[iaQ_\lambda{}^2]d^4Q=-\delta_{\mu\nu}(\pi^2/2a^3)\epsilon(a),\\
&\int_{-\infty}^{\infty}Q_\mu{}^2\exp[iaQ_\lambda{}^2]d^4Q=-(2\pi^2/a^3)\epsilon(a).
\end{aligned} \tag{4.20}$$

Thus integrating with respect to Q,

$$\mathrm{K}(p)=\frac{1}{32\pi^2}\int da\int db\exp\left[i(a+b)\kappa_0{}^2+i\frac{ab}{a+b}p_\lambda{}^2\right] \times\frac{\epsilon(b)\epsilon(a+b)}{(a+b)^2}\left[-\frac{ab}{(a+b)^2}p_\lambda{}^2-\kappa_0{}^2+\frac{2i}{(a+b)}\right]. \tag{4.21}$$

Symmetrizing with respect to a and b,

$$\epsilon(b)=\tfrac{1}{2}(\epsilon(a)+\epsilon(b)). \tag{4.22}$$

Making the substitution,

$$a=\tfrac{1}{2}z(1+y),\quad b=\tfrac{1}{2}z(1-y). \tag{4.23}$$

Then

$$\tfrac{1}{2}(\epsilon(a)+\epsilon(b))=\begin{cases}\epsilon(z) & \text{for } |y|<1,\\ 0 & \text{for } |y|>1,\end{cases} \tag{4.24}$$

and

$$dadb=\tfrac{1}{2}z\epsilon(z)dzdy. \tag{4.25}$$

Thus

$$\mathrm{K}(p)=\frac{1}{64}\left(\frac{1}{2\pi}\right)^2\int_{-1}^{+1}dy\int_{-\infty}^{\infty}dz\frac{\epsilon(z)}{z}\times\exp\left[iz\left(\kappa_0^2+\frac{1-y^2}{4}p_\lambda^2\right)\right]\times\left\{\frac{8i}{z}-(1-y^2)p_\lambda^2-4\kappa_0^2\right\}. \tag{4.26}$$

Let

$$z=(\omega/\kappa_0^2), \tag{4.27}$$

and

$$\mu=(\kappa_0/\kappa). \tag{4.28}$$

Then substituting for p_λ^2 from (4.9),

$$\mathrm{K}(\kappa)=\frac{\kappa^2}{64}\left(\frac{1}{2\pi}\right)^2\int_{-1}^{+1}dy\left[\frac{8i\mu^2}{\omega}-4\mu^2+1-y^2\right]\times\int_{-\infty}^{\infty}d\omega\frac{1}{|\omega|}\exp\left[i\omega\left(1-\frac{1-y^2}{4\mu^2}\right)\right] \tag{4.29}$$

$$=\frac{\kappa^2}{64}\left(\frac{1}{2\pi}\right)^2\int_{-1}^{+1}dy\left(A+\frac{iB}{\omega}\right)\times\int_{-\infty}^{\infty}d\omega\frac{1}{|\omega|}\exp[iC\omega], \tag{4.30}$$

where

$$A=1-y^2-4\mu^2,\quad B=8\mu^2,\quad C=1-(1-y^2)/4\mu^2. \tag{4.31}$$

The imaginary terms in the integrand are odd and can be regarded as giving no contribution to the integral. Thus

$$\int_{-\infty}^{\infty}\left(A+\frac{iB}{\omega}\right)\frac{1}{|\omega|}\exp[iC\omega]d\omega=2\int_0^{\infty}(A-BC)\frac{\cos C\omega}{\omega}d\omega-2BC, \tag{4.32}$$

and

$$\mathrm{K}(\kappa)=\frac{\kappa^2}{32}\left(\frac{1}{2\pi}\right)^2\int_{-1}^{+1}\left\{(A-BC)\times\left(\log\frac{1}{\gamma\omega_0}-\log C\right)-BC\right\}dy \tag{4.33}$$

$$=\frac{\kappa^2}{32\pi^2}\left[(1-6\mu^2)\log\frac{1}{\gamma\omega_0}+\text{finite terms}\right]. \tag{4.34}$$

Therefore,

$$\eta(x)=\varphi(x)\left(\frac{\kappa^2f^2}{4\pi\hbar c}\right)\left(\frac{-1}{8\pi}\right)\times\left[(1-6\mu^2)\log\frac{1}{\gamma\omega_0}+\text{f. t.}\right]. \tag{4.35}$$

And by (4.2),

$$\mathfrak{H}_{13}^{s}(x)=2\kappa\kappa_1\{\varphi^2(x)\}_1, \tag{4.36}$$

where

$$\kappa_1=\kappa\left(\frac{f^2}{4\pi\hbar c}\right)\left(\frac{-1}{8\pi}\right)\left[(1-6\mu^2)\log\frac{1}{\gamma\omega_0}+\text{f. t.}\right]. \tag{4.37}$$

The scalar meson g self-energy is given by

$$\mathfrak{H}_{23}^{s}(x)=(-i/8\hbar c^3\kappa^2)\int_{-\infty}^{\infty}\langle[j_\mu(x),\,j_\nu(x')]\rangle_0\times\{\varphi_\mu(x),\,\varphi_\nu(x')\}_1\epsilon(\sigma,\,\sigma')d\omega' \tag{4.38}$$

$$=\{\varphi_\mu(x),\,\eta_\mu^{s}(x)\}_1, \tag{4.39}$$

where by (2.36),

$$\eta_\mu^{s}(x)=(-i/8\hbar c^3\kappa^2)\int_{-\infty}^{\infty}\langle[j_\mu(x),\,j_\nu(x')]\rangle_0\times\varphi_\nu(x')\epsilon(\sigma,\,\sigma')d\omega' \tag{4.40}$$

$$\begin{aligned}=(g^2/\hbar c\kappa^2)\int_{-\infty}^{\infty}&[\bar{\Delta}_{0\mu}(x-x')\Delta_{0\nu}^{(1)}(x-x')\\&+\bar{\Delta}_{0\nu}(x-x')\Delta_{0\mu}^{(1)}(x-x')\\&-\delta_{\mu\nu}\{\bar{\Delta}_{0\lambda}(x-x')\Delta_{0\lambda}^{(1)}(x-x')\\&+\kappa_0^2\bar{\Delta}_0(x-x')\Delta_0^{(1)}(x-x')\}]\varphi_\nu(x')d\omega'\end{aligned}$$

$$=(g^2/\hbar c\kappa^2)\int_{-\infty}^{\infty}\mathrm{K}_{\mu\nu}^{s}(x-x')\varphi_\nu(x')d\omega'. \tag{4.41}$$

Evaluating for a particular component of $\varphi(x)$,

$$\begin{aligned}\eta_\mu^{s}(x)&=(g^2/\hbar c\kappa^2)(1/2\pi)^4\int d\omega_\xi'\int d^4k\mathrm{K}_{\mu\nu}^{s}(k)\varphi(p)ip_\nu\times\exp[ip_\lambda x_\lambda]\exp[i\xi_\sigma\cdot k_\sigma-p_\sigma]\\&=(g^2/\hbar c\kappa^2)\varphi(p)ip_\nu\exp[ip_\lambda x_\lambda]\mathrm{K}_{\mu\nu}^{s}(p)\\&=(g^2/\hbar c\kappa^2)\varphi_\nu(x)\mathrm{K}_{\mu\nu}^{s}(p).\end{aligned} \tag{4.42}$$

In addition to (4.9), there is the relation

$$p_\mu p_\nu\varphi(p)ip_\nu\exp[ip_\lambda x_\lambda]=-\kappa^2\varphi(p)ip_\mu\exp[ip_\lambda x_\lambda]=-\kappa^2\varphi_\mu(x). \tag{4.43}$$

Thus for terms in the integrand of $\mathrm{K}_{\mu\nu}^{s}(p)$,

$$p_\mu p_\nu=-\kappa^2\delta_{\mu\nu}. \tag{4.44}$$

$\mathrm{K}_{\mu\nu}{}^{s}(p)$ can be integrated by the same method as $\mathrm{K}(p)$. Introducing the variables a, b, and Q and integrating over Q,

$$\mathrm{K}_{\mu\nu}{}^{s}(p)=\frac{1}{32\pi^2}\int da\int db \times\exp\left[i(a+b)\kappa_0{}^2+i\frac{ab}{a+b}p_\lambda{}^2\right]\frac{\epsilon(b)\epsilon(a+b)}{(a+b)^2} \times\left[\delta_{\mu\nu}\left\{\frac{-i}{(a+b)}+\frac{ab}{(a+b)}p_\lambda{}^2-\kappa^2\right\}-p_\nu p_\mu\frac{2ab}{(a+b)^2}\right]. \quad (4.45)$$

Introducing variables y and ω and eliminating p_λ by (4.9) and (4.44)

$$\mathrm{K}_{\mu\nu}{}^{s}(x)=\frac{\kappa^2}{64}\left(\frac{1}{2\pi}\right)^2\delta_{\mu\nu}\int_{-1}^{+1}dy\left[\frac{-4i\mu^2}{\omega}-4\mu^2+1-y^2\right] \times\int_{-\infty}^{\infty}d\omega\frac{1}{|\omega|}\exp\left[i\omega\left(1-\frac{1-y^2}{4\mu^2}\right)\right], \quad (4.46)$$

which can be evaluated like (4.30) with

$$A=1-y^2-4\mu^2,\quad B=-4\mu^2,\quad C=1-(1-y^2)/4\mu^2. \quad (4.47)$$

In this case $A-BC=0$, giving the finite result

$$\mathrm{K}_{\mu\nu}{}^{s}(\kappa)=\frac{\kappa^2}{32\pi^2}\delta_{\mu\nu}[2\mu^2-\tfrac{1}{3}]. \quad (4.48)$$

Thus

$$\eta_\mu{}^{s}(x)=\varphi_\mu(x)\left(\frac{g^2}{4\pi\hbar c}\right)\left(\frac{1}{8\pi}\right)[2\mu^2-\tfrac{1}{3}], \quad (4.49)$$

and

$$\mathfrak{IC}_{23}{}^{s}(x)=-2(\kappa_2/\kappa)\{\varphi_\mu{}^2(x)\}_1, \quad (4.50)$$

where

$$\kappa_2=\kappa\left(\frac{g^2}{4\pi\hbar c}\right)\left(\frac{1}{8\pi}\right)[\tfrac{1}{3}-2\mu^2]. \quad (4.51)$$

Now

$$\varphi(x)=\sum_k\varphi^{(+)}(k)\exp[i(k_r x_r-k_0x_0)] +\varphi^{(-)}(k)\exp[i(k_r x_r+k_0x_0)], \quad (4.52)$$

where

$$k_0=(k_r{}^2+\kappa^2)^{\frac{1}{2}}. \quad (4.53)$$

Consider $\{\varphi^2(x)\}_1$ as an expression in terms of $\varphi(k)$. Since it is a term in an energy density, only terms with zero exponential in the space variables need be included. Also $\{\varphi^2(x)\}_1$ operates on one meson which must be annihilated and subsequently recreated by the two operators $\varphi(x)$. Thus the exponential in the time factor is also zero and

$$\{\varphi^2(x)\}_1=\sum_k\varphi^{(-)}(k)\varphi^{(+)}(k). \quad (4.54)$$

Now

$$(\partial\varphi(x)/\partial x_r)=\sum ik_r\varphi^{(+)}(k)\exp[i(k_r x_r-k_0x_0)] +ik_r\varphi^{(-)}(k)\exp[i(k_r x_r+k_0x_0)], \quad (4.55)$$

and

$$(\partial\varphi(x)/\partial x_4)=\sum -k_0\varphi^{(+)}(k)\exp[i(k_r x_r-k_0x_0)] +k_0\varphi^{(-)}(k)\exp[i(k_r x_r+k_0x_0)]. \quad (4.56)$$

Thus

$$\{\varphi_\mu{}^2(x)\}_1=\sum(k_r{}^2-k_0{}^2)\varphi^{(-)}(k)\varphi^{(+)}(k) =-\kappa^2\{\varphi^2(x)\}_1. \quad (4.57)$$

So that the g self-energy of the scalar meson can also be written in the form

$$\mathfrak{IC}_{23}{}^{s}=2\kappa_2\kappa\{\varphi^2(x)\}_1. \quad (4.58)$$

The Schrödinger Eq. (3.4) can now be written

$$ihc\delta\Psi/\delta\sigma=\{\mathfrak{IC}_e{}^{s}(\varphi)+\mathfrak{IC}_m{}^{s}(\varphi)\}\Psi, \quad (4.59)$$

where

$$\mathfrak{IC}_m{}^{s}(\varphi)=2(\kappa_1+\kappa_2)\kappa\varphi^2(x), \quad (4.60)$$

and

$$\mathfrak{IC}_e{}^{s}(\varphi)=\mathfrak{IC}_1{}^{s}(\varphi)+\mathfrak{IC}_2{}^{s}(\varphi) +\mathfrak{IC}_3{}^{s}(\varphi)+\mathfrak{IC}_4{}^{s}(\varphi)-\mathfrak{IC}_m{}^{s}(\varphi). \quad (4.61)$$

The field variable φ of which the various expressions $\mathfrak{IC}(\varphi)$ are functions, satisfies the equation of motion of the free meson field determined by the Hamiltonian (1.30). To obtain an equation from which the self-energies $\mathfrak{IC}_m(\varphi)$ have been eliminated make the transformation

$$\Psi(\sigma)=U_0(\sigma)\bar{\Psi}(\sigma), \quad (4.62)$$

where

$$ihc\delta U_0/\delta\sigma=\mathfrak{IC}_m{}^{s}(\varphi)U_0. \quad (4.63)$$

Then

$$ihc\delta\bar{\Psi}/\delta\sigma=\mathfrak{IC}_e{}^{s}(\bar{\varphi})\bar{\Psi}, \quad (4.64)$$

where

$$\bar{\varphi}=U_0{}^{-1}\varphi U_0. \quad (4.65)$$

Define $R_\varphi(\sigma)$ by the equation

$$ihc\delta R_\varphi/\delta\sigma=\mathfrak{IC}_{\mathrm{free}}{}^{s}(\varphi_s)R_\varphi, \quad (4.66)$$

$\mathfrak{IC}_{\mathrm{free}}{}^{s}(\varphi_s)$ being given by (1.30). The variables φ can be regarded as the Heisenberg variables of the free field and R_φ is the transformation which takes them into the Schrödinger variables of the free field by the relation

$$\varphi=R_\varphi{}^{-1}\varphi_s R_\varphi. \quad (4.67)$$

Thus

$$\bar{\varphi}=V^{-1}\varphi_s V, \quad (4.68)$$

where

$$V=R_\varphi U_0. \quad (4.69)$$

By (4.63), (4.66), and (4.69),

$$ihc\delta V/\delta\sigma=\mathfrak{IC}_{\mathrm{free}}{}^{s}(\varphi_s)V+R_\varphi\mathfrak{IC}_m{}^{s}(\varphi)U_0 =\{\mathfrak{IC}_{\mathrm{free}}{}^{s}(\varphi_s)+\mathfrak{IC}_m{}^{s}(\varphi_s)\}V. \quad (4.70)$$

Thus by (4.68), $\bar{\varphi}$ satisfies the equation of motion determined by the Hamiltonian $\mathfrak{H}_{free}^{s}+\mathfrak{H}_{m}^{s}$. But by (4.60) and (1.30) this is equal to $\mathfrak{H}_{free}^{s}$ with κ replaced by $\kappa+\kappa_1+\kappa_2$. Thus the field variable of Eq. (4.64) from which the meson self-energy terms have been eliminated satisfies the equation of motion of the free meson field with the renormalized mass $\kappa+\kappa_1+\kappa_2$ (κ_1, κ_2 small). This is only a formal renormalization since κ_1 is given infinite by the theory. The renormalized mass is put equal to the observed mass since it is the "bare" particle plus the vacuum effects which is actually observed.

The vector meson f self-energy arises from

$$\mathfrak{H}_{13}^{v}(x)=(-i/8\hbar c^3)\int\langle[j_\mu(x),\, j_\nu(x')]\rangle_0 \times\{\varphi_\mu(x),\, \varphi_\nu(x')\}_1\epsilon(\sigma,\,\sigma')d\omega' \quad (4.71)$$

$$=\{\varphi_\mu(x),\, \eta_\mu^{v}(x)\}_1, \quad (4.72)$$

where

$$\eta_\mu^{v}(x)=(-i/8\hbar c^3)\int\langle[j_\mu(x),\, j_\nu(x')]\rangle_0 \times\varphi_\nu(x')\epsilon(x-x')d\omega'$$

$$=(f^2/\hbar c)\int \mathrm{K}_{\mu\nu}^{v}(x-x')\varphi_\nu(x')d\omega'. \quad (4.73)$$

$\mathrm{K}_{\mu\nu}^{v}(x)$ is the same expression as occurred in (4.41) in the scalar g self-energy. As for (4.8),

$$\eta_\mu^{v}(x)=(f^2/\hbar c)\mathrm{K}_{\mu\nu}^{v}(p)\varphi_\nu(x). \quad (4.74)$$

From the supplementary condition

$$(\partial\varphi_\nu/\partial x_\nu)\Psi=0, \quad ip_\nu\varphi_\nu(p)\exp[ip_\lambda x_\lambda]\Psi=0. \quad (4.75)$$

Thus, in this case, for the terms in the integrand of $\mathrm{K}_{\mu\nu}^{v}(p)$

$$p_\mu p_\nu=0. \quad (4.76)$$

This relation replaces (4.44) in the scalar g case. Equation (4.45) is still valid. Introducing the variables y and ω and eliminating p_λ by (4.9) and (4.76),

$$\mathrm{K}_{\mu\nu}^{v}(\kappa)=\frac{\kappa^2}{64}\left(\frac{1}{2\pi}\right)^2\delta_{\mu\nu}\int_{-1}^{+1}dy\left[\frac{-4i\mu^2}{\omega}-4\mu^2-1+y^2\right] \times\int d\omega\frac{1}{|\omega|}\exp\left[i\omega\left(1-\frac{1-y^2}{4\mu^2}\right)\right]. \quad (4.77)$$

This integral is of the standard form (4.30) with

$$A=-1+y^2-4\mu^2, \quad B=-4\mu^2, \quad C=1-(1-y^2)/4\mu^2. \quad (4.78)$$

Thus

$$\mathrm{K}_{\mu\nu}^{v}(\kappa)=\frac{\kappa^2}{32}\left(\frac{1}{2\pi}\right)^2\delta_{\mu\nu}\left[-\frac{8}{3}\log\frac{1}{\gamma\omega_0}+2\int_{-1}^{+1}(1-y^2) \times\log\left(1-\frac{1-y^2}{4\mu^2}\right)dy+8\mu^2-\frac{4}{3}\right] \quad (4.79)$$

$$=-\frac{\kappa^2}{16\pi^2}\delta_{\mu\nu}\left[\frac{1}{3}\log\frac{1}{\gamma\omega_0}+\text{f. t.}\right] \quad (4.80)$$

and

$$\eta_\mu^{v}(x)=\varphi_\mu(x)\left(\frac{\kappa^2 f^2}{4\pi\hbar c}\right)\left(\frac{-1}{4\pi}\right)\left[\frac{1}{3}\log\frac{1}{\gamma\omega_0}+\text{f. t.}\right]. \quad (4.81)$$

Hence

$$\mathfrak{H}_{13}^{v}(x)=2\kappa\kappa_3\{\varphi_\mu^2(x)\}_1, \quad (4.82)$$

and

$$\kappa_3=\kappa\left(\frac{f^2}{4\pi\hbar c}\right)\left(\frac{-1}{4\pi}\right)\left[\frac{1}{3}\log\frac{1}{\gamma\omega_0}+\text{f. t.}\right]. \quad (4.83)$$

In the particular case when $\kappa=0$ the only non-zero term in $\mathfrak{H}_{13}^{v}(x)$ comes from the term $8\mu^2$ in the square bracket of (4.79). Then

$$\kappa_{\mu\nu}^{v}(\kappa)=\frac{\kappa_0^2}{4}\left(\frac{1}{2\pi}\right)^2\delta_{\mu\nu},$$

which leads to

$$\mathfrak{H}_{13}^{v}(x)=\kappa_0^2\left(\frac{f^2}{4\pi\hbar c}\right)\frac{1}{2\pi}\{\varphi_\mu^2(x)\}_1. \quad (4.84)$$

This is the finite value for the photon self-energy obtained by Wentzel.[6]

The strongest singularities of the Δ-functions are

$$\bar{\Delta}(x)=(-1/4\pi)\delta(x_\mu^2)+\cdots, \quad (4.85)$$

$$\Delta^{(1)}(x)=(-1/2\pi x_\mu^2)+\cdots. \quad (4.86)$$

Thus the integral of a product $\bar{\Delta}(x)\Delta^{(1)}(x)$ through the origin is not regular and will give different values for different methods of integration. For unobservable effects such as meson self-energies, which are to be transformed away, only the form of the expression is really significant. However, for observable effects some precise definition of the integrals is necessary. The vector meson f self-energy is an observable effect when $\kappa=0$, since it then reduces to the photon self-energy which must be zero. Pauli[7] has proposed a procedure for regularizing the integrals which will be given here in some detail.

It can be shown that both $\bar{\Delta}(x)$ and $\Delta^{(1)}(x)$ are functions of $\kappa^2x_\mu^2$ so that a regular function $\mathbf{K}$ can be obtained from $\mathrm{K}(\kappa^2x_\mu^2)$ defined by

$$\mathbf{K}=\int_0^\infty\rho(\alpha)\mathrm{K}(\alpha x_\mu^2)d\alpha, \quad (4.87)$$

where

$$\int_0^\infty \rho(\alpha)d\alpha=0. \tag{4.88}$$

and

$$\int_0^\infty \alpha\rho(\alpha)d\alpha=0. \tag{4.89}$$

Also

$$\rho(\alpha)=\delta(\alpha-\kappa^2)+\rho_1(\alpha), \tag{4.90}$$

and $\rho_1(\alpha)=0$ for finite α and $\rho_1(\alpha)$ is such that in the limit

$$\int_0^\infty (\rho_1(\alpha)/\alpha)d\alpha=0. \tag{4.91}$$

If $\rho(\alpha)$ is expressed in terms of discreet masses

$$\rho_1(\alpha)=\sum C_i\delta(\alpha-\kappa_i^2). \tag{4.92}$$

Then

$$1+\sum C_i=0, \tag{4.93}$$

and

$$\kappa^2+\sum C_i\kappa_i^2=0. \tag{4.94}$$

The regularization of the matrix element for any effect can thus be regarded as subtracting the matrix element for the same effect due to an interaction with similar particles with masses corresponding to κ_i and weight factors C_i and in the final limit letting the masses of the subsidiary particles tend to infinity. The procedure is thus a generalization of the ideas of Podolsky[10] and Feynman.[11] In this case, however, the subsidiary fields are introduced purely as a mathematical device with no suggestion of physical reality.

To regularize a term $\exp[ix\kappa_0^2]$ in $\kappa_{\mu\nu}$ it must be replaced by

$$R(x)=\int_0^\infty \rho(\alpha)\exp[i\alpha x]d\alpha, \tag{4.95}$$

where by (4.88) and (4.89),

$$R(0)=0, \tag{4.96}$$

and

$$R'(0)=0. \tag{4.97}$$

Also

$$R'(x)=\int_0^\infty i\alpha\rho(\alpha)\exp[i\alpha x]d\alpha. \tag{4.98}$$

Thus a term $\kappa_0^2\exp[ix\kappa_0^2]$ occurring in $\mathbf{K}_{\mu\nu}$ is regularized by replacing it by $-iR'(x)$. Applying this procedure to (4.45) gives

$$\mathbf{K}_{\mu\nu}(p)=\frac{1}{32\pi^2}\int da\int db\frac{\epsilon(a)\epsilon(a+b)}{(a+b)^2}\exp\left[ip_\lambda^2\frac{ab}{a+b}\right]$$
$$\times\left\{\delta_{\mu\nu}\left[\left(\frac{-i}{a+b}+\frac{ab}{(a+b)^2}p_\lambda^2\right)R(a+b)\right.\right.$$
$$\left.+iR'(a+b)\right]-p_\nu p_\mu\frac{2ab}{(a+b)^2}R(a+b)\Bigg\}. \tag{4.99}$$

By symmetrizing with respect to a and b and introducing the variables y and z

$$\mathbf{K}_{\mu\nu}(p)=\frac{1}{32}\cdot\frac{1}{2\pi^2}\int_{-1}^{+1}dy\int_{-\infty}^{\infty}dz\epsilon(z)$$
$$\times\left\{\delta_{\mu\nu}\frac{d}{dz}\left[i\frac{R(z)}{z}\exp\left[\frac{i}{4}(1-y^2)p_\lambda^2z\right]\right]\right.$$
$$+\tfrac{1}{2}(p_\lambda^2\delta_{\mu\nu}-p_\mu p_\nu)(1-y^2)\frac{R(z)}{z}$$
$$\left.\times\exp\left[\frac{i}{4}(1-y^2)p_\lambda^2z\right]\right\}$$
$$=\frac{1}{32}\cdot\frac{1}{2\pi^2}\int_{-1}^{+1}dy\int_{-\infty}^{\infty}dz\left\{\delta_{\mu\nu}\left(\frac{-d\epsilon(z)}{dz}\right)\right.$$
$$\times\left[i\frac{R(z)}{z}\exp\left[\frac{i}{4}(1-y^2)p_\lambda^2z\right]\right]$$
$$+\tfrac{1}{2}\epsilon(z)(p_\lambda^2\delta_{\mu\nu}-p_\mu p_\nu)(1-y^2)\frac{R(z)}{z}$$
$$\left.\times\exp\left[\frac{i}{4}(1-y^2)p_\lambda^2z\right]\right\}. \tag{4.100}$$

By (2.49) the first term is

$$-2i(R(z)/z)_{z=0}=-2R'(0).$$

This is zero by (4.97). Thus

$$\mathbf{K}_{\mu\nu}(p)=\frac{1}{32}\cdot\frac{1}{4\pi^2}\int_{-\infty}^{\infty}dz\frac{\epsilon(z)}{z}R(z)\int_{-1}^{+1}dy(1-y^2)$$
$$\times\exp\left[\frac{i}{4}(1-y^2)p_\lambda^2z\right](\delta_{\mu\nu}p_\lambda^2-p_\mu p_\nu)$$
$$=\frac{1}{32}\cdot\frac{1}{4\pi^2}(\delta_{\mu\nu}p_\lambda^2-p_\mu p_\nu)F(p_\lambda^2). \tag{4.101}$$

Thus

$$\eta_\mu{}^\nu(x)=\varphi_\nu(x)\frac{f^2}{\hbar c}\frac{1}{32}\cdot\left(\frac{1}{2\pi}\right)^2(\delta_{\mu\nu}p_\lambda^2-p_\mu p_\nu)F(p_\lambda^2) \tag{4.102}$$

$$=-\frac{f^2}{\hbar c}\frac{1}{32}\cdot\left(\frac{1}{2\pi}\right)^2\kappa^2F(-\kappa^2)\varphi_\mu(x). \tag{4.103}$$

This is zero in the photon case ($\kappa=0$) as required and is infinite in the meson case ($\kappa\neq0$).

Taking the regularized form of $\mathbf{K}_{\mu\nu}(p)$ by (4.9) and (4.44)

$$\eta_\mu{}^\mu(x)=0. \tag{4.104}$$

Thus the regularized scalar meson g self-energy is

[10] F. Podolsky, Rev. Mod. Phys. **20**, 40 (1948).
[11] R. P. Feynman, Phys. Rev. **74**, 1430 (1948).

zero. The scalar meson f self-energy and the vector meson g self-energy remain infinite with or without regularization, unless extra conditions are imposed.

The vector meson g self-energy is given by

$$\mathcal{H}_{23}{}^{\nu}(x)=(-i/8\hbar c\kappa^2)\int\langle[m_{\mu\nu}(x),\, m_{\pi\rho}(x')]\rangle_0 \times\{\varphi_{\nu\mu}(x),\, \varphi_{\rho\pi}(x')\}_1\epsilon(x-x')d\omega' \quad (4.105)$$

$$=\{\varphi_{\nu\mu}(x),\, \eta_{\mu\nu}{}^{\nu}(x)\}_1, \quad (4.106)$$

where

$$\eta_{\mu\nu}{}^{\nu}(x)=(-i/8\hbar c\kappa^2)\int\langle[m_{\mu\nu}(x),\, m_{\pi\rho}(x')]\rangle_0 \times\varphi_{\rho\pi}(x')\epsilon(x-x')d\omega'$$

$$=(g^2/\hbar c\kappa^2)\int \mathrm{K}_{\mu\nu\pi\rho}{}^{\nu}(x-x')\varphi_{\rho\pi}(x')d\omega'$$

$$=(g^2/\hbar c\kappa^2)\mathrm{K}_{\mu\nu\pi\rho}{}^{\nu}(p)\varphi_{\rho\pi}(x). \quad (4.107)$$

For factors in the integrand of $\kappa_{\mu\nu\pi\rho}{}^{\nu}(p)$, Eq. (4.9) is still valid and in place of (4.44),

$$p_\pi p_\mu=-\kappa^2\delta_{\pi\mu}. \quad (4.108)$$

Also from the supplementary condition, in the integrand of $\kappa_{\mu\nu\pi\rho}{}^{\nu}(p)$ effectively

$$p_\rho=0. \quad (4.109)$$

From (2.37),

$$\mathrm{K}_{\mu\nu\pi\rho}{}^{\nu}(x)=\delta_{\rho\nu}\mathrm{K}_{\pi\mu}{}'(x)-\delta_{\rho\mu}\mathrm{K}_{\pi\nu}{}'(x)+\delta_{\pi\mu}\mathrm{K}_{\rho\nu}{}'(x) -\delta_{\pi\nu}\mathrm{K}_{\rho\mu}{}'(x)+(\delta_{\rho\mu}\delta_{\pi\nu}-\delta_{\pi\mu}\delta_{\rho\nu})\mathrm{K}(x), \quad (4.110)$$

where $\mathrm{K}(x)$ is defined in (4.10) and, with the notation (2.34),

$$\mathrm{K}_{\mu\nu}{}'(x)=\Delta_{0\mu}{}^{(1)}(x)\bar{\Delta}_{0\nu}(x)+\Delta_{0\nu}{}^{(1)}(x)\bar{\Delta}_{0\mu}(x). \quad (4.111)$$

By the usual method

$$\mathrm{K}_{\mu\nu}{}'(p)=\frac{1}{64\pi^2}\int_{-1}^{+1}dy\int_{-\infty}^{\infty}dz\epsilon(z) \times\exp\left[iz\left(\kappa_0{}^2+\frac{1-y^2}{4}p_\lambda{}^2\right)\right] \times\left\{\frac{i\delta_{\mu\nu}}{z^2}-\frac{1-y^2}{2z}p_\mu p_\nu\right\}, \quad (4.112)$$

and from (4.26),

$$\mathrm{K}(p)=\frac{1}{64\pi^2}\int_{-1}^{+1}dy\int_{-\infty}^{\infty}dz\epsilon(z) \times\exp\left[iz\left(\kappa_0{}^2+\frac{1-y^2}{4}p_\lambda{}^2\right)\right] \times\left\{\frac{2i}{z^2}-\frac{\kappa_0{}^2}{z}-\frac{(1-y^2)}{4z}p_\lambda{}^2\right\}. \quad (4.113)$$

Introducing ω and substituting for p_λ from (4.9), (4.108), and (4.109)

$$\mathrm{K}_{\mu\nu\pi\rho}{}^{\nu}(\kappa)=-\frac{\kappa^2}{64}\left(\frac{1}{2\pi}\right)^2\int_{-1}^{+1}dy(4\mu^2+1-y^2) \times\int_{-\infty}^{\infty}d\omega\frac{1}{|\omega|}\exp\left[i\omega\left(1-\frac{1-y^2}{4\mu^2}\right)\right] \times(\delta_{\rho\mu}\delta_{\pi\nu}-\delta_{\pi\mu}\delta_{\rho\nu}). \quad (4.114)$$

This is of the standard form (4.30) with

$$A=4\mu^2+1-y^2,\quad B=0,\quad C=1-(1-y^2)/4\mu^2, \quad (4.115)$$

and yields

$$\mathrm{K}_{\mu\nu\pi\rho}{}^{\nu}(p)=\frac{-\kappa^2}{32\pi^2}\left[(\tfrac{1}{3}+2\mu^2)\log\frac{1}{\gamma\omega_0}+\text{f. t.}\right] \times(\delta_{\rho\mu}\delta_{\pi\nu}-\delta_{\pi\mu}\delta_{\rho\nu}). \quad (4.116)$$

Thus

$$\eta_{\mu\nu}{}^{\nu}(x)=-\left(\frac{g^2}{4\pi\hbar c}\right)\left(\frac{1}{8\pi}\right)\left[(\tfrac{1}{3}+2\mu^2)\log\frac{1}{\gamma\omega_0}+\text{f. t.}\right] \times(\varphi_{\mu\nu}(x)-\varphi_{\nu\mu}(x)), \quad (4.117)$$

and

$$\mathcal{H}_{23}{}^{\nu}(x)=-2(\kappa_4/\kappa)\{(\varphi_{\mu\nu}(x)-\varphi_{\nu\mu}(x))^2\}_1, \quad (4.118)$$

where

$$\kappa_4=\kappa\left(\frac{g^2}{4\pi\hbar c}\right)\left(\frac{1}{8\pi}\right)\left[(\tfrac{1}{3}+2\mu^2)\log\frac{1}{\gamma\omega_0}+\text{f. t.}\right]. \quad (4.119)$$

Now

$$\varphi_\mu(x)=\sum_k\varphi_\mu(k)\exp[ik_\mu x_\mu]. \quad (4.120)$$

As in the case of (4.57)

$$\{\varphi_{\mu\nu}{}^2(x)\}_1=\sum k_\nu{}^2\varphi_\mu{}^{(-)}(k)\varphi_\mu{}^{(+)}(k) =-\kappa^2\{\varphi_\mu{}^2(x)\}_1. \quad (4.121)$$

Similarly

$$\{\varphi_{\nu\mu}(x)\varphi_{\mu\nu}(x)\}_1=\sum k_\mu k_\nu\{\varphi_\nu{}^{(+)}(k)\varphi_\mu{}^{(-)}(k) +\varphi_\nu{}^{(-)}(k)\varphi_\mu{}^{(+)}(k)\}. \quad (4.122)$$

But by the supplementary condition

$$k_\nu\varphi_\nu{}^{(+)}(k)=0,\quad\text{and}\quad k_\nu\varphi_\nu{}^{(-)}(k)=0. \quad (4.123)$$

Thus

$$\{(\varphi_{\mu\nu}(x)-\varphi_{\nu\mu}(x))^2\}_1 =2\{\varphi_{\mu\nu}{}^2(x)-\varphi_{\mu\nu}(x)\varphi_{\nu\mu}(x)\}_1=-2\kappa^2\{\varphi_\mu{}^2(x)\}_1. \quad (4.124)$$

By a similar argument it can be shown that

$$\kappa^2\{\varphi_\mu{}^2(x)\}_1=\kappa^2\{A_\mu{}^2(x)\}_1+\kappa^2\{B^2(x)\}_1, \quad (4.125)$$

which is of the form of the mass dependent terms in $\mathcal{H}_{free}^{v}(x)$ by (1.58). Define

$$\mathcal{H}_0^{v}(x)=2(\kappa_3+\kappa_4)\kappa\varphi_\mu^2(x). \tag{4.126}$$

Then by replacing the label s by the label v in the derivation of (4.64), the wave equation can be transformed into

$$i\hbar c\delta\Psi/\delta\sigma=\mathcal{H}_e^{v}(\bar{\varphi}_\mu)\Psi, \tag{4.127}$$

which is free from the infinities due to meson self-energies and in which the meson field variables satisfy the equations of motion of the free field with renormalized mass, $\kappa+\kappa_3+\kappa_4$.

The cross terms which arise from $\mathcal{H}_3^{s}(x)$ and $\mathcal{H}_3^{v}(x)$ have not yet been considered. These give rise to the fg meson self-energy through $\mathcal{H}_{33}^{s}(x)$ and $\mathcal{H}_{33}^{v}(x)$. From (2.38) it follows immediately that $\mathcal{H}_{33}^{s}(x)$ is zero. It can be shown after a short calculation using the properties of the Δ-functions, (2.6), and (2.39) that $\mathcal{H}_{33}^{v}(x)$ is also zero.

V. THE NUCLEON SELF-ENERGIES

The nucleon f self-energy caused by interaction with scalar mesons is the one-nucleon part of $\mathcal{H}_{1,2}^{s}(x)$ which is given by (3.5), (3.10) and the discussion following these equations.

$$\mathcal{H}_{fse}^{s}(x)=(-i/8c^2)\times\int_{-\infty}^{\infty}[\omega(x),\omega(x')]\Delta^{(1)}(x-x')\epsilon(x-x')d\omega'-(1/4c^2)\int_{-\infty}^{\infty}\{\omega(x),\omega(x')\}_1\times\bar{\Delta}(x-x')d\omega'. \tag{5.1}$$

By (2.31 and (2.45)

$$\begin{aligned}\mathcal{H}_{fse}^{s}(x)=(f^2/8)\int_{-\infty}^{\infty}\{&[\bar{\psi}(x),S^{(1)}(x-x')\psi(x')]\bar{\Delta}(x-x')\\&+[\bar{\psi}(x),\bar{S}(x-x')\psi(x')]\Delta^{(1)}(x-x')\\&+[\bar{\psi}(x')S^{(1)}(x-x'),\psi(x)]\bar{\Delta}(x-x')\\&+[\bar{\psi}(x')\bar{S}(x'-x),\psi(x)]\Delta^{(1)}(x-x')\}d\omega'\end{aligned} \tag{5.2}$$

$$=\tfrac{1}{4}[\bar{\psi}(x),\zeta_1(x)]+[\bar{\zeta}_1(x),\psi(x)], \tag{5.3}$$

where

$$\begin{aligned}\zeta_1(x)=\tfrac{1}{2}f^2\int\{&S^{(1)}(x-x')\bar{\Delta}(x-x')\\&+\bar{S}(x-x')\Delta^{(1)}(x-x')\}\psi(x')d\omega'\end{aligned} \tag{5.4}$$

$$=\tfrac{1}{2}f^2\int K_1(x-x')\psi(x')d\omega'. \tag{5.5}$$

The last equation defines $K_1(x-x')$. As for (4.8)

$$\zeta_1(x)=\tfrac{1}{2}f^2\psi(x)\kappa_1(p). \tag{5.6}$$

Since $\psi(x)$ satisfies the Dirac Eq. (1.18),

$$i\gamma_\mu p_\mu=-\kappa_0, \tag{5.7}$$

and

$$p_\lambda{}^2=-\kappa_0{}^2. \tag{5.8}$$

Expanding the S-functions, it follows from (5.5) with the notation (2.34) that

$$\begin{aligned}K_1(\xi)=\gamma_\lambda[&\bar{\Delta}(\xi)\Delta_{0\lambda}{}^{(1)}(\xi)+\Delta^{(1)}(\xi)\bar{\Delta}_{0\lambda}(\xi)]\\&-\kappa^0[\bar{\Delta}(\xi)\Delta_0{}^{(1)}(\xi)+\Delta^{(1)}(\xi)\bar{\Delta}_0(\xi)].\end{aligned} \tag{5.9}$$

Substituting for $\bar{\Delta}$ and $\Delta^{(1)}$ from (4.11) and (4.12),

$$K_1(p)=\left(\frac{1}{2\pi}\right)^3\int d_4q\left\{\left[\frac{\delta(q_\lambda{}^2+\kappa_0{}^2)}{(p_\lambda-q_\lambda)^2+\alpha^2}+\frac{\delta((p_\lambda-q_\lambda)^2+\kappa^2)}{q_\lambda{}^2+\kappa_0{}^2}\right](i\gamma_\lambda q_\lambda-\kappa_0)\right\}. \tag{5.10}$$

This can be evaluated by the transformations (4.15), (4.16) (4.18), and (4.23) used for the meson self-energy. Eliminating p_λ by (5.7) and (5.8),

$$K_1(\kappa_0)=\frac{-\kappa_0}{64\pi^2}\int_{-1}^{+1}dy(3-y)\int_{-\infty}^{\infty}d\omega\frac{1}{|\omega|}\times\exp\left[i\omega\left\{\left(\frac{1+y}{2}\right)^2+\frac{1-y}{2\mu^2}\right\}\right]. \tag{5.11}$$

Now

$$(3-y)=\frac{1}{2}\frac{d}{dy}(7-y)(1+y). \tag{5.12}$$

Integrating (5.11) by parts,

$$\begin{aligned}K_1(\kappa_0)&=-\frac{\kappa_0}{32\pi^2}\left[6\int_0^{\infty}\frac{\cos\omega}{\omega}d\omega+\int_{-1}^{+1}\frac{(7-y)(1+y)\{(1+y)\mu^2-1\}}{(1+y)^2\mu^2+1-y}dy\right] &(5.13)\\&=-\frac{\kappa_0}{32\pi^2}\left[6\log\frac{1}{\gamma\omega_0}+\text{f. t.}\right] &(5.14)\end{aligned}$$

since the integrand in the second integral in (5.13) is finite. Thus

$$\begin{aligned}\zeta_1(x)&=-\hbar c\kappa_0\left(\frac{f^2}{4\pi\hbar c}\right)\left[\frac{3}{8\pi}\log\frac{1}{\gamma\omega_0}+\text{f. t.}\right]\psi(x) &(5.15)\\&=-\hbar c\kappa_0{}^{(1)}\psi(x), &(5.16)\end{aligned}$$

where

$$\kappa_0{}^{(1)}=-\kappa_0\left(\frac{f^2}{4\pi\hbar c}\right)\left[\frac{3}{8\pi}\log\frac{1}{\gamma\omega_0}+\text{f. t.}\right]. \tag{5.17}$$

Thus by (5.3)

$$\mathcal{H}_{fse}{}^{s}(x)=\tfrac{1}{2}\hbar c\kappa_0{}^{(1)}(\bar{\psi}(x)\psi(x)-\psi(x)\bar{\psi}(x)). \quad (5.18)$$

This term can be eliminated from the Schrödinger Eq. (3.4) by the same transformation as was used for the meson self-energies, (4.62) and (4.63), with $\mathcal{H}_m{}^{s}(x)$ replaced by $\mathcal{H}_{fse}{}^{s}(x)$. By the same argument as that which lead to (4.70) the new field variable ψ will satisfy the equation of motion determined by the Hamiltonian $\mathcal{H}_{\text{free}}(x)+\mathcal{H}_{fse}(x)$. But the mass terms in $\mathcal{H}_{\text{free}}(x)$ are

$$\tfrac{1}{2}\hbar c\kappa_0(\bar{\psi}(x)\psi(x)-\psi(x)\bar{\psi}(x)),$$

as can be seen from the Lagrangian (1.16). Thus the new field variables will satisfy the equation of the free field with the renormalized mass $\kappa_0+\kappa_0{}^{(1)}$.

The nucleon g self-energy due to scalar mesons is the one particle part of $\mathcal{H}_{22}{}^{s}(x)+\mathcal{H}_{4}{}^{s}(x)$ which was derived in (3.13). The required commutators are given by (2.31) and (2.45). A calculation similar to that outlined above, complicated slightly by the additional γ_μ factors, gives

$$\mathcal{H}_{gse}{}^{s}(x)=\tfrac{1}{2}\hbar c\kappa_0{}^{(2)}(\bar{\psi}(x)\psi(x)-\psi(x)\bar{\psi}(x)), \quad (5.19)$$

where $\kappa_0{}^{(2)}$ is finite and remains finite in the limit $\mu\to 0$ that is, when the meson mass becomes infinite. The scalar fg nucleon self-energy can be shown to be zero by a similar calculation.

The vector f nucleon self-energy is the one-nucleon part of $\mathcal{H}_{12}{}^{v}(x)+\mathcal{H}_{41}{}^{v}(x)$ which was derived in (3.21). This splits into two parts, one containing pure Δ-functions and the other containing double differentials of Δ-functions. The latter is identical with the scalar g nucleon self-energy which is finite. Thus the infinity is contained in the first part. Substituting for the commutators from (2.31) and (2.45) and evaluating as above,

$$\mathcal{H}_{fse}{}^{v}(x)=\tfrac{1}{2}\hbar c\kappa_0{}^{(3)}(\bar{\psi}(\kappa)\psi(x)-\psi(x)\bar{\psi}(x)), \quad (5.20)$$

where

$$\kappa_0{}^{(3)}=\kappa_0\left(\frac{f^2}{4\pi\hbar c}\right)\left[\frac{3}{4\pi}\log\frac{1}{\gamma\omega_0}+\text{f. t.}\right]. \quad (5.21)$$

It is important that $\kappa_0{}^{(1)}$ and $\kappa_0{}^{(3)}$ differ in their infinite term only by a factor $-\frac{1}{2}$ so that $2\kappa_0{}^{(1)}+\kappa_0{}^{(3)}$ is finite. This is the basis of the Pais f-field theory[8] in which a finite electron self-energy is obtained by adding a scalar meson field to the photon field with the coupling constant,

$$f^2=2e^2. \quad (5.22)$$

Also, since the infinite part of $\kappa_0{}^{(3)}$ is independent of κ and the finite part remains finite when $\kappa\to\infty$, a finite electron self-energy is obtained by subtracting a vector meson field with coupling constant

$$f=e. \quad (5.23)$$

This is the basis of the theories of Podolsky[10] and Feynman.[11] Difficulties arise over the interpretation of the meson field if it is regarded as having any physical reality since the theory necessarily involves either negative energies or negative "probabilities."

The vector g and fg nucleon self-energies, given by the one-nucleon parts of $\mathcal{H}_{22}{}^{v}(x)+\mathcal{H}_{42}{}^{v}(x)$, (3.24), and $\mathcal{H}_{32}{}^{v}(x)$, respectively, are

$$\mathcal{H}_{gse}{}^{v}(x)=\tfrac{1}{2}\hbar c\kappa_0{}^{(4)}(\bar{\psi}(x)\psi(x)-\psi(x)\bar{\psi}(x)), \quad (5.24)$$

and

$$\mathcal{H}_{fgse}{}^{v}(x)=\tfrac{1}{2}\hbar c\kappa_0{}^{(5)}(\bar{\psi}(x)\psi(x)-\psi(x)\bar{\psi}(x)), \quad (5.25)$$

where

$$\kappa_0{}^{(4)}=\kappa_0\left(\frac{g^2}{4\pi\hbar c}\right)\frac{\mu^2}{4\pi}\left[\left(8+\frac{3}{\mu^2}\right)\log\frac{1}{\gamma\omega_0}+\text{f. t.}\right], \quad (5.26)$$

and

$$\kappa_0{}^{(5)}=-\kappa_0\left(\frac{fg}{4\pi\hbar c}\right)\left[\frac{3}{2\pi\mu}\log\frac{1}{\gamma\omega_0}+\text{f. t.}\right]. \quad (5.27)$$

All the nucleon self-energies are of the same form as (5.18) and can be eliminated from the Schrödinger Eqs. (3.4) or (3.14) by transformations of the type described in the discussion following Eq. (5.18). The new nucleon field variable, $\psi(x)$, will satisfy the equation of motion of the free field with renormalized mass, in the scalar case,

$$\bar{\kappa}_0=\kappa_0+\kappa_0{}^{(1)}+\kappa_0{}^{(2)}, \quad (5.28)$$

and in the vector case

$$\bar{\kappa}_0{}'=\kappa_0+\kappa_0{}^{(3)}+\kappa_0{}^{(4)}+\kappa_0{}^{(5)}. \quad (5.29)$$

These are equated to the experimental mass.

The transformations for eliminating the meson self-energies and the nucleon self-energies are independent. If $\mathcal{H}_n{}^{s}(x)$ is defined by

$$\mathcal{H}_n{}^{s}(x)=\mathcal{H}_{fse}{}^{s}(x)+\mathcal{H}_{gse}{}^{s}(x), \quad (5.30)$$

and both transformations are performed, the Schrödinger equation for the transformed state vector, $\Psi(\sigma)$, is

$$ihc\delta\Psi/\delta\sigma(x)=\mathcal{H}^{s}(x)\Psi(\sigma), \quad (5.31)$$

where

$$\mathcal{H}^{s}(x)=\mathcal{H}_e{}^{s}(x)-\mathcal{H}_n{}^{s}(x). \quad (5.32)$$

$\mathcal{H}_e{}^{s}(x)$ is defined by (4.61). The matrix elements of $\mathcal{H}^{s}(x)$ are free from infinites. $\mathcal{H}^{s}$ is a function of the transformed variable $\varphi(x)$ and $\psi(x)$, each of which satisfies its respective free-field equation with renormalized mass. A similar equation can be obtained in the vector case. Since all the integrals for the mass renormalizations are independent of the choice of n_μ, this is an invariant result. The transformations do not alter the form of the supplementary condition.

VI. THE YUKAWA POTENTIALS

One real effect which of course has not been eliminated from (5.31) is the Yukawa potentials between nucleons. These have been known for many years but it is of interest that the derivation of the expression for the potential in configuration space from the interaction operator in field theory, which has previously been rather awkward, is very neat when the theory is developed in this Schwinger form.

The f scalar nucleon interaction is the two-nucleon part of $\mathfrak{IC}_{12}{}^{s}(x)$ (5.1). Since, by (2.31), $[\omega(x), \omega(x')]$ is a one-nucleon operator, only the second term need be considered.

$$\mathfrak{IC}_{fint}{}^{s}(x) = -(1/4c^2)\int_{-\infty}^{\infty}\{\omega(x), \omega(x')\}_2\bar{\Delta}(x-x')d\omega'. \quad (6.1)$$

Now $\omega(x)$ can be expressed as

$$\omega(x) = fc\bar{\psi}(x)\psi(x) + \text{c. number}. \quad (6.2)$$

Thus

$$\mathfrak{IC}_{fint}{}^{s}(x) = -(f^2/4)\int\{\bar{\psi}(x)\psi(x), \bar{\psi}(x')\psi(x')\}_2 \times\bar{\Delta}(x-x')d\omega' \quad (6.3)$$

$$= (f^2/2)\int\bar{\psi}(x)\bar{\psi}(x')\psi(x)\psi(x') \times\bar{\Delta}(x-x')d\omega'. \quad (6.4)$$

In the second equation a one-nucleon term has been dropped. Substituting for $\bar{\Delta}(x-x')$ from (2.56),

$$\mathfrak{IC}_{fint}{}^{s}(x) = \frac{f^2}{2}\left(\frac{1}{2\pi}\right)^4\int d^4x'\int d^4k \times\bar{\psi}(x)\bar{\psi}(x')\psi(x)\psi(x')\frac{\exp[ik_\mu\cdot x_\mu - x_\mu']}{k_\mu{}^2+\kappa_0{}^2}. \quad (6.5)$$

If recoil is neglected, $\bar{\psi}(x')\psi(x')$ is independent of x_0' and the integration over x_0 and k_0 can be performed

$$\mathfrak{IC}_{fint}{}^{s}(x) = \frac{f^2}{2}\left(\frac{1}{2\pi}\right)^3\int d^3x'\int d^3k \times\bar{\psi}(x)\bar{\psi}(x')\psi(x)\psi(x')\frac{\exp[i\mathbf{k}\cdot\mathbf{x}-\mathbf{x}']}{|\mathbf{k}|^2+\kappa_0{}^2}. \quad (6.6)$$

But[12]

$$\left(\frac{1}{2\pi}\right)^3\int\frac{\exp[i\mathbf{k}\cdot\mathbf{x}-\mathbf{x}']}{|\mathbf{k}|^2+\kappa_0{}^2}d^3k = \frac{1}{4\pi}\frac{\exp[-\kappa_0|\mathbf{x}-\mathbf{x}'|]}{|\mathbf{x}-\mathbf{x}'|} = J(|\mathbf{x}-\mathbf{x}'|), \quad (6.7)$$

and

$$\bar{\psi}(x)\bar{\psi}(x')\psi(x)\psi(x') = \psi^*(x)\psi^*(x')\gamma_4\gamma_4'\psi(x)\psi(x'), \quad (6.8)$$

where γ_4 operates on $\psi(x)$ and γ_4' on $\psi(x')$. Thus

$$\mathfrak{IC}_{fint}{}^{s}(x) = (f^2/2)\int\psi^*(x)\psi^*(x')\gamma_4\gamma_4'\psi(x)\psi(x') \times J(|\mathbf{x}-\mathbf{x}'|)d^3x'. \quad (6.9)$$

This field theory operator expresses the interaction between nucleons in terms of annihilation and creation operators. The Yukawa potential in configuration space is that from which $\mathfrak{IC}_{fint}{}^{s}(x)$ can be derived by the process of second quantization. If $V(\mathbf{x}-\mathbf{x}')$ is the Yukawa potential then

$$\int_{-\infty}^{\infty}\mathfrak{IC}_{fint}(x)d^3x = \frac{1}{2}\int\psi^*(x)\psi^*(x')V(\mathbf{x}-\mathbf{x}')\psi(x)\psi(x')d^3xd^3x'. \quad (6.10)$$

Thus by (6.9)

$$V_f'(\mathbf{x}-\mathbf{x}') = f^2\gamma_4\gamma_4'J(|\mathbf{x}-\mathbf{x}'|), \quad (6.11)$$

which agrees with result given by Kemmer.[13] The g scalar and the f and g vector potentials can be derived similarly. Exchange effects have been neglected.

ACKNOWLEDGMENTS

In conclusion the author would like to thank Dr. N. Kemmer for his interest and helpful criticism and acknowledge his indebtedness to Professor W. Pauli for the ideas taken from his very stimulating lectures.

[12] G. Wentzel, *Einfuhrung in die Quantentheorie der Wellenfelder* (Edwards Brothers, Inc., Ann Arbor, Michigan, 1946), Eq. (7.15).
[13] N. Kemmer, Proc. Roy. Soc. A **166**, 127 (1938).

The Rotational Stark Spectrum of Linear Molecules

HAROLD KENNETH HUGHES
Technical Service Department, Socony-Vacuum Laboratories, Brooklyn, New York
(Received July 20, 1949)

In the electric resonance method of radiofrequency spectroscopy various molecular and nuclear parameters of linear polar molecules may be determined from observations of the $1, 0 \rightarrow 1, \pm 1$ transition. An equation is given for the energy difference of these two states which is good to terms in λ^6 up to values of $\lambda = 1.0$, where λ is a quantity which is proportional to the electric field strength. From this equation, expressions are derived for the permanent electric dipole moment and the moment of inertia in terms of experimentally determined parameters.

I. INTRODUCTION

IN the investigation of molecular and nuclear structure by the electric resonance method of radiofrequency spectroscopy[1-3] the practice has been, up to the present time, to interpret the experimental results with the aid of Brouwer's equation.[4] This perturbation equation describes the rotational energy levels of a linear polar molecule which is rotating in the presence of an electric field. Representing the rotational quantum number by R and the electric quantum number by p, the energy of the $R=1$, $p=0$ state was stated by Brouwer to be

$$\epsilon = 2 + (1/10)\lambda^2 - (73/7900)\lambda^4 + \cdots, \qquad (1)$$

where ϵ is in units of $\hbar^2/2I$, I is the moment of inertia in g-cm^2, $\lambda = \mu E/(\hbar^2/2I)$, μ is the permanent electric dipole moment in e.s.u. and E in the electric field strength in e.s.u.

However, there is an error[5] in Brouwer's published value for the coefficient of the λ^4-term in Eq. (1) and the correct energy of the 1,0 state, to this degree of approximation, is given by the expression

$$\epsilon = 2 + (1/10)\lambda^2 - (73/7000)\lambda^4 + \cdots. \qquad (2)$$

Brouwer's equation for the $1, \pm 1$ state is given correctly in reference 1.

In considering the effect of this error on the reported values for the moment of inertia and the electric dipole moment of CsF, the author discovered that Brouwer's equations are not sufficiently accurate for use with the $1, 0 \rightarrow 1, \pm 1$ transition at values of λ as high as 0.8. It is the purpose of this paper to extend his equations by the addition of terms in λ^6. These yield values of $\Delta\epsilon$ for the transition which are good to within 0.008 percent up to $\lambda = 0.8$. The error at $\lambda = 1$ is only 0.04 percent. These new equations are adequate for the interpretation of all data collected up to the present and should serve well for experiments now in progress and being designed.

When there are terms in the Hamiltonian arising from a nuclear electric quadrupole moment or from an I·R type of coupling, the equations in this paper can still be applied. When these terms are small, it is only necessary to calculate the unperturbed center of gravity of the split lines. When the quadrupole coupling is large, this is determined at low fields and then the unperturbed position of a high field Stark line calculated.

II. ENERGY OF THE 1,0 AND 1, ±1 STATES

To obtain values of $\Delta\epsilon$ reliable to within 0.04 percent, the exact energies of the two levels which are involved in the transition have been calculated to seven significant figures by Lamb's equation.[1] The results for values of λ between 0 and 1.0, in steps of 0.1, are tabulated in Table I, together with the corresponding energies as calculated by Brouwer's corrected equations.

In the analysis of data from observations of the $1,0 \rightarrow 1, \pm 1$ transition, it is desirable to have an analytic expression for the energy. Lamb's equation for the energy eigenvalues is in the form of a continued fraction which is not well suited to rapid use. Therefore, empirical equations have been prepared which fit Lamb's equation very well up to $\lambda = 1.0$. For the 1,0

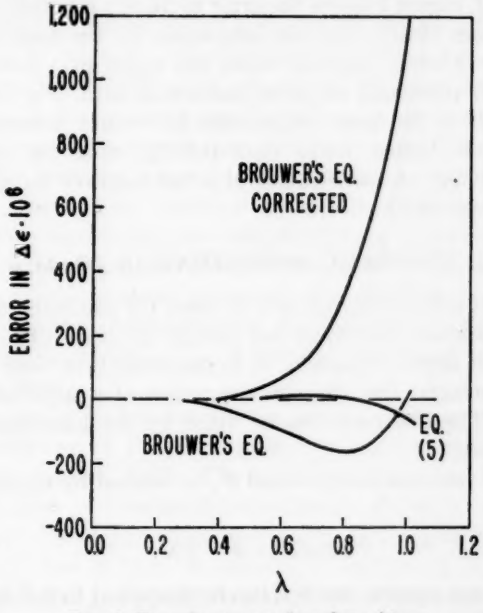

FIG. 1. Error in $\Delta\epsilon$ as a function of λ.

[1] H. K. Hughes, Phys. Rev. **72**, 614 (1947).
[2] J. W. Trischka, Phys. Rev. **74**, 718 (1948).
[3] U. Fano, J. Research Nat. Bur. of Stand. **40**, 215 (1948).
[4] F. Brouwer, Dissertation, Amsterdam, 1930.
[5] The author is indebted to Professor J. W. Trischka of Syracuse University for communicating this observation.

TABLE I. Energy of the 1,0 and 1, ±1 states in units of $\hbar^2/2I$.

λ	1,0 state			1, ±1 state	
	Brouwer corrected	Lamb	Eq. (3)	Brouwer	Lamb and Eq. (4)
0.0	2.0000000	2.0000000	2.0000000	2.0000000	2.0000000
0.1	2.0009990	2.0009990	2.0009990	1.999500	1.999500
0.2	2.0039833	2.0039834	2.0039834	1.9980005	1.9980005
0.3	2.008916	2.008917	2.008917	1.995503	1.995503
0.4	2.015733	2.015739	2.015738	1.992009	1.992009
0.5	2.024348	2.024369	2.024367	1.987521	1.987521
0.6	2.034648	2.034710	2.034706	1.982044	1.982044
0.7	2.046496	2.046647	2.046642	1.975582	1.975581
0.8	2.059729	2.060057	2.060054	1.968139	1.968138
0.9	2.074158	2.074807	2.074817	1.959723	1.959720
1.0	2.089571	2.090761	2.090811	1.950339	1.950334

state, we have

$$\epsilon=2+(1/10)\lambda^2-(73/7000)\lambda^2+0.00124\lambda^6. \quad (3)$$

Up to $\lambda=0.8$ a somewhat better fit is obtained using 0.00126 as the coefficient of the λ^6-term.

For the 1, ±1 state, values of ϵ derived from the equation,

$$\epsilon=2-(1/20)\lambda^2+(19/56{,}000)\lambda^4-5\cdot10^{-6}\lambda^6, \quad (4)$$

are identical, to seven significant figures, with those derived from Lamb's equation.

Values of $\Delta\epsilon$ are given in Table II. The last column is computed from the equation

$$\Delta\epsilon=0.15\lambda^2-0.010768\lambda^4+0.00125\lambda^6. \quad (5)$$

The error in Eq. (5) rises to a maximum of 0.0076 percent at about $\lambda=0.6$, drops to zero near $\lambda=0.8$ and thereafter increases steadily. At $\lambda=1.0$, the error is, however, still only 0.039 percent. In comparison with these figures, the error in Brouwer's corrected fourth degree equation rises steadily and is 0.85 percent at $\lambda=1.0$. Figure 1 shows the error in $\Delta\epsilon$ as a function of λ. It is seen clearly that the best value for the coefficient of the λ^6-term depends upon the range in λ covered by any particular set of experimental data. The value 0.00125 is the best compromise for values between 0 and 0.9. Values lower than 0.00125 raise the error moderately at lower values of λ but improve the fit at the upper end.

III. QUADRATIC APPROXIMATION TO $\Delta\epsilon/\lambda^2$

Over a limited range of λ or when the precision of the experimental data does not justify the labor of fitting a sixth degree equation, it is convenient to draw the best straight line through the points of a $\Delta\epsilon/\lambda^2$ *vs.* λ^2 plot. The line may also be fitted by the least-squares method.

Let two constants, α' and β', be defined by the equation

$$(\Delta\epsilon/\lambda^2)=\alpha'-\beta'\lambda^2. \quad (6)$$

The least-squares method has been applied to the determination of α' and β', using the data in the third column of Table II. Over the range $\lambda=0.1$ to 0.8, $\alpha'=0.1499$ and $\beta'=0.00998$. Between the limits of 0.5 and 0.8, the best fit is obtained with $\alpha'=0.1498$ and $\beta'=0.00966$. These values are to be compared with $\alpha'=0.1500$, $\beta'=0.00958$ for Brouwer's original equation and with $\alpha'=0.1500$, $\beta'=0.01077$ for the corrected version. It is readily seen that the incorrect equation actually gives the better fit to the true values. α' is changed but little by varying the range; β', however, does show a significant dependence on this factor.

TABLE II. Values of $\Delta\epsilon$ for the 1,0→1, ±1 transition.

λ	Brouwer corrected	Lamb	Eq. (5)
0.0	0.000000	0.000000	0.000000
0.1	0.001499	0.0014990	0.001499
0.2	0.005983	0.0059829	0.005983
0.3	0.013413	0.013414	0.013414
0.4	0.023724	0.023730	0.023729
0.5	0.036827	0.036848	0.036847
0.6	0.052604	0.052666	0.052662
0.7	0.070915	0.071066	0.071062
0.8	0.091590	0.091919	0.091918
0.9	0.114435	0.115087	0.115099
1.0	0.139232	0.140427	0.140482

IV. EQUATIONS FOR THE MOMENT OF INERTIA AND THE ELECTRIC DIPOLE MOMENT

The data in experiments based on the electric resonance method of radiofrequency spectroscopy consist of values of the electric field strength in volts per cm and the corresponding resonant frequency in cycles per second. From these, two experimentally determined constants, α and β, defined by the equation

$$f/E^2=\alpha-\beta E^2+\gamma E^4 \quad (7)$$

are derived by the least-squares method. From Eqs. (6) and (7) the following expressions are obtained for the electric dipole moment, μ, in e.s.u. and the moment of inertia, I, in gm-cm².

$$\mu^2=300^2h^2(\alpha/\alpha')^3(\beta'/\beta). \quad (8)$$

$$I=(h/4\pi)(\beta/\beta')(\alpha'/\alpha)^2. \quad (9)$$

In reference 1 the values of α and β, derived from a series of experiments between $\lambda=0.1$ and 0.8, were reported as follows: $\alpha=448\pm5.4$ and $\beta=(1.91\pm0.23)\times10^{-5}$. Inserting these values and the values of α' and β', derived above for this range, into Eqs. (8) and (9), there is obtained:

$$\mu=7.42\pm0.47 \text{ debye},$$

and

$$I=(180\pm22)10^{-40} \text{ g-cm}^2.$$

The inter-nuclear distance, r, derived from I is

$$r=(2.55\pm0.16)10^{-8} \text{ cm}.$$

B, the rotational constant, is:

$$B=(1/hc)(h^2/2I)=0.156 \text{ cm}^{-1}.$$

It is likely that these figures which are weighted averages for the unresolved vibrational states, correspond approximately to those for the $v=1$ or $v=2$ vibrational states which Trischka[2] resolved.

V. ACKNOWLEDGMENTS

I wish to thank Professor P. Kusch and Professor Charles Townes of Columbia University for suggesting improvements in this paper.

PHYSICAL REVIEW VOLUME 76, NUMBER 11 DECEMBER 1, 1949

On the Interactions of Mesons with the Electromagnetic Field

M. NEUMAN* AND W. H. FURRY
Harvard University, Cambridge, Massachusetts
(Received July 11, 1949)

By means of the formalism of Duffin and Kemmer there is constructed for mesons interacting with the electromagnetic field a theory that is manifestly Lorentz invariant and also gauge invariant and invariant under charge conjugation. The transformation to an interaction representation is accomplished by a procedure necessarily somewhat more complicated than that used by Schwinger for the quantum electrodynamics of electrons. The longitudinal components of the electromagnetic field are eliminated in a covariant manner.

The resulting interaction Hamiltonian is analyzed into terms corresponding to self-energies and terms describing interactions. By a suitable interpretation of ambiguous expressions, the photon self-energy is shown to vanish. Expressions are found for the polarization of the mesic vacuum by a given electromagnetic field. In the case of mesons of spin 1, not only the term proportional to the original current, but also that proportional to its d'Alembertian has an infinite factor. A formal procedure for the unambiguous exclusion of such infinite contributions is suggested. Explicit expressions are found for the self-energies of scalar and vector mesons. These self-energies can be eliminated by renormalization of mass.

INTRODUCTION

IN the last few years the theory of quantum electrodynamics, or the interaction of electrons and positrons with the quantized electromagnetic field, has been advanced into a rather satisfactory condition. The new developments of the theory have been found to agree well with the latest experimental results.

Although precise experimental data on electromagnetic effects are available only for electrons, there is good reason to believe in the existence of charged mesons of spin 0, and there is at least considerable speculation about similar particles of spin 1. Thus an appreciable interest attaches to the various theoretical discussions of such particles.

In the present paper the theory for mesons of spins 0 and 1 is developed throughout on the basis of Kemmer's formulation of the wave equations of these particles. In this formulation the equations of motion and the expression for the current are formally precisely like those for the Dirac electron, and charge conjugation can be defined in a very similar way. We thus have the possibility of developing the theory in the closest possible analogy to Schwinger's treatment of quantum electrodynamics.

There are a number of necessary differences in the treatment, and in all such respects the electron case is the simpler. A main source of additional complication is the fact that in the Kemmer case not all components of the wave function are dynamically independent. When properly formulated, the commutation relations involve only the dynamically independent parts of the wave function. The remaining part of the wave function is expressed by means of space-like derivatives of the dynamically independent part.

The introduction of an interaction representation, which is accomplished in the Dirac case by a unitary transformation, here requires, in addition, a redefinition of the particle wave function. Because the interaction Hamiltonian density involves space-like derivatives of the dynamically independent wave function, a more precise statement of the meaning of differential operators in various representations is necessary. The interaction Hamiltonian density in the Kemmer case is not precisely the negative of the coupling term in the Lagrangian, as it is in quantum electrodynamics.

The Kemmer case resembles the Dirac case in that it is possible, by identical physical considerations, to resolve the ambiguities inherent in the interpretation of divergent integrals in such a way that the self-energy of a photon is found to vanish. The elimination of the longitudinal components of the electromagnetic field is also accomplished in essentially the same way in both cases.

A major difference in the results appears in the polarization of the vacuum due to fluctuations in the vector meson field. The possibility of the simple procedure of charge renormalization depends on the absence of higher order derivatives in the polarization kernel, and is thus an accidental feature of fields of spins 0 and $\frac{1}{2}$. For the vector meson case an unambiguous procedure for eliminating the infinite polarization

* Now at Institute for Advanced Study, Princeton, New Jersey.

suggests itself, but is not capable of interpretation in terms of charge renormalization alone.

I. THE ISOLATED MESON FIELD

It has been shown by Duffin[1] and Kemmer[2] that the equations for particles of spins 0 and 1 are representations of the equation

$$\left(\beta_\mu\frac{\partial}{\partial x_\mu}+\kappa\right)\psi(x)=0, \tag{1.1}$$

with the β_μ's obeying the relations

$$\beta_\mu\beta_\nu\beta_\sigma+\beta_\sigma\beta_\nu\beta_\mu=\delta_{\mu\nu}\beta_\sigma+\beta_\mu\delta_{\nu\sigma}. \tag{1.2}$$

The adjoint equation

$$\frac{\partial}{\partial x_\mu}\bar{\psi}\beta_\mu-\kappa\bar{\psi}=0 \tag{1.1'}$$

is satisfied by the spinor $\bar{\psi}(x)=\psi^*(x)\eta_4$, where $\eta_\mu=2\beta_\mu^2-1$. The charge-conjugate wave function is defined by $\phi(x)=C\bar{\psi}(x)$, where C is a unitary, symmetric matrix, such that $\beta_\mu^T=-C^{-1}\beta_\mu C$. The alleged properties of C may be inferred from the fact that in a representation in which β_i is real and β_4 pure imaginary $C=\eta_4$. If all the β_μ's are taken as real, then $C=\eta_1\eta_2\eta_3\eta_4$.

We now introduce a space-like surface σ into the Minkowski world by means of the equations

$$x_\mu=x_\mu(u_i),\quad \mu=1,\cdots,4,\quad i=1,2,3, \tag{1.3}$$

and associate with every set of parametric coordinates u_i a unit normal vector $\lambda_\mu(u)$ sensed towards the future and a tensor $I_{\mu\nu}(u)=\delta_{\mu\nu}+\lambda_\mu(u)\lambda_\nu(u)$. It will be noticed that

$$\lambda_\mu(u)I_{\mu\nu}(u)=0,\quad I_{\mu\alpha}(u)I_{\alpha\nu}(u)=I_{\mu\nu}(u). \tag{1.4}$$

Let $B_\alpha(x)$ be a vector field defined everywhere in space. Its value at u is $B_\alpha[x(u)]$ and its projection on the normal $\lambda_\mu(u)$,

$$B_N[x(u)]=\lambda_\alpha(u)B_\alpha[x(u)].$$

By $(\partial/\partial x_\nu)B_N[x(u)]$ we shall understand

$$\lim_{x_\nu'\to x_\nu(u)}\lambda_\alpha(u)\frac{B_\alpha[x_1(u),\cdots,x_\nu',\cdots x_4(u)]-B_\alpha[x(u)]}{x_\nu'-x_\nu}.$$

The point x_ν' need not lie on σ. This definition of a derivative involves the comparison of the projection of a vector at the point u, on the normal at that point, with the projection on the same normal of a vector at some neighboring point, not necessarily on the surface. As a result of this definition, we may write

$$\frac{\partial B_N[x(u)]}{\partial x_\nu}=\lambda_\alpha(u)\frac{\partial B_\alpha[x(u)]}{\partial x_\nu}. \tag{1.5}$$

[1] R. J. Duffin, Phys. Rev. 54, 905 (1938).
[2] N. Kemmer, Proc. Roy. Soc. 173, 97 (1939).

The two matrices β_N^2 and $1+\beta_N^2$ obeying the relations

$$\begin{aligned}(1+\beta_N^2)^2&=1+\beta_N^2;\\ (\beta_N^2)^2&=-\beta_N^2;\\ \beta_N^2(1+\beta_N^2)&=0;\end{aligned} \tag{1.6a}$$

$$\begin{aligned}(\beta_N^2+1)\beta_\mu(\beta_N^2+1)&=0;\\ (\beta_N^2+1)\beta_\mu&=-I_{\mu\nu}\beta_\nu\beta_N^2;\\ \beta_\mu(\beta_N^2+1)&=-I_{\mu\nu}\beta_N^2\beta_\nu;\end{aligned} \tag{1.6b}$$

are now used to decompose $\psi[x(u)]$ into two projections

$$\psi[x(u)]=-\beta_N^2\psi[x(u)]+[1+\beta_N^2]\psi[x(u)]. \tag{1.7}$$

The two are not independent but related through (1.1) according to

$$[1+\beta_N^2]\psi[x(u)]=\frac{1}{\kappa}I_{\sigma\rho}\beta_\sigma\frac{\partial}{\partial x_\rho}\beta_N^2\psi[x(u)], \tag{1.8}$$

as may be seen by multiplying (1.1) with (β_N^2+1) and using (1.6b). The operator $I_{\sigma\rho}(\partial/\partial x_\rho)$ compares the value of a function at the point with its value at a neighboring point lying on the plane tangent to the surface at u. It thus may be regarded as the local spatial derivative.

The nature of the two projections becomes clearer from the role they play in the solution of the initial value problem for (1.1). Let $\beta_N\psi[x(u)]=-\beta_N\beta_N^2\psi[x(u)]$ be prescribed on σ. This does not determine $\psi[x(u)]$, for the application of (1.8) would require the knowledge of $\beta_N^2\psi$ on the planes tangent to σ. We shall show, however, that $\beta_N\psi[x(u)]$ is sufficient to fix—in virtue of (1.1)—the function $\psi(x)$ everywhere in space. Thus $\beta_N^2\psi[x(u)]$ will emerge as the dynamically independent projection of the spinor, for upon solution of the initial value problem, (1.8) may be applied. (If the surface is specialized to a plane, (1.8) may, of course, be applied directly.) The expression

$$-\frac{1}{\kappa}\int_\sigma S[x-x(u)]\beta_N\psi[x(u)](du)$$

$$\equiv-\frac{1}{\kappa}\int_\sigma S(x-x')\beta_\mu\psi(x')d\sigma_\mu'$$

with

$$S(x)=\beta_\alpha\frac{\partial}{\partial x_\alpha}\left(\beta_\beta\frac{\partial}{\partial x_\beta}-\kappa\right)\Delta(x),\quad d\sigma_\mu=\lambda_\mu(u)(du) \tag{1.9}$$

is readily seen to obey the Kemmer and the Gordon-Klein equations. To constitute a representation of $\psi(x)$ t must also incorporate the correct boundary conditions as expressed by

$$\beta_N^2\psi[x(u)]=-\frac{1}{\kappa}\int_\sigma\beta_N^2(u)S[x(u)-x(u')]$$

$$\times\beta_N(u')\psi[x(u')](du'). \tag{1.10}$$

A direct calculation, making use of the properties of $\Delta(x)$ in the form

$$I_{\alpha\beta}(u)\frac{\partial^2\Delta[x(u)]}{\partial x_\alpha \partial x_\beta}-\left(\lambda_\alpha(u)\frac{\partial}{\partial x_\alpha}\right)^2\Delta[x(u)]$$

$$-\kappa^2\Delta[x(u)]=0 \quad (1.11a)$$

$$\Delta[x(u)-x(u')]=0 \quad (1.11b)$$

$$I_{\alpha\beta}(u)\frac{\partial\Delta[x(u)]}{\partial x_\beta}=0 \quad (1.11c)$$

confirms (1.10). The representation

$$\psi(x)=\frac{1}{\kappa}\int_\sigma S(x-x')\beta_\mu\psi(x')d\sigma_\mu' \quad (1.12)$$

is therefore seen to be valid.

Consistent with the statement regarding the projections of $\psi(x)$ are the commutation relations for the Kemmer field. A canonical formulation of the theory leads to the expression of the latter as

$$i\int d\sigma_\mu'[\psi_\alpha(x),(\bar\psi(x')\beta_\mu)_\beta]=\begin{cases}\delta_{\alpha\beta}\text{; if left side does not}\\ \quad\text{vanish identically}\\ 0\text{; otherwise.}\end{cases}$$

The qualifying text is incorporated into the formula by writing it as

$$i\int d\sigma_\mu'[(\beta_N\psi(x))_\sigma,(\bar\psi(x')\beta_\mu)_\rho]=(\beta_N[x(u)])_{\sigma\rho}, \quad (1.13)$$

where only the dynamically independent projection is quantized. Equation (1.13) in conjunction with (1.12) yields

$$[(\beta_N^2\psi(x))_\alpha,\bar\psi_\beta(x')]=-\frac{i}{\kappa}(\beta_N^2S(x-x'))_{\alpha\beta}. \quad (1.14)$$

Applying $[1-(1/\kappa)I_{\sigma\rho}\beta_\sigma(\partial/\partial x_\rho)]_{\cdot\alpha}$ to both sides of (1.14) and taking account of (1.8) and an identical expression involving $S(x)$, we obtain

$$[\psi_\alpha(x),\bar\psi_\beta(x')]=(i/\kappa)S_{\alpha\beta}(x-x'), \quad (1.15)$$

for the commutator of field quantities at two arbitrary points.

Commutators involving field variables on the same space-like surface may be evaluated with the aid of (1.8) and (1.13). We thus find for the current vector $j_\mu=(iec/2)(\bar\psi\beta_\mu\psi-\bar\phi\beta_\mu\phi)$ that

$$\int d\sigma_\alpha' g(x')[j_\alpha(x'),j_\mu(x)]=\frac{ie^2c^2}{\kappa}[M_{\mu\alpha}(x)+M_{\alpha\mu}(x)]\frac{\partial g(x)}{\partial x_\alpha} \quad (1.16)$$

where $g(x)$ is an arbitrary function and

$$M_{\mu\nu}(x)=\tfrac{1}{2}[\bar\psi(x)\beta_\mu(\beta_N^2+1)\beta_\nu\psi(x)+\bar\phi(x)\beta_\mu(\beta_N^2+1)\beta_\nu\phi(x)]. \quad (1.17)$$

Equation (1.16) is seen to imply that any component of the current commutes with the total charge on the same space-like surface. Since the latter quantity is a constant of motion, the two must commute even when x does not lie on σ. The properties of $M_{\mu\nu}$,

$$\lambda_\mu(u)M_{\mu\nu}[x(u)]=\lambda_\nu(u)M_{\mu\nu}[x(u)]=0 \quad (1.18a)$$

$$\int d\sigma_\alpha' g(x')[j_\alpha(x'),M_{\mu\nu}(x)]=0, \quad (1.18b)$$

will be found useful in later calculations. For the commutator of components of the current four vector at two arbitrary points we obtain

$$[j_\mu(x),j_\nu(x')]=-\frac{ie^2c^2}{2\kappa}\{[\bar\psi(x)\beta_\mu S(x-x')\beta_\nu\psi(x')+\bar\phi(x)\beta_\mu S(x-x')\beta_\nu\phi(x')]-[\bar\psi(x')\beta_\nu S(x'-x)\beta_\mu\psi(x)+\bar\phi(x')\beta_\nu S(x'-x)\beta_\mu\phi(x)]\}. \quad (1.19)$$

The constants of motion generate the usual infinitesimal transformations when applied to $\psi(x)$. It is to be emphasized, however, that this result depends on our definition of a derivative of a component of a vector along the normal to a surface. Thus in the case of linear momenta

$$\frac{i}{\hbar}[\beta_N^2\psi(x),P_\nu]=i\int d\sigma_\alpha'[\beta_N^2\psi(x),(\bar\psi(x')\beta_\alpha)_\sigma]\frac{\partial\psi_\sigma(x')}{\partial x_\nu'}$$

$$=\beta_N^2\frac{\partial\psi(x)}{\partial x_\nu}=\frac{\partial}{\partial x_\nu}\beta_N^2\psi(x),$$

where (1.5) was used. From this we obtain

$$\frac{i}{\hbar}[\psi(x),P_\nu]=\frac{\partial\psi(x)}{\partial x_\nu} \quad (1.20)$$

by a step employed in arriving at (1.15).

Equation (1.20) permits the characterization of the vacuum—the lowest eigenstate of P_N—through

$$\psi^+(x)\phi_0=0,\quad \phi^+(x)\phi_0=0, \quad (1.21)$$

where $+$ denotes the positive frequency component of the field variable and ϕ_0 is the state vector of the system. In obtaining vacuum expectation values of dynamical variables we shall have occasion to use the following traces of products of β_μ matrices due to

Harish-Chandra[3]

$$\begin{aligned}
&\mathrm{Tr}\beta_\alpha\beta_\beta=\binom{2}{6}\delta_{\alpha\beta}\\
&\mathrm{Tr}\beta_\mu\beta_\nu\beta_\alpha\beta_\beta=\binom{1}{3}(\delta_{\mu\nu}\delta_{\alpha\beta}+\delta_{\nu\alpha}\delta_{\mu\beta})\\
&\mathrm{Tr}\beta_\mu\beta_\sigma\beta_\rho\beta_\nu\beta_\alpha\beta_\beta=\binom{1}{1}(\delta_{\mu\sigma}\delta_{\nu\rho}\delta_{\alpha\beta}+\delta_{\sigma\rho}\delta_{\nu\alpha}\delta_{\mu\beta})\\
&\qquad+\binom{0}{2}(\delta_{\mu\sigma}\delta_{\rho\beta}\delta_{\nu\alpha}+\delta_{\rho\nu}\delta_{\sigma\alpha}\delta_{\mu\beta}\\
&\qquad\qquad+\delta_{\alpha\beta}\delta_{\mu\nu}\delta_{\sigma\rho}-\delta_{\mu\nu}\delta_{\sigma\alpha}\delta_{\rho\beta}).
\end{aligned}\tag{1.22}$$

The upper and lower numbers in the bracket refer to representations of five and ten rows, respectively. Traces of products of odd numbers of β_μ's vanish. The vacuum expectation value of the symmetrized stress tensor is given by

$$\begin{aligned}
\langle\Theta_{\mu\nu}(x)\rangle_0&=-\frac{mc^2}{2}\langle\bar\psi(x)(\beta_\mu\beta_\nu+\beta_\nu\beta_\mu-\delta_{\mu\nu})\psi(x)\\
&\qquad+\bar\phi(x)(\beta_\mu\beta_\nu+\beta_\nu\beta_\mu-\delta_{\mu\nu})\phi(x)\rangle_0\\
&=-\frac{\hbar c}{2}\binom{2}{6}\frac{\kappa^2}{4}\Delta^{(1)}(0)\delta_{\mu\nu}.
\end{aligned}\tag{1.23}$$

and of the current, by

$$\langle j_\mu(x)\rangle_0=-\frac{iec}{2}\binom{2}{6}\frac{\partial\Delta^{(1)}(\xi)}{\partial\xi_\mu}\Big]_{\xi\to0}.\tag{1.24}$$

The latter quantity is taken to vanish because of the even nature of $\Delta^{(1)}(x)$.

II. THE INTERACTION OF THE MESIC AND ELECTROMAGNETIC FIELDS

The equation of the meson field in the Heisenberg representation is taken to be

$$\cdot[\beta_\mu\nabla_\mu-(ie/\hbar c)\beta_\mu\underline{A}_\mu+\kappa]\underline{\psi}=0.\tag{2.1}$$

The symbol ∇_μ denotes a total derivative operator:

$$\nabla_\mu F(x_1\sigma)=\frac{\partial F(x_1\sigma)}{\partial x_\mu}+\int_\sigma d\sigma_\mu'\frac{\delta F(x_1\sigma)}{\delta\sigma(x')}.\tag{2.2}$$

In particular, if

$$F(x_1\sigma)=U^{-1}[\sigma]F(x)U[\sigma]\tag{2.3a}$$

$$ihc\frac{\delta U[\sigma]}{\delta\sigma(x)}=H(x)U[\sigma],\tag{2.3b}$$

then

$$\begin{aligned}
\nabla_\mu F(x_1\sigma)&=U^{-1}[\sigma]\frac{\partial F(x)}{\partial x_\mu}U[\sigma]\\
&\quad-\frac{i}{\hbar c}U^{-1}[\sigma]\int_\sigma[F(x),H(x')]d\sigma_\mu'U[\sigma]\\
&=\frac{i}{\hbar}U^{-1}[\sigma][F(x),P_\mu-\frac{1}{c}\int_\sigma d\sigma_\mu'H(x')]U[\sigma].
\end{aligned}\tag{2.4}$$

The definition (2.2) does not require that x lie on σ. The arguments x and σ are therefore treated as independent. It will be understood—unless otherwise stipulated—that the differentiated quantities in (2.4) are evaluated with x on σ. The differential operator $(\partial/\partial x_\mu)$ moves the point off the surface, $(\delta/\delta\sigma(x))$ indents it at x, ∇_μ displaces the surface and the point rigidly in the direction x_μ. The dependence of a field variable on x is determined by the structure of the isolated field, that on σ is due to interaction between fields. It will be noticed that the integration in the second term of the right member of (2.4) is extended over the argument of the Hamiltonian density rather than that of $F(x)$—an indifferent matter in the Dirac case, but significant when space-like derivatives occur in the field quantities—and that

$$P_\mu-(1/c)\int_\sigma d\sigma_\mu'H(x')$$

emerges directly as a displacement operator for ∇_μ.

We take $\underline{\psi}$ of (2.1) to be of the form $U^{-1}[\sigma]\psi'(x)U[\sigma]$. The situation is more complicated here than in the Dirac case, in that $\psi'(x)$ cannot be identified with $\psi(x)$, the spinor of the isolated field. For the procedure leading to (1.8) when applied to (2.1) yields

$$\begin{aligned}
&U^{-1}[\sigma]\psi'(x)U[\sigma]\\
&=-\left[1-\frac{1}{\kappa}I_{\sigma\rho}\beta_\sigma\frac{\partial}{\partial x_\rho}\right]U^{-1}[\sigma]\beta_N{}^2\psi'(x)U[\sigma]\\
&\quad-\frac{1}{\kappa}\frac{ie}{hc}I_{\sigma\rho}U^{-1}[\sigma]\beta_\sigma A_\rho(x)\beta_N{}^2\psi'(x)U[\sigma],
\end{aligned}\tag{2.5}$$

where we have made use of the fact that

$$I_{\mu\nu}\nabla_\nu F(x_1\sigma)=I_{\mu\nu}\frac{\partial}{\partial x_\nu}F(x_1\sigma)\tag{2.6}$$

in virtue of (1.4). This implies

$$\psi'(x)=-\left[1-\frac{1}{\kappa}I_{\sigma\rho}\beta_\sigma\left(\frac{\partial}{\partial x_\rho}-\frac{ie}{hc}A_\rho\right)\right]\beta_N{}^2\psi'(x).\tag{2.7}$$

[3] Harish-Chandra, Proc. Roy. Soc. **186**, 502 (1946).

The spinor $\psi'(x)$ differs from $\psi(x)$ by a term containing A_μ. We therefore take

$$\psi'(x)=\psi(x)+(1/\kappa)(ie/\hbar c)(\beta_N{}^2+1)\beta_\mu A_\mu(x)\psi(x), \quad (2.8a)$$

where (1.6b) was used.

Equation (2.8a) is consistent with (1.8), since

$$\beta_N{}^2\psi'(x)=\beta_N{}^2\psi(x) \quad (2.9a)$$

in virtue of (1.6a). It is also seen from (2.8a) that

$$(\beta_N{}^2+1)\psi'(x)=(\beta_N{}^2+1)\psi(x) +(1/\kappa)(ie/\hbar c)(\beta_N{}^2+1)\beta_\mu A_\mu(x)\psi(x). \quad (2.9b)$$

The transition from the Heisenberg to the interaction representation thus involves not only a unitary transformation but also a redefinition of the $(\beta_N{}^2+1)$ projection of the spinor. For the Pauli adjoint of ψ we similarly obtain

$$\bar\psi'(x)=\bar\psi(x)-(1/\kappa)(ie/\hbar c)\bar\psi(x)\beta_\mu A_\mu(x)(\beta_N{}^2+1). \quad (2.8b)$$

It follows from (2.8a, b) that $j_\mu'(x)=(iec/2)(\bar\psi'(x)\beta_\mu\psi'(x) -\bar\phi(x)\beta_\mu\phi'(x))$ is related to $j_\mu(x)$ by

$$j_\mu'(x)=j_\mu(x)-c\cdot(e^2/mc^2)[M_{\mu\nu}(x)+M_{\nu\mu}(x)]A_\nu(x), \quad (2.10)$$

where the terms quadratic in $A_\nu(x)$ vanish in virtue of (1.6b).

Our next task is to find an interaction Hamiltonian that would lead from (2.1) to (1.1) in virtue of (2.3). The scalar product of the current and electromagnetic four-vectors readily suggests itself. The question, of course, is whether $j_\mu(x)$ or $j_\mu'(x)$ constitutes an appropriate choice. On examination it is found that**

$$H(x)=-(1/c)\cdot\tfrac{1}{2}(j_\mu(x)+j_\mu'(x))A_\mu(x) =-(1/c)j_\mu(x)A_\mu(x) +(e^2/mc^2)M_{\mu\nu}(x)A_\mu(x)A_\nu(x). \quad (2.11)$$

To verify the suitability of (2.11) to play the role of an interaction Hamiltonian we note that in accordance with (1.1)

$$(\beta_\mu\nabla_\mu+\kappa)U^{-1}[\sigma]\psi(x)U[\sigma]$$

$$=(i/\hbar c)U^{-1}[\sigma]\int_\sigma d\sigma_\mu'[H(x'),\ \beta_\mu\psi(x)]U[\sigma]$$

$$=-U^{-1}[\sigma]\beta_N{}^2\left[1-(1/\kappa)I_{\sigma\rho}\beta_\sigma\frac{\partial}{\partial x_\rho}\right] \times[(ie/\hbar c)\beta_\nu A_\nu(x)-(1/\hbar c)(e^2/mc^2) \times\beta_\alpha(\beta_N{}^2+1)\beta_\beta A_\alpha(x)A_\beta(x)]\psi(x)U[\sigma] \quad (2.12)$$

by a straightforward application of (1.8) and (1.13). The two terms of the right member of (2.12) arising from the commutator of $\beta_N\psi(x)$ with $j_\mu A_\mu$ are now rearranged with the aid of (1.6b) and (2.6), in the following manner:

$$U^{-1}[\sigma]\beta_N{}^2\left[1-(1/\kappa)I_{\sigma\rho}\beta_\sigma\frac{\partial}{\partial x_\rho}\right](ie/\hbar c)\beta_\nu A_\nu(x)\psi(x)U[\sigma]$$

$$=U^{-1}[\sigma](\beta_N{}^2+1)(ie/\hbar c)\beta_\nu A_\nu(x)\psi(x)U[\sigma] -I_{\sigma\rho}\nabla_\rho U^{-1}[\sigma](1/\kappa)(ie/\hbar c)\beta_N{}^2\beta_\sigma\beta_\nu A_\nu(x)\psi(x)U[\sigma] -(ie/\hbar c)U^{-1}[\sigma]\beta_\nu A_\nu(x)\psi(x)U[\sigma]$$

$$=(\beta_\sigma\nabla_\sigma+\kappa)U^{-1}[\sigma](1/\kappa)(ie/\hbar c)(\beta_N{}^2+1) \times\beta_\nu A_\nu(x)\psi(x)U[\sigma] -(ie/\hbar c)U^{-1}[\sigma]\beta_\nu A_\nu(x)\psi(x)U[\sigma]. \quad (2.13)$$

The first term of the right member of (2.13) is the term that must be added to $(\beta_\sigma\nabla_\sigma+\kappa)U^{-1}[\sigma]\psi(x)U[\sigma]$ in order to obtain $(\beta_\sigma\nabla_\sigma+\kappa)U^{-1}[\sigma]\psi'(x)U[\sigma]$ in accordance with (2.8a); the second is part of the explicit interaction term of (2.1). The term necessary for the redefinition of $\psi(x)$ in the latter arises from the commutator of $M_{\mu\nu}A_\mu A_\nu$ with $\beta_N\psi(x)$. For

$$-U^{-1}[\sigma](1/\hbar c)(e^2/mc^2)\beta_N{}^2\beta_\alpha(\beta_N{}^2+1) \times\beta_\beta A_\alpha(x)A_\beta(x)\psi(x)U[\sigma] =-(ie/\hbar c)U^{-1}[\sigma]\beta_\nu A_\nu(x)(1/\kappa)(ie/\hbar c) \times(\beta_N{}^2+1)\beta_\alpha A_\alpha(x)\psi(x)U[\sigma] \quad (2.14)$$

in virtue of (1.6b). Still to be accounted for is the fourth term of the right member of (2.12), which however is seen to vanish,

$$I_{\sigma\rho}(\partial/\partial x_\rho)\beta_N{}^2\beta_\sigma\beta_\alpha(\beta_N{}^2+1)\beta_\beta A_\alpha(x)A_\beta(x)\psi(x) =-(\partial/\partial x_\rho)\beta_\rho(\beta_N{}^2+1)\beta_\alpha(\beta_N{}^2+1)\beta_\beta A_\alpha(x)A_\beta(x)\psi(x)=0,$$

according to (1.6b). Thus (2.12) is identical with

$$(\beta_\mu\nabla_\mu+\kappa)U^{-1}[\sigma][\psi(x)+(1/\kappa)(ie/\hbar c) \times(\beta_N{}^2+1)\beta_\nu A_\nu(x)\psi(x)]U[\sigma] =(ie/\hbar c)U^{-1}[\sigma]\beta_\nu A_\nu(x)[\psi(x)+(1/\kappa)(ie/\hbar c) \times(\beta_N{}^2+1)\beta_\nu A_\nu(x)\psi(x)]U[\sigma], \quad (2.15)$$

which is the content of (2.1).

We now turn to the equations of the electromagnetic field. Since the Lorentz condition as usually stated does not confine the point x to the surface σ, we shall—in this section—remove this restriction from our definition (2.2) of ∇_μ and obtain Maxwell's equations of comparable generality. Denoting by $F_{\mu\nu}(x)$ the electro-

** A procedure of this type seems to lead to correct Hamiltonians in mesonuclear couplings, whenever a redefinition of the field variable is involved.

magnetic field strengths, we obtain

$$\begin{aligned}\nabla_\mu U^{-1}[\sigma]F_{\mu\nu}(x)U[\sigma]&=-\frac{\partial}{\partial x_\nu}U^{-1}[\sigma]\frac{\partial A_\mu(x)}{\partial x_\mu}U[\sigma]\\&+\frac{i}{\hbar c}U^{-1}[\sigma]\int_\sigma d\sigma_\mu'[H(x'),F_{\mu\nu}(x)]U[\sigma]\\&=-\frac{1}{c}U^{-1}[\sigma]\int_\sigma d\sigma_\mu' j_\nu'(x')\frac{\partial D(x-x')}{\partial x_\mu}U[\sigma]\\&-\frac{\partial}{\partial x_\nu}U^{-1}[\sigma]\Big[\frac{\partial A_\mu(x)}{\partial x_\mu}\\&\qquad-\frac{1}{c}\int d\sigma_\mu' j_\mu(x')D(x-x')\Big]U[\sigma]\end{aligned}\tag{2.16}$$

by a straightforward evaluation of the commutator. If we admit only those state vectors ϕ_0 that satisfy

$$U^{-1}[\sigma]\Big[\frac{\partial A_\mu(x)}{\partial x_\mu}-\frac{1}{c}\int d\sigma_\mu' j_\mu(x')D(x-x')\Big]U[\sigma]\phi_0=0,\tag{2.17}$$

then (2.16) assumes the Maxwellian form

$$\Big\{\nabla_\mu U^{-1}[\sigma]F_{\mu\nu}(x)U[\sigma]+\frac{1}{c}U^{-1}[\sigma]\times\int d\sigma_\mu' j_\nu'(x')\frac{\partial D(x-x')}{\partial x_\mu}U[\sigma]\Big\}\phi_0=0.\tag{2.18}$$

It is clear that from the properties of the $D(x)$ function that (2.18) reduces to the conventional Maxwell equations if x is taken to lie on σ.

We now proceed to eliminate the longitudinal components of the electromagnetic field from the equation

$$ihc\frac{\delta U'[\sigma]}{\delta\sigma(x)}=\Big\{-\frac{1}{c}j_\mu(x)A_\mu(x)+\frac{e^2}{mc^2}M_{\mu\nu}(x)A_\mu(x)A_\nu(x)\Big\}U'[\sigma].\tag{2.19}$$

It has been shown by Schwinger[4] that the four-vector $A_\mu(x)$ can be decomposed into three kinematically independent fields according to

$$A_\mu(x)=\lambda_\mu(u)\frac{\partial\Lambda(x)}{\partial x_N}-I_{\mu\nu}(u)\frac{\partial\Lambda'(x)}{\partial x_\nu}+\mathfrak{A}_\mu(x).\tag{2.20}$$

[4] J. Schwinger, Phys. Rev. 74, 1439 (1948).

The commutation relations obeyed by $\Lambda(x)$ and $\Lambda'(x)$ are found in the cited reference. The vector $\lambda_\mu(u)$ and the tensor $I_{\mu\nu}(u)$ are defined with respect to the orientation of the space-like surface, rather than a constant direction. This will introduce a considerable simplification in our final result. Substituting (2.20) in (2.19) we obtain

$$\begin{aligned}ihc\frac{\delta U'[\sigma]}{\delta\sigma(x)}=\Big\{&-\frac{1}{c}j_\mu(x)\mathfrak{A}_\mu(x)+\frac{e^2}{mc^2}M_{\mu\nu}(x)\mathfrak{A}_\mu(x)\mathfrak{A}_\nu(x)\\&+\frac{1}{c}j_\mu(x)\frac{\partial\Lambda'(x)}{\partial x_\mu}+\frac{e^2}{mc^2}M_{\mu\nu}(x)\frac{\partial\Lambda'(x)}{\partial x_\mu}\frac{\partial\Lambda'(x)}{\partial x_\nu}\\&-\frac{e^2}{mc^2}(M_{\mu\nu}(x)+M_{\nu\mu}(x)\mathfrak{A}_\mu(x)\frac{\partial\Lambda'(x)}{\partial x_\nu}\\&-\frac{1}{c}j_N(x)\frac{\partial(\Lambda(x)-\Lambda'(x))}{\partial x_N}\Big\}U'[\sigma].\end{aligned}\tag{2.21}$$

The operator $U'[\sigma]$ is now subjected to the transformation

$$\begin{aligned}U'[\sigma]&=e^{-iG[\sigma]}U[\sigma];\\G[\sigma]&=\frac{1}{\hbar c}\frac{1}{c}\int\Lambda'(x')j_\mu(x')d\sigma_\mu'.\end{aligned}\tag{2.22}$$

Making use of (1.16), (1.18), and of the commutators for the electromagnetic field variables appearing in reference 4, we obtain the following expressions:

$$\begin{aligned}e^{iG[\sigma]}\frac{\delta}{\delta\sigma(x)}e^{-iG[\sigma]}&=\frac{\delta}{\delta\sigma(x)}-\frac{i}{\hbar c}\frac{1}{c}j_\mu(x)\frac{\partial\Lambda'(x)}{\partial x_\mu}\\&+\frac{i}{\hbar c}\frac{e^2}{mc^2}M_{\mu\sigma}(x)\frac{\partial\Lambda'(x)}{\partial x_\mu}\frac{\partial\Lambda'(x)}{\partial x_\sigma}-\frac{i}{2c}\frac{1}{\hbar c}j_\mu(x)V_\mu(x)\\&+\frac{i}{2c}\frac{1}{\hbar}\frac{e^2}{mc^2}(M_{\mu\sigma}(x)+M_{\sigma\mu}(x))V_\mu(x)\frac{\partial\Lambda'(x)}{\partial x_\sigma}\\&+\frac{i}{4\hbar c}\frac{e^2}{mc^2}M_{\mu\sigma}(x)V_\mu(x)V_\sigma(x),\end{aligned}\tag{2.23a}$$

$$e^{iG[\sigma]}j_\mu(x)e^{-iG[\sigma]}=j_\mu(x)-c\frac{e^2}{mc^2}(M_{\mu\sigma}(x)+M_{\sigma\mu}(x))\frac{\partial\Lambda'(x)}{\partial x_\mu}-\frac{c}{2}\frac{e^2}{mc^2}(M_{\mu\sigma}(x)+M_{\sigma\mu}(x))V_\sigma(x),\tag{2.23b}$$

$$e^{iG[\sigma]}\Lambda'(x)e^{-iG[\sigma]}=\Lambda'(x)-\frac{1}{c}\int_\sigma d\sigma_\mu' j_\mu(x')\mathfrak{D}(x-x'),\tag{2.23c}$$

where

$$V_\mu(x)=-\frac{1}{c}\int d\sigma_\nu' j_\nu(x')\frac{\partial \mathfrak{D}(x-x')}{\partial x_\mu'}, \quad (2.24a)$$

$$\partial^2\mathfrak{D}(x)/\partial x_N^2=D(x). \quad (2.24b)$$

With the aid of (2.23) we express (2.21) in the form

$$ihc\frac{\delta U[\sigma]}{\delta\sigma(x)}=\Big\{-\frac{1}{c}j_\mu(x)\mathfrak{A}_\mu(x)+\frac{e^2}{mc^2}M_{\mu\nu}(x)\mathfrak{A}_\mu(x)\mathfrak{A}_\nu(x)$$
$$+\frac{1}{2}j_N(x)V_N(x)+\frac{1}{2}\frac{1}{c}I_{\mu\nu}j_\mu(x)V_\nu(x)-\frac{1}{2}\frac{e^2}{mc^2}(M_{\mu\nu}(x)$$
$$+M_{\nu\mu}(x))\mathfrak{A}_\mu(x)V_\nu(x)+\frac{1}{4}\frac{e^2}{mc^2}M_{\mu\nu}(x)V_\mu(x)V_\nu(x)$$
$$-\frac{1}{c}j_N(x)\frac{\partial(\Lambda(x)-\Lambda'(x))}{\partial x_N}\Big\}U[\sigma]. \quad (2.25)$$

We can now infer the gauge invariance of (2.19) from (2.25). For (2.20) reduces to a gauge transformation of the electromagnetic potentials if $\Lambda'(x)=\Lambda(x)$ is taken to be a c-function. The latter assumption is equivalent to replacing the function $\mathfrak{D}(x)$, by zero, wherever it occurs in (2.25). As a result, the terms involving V_μ vanish and (2.25) assumes the form of (2.19). The gauge invariance of the Lorentz condition (2.17) is apparent from (2.23b) and (1.18a).

Equation (2.25) may be simplified by exploiting the fact that λ_μ is the normal to σ. Thus $I_{\mu\nu}V_\nu=0$ by (2.24) and (1.11c). Moreover,

$$M_{\mu\nu}V_\nu=M_{\mu\nu}I_{\nu\alpha}V_\alpha-M_{\mu\nu}\lambda_\nu\lambda_\alpha V_\alpha=0,$$

in virtue of (1.18a). The last term of the right member of (2.25) can be shown—as in the case of quantum electrodynamics[4]—to vanish by the Lorentz condition, if (2.25) is applied to the state vector. Equation (2.25) thus reduces to

$$ihc\frac{\delta\psi[\sigma]}{\delta\sigma(x)}=\Big\{-\frac{1}{c}j_\mu(x)\mathfrak{A}_\mu(x)+\frac{e^2}{mc^2}M_{\mu\nu}(x)\mathfrak{A}_\mu(x)\mathfrak{A}_\nu(x)$$
$$+\frac{1}{2}j_N(x)V_N(x)\Big\}\psi[\sigma] \quad (2.26)$$

where $\psi[\sigma]=U[\sigma]\phi_0$, and the $\mathfrak{A}_\mu$ four-vector of the pure radiation field is subject to the commutation relations[4]

$$[\mathfrak{A}_\mu(x),\mathfrak{A}_\nu(x')]=ihc\delta_{\mu\nu}D(x-x')-ihc\frac{\partial}{\partial x_\nu'}\lambda_\mu\frac{\partial\mathfrak{D}(x-x')}{\partial x_N'}$$
$$-ihc\frac{\partial}{\partial x_\mu}I_{\nu\sigma}\frac{\partial\mathfrak{D}(x-x')}{\partial x_\sigma}. \quad (2.27)$$

The term $\frac{1}{2}j_NV_N$ represents—as discussed in reference 4—the Coulomb interaction between charged particles.

III. THE SECOND-ORDER HAMILTONIAN

In order to eliminate terms linear in e from (2.26), we subject $\psi[\sigma]$ to the transformation

$$\psi[\sigma]\to e^{-iS[\sigma]}\psi[\sigma];$$
$$S[\sigma]=-\frac{1}{\hbar c^2}\int_{-\infty}^{\sigma}j_\mu(x')\mathfrak{A}_\mu(x')d\omega'. \quad (3.1)$$

Equation (2.26) then becomes, to the second order of approximation,

$$ihc\frac{\delta\psi[\sigma]}{\delta\sigma(x)}=\Big\{-\frac{i}{2c}[S[\sigma],j_\mu(x)\mathfrak{A}_\mu(x)]$$
$$+\frac{e^2}{mc^2}M_{\mu\nu}(x)\mathfrak{A}_\mu(x)\mathfrak{A}_\nu(x)+\frac{1}{2}j_N(x)V_N(x)\Big\}\psi[\sigma]. \quad (3.2)$$

The first term of the right member of (3.2) may be written as

$$-\frac{i}{2c}[S[\sigma],j_\mu(x)\mathfrak{A}_\mu(x)]=-\frac{1}{4c}\{\delta j_\mu(x),\mathfrak{A}_\mu(x)\}$$
$$-\frac{1}{4c}\{\delta\mathfrak{A}_\mu(x),j_\mu(x)\} \quad (3.3)$$

where δ denotes an infinitesimal transformation generated by $S[\sigma]$. It is readily seen that

$$\delta\mathfrak{A}_\mu(x)=-\frac{i}{\hbar c^2}\int_{-\infty}^{\sigma}j_\nu(x')[\mathfrak{A}_\nu(x'),\mathfrak{A}_\mu(x)]d\omega'$$
$$=\frac{1}{c}\int_{-\infty}^{+\infty}\bar{D}(x-x')j_\mu(x')d\omega'+\lambda_\mu V_N(x)$$
$$+\frac{\partial}{\partial x_\mu}\frac{1}{c}\int_{-\infty}^{\sigma}d\omega' j_\nu(x')I_{\nu\sigma}\frac{\partial\mathfrak{D}(x-x')}{\partial x_\sigma} \quad (3.4)$$

in virtue of (2.27), and that

$$\delta j_\mu=\frac{i}{\hbar c^2}\int_{-\infty}^{\sigma}[j_\mu(x),j_\nu(x')]\mathfrak{A}_\nu(x')d\omega'. \quad (3.5)$$

The first term of the right member of (3.4), obtained by symmetrizing the integral between past and future and exploiting the fact that only virtual processes are considered, is recognized as δA_μ; the second when inserted into (3.3) will cancel the Coulomb term of (3.2), the third may be removed to this order, by a change of gauge. The right member of (3.5) may be combined with the $M_{\mu\nu}$ term of (3.2) by defining an infinitesimal transformation of the current:

$$\delta^*j_\mu(x)=e^{iS[\sigma]}j_\mu'(x)e^{-iS[\sigma]}-j_\mu(x)$$
$$\cong\frac{i}{hc^2}\int_{-\infty}^{\sigma}[j_\mu(x),j_\nu(x')]\mathfrak{A}_\nu(x')d\omega'$$
$$-\frac{e^2}{mc}(M_{\mu\nu}(x)+M_{\nu\mu}(x))\mathfrak{A}_\nu(x). \quad (3.6)$$

The resulting equation is then of the form

$$i\hbar c\frac{\delta\psi[\sigma]}{\delta\sigma(x)}=\left[-\frac{1}{4c}\{\delta^*j_\mu(x),\mathfrak{A}_\mu(x)\}\right.$$
$$\left.-\frac{1}{4c}\{\delta A_\mu(x),j_\mu(x)\}\right]\psi[\sigma]. \quad (3.7)$$

It is evident from (3.6) and (1.16) that $\delta^*j_\mu(x)$ is gauge invariant. The differential conservation law

$$\nabla_\mu\delta^*j_\mu(x)=0 \quad (3.8)$$

may be inferred from (2.1).

Our next task is to analyze (3.7) into photon and meson self-energy terms and terms representing the coupling of photons with mesons and the interaction between mesons. It is important to show in this connection that the terms depending explicitly on the orientation of the surface cancel. The quantities needed in setting up these expressions are

$$\langle\delta^*j_\mu(x)\rangle_0,\quad \epsilon(x-x')[j_\mu(x),\ j_\nu(x')]_1,\quad \{j_\mu(x),\ j_\nu(x')\}_1.$$

To find $\langle\delta^*j_\mu(x)\rangle_0$ we calculate, using (1.22), (1.19), (1.21),

$$\langle M_{\mu\alpha}(x)+M_{\alpha\mu}(x)\rangle_0$$
$$=\frac{1}{2\kappa}\mathrm{Tr}\{[\beta_\mu(\beta_N^2+1)\beta_\nu+\beta_\nu(\beta_N^2+1)\beta_\mu]S^{(1)}(\xi)\}_{\xi\to0}$$
$$=\binom{1}{1}\kappa I_{\mu\nu}\Delta^{(1)}(0)+\binom{0}{1}\frac{2}{\kappa}[\Delta_{\mu\nu}{}^{(1)}(0)+\lambda_\mu\Delta_{\nu N}{}^{(1)}(0)$$
$$+\lambda_\nu\Delta_{\mu N}{}^{(1)}(0)-\delta_{\mu\nu}\Delta_{NN}{}^{(1)}(0)] \quad (3.9)$$

$$\langle[j_\mu(x),j_\nu(x')]\rangle_0$$
$$=-\frac{i}{2}\left(\frac{ec}{\kappa}\right)^2\mathrm{Tr}[\beta_\mu S(x-x')\beta_\nu S^{(1)}(x'-x)$$
$$-\beta_\nu S(x'-x)\beta_\mu S^{(1)}(x-x')]$$
$$=-ie^2c^2\left\{\binom{1}{1}[\Delta^{(1)}(x-x')\Delta_{\mu\nu}(x-x')\right.$$
$$+\Delta(x-x')\Delta_{\mu\nu}{}^{(1)}(x-x')]-\binom{1}{3}[\Delta_\mu(x-x')$$
$$\times\Delta_\nu{}^{(1)}(x-x')+\Delta_\nu(x-x')\Delta_\mu{}^{(1)}(x-x')]$$
$$+\binom{0}{1}\frac{2}{\kappa^2}[(\Delta_{\mu\sigma}(x-x')\Delta_{\nu\sigma}{}^{(1)}(x-x')+\Delta_{\nu\sigma}(x-x')$$
$$\times\Delta_{\mu\sigma}{}^{(1)}(x-x'))+\delta_{\mu\nu}(\kappa^2\Delta(x-x')\Delta^{(1)}(x-x')$$
$$\left.-\Delta_{\sigma\rho}(x-x')\Delta_{\sigma\rho}{}^{(1)}(x-x'))]\right\}, \quad (3.10)$$

where $\Delta_{\alpha\beta}(x)=(\partial^2\Delta(x)/\partial x_\alpha\partial x_\beta)$ and $\Delta_{\alpha\beta}(0)$ is to be understood as $(\partial^2\Delta(\xi)/\partial\xi_\alpha\partial\xi_\beta)_{\xi\to0}$. The $\Delta(x)$ function in (3.10) is now expressed in terms of $\bar\Delta(x)$ by means of the identities

$$\Delta(x-x')=-2\epsilon(x-x')\bar\Delta(x-x') \quad (3.11a)$$
$$\Delta_\mu(x-x')=-2\epsilon(x-x')\bar\Delta_\mu(x-x') \quad (3.11b)$$
$$\Delta_{\mu\nu}(x-x')=-2\epsilon(x-x')\bar\Delta_{\mu\nu}(x-x')$$
$$+2\epsilon(x-x')\lambda_\mu\lambda_\nu\delta(x-x'). \quad (3.11c)$$

The second term of the right member of (3.11c) gives rise to a group of terms in (3.10) which inserted into (3.6) precisely cancel the surface dependent terms of (3.9) and we finally obtain

$$\langle\delta^*j_\mu(x)\rangle_0=-\frac{e^2}{\hbar}\binom{1}{1}\Delta^{(1)}(0)\mathfrak{A}_\mu(x)$$
$$-\frac{e^2}{\hbar}\frac{2}{\kappa^2}\binom{0}{1}\Delta_{\mu\nu}{}^{(1)}(0)\mathfrak{A}_\nu(x)-\frac{e^2}{\hbar}\binom{1}{1}\int_{-\infty}^{+\infty}[\Delta^{(1)}(x-x')$$
$$\times\bar\Delta_{\mu\nu}(x-x')+\bar\Delta(x-x')\Delta_{\mu\nu}{}^{(1)}(x-x')]\mathfrak{A}_\nu(x')d\omega'$$
$$+\frac{e^2}{\hbar}\binom{1}{3}\int_{-\infty}^{+\infty}[\Delta_\mu{}^{(1)}(x-x')\bar\Delta_\nu(x-x')$$
$$+\Delta_\nu{}^{(1)}(x-x')\bar\Delta_\mu(x-x')]\mathfrak{A}_\nu(x')d\omega'$$
$$-\frac{e^2}{\hbar}\binom{0}{1}\frac{2}{\kappa^2}\int_{-\infty}^{+\infty}\{[\Delta_{\mu\sigma}{}^{(1)}(x-x')\bar\Delta_{\nu\sigma}(x-x')$$
$$+\Delta_{\nu\sigma}{}^{(1)}(x-x')\bar\Delta_{\mu\sigma}(x-x')]+\delta_{\mu\nu}[\kappa^2\Delta^{(1)}(x-x')\bar\Delta(x-x')$$
$$-\Delta_{\sigma\rho}{}^{(1)}(x-x')\bar\Delta_{\sigma\rho}(x-x')]\}\mathfrak{A}_\nu(x')d\omega'. \quad (3.12)$$

Making use of (1.19) and the readily verified identity

$$S(x)=-2\epsilon(x)\bar S(x)+2\beta_N{}^2\epsilon(x)\delta(x), \quad (3.13)$$

we also find that

$$\epsilon(x-x')[j_\mu(x),j_\nu(x')]$$
$$=\tfrac{1}{2}ie^2c^2[\{\bar\psi(x),\beta_\mu\bar S(x-x')\beta_\nu\psi(x')\}$$
$$+\{\bar\psi(x')\beta_\nu\bar S(x'-x)\beta_\mu\psi(x)\}$$
$$-\delta(x-x')B_{\mu\nu}(x)], \quad (3.14)$$

where

$$B_{\mu\nu}(x)=\{\bar\psi(x),(\beta_\mu\beta_N{}^2\beta_\nu+\beta_\nu\beta_N{}^2\beta_\mu)\psi(x)\}. \quad (3.15)$$

Another straightforward calculation yields

$$\{j_\mu(x),j_\nu(x')\}_1=-\frac{e^2c^2}{\kappa}\frac{1}{2}[\{\bar\psi(x),\beta_\mu S^{(1)}(x-x')\beta_\nu\psi(x')\}$$
$$+\{\bar\psi(x')\beta_\nu S^{(1)}(x'-x)\beta_\mu,\psi(x)\}]. \quad (3.16)$$

We shall now set up the expression for the meson self-energy. This is readily seen to be

$$H_{1,0}(x)=-\frac{1}{4c^2}\int_{-\infty}^{+\infty}\bar{D}(x-x')\{j_\mu(x),j_\mu(x')\}_1 d\omega'$$
$$-\frac{i}{4\hbar c^3}\int_{-\infty}^{\sigma}\langle[j_\mu(x),j_\alpha(x')]\rangle_1\langle\{\mathfrak{A}_\alpha(x'),\mathfrak{A}_\mu(x)\}\rangle_0 d\omega'$$
$$+\frac{1}{4}\frac{e^2}{mc^2}\langle M_{\mu\alpha}(x)+M_{\alpha\mu}(x)\rangle_1\langle\{\mathfrak{A}_\alpha(x),\mathfrak{A}_\mu(x)\}\rangle_0. \quad (3.17)$$

The first subscript of H refers to the number of mesons; the second, to the number of light quanta present. The vacuum expectation value of the anticommutator[5] is given by

$$\langle\{\mathfrak{A}_\mu(x),\mathfrak{A}_\alpha(x')\}\rangle_0=\hbar c\delta_{\mu\alpha}D^{(1)}(x-x')$$
$$-\hbar c\frac{\partial}{\partial x_\alpha}I_{\mu\beta}\frac{\partial\mathfrak{D}^{(1)}(x-x')}{\partial x_\beta}-\hbar c\frac{\partial}{\partial x_\mu}\lambda_\alpha\frac{\partial\mathfrak{D}^{(1)}(x-x')}{\partial x_N}. \quad (3.18)$$

Substituting (3.18) into the second term of the right member of (3.17), we obtain

$$-\frac{i}{4c^2}\int_{-\infty}^{\sigma}\langle[j_\mu(x),j_\mu(x')]\rangle_0 D^{(1)}(x-x')d\omega'$$
$$-\frac{i}{4c^2}\int d\sigma_\alpha'\langle[j_\alpha(x'),j_\mu(x)]\rangle_1 I_{\mu\sigma}\frac{\partial\mathfrak{D}^{(1)}(x-x')}{\partial x_\sigma'}$$
$$=-\frac{i}{8c^2}\int_{-\infty}^{+\infty}\epsilon(x-x')\langle[j_\mu(x),j_\mu(x')]\rangle_0 D^{(1)}(x-x')$$
$$+\frac{\hbar c}{4}\frac{e^2}{mc^2}(M_{\mu\nu}(x)+M_{\nu\mu}(x))\frac{\partial^2\mathfrak{D}^{(1)}(\xi)}{\partial\xi_\mu\partial\xi_\nu}\Big]_{\xi\to 0}. \quad (3.19)$$

In the first step we removed the term arising from $(\partial/\partial x_\mu)\lambda_\alpha(\partial/\partial x_N)\mathfrak{D}^{(1)}(x-x')$ by a change of gauge, and applied Gauss' theorem to the preceding term; in the subsequent step a symmetrization with respect to past and future was carried out and a commutator evaluated with the aid of (1.16). According to (1.18a)

$$\frac{1}{4}\frac{e^2}{mc^2}\langle M_{\mu\alpha}(x)+M_{\alpha\mu}(x)\rangle_1\langle\{\mathfrak{A}_\alpha(x),\mathfrak{A}_\mu(x)\}\rangle_0$$
$$=\frac{\hbar c}{2}\frac{e^2}{mc^2}D^{(1)}(0)-\frac{\hbar c}{4}\frac{e^2}{mc^2}$$
$$\times\langle M_{\mu\nu}(x)+M_{\nu\mu}(x)\rangle\frac{\partial^2\mathfrak{D}^{(1)}(\xi)}{\partial\xi_\mu\partial\xi_\nu}\Big]_{\xi\to 0}. \quad (3.20)$$

thus canceling the $\mathfrak{D}^{(1)}$ dependent term of (3.19).

[5] J. Schwinger, Phys. Rev. 75, 651 (1949).

Equation (3.17) then becomes

$$H_{1,0}(x)=\frac{\hbar c}{2}\langle M_{\mu\mu}(x)\rangle_1 D^{(1)}(0)-\frac{1}{4c^2}\int_{-\infty}^{+\infty}\bar{D}(x-x')$$
$$\times\{j_\mu(x),j_\mu(x')\}_1 d\omega'-\frac{i}{8c^2}\int_{-\infty}^{+\infty}\epsilon(x-x')$$
$$\times[j_\mu(x),j_\mu(x')]_1 D^{(1)}(x-x')d\omega'. \quad (3.21)$$

Inserting (3.14) and (3.16) into (3.21) we find that the terms arising from $B_{\mu\nu}(x)$ cancel the surface dependent terms of $M_{\mu\mu}(x)$ and we finally obtain

$$H_{1,0}(x)=\frac{e^2}{2\kappa}\langle N_{\mu\mu}(x)\rangle_1+\frac{e^2}{4\kappa}\frac{1}{2}[\{\bar{\psi}(x),\chi(x)\}_1$$
$$+\{\bar{\chi}(x),\psi(x)\}_1], \quad (3.22)$$

where

$$N_{\mu\nu}(x)=\tfrac{1}{2}[\bar{\psi}(x)\beta_\mu\beta_\nu\psi(x)+\bar{\phi}(x)\beta_\mu\beta_\nu\phi(x)] \quad (3.23)$$

and

$$\chi(x)=\int_{-\infty}^{+\infty}\beta_\mu[\bar{D}(x-x')S^{(1)}(x-x')$$
$$+D^{(1)}(x-x')\bar{S}(x-x')]\beta_\mu\psi(x')d\omega'.$$

A somewhat similar procedure leads to an expression for the Hamiltonian representing the coupling between mesons and photons of the form

$$H_{1,1}(x)=\frac{e^2}{4mc^2}[N_{\mu\nu}(x)+N_{\nu\mu}(x)]_1\{\mathfrak{A}_\mu(x),\mathfrak{A}_\nu(x)\}_1$$
$$+\frac{e^2}{4mc^2}\frac{1}{2}\int_{-\infty}^{+\infty}[\{\bar{\psi}(x),\beta_\mu\bar{S}(x-x')\beta_\nu\psi(x')\}_1$$
$$+\{\bar{\psi}(x')\beta_\nu\bar{S}(x'-x)\beta_\mu,\psi(x)\}_1]$$
$$\times\{\mathfrak{A}_\mu(x),\mathfrak{A}_\nu(x')\}_1 d\omega', \quad (3.24)$$

where we again notice that the surface dependent terms have canceled. The interaction between mesons is given by

$$H_{20}=-\frac{1}{4c^2}\int_{-\infty}^{+\infty}\bar{D}(x-x')\{j_\mu(x),j_\mu(x')\}_2 d\omega'. \quad (3.25)$$

IV. VACUUM POLARIZATION AND PHOTON SELF-ENERGY

In the previous section we obtained an expression (3.12) for the vacuum expectation value of the current induced by a pure radiation field. It is clear, however, that the current due to an external field is formally identical with (3.12),

$$\langle\delta^* j_\mu(x)\rangle_0=-\frac{e^2}{\hbar}\int_{-\infty}^{+\infty}K_{\mu\nu}(x-x')A_\nu(x')d\omega', \quad (4.1)$$

the potentials A_ν replacing $\mathfrak{A}_\nu$. The first two terms of the right member of (3.12) are incorporated into $K_{\mu\nu}$ by means of four-dimensional Dirac delta-functions.

We now introduce the notation

$$\langle \delta^* j_\mu^{(i)}(x)\rangle_0 = -\frac{e^2}{\hbar}\int_{-\infty}^{+\infty} K_{\mu\nu}^{(i)}(x-x')A_\nu(x')d\omega'; \qquad i=1,2 \quad (4.2)$$

with $\delta^* j_\mu^{(1)}(x)$ and $\delta^* j_\mu^{(2)}(x)$ standing for the currents associated with the scalar particle and half the current that must added to $\delta^* j_\mu^{(1)}(x)$ in order to obtain that of a vector particle, respectively. It is readily verified on the basis of (3.12) that $\delta^* j_\mu^{(1)}$, $\delta^* j_\mu^{(2)}$ are separately conserved and gauge invariant and may therefore be regarded as two independent components of the vector meson current. The latter, specific to this particle, is of fourth order in the derivatives; the former, common to the particles of spins 0 and 1, is only of second order. We shall show in this section that

$$K_{\mu\nu}^{(i)}(x) = \left[\frac{\partial}{\partial x_\mu}\frac{\partial}{\partial x_\nu} - \delta_{\mu\nu}\Box^2\right]S^{(i)}(x), \qquad (4.3)$$

where $S^{(i)}(x)$ are functions whose form will appear after a lengthy calculation. A partial integration will then yield

$$\langle \delta^* j_\mu^{(i)}\rangle_0 = -\frac{e^2}{\hbar}\int_{-\infty}^{+\infty} S^{(i)}(x-x') \times\left[\frac{\partial}{\partial x_\mu'}\frac{\partial}{\partial x_\nu'} - \delta_{\mu\nu}\Box'^2\right]A_\nu(x')d\omega' \quad (4.4)$$

implying a vanishing photon self-energy and a polarization of the mesic vacuum by an external source:

$$\begin{aligned}\langle \delta^* j_\mu(x)\rangle_{0;\text{spin }0} &= -4\pi\alpha\int_{-\infty}^{+\infty} S^{(1)}(x-x')J_\mu(x')d\omega' \\ \langle \delta^* j_\mu(x)\rangle_{0;\text{spin }1} &= -4\pi\alpha\int_{-\infty}^{+\infty}[S^{(1)}(x-x') \\ &\qquad +2S^{(2)}(x-x')]J_\mu(x')d\omega'.\end{aligned} \qquad (4.5)$$

We shall follow a method employed by Schwinger[6] in demonstrating the structure (4.3) and the construction of $S^{(i)}(x)$.

We turn now to the proof of (4.3). Employing the Fourier representations[5] of $\bar{\Delta}(x)$, $\Delta^{(1)}(x)$, $\delta(x)$, we may write

$$K_{\mu\nu}^{(1)}(x) = -\frac{1}{(2\pi)^7}\int (dk')(dk'')e^{i(k'+k'')x} \times\left\{\frac{\delta(k'^2+\kappa^2)}{k''^2+\kappa^2}[(k_\mu''k_\nu''+k_\mu'k_\nu') - (k_\mu'k_\nu''+k_\mu''k_\nu')] - \delta_{\mu\nu}\delta(k'^2+\kappa^2)\right\}. \quad (4.6)$$

[6] J. Schwinger, Phys. Rev. **76**, 790 (1949).

The identities

$$\delta(\kappa^2+k'^2)-\delta(\kappa^2+k''^2) = \frac{k'^2-k''^2}{2}\int_{-1}^{+1}\delta'\left[\kappa^2+\frac{k'^2+k''^2}{2}+\frac{k'^2-k''^2}{2}v\right] \quad (4.7a)$$

$$\begin{aligned}\delta(\kappa^2+k'^2)+\delta(\kappa^2+k''^2) &= \int_{-1}^{+1}dv\delta\left[\kappa^2+\frac{k'^2+k''^2}{2}+\frac{k'^2-k''^2}{2}v\right] \\ &\quad +\frac{k'^2-k''^2}{2}\int_{-1}^{+1}dv\cdot v\cdot\delta' \\ &\quad \times\left[\kappa^2+\frac{k'^2+k''^2}{2}+\frac{k'^2-k''^2}{2}v\right]\end{aligned} \quad (4.7b)$$

and the observation that the coefficients of $\delta(k'^2+\kappa^2)/(k''^2+\kappa^2)$, $\delta(k'^2+\kappa^2)$ in (4.6) are symmetric in k' and k'' permit us to write this expression in the form

$$\begin{aligned}K_{\mu\nu}^{(1)}(x) &= \frac{1}{(2\pi)^7}\frac{1}{4}\int (dk')(dk'')e^{i(k'+k'')x} \\ &\quad\times\int_{-1}^{+1}dv\delta'\left[\kappa^2+\frac{k'^2+k''^2}{2}+\frac{k'^2-k''^2}{2}v\right] \\ &\quad\times[(k_\mu''k_\nu''+k_\mu'k_\nu')-(k_\mu'k_\nu''+k_\mu''k_\nu') \\ &\quad +\delta_{\mu\nu}v(k'^2-k''^2)]+\frac{1}{(2\pi)^7}\frac{1}{2}\delta_{\mu\nu}\int (dk')(dk'')e^{i(k'+k'')x} \\ &\quad\times\int_{-1}^{+1}\delta\left[\kappa^2+\frac{k'^2+k''^2}{2}+\frac{k'^2-k''^2}{2}v\right]dv.\end{aligned} \quad (4.8)$$

New variables

$$k'=p+(k/2)(1-v), \quad k''=-p+(k/2)(1+v) \quad (4.9)$$

are now introduced and (4.8) becomes

$$\begin{aligned}K_{\mu\nu}^{(1)}(x) &= \frac{1}{(2\pi)^7}\frac{1}{4}\int (dk)(k_\mu k_\nu-\delta_{\mu\nu}k^2)e^{ikx} \\ &\quad\times\int (dp)\int_{-1}^{+1}dv\cdot v^2\cdot\delta'\left[p^2+\kappa^2\left(1+\frac{k^2}{4\kappa^2}(1-v^2)\right)\right] \\ &\quad+\frac{1}{(2\pi)^7}\frac{1}{4}\int (dk)e^{ikx}\int (dp)\int_{-1}^{+1}dv \\ &\quad\times\left\{\delta'\left[p^2+\kappa^2\left(1+\frac{k^2}{4\kappa^2}(1-v^2)\right)\right]4p_\mu p_\nu \right. \\ &\qquad\left.+\delta\left[p^2+\kappa^2\left(1+\frac{k^2}{4\kappa^2}(1-v^2)\right)\right]2\delta_{\mu\nu}\right\}.\end{aligned} \quad (4.10)$$

The physical requirement of conservation of current

calls for the vanishing of the second term of this sum:

$$\int(dp)\int_{-1}^{+1}dv\left\{\delta'\left[p^2+\kappa^2\left(1+\frac{k^2}{4\kappa^2}(1-v^2)\right)\right]4p_\mu p_\nu + \delta\left[p^2+\kappa^2\left(1+\frac{k^2\,I}{4\kappa^2}(1-v^2)\right)\right]2\delta_{\mu\nu}\right\}=0. \quad (4.11)$$

This requirement will be met if we evaluate the first integral of (4.11) in the following manner

$$4\int(dp)\int_{-1}^{+1}dvp_\mu p_\nu\delta'\left[p^2+\kappa^2\left(1+\frac{k^2}{4\kappa^2}(1-v^2)\right)\right]$$
$$=2\int(dp)\int_{-1}^{+1}dvp_\mu\frac{\partial}{\partial p_\nu}\delta\left[p^2+\kappa^2\left(1+\frac{k^2}{4\kappa^2}(1-v^2)\right)\right]$$
$$=-2\delta_{\mu\nu}\int(dp)\int_{-1}^{+1}dv\delta\left[p^2+\kappa^2\left(1+\frac{k^2}{4\kappa^2}(1-v^2)\right)\right].$$

$S^{(1)}(x)$ is therefore seen to be

$$S^{(1)}(x)=-\frac{1}{(2\pi)^7}\frac{1}{4}\int(dk)e^{ikx}\int(dp)\int_{-1}^{+1}dv\cdot v^2 \times\delta'\left[p^2+\kappa^2\left(1+\frac{k^2}{4\kappa^2}(1-v^2)\right)\right]. \quad (4.12)$$

The function $K_{\mu\nu}^{(2)}(x)$, expressed in terms of Fourier representations, is of the form

$$K_{\mu\nu}^{(2)}(x)=\frac{1}{(2\pi)^7}\frac{1}{\kappa^2}\int(dk')(dk'')e^{i(k'+k'')x} \times\left\{\frac{\delta(k'^2+\kappa^2)}{k''^2+\kappa^2}(k'k''+\kappa^2)[(k_\mu'k_\nu''+k_\mu''k_\nu') - \delta_{\mu\nu}k'(k'+k'')]-\delta(k'^2+\kappa^2)k_\mu'k_\nu'\right\}. \quad (4.13)$$

This expression, unlike (4.6), does not have the coefficients of $\delta(k'^2+\kappa^2)/(k''^2+\kappa^2)$ and $\delta(k'^2+\kappa^2)$ symmetric in k' and k''. We find it convenient to remedy this situation by writing

$$-\delta_{\mu\nu}k'(k'+k'')=-\delta_{\mu\nu}k'(k'+k'')\left[1+\frac{k''^2-k'^2}{(k'+k'')^2}\right] +\delta_{\mu\nu}k'(k'+k'')\frac{k''^2-k'^2}{(k'+k'')^2}$$
$$=-\delta_{\mu\nu}\frac{2[k'(k'+k'')][k''(k'+k'')]}{(k'+k'')^2} +\delta_{\mu\nu}[k'(k'+k'')]\frac{k''^2-k'^2}{(k'+k'')^2}. \quad (4.14)$$

The first term of the right member of (4.14) possesses the desired symmetry property. The second is combined with the last term of the curly bracket in (4.13), also devoid of this property, to yield the expression

$$\frac{2\delta_{\mu\nu}}{(2\pi)^7}\int(dk)\frac{e^{ikx}}{k^2}\int(dk')\delta(k'^2+\kappa^2)(k'k). \quad (4.15)$$

In obtaining (4.15) we introduced a change of variables

$$k'=k'; \quad k=k'+k''$$

and exploited the symmetry of the domain of integration of the k' variable to carry out the replacement

$$k_\mu'k_\nu'\xrightarrow{\delta_{\mu\nu}}\frac{\delta_{\mu\nu}}{4}k'^2.$$

The conservation of current is readily seen to require that (4.15) vanish. Such an interpretation of this ambiguous integral is clearly possible because of the odd nature of the integrand in the k' variable. As a result of this interpretation (4.13) becomes

$$K_{\mu\nu}^{(2)}(x)=\frac{1}{(2\pi)^7}\frac{1}{\kappa^2}\int(dk')(dk'')e^{i(k'+k'')x} \times\frac{\delta(k'^2+\kappa^2)}{k''^2+\kappa^2}(k'k''+\kappa^2)P_{\mu\nu}(k',k''), \quad (4.16)$$

where

$$P_{\mu\nu}(k',k'')=(k_\mu'k_\nu''+k_\mu''k_\nu') -\delta_{\mu\nu}\frac{2[k'(k'+k'')][k''(k'+k'')]}{(k'+k'')^2}. \quad (4.17)$$

Since $P_{\mu\nu}(k',k'')=P_{\mu\nu}(k'',k')$ we may carry out the replacement

$$\frac{\delta(k'^2+\kappa^2)}{k''^2+\kappa^2}(k'k''+\kappa^2) \rightarrow-\frac{1}{2}\frac{1}{k'^2-k''^2}[\delta(k'^2+\kappa^2)(k'k''-k'^2) -\delta(k''^2+\kappa^2)(k'k''-k''^2)]. \quad (4.18)$$

A more compact expression for (4.18) is obtained by noticing the identity

$$\delta(k'^2+\kappa^2)(k'k''-k'^2)-\delta(k''^2+\kappa^2)(k'k''-k''^2)$$
$$=\frac{k'^2-k''^2}{2}\left[\int_{-1}^{+1}dv\delta'\left(\kappa^2+\frac{k'^2+k''^2}{2}+\frac{k'^2-k''^2}{2}v\right) \times\left(k'k''-\frac{k'^2+k''^2}{2}-\frac{k'^2-k''^2}{2}v\right) -\int_{-1}^{+1}dv\delta\left(\kappa^2+\frac{k'^2+k''^2}{2}+\frac{k'^2-k''^2}{2}v\right)\right]. \quad (4.19)$$

Equation (4.16) then assumes the form

$$K_{\mu\nu}^{(1)}(x)=-\frac{1}{4\kappa^2}\frac{1}{(2\pi)^7}\int(dk')(dk'')e^{i(k'+k'')x}$$
$$\times\int_{-1}^{+1}dv\delta'\left[\kappa^2+\frac{k'^2+k''^2}{2}-\frac{k'^2-k''^2}{2}v\right]$$
$$\times\left(k'k''-\frac{k'^2+k''^2}{2}-\frac{k'^2-k''^2}{2}v\right)P_{\mu\nu}(k'k'')$$
$$+\frac{1}{4\kappa^2}\frac{1}{(2\pi)^7}\int(dk')(dk'')e^{i(k'+k'')x}\int_{-1}^{+1}dv$$
$$\times\delta'\left[\kappa^2+\frac{k'^2+k''^2}{2}+\frac{k'^2-k''^2}{2}v\right]P_{\mu\nu}(k'k''). \quad (4.20)$$

The form (4.3) of (4.20) becomes immediately evident after the change of variables (4.9), with $S^{(2)}(x)$ given by

$$S^{(2)}(x)=-\frac{1}{8\kappa^2}\frac{1}{(2\pi)^7}\int(dk)e^{ikx}\int(dp)$$
$$\times\left\{\int_{-1}^{+1}dv(1-v^2)\delta\left[p^2+\kappa^2\left(1+\frac{k^2}{4\kappa^2}(1-v^2)\right)\right]\right.$$
$$+\int_{-1}^{+1}dv(2-3v^2)p^2$$
$$\left.\times\delta'\left[p^2+\kappa^2\left(1+\frac{k^2}{4\kappa^2}(1-v^2)\right)\right]\right\}. \quad (4.21)$$

We now proceed with the explicit construction of $S^{(4)}(x)$. In the course of it, we shall make use of the following expressions:

$$\int(dp)\delta(p^2+\kappa^2)=2\pi\left[P_mP_0-\kappa^2\log\frac{P_m+P_0}{\kappa}\right] \quad (4.22)$$

$$\int(dp)\delta'(p^2+\kappa^2)=-2\pi\left[\log\frac{P_0+P_m}{\kappa}-1\right] \quad (4.23)$$

$$\int(dp)\delta''(p^2+\lambda^2)=\frac{\pi}{\lambda^2}, \quad (4.24)$$

where $P_m=|\mathbf{P}|$ is the upper limit for the magnitude of the $\mathbf{P}$ vector and $P_0=(P_m{}^2+\kappa^2)^{\frac{1}{2}}$. The result will be expressed in terms of $F_n(x)$ functions[6] defined as

$$F_n(x)=\int_0^1 dvv^{2n}\frac{1}{(2\pi)^4}\int(dp)\frac{e^{ipx}}{1+\frac{p^2}{4\kappa^2}(1-v^2)}. \quad (4.25)$$

In this connection the identity

$$F_n(x)=\frac{\kappa^2}{(2\pi)^5}\int(dk)e^{ikx}\int_{-1}^{+1}dv\cdot v^{2n}\int(dp)$$
$$\times\delta''\left[p^2+\kappa^2\left(1+\frac{k^2}{4\kappa^2}(1-v^2)\right)\right] \quad (4.26)$$

should also be noticed. For $S^{(1)}(x)$ we obtain

$$S^{(1)}(x)=-\frac{1}{4}\frac{1}{(2\pi)^7}\frac{2}{3}\int(dk)e^{ikx}\int(dp)\delta'[p^2+\kappa^2]$$
$$-\frac{1}{24}\frac{1}{(2\pi)^7}\int k^2(dk)e^{ikx}\int_{-1}^{+1}dv\cdot v^4\int dp$$
$$\times\delta''\left[p^2+\kappa^2\left(1+\frac{k^2}{4\kappa^2}(1-v^2)\right)\right]$$
$$=\frac{1}{24\pi^2}\delta(x)\left[\log\frac{P_0+P_m}{\kappa}-1\right]$$
$$+\frac{1}{96\pi^2}\left(\frac{\Box}{\kappa}\right)^2F_2(x) \quad (4.27)$$

where use has been made of (4.23) and (4.26). To construct $S^{(2)}(x)$ we carry out the following partial differentiations on the terms occurring in (4.21):

$$\int_{-1}^{+1}dv(1-v^2)\delta\left[p^2+\kappa^2\left(1+\frac{k^2}{4\kappa^2}(1-v^2)\right)\right]$$
$$=-\frac{4}{3}\delta[p^2+\kappa^2]+\frac{4}{15}k^2\delta'(p^2+\kappa^2)+\frac{(k^2)^2}{60}\int dv(5v^4-v^6)$$
$$\times\delta''\left[p^2+\kappa^2\left(1+\frac{k^2}{4\kappa^2}(1-v^2)\right)\right] \quad (4.28a)$$

$$\int_{-1}^{+1}dv(2-3v^2)p^2\delta'\left[p^2+\kappa^2\left(1+\frac{k^2}{4\kappa^2}(1-v^2)\right)\right]$$
$$=2p^2\delta'(p^2+\kappa^2)+\frac{7}{15}k^2p^2\delta''(p^2+\kappa^2)$$
$$+\frac{(k^2)^2}{60}\int_{-1}^{+1}dv(10v^4-3v^6)p^2$$
$$\times\delta'''\left[p^2+\kappa^2\left(1+\frac{k^2}{4\kappa^2}(1-v^2)\right)\right]. \quad (4.28b)$$

The factor p^2 multiplying the first two terms of the right member of (4.28b) is absorbed by means of the identities

$$x\delta'(x)=-\delta(x);\quad x\delta''(x)=-2\delta'(x)$$

and in the case of the third member through a partial integration

$$p^2\delta'''(p^2+\kappa^2\lambda^2)=\frac{1}{2}p_\alpha\frac{\partial}{\partial p_\alpha}\delta''(p^2+\kappa^2\lambda^2)\rightarrow-2\delta''[p^2+\kappa^2\lambda^2].$$

The function $S^{(2)}(x)$ then becomes

$$\begin{aligned}S^{(2)}(x)=&\frac{1}{24\kappa^2}\frac{1}{(2\pi)^7}\int(dk)e^{ikx}\int(dp)\\&\times\{2[\delta(p^2+\kappa^2)+3\kappa^2\delta'(p^2+\kappa^2)]\\&+k^2\left[2\delta'(p^2+\kappa^2)+\frac{7}{5}\kappa^2\delta''(p^2+\kappa^2)\right]\\&+\frac{3}{4}(k^2)^2\int_{-1}^{+1}dv\left(v^4-\frac{v^6}{3}\right)\\&\times\delta''\left[p^2+\kappa^2\left(1+\frac{k^2}{4\kappa^2}(1-v^2)\right)\right]\Big\}.\end{aligned}\tag{4.29}$$

With the aid of (4.22), (4.23) and (4.26), Eq. (4.29) may be expressed as

$$\begin{aligned}S^{(2)}(x)=&\frac{1}{48\pi^2}\left[\frac{P_0P_m}{\kappa^2}-4\log\frac{P_0+P_m}{\kappa}+3\right]\delta(x)\\&+\frac{1}{48\pi^2}\left[\log\frac{P_0+P_m}{\kappa}-\frac{27}{20}\right]\left(\frac{\Box}{\kappa}\right)^2\delta(x)\\&+\frac{1}{128\pi^2}\left(\frac{\Box^2}{\kappa^2}\right)^2\left[F_2(x)-\frac{F_3(x)}{3}\right].\end{aligned}\tag{4.30}$$

Substituting $S^{(i)}(x)$ into (4.4) we obtain

$$\begin{aligned}\langle\delta^*j_\mu^{(1)}(x)\rangle_0=&-\frac{\alpha}{6\pi}\left[\log\frac{P_0+P_m}{\kappa}-1\right]J_\mu(x)\\&-\frac{\alpha}{24\pi}\int F_2(x-x')\Box'^2J_\mu(x')d\omega',\end{aligned}\tag{4.31a}$$

$$\begin{aligned}\langle\delta^*j_\mu^{(2)}(x)\rangle_0=&-\frac{\alpha}{12\pi}\left[\frac{P_0P_m}{\kappa^2}-4\log\frac{P_0+P_m}{\kappa}+3\right]J_\mu(x)\\&-\frac{\alpha}{12\pi}\left[\log\frac{P_0+P_m}{\kappa}-\frac{27}{20}\right]\left(\frac{\Box}{\kappa}\right)^2J_\mu(x)\\&-\frac{\alpha}{32\pi}\int[F_2(x-x')-\tfrac{1}{3}F_3(x-x')]\\&\times\left(\frac{\Box'}{\kappa}\right)^2J_\mu(x')d\omega'.\end{aligned}\tag{4.31b}$$

For reasons discussed in a previous note,[7] the first term of $\langle\delta^*j_\mu^{(1)}(x)\rangle_0$ and the first two terms of $\langle\delta^*j_\mu^{(2)}(x)\rangle_0$ are regarded as devoid of physical significance and the observable scalar and vector currents are taken to be

$$\begin{aligned}&\langle\delta^*j_\mu(x)\rangle_{0;\text{ spin }0}\\&=-\frac{\alpha}{24\pi}\int F_2(x-x')\left(\frac{\Box'}{\kappa}\right)^2J_\mu(x')d\omega'\end{aligned}\tag{4.32a}$$

$$\begin{aligned}&\langle\delta^*j_\mu(x)\rangle_{0;\text{ spin }1}\\&=-\frac{\alpha}{24\pi}\int F_2(x-x')\left(\frac{\Box'}{\kappa}\right)^2J_\mu(x')d\omega'\\&\quad-\frac{\alpha}{16\pi}\int[F_2(x-x')-\tfrac{1}{3}F_3(x-x')]\\&\quad\times\left(\frac{\Box'^2}{\pi^2}\right)^2J_\mu(x')d\omega'.\end{aligned}\tag{4.32b}$$

V. MESON SELF-ENERGY AND MASS RENORMALIZATION

In this section we shall obtain the explicit expression for (3.22). It will turn out to be of a somewhat more involved nature than its electrodynamic analogue. This is due to the fact that

$$\mathfrak{B}=\beta_\mu\beta_\mu$$

is a matrix rather than a number. When transformed back to the Heisenberg representation, it will nonetheless be recognized as a mass correction term. By transcribing the latter into representations of rank 5 and 10 of the β_μ's we shall obtain the self-energy of the scalar and vector particle, respectively.

A technique identical with the one employed by Schwinger[6] permits us to write

$$H_{1,0}(x)=\frac{e^2}{4\kappa}\frac{1}{2}[\{\bar\psi(x),\Theta(x)\}+\{\Theta(x),\psi(x)\}]\tag{5.1}$$

where

$$\Theta(x)=\int K(x-x')\psi(x')d\omega'\tag{5.2}$$

and

$$K(x)=K\delta(x).\tag{5.3}$$

The constant K, evaluated in a straightforward manner, yields

$$K=\frac{\kappa^2}{8\pi^2}(c_0+c_1\mathfrak{B}+c_2\mathfrak{B}^2)=\frac{\kappa^2}{8\pi^2}\mathfrak{C}\tag{5.4}$$

[7] W. H. Furry and M. Neuman, Phys. Rev. **76**, 432 (1949).
Note added in proof: The reduction of Eq. (4.31a, b) to Eq. (4.32a, b) is also given by the procedure of "invariant regularization": W. Pauli and F. Villars, Rev. Mod. Phys. **21**, 434 (1949).

where

$$c_0=-\frac{5}{3}\log\frac{P_0+P_m}{\kappa}+\frac{19}{18}$$

$$c_1=-\frac{1}{2}\frac{P_0P_m}{\kappa^2}+\frac{5}{3}\log\frac{P_0+P_m}{\kappa}-\frac{4}{9} \tag{5.5}$$

$$c_2=+\frac{1}{2}\frac{P_0P_m}{\kappa^2}-\frac{1}{3}\log\frac{P_0+P_m}{\kappa}-\frac{1}{9}.$$

The expression for the self-energy is therefore seen to be

$$H_{1,0}=\frac{\alpha}{4\pi}mc^2\frac{1}{2}[c_0\{\bar\psi(x),\psi(x)\}+c_1\{\bar\psi(x),\mathfrak{B}\psi(x)\}+c_2\partial\{\bar\psi(x),\mathfrak{B}^2\psi(x)\}]. \tag{5.6}$$

We now carry out a unitary transformation on $\psi(x)$

$$\psi(x)\rightarrow W^{-1}[\sigma]\psi(x)W[\sigma]$$

with

$$ihc\frac{\delta W[\sigma]}{\delta\sigma(x)}=H_{1,0}(x)W[\sigma]$$

and find that

$$(\beta_\mu\nabla_\mu+\kappa)W^{-1}[\sigma]\psi(x)W[\sigma]$$

$$=\frac{i}{\hbar c}W^{-1}[\sigma]\int d\sigma_\mu'[H_{1,0}(x'),\beta_\mu\psi(x)]W[\sigma]$$

$$=\frac{\alpha}{4\pi}\kappa\beta_N{}^2\left[1-\frac{1}{\kappa}I_{\sigma\rho}\beta_\sigma\frac{\partial}{\partial x_\rho}\right]W^{-1}[\sigma]\mathfrak{C}\psi(x)W[\sigma]. \tag{5.7}$$

It is now observed that

$$(\beta_\mu\nabla_\mu+\kappa)\frac{\alpha}{4\pi}(\beta_N{}^2+1)W^{-1}[\sigma]\mathfrak{C}\psi(x)W[\sigma]$$

$$=\frac{\alpha}{4\pi}\kappa\beta_N{}^2\left[1-\frac{1}{\kappa}I_{\sigma\rho}\beta_\sigma\frac{\partial}{\partial x_\rho}\right]W^{-1}[\sigma]\mathfrak{C}\psi(x)W[\sigma]$$

$$+\frac{\alpha}{4\pi}\kappa W^{-1}[\sigma]\mathfrak{C}\psi(x)W[\sigma], \tag{5.8}$$

according to (1.6b) and (2.6). Equation (5.7) may then be written as

$$(\beta_\mu\nabla_\mu+\kappa)W^{-1}[\sigma]\left\{\psi(x)-(\beta_N{}^2+1)\frac{\alpha}{4\pi}\mathfrak{C}\psi(x)\right\}W[\sigma]$$

$$=-\kappa\frac{\alpha}{4\pi}W^{-1}[\sigma]\mathfrak{C}\psi(x)W[\sigma]. \tag{5.9}$$

A new spinor $\psi''(x)$, differing from $\psi(x)$ in its $(\beta_N{}^2+1)$ projection, is now defined:

$$\psi''(x)=\psi(x)-(\beta_N{}^2+1)\frac{\alpha}{4\pi}\mathfrak{C}\psi(x). \tag{5.10}$$

Exact to the first order in α, (5.9) may be put in the form

$$\left[\beta_\mu\nabla_\mu+\kappa\left(1+\frac{\alpha}{4\pi}\mathfrak{C}\right)\right]W^{-1}[\sigma]\psi''(x)W[\sigma]=0. \tag{5.11}$$

The definition (5.10) is inherent in (5.11) and need not be carried separately.

An elegant scheme due to Harish-Chandra[3] provides a simple means for transcribing (5.11) into particular representations of the β_μ-matrices. The transcription yields

$$\frac{\partial U(x)}{\partial x_\mu}=\kappa\left[1+\frac{\alpha}{4\pi}(c_0+c_1+c_2)\right]U_\mu(x) \tag{5.12a}$$

$$\frac{\partial U_\mu}{\partial x_\mu}=\kappa\left[1+\frac{\alpha}{4\pi}(c_0+4c_1+16c_2)\right]U(x) \tag{5.12b}$$

for the scalar and

$$\frac{\partial U_\mu}{\partial x_\nu}-\frac{\partial U_\nu}{\partial x_\mu}=\kappa\left[1+\frac{\alpha}{4\pi}(c_0+2c_1+4c_2)\right]G_{\mu\nu}(x) \tag{5.13a}$$

$$\frac{\partial G_{\mu\nu}(x)}{\partial x_\mu}=\kappa\left[1+\frac{\alpha}{4\pi}(c_0+3c_1+9c_2)\right]U_\nu(x) \tag{5.13b}$$

for the vector meson. Substituting (5.12a) and (5.13a) into (5.12b) and (5.13b), respectively, we obtain (exact to the first order in α)

$$\Box^2U(x)-(\kappa+\delta\kappa)^2U(x)=0 \tag{5.14}$$

$$\frac{\delta\kappa}{\kappa}=\frac{\alpha}{8\pi}(2c_0+5c_1+17c_2)$$

$$=\frac{32}{4\pi}\left[\frac{P_0P_m}{\kappa^2}+\log\frac{P_0+P_m}{\kappa}-\frac{1}{3}\right] \tag{5.15}$$

for a particle of spin 0, and

$$\Box^2U_\alpha(x)-\frac{\partial}{\partial x_\alpha}\left(\frac{\partial U_\mu(x)}{\partial x_\mu}\right)-(\kappa+\delta\kappa)^2U_\alpha(x)=0 \tag{5.16}$$

$$\frac{\delta\kappa}{\kappa}=\frac{\alpha}{8\pi}(2c_0+5c_1+13c_2)$$

$$=\frac{\alpha}{12\pi}\left[6\frac{P_0P_m}{\kappa^2}+11\log\frac{P_0+P_m}{\kappa}-\frac{7}{3}\right] \tag{5.17}$$

for a particle of spin 1.

Bosons in an Electromagnetic Field

R. G. MOORHOUSE
Trinity College, Cambridge, England
(Received May 31, 1949)

The interaction representation for bosons of spin 0 or 1 in an electromagnetic field is given, using β-matrix theory. The gauge invariance of the scheme is proved. The photon self-energy is shown to be zero, and the meson self-energy is evaluated. The vacuum polarization is evaluated for a particular representation of the β-matrices.

1. INTRODUCTION

THE theories of radiative corrections in quantum electrodynamics, developed by Feynman,[1] Schwinger,[2] Dyson,[3] and various Japanese authors,[4] in explaining experimental results and in getting rid of infinities have had an unqualified success. Perhaps the most natural extension to other interactions is to the case of mesons in an electromagnetic field, because here the coupling constant is small and on traditional ideas of perturbation theory one would expect to get a sensible result. Tomonaga and his collaborators have gone some part of the way by giving the interaction representation for scalar and vector mesons. Here a generalization of this work by the use of β-matrix theory is given and the phenomena of meson self-energy and vacuum polarization dealt with. The paper is mainly concerned with showing that despite mathematical differences the work of Schwinger has an exact parallel in the case of bosons in an electromagnetic field.

2. EQUATION OF MOTION

In the β-matrix formalism,[5] the free meson wave function $\psi(x)$ obeys the equation

$$(\partial/\partial x_\mu)\beta_\mu\psi(x)+\kappa\psi(x)=0, \tag{2.1}$$

where

$$\beta_\mu\beta_\nu\beta_\rho+\beta_\rho\beta_\nu\beta_\mu=\beta_\mu\delta_{\nu\rho}+\beta_\rho\delta_{\nu\mu}.$$

We define

$$\bar{\psi}=\psi_T{}^*\eta_4, \tag{2.2}$$

where* denotes conjugate complex, and $_T$ denotes transpose.

$$\eta_4=2\beta_4{}^2-1. \tag{2.3}$$

The free field commutation relations are

$$[\psi_\mu(x),\bar{\psi}_\nu(x')]=-iT_{\mu\nu}(x-x'), \tag{2.4}$$

where[6]

$$T_{\mu\nu}(x-x')=(\beta_\lambda(\partial/\partial x_\lambda)-(1/\kappa)\beta_\lambda\beta_\rho(\partial^2/\partial x_\lambda\partial x_\rho))_{\mu\nu}\times\Delta(x-x'), \tag{2.5}$$

and Δ is the function of Schwinger obeying the wave equation for Compton wave-length $1/\kappa$.

$$[A_\mu(x),A_\nu(x')]=i\hbar cD(x-x')\delta_{\mu\nu}. \tag{2.6}$$

Since there are only two non-trivial irreducible representations of the β's of different ranks there is a C such that

$$C_T{}^*C=1,\quad \beta_{T\mu}=\beta_\mu{}^*=-C^{-1}\beta_\mu C, \tag{2.7}$$

and one finds $C_T=C$. Define

$$\psi'=C\bar{\psi}_T=C\eta_{T4}\psi^*, \tag{2.8}$$

then

$$\bar{\psi}'=\psi_T\eta_4{}^*C_T{}^*\eta_4=\psi_TC^{-1}C\eta_{T4}C^{-1}\eta_4.$$

But

$$C^{-1}\eta_{T4}C^{-1}=2(C\beta_{T4}C^{-1})(C\beta_{T4}C^{-1})-1=\eta_4,$$

and

$$\eta_4{}^2=1$$

Therefore

$$\bar{\psi}'=\psi_TC^{-1}. \tag{2.9}$$

Also

$$\partial/\partial x_\mu\cdot\beta_\mu\psi'+\kappa\psi'=0. \tag{2.10}$$

It can easily be deduced from the above definitions that

$$[\psi_\mu'(x),\bar{\psi}_\nu'(x')]=-iT_{\mu\nu}(x-x'). \tag{2.11}$$

The ψ', $\bar{\psi}'$ are the charge conjugate functions and if we define the current operator for the free meson field

$$s_\mu(x)=(iec/2)(\bar{\psi}(x)\beta_\mu\psi(x)-\bar{\psi}'(x)\beta_\mu\psi'(x)), \tag{2.12}$$

its expectation value in the vacuum is zero. For it can easily be shown, that

$$\begin{aligned}\langle\{\psi_\mu(x),\bar{\psi}_\nu(x')\}\rangle_0&=-T_{\mu\nu}{}^{(1)}(x-x'),\\ \langle\{\psi_\mu'(x),\bar{\psi}_\nu'(x')\}\rangle_0&=-T_{\mu\nu}{}^{(1)}(x-x'),\end{aligned} \tag{2.13}$$

where

$$\{a,b\}=ab+ba.$$

The free electromagnetic field variables are dealt with exactly as Schwinger does.

Tomonaga[4] and his collaborators have written down in the interaction representation the equation of motion and supplementary condition for meson fields interacting with the electromagnetic field. Except for the charge symmetrization, the following equations contain theirs, and can be obtained in the same manner.

[1] R. P. Feynman, Phys. Rev. **74**, 1430 (1948).
[2] J. Schwinger, Phys. Rev. **74**, 1939 (1948); **75**, 651, 898 (1949).
[3] F. J. Dyson, Phys. Rev. **75**, 486 (1949) and unpublished work.
[4] Many papers in Prog. Theor. Phys., in particular, S. Kanesawa and S. Tomonaga, Prog. Theor. Phys. **3**, 101 (1948).
[5] N. Kemmer, Proc. Roy. Soc. **A173**, 91 (1939).
[6] W. Pauli, Rev. Mod. Phys. **13**, 203 (1941).

$$ihc\frac{\delta\Psi(\sigma)}{\delta\sigma(x)}=\left(-\frac{1}{c}s_\mu(x)A_\mu(x)-\frac{ie}{\kappa\hbar c^2}q_{\mu\nu}(x)A_\mu(x)A_\nu(x)\right)\Psi(\sigma)$$
$$\equiv H(x,\sigma)\Psi(\sigma), \quad (2.14)$$

$$\left(\frac{\partial A_\mu(x)}{\partial x_\mu}+\frac{1}{c}\int_\sigma s_\mu(x')D(x'-x)d\sigma_\mu'\right)\Psi(\sigma)=0, \quad (2.15)$$

where

$$q_{\mu\nu}(x)=(iec/2)(\bar\psi(x)\beta_\mu\beta_\lambda\beta_\rho\beta_\nu\psi(x)N_\lambda N_\rho$$
$$+\bar\psi'(x)\beta_\mu\beta_\lambda\beta_\rho\beta_\nu\psi'(x)N_\lambda N_\rho$$
$$+\bar\psi(x)\beta_\mu\beta_\nu\psi(x)+\bar\psi'(x)\beta_\mu\beta_\nu\psi'(x)). \quad (2.16)$$

N_λ is the usual vector normal to the surface at σ. $N_\lambda^2=-1$. The integrability of (2.14), and the compatability of all the Eqs. (2.15) and (2.14) can be shown without going out of the β-matrix formalism. Thus the theory need not be confined to the irreducible representations of the β's of spin 0 and spin 1. The proof follows familiar lines laid down by Tomonaga and others, and will not be given here.

The field quantities obey the commutation relations for the free fields.

3. GAUGE INVARIANCE

The equations of the theory are all invariant under a gauge transformation, except for the equation of motion which becomes

$$ihc\frac{\delta\Psi(\sigma)}{\delta\sigma(x)}=\left(H(x,\sigma)+\frac{\partial}{\partial x_\mu}\left(\frac{1}{c}s_\mu(x)\Lambda(x)\right)\right.$$
$$-\frac{ie}{\kappa\hbar c^2}q_{\mu\nu}(x)\left(A_\mu(x)\frac{\partial\Lambda(x)}{\partial x_\nu}\right.$$
$$\left.\left.+\frac{\partial\Lambda(x)}{\partial x_\mu}A_\nu(x)-\frac{\partial\Lambda(x)}{\partial x_\mu}\frac{\partial\Lambda(x)}{\partial x_\nu}\right)\right)\Psi(\sigma) \quad (3.1)$$

using Schwinger's notation.

If we make the transformation

$$\Psi(\sigma)\to e^{-iG(\sigma)}\Psi(\sigma), \qquad G(\sigma)=\frac{1}{\hbar c}\int_\sigma\frac{1}{c}s_\mu(x)\Lambda(x), \quad (3.2)$$

$$ihc\frac{\delta\Psi}{\delta\sigma(x)}+ihce^{iG}\frac{\delta e^{-iG}}{\delta\sigma(x)}\Psi$$
$$=e^{iG}\left(H(x,\sigma)+\frac{\partial}{\partial x_\mu}\left(\frac{1}{c}s_\mu(x)\Lambda(x)\right)\right.$$
$$-\frac{ie}{\kappa\hbar c^2}q_{\mu\nu}(x)\left(A_\mu(x)\frac{\partial\Lambda(x)}{\partial x_\nu}\right.$$
$$\left.\left.+\frac{\partial\Lambda(x)}{\partial x_\mu}A_\nu(x)-\frac{\partial\Lambda(x)}{\partial x_\mu}\frac{\partial\Lambda(x)}{\partial x_\nu}\right)\right)e^{-iG}\Psi(\sigma), \quad (3.3)$$

$$ihce^{iG}\frac{\delta e^{-iG}}{\delta\sigma(x)}=\frac{\partial}{\partial x_\mu}\left(\frac{1}{c}s_\mu(x)\Lambda(x)\right)$$
$$+\frac{i}{2\hbar c^3}\int_\sigma\left[s_\mu(x')\Lambda(x'),\, s_\nu(x)\frac{\partial\Lambda(x)}{\partial x_\nu}\right]d\sigma_\nu'$$
$$+\frac{i}{3!}\left[G,\left[G,\frac{\delta G}{\delta\sigma(x)}\right]\right]+\cdots, \quad (3.4)$$

$$[s_\mu(x'),\, s_\nu(x)]=ie^2c^2((\bar\psi(x)\beta_\mu T(x'-x)\beta_\nu\psi(x))$$
$$-(\bar\psi(x)\beta_\nu T(x-x')\beta_\mu\psi(x'))). \quad (3.5)$$

We change to a system of axes where the time axis is perpendicular to σ at x and use the fact that for x' and x with space like separation

$$\frac{\partial\Delta(x'-x)}{\partial x_i'}=\frac{\partial^2\Delta(x'-x)}{\partial x_i'\partial x_j'}=\frac{\partial^2\Delta(x'-x)}{\partial x_4'^2}=0.$$

Then the second term on the right-hand side of (3.4) is

$$-\frac{e^2}{2hc}\int_\sigma d\sigma_4'\left(\bar\psi(x')\beta_4^2\beta_\nu\frac{\partial\Delta(x'-x)}{\partial x_4'}\psi(x)-\bar\psi(x)\beta_\nu\beta_4^2\frac{\partial\Delta(x'-x)}{\partial x_4'}\psi(x')-\frac{1}{\kappa}\bar\psi(x')\beta_4^2\beta_i\beta_\nu\frac{\partial^2\Delta(x'-x)}{\partial x_i'\partial x_4'}\psi(x)\right.$$
$$\left.-\frac{1}{\kappa}\bar\psi(x)\beta_\nu\beta_i\beta_4^2\frac{\partial^2\Delta(x'-x)}{\partial x_4'\partial x_i'}\psi(x)\right)\Lambda(x')\frac{\partial\Delta(x)}{\partial x_\nu}=-\frac{e^2}{2hc\kappa}\int\left(\bar\psi(x')\beta_4^2\beta_i\beta_\nu\frac{\partial\Delta(x'-x)}{\partial x_4'}\psi(x)\right.$$
$$\left.+\bar\psi(x)\beta_\nu\beta_i\beta_4^2\frac{\partial\Delta(x'-x)}{\partial x_4'}\psi(x')\right)\frac{\partial\Delta(x')}{\partial x_i'}\frac{\partial\Delta(x)}{\partial x_\nu}d\sigma_4'=\frac{e^2}{\hbar c\kappa}\bar\psi(x)\beta_4^2\beta_\nu\beta_j\psi(x)\frac{\partial\Delta(x)}{\partial x_i}\frac{\partial\Delta(x)}{\partial x_j}. \quad (3.6)$$

In the above the following equations have been used

$$\kappa\psi=-(\partial/\partial x_i)\beta_i\beta_4^2\psi+\kappa\beta_4^2\psi, \qquad \kappa\bar\psi=(\partial/\partial x_i)\bar\psi\beta_4^2\beta_i+\kappa\bar\psi\beta_4^2. \quad (3.7)$$

It is obvious that $\bar\psi(x)\beta_4^2\beta_i\beta_j\psi(x)$ commutes with $s_4(x')$ for x' and x having space-like separation. Thus the third and higher terms in the expansion (3.4) are zero. The terms on the right-hand side of (3.3) are evaluated by a similar process, so that collecting results:

$$ihce^{iG}\frac{\delta e^{-iG}}{\delta\sigma(x)}=\frac{\partial}{\partial x_\mu}\left(\frac{1}{c}s_\mu(x)\Lambda(x)\right)+\frac{e^2}{\hbar c\kappa}\bar\psi(x)\beta_4^2\beta_i\beta_j\psi(x)\frac{\partial\Lambda(x)}{\partial x_i}\frac{\partial\Lambda(x)}{\partial x_j}, \quad (3.8)$$

$$e^{iG}H(x\sigma)e^{-iG}=H(x\sigma)+\frac{e^2}{\hbar c\kappa}(\bar\psi(x)\beta_4^2\beta_i\beta_j\psi(x))\left(A_j\frac{\partial\Lambda}{\partial x_i}+A_i\frac{\partial\Lambda}{\partial x_j}\right), \quad (3.9)$$

$$e^{iG}\frac{1}{c}s_\mu(x)\frac{\partial\Lambda(x)}{\partial x_\mu}e^{-iG}=\frac{1}{c}s_\mu(x)\frac{\partial\Lambda(x)}{\partial x_\mu}-\frac{2e^2}{\hbar c\kappa}\bar\psi(x)\times\beta_4^2\beta_i\beta_j\psi(x)\frac{\partial\Lambda(x)}{\partial x_i}\frac{\partial\Lambda(x)}{\partial x_j}, \quad (3.10)$$

$$e^{iG}q_{\nu\mu}(x)e^{-iG}=q_{\mu\nu}(x). \quad (3.11)$$

Equation (3.11) uses the fact that in the coordinates where the time axis is perpendicular to σ at x

$$X_{\mu\nu}q_{\mu\nu}(x)=iecX_{ij}\bar\psi(x)\beta_4^2\beta_i\beta_j\psi(x).$$

Thus taking together Eqs. (3.8)–(3.11) we see that Eq. (3.4) is, in the coordinates we have chosen

$$i\hbar c(\delta\Psi(\sigma)/\delta\sigma(x))=H(x,\sigma)\Psi(\sigma).$$

This equation is unaltered in form when we now transform back to the coordinate system from which we started.

Thus the equation of motion is essentially unaltered under a gauge transformation.

4. VACUUM POLARIZATION

We must first consider what the current is in the interaction representation. Before the transformation to the interaction representation is made the current can be written

$$\begin{aligned}\bar\psi\beta_\mu\psi=&\bar\psi(x)\beta_4^2\beta_\mu\beta_4\psi(x)-(1/\kappa)\bar\psi(x)\beta_4^2\beta_i\beta_4^2(\partial\psi(x)/\partial x_i)\\&+(1/\kappa)(\partial\bar\psi(x)/\partial x_i)\beta_4^2\beta_i\beta_\mu\beta_4^2\psi(x)\\&+(1/\kappa)(ie/\hbar c)A_i(x)\bar\psi(x)\beta_4^2\beta_i\beta_\mu\beta_4^2\psi(x)\\&+(1/\kappa)\bar\psi(x)\beta_4^2\beta_\mu\beta_i\beta_4^2\psi(x)(ie/\hbar c)A_i(x). \quad (4.1)\end{aligned}$$

To get (4.1) the equations

$$\kappa\bar\psi=\frac{\partial}{\partial x_i}\bar\psi\beta_4^2\beta_i+\frac{ie}{\hbar c}A_i\bar\psi\beta_4^2\beta_i+\kappa\bar\psi\beta_4^2,$$

$$\kappa\psi=-\frac{\partial}{\partial x_i}\beta_i\beta_4^2\psi+\frac{ie}{\hbar c}A_i\beta_i\beta_4^2\psi+\kappa\beta_4^2\psi$$

were used. (Greek suffixes run from 1 to 4, Latin from 1 to 3). When the transformation to the interaction representation is made, it is the independent quantities $\beta_4^2\psi(x)$, $\bar\psi(x)\beta_4^2$ (taking the x_4 axis perpendicular to σ at x) which are unchanged in form, with the ψ, $\bar\psi$ now obeying the free field equations. Thus (4.1) is transformed to

$$\bar\psi\beta_\mu\psi+(1/\kappa)(ie/\hbar c)A_i\bar\psi\beta_4^2(\beta_i\beta_\mu+\beta_\mu\beta_i)\beta_4^2\psi.$$

Here

$$A_i=A_\mu \text{ for } \mu=1,2,3, \qquad A_i=0 \text{ for } \mu=4.$$

For a more general coordinate system, that is, one whose x_4 axis is not necessarily perpendicular to σ at x this is

$$\bar\psi\beta_\mu\psi+(1/\kappa)(ie/\hbar c)A_\nu\bar\psi(\beta_\nu\beta_\lambda\beta_\rho\beta_\mu N_\lambda N_\rho+\beta_\nu\beta_\mu+\beta_\mu\beta_\lambda\beta_\rho\beta_\nu N_\lambda N_\rho+\beta_\mu\beta_\nu)\psi.$$

Similarly for the charge conjugate. So in the interaction representation the current is

$$j_\mu(x)=s_\mu(x)+(1/\kappa)(ie/\hbar c)A_\nu(x)(q_{\mu\nu}(x)+q_{\mu\nu}(x)), \quad (4.2)$$

where $s_\mu(x)$ is defined in (2.12).

Now the solution of the equation of motion (2.14) is

$$\Psi(\sigma)=\left(1-\frac{i}{\hbar c}\int_{-\infty}^{\sigma}H(x\sigma')\right)\Psi_0, \quad (4.3)$$

where $\Psi(\sigma)\to\Psi_0$ as $\sigma\to-\infty$. To the first order in e

$$\begin{aligned}\Psi(\sigma)&=\left(1+\frac{i}{\hbar c^2}\int_{-\infty}^{\sigma}s_\mu(x')A_\mu(x')d\omega'\right)\Psi_0\\&\equiv U(\sigma)\Psi_0.\end{aligned}$$

The vacuum polarization is the current induced in what was initially a vacuum by virtue of the "switching on" of the interaction. Thus if Ψ_0 is a vacuum state, what we require to the first order in e is

$$\begin{aligned}&(\Psi_0, U^{-1}(\sigma)(s_\mu(x)+(1/\kappa)(ie/\hbar c)A_\nu(x)\\&\qquad\times(q_{\nu\mu}(x)+q_{\mu\nu}(x)))U(\sigma)\Psi_0)\\&=\frac{i}{\hbar c^2}\int_{-\infty}^{\sigma}\langle[[s_\mu(x),s_\nu(x')]]_0A_\nu(x')\\&\qquad+(1/\kappa)(ie/\hbar c)A_\nu(x)(q_{\nu\mu}(x)+q_{\mu\nu}(x))_0\\&\qquad\equiv\langle j_\mu(x)\rangle. \quad (4.4)\end{aligned}$$

We must have $\langle j_\mu(x)\rangle$ zero for $A_\mu(x)=-\partial\Lambda(x)/\partial x_\mu$, where Λ is a scalar function, otherwise the current would have an expectation value when there was no real field. We take a Lorentz system where the time axis is perpendicular to σ at x and get

$$\begin{aligned}\langle j_\mu(x)\rangle=&-\frac{i}{\hbar c^2}\int_\sigma d\sigma_\nu'\langle[[s_\mu(x),s_\nu(x')]]\Lambda(x')\\&-\frac{1}{\kappa}\frac{ie}{\hbar c}\frac{\partial\Lambda(x)}{\partial x_\nu}\langle q_{\nu\mu}(x)+q_{\mu\nu}(x)\rangle_0\\=&\frac{e^2}{\hbar}\int d\sigma_4'\Big\langle\bar\psi(x)\beta_\mu\Big(\beta_4\frac{\partial}{\partial x_4'}+\frac{1}{\kappa}\beta_j\beta_4\frac{\partial^2}{\partial x_j'\partial x_4'}\Big)\\&\times\Delta(x'-x)\beta_4\psi(x')-\bar\psi(x')\beta_4\Big(\beta_4\frac{\partial}{\partial x_4'}\\&-\frac{1}{\kappa}\beta_4\beta_j\frac{\partial^2}{\partial x_j'\partial x_4'}\Big)\Delta(x'-x)\beta_\mu\psi(x)\Big\rangle_0\Lambda(x')\\&+\frac{1}{\kappa}\frac{e^2}{\hbar}\frac{\partial\Lambda(x)}{\partial x_j}\langle\bar\psi(x)\beta_4^2(\beta_\mu\beta_j+\beta_j\beta_\mu)\beta_4^2\psi(x)\rangle_0\\=&-\frac{e^2}{\kappa\hbar}\int_\sigma d\sigma_4'\Big(\bar\psi(x)\beta_\mu\beta_j\frac{\partial\Delta(x'-x)}{\partial x_4'}\beta_4^2\psi(x')\\&+\bar\psi(x')\beta_4^2\beta_j\beta_\mu\psi(x)\frac{\partial\Delta(x'-x)}{\partial x_4'}\Big)\frac{\partial\Delta(x')}{\partial x_j'}\\&+\frac{1}{\kappa}\frac{e^2}{\hbar}\frac{\partial\Lambda(x)}{\partial x_j}\langle\bar\psi(x)\beta_4^2(\beta_\mu\beta_j+\beta_j\beta_\mu)\beta_4^2\psi(x)\rangle_0\\=&0.\end{aligned}$$

In the above we have used the facts that for x' and x lying on a space like surface

$$\frac{\partial}{\partial x_i'}\Delta(x'-x)=\frac{\partial^2\Delta(x'-x)}{\partial x_i'\partial x_j'}=\frac{\partial^2\Delta(x'-x)}{\partial x'_4{}^2}=0,$$

and that

$$\beta_4\beta_i\beta_4=0.$$

This essentially proves that the photon self-energy is zero. For take, in order to evaluate (4.4), a Fourier component of $A_\nu(x')$, say $A_\nu(x)e^{-ip(x'-x)}$ and take any particular representation of the β's. Then from covariance reasons (4.4) is $F_1(p^2)\delta_{\mu\nu}A_\nu(x)+F_2(p^2)p_\mu p_\nu A_\nu(x)$. For a free photon $p^2=0$ and $p_\nu A_\nu(x)=0$, so that this becomes $F_1(0)A_\nu(x)\delta_{\mu\nu}$. But the "free photon" conditions are obeyed when $A_\nu(x)=-\partial\Lambda(x)/\partial x_\nu$ and $\Lambda(x)=e^{ipx}$, $p^2=0$. So that by what has just been proved, we must have $F_1(0)\equiv 0$ and thus the photon self-energy zero. Wentzel[7] has objected to Schwinger's proof of the vanishing of the photon self-energy, on the grounds that the partial integration is not allowable. Pauli,[8] however, has adopted a technique of regularizing improper functions which meets Wentzel's objections, and so there is reason to believe that the kind of partial integration given above is a proper procedure.

To evaluate the vacuum polarization we use the fact that we are dealing with virtual processes and so

$$\langle j_\mu(x)\rangle=\frac{e^2}{2\hbar}\int_{-\infty}^{\infty}\epsilon(x-x')Sp\Big(\tfrac{1}{2}\beta_\lambda\beta_\nu\beta_\rho\beta_\mu\times\Big(\frac{\partial\Delta(x'-x)}{\partial x_\rho'}\frac{\partial\Delta^{(1)}(x'-x)}{\partial x_\lambda'}+\frac{\partial\Delta(x'-x)}{\partial x_\lambda'}\frac{\partial\Delta^{(1)}(x'-x)}{\partial x_\rho'}\Big)$$
$$-\frac{1}{2}\frac{1}{\kappa^2}\beta_\sigma\beta_\tau\beta_\nu\beta_\rho\beta_\lambda\beta_\mu\Big(\frac{\partial^2\Delta^{(1)}(x'-x)}{\partial x_\sigma'\partial x_\tau'}\frac{\partial^2\Delta(x'-x)}{\partial x_\rho'\partial x_\lambda'}+\frac{\partial^2\Delta^{(1)}(x'-x)}{\partial x_\rho'\partial x_\lambda'}\frac{\partial^2\Delta(x'-x)}{\partial x_\sigma'\partial x_\tau'}\Big)\Big)A_\nu(x')$$
$$-\frac{e^2}{2k\hbar}\langle-\bar\psi(x)\beta_\mu\beta_4{}^2\beta_\nu\psi(x)+\bar\psi(x)\beta_\mu\beta_\nu\psi(x)$$
$$-\bar\psi'(x)\beta_\nu\beta_4{}^2\beta_\mu\psi'(x)+\bar\psi'(x)\beta_\nu\beta_\mu\psi'(x)-\bar\psi(x)\beta_\nu\beta_4{}^2\beta_\mu\psi(x)$$
$$+\bar\psi(x)\beta_\nu\beta_\mu\psi(x)-\bar\psi'(x)\beta_\mu\beta_4{}^2\beta_\nu\psi'(x)$$
$$+\bar\psi'(x)\beta_\mu\beta_\nu\psi'(x)\rangle_0A_\nu(x).$$

It can be shown that

$$\int_{-\infty}^{\infty}\Big(\frac{1}{2}\epsilon(x'-x)\frac{\partial^2\Delta(x'-x)}{\partial x_\mu'\partial x_\nu'}-\frac{1}{2}\frac{\partial^2\epsilon(x'-x)\Delta(x'-x)}{\partial x_\rho'\partial x_\nu'}\Big)\times B(x')d\omega'=-\delta_{\mu4}\delta_{\nu4}B(x),\quad(4.5)$$

[7] G. Wentzel, Phys. Rev. 74, 1070 (1948).
[8] W. Pauli, unpublished.

$$\langle j_\mu(x)\rangle=\frac{e^2}{2\hbar}\int_{-\infty}^{\infty}Sp\Big(\beta_\lambda\beta_\nu\beta_\rho\beta_\mu\Big(\frac{\partial\bar\Delta(x'-x)}{\partial x_\rho'}\times\frac{\partial\Delta^{(1)}(x'-x)}{\partial x_\lambda'}+\frac{\partial\bar\Delta(x'-x)}{\partial x_\lambda'}\frac{\partial\Delta^{(1)}(x'-x)}{\partial x_\rho'}\Big)$$
$$-\frac{1}{\kappa^2}\beta_\sigma\beta_\tau\beta_\nu\beta_\rho\beta_\lambda\beta_\mu\Big(\frac{\partial^2\Delta^{(1)}(x'-x)}{\partial x_\sigma'\partial x_\tau'}\frac{\partial^2\bar\Delta(x'-x)}{\partial x_\rho'\partial x_\lambda'}+\frac{\partial^2\Delta^{(1)}(x'-x)}{\partial x_\rho'\partial x_\lambda'}\frac{\partial^2\bar\Delta(x'-x)}{\partial x_\sigma'\partial x_\tau'}\Big)$$
$$-\frac{e^2}{2\kappa^2\hbar}S\Big(\beta_\mu\beta_\nu\beta_\rho\beta_\lambda\frac{\partial^2\Delta^{(1)}(x'-x)}{\partial x_\rho'\partial x_\lambda'}+\beta_\nu\beta_\mu\beta_\rho\beta_\lambda\frac{\partial^2\Delta^{(1)}(x'-x)}{\partial x_\rho'\partial x_\lambda'}\Big)\delta(x'-x)\Big)A_\nu(x')d\omega'.$$

$\delta(x'-x)$ here denotes the 4-dimensional δ-function $\delta(x_1)\delta(x_2)\partial(x_3)\delta(x_4)$. We take the spin 0 case as an example. The spurs of the matrix products are evaluated by the method given by Harish-Chandra[9]

$$\langle j_\mu(x)\rangle=\frac{e^2}{\hbar}\int_{-\infty}^{\infty}d\omega'A_\nu(x')\Big(\frac{\partial\bar\Delta(x'-x)}{\partial x_\mu'}\frac{\partial\Delta^{(1)}(x'-x)}{\partial x_\nu'}$$
$$+\frac{\partial\bar\Delta^{(1)}(x'-x)}{\partial x_\nu'}\frac{\partial\bar\Delta(x'-x)}{\partial x_\nu'}-\bar\Delta(x'-x)\frac{\partial^2\Delta^{(1)}(x'-x)}{\partial x_\mu'\partial x_\nu'}$$
$$-\Delta^{(1)}(x'-x)\frac{\partial^2\bar\Delta(x'-x)}{\partial x_\nu'\partial x_\mu'}-\delta_{\mu\nu}\Delta^{(1)}(x'-x)\delta(x'-x)\Big).$$

Put

$$K_{\mu\nu}(\xi)=\frac{\partial\Delta^{(1)}(\xi)}{\partial\xi_\mu}\frac{\partial\bar\Delta(\xi)}{\partial\xi_\nu}+\frac{\partial\Delta^{(1)}(\xi)}{\partial\xi_\nu}\frac{\partial\bar\Delta(\xi)}{\partial\xi_\mu}$$
$$-\bar\Delta(\xi)\frac{\partial^2\Delta^{(1)}(\xi)}{\partial\xi_\mu\partial\xi_\nu}-\Delta^{(1)}(\xi)\frac{\partial^2\bar\Delta(\xi)}{\partial\xi_\mu\partial\xi_\nu}-\Delta^{(1)}(\xi)\delta(\xi),$$

$$K_{\mu\nu}(\mathrm{p})=\int_{-\infty}^{\infty}K_{\mu\nu}(\xi)e^{-\epsilon\rho\xi}d^4\xi,$$

$$K_{\mu\nu}(\mathrm{p})=\frac{1}{(2\pi)^3}\int_{-\infty}^{\infty}d^4q\frac{\delta(q^2+\kappa^2)}{(q-p)^2+\kappa^2}((q_\mu-p_\mu)q_\nu+(q_\nu-p_\nu)q_\mu+q_\mu q_\nu+(q_\mu-p_\mu)(q_\nu-p_\nu)-\delta_{\mu\nu}((q-p)^2+\kappa^2)),\quad(4.6)$$

$$\delta(q^2+\kappa^2)=\frac{1}{2\pi}\int_{-\infty}^{\infty}\exp[ia(q^2+\kappa^2)]da,$$

$$\frac{1}{q^2+\hbar^2}=\frac{-i}{2}\int_{-\infty}^{\infty}\frac{b}{|b|}\exp[ib(q^2+\kappa^2)]db.$$

[9] Harish-Chandra, Proc. Roy. Soc. 186, 502 (1946).

$$K_{\mu\nu}(p)=-\frac{i}{4\pi(2\pi)^3}\int_{-\infty}^{\infty}dadb\frac{b}{|b|}$$
$$\times\exp\left(i(a+b)Q^2+\frac{iab}{a+b}p^2+i(a+b)\kappa^2\right)$$
$$\times\left(\left(\frac{a-b}{a+b}\right)^2 p_\mu p_\nu-\frac{2(a-b)}{(a+b)}\right.$$
$$\left.\times(Q_\mu p_\nu+Q_\nu p_\mu)+4Q_\mu Q_\nu\right)$$
$$-\frac{1}{(2\pi)^4}\int_{-\infty}^{\infty}dad^4q\exp(\partial aq^2+ia\kappa^2)\delta_{\mu\nu} \quad (4.7)$$
$$=\frac{1}{64\pi^2}\int_{-\infty}^{\infty}dz\int_{-1}^{1}dy\frac{z}{|z|}$$
$$\times\exp\left(\frac{i}{4}z(1-y^2)p^2+iz\kappa^2\right)\left(\frac{y^2}{z}p_\mu p_\nu+2\delta_{\mu\nu}\frac{i}{z^2}\right)$$
$$-\frac{i\pi^2}{(2\pi)^4}\int_{-\infty}^{\infty}da\frac{a}{|a|}\frac{\exp iak^2}{a^2}, \quad (4.8)$$
$$=\frac{1}{64\pi^2}\int_{-\infty}^{\infty}dz\int_{-1}^{1}dy\frac{z}{|z|}$$
$$\times\exp\left(\frac{1}{4}z(1-y^2)p^2+iz\kappa^2\right)\frac{y^2}{z}(p_\mu p_\nu-\delta_{\mu\nu}p^2). \quad (4.9)$$

Equation (4.8) is got from (4.7) by the substitution

$$a=\tfrac{1}{2}z(1+y), \quad b=\tfrac{1}{2}z(1-y).$$

Equation (4.9) is got from (4.8) by a partial integration with respect to y. Equation (4.8) shows directly that the photon self-energy is zero, because for a free photon $p^2=0$ and the $p_\mu p_\nu$ term gives zero because of the gauge condition. If $A_\nu(x)$ is an external field varying sufficiently slowly

$$\langle j_\mu(x)\rangle=\frac{1}{3}\frac{e^2}{16\pi^2\hbar c}(-\gamma-\log\kappa^2\epsilon)J_\mu(x)$$
$$-\frac{e^2}{32\pi^2\hbar c}\frac{1}{15k^2}\Box^2 J_\mu(x), \quad \epsilon\to 0.$$

It is interesting that Wentzel's objection does not hold in the spin 0 case.

5. MESON SELF-ENERGY

In the evaluation of the electron self-energy by Schwinger and Feynman a "false vacuum" of the electromagnetic field is used. The use of this false vacuum does not seem to affect physical results, and it gives the same electron self-energy as is got by traditional methods. In the electron self-energy case Schwinger justifies its use by an argument involving gauge transformations. A similar argument to justify the false vacuum has been carried through in the meson self-energy case. The mathematics of this argument varies from Schwinger's in the kind of way that the treatment given here of gauge invariance and vacuum polarization varies from the electron case. The argument is thus straightforward and tedious. In this section the validity of the false vacuum will be assumed.

For a system consisting of one meson the first-order term $-(1/c)s_\mu(x)A_\mu(x)$ in $H(x\sigma)$ (Eq. (2.14)), gives only virtual transitions. So this term can be eliminated from the equation of motion by the usual canonical transformation. Thus taking into account the virtual nature of the processes involved the equation of motion becomes, to the second order in the coupling constant

$$i\hbar c\frac{\delta\Psi(\sigma)}{\delta\sigma(x)}=\left(-\frac{i}{4\hbar c^3}\int_{-\infty}^{\infty}[s_\mu(x)A_\mu(x),\, s_\nu(x')A_\nu(x')]\right.$$
$$\left.\times\epsilon(\sigma\sigma')d\omega'-\frac{ie}{\kappa\hbar c^2}q_{\mu\nu}(x)A_\mu(x)A_\nu(x)\right)\psi(\sigma). \quad (5.1)$$

To evaluate the meson self-energy we must pick out the one particle part of the operator on the R.H.S. of (5.1). After some reduction it turns out to be

$$-\frac{e^2}{4}\int_{-\infty}^{\infty}\bar{D}(x-x')[\bar{\psi}(x)\beta_\mu T^{(1)}(x-x')\beta_\mu\psi(x')$$
$$+\bar{\psi}(x')\beta_\mu T^{(1)}(x'-x)\beta_\mu\psi(x))_1$$
$$-\frac{e^2}{4}\int_{-\infty}^{\infty}D^{(1)}(x-x')(\bar{\psi}(x)\beta_\mu\bar{T}(x-x')\beta_\mu\psi(x')$$
$$+\bar{\psi}(x')\beta_\mu\bar{T}(x'-x)\beta_\mu\psi(x))_1 \quad (5.2)$$
$$+\frac{e^2}{2k}\int_{-\infty}^{\infty}(\bar{\psi}(x)\beta_\mu\beta_\mu D^{(1)}(x'-x)\psi(x))_1\delta(x'-x),$$

where

$$\left.\begin{matrix}\bar{T}(\xi)\\ T^{(1)}(\xi)\end{matrix}\right\}=\left(\beta_\mu\frac{\partial}{\partial\xi_\sigma}-\frac{1}{\kappa}\beta_\mu\beta_\nu\frac{\partial^2}{\partial\xi_\mu\partial\xi_\nu}\right)\left\{\begin{matrix}\bar{\Delta}(\xi)\\ \Delta^{(1)}(\xi)\end{matrix}\right. \quad (5.3)$$

Put

$$L(\xi)=\beta_\mu\bar{D}(\xi)T^{(1)}(\xi)\beta_\mu+\beta_\mu D^{(1)}(\xi)\bar{T}(\xi)\beta_\mu$$
$$-(1/\kappa)\beta_\mu\beta_\mu D^{(1)}(\xi)\delta(\xi), \quad (5.4)$$

and take a momentum representation defined by

$$L(p)=\int_{-\infty}^{\infty} L(\xi)e^{-ip\xi}d^4(\xi), \tag{5.5}$$

$$L(p)=\frac{1}{(2\pi)^3}\int d^4q\left(\frac{\delta(q^2+\hbar^2)}{(q-p)^2}+\frac{\delta(q-p)^2}{q^2+\hbar^2}\right)\beta_\mu \times\left(\beta_\rho iq_\rho-\frac{1}{\kappa}\beta_\rho\beta_\lambda iq_\rho iq_\lambda\right)\beta_\mu -\frac{1}{\kappa}\frac{1}{(2\pi)^3}\int\delta(q^2)d^4q\beta_\mu\beta_\nu. \tag{5.6}$$

We use Fourier integrals (4.6) for all the inverse and δ-functions in the above, and the fact that for a self-energy evaluation $\beta_\rho ip_\rho+\kappa=0$ when the β_ρ is operating on the right or on the left of the $L(\xi)$.

$$L=-\frac{1}{3}\frac{\kappa}{64\pi^2}(\gamma+\log\kappa^2\epsilon)(20+4\beta_\mu\beta_\mu(\beta_\nu\beta_\nu-5)) +\frac{\kappa}{64\pi^2}(-16+4\beta_\mu\beta_\mu(\beta_\nu\beta_\nu-5)) -\frac{1}{3}\frac{i}{32\pi^2\kappa z^2}\beta_\mu\beta_\mu(\beta_\nu\beta_\nu+7),$$

$$\epsilon\to 0,\quad z\to 0.$$

z is a quantity of the dimensions of a length.

In the scalar meson and vector meson cases $\beta_\mu\beta_\mu(\beta_\nu\beta_\nu-5)$ takes the values -4 and -6, respectively. Some justification is perhaps needed for the way in which the last term in (5.4) has been treated by expressing it in the form of a Fourier integral, and then reversing orders of integration. It might seem more natural to say that this term was proportional to $D^{(1)}(0)$, which may be evaluated as a quadratically divergent quantity. But though a term of the form $D^{(1)}(\xi)\delta(\xi)$ only appears explicitly in the last term of (5.4) it may be implicit in the other terms. For example, if the scalar meson representation of the β's is taken then part of the second term of 5.4 is of the type $(\partial^2\Delta(\xi)/\partial x_\rho\partial x_\rho)D^{(1)}(\xi)$. And this is $(\kappa^2\bar{\Delta}(\xi)-\delta(\xi))\times D^{(1)}(\xi)$. So it is reasonable to treat the last term in (5.4) on the same footing as all the rest.

Thus finally one gets for the self-energy operator

$$-\frac{e^2}{4}(\bar{\psi}(x)L\psi(x))_1. \tag{5.7}$$

That this is a mass renormalization can be seen by taking particular representations of the β's. In the scalar and vector cases (5.7) is respectively

$$a\phi^x(x)\phi(x)+b\frac{\partial\phi^*(x)}{\partial x_\mu}\frac{\partial\phi(x)}{\partial x_\mu},$$

and

$$A\phi_\mu{}^*(x)\phi_\mu(x)+B\left(\frac{\partial\phi_\mu{}^*}{\partial x_\nu}-\frac{\partial\phi_\nu{}^*}{\partial x_\mu}\right)\left(\frac{\partial\phi_\mu}{\partial x_\nu}-\frac{\partial\phi_\nu}{\partial x_\mu}\right),$$

and these give rise to a mass renormalization to the first order in e^2.

6. CONCLUSION

It is seen that the interaction representation can be used to describe the electromagnetic field interacting with the charged mesons described by β-matrix theory. The expression for the vacuum polarization can be evaluated explicitly taking any particular meson of the general type dealt with. In particular it is found that the photon self-energy with respect to any of these mesons is zero. The meson self-energy is evaluated.

The question of radiative corrections to observable processes is rather more complicated than in quantum electrodynamics, and it is hoped to deal with some such corrections in a succeeding paper.

In conclusion I would like to thank Dr. N. Kemmer for his help and encouragement in this work.

Measurement of Electron-Ion Recombination*

MANFRED A. BIONDI** AND SANBORN C. BROWN
Research Laboratory of Electronics, Massachusetts Institute of Technology, Cambridge, Massachusetts
(Received August 5, 1949)

Microwave techniques are applied to the measurement of the recombination between electrons and positive ions. The measured recombination coefficients for monatomic gases range from 1.7×10^{-8} cc/ion-sec. for helium to 3×10^{-7} cc/ion-sec. for argon. The recombination coefficients for diatomic gases range from 2.5×10^{-6} cc/ion-sec. for hydrogen to 2.8×10^{-7} cc/ion-sec. for oxygen. At electron temperatures of 300°K, the recombination is found to be independent of pressure for the monatomic gases. A pressure dependence is observed in diatomic gases, the recombination increasing with increasing pressure in nitrogen and oxygen.

RECOMBINATION between electrons and positive ions has been studied semiquantitatively over a period of years. In the present experiment, microwave techniques are used to obtain quantitative measurements of recombination coefficients for a number of monatomic and diatomic gases.

I. EXPERIMENTAL METHOD

The recombination is measured by observing the decay of electron density from an initially ionized gas. The details of the method have been described in an earlier paper.[1] The electron density is determined from the change in resonant frequency of a microwave cavity enclosing the electrons. Under proper experimental conditions, the change of resonant frequency, $\Delta\nu$, is linearly proportional to the electron density within the cavity

$$\Delta\nu=\nu-\nu_0=Cn_-,$$

where ν is the resonant frequency of the cavity containing electrons; ν_0 is the resonant frequency of the cavity in the absence of electrons; C is a geometrical coefficient which takes into account the distribution of electrons and electric field within the cavity, and n_- is the average electron density within the cavity.

The gas sample is contained in a quartz bottle placed within a TM_{010}-mode cavity which is resonant at approximately 3000 Mc/sec. An electrodeless discharge is produced within the bottle by the application of a large microwave field to the cavity by means of a magnetron. The discharge is terminated by turning off the magnetron, and the electrons and ions remaining come to equilibrium with the gas in less than 50 μsec. Their energies from this time on are therefore thermal. If the gas pressure is sufficiently high, the diffusion loss of electrons and ions to the walls of the bottle will be small compared to the loss by volume recombination. As a result, the electron density decays with time in a manner characteristic of recombination loss. We determine the decay of electron density during the interval by measuring the resonant frequency of the cavity as a function of time.

II. MEASUREMENTS

The rate of removal of electrons or ions by recombination is given by

$$\partial n_-/\partial t=\partial n_+/\partial t=-\alpha n_+n_-$$

where n refers to charge density and α is the recombination coefficient. Under experimental conditions, $n_+\simeq n_-$, so that we have

$$\partial n/\partial t=-\alpha n^2,$$

whose solution is

$$1/n=1/n_0+\alpha t,$$

where n_0 is the electron density at time $t=0$.

Experimentally, it was found that plots of $1/n$ *vs.* t were linear, and it was concluded that recombination was taking place. However, the recombination coefficients obtained from the data were several orders of magnitude greater than those previously reported in the literature. To test the hypothesis that recombination was taking place, a search was made for light emitted from the ionized gas after the ionizing field was removed. An afterglow was found which lasted for more than 4000 μsec. after the discharge was terminated. This prolonged afterglow is most simply explained on the basis of radiative recombination.

III. RECOMBINATION IN MONATOMIC GASES

The results of measurements of electron removal in helium have been presented previously.[1] The value of the recombination coefficient at an electron temperature $T=300$°K was found to be 1.7×10^{-8} cc/ion-sec. The value was obtained with several different samples of helium and is believed to be accurate to 5 percent.

Neon has been studied most extensively for two reasons; the commercially prepared gas samples are sufficiently pure to give reproducible results for many different samples of neon, and recombination is the dominant electron removal process over a wide range of experimental variables. An example of the accuracy possible in the determination of α is illustrated by the data shown in Fig. 1. The slope of the curve can be

* This work has been supported in part by the Signal Corps, the Air Materiel Command, and ONR.
** Now at Westinghouse Research Laboratories, East Pittsburgh, Pennsylvania.
[1] M. A. Biondi and S. C. Brown, Phys. Rev. 75, 1700 (1949).

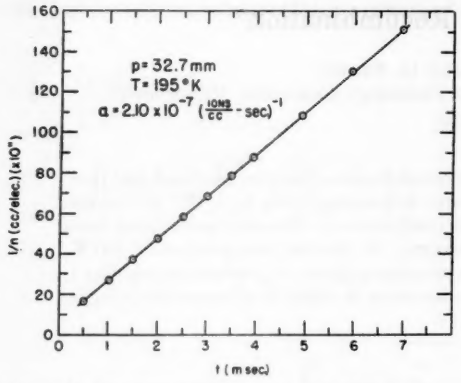

FIG. 1. Electron-ion recombination in neon at $T=195°K$.

determined very accurately so that the measurements of the recombination as a function of energy, which will be discussed shortly, are quite accurate.

The variation of the recombination coefficient with pressure was studied first. At $T=300°K$, there was no observed variation over the range $p=15$ mm Hg to 30 mm Hg. The value of α is $2.07\pm0.05\times10^{-7}$ cc/ion-sec. Next, the variation of α was studied over a temperature range from $T=300°K$ to 410°K. No change in α with temperature was found. (The maximum change observed was 5 percent but did not follow a consistent trend.)

No variation having been found in the recombination coefficient at elevated temperatures, the behavior of α as a function of pressure was studied at the temperature of dry ice (195°K) and liquid nitrogen (77°K). At 195°K, no variation in α with pressure was found, and the value of α was found to be the same at 195°K as at 300°K. At 77°K, a change in the behavior was noted. The value of the recombination coefficient increased with increasing pressure; however, at low pressures, the value of α approached the same value as at 195° and 300°K. These results are shown in Figs. 2 and 3. Figure 2 indicates that the recombination is independent of pressure at 195°K and 300°K over the measured range. At 77°K, a strong pressure dependence develops; however, the residual value of α (the value of α in the limit $p\rightarrow0$) is the same as for $T=195°$ and 300°K. Empirically, it is found that the recombination coefficient at 77°K is given by

$$\alpha=\alpha_r+Ae^{bp},$$

where

$$\alpha_r=1.94\times10^{-7} \text{ cc/ion-sec.}$$
$$A=0.13\times10^{-7} \text{ cc/ion-sec.}$$
$$b=0.16 \text{ (mm Hg)}^{-1}.$$

α_r is called the residual part of the recombination coefficient since it does not seem to depend on energy or pressure. The pressure dependent part, $\alpha(p)=Ae^{bp}$, is shown in Fig. 4. No physical explanation for the exponential character of the pressure dependent part of α is available at present; however, attempts to fit the data to a $p^n(n=1, 2, 3, 4)$ type of dependence do not give a reasonable result.

The measurements of argon are of a less satisfactory nature because we have been unable to obtain sufficiently pure gas samples to give adequately reproducible results. However, by averaging the data obtained from a number of samples of argon, we find that the residual part of the recombination coefficient is approximately

$$\alpha_r=3\times10^{-7} \text{ cc/ion-sec.}$$

at $T=300°K$.

The values of the coefficient of recombination between thermal electrons and ions are several orders of magnitude greater than those previously reported in the literature.[2,3] The value of α increases with increasing mass number. Except at low temperatures, α appears to be independent of pressure over the measured range, and in neon is also independent of temperature.

IV. RECOMBINATION IN DIATOMIC GASES

Over the measured range, the recombination coefficient for hydrogen is found to be independent of pressure at $T=300°K$. The results are shown in Fig. 5. Studies of the energy dependence of α for hydrogen in the temperature range from 303°K to 413°K indicate that α varies as $1/T^k$ where the value of k is between 0.8 and 0.9.

The recombination coefficient for nitrogen is about half the value for hydrogen and a rise in the recombination coefficient is noted with increasing pressure (see Fig. 5). A more marked pressure dependence is observed in oxygen and the residual value of α is about one-fifth the value for nitrogen.

The behavior of the recombination coefficients for diatomic gases is quite different from that for monatomic gases. We find a dependence of α on temperature for hydrogen, while for neon we found that the residual value of α is independent of temperature. In addition,

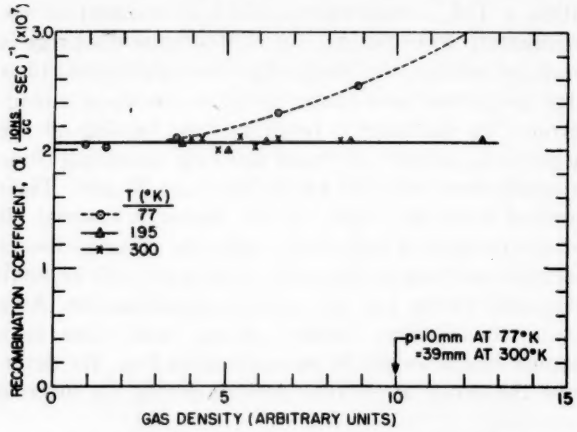

FIG. 2. Recombination in neon as a function of gas density and temperature.

[2] F. L. Mohler, Phys. Rev. 31, 187 (1928).
[3] C. Kenty, Phys. Rev. 32, 624 (1928).

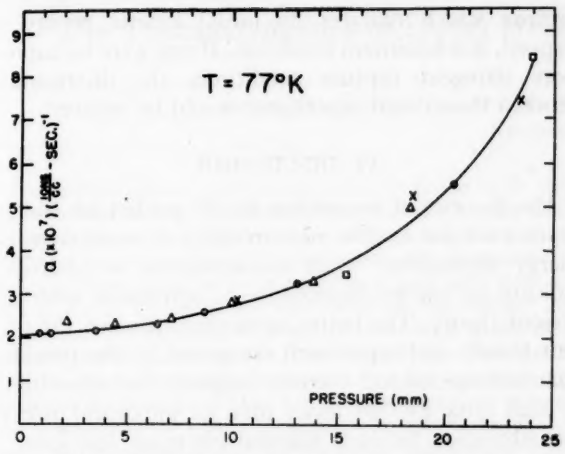

FIG. 3. Recombination in neon at the temperature of liquid nitrogen.

the recombination coefficients are observed to increase with increasing atomic number for monatomic gases while they decrease with increasing atomic number for diatomic gases.

The lack of pressure dependence for the recombination at low pressures indicates that this recombination is a two-body process involving the direct capture of the electron by the ion. In monatomic gases, the capture is believed to be by radiative transitions of the electron into excited levels of the resulting atom. However, the fact that the recombination coefficient for hydrogen is more than 100 times that of helium indicates that there exists for diatomic ions a capture mechanism which is much more efficient than radiative capture. The spacing of the vibration and rotation levels of diatomic ions is the same order of magnitude as the average electron energy. It is suggested that these levels offer an efficient means of absorbing the electron's initial kinetic energy into vibration and rotation energy of the resulting excited molecule. The subsequent radiation of quanta removes enough energy from the excited molecule to prevent dissociation into an electron and an ion.

V. THEORY

The existing theories of recombination[4–6] predict electron-ion recombination coefficients which are 10^4 times smaller than the values reported here. The theories formulate quantum mechanically the transition probability of electrons with positive initial energy into excited levels of the resulting atom. From these theories, it is concluded that the significant contributions to the recombination come from transitions to ground state and the low lying excited levels. Craggs and Hopwood[6] compare their measurement of the recombination of electrons with H^+ with theory and conclude that transitions to ground state are sufficient to account for their observed value. In the present experiment, we do not arrive at this conclusion. We shall calculate the recombination arising from the transitions of electrons into the highest excited states by computing the continuous radiation emitted by an electron accelerated in the field of the ion.

The calculations of Kramers and Eddington[7] on opacity and absorption cross sections may be adapted to this method. If we require that an electron of initial velocity, v, radiate its initial kinetic energy or more in order to be captured, we can calculate a critical capture orbit, and, from this, the capture cross section. The capture cross section for thermal electrons is given by

$$\sigma = 8.64\left\{\frac{Z_e^{8/5}e^4}{m^2c^{6/5}v^{14/5}}\right\}\text{cm}^2$$

where σ is the capture cross section; Z_e is the effective charge of the ion; e and m are the electron charge and mass, respectively, and c is the velocity of light.

The coefficient of recombination for monoenergetic electrons of velocity, v, is given by $\alpha(v)=\sigma v$. The observable recombination coefficient $\alpha(T)$ is obtained by averaging the recombination over the Maxwellian energy distribution of the electrons; thus

$$\alpha(T) = 14.5(m/2kT)^{0.9}\left\{\frac{Z_e^{8/5}e^4}{m^2c^{6/5}}\right\}\text{cc/ion-sec.}, \qquad (1)$$

where T is the electron temperature.

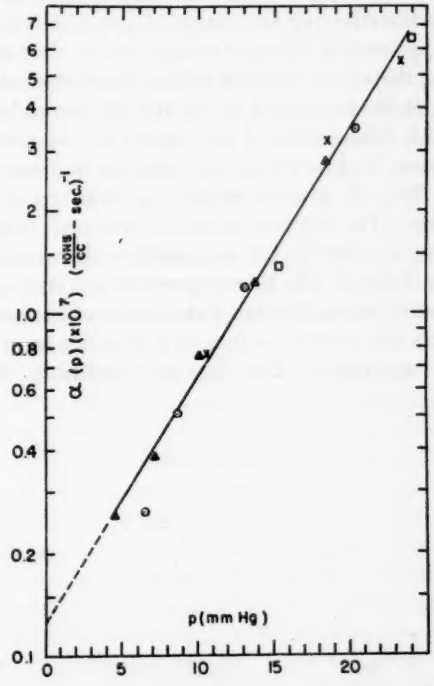

FIG. 4. The pressure-dependent part of the recombination coefficient for neon at $T=77°$K.

[4] See, for example, P. M. Morse and E. C. G. Stueckelberg, Phys. Rev. **35**, 116 (1930).
[5] H. Zanstra, Proc. Roy. Soc. **A186**, 236 (1946).
[6] J. D. Craggs and W. Hopwood, Proc. Phys. Soc. **59**, 771 (1947).
[7] A. S. Eddington, *The Internal Constitution of the Stars* (Cambridge University Press, London, 1926), p. 224.

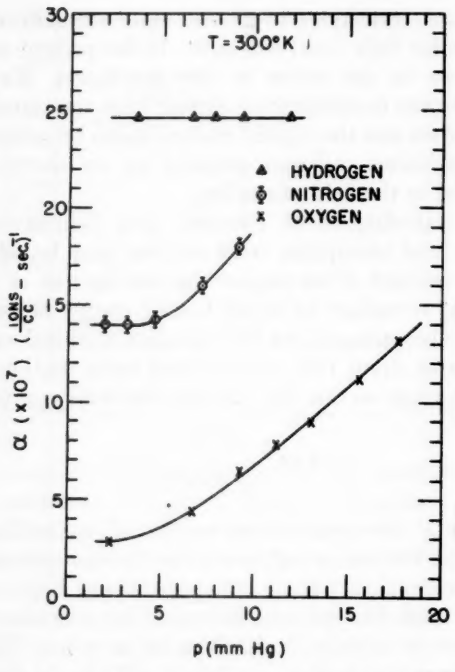

FIG. 5. Recombination in diatomic gases at $T=300°K$.

It is found that according to the classical calculation, the electron's orbit penetrates the electronic shell of the ion and hence the electron is accelerated in a field arising from a variable charge. Using the quantum-mechanical model of the helium ion and the Thomas-Fermi model for the neon and argon ions, we may calculate the effective ion charge, Z_e, at the distance of closest approach of the electron to the ion. For thermal electrons, the value of Z_e for helium is approximately 2, for neon, it lies between 8 and 9 and for argon, between 11 and 13. Since most of the energy is radiated while the electron is close to the ion, the use of these values of Z_e in Eq. (1) introduces only a small error in the calculation. The values of $\alpha(T)$ obtained from this theory for $T=300°K$ are compared with experimental values in Table I. The theory predicts an order of magnitude more recombination than is observed; however, it predicts the relative values of α in going from He to A quite accurately. The capture condition, that an electron which radiates its initial kinetic energy is trapped, is a minimum condition. If one were to impose more stringent capture conditions, the discrepancy between theory and experiment would be reduced.

VI. DISCUSSION

The theories of recombination all predict an energy dependence for α. The measurements in neon show no energy dependence while measurements in hydrogen indicate an energy dependence in agreement with the present theory. The better agreement between the present theory and experiment compared to the previous quantum-mechanical theories suggests that transitions to high lying excited levels play an important role in recombination between thermal electrons and ions. A quantum-mechanical theory which accurately takes into account this process is necessary.

The measured recombination coefficients for monatomic and diatomic gases lie in the range 10^{-8} to 10^{-6} cc/ion-sec. These values are several orders of magnitude greater than previous experimental values and are of the order of previously reported values of positive ion–negative ion recombination coefficients. However, the present experiment measures the removal of electrons since the apparatus is sensitive to electrons and ions in the inverse ratio of their masses.

TABLE I. Recombination coefficients at $T=300°K$.

Gas	$\alpha[T]$(theory)	α(measured)	Ratio of values
He	2.0×10^{-7}	1.7×10^{-8}	12
Ne	2.2×10^{-6}	2.03×10^{-7}	11
A	3.3×10^{-6}	3×10^{-7}	11

The gas samples used were obtained from the Air Reduction Sales Company. The vacuum system was of glass and quartz and used a mercury McLeod gauge and a mercury cut-off. The system was thoroughly outgassed before each run and held for several hours at 10^{-7} mm Hg when isolated from the pumps. The helium and neon samples were purified by a liquid nitrogen-cooled charcoal trap while the other gases were passed through two liquid nitrogen traps.

The Thermodynamics of Liquid Helium on the Basis of the Two-Fluid Theory

O. K. RICE
Department of Chemistry, University of North Carolina, Chapel Hill, North Carolina
(Received June 27, 1949)

The thermodynamics of liquid helium is developed in the light of the two-fluid theory, which says that below the λ-point liquid helium consists of two "phases," one a superfluid phase and one a phase of normal fluid; and the thermodynamic consequences of assuming these phases to be in equilibrium with each other are worked out. It is pointed out that there is some evidence that these phases are separated not only in momentum space, as in London's theory based on the Bose-Einstein gas, but also in ordinary space. The specific heat just above the λ-point is considered on the assumption that in this region superfluid is beginning to appear in the form of small globules; it is estimated that these globules contain around 60 to 80 helium atoms. The thermodynamic properties below the λ-point are used to estimate the entropy of mixing of the two fluids in this region. The results suggest that in this region the superfluid forms a "partially condensed system," having possibly a fibroid structure. The nature of the second-order transition at the λ-point is considered in the light of this picture. A new relation is derived for the change of the λ-point with pressure, and the change with concentration of He^3 is also considered. The thermodynamic results, though discussed in the light of the hypothesis that the two phases separate in ordinary space as well as momentum space, depend for the most part only on pure thermodynamics and the mere existence of two phases.

1. INTRODUCTION

IN discussing the properties of liquid helium Tisza[1] has suggested the hypothesis that below the λ-point helium may be considered to be a mixture of a "normal" and a "superfluid" phase. These phases were presumably thought of as separated in momentum space, in conformity with London's[2] theory that the λ-point is a manifestation of the condensation in momentum space which is characteristic of a Bose-Einstein gas. Recently London and Rice[3] have considered experimental data[4] on the vapor pressures of solutions of He^3 in He^4, and have interpreted these data as indicating that each atom of He^3 in these solutions is surrounded by a globule of superfluid He^4.

It now appears,[5] however, that the experimental data on which these conclusions were based, were not obtained under conditions such that equilibrium was established. More recent experiments[6] indicate that the partial pressure of He^3 and He^4 in equilibrium with the liquid solution are such as would be predicted from Raoult's law, provided that the He^3 dissolves only in the normal part of the He^4 and is excluded from the superfluid. While this conclusion is diametrically opposite to that reached by London and Rice from the earlier experiment, it suggests, remarkably enough, one thing that might also have been inferred from their conclusions; namely, it makes it seem probable that there is a separation of superfluid and normal liquid in ordinary space, as well as in momentum space.

This idea is indeed hard to prove, but it does not appear inherently unreasonable. The exact energy levels for the helium depend upon the boundary conditions to which the corresponding wave functions are subjected. These are very simple in the case of the perfect gas; the only boundary conditions are those arising at the walls of the container, and the large extension in space results in a very low lying level of definite energy into which many atoms can go when the Bose-Einstein condensation takes place. On the other hand, the boundary conditions in a liquid of interacting atoms are much more complicated. It is unlikely that single wave functions can extend, without interference or scattering, from wall to wall. Thus the lower energy levels would be in general, raised, and there would scarcely be one lowest energy level into which, ultimately, all of the atoms could go. It is not at all impossible that more favorable boundary conditions, with lower total energy, would be attained by segregation of those atoms which are in the lowest levels available to them. These segregated atoms would thus form the superfluid. Near the λ-point this segregated superfluid would nevertheless be pretty well scattered through the body of the normal fluid, except for its tendency to collect near the walls, giving rise to the Rollin film. It is to be noted that this hypothesis is not in conflict with London's idea of the Bose-Einstein condensation, but is merely meant to supplement it.

While it is admitted that the hypothesis that the superfluid and normal phase separate in ordinary space is highly speculative, it seems desirable to explore every lead in the rather difficult problem of liquid helium, and we shall attempt to characterize it more closely with the aid of the specific heat data, which have been collected by Keesom.[7] Above the λ-point, the specific heat is practically constant at 0.55 cal. g^{-1} deg.$^{-7}$ until the temperature has been reduced to about 0.1° above the λ-point, at which point, as the temperature is further reduced, it increases rapidly to a value of perhaps 1.2 cal. g^{-1} deg.$^{-1}$ at the λ-point. At the λ-point it is

[1] L. Tisza, Phys. Rev. **72**, 838 (1947); Nature **141**, 913 (1938), and other papers. See also L. Landau, J. Phys. U.S.S.R. **5**, 71 (1941).
[2] F. London, Nature **141**, 643 (1938); Phys. Rev. **54**, 947 (1938).
[3] F. London and O. K. Rice, Phys. Rev. **73**, 1188 (1948).
[4] Fairbank, Lane, Aldrich, and Nier, Phys. Rev. **73**, 729 (1948).
[5] Lane, Fairbank, Aldrich, and Nier, Phys. Rev. **75**, 46 (1949).
[6] Taconis, Beenakker, Nier, and Aldrich, Phys. Rev. **75**, 1966 (1949).
[7] W. H. Keesom, *Helium* (Elsevier Publishing Company, Inc., New York, 1942). See especially Fig. 4.15, p. 215, and Table 4.21, p. 217.

generally supposed that it takes a jump-up of about 1.7 to 1.9 cal. g^{-1} deg.$^{-1}$. Below the λ-point it decreases fairly rapidly, becoming practically zero a degree or so below.

An ideal gas obeying the Bose-Einstein statistics shows no break in the specific heat curve at the Einstein condensation temperature, but only a change in slope. The specific heat shows an increase as the temperature is decreased to the condensation temperature, but the increase is slight, and does not resemble that actually found as the λ-point in helium is approached. It is not too difficult to find special models[8] which will give a break at the λ-point, and will in general give a fair representation of the specific heat curve, though as far as I know the curve just above the λ-point has not been reproduced very well. The possibilities along this line can hardly be said to have been exhausted; nevertheless, it seems worth while to see what can be done with the assumption that the superfluid is separated in space from the normal liquid.

Since there is no visible separation of phases, but, rather, the phase present in smaller amount is presumably scattered in the form of rather small droplets or globules, the problem becomes one of heterophase fluctuations of the type discussed by Frenkel.[9] The λ-transition is a second-order transition, which means that there is no latent heat, so that the appearance, as fluctuations, of small particles or globules of the other phase would not be expected to affect the specific heat appreciably. However, the fluctuations may involve, rather, appearance of one of the extreme types, superfluid or normal fluid, in a phase which consists principally of the other type.

We shall attempt to apply a theory of the type indicated in the preceding paragraph to a discussion of the specific heat curve just above the λ-point. Below the λ-point, however, there appear to be complications, and we shall give what amounts to a thermodynamic analysis of the experimental data on the basis of a two-fluid or two-component theory. It may be remarked that this thermodynamic treatment is independent of whether or not the superfluid and the normal fluid separate in ordinary space. It may, however, be interpreted in terms of such a separation, and this leads to a further interpretation of the λ-point.

2. THE SPECIFIC HEAT ABOVE THE λ-POINT

Above the λ-point we may consider liquid helium to consist of a very dilute solution of superfluid in ordinary helium. In accordance with the ideas discussed in Section 1, we shall suppose the superfluid to occur in the form of droplets or globules of finite size. There will be an effective lower limit to their size, since according to the hypothesis molecularly dispersed superfluid is not stable. On the other hand, the entropy of mixing of these globules with the normal fluid will be a factor working to cause breaking up of the globules, so that globules appreciably larger than this minimum size will also not be stable. Naturally, we would expect a range of globule sizes; however, we will consider later how this affects the results, and for the present shall consider the globules to be of uniform size.

We shall distinguish thermodynamic quantities belonging to the normal or ordinary fluid by use of a subscript 1, while for the superfluid we shall use the subscript 2. We shall then use the following notation ($i=1$, or 2):

x_i = mole fraction of component i
μ_i = chemical potential of component i
n = number of atoms in a globule of superfluid
H_1 = enthalpy of 1 mole of ordinary helium, based on $H_2=0$
S_1 = entropy of 1 mole of ordinary helium, based on $S_2=0$
F = total Gibbs free energy per mole
R = gas constant
T = absolute temperature = 2.186°K.
T_λ = λ-temperature
S_λ = entropy of helium at $T_\lambda=1.62$ cal. mole^{-1} deg.$^{-1}$ (expt. value)[1,10]
H_λ = enthalpy of helium at $T_\lambda=3.01$ cal. mole^{-1} (expt. value).[10]

We shall suppose that the superfluid occurs in globules of size n, as indicated, and we may then say that in 1 mole of helium the number of moles of superfluid globules is x_2/n. The number of moles of ordinary helium atoms is $x_1=1-x_2$. The "true" mole fraction of superfluid is thus $(x_2/n)/(1-x_2+x_2/n)\sim x_2/n$, while the true mole fraction of normal helium is $(1-x_2)/(1-x_2+x_2/n)\sim 1-x_2/n$, to terms of the first power in x_2. We then write for the free energy of one mole, assuming that H_2 and S_2 remain equal to zero, independently of temperature,[11] and that the heat of mixing

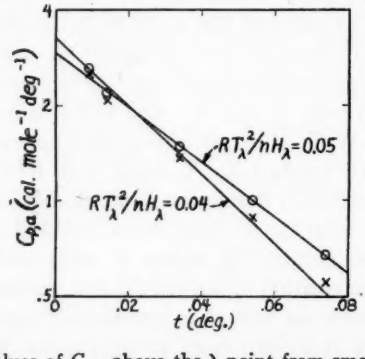

FIG. 1. Values of $C_{p,a}$ above the λ-point from smoothed values of C_p given in Table 4.21 of reference 7. Circles calculated on assumption that $C_p-C_{p,a}=2.20$ cal. mole^{-1} deg.$^{-1}$. Crosses calculated on assumption that $C_p-C_{p,a}=2.32$ cal. mole^{-1} deg.$^{-1}$, to show effect of small errors. $t=T-T_\lambda$ with $T_\lambda=2.190$°K. Lines show calculated slopes of $C_{p,a}$ *vs.* t curves on the logarithmic scale.

[8] See, e.g., F. London, J. Phys. Chem. **43**, 49 (1939); A. Bijl, Physica **7**, 869 (1940); Bijl, de Boer, and Michels, Physica **8**, 655 (1941).

[9] J. Frenkel, J. Chem. Phys. **7**, 538 (1939).

[10] F. London, Rev. Mod. Phys. **17**, 310 (1945). H_λ may be obtained from S_λ. According to London, the entropy of helium below the λ-point is equal to $\alpha T^{5.6}$, where α is a constant. Since $dH=TdS$ we have $dH=5.6\alpha T^{5.6}dT$. Integrating,

$$H_\lambda=(5.6/6.6)\alpha T_\lambda^{6.6}=(5.6/6.6)T_\lambda S_\lambda.$$

[11] Compare Tisza, reference 1, p. 845.

is negligible,

$$F=x_1(H_1-TS_1)+(x_2/n)RT\ln(x_2/n)+x_1RT\ln(1-x_2/n). \quad (1)$$

The last two terms represent the entropy of mixing.[12] F must be made a minimum with respect to variation of x_2. Remembering $dx_2=-dx_1$, we find

$$0=\partial F/\partial x_2=-(H_1-TS_1)+(RT/n)\ln(x_2/n)+RT/n-RT\ln(1-x_2/n)-x_1(1-x_2/n)^{-1}(RT/n)\cong-(H_1-TS_1)+(RT/n)\ln(x_2/n). \quad (2)$$

From Eq. (2) we get

$$x_2=n\exp(nH_1/RT)\exp(-nS_1/R). \quad (3)$$

With H_2 always equal to zero, the total enthalpy may be set equal to x_1H_1. We then have

$$C_p=x_1(\partial H_1/\partial T)_p+H_1(\partial x_1/\partial T)_p \quad (4)$$

where C_p, the specific heat at constant pressure, is essentially equal, in the neighborhood of the λ-point to the specific heat of the liquid at its vapor pressure. Since $x_1\sim1$ near the λ-point, the first term represents the normal specific heat, the second term the anomaly. We may then write

$$C_{p,a}=H_1(\partial x_1/\partial T)_p=-H_1(\partial x_2/\partial T)_p=nH_1{}^2x_2/RT^2 \quad (5)$$

from Eq. (3), taking into account the fact that

$$(\partial H_1/\partial T)_p=T(\partial S_1/\partial T)_p. \quad (6)$$

$C_{p,a}$ is thus directly proportional to x_2. Because of Eq. (6) it is possible to ignore the dependence of H_1 and S_1 on T in Eq. (3), in considering the dependence of x_2 on T over a small range. If we replace T by $T+t$, where t is a small increment, we may write Eq. (3) in the approximate form

$$x_2=n\exp(nH_\lambda/RT_\lambda)\exp(-nS_\lambda/R)\times\exp(-nH_\lambda t/RT_\lambda{}^2). \quad (7)$$

From reference 7, it appears that the specific heat anomaly has a roughly exponential dependence on t just above the λ-point. From Table 4.21 of reference 7 (see Fig. 1) we find that $C_{p,a}$ drops by a factor e in about 0.05°, so

$$0.05nH_\lambda/RT_\lambda{}^2=1. \quad (8)$$

Since H_λ and T_λ are given above, we can now calculate n, and we obtain $n=63$.

From the value of n and using Eq. (5) and Eq. (7), together with the above given values of H_λ, S_λ and T_λ, it is possible to calculate $C_{p,a}$ at the λ-point; this comes out to be 1.6 cal. mole^{-1} deg.$^{-1}$. Experimentally, as seen from Fig. 1, it is about 3 cal. mole^{-1} deg.$^{-1}$. The discrepancy is in the direction to be expected both from the matter discussed in footnote 12 and from the fact that not all the globules will have exactly the same size. Each different size of globule may be considered to be an independent species, since a different state of the system is produced by interchanging two globules of different size. Each one of these species will, therefore, be in equilibrium with the solvent, independently of the others; therefore, if η is the effective range of values of n, the value of x_2 will be multiplied by approximately η, and $C_{p,a}$ will be multiplied by the same factor. In this light the discrepancy between the calculated and experimental values of $C_{p,a}$ at the λ-point obviously appears to be too small. The calculated value of x_2 and hence of $C_{p,a}$ is, however, sensitive to the exact shape of the specific heat curve. Had we estimated 0.04 instead of 0.05, in Eq. (8), we would have obtained $n=79$ and $C_{p,a}=0.33$. This is probably within the possible range of experimental error. The estimate of x_2 and $C_{p,a}$ will also be affected by errors in H_λ and S_λ. Especially if their ratio should be in error by a few percent, $C_{p,a}$ would be altered by an appreciable factor.

Some indication of the probable order of magnitude of η may be obtained by noting how the right-hand side of Eq. (7) varies with n when $t=0$. This is directly proportional to $C_{p,a}/n$ at the λ-point, and as may be seen from the values of $C_{p,a}$ just quoted, $C_{p,a}/n$ varies by a factor of about 5 or 6 as n goes from 63 to 79. We may reasonably say, then, that the effective value of η is of the order of 10.

It will be desirable at this point to make an estimate of x_2 at the λ-point from the experimental value of $C_{p,a}$ at the λ-point. For this purpose we may use Eq. (5), with the average value of n, regardless of the size of η, provided we include in x_2 the total amount of superfluid contributed by globules of all sizes. With $n=79$ and using $C_{p,a}=3$ cal. mole^{-1} deg.$^{-1}$ we find that the "experimental" value of x_2 at the λ-point is 0.04.

3. THE THERMODYNAMIC PROPERTIES BELOW THE λ-POINT

In this section we shall, in addition to that given at the beginning of Section 2, make use of the following

[12] It has been assumed that the entropy of mixing is to be calculated as for a perfect solution. It is possible for the entropy of mixing to deviate considerably from this value when the forces between solvent and solute differ considerably from those between solvent molecules [see, e.g., O. K. Rice, J. Chem. Phys. 15, 875 (1947)]. Not much is known about the case in which the solute consists of an aggregate of molecules which interact with solvent molecules about as the latter interact with each other, but this problem has been discussed in the case in which the aggregate consists of a diatomic molecule dispersed in a monatomic liquid. [See R. H. Fowler and E. A. Guggenheim, *Statistical Thermodynamics* (The Cambridge University Press, New York, 1939), pp. 366 ff.] For a dilute solution of double molecules in single molecules, the formula reduces to that for a monatomic solute except that the mole fraction of diatomic molecules (corresponding to x_2/n with $n=2$) in the logarithm is multiplied by $2/z$, where z is the coordination number in the liquid. $z/2$ is the number of possible orientations of the diatomic molecules, in which each atom in the solute molecule takes the position which would, in pure solvents, be occupied by a solvent atom. With a more symmetrical, even though larger, solute the factor might be expected to be closer to 1. Surface effects are also neglected.

notation:

$\bar{S}_2$ = partial molal entropy of superfluid (equals zero, except for contribution of entropy of mixing)
$\bar{H}_2$ = partial molal enthalpy
$\bar{V}_2$ = partial molal volume of superfluid
S = total entropy of liquid per mole
V = total volume of liquid per mole
p = pressure.

S_1, H_1, S_2, and H_2 (the latter two equal to zero) continue to refer to intrinsic properties of the two "components," i.e., properties of these components in "pure" form.

We make use of the thermodynamic equations,

$$d\mu_2 = -\bar{S}_2 dT + \bar{V}_2 dp + (\partial\mu_2/\partial x_2)_{p,T} dx_2 \tag{9}$$

and

$$dF = -SdT + Vdp. \tag{10}$$

If the normal liquid and the superfluid are in equilibrium with each other, we will have $\mu_2 = \mu_1 = F$. Therefore, from Eqs. (9) and (10), we get at constant pressure[13]

$$(\partial\mu_2/\partial x_2)_{T,p} dx_2/dT = -(S - \bar{S}_2). \tag{11}$$

Equation (11) will hold above as well as below the λ-point, and by introducing the proper expression for $\bar{S}_2$ and μ_2 could be used to get the results of Section 2. Below the λ-point, however, $\bar{S}_2$ and μ_2 apparently do not have the standard form. We shall, therefore, use the experimental results to reverse the procedure.

According to the hypotheses made by Tisza the entropy S below the λ-point is proportional to the amount of helium which has gone over from superfluid to normal fluid, so that we might write $x_1 = S/S_\lambda$. Of course, this is not strictly true, because the entropy of the normal fluid will itself depend upon the temperature, and the entropy of mixing also contributes. However, we may accept it as an approximation. As we have already noted,[10] the entropy is empirically found to be proportional to T^r where r is about 5.6, so that we have

$$1 - x_2 = x_1 = S/S_\lambda = (T/T_\lambda)^r. \tag{12}$$

We therefore have $dx_2/dT = -rx_1/T$. Introducing this and $S = S_\lambda x_1$ into Eq. (11) we obtain

$$(\partial\mu_2/\partial x_2)_{T,p} rx_1/T = S_\lambda x_1 - \bar{S}_2.$$

Since $\mu_2 = \bar{H}_2 - T\bar{S}_2$, and since $\bar{H}_2$ can be taken as zero, we finally obtain

$$(\partial\bar{S}_2/\partial x_1)_{T,p} rx_1 = S_\lambda x_1 - \bar{S}_2. \tag{13}$$

Actually this equation has been derived only for the equilibrium point at any given T and p. It seems reasonable, however, to regard it as a differential equation with x_1 the independent variable and $\bar{S}_2$ the dependent variable. The solution of this equation is

$$\bar{S}_2 = S_\lambda x_1/(r+1) + a/x_1^{1/r}$$

where a is a constant. Since $\bar{S}_2$ must become zero when $x_1 = 0$, we must have $a = 0$. Hence

$$\bar{S}_2 = S_\lambda x_1/(r+1). \tag{14}$$

Equation (14), which may be said to be an empirical expression of the thermodynamic properties of helium II, on the basis of the two-fluid theory, has a rather unusual form. Recalling that $\bar{S}_2$ is solely dependent upon entropy of mixing, we do expect that, when x_2 is nearly 1, and x_1 is consequently very small, we shall find $\bar{S}_2$ to be proportional to x_1. However, when x_2 is small (as it is near the λ-point) we expect $\bar{S}_2$ to vary as $-\ln x_2$, and hence to become infinite as x_2 goes to zero. The fact that $\bar{S}_2$ appears to be approaching a finite value as the λ-point is approached, suggests that in some respects, the superfluid resembles a condensed phase; at least, it does not approach a state of infinite dilution as ordinary solutions do. On the other hand, the fact that the entropy does depend on the concentration suggests that it is not a separate phase of the usual type. Rather it must be partially condensed and at the same time partially dispersed in some way. Possibly it has some kind of branched and interlacing fiber structure. A somewhat similar suggestion has been made by Landau[14] for superconductors. We shall describe a state of this sort as a "partially condensed phase."

It will now be of interest to compare the value of $\bar{S}_2$ at the λ-point (where $x_1 \sim 1$) obtained from Eq. (14) with the value obtained from the considerations of Section 2. Since the total free energy per mole is given by $F = x_1\mu_1 + x_2\mu_2$, we infer from Eq. (1) that in the region just above the λ-point

$$\mu_2 = (RT/n) \ln(x_2/n) \tag{15}$$

or, since $\bar{H}_2 = 0$

$$\bar{S}_2 = -(R/n) \ln(x_2/n). \tag{16}$$

This holds in the region where x_2 is small, as does Eq. (1), and it can be obtained, if desired, by more rigorous methods. x_2/n is the (approximate) mole fraction of superfluid globules, while x_2 is the mole fraction of superfluid counted in terms of single helium atoms. Equation (16) presupposes that there is only one size of globules. If, however, n has an approximate range of η, then the mole fraction of any one of these sizes would be $x_2/n\eta$. Instead of the one term on the right-hand side of Eq. (1) which is proportional to x_2 there would be η such terms, and each one would have the approximate form $(x_2/n\eta)RT \ln(x_2/n\eta)$. Instead of Eq. (16) we, therefore, obtain the approximate relation

$$\bar{S}_2 = -(R/n) \ln(x_2/n\eta). \tag{17}$$

[13] Helium under its own vapor pressure is essentially at zero pressure below the λ-point.

[14] L. Landau, Physik. Zeits. Sowjetunion **11**, 129 (1937), J. Phys. U.R.S.S. **7**, 99 (1943); E. R. Andrew, Proc. Roy. Soc. London **A194**, 98 (1948); I am indebted to Professor D. H. Andrews of Johns Hopkins University for discussing this matter with me.

Evaluating $\bar{S}_2$ at the λ-point, we find from Eq. (17), using the value of x_2 obtained at the end of Section 2

$$\bar{S}_2 \cong -(1.986/79)\ln(0.04/79\times 10)=0.25. \quad (18)$$

From Eq. (14), using $x_1=1$, on the assumption that at the λ-point the fibrous structure of superfluid has disappeared (since the globules are not to be counted as part of the fibrous structure which contributes to the entropy given by Eq. (14)), we get

$$\bar{S}_2 \cong 1.62/6.6=0.25. \quad (19)$$

We thus find the remarkable result that the entropy of mixing gives essentially the same value of $\bar{S}_2$ at the λ-point for the globules which we assume to occur above the λ-point as for the fibrous structure we assume below the λ-point. They should thus both be in equilibrium at the λ-point if they both have the same intrinsic entropy of zero, and the same enthalpy. Of course, Eqs. (18) and (19) rest on approximations, but if the equality is not quite correct it would require a relatively small difference in the enthalpies of the two kinds of superfluid to effect the balance, since the value of $\bar{S}_2$ itself is not large.

As we go below the λ-point, x_2 increasing, the value of $\bar{S}_2$ calculated from Eq. (14) decreases less rapidly than that calculated from Eq. (17). Thus the partial molal entropy of mixing of the fibrous structure will be greater than that of the globules. It seems remarkable that the entropy of mixing of a partially condensed phase should be greater than that of a fully dispersed set of globules, even though the latter are beginning to be present in appreciable concentration. It would seem that this could only be understood if the average diameter of the fibers be supposed to be considerably smaller than the average diameter of the globules, and that this diameter be subject to variation. Then the possibility of different modes of variation of the diameter of the fibers, together with differing methods of twisting and interlacing, might give rise to a relatively high entropy. It is difficult, however, to see how a quantitative calculation could be made.

4. THE NATURE OF THE λ-TRANSITION

If we accept the picture drawn in the last two sections, we can use it to describe the λ-transition in liquid helium. The λ-transition may be considered as a condensation in which the "condensate" is the partially condensed phase with the fibrous structure. The onset of the condensation occurs at that temperature at which the difference between H_1 and TS_1 is just balanced by $\bar{S}_2$ as given by Eq. (14) with $x_1=1$ (H_2 and S_2 of course being zero). (The temperature may be altered, but only very slightly, by the presence of the globules). The temperature T_λ at which the condensation begins is definite and sharp because $\bar{S}_2$ remains finite when $x_1=1$. $\bar{S}_1$ is, of course, just equal to S_1 under these conditions. The condensation merely begins at T_λ and does not all take place at that temperature because $\bar{S}_2$ and $\bar{S}_1$ do depend on the composition, i.e., there is an entropy of mixing. Thus the transition is second order, rather than first order.

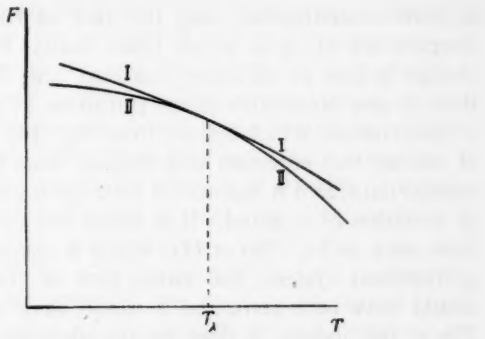

FIG. 2. The free energy as a function of the temperature for liquid He I and He II.

One would expect the globules to continue to form below the transition temperature. If it were not for them the specific heat would presumably decrease more rapidly than it does near the λ-point, a fact we have neglected in the above discussion. However, the effect of the globules probably persists only a little distance below the λ-point. As the partially condensed phase appears, the free volume available to the globules no doubt decreases, so that their entropy of mixing goes down; hence the formation of globules will cease to be favored.

These remarks are particularly interesting in connection with the earlier discussions of the λ-point.[15] If we plot the free energy F as a function of the temperature T for liquid He I and He II (Fig. 2) we get two curves which do not cross, but have a common tangent at the λ-point.[16] If we conceive of He I and He II as two separate phases, each with its own continuous specific heat and compressibility (and hence a continuous curvature for each of the F curves, as well as a continuous slope), these curves could be continued into "metastable" regions, as indicated in Fig. 2. However, if this were done, the free energy for He II would lie below that of He I above as well as below the λ-point. The conclusion which has been reached is that it is impossible to extend the curve for He II above the λ-point. According to our picture this is readily understood. He II contains partially condensed superfluid below the λ-point. At the λ-point the concentration of this partially condensed portion reaches zero; it cannot become negative. This is not essentially different from suggestions which have been made previously, but the behavior of the system is very clearly brought out by the present considerations.

The transition is second order, involving no change in entropy or volume, because at the first temperature at which it appears the condensed phase appears only

[15] See, e.g., Keesom, reference 7, pp. 258–260.

[16] This follows because $(\partial F/\partial T)_p=-S$ and $(\partial F/\partial p)_T=V$. There is a discontinuity in neither S nor V at a second-order transition.

at zero concentration, and the rate of change with temperature of x_2 is at all times finite. The rate of change is also at all times non-zero, and this is why there is any observable phase transition at all. This is a characteristic which follows from Eq. (14). (Actually, of course, this equation was derived from the experimental data, and it has such a form as to give the type of variation of x_2 noted.) If $\bar{S}_2$ below the λ-point had a form such as Eq. (16) or (17) which is characteristic of a dispersed system, the initial rate of change of x_2 would have been zero, and it would have occurred at $T=\infty$ (as, indeed, it does for the globules above the λ-point); thus, there would not have been an observable transition. It is the difference in behavior at $x_2=0$ of Eq. (14) on the one hand, and Eq. (16) or (17) on the other which is crucial.

The more general remarks on the character of the λ-transition as related to the properties of $\bar{S}_2$ are tantamount to a thermodynamic analysis of the two-fluid theory of liquid helium. Though couched in terms of a specific mechanism the thermodynamic conclusions of this paper must be correct if only the two-fluid theory has validity. Thus many of the conclusions may be considered to have a degree of certainty greater than that of the actual mechanism proposed. This will be true of the deductions of the next two sections.

5. THE CHANGE OF THE λ-POINT WITH PRESSURE

The change of the λ-point with pressure dT_λ/dp, or more conveniently, the inverse dp/dT_λ may be related to certain properties of the two phases. Thus by thermodynamic arguments Keesom[17] and Ehrenfest[18] have derived the equation

$$dp/dT_\lambda=\Delta C_p/TV\Delta\alpha, \tag{20}$$

where ΔC_p is the difference in specific heats, $C_{p\mathrm{II}}-C_{p\mathrm{I}}$, and $\Delta\alpha$ is the difference in coefficients of expansion, $\alpha_{\mathrm{II}}-\alpha_{\mathrm{I}}$, the subscript II referring to helium just below the λ-point, and the subscript I referring to it just above the λ-point. The application of this equation has been considered by Keesom[19] in some detail. Keesom takes

$$dp/dT_\lambda=-80.8 \text{ atmos./deg.}, \tag{21a}$$

$$\Delta C_p=7.6 \text{ cal. deg.}^{-1} \text{ mole}^{-1}, \tag{21b}$$

$$V=27.4 \text{ cc/mole}, \tag{21c}$$

and

$$\alpha_{\mathrm{I}}=0.0222 \text{ deg.}^{-1}. \tag{21d}$$

From these experimental values and Eq. (20) he calculates

$$\alpha_{\mathrm{II}}=-0.0426 \text{ deg.}^{-1}. \tag{21e}$$

A line, with slope corresponding to this value, has been placed[19] on the density *vs.* temperature diagram of liquid helium, and this diagram suggests that α_{II} should be perhaps two-thirds of the value given in Eq. (21e). However, this agreement is probably within the limit of the experimental accuracy, and in view of the thermodynamic origin of Eq. (20) it seems certain that it is correct.

The present paper suggests that there should be another relation, based on the hypothesis that the λ-point occurs when

$$F_\lambda=\mu_{2,\lambda}, \tag{22}$$

where the subscript λ is used to indicate the value at the λ-point, and, in particular, for μ_2 and $\bar{S}_2$, the value obtained by setting $x_1=1$ in Eq. (14). Hence as we go along the λ-line

$$dF_\lambda=d\mu_{2,\lambda}$$

or

$$-S_\lambda dT+V_\lambda dp=-\bar{S}_{2,\lambda}dT+\bar{V}_{2,\lambda}dp, \tag{23}$$

whence[20]

$$dp/dT_\lambda=(S_\lambda-\bar{S}_{2,\lambda})/(V_\lambda-\bar{V}_{2,\lambda}). \tag{24}$$

From Eq. (14) we get

$$\frac{dp}{dT_\lambda}=\frac{S_\lambda r}{(r+1)(V_\lambda-\bar{V}_{2,\lambda})}. \tag{25}$$

At first sight it seems natural to suppose $\bar{V}_{2,\lambda}$ should be set equal to the volume of helium at the given pressure and 0°K (this amounts to taking $\bar{V}_{2,\lambda}=V_2$). If we do this, we estimate from density tables[21] that at low pressures $V_\lambda-\bar{V}_{2,\lambda}=-0.19$ cc. mole^{-1}. Using $r=5.6$, and converting to atmospheres, we obtain from Eq. (25), $dp/dT_\lambda=-300$ atmos./deg., very different from Eq. (21a).

However, it does not seem legitimate to assume that[22] $\bar{V}_{2,\lambda}=V_2$. If $\bar{V}_{2,\lambda}$ were equal to V_2, it would seem reasonable to suppose that at any temperature $V-V_2$ should be proportional to the amount of normal fluid present, and this is taken to be roughly proportional to $(T/T_\lambda)^r$. We would thus have

$$V-V_2=(V_\lambda-V_2)(T/T_\lambda)^r \tag{26}$$

and

$$(\partial V/\partial T)_p=r(V-V_2)/T. \tag{27}$$

Evaluating this at the λ-point we find

$$\alpha=V^{-1}(\partial V/\partial T)_p=-0.0177 \text{ deg.}^{-1}, \tag{28}$$

much less than the value of Eq. (21e).

[17] W. H. Keesom, Proc. Roy. Acad. Amsterdam **36**, 147 (1933).
[18] P. Ehrenfest, Proc. Roy. Acad. Amsterdam **36**, 153 (1933).
[19] Keesom, reference 7, p. 256.

[20] We note that $\mu_2=\bar{H}_2-T\bar{S}_2$. We have been setting $\bar{H}_2=H_2=0$, which is satisfactory at constant (essentially zero) pressure, which we have been considering heretofore, and this gives a good reference point for H. However, $\bar{H}_2$ may vary with pressure. We shall suppose that it is equal to H_2 and independent of temperature, which also makes $\bar{S}_2$ independent of temperature, which is usual for an entropy of mixing, though it could not be predicted from Eq. (14). It must be remembered that the latter is a rough empirical representation; in any event, it does not necessarily demand a change in $\bar{S}_2$ with temperature.
[21] Keesom, reference 7, p. 207.
[22] I am much indebted to Professor P. M. Gross of Duke University for suggesting this to me.

Actually it must be noted also that $V-V_2$ should be more closely related to $\alpha_{II}-\alpha_I$ than to α_{II} itself, since the volume of the normal part of the fluid would change with temperature in the normal way below the λ-point and have to be corrected for. We have in fact

$$\begin{aligned}\alpha_{II}&=V^{-1}(\partial V/\partial T)_p\\&=V^{-1}(\partial V/\partial x_2)_{T,p}dx_2/dT+V^{-1}(\partial V/\partial T)_{x_2,p}\\&\cong -V^{-1}r(T/T_\lambda)^rT^{-1}(\partial V/\partial x_2)_{T,p}+\alpha_I,\end{aligned}$$

if we set $x_1=1-x_2=(T/T_\lambda)^r$, and assume that we are at, or sufficiently near, the λ-point so that the last term in the middle line is approximated by α_I. At the λ-point we have

$$\alpha_{II}-\alpha_I=-r(\partial V/\partial x_2)_{T,p}V_\lambda^{-1}T_\lambda^{-1}.$$

Now $V=x_1\bar{V}_1+x_2\bar{V}_2$ and

$$\begin{aligned}(\partial V/\partial x_2)_{T,p}=&-\bar{V}_1+x_1(\partial\bar{V}_1/\partial x_2)_{T,p}+\bar{V}_2\\&+x_2(\partial\bar{V}_2/\partial x_2)_{T,p}=\bar{V}_2-\bar{V}_1.\end{aligned}$$

Now with $x_1\sim 1$ we have $\bar{V}_1=V$, hence at the λ-point we may write approximately

$$\alpha_{II}-\alpha_I=r(V_\lambda-\bar{V}_{2,\lambda})V_\lambda^{-1}T_\lambda^{-1}. \tag{29}$$

Comparing this with Eq. (27) and comparing Eq. (28) with Eqs. (21d) and (21e) suggests that in using Eq. (24) we should evaluate $V_\lambda-\bar{V}_{2,\lambda}$ by multiplying $V-V_2$ by $(0.0222+0.0426)/0.0177$. If this be done we get $-dp/dT_\lambda=82$, in excellent agreement with Eq. (21a). As we have noted, the value of α_{II} given in Eq. (21e) may be a little large, but in any event the discrepancy is no greater for Eq. (24) than for Eq. (20).

The one strange feature is that $\bar{V}_2$ should vary with temperature as much as it evidently does. The difference between $\bar{V}_2$ and V_2 might be ascribed to a surface effect, a little extra space being necessary between the filaments of superfluid and the normal fluid. However, the difference would in any case be expected to remain fairly constant until the concentration of superfluid was so great that the filaments began to coalesce. It must be remembered, however, that the normal fluid must change its properties appreciably in the 0.6° or 0.7° range of temperature in which the greater part of the transition occurs. The specific heat just above the λ-point (sufficiently far above so that $C_{p,a}=0$) is sufficient to remove all the enthalpy of the liquid at the λ-point in a drop of about 1.4°.

6. EFFECT OF He^3 ON THE λ-POINT

If the results[6] which indicate that He^3 dissolves only in the normal fluid, not the superfluid, are correct, it should be possible to predict the effect of solution of He^3 on the λ-point. We use Eq. (22), modified to read

$$\mu_4=\mu_{2,\lambda}. \tag{30}$$

By μ_4 we mean the partial molal free energy or chemical potential of He^4, considered as a single component, in the solution of He^3 and He^4. Since He^3 is insoluble in the superfluid, $\mu_{2,\lambda}$ is unaltered (except as an accompanying temperature change may affect it) by addition of He^3, as the subscript λ implies that the superfluid is at constant (essentially zero) mole fraction; however, μ_4 will depend directly upon x_3, the mole fraction of He^3, or x_4 the mole fraction of He^4. We note that $x_4=x_1+x_2$ where x_1 and x_2 have their usual significance. At constant pressure we may write $d\mu_4=-\bar{S}_4dT+(\partial\mu_4/\partial x_3)_Tdx_3$. At the λ-point we may neglect the small concentration of globules of superfluid and set $x_4=x_1$. Assuming a perfect solution we then have

$$\mu_4=\mu_4^0+RT\ln x_4 \tag{31}$$

where μ_4^0 is the value of μ_4 when $x_4=1$. Whence

$$(\partial\mu_4/\partial x_3)_T=-RT/x_4\cong -RT \tag{32}$$

if the solution is dilute in He^3. Under these circumstances we will also have $\bar{S}_4\sim S_\lambda$. Setting $d\mu_4=d\mu_{2,\lambda}$ and using $d\mu_{2,\lambda}=-\bar{S}_{2,\lambda}dT$ we find

$$(\partial T_\lambda/\partial x_3)_p=-RT/(S_\lambda-\bar{S}_{2,\lambda}). \tag{33}$$

Using Eq. (14) we get

$$(\partial T_\lambda/\partial x_3)_p=-RT(r+1)/rS_\lambda. \tag{34}$$

The λ-point is lowered by addition of He^3, as is to be expected. It is to be hoped that experimental data will soon be available to test Eq. (34).

I wish to acknowledge the stimulation I have received from some earlier conversations with Professor F. London.

Note added July 30, 1949.—Dr. B. Weinstock of the Argonne National Laboratory has kindly sent me a copy of a note which has been submitted to the Physical Review by B. M. Abraham, B. Weinstock, and D. W. Osborne,[23] in which a report is given of measurements of T_λ as a function of x_3. Accompanying this is a note by J. W. Stout, in which a thermodynamic calculation of dT_λ/dx_3 is given,[24] which bears the same relation to Eq. (34) as the Keesom-Ehrenfest equation, Eq. (20) above, bears to Eq. (25). Stout calculates that the value of dT_λ/dx_3 for $x_3=0$ should be -3.4 deg. per mole fraction, which seems to fit the experiments. From Eq. (34) we find $dT_\lambda/dx_3=-3.16$, in excellent agreement with the thermodynamically calculated value. Had Stout used the value of r used here the agreement would have been almost exact.

---

[23] Abraham, Weinstock, and Osborne, Phys. Rev. **76**, 864 (1949).
[24] See J. W. Stout, Phys. Rev. **74**, 605 (1948), and reference 23.

On the Approach to Statistical Equilibrium

ARNOLD J. F. SIEGERT
Physics Department, Northwestern University, Evanston, Illinois
(Received August 12, 1949)

We consider as a random process the distribution of a gas in momentum space as function of the time. The probability of changes of the distribution in infinitesimal time intervals is assumed to be given by the "Stosszahlansatz." For the Rayleigh model of a gas we derive the probability of a distribution as a function of the time. For the Boltzmann gas with microscopic reversibility we show that the probability of a distribution approaches the stationary value in the limit of infinite time.

IN the usual derivation of the H-theorem the probability description is abandoned when, for the purpose of the calculation, the collision probability postulate ("Stosszahlansatz") is used as giving an expression for the number of collisions. Only the final result of the calculation is again interpreted as a probability statement. It therefore seemed to us of interest to attempt a discussion of the approach to equilibrium adhering to the probability description throughout the calculation, and, by treating the "distribution" or "Z state" —i.e., the set $n(t)$ of occupation numbers $n_i(t)$ in momentum space cell i at time t—as a random process[1] to obtain the probability of a distribution as a function of the time, or at least to investigate whether this probability approaches a limit for infinite time. The "Stosszahlansatz" is used in its original significance as a postulate expressing the probability of a change of the distribution in an infinitesimal time interval in terms of the occupation numbers and a matrix α whose off diagonal elements are the probabilities of individual collisions.

In Section I we have derived a formal expression for the probability function and discussed its limit for $t\rightarrow\infty$. Limit theorems of a more general scope[2] are probably known, but are not needed for our purpose.

In Section II we consider the random process generated by the simplified "Stosszahlansatz" describing the Rayleigh model[3] of a gas, which consists of non-interacting independent molecules. Changes in the system are caused by collisions with the atoms of another gas which is not considered as part of the system and whose distribution is assumed to be unchanged throughout the process. The elementary transition probabilities for the model are then linear in the occupation numbers. The probability function for its distribution can be expressed explicitly if α can be diagonalized, which is shown to be the case, if e.g., the Rayleigh gas interacts with a gas in thermal equilibrium by binary collisions. The Stosszahlansatz of Section II also applies to the continuous time variant of a two-cell problem, which was suggested by Ehrenfest[4] as an entropy-model, further discussed by Schroedinger and Kohlrausch[5] and solved by Kac[6] (in its original form with discrete time variable) and later by the author[7] (with a continuous time variable). Another model with the simplified Stosszahlansatz is Ehrenfest's "wind tree" model.[8] The problem of concentration fluctuations[9] is also of this type, if n_i is interpreted as the number of colloidal particles in cell i in coordinate space, and if all intervals of observation times are long compared with the time it takes for the colloidal particles to come to Maxwell Boltzmann equilibrium in momentum space. This assumption makes it possible to consider the process as Markoffian in the occupation numbers in coordinate space cells (rather than in the occupation numbers in phase space). It was pointed out by M. Kac (private communication) that this process is actually (even with the above approximation) Markoffian in the whole set of occupation numbers, and that the occupation number of one cell is not (as is usually assumed) a Markoffian random process.

In Section III we have solved explicitly a simple two-cell problem with transition probabilities which are quadratic functions of the occupation numbers, as a model of a system with binary collisions.

In Section IV we have discussed the random process generated by the Boltzmann Stosszahlansatz with microscopic reversibility (symmetry of α). We have shown that the conditional probability of any distribution n, which can be reached from the initial distribution m by a succession of allowed binary collisions, approaches the multinomial coefficient for $t\rightarrow\infty$.

I

We consider a system described by a set of occupation numbers $n_1(t)$, $n_2(t)\cdots n_K(t)$, with

$$\sum_{i=1}^{K} n_i = N$$

[1] Terminology of M. C. Wang and G. E. Uhlenbeck, Rev. Mod. Phys. **17**, 323 (1945).
[2] Some far reaching limit theorems for random processes with a discrete time variable have been derived by R. v. Mises, *Wahrscheinlichkeitsrechnung* (Berlin, 1931).
[3] Lord Rayleigh, Scient. Papers III, p. 473, also M. C. Wang, Dissertation, Ann Arbor, Michigan, 1942.
[4] P. and T. Ehrenfest, Physik Zeits. **8**, 311 (1907); also Wang and Uhlenbeck, reference 1.
[5] E. Schroedinger and F. Kohlrausch, Physik Zeits. **27**, 306 (1926).
[6] M. Kac, Am. Math. Monthly **54**, 369 (1947).
[7] A. J. F. Siegert, LADC 438.
[8] P. and T. Ehrenfest, Encyclopaedie der Math. Wissenschaften **IV**, 32, p. 19; A. J. F. Siegert, Phys. Rev. **75**, 1322 (1949).
[9] M. v. Smoluchowski, Physik Zeits. **17**, 557 (1916); see also S. Chandrasekhar, Rev. Mod. Phys. **15**, 1 (1943).

["distribution" or "Z state"] where $n_i(t)$ is the number of elements (e.g., atoms or molecules) in state i, where the state i may, e.g., be a cell in momentum space. The conditional probability

$$P(m/n, t) \equiv P(m_1, m_2 \cdots / n_1, n_2, \cdots; t)$$

is the probability that $n_i(t) = n_i$ if $n_i(0) = m_i$. We will try to calculate $P(m/n, t)$ from the probability of the change of the system in an infinitesimal time interval Δt: $P(m/n, \Delta t)$[10] assuming that

$$P(m/n, \Delta t) = (m|1|n) + (m|Q|n)\Delta t + o(\Delta t) \quad (1)$$

where $o(\Delta t)$ is defined by

$$\lim_{\Delta t \to 0} o(\Delta t)/\Delta t = 0$$

and where

$$(m|1|n) = \prod_i \delta_{m_i, n_i}.$$

This presupposes that $n(t)$ is K-dimensional Markoffian, i.e., that the probability of any change of the system in the time interval $(0, \Delta t)$ depends only on the occupation numbers at time zero. It is also assumed that the process is stationary, i.e., that $P(m/n, \Delta t)$ does not depend on the choice of the zero time. It is convenient to consider $P(m/n, t)$, $(m|Q|n)$ and $(m|1|n)$ as matrices $P(t)$, Q and 1 (unit matrix) with $2K$ indices which run from 0 to N. The matrix Q is arbitrary except for the properties:

$$(m|Q|n) = 0 \text{ unless } \sum_i m_i = \sum_i n_i = N \quad (2)$$

$$\sum_n (m|Q|n) = 0 \quad (3)$$

where $\sum_n$ is $\sum_{n_1 n_2 \cdots n_K}$ and

$$(m|Q|n) \geq 0 \text{ real}, \quad (4)$$

except if $n_i = m_i$ for all i. Q is independent of the time.

The above assumptions lead to two systems of differential equations:[11]

$$dP/dt = PQ, \quad (5)$$

$$dP/dt = QP \quad (6)$$

to be solved with the initial condition

$$P(0) = 1. \quad (7)$$

The formal solution is

$$P = \exp Qt. \quad (8)$$

[10] This change can be visualized as an elementary step of a random walk in the K-dimensional lattice formed by the points n on the hyperplane defined by $\Sigma_k n_k = N$.

[11] Special case of Eqs. (52) and (57), A. Kolmogoroff, Math. Ann. **104**, 415 (1931). The proof is based on the Smoluchowski equation

$$P(t+t') = P(t)P(t') \text{ for } t' \geq 0,$$

which implies that the validity of the above equations is restricted to cases where the state of the system can be ascertained between changes without disturbing the process.

The solution can be made explicit if Q can be diagonalized by means of a matrix C such that

$$(m|Q|n) = \sum_l (m|C^{-1}|l)\Lambda(l_1 l_2 \cdots l_K)(l|C|n). \quad (9)$$

If C can be found, we get

$$P(m/n, t) = \sum_l (m|C^{-1}|l)[\exp\Lambda(l)t] \cdot (l|C|n). \quad (10)$$

Because of Eq. (3), there is at least one right eigenvector to the eigenvalue $\Lambda(l_0) = 0$:

$$(n|C^{-1}|l_0) = b(l_0) \text{ (independent of } n).$$

If there is only one eigenvalue with vanishing real part we get, for $t \to \infty$

$$P(m/n_1 \infty) = b(l_0)(l_0|C|n) = (l_0|C|n)/\sum_{n'} (l_0|C|n') \quad (10')$$

since all $Re\Lambda(l) \leq 0$ (see Appendix I). In this case, therefore, an equilibrium probability function is approached, which is independent of the initial distribution m.

The eigenvalue zero of Q is degenerate, however, if e.g. the matrix Q is reducible by a mere rearrangement of rows and columns. Reducibility means that from a given initial point m in the K-dimensional lattice only the points n which belong to a sub-lattice can be reached, either directly or by any succession of steps. Reducibility can be caused by, e.g., conservation of energy and momentum. The above considerations are then applied to the sub-matrix and the sub-lattice, and if the eigenvalue zero of the sub-matrix is non-degenerate equilibrium is reached and is independent of the choice of the initial point m in the sublattice.

To apply these considerations to special cases, we will therefore have to prove in each case that Q can be diagonalized by a similarity transformation and that the eigenvalue zero of Q (or of its sub-matrices) is non-degenerate.

II

As a special case we consider a matrix Q representing changes in a system whose elements do not interact with each other, but change states independently, e.g., by collisions with a different set of molecules. This form of the "Stosszahlansatz" describes the Rayleigh model of a gas[3] and Ehrenfest's "wind-tree" model[8] (in momentum space), also the continuous variant of Ehrenfest's two box entropy model[7] and Smoluchowski's concentration fluctuations[9] (in coordinate space).

The matrix elements of Q are given by

$$(m|Q|n) = \sum_{\substack{i,k \\ i \neq k}}{}' \alpha_{ki} m_i \delta_{n_i, m_i - 1} \delta_{n_k, m_k + 1} \prod_{\substack{r \\ r \neq k, i}} \delta_{n_r, m_r} + \sum_i \alpha_{ii} m_i \prod_r \delta_{n_r, m_r}, \quad (11)$$

where $\alpha_{ki}\Delta t$ is the probability that a particle goes from

state i to state k in Δt. The off-diagonal matrix elements α_{ki} are arbitrary except for the conditions

$$\alpha_{ki} \geqslant 0 \text{ for } k \neq i \tag{12}$$

and the diagonal elements are defined by

$$\sum_k \alpha_{ki} = 0 \tag{13}$$

and it is assumed that α can be diagonalized by a matrix c such that

$$\alpha_{ki} = \sum_l c_{kl} \lambda_l c^{-1}{}_{li}. \tag{14}$$

We shall prove that under these assumptions Q is diagonalized by a certain matrix representation C of c, defined by Eqs. (24) and (25). To show this we define the generating polynomials

$$G_m(x, t) \equiv \sum_n P(m/n, t) \prod_j x_j{}^{n_j}, \tag{15}$$

$$Q_m(x) = \sum_n (m|Q|n) \prod_j x_j{}^{n_j}, \tag{16}$$

where x stands for $x_1, x_2, \cdots x_k$, and note that

$$Q_m(x) = \sum_{\substack{i,k \\ i \neq k}}{}' \alpha_{ki} m_i x_i{}^{m_i - 1} x_k{}^{m_k + 1} \prod_{\substack{j \\ j \neq k, i}} x_j{}^{m_j} + \sum_i \alpha_{ii} m_i \prod_j x_j{}^{m_j}$$

$$= \sum_{\substack{i,k \\ i \neq k}}{}' x_k \alpha_{ki} \frac{\partial}{\partial x_i} \prod_j x_j{}^{m_j} + \sum_i \alpha_{ii} x_i \frac{\partial}{\partial x_i} \prod_j x_j{}^{m_j} \tag{17}$$

or

$$Q_m(x) = \sum_{i,k} x_k \alpha_{ki} \frac{\partial}{\partial x_i} \prod_j x_j{}^{m_j}. \tag{18}$$

Equation (5) then yields

$$\frac{\partial G_m(x, t)}{\partial t} = \sum_{n'} P(m/n', t) \sum_n (n'|Q|n) \prod_j x_j{}^{n_j}$$

$$= \sum_{n'} P(m/n', t) \sum_{i,k} x_k \alpha_{ki} \frac{\partial}{\partial x_i} \prod_j x_j{}^{n_j} \tag{19}$$

$$= \sum_{i,k} x_k \alpha_{ki} \frac{\partial}{\partial x_i} G_m(x, t)$$

to be solved with initial conditions

$$G_m(x, 0) = \prod_j x_j{}^{m_j}. \tag{20}$$

It is convenient for our purposes to solve this equation by introducing a function

$$G(y, x, t) = N! \sum_m \prod_j \frac{y_j{}^{m_j}}{m_j!} G_m(x, t), \tag{21}$$

which satisfies the same differential equation as $G_m(x, t)$ with initial condition

$$G(y, x, 0) = (\sum_j y_j x_j)^N. \tag{22}$$

The solution is*

$$G(y, x, t) = [\sum_{i,j} x_i (e^{\alpha t})_{ij} y_j]^N$$

$$= [\sum_{ikj} x_i c_{ik} e^{\lambda_k t} c^{-1}{}_{kj} y_j]^N. \tag{23}$$

To obtain Q and P in the forms (9) and (10), respectively, we define a matrix representation $C(c)$ by

$$\prod_k u_k{}^{l_k} = \sum_n (l|C(c)|n) \prod_j x_j{}^{n_j} \tag{24}$$

with

$$u_k = \sum_i x_i c_{ik}. \tag{25}$$

We note that

$$[C(c)]^{-1} = C(c^{-1}), \tag{26}$$

$$\frac{N!}{\prod l_k!} \prod_k v_k{}^{l_k} = \sum_m \frac{N!}{\prod_r m_r!} \prod_r y_r{}^{m_r} (m|C(c^{-1})|l), \tag{27}$$

if

$$v_k = \sum_j c^{-1}{}_{kj} y_j. \tag{28}$$

We thus get

$$G(y, x, t) = [\sum_k u_k e^{\lambda_k t} v_k]^N$$

$$= \sum_l{}' \frac{N!}{\prod_k l_k!} \prod_k (u_k e^{\lambda_k t} v_k)^{l_k}$$

$$= \sum_l \frac{N!}{\prod_k l_k!} \prod_k u_k{}^{l_k} \exp(\sum_k \lambda_k l_k t) \prod_k v_k{}^{l_k}$$

$$= \sum_{m, n, l} \frac{N!}{\prod_r m_r!} \prod_r y_r{}^{m_r} (m|C(c^{-1})|l)$$

$$\times \exp(\sum_k \lambda_k l_k t)(l|C(c)|n) \prod_j x_j{}^{n_j}, \tag{29}$$

and using Eqs. (21), (15), and (26)

$$P(m/n, t) = \sum_l (m|C^{-1}|l) \exp(\sum_k \lambda_k l_k t)(l|C|n) \tag{30}$$

and

$$(m|Q|n) = \sum_l (m|C^{-1}|l)(\sum_k \lambda_k l_k)(l|C|n). \tag{31}$$

* See Appendix II for an alternative proof.

As a simple example we consider the most general two-state model, assuming

$$\alpha=\begin{pmatrix}-\gamma & \beta\\ \gamma & -\beta\end{pmatrix}. \tag{32}$$

The eigenvalues of α are $\lambda_1=0$ and $\lambda_2=-(\beta+\gamma)$ and the transformation matrix c is obtained as

$$c=\begin{pmatrix}\beta & 1\\ \gamma & -1\end{pmatrix} \text{ with } c^{-1}=\frac{1}{\beta+\gamma}\begin{pmatrix}1 & 1\\ \gamma & -\beta\end{pmatrix}. \tag{33}$$

Equation (23) becomes

$$\begin{aligned}G(y,x,t)&=(\beta+\gamma)^{-N}\{(\beta x_1+\gamma x_2)(y_1+y_2)\\ &\quad+(x_1-x_2)e^{-(\beta+\gamma)t}\\ &=(\beta+\gamma)^{-N}\{y_1[(\beta x_1+\gamma x_2)+\gamma(x_1-x_2)e^{-(\beta+\gamma)t}]\\ &\quad+y_2[(\beta x_1+\gamma x_2)-\beta(x_1-x_2)e^{-(\beta+\gamma)t}]\}^N\end{aligned} \tag{34}$$

and we get for $G_m(x,t)$:

$$\begin{aligned}G_m(x,t)&=(\beta+\gamma)^{-N}[(\beta x_1+\gamma x_2)+\gamma(x_1-x_2)e^{-(\beta+\gamma)t}]^{m_1}\\ &\quad\times[(\beta x_1+\gamma x_2)-\beta(x_1-x_2)e^{-(\beta+\gamma)t}]^{m_2}.\end{aligned} \tag{35}$$

For large times, $G_m(x,t)$ approaches

$$G_m(x,\infty)=\left[\frac{\beta x_1+\gamma x_2}{\beta+\gamma}\right]^N$$

and we get

$$P(m/n,\infty)=\frac{N!}{n_1!n_2!}\frac{\beta^{n_1}\gamma^{n_2}}{(\beta+\gamma)^N} \quad (\text{with } n_1+n_2=N). \tag{36}$$

The probabilities derived in references 4 and 5 can be obtained from Eq. (35).

We may interpret this example as describing a system of non-interacting spins in a constant magnetic field brought to thermal equilibrium, described by Eq. (36), by a temperature reservoir. The temperature T is defined by

$$\beta/\gamma=e^{(\epsilon_2-\epsilon_1)/kT},$$

where ϵ_1 and ϵ_2 are the energies of states 1 and 2, respectively, and k is the Boltzmann constant. The matrix α representing the effect of the temperature reservoir on the system must, therefore, be of the form

$$\alpha=\gamma\begin{pmatrix}-1 & e^{(\epsilon_2-\epsilon_1)/kT}\\ 1 & -e^{(\epsilon_2-\epsilon_1)/kT}\end{pmatrix}. \tag{37}$$

Just as in the case of Brownian motion,[12] the probability of changes of the system in Δt is thus derived from the validity of the Boltzmann law for the stationary distribution.

As a more general example we consider the case of a system which is brought to equilibrium by binary collisions with the atoms of a Boltzmann-gas. In this case α has the property

$$\alpha_{ki}=\alpha_{ik}e^{(\epsilon_i-\epsilon_k)/kT}, \tag{38}$$

where ϵ_i is the energy of state i, in addition to the properties expressed by Eqs. (12) and (13). To prove that α can be diagonalized we show that it can be symmetrized by a similarity transformation. We define the diagonal matrix ρ by

$$\rho_{ik}=e^{\epsilon_i/2kT}\delta_{ik} \tag{39}$$

and the symmetric real matrix σ by

$$\sigma=\rho\alpha\rho^{-1}. \tag{40}$$

σ can be diagonalized by a real matrix b, such that

$$\sigma=b\lambda b^{-1} \tag{41}$$

with λ real and diagonal, and with b real and $(b^{-1})_{il}=b_{li}$, thus

$$\alpha=\rho^{-1}\sigma\rho=\rho^{-1}b\lambda b^{-1}\rho=c^{-1}\lambda c, \tag{42}$$

where

$$c=b^{-1}\rho. \tag{43}$$

Next we show that the eigenvalue $\lambda_1=0$ is non-degenerate (unless α can be reduced by a mere re-arrangement of rows and columns) and derive the form of the eigen vector c_{il}. From

$$\lambda_l=\sum_{ik} b_{il}\sigma_{ik}b_{kl} \tag{46}$$

and

$$\sigma_{ii}=\alpha_{ii}=-\sum_{\substack{k\\ k\neq i}}{}' \alpha_{ki}=-\sum_{\substack{k\\ k\neq i}}{}' \rho_k^{-1}\sigma_{ki}\rho_i \tag{45}$$

we get, using the symmetry of σ,

$$\lambda_l=-\sum_{\substack{i,k\\ i\neq k}} b_{il}\rho_k^{-1}\sigma_{ik}\rho_i b_{il}+\sum_{\substack{i,k\\ i\neq k}} b_{il}\sigma_{ik}b_{kl} \tag{46}$$

and by interchanging indices

$$\lambda_l=-\sum_{\substack{i,k\\ i\neq k}} b_{kl}\rho_i^{-1}\sigma_{ik}\rho_k b_{kl}+\sum_{\substack{i,k\\ i\neq k}} b_{il}\sigma_{ik}b_{kl}. \tag{47}$$

Adding these expressions we get

$$\lambda_l=-\tfrac{1}{2}\sum_{\substack{i,k\\ i\neq k}}(b_{il}^2\rho_i\rho_k^{-1}-2b_{il}b_{kl}+b_{kl}^2\rho_i^{-1}\rho_k)\sigma_{ik} \tag{48}$$

$$=-\tfrac{1}{2}\sum_{\substack{i,k\\ i\neq k}}(b_{il}^2\rho_i^2-2b_{il}b_{kl}\rho_i\rho_k+b_{kl}^2\rho_k^2)\sigma_{ik}\rho_i^{-1}\rho_k^{-1} \tag{49}$$

$$=-\tfrac{1}{2}\sum_{\substack{i,k\\ i\neq k}}(b_{il}\rho_i-b_{kl}\rho_k)^2\sigma_{ik}(\rho_i\rho_k)^{-1}. \tag{50}$$

From this follows $\lambda_l\leqslant 0$, and if $\lambda_l=0$ $\rho_i b_{i1}=\rho_k b_{k1}$ unless $\sigma_{ik}=0$. Thus, if there exists at least one sequence of non-vanishing elements $\sigma_{ik_1}, \sigma_{k_1k_2}, \cdots\sigma_{k_{m-1},k_m}, \sigma_{k_mk}$ between any pair ik we get $\rho_i b_{i1}=\rho_{k_1} b_{k_11}=\cdots=\rho_k b_{k1}$

[12] H. A. Kramers, Physica 7, 284 (1940).

or $b_{k1}=\rho_k^{-1}s$ where s is determined by

$$\sum_j b_{j1}^2=1=s^2\sum_j \rho_j^{-2}. \tag{51}$$

For the probability p_{ik} of an individual particle to go from state i to state k in time t we thus get

$$p_{ik}(t)\equiv(e^{\alpha t})_{ki}=(c^{-1}e^{\lambda}tc)_{ki}=\sum_j \rho_k^{-1}b_{kj}e^{\lambda_j t}b_{ji}^{-1}\rho_i \tag{52}$$

and for $t\to\infty$ only the term $j=1$ remains, so that

$$\begin{aligned} w_k\equiv p_{ik}(\infty)&=\rho_k^{-1}b_{k1}b^{-1}{}_{1i}\rho_i=\rho_k^{-2}s^2\\ &=e^{-\epsilon_k/kT}/\sum_j e^{-\epsilon_j/kT}. \end{aligned} \tag{53}$$

Correspondingly one gets for the generating function (23)

$$G(y, x, t)\equiv(\sum_{i,k} x_i p_{ki}(t)y_k)^N \tag{54}$$

which becomes for $t\to\infty$

$$G(y, x, \infty)=(\sum_{i,k} x_i w_i y_k)^N=(\sum y_k)^N(\sum x_i w_i)^N \tag{55}$$

so that

$$P(m/n, \infty)=\frac{N!}{\prod_i n_i!}\prod_i w_i^{n_i} \tag{56}$$

which represents the canonical ensemble.

III

The cases discussed in Section II represent systems which change due to an outside influence. The elements of the system change states independent of each other, i.e. the system is actually an ensemble. If the system changes by interaction between the elements, $(n|Q|n')$ is no longer linear in the variables n_i, but can be, for instance, of second order (e.g. with Boltzmann's "Stosszahlansatz"). The solution for a simple model of this type is calculated. It is assumed that the elements can be in only two states, and that two elements in state 1 can interact and both change to state 2 and vice versa. The matrix Q is then given by

$$\begin{aligned} &(n_1n_2|Q|n_1'n_2')\\ &=\beta\{n_1(n_1-1)\delta(n_1', n_1-2)\delta(n_2', n_2+2)\\ &\quad+n_2(n_2-1)\delta(n_2', n_2-2)\delta(n_1', n_1+2)\\ &\quad-[n_1(n_1-1)+n_2(n_2-1)]\delta(n_1', n_1)\delta(n_2', n_2)\}, \end{aligned} \tag{57}$$

where β is a constant. It then follows that

$$\begin{aligned} \sum_{n_1'n_2'}{}' (n_1n_2|Q|n_1'n_2')x_1^{n_1'}x_2^{n_2'}\\ =\beta(x_2^2-x_1^2)\left(\frac{\partial^2}{\partial x_1^2}-\frac{\partial^2}{\partial x_2^2}\right)x_1^{n_1}x_2^{n_2} \end{aligned} \tag{58}$$

and, for the generating function, we get

$$\frac{\partial G_m(x, t)}{\partial t}=\beta(x_2^2-x_1^2)\left(\frac{\partial^2}{\partial x_1^2}-\frac{\partial^2}{\partial x_2^2}\right)G_m(x, t), \tag{59}$$

with initial condition

$$G_m(x, 0)=x_1^{m_1}x_2^{m_2}. \tag{60}$$

The solution is

$$\begin{aligned} G_m(x, t)=\sum_{\substack{l_1, l_2\\ l_1+l_2=N}}{}' (m|C^{-1}|l)e^{-4\beta l_1 l_2 t}(x_1+x_2)^{l_1}\\ \times(x_1-x_2)^{l_2} \end{aligned} \tag{61}$$

with $(m|C^{-1}|l)$ defined by

$$x_1^{m_1}x_2^{m_2}=\sum_{\substack{l_1, l_2\\ l_1+l_2=N}}{}' (m|C^{-1}|l)(x_1+x_2)^{l_1}(x_1-x_2)^{l_2} \tag{62}$$

in order to satisfy the initial condition. For $t\to\infty$, $G_m(x, t)$ approaches

$$\begin{aligned} G_m(x, \infty)=(m|C^{-1}|0, N)(x_1-x_2)^N\\ +(m|C^{-1}|N, 0)(x_1+x_2)^N, \end{aligned} \tag{63}$$

and since

$$(m|C^{-1}|N, 0)=2^{-N},\quad (m|C^{-1}|0, N)=2^{-N}(-)^{m_2}, \tag{64}$$

we get

$$G_m(x, \infty)=2^{-N}\{(-)^{m_2}(x_1-x_2)^N+(x_1+x_2)^N\} \tag{65}$$

and

$$P(m_1m_2/n_1n_2, \infty)=2^{-N}[1+(-)^{m_2+n_2}]\frac{N!}{n_1!n_2!} \tag{66}$$

with $m_1+m_2=n_1+n_2=N$. Except for the conservation of parity the binomial distribution is approached for $t\to\infty$.

IV

The problem of the approach to equilibrium of a gas with Boltzmann Stosszahlansatz—interpreted as a collision probability postulate—can be formulated in the same way. The matrix Q is given by

$$\begin{aligned} (m|Q|n)=\tfrac{1}{2}\{\sum_{\substack{ijkl\\ ij\neq k, l}} \alpha_{kl, ij}m_im_j\delta_{n_i, m_i-1}\\ \times\delta_{n_jm_j-1}\delta_{n_k, m_k+1}\delta_{n_l, m_l+1}\prod_r \delta_{n_r, m_r}\\ +\sum_{ij}\alpha_{ij, ij}m_im_j\prod_r \delta_{n_r m_r}\}, \end{aligned} \tag{67}$$

where $2\alpha_{kl, ij}\Delta t$, for $k, l\neq i, j$, is the probability of a collision $i, j\to k, l$ in Δt and $\alpha_{ij, ij}$ is defined by

$$\sum_{kl}\alpha_{kl, ij}=0 \tag{68}$$

$\alpha_{kl,ij}$ has the properties

$$\alpha_{kl,ii}=0, \tag{69}$$

$$\alpha_{kl,ij}=\alpha_{kl,ji}=\alpha_{lk,ij}, \tag{70}$$

$$\alpha_{kl,ij}\geqslant 0 \tag{71}$$

for $k,l\neq i,j$.

We also assume microscopic reversibility, i.e.,

$$\alpha_{kl,ij}=\alpha_{ij,kl}.^{13} \tag{72}$$

The matrix Q can be symmetrized by a similarity transformation

$$S=RQR^{-1}, \tag{73}$$

where R is defined by

$$(m|R|m')=(N!/\prod_r m_r!)^{\frac{1}{2}}\prod_r \delta_{m_r m_r'}. \tag{74}$$

To a submatrix of Q which can not be reduced by a mere interchange of rows and columns corresponds a similarly irreducible sub-matrix of S, since an element of S can be equal to zero only if the corresponding element of Q vanishes. Such a sub-matrix of Q defines a sublattice of distributions n such that each n can be reached from any other distribution m of the sub-lattice through a succession of steps mn', $n'n''\cdots n^{(s)}n$, for which the corresponding matrix elements $(m|Q|n')$, $(n'|Q|n'')\cdots(n^{(s)}|Q|n)$ are different from zero (i.e. through a sequence of allowed binary collisions). Equilibrium is reached in the sub-lattice according to Eq. (10′), since the eigenvalue zero is non-degenerate under these conditions. We get

$$P(m/n,\infty)=b_{l_0}(l_0|C|n) \tag{75}$$

for all distributions n which are in the same sub-lattice as m, where

$$(l_0|C|n)=(n|C^{-1}|l_0)(n|R^2|n)=b_{l_0}N!/\prod_r n_r! \tag{76}$$

and

$$b_{l_0}{}^2=[\sum_n{}' N!/\prod_r n_r!]^{-1} \tag{77}$$

the sum being extended over all distributions in the sub-lattice.

It would be of interest to see whether assumptions can be made concerning the matrix α such that the sub-lattice defined above becomes identical with the sub-lattice of all distributions with the same energy and momentum. The attempt to assign a discrete set of momenta and energies to the cells such that energy and momentum relations allow collisions between all pairs of particles lead, however, to number theoretical questions inherent in the discrete model which seem irrelevant to the physical problem.

[13] With these assumptions, the moments of $P(m/nt)$ satisfy a system of linear differential equations, see Appendix III.

APPENDIX I

In order that the right-hand side of Eq. (10) can be interpreted as a probability it is necessary that all $\Lambda(l)$ have non-positive real parts. This can be shown without using the assumption that Q can be diagonalized on the basis of Eqs. (3) and (4) only.

Suppose we have solved the system of equations

$$\sum_n (m|Q|n)(n|B|l)=(m|B|l)\Lambda(l),$$

which may be written in the form

$$-(m|B|l)\sum_{n\neq m}{}'(m|Q|n)+\sum_{n\neq m}{}'(m|Q|n)(n|B|l)=(m|B|l)\Lambda(l).$$

Now we chose among all $(m|B|l)$, for a chosen l, one, $(m_0|B|l)$ for which $|(m_0|B|l)|\geqslant|(n|B|l)|$ for all n. This may be assumed to be real without restricting generality. The equation for this index m_0 can be written as

$$\sum_{n\neq m_0} (m_0|Q|n)\left[\frac{(n|B|l)}{(m_0|B|l)}-1\right]=\Lambda(l).$$

Since $(m_0|B|l)\geqslant|(n|B|l)|\geqslant Re(n|B|l)$ we see that $Re\Lambda(l)\leqslant 0$ as required.

APPENDIX II

Equation (23) can also be derived using the independence of the particles: Let

$$(k_\sigma'|1|k_\sigma)+(k_\sigma'|\alpha|k_\sigma)\Delta t$$

denote the conditional probability that the particle numbered by σ and originally in cell k_σ, is after an infinitesimal time Δt in cell k_σ'. The conditional probability that particle σ is in cell k_σ' at t if it was in k_σ at $t=0$ is then given by the matrix

$$(k_\sigma'|e^{\alpha t}|k_\sigma)$$

and we get for the conditional probability $p(k_1k_2\cdots k_N/n,t)$ that $n_i(t)=n_i$, if the particles are at $t=0$ in the cells $k_1\cdots k_N$

$$p(k_1,k_2,\cdots k_N/n,t)=\sum_{k_1'\cdots k_N'}\prod_\sigma(k_\sigma'|e^{\alpha t}|k_\sigma)\prod_i(n_i|1|\sum_\sigma \delta_{i,k_\sigma'})$$

and for the generating function

$$\begin{aligned}g(k_1,k_2,\cdots/x,t)&\equiv\sum_n\prod_i x_i^{n_i}p(k_1\cdots k_N/n,t)\\&=\sum_{k_1'\cdots k_N'}\prod_\sigma(k_\sigma'|e^{\alpha t}|k_\sigma)\prod_i x_i^{\sum_\sigma\delta_{i,k_\sigma'}}\\&=\sum_{k_1'\cdots k_N'}\prod_\sigma\prod_i x_i^{\delta_{i,k_\sigma'}}(k_\sigma'|e^{\alpha t}|k_\sigma)\\&=\prod_\sigma(\sum_i x_i(i|e^{\alpha t}|k_\sigma))\\&=\prod_k[\sum_i x_i(i|e^{\alpha t}|k)]^{m_k}.\end{aligned}$$

This expression depends only on the number m_k of particles in cell k at time $t=0$ and not on the individual values k_σ. We have, therefore,

$$g(k_1\cdots k_N/x,t)=G_m(x,t)=\prod_k[\sum_i x_i(e^{\alpha t})_{ik}]^{m_k}$$

from which (22) follows using the definition (21). A still simpler derivation is obtained by introducing the random variables $n_k^{(\sigma)}$, with $n_k^{(\sigma)}=1$ if particle σ is in cell k, and zero otherwise. The generating functions for these variables are

$$P(0,0,\cdots,1,0\cdots/n^{(\sigma)},t)\prod_i x_i^{n_i^{(\sigma)}}=\sum_i x_i(e^{\alpha t})_{ik}$$

with the unity on the left-hand side in the kth place. Since $n_i=\sum_\sigma n_i^{(\sigma)}$, the above result for $G_m(x,t)$ follows from the independence of the particles.

APPENDIX III

The role of the non-linear Boltzmann equation in this formalism can be demonstrated by deriving the equation for the average $\bar{n}_k$.

We define the generating functions $Q_m(x)$ and $G_m(x, t)$ by Eqs. (15) and (16) and obtain

$$Q_m(x)=\tfrac{1}{2}\{\sum_{\substack{ijkl\\ij\neq kl}}\alpha_{kl;ij}m_im_jx_i^{m_i-1}x_j^{m_j-1}x_k^{m_k+1}x_l^{m_l+1}\prod_{r\neq ij,\,k,\,l}x_r^{m_r}$$

$$+\sum_{ij}\alpha_{ij,\,ij}m_im_j\prod_r x_r^{m_r}\}=\tfrac{1}{2}\sum_{ijkl}x_kx_l\alpha_{kl;ij}\frac{\partial^2}{\partial x_i\partial x_j}\prod_r x_r^{m_r}$$

and, therefore,

$$\frac{\partial G_m(x,t)}{\partial t}=\frac{1}{2}\sum_{ijkl}x_kx_l\alpha_{kl;ij}\frac{\partial^2}{\partial x_i\partial x_j}G_m(x,t).$$

For the averages

$$\bar{n}_s(t)=\left(\frac{\partial G_m}{\partial x_s}\right)_{x_1=x_2\cdots=x_K=1}$$

one obtains

$$\frac{d\bar{n}_s}{dt}=\sum_{ij,\,k}\alpha_{ks,\,ij}\langle n_in_j\rangle_{Av}$$

using Eqs. (68) and (70). Since

$$\alpha_{ks,\,ks}=-\sum_{ij(ij\neq ks)}\alpha_{ijks},$$

this can be written as

$$\frac{d\bar{n}_s}{dt}=\sum_{\substack{ijk\\ij\neq ks}}(\alpha_{ks,\,ij}\langle n_in_j\rangle_{Av}-\alpha_{ijks}\langle n_kn_s\rangle_{Av}).^{14}$$

This becomes the Boltzmann equation

$$\frac{d\bar{n}_s}{dt}=\sum_{\substack{ijk\\ij\neq ks}}[\alpha_{ks,\,ij}\bar{n}_i\bar{n}_j-\alpha_{ijks}\bar{n}_k\bar{n}_s]$$

if the correlations

$$\langle n_in_j\rangle_{Av}-\bar{n}_i\bar{n}_j\equiv\langle(n_i-\bar{n}_i)(n_j-\bar{n}_j)\rangle_{Av}$$

are neglected. Similar linear expressions can be derived for the time derivatives of higher moments. The non-linear Boltzmann equation is thus an approximation to the first one of a "hierarchy" of linear differential equations.

[14] This equation for the ensemble averages is thus in agreement with the transport equation for time averages derived by J. G. Kirkwood, J. Chem. Phys. **15**, 72 (1947), from essentially the same principles which underly the Stosszahlansatz.

PHYSICAL REVIEW VOLUME 76, NUMBER 11 DECEMBER 1, 1949

Structure of the Mercury Bands λ2540 and λ2476

S. MROZOWSKI
*Department of Physics, University of Chicago, Chicago, Illinois**

(Received August 22, 1949)

The structure of the band of Hg_2 at λ2540 and of the group of bands of Hg_2^+ at λ2476 was investigated under high dispersion. The band λ2540 was found to be limited by heads from both sides and to possess a number of sharp peaks on the long wave-length side. The bands at λ2476 were found to form a sequence with a gradually changing difference of the rotational constants of the upper and the lower energy states from negative to positive values. A number of peaks similar to those in λ2540 and band heads on both ends of bands are observed. An interpretation of the results is given in terms of the expected energy states of molecules of Hg_2 and Hg_2^+.

THE structure of the well-known mercury bands at λ2540 and λ2476 has been investigated under high dispersion. The photographs were taken several years ago and a short report on the results was made sometime later.[1] In this paper a more detailed account of the experiments will be given.

Both bands were investigated under very high resolution obtained in the second order of the 30-foot University of Chicago grating. The dispersion was about 0.44A per mm and the resolving power about 300,000. Unfortunately the mercury bands cannot be obtained under conditions which would give the full benefit of such a high resolving power. Due to temperature and pressure limitations the band λ2540 can be obtained in absorption with sufficient intensity only under conditions when the interesting finer details are wiped out to some extent by the temperature and pressure broadenings. In emission however the author succeeded in observing both bands under much more favorable conditions, and many fine details were obtained. The resolving power of the grating was still not utilized to the full extent (about the half of the resolving power would be sufficient to observe all details).

The band λ2540 was observed in absorption using a hydrogen discharge tube as a source of the continuum. The absorption tube (about 1 foot long) containing a few drops of mercury was sealed off under vacuum. A series of pictures was taken for different pressures of the saturated mercury vapor. The curve 3 in Fig. 1 gives the structure observed in absorption at temperatures below 200°C. At higher temperatures the band is more and more suppressed by the increasing continuous absorption extending from the resonance line λ2537 toward the longer wave-lengths and the structure becomes gradually wiped out. The gap in the absorption between λ2539.6 and λ2539.8 is very characteristic and was partly obtained by former investigators, as can be seen from a comparison of the curve 3 with the curves 1 and 2 in Fig. 1. Curve 1 was given in a paper by Wood

* Now at the Department of Physics, University of Buffalo, Buffalo, New York.

[1] S. Mrozowski, Phys. Rev. **73**, 1233 (1948).

TABLE I. Position of peaks in the band λ2540.

2540.524 edge
.467 peak
.453 peak
.424 peak
.378 peak
.345 peak
.290 peak
.235 peak
2539.823 edge

and Voss[2] and curve 12 by Kuhn and Freudenberg;[3] both curves represent the results of observations made using a much lower resolving power. Also much higher vapor pressures of mercury were used by these authors and therefore the absence of absorption in the gap could not be detected.

The peculiar structure of the band λ2540 was obtained with many more details in emission. Both bands λ2540 and λ2476 were excited in a very strongly water-cooled vacuum mercury arc of a special design.[4] The observation occurred end-on; the current was about 8–10 amps. How low the temperature and pressure are can be seen from the fact that under these conditions a maximum sidewise excitation of the mercury resonance radiation is obtained and that the hyperfine structures of the triplet λ5461, λ4358 and λ4047 for an end-on observation are complete and unreversed. The structure of the band λ2540 obtained in emission is given in curve 4, Fig. 1. A number of peaks are observed which seemingly converge toward the long wave-length limit. The exact wave-lengths of the peaks and of the band edges are given in Table I.

The gap at λ2539.7 is found to be limited by band edges as sharply as in absorption. As it will be mentioned below the peak at 2539.62 represents the edge of another vibrational band, so that the band λ2540 seems to be limited by edges (band heads?) from both ends. A similar behavior is found also in some bands of the group at λ2476 (see below).

The band λ2540 belongs to the transition $A^3 0_u^+ \rightarrow X^1\Sigma_g^+$ in the Hg_2 molecule.[5] For this transition a whole system of bands is observed. In absorption weaker bands are found at λ2542.5,[6] λ2541.5,[3,6] λ2539.5[3,6] and λ2538.5[3,7] (plus a number on the short wave-length side of the resonance line of an uncertain origin),[7] bands which are observed also in emission besides a great number of other bands.[8,9] One might be tempted to consider this group of absorption bands as a progression and accept the difference of 15 cm^{-1} as the vibrational quantum of the lower or of the upper electronic state. In such case however the band λ2540 would not be the 0→0 transition and a vibrational isotope splitting of the band heads would be expected. In fact in order to explain roughly the structure observed by the complex isotopic structure of the mercury, a distance of the band origin from the band λ2540 of around 300 cm^{-1} (toward the long wave-lengths) would be sufficient. This value should be considerably decreased by the presence of the nuclear isotope shift effect which in case of the Hg_2 molecules might be even greater than for the atomic transition $^3P_1 \rightarrow {}^1S_0$. Furthermore the structure would be changed by the nuclear isotope shifts and hyperfine splittings in the right direction, that is so as to resemble the observed intensity distribution. However the absence of other progressions in the absorption seems to favor rather an explanation of the peaks in terms of the band λ2540 being an $\Delta v = 0$ sequence of overlapping bands (due to equality of the vibrational quanta in the upper and lower states). Both assumptions do not explain why the short wave-length limit of the band λ2540 is single and the conclusion seems inevitable that the band λ2540 is a single band with a relatively small vibrational isotope effect.

For a $\Sigma \rightarrow \Sigma$ transition (or $0 \rightarrow \Sigma$) no Q branch is expected. Furthermore if we accept for the normal state of the molecule of mercury $B'' = 0.015$ cm^{-1} (assuming $r'' = 3.3$A), and assume a quite small change in nuclear distance in excitation $B' = 0.95 \times B''$, we find the distance of the zero line from the head to be around 0.3 cm^{-1}. It is hard to see how under these conditions a sharp peak at the edge can be formed. This gives further support to the view that the observed peaks cannot be band heads. The distance of the rotational

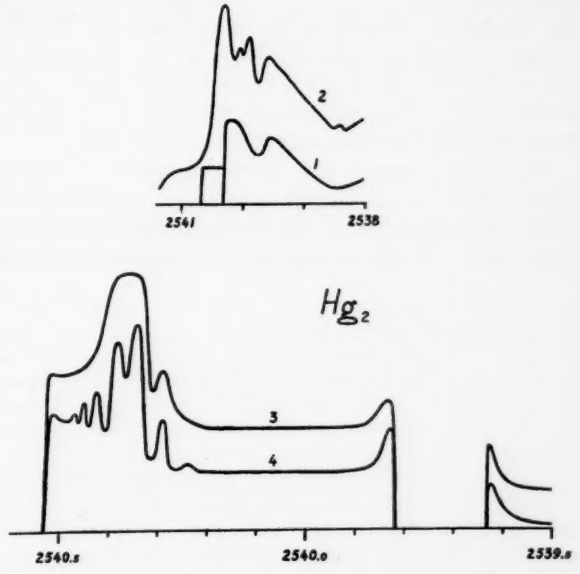

FIG. 1. Structure of the band of Hg_2 at λ2540 as observed in absorption by (1) Wood and Voss, (2) Kuhn and Freudenberg, and (3) in this work. (4) is the structure observed in this work in emission

[2] R. W. Wood and V. Voss, Proc. Roy. Soc. **A119**, 698 (1928).
[3] H. Kuhn and K. Freudenberg, Zeits. f. Physik **76**, 38 (1932).
[4] S. Mrozowski, Zeits. f. Physik **95**, 524 (1935).
[5] See, for instance, S. Mrozowski, Rev. Mod. Phys. **16**, 161 (1944).
[6] Observed by the author.
[7] D. K. Bhattacharyya and J. Murari, Ind. J. Phys. **19**, 20 (1945).
[8] H. Hulubei, Comptes Rendus **193**, 154 (1931).
[9] Lord Rayleigh, Nature **127**, 125 (1931).

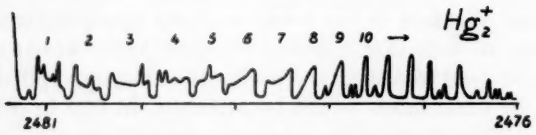

FIG. 2. Structure of the group of bands of Hg_2^+ at λ2476 as observed in this work in emission.

lines in the region where the two strongest peaks are observed should be about 0.15 cm^{-1} or less, that is one quarter of the observed distance of the peaks or less. It seems therefore probable that peaks are formed by overlapping of a number of lines belonging to different branches and to different isotopic bands. The rotational structure is sharp in the neighborhood of the zero line and only there peaks are observed; farther from the zero line probably a rotational pre-dissociation is setting in (both states having a very weak binding) and this pre-dissociation is responsible for the flatness of the rest of the band. The short wave-length edge must be due to higher order terms causing a turning back of the R branch.

The interpretation of the structure of the band λ2540 finds support in the study of the structure of the group of bands known as the band λ2476. The structure of this band as observed on our plates is presented schematically in Fig. 2. All the bands from No. 10 and up are sharp; below we notice an interesting transition effect: the bands 9 and 8 are asymmetric, with an increasing broadening. Starting from band 7 down all bands have a second (long wave-length) edge which is limiting the width of the bands. The intensity distribution inside each band changes gradually: first the intensity decreases toward long wave-lengths (7 to 5), then becomes flat in the band 4, finally reverses its trend in bands 3 to 1. Evidently in this series of bands the difference of the rotational constants $B'-B''$ changes its sign around the band 4. The presence of the second head shows the influence of the higher order terms in the rotational energy. The band 3 is similar in its intensity distribution to the band λ2540.

The peaks observed in a number of bands or between them might have partly the same origin as in the band λ2540. Anyway it can be definitely stated that there is no evidence for the occurrence of a returning series of bands. The existence of such a returning series of band heads overlapping the bands in the short wave-length region and gradually going out of step toward the long wave-lengths was given by Winans[10] as an explanation of the gradual broadening of the bands below 10 and a later increase of sharpness below band 3. It might be interesting to note that the band 3 has been mistakenly interpreted by Brzozowska[11] and by Winans[10] as two consecutive separate bands in the series. The band No. 21 of Brzozowska (0→0 of Winans) could not be observed in this work due to the presence of a strong ghost of the line λ2482 of Hg.

The group of bands at λ2476 is emitted undoubtedly by the ionized molecule of mercury Hg_2^+[12,13] A look at the level schemes of Hg I and Hg II shows that the only transition responsible for this band system can be the resonance transition $^3P_1 \rightarrow {}^1S_0$ in the neutral atom.[13] The energy states of the ion Hg_2^+ should have a larger binding energy than the corresponding ones of the neutral molecule due to charge exchange interaction. The excited state of the ion Hg_2^+ corresponding to the molecular state $A^3O_u^+$ should have a little weaker binding than the ground state of the ion due to the repulsion of the ion Hg^+ with the core of the excited atom. This explains why this band system is located on the short wave-length side of the resonance line. The rotational constants for both levels being about equal, the group of bands at λ2476 has to be interpreted in agreement with Mulliken's suggestion as a sequence of bands.[10] The vibrational quanta of both states are therefore around 100 cm^{-1}, that is considerably larger than for the band system of Hg_2 around λ2540 (both upper and normal states about 15 cm^{-1}). The sequence is probably a $\Delta v=0$ sequence and so the absence of isotopic effects is understandable. Since the substitution of an Hg^+ ion for a neutral atom does not change the type of transition in the other atom of the molecule, no Q branches are expected in these bands. The sharp peaks in the bands must therefore be attributed again to groupings of rotational lines, as it was done in the case of the band λ2540.

[10] J. G. Winans, Phys. Rev. **42**, 800 (1932).
[11] J. Brzozowska, Zeits. f. Physik **63**, 577 (1930).
[12] L. Job, Acta Phys. Polonica **2**, 31 (1933).
[13] T. C. Chow and K. T. Chao, Chinese J. Phys. **2**, 22 (1936).

Letters to the Editor

PUBLICATION of brief reports of important discoveries in physics may be secured by addressing them to this department. The closing date for this department is five weeks prior to the date of issue. No proof will be sent to the authors. The Board of Editors does not hold itself responsible for the opinions expressed by the correspondents. Communications should not exceed 600 words in length.

On the Occurrence of Vanadium 50 in Nature

DAVID C. HESS, JR. AND MARK G. INGHRAM
Argonne National Laboratory and University of Chicago, Chicago, Illinois
October 24, 1949

THE isotopic composition of vanadium was first studied by Aston[1] who showed it to consist principally of V^{51}. No work has since been reported on the naturally occurring isotopes of this element. The artificially produced radio-isotopes of vanadium listed by Seaborg and Perlman are: V^{47}—33 minutes, V^{48}—16 days, V^{49}—600 days, and V^{52}—3.8 minutes.[2] Recently Cork, Keller, and Stoddard have observed 635-day and 16-hour activities in vanadium which had been subjected to neutron bombardment in the Clinton pile.[3] The production of the 600-day activity by pile neutron irradiation of V^{51} is inconsistent with the assignment of this activity to V^{49}. As has been pointed out to us by Katharine Way, one of the possible explanations for this inconsistency is that vanadium has more than one naturally occurring isotope. This possibility is also indicated by consideration of the curve of greatest stability.

In order to test this hypothesis the isotopic composition of vanadium has been restudied and a new isotope found to be present at mass 50. The results are tabulated in Table I. Two 60° single focusing mass spectrometers were used, one equipped with a standard electron bombardment type of source and the other with a surface ionization source in which the vanadium was ionized by evaporation from a hot platinum filament. In the case of the source using electron bombardment the ratio of the abundance of the isotope at mass 50 to the one at mass 51 was determined from three different ion groups, V^+, V^{++} and VCl^{++}. In the case of the surface ionization source two ion groups were used, V^+ and VO^+. The fifth column lists the ratios observed in the five cases studied along with the mean deviation of the results. The sixth column lists the ions of impurities for which small corrections must be applied to the observed ratios. These corrections amount to about 0.018, 0.027 and 0.013 in the cases of C_2^+, Cr^+ and Zn^+, respectively. The results indicate that V^{50} exists in nature to about 0.25 percent. This conclusion is confirmed by the fact that the abundance ratios measured with five different ions are consistent, and that two different types of sources gave the same results. In addition two samples of different chemical purity gave the same result and the ratio was found to be independent of sample pressure and peak intensity. Finally, large fractionations of adjacent elements were observed with time with the surface ionization source, but no fractionation was detectable in the 50/51 ratio. All of these facts would be extremely improbable unless both peaks were due to the same element.

TABLE I. Abundance of the vanadium isotopes.

Ion source	Sample form	Ion group studied	No. of results	Observed 50/51 ×100	Impurity peaks
Electron bombardment	$VOCl_3$	V^{++}	13	0.274±0.004	C_2^+
Electron bombardment	$VOCl_3$	V^+	8	0.256±0.004	——
Electron bombardment	$VOCl_3$	VCl^{++}	12	0.254±0.005	——
Surface ionization	V_2O_5	V^+	19	0.268±0.026	Cr^+
Surface ionization	V_2O_5	VO^+	29	0.271±0.027	Zn^+

The probable explanation of Cork's results are that the 635-day activity was produced by an $(n,2n)$ reaction on V^{50}, and that the 16-hour activity is an excited state of V^{50}.

Further work is in progress in an attempt to detect natural radioactivity in V^{50} and to determine more carefully the abundance of this isotope.

[1] F. W. Aston, Phil. Mag. **47**, 397 (1924).
[2] G. T. Seaborg and I. Perlman, Rev. Mod. Phys. **20**, 593 (1948).
[3] Cork, Keller, and Stoddard, Phys. Rev. **76**, 575 (1949).

On the Relative Yields of Fission Cesium Isotopes

MARK G. INGHRAM, DAVID C. HESS, JR., AND JOHN H. REYNOLDS
Argonne National Laboratory, Chicago, Illinois
October 13, 1949

THE radioactive isotopes of cesium formed in fission have been studied by a number of investigators.[1,2] The purpose of this letter is to report on mass spectrometric measurements of the abundances of the long lived fission cesium isotopes.

A sample of fission cesium was isolated from uranium fission products by G. W. Parker and J. W. Ruch of the Oak Ridge National Laboratory. The usual method of electron bombardment ionization could not be used due to the small size of the samples obtainable. The mass spectrometer measurements were made with a surface ionization type of source in a 60° direction focusing mass spectrometer using techniques previously described.[3] Since the isotopes of cesium fractionate in the process of surface ionization, it was necessary to correct for this effect. The total magnitude of this effect in the measurements reported was 5 percent so that the corrected ratios should be accurate to about this value. The results of this analysis are given in Table I. The results tabulated are the relative yields deduced from the observed abundances of the isotopes by correcting for fractionation, neutron absorption and radioactive decay.

TABLE I. Isotopic composition of fission cesium.

Mass	133	134	135	136	137
Observed yield	≤1.03	——	1.28	<0.0001	1.000
Predicted yield	0.714	——	0.952	——	1.000

The predicted relative yields given in Table I are based on a smooth extrapolation of the published fission yield curve obtained by radiochemical methods.[1] Both yields are normalized to $Cs^{137}=1.000$. It appears from Table I that the yields as measured by the mass spectrometer are quite different from those predicted from the fission yield curve. The explanation of the observed yields is not clear, however, several comments are pertinent. The yield at mass 133 can be considered only as a maximum, since the normal cesium which is inevitably introduced during the purification process increases the apparent yield at this position, and there is no way to correct for this isotopic dilution. A small peak was observed at mass 134, but does not indicate that this isotope was formed directly in fission since the magnitude of the peak can be explained by the neutron absorption of Cs^{133} which has an activation cross section of about 26 barns. The higher value observed for the ratio of the yield at 135 to 137 must be attributed to the fission process itself. An analogous result has been obtained in xenon by Thode and Graham[4] who find a high yield in Xe at mass 134 when compared with the yield at 131 and 132.

In order to study the activity of Cs^{135} a mass spectrographic separation of the cesium isotopes was made with the mass spectrograph which has been described by Lewis and Hayden.[5] Photographic transfers were obtained using different intervals of exposure. With the deposit obtained, a transfer was obtained due to the 33 year Cs^{137} after 10 minutes. However, after 4 months transfer, the activity of Cs^{135} was still undetected, although the darkening due to the small amount of 1.7 *y* Cs^{134} present was quite pronounced. This proves that the half-life of Cs^{135} is at least 1.8×10^4 times longer than Cs^{137}, i.e., is greater than 6×10^5 years. This result is not in disagreement with the results of Sugarman in which he has detected the activity due to Cs^{135} and assigned a half-life of 2.1×10^6 years.

[1] Plutonium Project Fission Table, Rev. Mod. Phys. **18**, 513 (1946).
[2] N. Sugarman, Phys. Rev. **75**, 1473 (1949).
[3] M. G. Inghram, R. J. Hayden, and D. C. Hess, Jr., Phys. Rev. **72**, 967 (1947).
[4] H. G. Thode and N. L. Graham, Can. J. Research **A25**, 1 (1947).
[5] L. G. Lewis and R. J. Hayden, Rev. Sci. Inst. **19**, 599 (1948).

Internal Conversion Coefficient and Mass Assignment of the 57-Min. Se Isomer

I. Bergström and S. Thulin
Nobel Institute for Physics, Stockholm, Sweden
October 14, 1949

THE internal conversion lines of the 57-min. Se isomer have been measured by A. C. Helmholz.[1] It was not possible, however, to calculate the internal conversion coefficient because of the contamination of other Se activities produced in the Se+*d* reaction. According to Seaborg's tables[2] the mass number 81 of this activity is still somewhat uncertain (class B).

The electromagnetic isotope separator of this institute has been used to separate deuteron bombarded Se. In this way it is possible to obtain carrier free activities deposited on very thin foils. As Fig. 1 shows, the ordinary isotope lines can also be focused as circular spots of a size convenient for β-spectrometer measurements. After the separation, the collector plate (Fig. 1) was cut into strips corresponding to the different mass numbers between 77 and 83. We found the complex activity of the chain $Se^{83} \rightarrow Br^{83} \rightarrow Kr^{83}$ at mass number 83. The 57-min. activity of mass number 81 (no activity at 79) was sufficient for β-spectrometer investigation. Figure 2 shows the β-spectrum of this isotope recorded 60 minutes after the separation, when transient equilibrium is practically reached. The β-spectrometer data are summarized in Table I.

TABLE I. Summary of the β-spectrometer data.

Isotope	Upper limit Fermi plot Mev	β-lines	$H\rho$	Energy kev	$h\gamma$ kev	K/L	Half-life min.
Se^{*81}		K	1060	90.5	104±2	≈3.9	57±1
		L	1131	102.4	104±2		
Se^{81}	1.38±0.05						

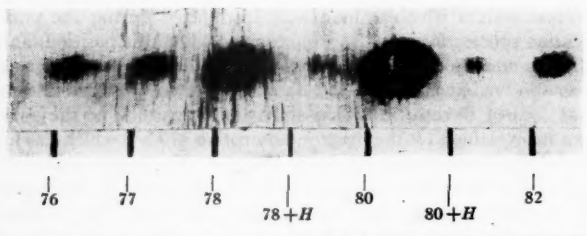

FIG. 1. Circular focused mass spectrum of Se deposited on a thin Al-plate. Spot distance 11 mm.

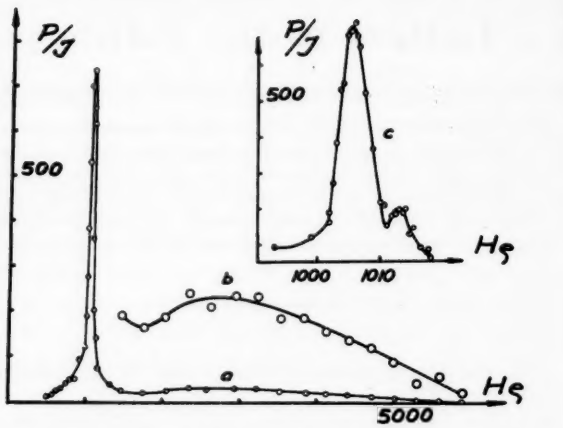

FIG. 2. a. β-spectrum of the separated activity on mass number 81. b. The continuum drawn to a five times larger P/I scale than a. c. The lines drawn to an eight times larger $H\rho$-scale than a.

To get the total internal conversion coefficient $[(Ne/(Ne+N\gamma) \cdot 100)]$ the ratio of the surfaces under the lines and the continuum have to be multiplied by the factor $[\lambda Se^{81}/(\lambda Se^{81} - \lambda Se^{*81})]$, because of radioactive equilibrium requirements. If we use the values 57 and 19 min. of A. Langsdorff, Jr., and E. Segrè[3] for the half-lives, we arrive to a total impossible internal conversion coefficient of 120 percent. The half-lives 56.5 and 13.6 min. determined by H. Wäffler and O. Hirzel[4] seem, however, to fit our measurements much better and give the value 104 percent for the coefficient. We estimate the error in our measurements to be less than 10 percent. Thus the γ-ray corresponding to the isomeric transmission of Se^{81} seems to be almost completely converted.

[1] A. C. Helmholz, Phys. Rev. **60**, 415 (1941).
[2] G. T. Seaborg and I. Perlman, Rev. Mod. Phys. **20**, 600 (1948).
[3] A. Langsdorf, Jr. and E. Segrè, Phys. Rev. **57**, 105 (1940).
[4] H. Wäffler and O. Hirzel, Helv. Phys. Acta **XXI**, 200 (1948).

Interpretation of Underground Cosmic-Ray Data

K. Greisen
Cornell University, Ithaca, New York
October 13, 1949

THIS letter is intended to put on record some remarks made verbally by the writer and others within the last year, regarding the interpretation of underground experiments.

It is well known that the vertical cosmic-ray intensity follows the depth as a power law with exponent ≈1.9 down to a depth of about 300 meters water equivalent (when correction is made at the smaller depths for the decay of mu-mesons in the atmosphere), and with exponent ≈2.9 at depths beyond about 400 meters. On the other hand, the extensive air showers have a power-law energy spectrum with exponent ≈1.8 continuing to energies 10^5 times greater than the energy which a meson must have to penetrate to the greatest depth at which they have been detected (3000 m). The explanation of this anomaly in terms of increased energy loss of high energy mesons has been rejected.[1-3] Barnothy and Forro[3,4] have explained it on the hypothesis that the rays that penetrate great depths are not mesons but their neutral decay products, which occasionally produce short-range charged secondaries in or near the detecting apparatus. The writer[1] and Hayakawa[2] have offered the suggestion that mu-mesons are the penetrating particles, but are themselves decay products of pi-mesons produced high in the atmosphere. The original estimate of the lifetime of the pi-meson necessary to fit this picture was rather crude, but more refined calculations by Hayakawa and Tomonaga[5] and by Eyges

and Greisen[6] have verified that the mean life measured in Berkeley[7] has about the best value to fit the underground intensity curve.

We wish to remark that the hypotheses of Barnothy and Forro and of the writer are exactly equivalent in respect to the means of obtaining the proper form of the vertical intensity *vs.* depth relation, and to point out that the necessary parts of both hypotheses are the following: (1) An unstable particle of type A is produced high in the atmosphere with an energy spectrum $\sim E^{-1.8}$, and decays into a particle of type B that is capable of penetrating to great depths; (2) essentially no particles of type A are capable of penetrating to great depths—or $I_{A\epsilon A} \ll I_{B\epsilon B}$, where I and ϵ represent respectively the intensity and the efficiency of detecting the components at large depths; (3) particles of type B lose energy at an approximately constant rate in traversing matter—mainly in small units instead of transferring large fractions of their energy in single interactions; and (4) $\gamma c\tau_0 = kL$, where γ is the Lorentz factor for particles of type B just capable of penetrating to the depth where the kink occurs, τ_0 is the mean life at rest of particles of type A, L is the distance (6.4×10^5 cm near the top of the atmosphere) in which the atmospheric pressure decreases by a factor ϵ, and k is a factor varying from about $\frac{1}{2}$ to 1.5 depending on the cross section for absorption of particles of type A by processes other than decay.

All conditions 1 to 4 are met by the pi-mu-meson explanation, provided that pi-mesons of high energy have cross sections for nuclear interaction greater than 1/1000 of the geometric cross section of the nucleons. The hypothesis of neutral penetrating particles can of course be made to account for conditions 1, 3, and 4 because we have practically no independent information about the energy loss of the neutral particles in the ground. However, it is also necessary in this case to explain the absence of mu-mesons at great depths; i.e., one must assume either that the meson spectrum is sharply cut off at high energies, or that a new process of energy loss sets in. The cut-off must be so complete that the mesons become less than 1/400 as abundant as is predicted by extrapolation of the known part of the meson energy spectrum with the assumption of no new absorption processes.

Further information on the origin of the penetrating particles is obtainable from the zenith angle dependence of the underground intensity, but here again the hypotheses of Barnothy and Forro and of the writer predict identical results, again with the necessary assumptions 1 to 4 listed above. In inclined directions, the unstable component A is produced at greater altitudes than in the vertical direction, so that the probability of decay is greater by a factor $\sec\theta$ (because of the reduced density of the air, in case A is subject to other strong absorption processes, or because of the longer path to sea level in case A is not a strongly interacting particle). Therefore, if the dependence on depth h goes as $h^{-\gamma}$ above the kink and $h^{-(\gamma+1)}$ below the kink in the curve, the zenith dependence underground should go as $(\cos\theta)^{\gamma}$ both above *and* below the kink.* This is in agreement with the experimental results of Barnothy and Forro.[3] If they are indeed correct, they constitute clear proof not that the hypothesis of Barnothy and Forro or that of the writer is correct, but that the conditions 1 to 4 listed above are met by the penetrating particles and their parents.

Direct information about the ionizing or neutral nature of the rays found underground, and about the penetrating character or local origin of the charged rays observed, can be obtained in principle from accurate absorption curves. The data available at this date are however somewhat confusing. Barnothy and Forro have presented evidence that most of the rays are neutral. Miesowicz, Jurkiewicz, and Massalski,[8] however, have apparently shown that the neutral rays are simply low energy gamma-rays of local radioactive origin. The absorption curves that have been measured of the ionizing component underground[3,9-11] contain large statistical errors, irregularities that have required artificial explanations, and disagreements with each other. If the charged particles are those that have traversed all the earth above the counters, a meter of lead should only succeed in stopping 6 percent of the particles at 300 m.w.e., 2½ percent at 1000 m.w.e., and one percent at 3000 m.w.e. The absorption measured by Wilson[9] at 300 m.w.e. is small enough (though the statistical errors are large); but the absorption measured by Nishina and Miyazaki[11] at 3000 m.w.e. is much too great; and the ups and downs of the curves of Barnothy and Forro at 1000 m.w.e., if not due to statistical and unknown systematic errors, are also too great.

It seems impossible, therefore, to draw a specific and reliable conclusion about the nature and origin of the rays underground from the data now available.

[1] K. Greisen, Phys. Rev. **73**, 521 (1948).
[2] S. Hayakawa, Prog. Theor. Phys. **3**, 199 (1948).
[3] J. Barnothy and M. Forro, Phys. Rev. **74**, 1300 (1948).
[4] J. Barnothy, Zeits. f. Physik **115**, 140 (1940).
[5] S. Hayakawa and S. Tomonaga, Phys. Rev. **75**, 1958 (1949).
[6] Unpublished.
[7] J. R. Richardson, Phys. Rev. **74**, 1720 (1948). The uncertainties in the underground data, in the exponent γ of the spectrum, in the range-energy curve of mu-mesons and in the nuclear interaction of pi-mesons prevent attributing much precision to the agreement. The more recent Berkeley value of 1.7×10^{-6} sec. gives just as good a fit as Richardon's value of 0.9×10^{-6} sec. Mean life values greater than 4×10^{-6} or less than 0.4×10^{-6} do not fit the data well.
* Of course, for particles of type A with low energy, the probability of decay is practically 1 regardless of the zenith direction. The factor $\sec\theta$ applies only to high energy particles that have small probabilities of decaying.
[8] Miesowicz, Jurkiewicz, and Massalski, Phys. Rev. (to be published); see also J. Barnothy and M. Forro, Phys. Rev. **55**, 870 (1939).
[9] V. C. Wilson, Phys. Rev. **55**, 6 (1939).
[10] J. Barnothy and M. Forro, Phys. Rev. **55**, 870 (1939); Phys. Rev. **58**, 844 (1940).
[11] Y. Nishina and Y. Miyazaki (private communication).

Radiation from Zn^{65}

K. C. Mann, D. Rankin, and P. N. Daykin
Department of Physics, University of British Columbia, Vancouver, British Columbia, Canada
October 11, 1949

SOME preliminary measurements have been made in this laboratory on the energies of the beta- and gamma-radiations from Zn^{65}, using a beta-ray spectrometer of the thin lens type. The spectrometer has been equipped with a spiral baffle placed in the center of the spectrometer tube. A proper choice of the focusing magnet's current direction thus makes possible the selection for analysis of either positrons or negatrons. The source was in the form of a small square of zinc metal of surface density 25 milligrams/cm², irradiated with slow neutrons in the pile at Chalk River, Ontario. The total activity was one millicurie. Positron, negatron, and gamma-ray spectra were run. In the latter case, measurements were made of the energies of photoelectrons expelled from a uranium radiator of density 50 milligrams/cm². The resolution of the instrument is of the order of 3.5 percent in momentum. The energy calibration used both the F line of thorium B and the annihilation radiation of Zn^{65}. The estimated error on the basis of this calibration is thought to be about 0.5 percent in momentum. No corrections have been made for the finite thickness of the source or radiator, the importance of which has been discussed recently by Jensen, Laslett, and Pratt[1] and by Hornyak, Lauritsen, and Rasmussen.[2]

The results are shown in the accompanying figures. In all cases, the "normal" background, measured with the source in position in the spectrometer, and zero current in the focusing coils, averaged about 20 counts per minute, and this has been subtracted before plotting. Figure 1, (a) and (b), shows the positron distribution obtained and the calculated Fermi plot. Extrapolation of the latter leads to an end point of 0.325 ± 0.002 Mev which is in good agrement with the spectrometer measurements of Peacock.[3] Only one recognizable positron group is evident, although the effects of source thickness and scattering in the spectrometer would make difficult the detection of weak positron groups below say 0.15 Mev. Figure 2 shows the result obtained with the magnet

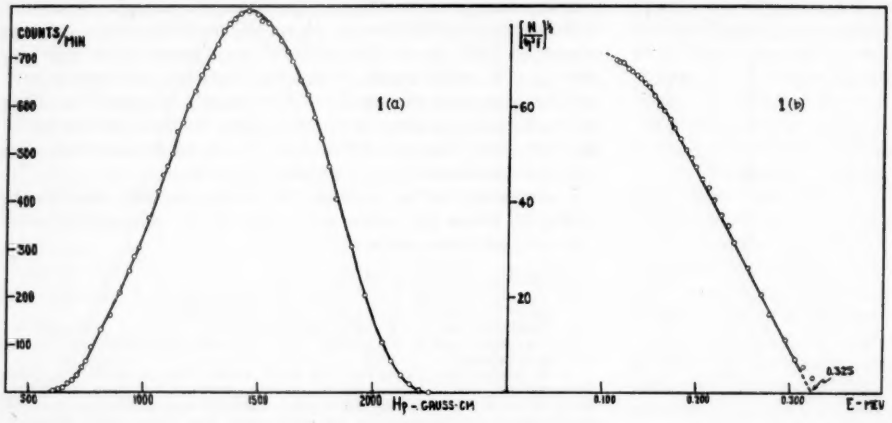

FIG. 1. (a) Positron spectrum and (b) Fermi plot of positrons from Zn^{65}.

current adjusted to transmit only negatrons. The strong conversion line corresponds to a 1.120±0.005-Mev transition. The continuous background can be attributed to Compton recoil electrons generated in the thick source. A Fermi plot failed to reveal any negatron group. It is therefore probable that orbital electron capture and positron emission are the only modes of decay of Zn^{65}. By extrapolating the continuous distribution to intercept the momentum axis, we obtain for the maximum energy of the Compton recoils the value of 0.92[8] Mev from which the energy of the responsible gamma-ray may be calculated to be 1.14±0.02 Mev. Therefore, we may assume with reasonable assurance that the transition giving rise to the conversion line also ejects the gamma-ray responsible for the Compton distribution.

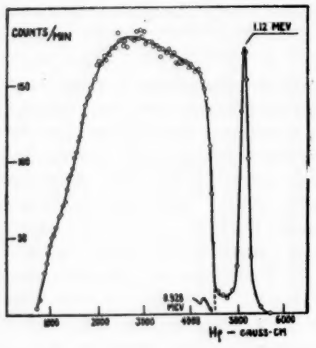

FIG. 2. Negatron spectrum of Zn^{65}.

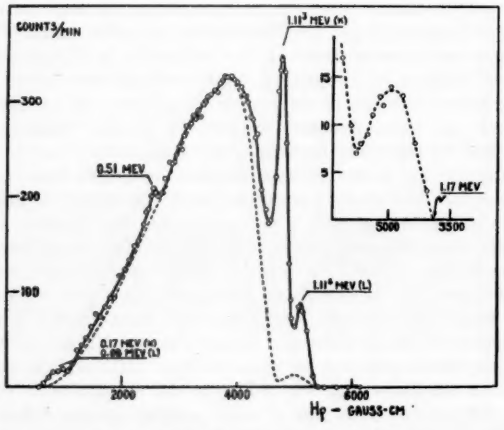

FIG. 3. Gamma-ray spectrum of Zn^{65}.

Figure 3 shows the gamma-ray spectrum taken with the uranium radiator. The solid curve is a composite curve of photo-electrons and Compton electrons combined. The broken curve is the Compton background alone, taken with the radiator removed. The measured energies of the photo-electrons plus the shell-binding energies of uranium (0.114 Mev and 0.020 Mev for K and L shells, respectively) lead to energies of 1.11[4]±0.005 Mev (a weighted average of 1.11[3] Mev for K shell and 1.11[6] Mev for L shell), 0.510±0.003 Mev which can be identified as annihilation radiation, and a somewhat weak peak at about 0.17±0.02 Mev or 0.08±0.02 Mev depending upon whether we assume their origin to be in the K or the L shell. The 1.11[4]-Mev gamma-ray can be identified with the conversion electron line of 1.12 Mev and is in good agreement with the work of Jensen, Laslett, and Pratt whose revised value for this transition has been reported as 1.11[8] Mev.[4] It id definitely lower than the value 1.14 Mev proposed by Deutsch, Roberts, and Elliott,[5] although the values are probably consistent within the error limits. The lowest energy gamma-ray has not been reported previously, and it is certainly near the limit of detection.

Examination of the Compton background curve in Fig. 3 shows a distinct distribution at the high energy end. This has been plotted on an expanded scale in the inset. It would appear to be caused by a gamma-ray of too low an intensity to produce a detectable photo-electron line. The maximum energy of the Comptons is at 1.17 Mev. The gamma-ray then has an energy of 1.38±0.03 Mev.

Further experiments are proceeding to make reasonably certain that these gamma-rays of low intensity are really those of Zn^{65} since the possibility of minute amounts of radioactive impurities cannot yet be discounted. We hope to be able to make a more detailed report in the near future.

We wish to acknowledge the generous support of the National Research Council of Canada. The work was made possible through a Grant-in-Aid of Research, and through the award of N.R.C. Studentships to two of us (D.R. and P.N.D.).

[1] Jensen, Laslett, and Pratt, Phys. Rev. **75**, 458 (1949).
[2] Hornyak, Lauritsen, and Rasmussen, Phys. Rev. **76**, 731 (1949).
[3] W. C. Peacock, Plut. Proj. Rep. Mon. N-432, **56** (December, 1947).
[4] Jensen, Laslett, and Pratt, Phys. Rev. **76**, 430 (1949).
[5] Deutsch, Roberts, and Elliott, Phys. Rev. **71**, 389(A) (1942).

Neutron-Proton Scattering

H. N. YADAV
Mathematics Department, University College, London, England
October 7, 1949

IN order to account for the coherent scattering of slow neutrons by para- and orthohydrogen molecules, as well as the observed binding energy of the deuteron, assuming a square well interaction,

different ranges need to be assumed for the central and the tensor part of the interaction in triplet states. Assuming such different ranges, however, Castillejo and Richardson[1] have been unable to account for the observed total cross section for neutrons of energy about 90 Mev.

To investigate whether better agreement could be obtained with a different well shape, similar calculations have been made employing a two-range Yukawa-well with ranges 0.80×10^{-13} cm and 1.60^{-13} cm for the central and tensor forces respectively for the triplet interaction. The appropriate constants were determined by the iteration method for these ranges to fit the data on the binding energy and the electrical quadrupole moment of the deuteron, and the proportion of D-wave thus obtained is 3.8 percent—in good agreement with that needed to explain the observed magnetic moment of the deuteron. For the interaction in singlet states a range of 1.18×10^{-13} cm was used to fit the data on p–p scattering.

The low energy scattering total cross sections have been obtained for incident neutrons of energy 0–3 Mev in agreement with the experimental results. But the high energy (83 Mev) total cross sections are large as usual, *viz.*, 14.6×10^{-26} cm² and 12.1×10^{-26} cm² for the symmetrical and Serber (interaction in even states only) types of interaction respectively. The following table gives the angular distribution in the two cases, in 10^{-26} cm²:

$\theta°$	0	15	30	60	90	120	150	165	180
Sym. $\sigma(\theta)$	1.49	1.43	1.30	0.97	0.81	1.06	2.08	2.65	2.97
Serber $\sigma(\theta)$	1.30	1.30	1.27	0.89	0.73	0.89	1.27	1.30	1.30

The validity of Born's approximation for high energy scattering in the triplet states has also been examined and it is found that in the present case it gives much smaller value for the cross section than that obtained by the exact method. The detailed account will be published elsewhere.

I wish to express my indebtedness to Professor H. S. W. Massey, F.R.S. for his keen interest in the calculation. I also wish to thank Dr. T. M. Hu and Mr. K. N. Hsu for many valuable discussions. Finally I express my thanks to the Government of Bihar (India) for extension of the scholarship enabling me to complete this work.

[1] L. Castillejo and H. T. Richardson, Phys. Rev. **76**, 1732 (1949).

Structure of the Line λ4686 of He II

K. Murakawa, S. Suwa, and T. Kamei
Institute of Science and Technology, Komaba, Meguro-ku, Tokyo, Japan
October 10, 1949

In order to test the theory of level shift in hydrogen-like atoms,[1,2] the structure of the line λ4686 of He II was studied. The light source was a cool aluminum hollow cathode discharge tube, which was filled with helium of about 1 mm Hg pressure. The fine structure was examined by the use of a silvered Fabry-Pérot etalon and a glass Lummer plate of thickness 4.7 mm.

The structure of the line λ4686 calculated according to the recent theory,[2] together with the observed structure, is shown in Fig. 1. Figure 2 is a reproduction of a photograph taken with a 2-mm etalon.

Mack and Austern[3] had previously resolved the components j and k, and obtained the value 0.16 ± 0.02 cm^{-1} as the mutual distance. The value obtained by us is 0.18 ± 0.006 cm^{-1}, and is nearer the one required by the theory (0.182 cm^{-1}). In addition to the resolution of the components j and k, the components l and m were also resolved in the present work, and the mutual distance was observed to be 0.14 ± 0.01 cm^{-1}, which is to be compared with the theoretical value 0.130_5 cm^{-1}. The observed structure is therefore in harmony with the theory,[1,2] but the accuracy of measurement is still insufficient for testing the level shift of the terms other than S terms.

One weak component not required by the theory was observed at -0.87 cm^{-1}. This was also observed by Paschen[4] in his former work, but rejected as doubtful in his later work. The line breadth of the component seems to be due to a light element, but the possibility of attributing it to the aluminum spectrum is not so definitely excluded.

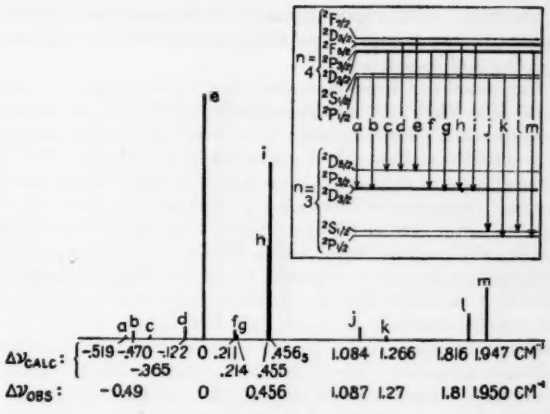

FIG. 1. Transition scheme and calculated and observed structure of He II λ4686.

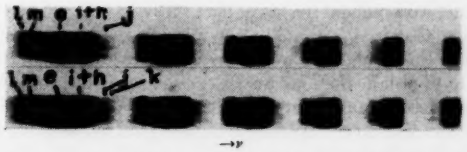

FIG. 2. Inference pattern of He II λ4686 taken with a 2-mm etalon.

In conclusion we wish to thank Professor M. Kiuchi who took deep interest in our work and kindly loaned us the helium gas.

[1] H. A. Bethe, Phys. Rev. **72**, 33 (1947). F. J. Dyson, Phys. Rev. **73**, 617 (1948).
[2] N. M. Kroll and W. E. Lamb, Phys. Rev. **75**, 388 (1949). J. B. French and V. F. Weisskopf, Phys. Rev. **75**, 1240 (1949).
[3] J. E. Mack and N. Austern, Phys. Rev. **72**, 972 (1947). See also G. R. Fowles, Phys. Rev. **73**, 639 (1948); **74**, 219 (1948).
[4] F. Paschen, Ann. d. Physik **50**, 901 (1916); **82**, 689 (1927).

Note on Wave Amplification by Interaction with a Stream of Electrons

L. R. Walker
Bell Telephone Laboratories, Murray Hill, New Jersey
October 10, 1949

In a recent paper, J. A. Roberts,[1] extending the work of V. A. Bailey[2] on the propagation of plane electromagnetic waves in an ionized gas, purports to show that plane waves with gain exist in infinite space filled with a uniform density of heavy positive ions and an equal density of electrons which move with uniform velocity in a given direction. The paper appears to be open to criticism, some of which extends to Bailey's original work.

Roberts' Eq. (1), a special case of one derived by Bailey, is said to be non-relativistic, but contains terms of order V^2/C^2, where V is the velocity of the electron stream. When the equation is derived again using the relativistic equations of motion for the electrons, further terms of order V^2/C^2 appear. The equation thus found may be readily factored and the resultant plane wave solutions show no gain. A similar conclusion may be reached by making a Lorentz transformation to a system in which the electrons are at rest. In this case the permissible plane wave solutions are found very simply and they may then be transformed back into the rest system. It would appear that an inconsistent neglect

of relativistic terms affects the nature of the plane wave solutions quite radically. A note will be submitted deriving the relativistic equation and its solutions.

The remarks of Roberts concerning growing waves in a cylindrical pipe filled with electrons moving parallel to the axis and upon traveling wave tubes seem to be based upon a misconception. It is stated that Ramo[3] in a discussion of this problem failed to discover a set of waves with negative attenuation. Ramo pointed out that two types of wave exist in such a tube; there are two "space charge" waves moving roughly with the electron stream velocity and two fast "field" waves. The latter solutions according to Ramo are cut off at a certain frequency. This is not strictly correct in the sense that the solutions below this frequency are not pure exponentials. However, such solutions are simply cut-off modes in the pipe perturbed by the electron stream, one increasing and decreasing in the direction of electron flow. The direction of power flow is opposed to the electron flow for these "field" waves. If a situation were to prevail in which the wave increasing in the direction of electron motion dominated the other three waves, clearly power would have to be supplied at the high level end. J. R. Pierce has shown in some unpublished calculations on traveling wave tubes, where a backward increasing wave may also exist, that it is possible by modulating the input stream and arranging the boundary conditions at the two ends of the tube correctly to obtain the four waves excited in such a way that the signal level at the upstream end is greater than that at the downstream end and power flows against the electron flow. However, the gain in such cases is very small compared to the exponential increase of the single backward cut-off wave and bears no simple relation to it. It is clear that the enormous gains cited by Roberts for the single wave would be quite unobtainable in practice. The use of retarding structures to produce approximate synchronism between the circuit wave and electron stream, with a consequent wave showing gain and power flow in the direction of electron flow is not simply a superfluous complication.

[1] J. A. Roberts, Phys. Rev. **76**, 340 (1949).
[2] V. A. Bailey, Nature **161**, 599 (1940); J. Roy. Soc. N.S.W. **82**, 107 (1948); Austr. J. Sci. Research **1**, 351 (1948).
[3] S. Ramo, Phys. Rev. **56**, 276 (1939).

A Naturally Occurring Odd-Odd Isotope of Vanadium

WALLACE T. LELAND*
Department of Physics, University of Minnesota, Minneapolis, Minnesota
October 24, 1949

As part of a program to investigate the isotope abundances of the heavier elements, an isotope of vanadium of mass 50 having an abundance of 0.23 ± 0.01 percent was discovered. The instrument used in the investigation was a 60 degree mass spectrometer of a design similar to one already described by Nier.[1] V^+ ions were obtained by electron bombardment of vanadium vapor produced by evaporation of the metal placed on a heated tungsten filament. That the isotope at mass 50 is actually vanadium and not due to an impurity is indicated by the following observations. (1) The ratio of the mass 50 peak to V^{51} remained constant while varying the temperature of the tungsten filament and consequently the rate of vanadium evaporation. Figure 1 shows the results obtained with two separate samples of vanadium. The intensity ratio of V^{51} to mass 50 is plotted against intensity of V^{51}. The scattering of the points is due to measurement errors introduced by time fluctuations in the vanadium vapor supply. It is seen that over the range of 20 in intensity covered, the ratio remained constant at about 425. (2) As indicated in Fig. 2, the variation in intensity of the mass 50 peak with energy of electrons producing the ions is the same as the variation characteristic of vanadium. (3) The mass spectrum in the region surrounding

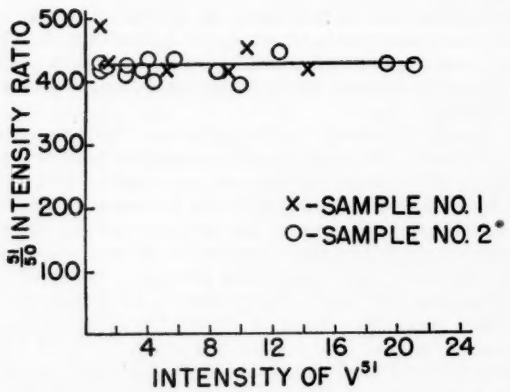

FIG. 1. The ratio of the V^{51} peak to the mass 50 peak is shown to be independent of the V^{51} intensity which in effect demonstrates the one to one correspondence of the mass 50 peak to the vapor pressure of vanadium.

masses 50 and 51 was void of peaks, thereby indicating the absence of impurities such as hydrocarbons or chromium and titanium which also have isotopes of mass 50. (4) Doubly charged ions were observed which gave the same ratio of intensities, namely $51^{++}/50^{++}$ equal to 425.

The existence of the odd-odd V^{50} with an abundance of 0.23 percent is unexpected. Aston[2] examined vanadium with his mass spectrograph in 1924 and reported it to be 100 percent V^{51}. His apparatus at that time, however, was not very sensitive, and the failure to detect V^{50} not surprising. In checking the literature, conflicting reports are found in regards to radioactive vanadium isotopes, and in the latest table of isotopes by Seaborg and Perlman[3] V^{50} is not listed. A recent article by Cork, Keller, and Stoddard[4] reports a 635-day activity produced in vanadium irradiated in a pile. This activity may be due to V^{49} previously reported as having a half-life of 600 days[5] and produced in their experiment by a $(n,2n)$ reaction on V^{50}. It would be interesting to examine chromium produced by a (d,n) reaction on vanadium since V^{50} would go into the 26.6-day Cr^{51} while V^{51} would end up as stable Cr^{52}.

Although the relatively high abundance of V^{50} speaks against it, one might expect that as in the case of K^{40} and other odd-odd nuclei heavier than N^{14},** V^{50} would be unstable. A check with a thin-walled beta-counter, however, failed to reveal any activity. A subsequent experiment wherein vanadium was placed on photographic plates for a period of 8 days also failed to reveal any ionizing events in excess of the cosmic-ray background.

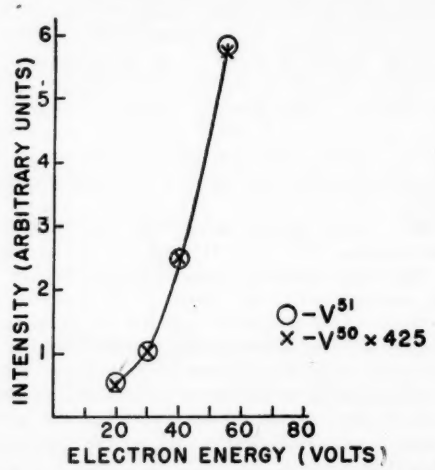

FIG. 2. The ionization efficiency curve for the mass 50 peak is shown to have the same shape as that of vanadium by the congruence of the two curves, the one for V^{51} and the other for the mass 50 peak times 425.

It is interesting to note in connection with the stability of V^{50} that on calculating the mass of Cr^{50}, V^{50}, and Ti^{50} using Wigner's[6] semi-empirical formula, one finds Cr^{50} and Ti^{50} to have practically identical mass with V^{50} about one-milli mass unit heavier. The presence of spin dependent forces not taken into account may, however, decrease the mass of V^{50}. It is possible that we are dealing with a situation wherein all three isobars, Cr^{50}, V^{50}, and Ti^{50}, have very nearly equal masses and, consequently, are stable or at least undetectably radioactive. A cloud chamber has been set up in which all three elements have been placed, and it is hoped that this will enable a critical examination as to their radioactivity.

I wish to thank Professor A. O. Nier for his constant interest and encouragement. Thanks are due also to Dr. W. D. Armstrong for the beta-counter work, to Phyllis Freier for the photographic plate work, and to Professor C. Critchfield for many helpful suggestions. The instrument used in this work was built with a grant from the Graduate School. The research was supported by the Joint Program of the ONR and the AEC. Assistance was also given by the University of Minnesota Technical Research Fund.

* AEC fellow.
** A possible exception to this rule is La^{138} reported by Inghram, Hayden, and Hess, Jr., Phys. Rev. **72**, 967 (1947).
[1] A. O. Nier, Rev. Sci. Inst. **18**, 398 (1947).
[2] F. W. Aston, Phil. Mag. **47**, 385 (1924).
[3] G. T. Seaborg and I. Perlman, Rev. Mod. Phys. **20**, 594 (1948).
[4] Cork, Keller, and Stoddard, Phys. Rev. (to be published).
[5] Walke, Williams, and Evans, Proc. Roy. Soc. (London) **A171**, 360 (1939).
[6] E. Wigner, University of Pennsylvania Bicentennial Conference (University of Pennsylvania Press, Philadelphia, Pennsylvania, 1941).

Nuclear and Molecular Information from the Microwave Spectrum of FCl*

D. A. Gilbert and A. Roberts
Physics Department,
and P. A. Griswold**
Department of Chemistry and Chemical Engineering,
State University of Iowa, Iowa City, Iowa
October 14, 1949

THE rotational transitions for $J=0\rightarrow1$ in FCl^{35} and FCl^{37} have been observed near 30,000 mc for both the ground vibrational state and the first excited vibrational state. A specially constructed Stark absorption cell resistant to fluorine corrosion was used. The hyperfine structure due to the electric quadrupole moment of the chlorine nuclei splits the $J=1$ levels so that the observed lines are triplets. The frequencies of the twelve resulting lines are given in Table I.

The hyperfine structure spacings do not agree with the theoretically predicted pattern for nuclear quadrupole splitting, even including second-order corrections. To explain this we assume an extra term in the Hamiltonian of the form $cI\cdot J$. Such a term has been found necessary to explain the spectrum of the alkali halides observed by Nierenberg and Ramsey,[1] and has also been introduced to explain small deviations from predicted frequencies in the NH_3 inversion spectrum.[2-4] The value of c for FCl^{35} is 0.036 ± 0.009 mc and 0.019 ± 0.009 mc for FCl^{37}. The magnetic field required at the Cl nucleus to produce interactions of this magnitude is unexpectedly large—about 70 gauss. It seems difficult to account for so large a field from molecular rotation alone, and the hypothesis of Van Vleck[1] that the field is due to coupling with higher electronic states is perhaps more plausible. The ratio $c^{35}/c^{37}=1.9\pm0.97$ is in agreement, within the rather large experimental error, with the ratio of the magnetic moments 1.2055 ± 0.003 taken from Goldsmith and Inglis.[5] Assuming the effective magnetic field is the same in both isotopic species these two ratios should be the same.

Table I. Observed transitions and frequencies.

Molecule	v	$J=0\rightarrow1$ F	Frequency, mc
FCl^{35}	0	$3/2\rightarrow1/2$	$30{,}873.004\pm0.042$
		$3/2\ \ 5/2$	$30{,}843.948\pm0.042$
		$3/2\ \ 3/2$	$30{,}807.413\pm0.042$
	1	$3/2\rightarrow1/2$	30,611.761 0.069
		$3/2\ \ 5/2$	30,582.614 0.069
		$3/2\ \ 3/2$	30,545.994 0.069
FCl^{37}	0	$3/2\rightarrow1/2$	$30{,}280.107\pm0.042$
		$3/2\ \ 5/2$	30,257.159 0.042
		$3/2\ \ 3/2$	30,228.359 0.042
	1	$3/2\rightarrow1/2$	30,026.195 0.069
		$3/2\ \ 5/2$	30,003.218 0.069
		$3/2\ \ 3/2$	29,974.470 0.069

Table II. Molecular constants of FCl.

	FCl^{35}	FCl^{37}
B_e	$15{,}483.688\pm0.026$ mc	$15{,}189.221\pm0.026$ mc
I_e	54.1822×10^{-40} g cm^2	55.2326
D_e	0.0263 mc*	0.0253
α	130.666 ± 0.029 mc	126.957 ± 0.029
r_e	1.62811×10^{-8} cm	
μ	0.881 ± 0.02 debye	
c	0.036 ± 0.009 mc	0.019 ± 0.009
eq$Q$	-145.94 ± 0.26 mc	-114.92 ± 0.26

* Calculated from the vibrational frequency given by A. L. Wahrhaftig, J. Chem. Phys. **10**, 248 (1942); also P. A. Griswold, thesis, State University of Iowa, 1949.

The values of the quadrupole coupling energy are $eqQ^{35}=-145.99\pm0.26$ mc and $eqQ^{37}=-114.92\pm0.26$ mc. The ratio $eqQ^{35}/eqQ^{37}=1.2704\pm0.004$ is only in fair agreement with the ratio of the quadrupole moments obtained by Davis and Zabel[6] from the spectrum of atomic chlorine, $Q^{35}/Q^{37}=1.2795\pm0.0026$. The existence of coupling with higher order electronic states also introduces a "pseudo-quadrupole" coupling[1,3] of unknown magnitude, indistinguishable from the nuclear coupling. Such a contribution to eq$Q$, being the same in both isotopic molecules, would tend to alter the observed ratios.

The ratio $Be^{37}/Be^{35}=0.9809821\pm0.0000024$ gives for the mass ratio $Cl^{35}/Cl^{37}=0.9459775\pm0.000004$. This agrees quite well with the value obtained by Townes *et al.*[7] from the microwave spectrum of ICl, 0.9459801 ± 0.000005. Both microwave determinations disgree with the best value from mass spectroscopy,[8] 0.9459445 ± 0.000007. We conclude that the latter is probably in error.

Stark effect measurements were made on the line $F=3/2\rightarrow3/2$, $M_F=3/2\rightarrow3/2$. The analysis of these data requires the solution of the secular equation for the case of intermediate field strength[9] $\mu^2E^2/B\sim eqQ$. The value of the molecular electric dipole moment appears in Table II along with other derived and measured molecular constants.

The bond in FCl is estimated at 80 percent covalent, 20 percent ionic, the latter figure being an average of the value obtained from electro-negativity difference and that obtained from the observed dipole moment. The large observed quadrupole coupling is in qualitative agreement with the value calculated on this basis, but somewhat larger than that obtained by assuming the covalent bond to be an s-p hybrid[10] and neglecting other contributions to q.

We are grateful to the Pennsylvania Salt Company, especially Dr. N. D. Peschko, for the gift of the FCl used in this work.

* Supported in part by ONR.
** Now at Smith College, Northampton, Massachusetts.
[1] W. A. Nierenberg and N. F. Ramsey, Phys. Rev. **72**, 1075 (1947).
[2] J. W. Simmons and W. Gordy, Phys. Rev. **73**, 713 (1948).
[3] R. S. Henderson, Phys. Rev. **74**, 107L (1948).
[4] J. M. Jauch, Phys. Rev. **74**, 1262A (1948).
[5] H. H. Goldsmith and D. R. Inglis, "The properties of atomic nuclei I," Brookhaven National Laboratory Report BNL-1-5 (1948).
[6] L. Davis and C. W. Zabel, Phys. Rev. **74**, 1211A (1948).
[7] Townes, Merritt, and Wright, Phys. Rev. **73**, 1334 (1948).
[8] Recalculated from Okuda *et al.*, Phys. Rev. **58**, 578 (1940), with H and C masses from K. T. Bainbridge, "Isotopic weights of the fundamental isotopes," National Research Council, Washington, D. C. (1948).
[9] F. Coester (to be published).
[10] C. H. Townes and B. P. Dailey, J. Chem. Phys. **17**, 782 (1949).

Spectral Analysis of 10-Mev Betatron Radiation by Nuclear Emulsion

P. K. S. WANG AND M. WIENER
National Bureau of Standards, Washington, D. C.
October 21, 1949

AN attempt to determine the spectrum of the 10-Mev betatron at the Naval Ordnance Laboratory has been made. We recorded and measured the proton tracks from the photo-disintegration of deuterium absorbed into the nuclear emulsions.[1,2]

The emulsions were Ilford C_2, 100μ thick. After eradication of accumulated background,[3] the plates were soaked in D_2O for 20 minutes at 25°C, before exposure. Tests indicate that D_2O is reproducibly absorbed to the extent of 80 percent of the weight of emulsion before soaking and is uniformly distributed in the various layers of the emulsion. These plates along with a control plate similarly soaked in H_2O were then exposed perpendicularly to the axis of the x-ray beam for an exposure of approximately 0.3 roentgens as measured by a Victoreen thimble chamber without external cap. The distance of the plates from the target was about 1.5 meters. The exposure lasted for 12 seconds. Along with another blank control plate, these plates were immediately developed in a mild hydroquinone developer perfected by Yagoda.[4] The fog background of the exposed plates was very slight. This facilitated the scanning of the plates and the measurement of the tracks. There were about 2000 tracks on each of the D_2O loaded plates and very few (~30) on an H_2O loaded plate. The blank control plate showed the usual background of accumulated stars and tracks.

We measured 500 tracks on the D_2O plates and selected those tracks (312) which had a slope $\leq 45°$ in the wet emulsion. On an equal area of an H_2O loaded plate, only 7 tracks were found. Since the 100μ emulsion swelled to 380μ after soaking and then shrank to 40μ after processing, the depth component, d, of the measured track length was multiplied by a factor, 9.5, in order to determine the original slope of the track in the wet emulsion. The uncorrected data on these 312 tracks are shown in Fig. 1, along with the control plate data.

The probability of a track starting and ending within the emulsion depends on its length and slope. This probability is equal to the ratio $(t-d)/t$, where t is the emulsion thickness after development (40μ). To correct for this, each track was given a statistical weight $t/(t-d)$. As we have limited our acceptable track angles to $\leq 45°$, this is a small correction in most instances. The weighted histogram is shown in Fig. 2.

The range-energy relationship was calculated from the variation of stopping power with energy[5] for the wet plate. This relationship was checked experimentally with recoils from D−D neutrons obtained using 0.75-Mev deuterons from the 3-Mev Van de Graaf machine at the Department of Terrestrial Magnetism of the Carnegie Institution. Our relationship is good to ±5 percent within the ranges we are considering. The rated maximum energy of the betatron is 10 Mev while the photon energy corresponding to the longest track is 11 Mev. According to information received, this is a reasonable value. In the following comparison with theory we assume the actual maximum energy to be 11.0 Mev.

The number of proton tracks, N_p, to be expected in our experiment within the range limits R_w and $R_w+\Delta R_w$ is related to the x-ray spectral intensity $I(E)\Delta E$ by the equation:

$$N_p=\frac{I(2E_p+2.2)}{2E_p+2.2}\sigma_{45°}^{135°}(2E_p+2.2)N_D 2(dE_p/dR_w)\Delta R_w At,$$

where

E_p = energy of proton in Mev,
N_D = number of deuterons per cm² emulsion,
$$=2\times 6.0\times 10^{23}\times\frac{(\text{g of } D_2O \text{ per cm}^2 \text{ emulsion})}{20},$$
dE_p/dR_w = stopping power of emulsion (Mev/μ),
$\sigma_{45°}^{135°}(E)$ = the cross section for photo-disintegration by a photon of energy E within our angular limits,
A = area of the emulsion examined,
t = time of exposure.

The theoretical histogram obtained using $I(E)\Delta E$ according to Schiff[6] with a suitable normalization and with the assumed maximum energy of 11.0 Mev is shown as a dotted line in Fig. 2 for comparison with the experimental data. The discrepancy at the low energies (<4.0 Mev) is at least partially due to the difficulty in finding all the short tracks. The excess over theory at

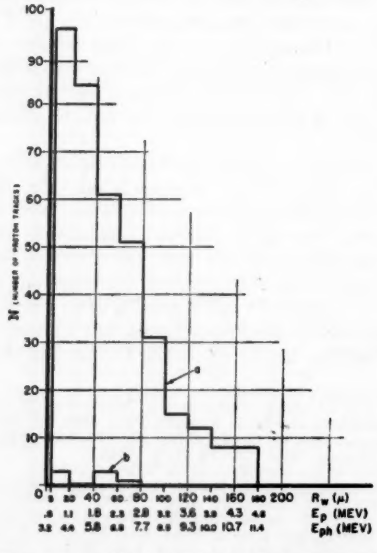

FIG. 1. (a) Histogram of data on D_2O loaded plates. Number of tracks, N, *vs.* range in wet emulsion, R_w, converted to energy of protons, E_p, and energy of incident photons, E_{ph}. (b) Histogram of data in H_2O loaded plate, equivalent area.

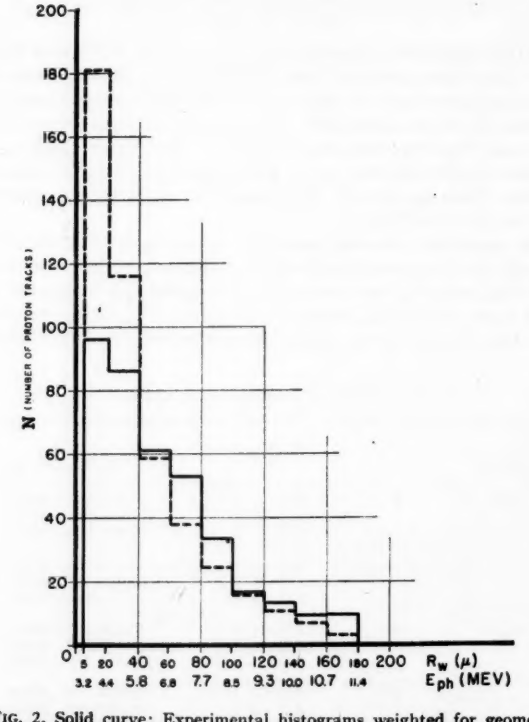

FIG. 2. Solid curve: Experimental histograms weighted for geometry. Dotted curve: Theoretical histogram from Schiff's calculations based on Bethe-Heitler theory and an assumed maximum energy of 11.0 Mev.

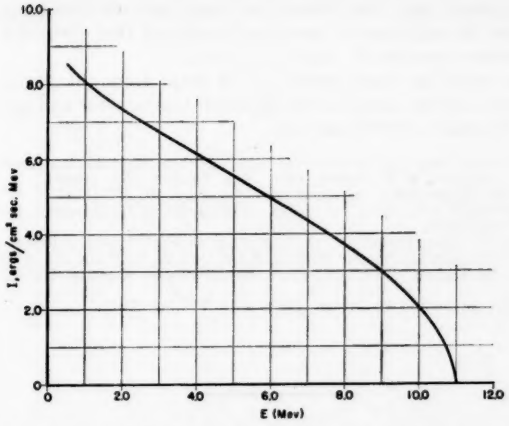

FIG. 3. Approximate intensity spectrum of the Naval Ordnance Laboratory betatron when run at "10 r/min. at 1 m," at 1.5 m from the target.

the high energies parallels results obtained at Illinois[7] at somewhat higher energies (20 Mev). If we assume the fit with Schiff's theory to be good enough, the comparison of the theoretical distribution with our experiment determines the approximate normalization factor. The intensity spectrum under the stated conditions in absolute units is given in Fig. 3.

We appreciate the kindness of Mr. D. T. O'Connor of the Naval Ordnance Laboratory for making the betatron available for our use. We wish also to extend our appreciation to Dr. U. Fano for several discussions and to Drs. N. P. Heydenburg and W. D. Whitehead for providing the D−D neutrons.

[1] W. Bosley, D. T. Cragg, *et al.*, Nature **161**, 1022 (1948).
[2] G. Goldhaber, Phys. Rev. **75**, 1725 (1949).
[3] M. Wiener and H. Yagoda, Phys. Rev. **76**, 469 (1949).
[4] H. Yagoda, Nucleonics **4**, 135 (1949).
[5] E.g., J. H. Webb, Phys. Rev. **74**, 511 (1948).
[6] L. I. Schiff, as reported by G. D. Adams, Phys. Rev. **74**, 1710 (1948).
[7] E. G. Fuller, Phys. Rev. **76**, 576 (1949).

The Excess of Negative over Positive Mesons Produced by High Energy Photons

K. A. BRUECKNER AND M. L. GOLDBERGER*
Radiation Laboratory, University of California, Berkeley, California
October 20, 1949

MESONS produced by the high energy photon beam from the University of California Radiation Laboratory 330 Mev synchrotron are found to show an excess of negatives over positives.[1] With a carbon target, observing mesons in the energy range 30–130 Mev at 90° to the photon beam, the ratio of negative to positive mesons is 1.7 ± 0.2 with no significant energy dependence.

A simple classical argument can be made to give an understanding of the reason for the negative excess. The photon can interact directly with the meson and proton through the current coupling

$$(\mathbf{j}\cdot\mathbf{A})(\text{meson})+(\mathbf{j}\cdot\mathbf{A})(\text{proton}).$$

The meson contribution is symmetrical for the production of positive and negative mesons. However, when positive mesons are produced, the proton is the initial nucleon at rest, and its current is zero. When negative mesons are produced, the proton is the final recoil nucleon giving a current contribution. Therefore, the cross sections for the production of positive and negative mesons are in the ratio

$$\frac{\sigma(\text{positives})}{\sigma(\text{negatives})}=\left[\frac{(\mathbf{j}\cdot\mathbf{A})(\text{meson})}{(\mathbf{j}\cdot\mathbf{A})(\text{meson})+(\mathbf{j}\cdot\mathbf{A})(\text{recoil proton})}\right]. \quad (1)$$

The current interaction is

$$\mathbf{j}\cdot\mathbf{A}=\frac{e\mathbf{v}\cdot\mathbf{A}}{1-(v/c)\cos\theta'}$$

where

$\mathbf{v}$ = velocity of particle
$\mathbf{A}$ = vector potential
$\cos\theta$ = angle between direction of particle and photon.

This differs from the non-relativistic expression, $e\mathbf{v}\cdot\mathbf{A}$, the factor $1-v/c\cos$ in the denominator taking account of the retardation effects in the interaction of charge with the electromagnetic field. Inserting this current expression and using over-all energy and momentum conservation, the positive to negative ratio can be written

$$\frac{\sigma(\text{positives})}{\sigma(\text{negatives})}=\left[1-\frac{\epsilon}{mc^2}\left(1-\frac{v}{c}\cos\theta\right)\right]^2, \quad (2)$$

where

ϵ = meson energy including rest energy
v = meson velocity
θ = angle between direction of meson and photon
m = nucleon rest mass.

Further calculations have been carried out using standard perturbation theory for scalar and pseudoscalar mesons to the lowest order in the coupling constants g and e, treating the nucleons as Dirac particles and taking into account the effects of the nucleon recoil. The result of these calculations, for the ratio of the cross sections for positive and negative mesons, is exactly the same as that derived by the above simple considerations. Similar calculations for vector mesons with vector coupling to the nucleon field are complicated by the strong magnetic moment interaction of the vector particle with the e.m. field. The ratio of negative to positive mesons is similar to that for the scalar meson fields but is somewhat larger.

The effects of the Coulomb field of the nucleus on the production of mesons have also been investigated and found to be less than 5 percent for mesons with energies above 30 Mev.

The ratio of the cross sections for the production of negative and positive mesons given by (1) varies from 1.55 at 40 Mev to 1.83 at 100 Mev, at 90° to the photon beam. This agrees, within the probable error with the experimentally observed ratio. Since the positive-negative ratio depends in a quite direct way on the currents carried by the mesons and nucleons, a more accurate determination of the ratio and its energy dependence could provide valuable evidence concerning the magnetic moments of the particles.

* Now at Department of Physics, Massachusetts Institute of Technology, Cambridge, Massachusetts.
[1] McMillan, Peterson, and White (to be published in Science).

The Beta-Spectra of Cu^{64}

L. M. LANGER, R. D. MOFFAT, AND H. C. PRICE, JR.
Indiana University, Bloomington, Indiana
October 21, 1949

IN a previous paper,[1] results were reported which indicated that the negatron and positron spectra of Cu^{64} have more particles at low energy than is predicted by the Fermi theory of beta-decay. It was later reported by Wu and Albert[2] that this deviation appeared to be a function of the source thickness over the same range of values for which no such effect had been observed in the earlier work. Subsequently, we made a study of autoradiographs of sources prepared from chemical solutions. It was found that in general such sources, though appearing to be uniform, may in many cases have variations in intensity of as much as 100 to 1. Under these circumstances, the *average* thickness of a source as reported by different investigators does not have much meaning.

In order to remove this difficulty, we have attempted to remeasure the Cu^{64} spectra using sources prepared by thermal evaporation of metallic Cu in vacuum. Two sources were used.

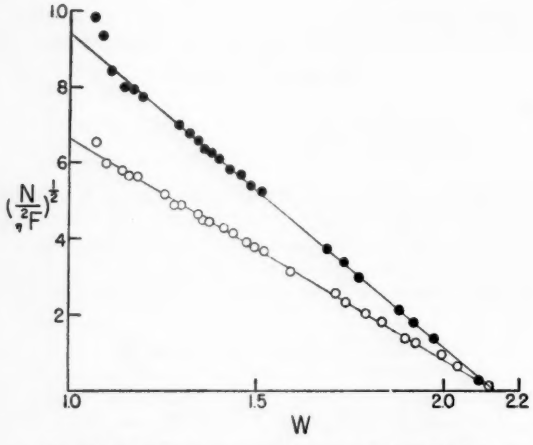

FIG. 1. Fermi plot of the negatron spectrum of Cu^{64}. Solid circles are for data obtained with the 75 $\mu g/cm^2$ source backed by 0.18 mg/cm^2 Al leaf. The open circles are for data obtained with the less than 5 $\mu g/cm^2$ source backed by 15 $\mu g/cm^2$ Zapon.

The thinnest one was less than 5 micrograms/cm^2 and was deposited on a Zapon backing of 15 micrograms/cm^2, at a distance of one inch from the evaporating filament. The autoradiograph of this source showed complete uniformity. The second source was twenty-five times stronger and consisted of 75 micrograms/cm^2 deposited at a distance of $\frac{1}{4}$ inch on a backing of 0.18 mg/cm^2 aluminum leaf. The autoradiograph of this source showed that the activity was uniformly distributed to within a factor of two.

Measurements were made in the 40-cm radius of curvature shaped magnetic field spectrometer.[3] A thin mica window counter was used for detecting particles with energies above 150 kev. A 6 microgram/cm^2—Zapon window counter was used for the region below 250 kev. The Zapon window was supported on a copper Lektromesh[4] grid, 0.004 inch thick having 0.006-inch openings which yield a transmission of 23 percent. The data were adjusted for intensity at one point in the overlapping energy region.

Figure 1 shows a Fermi plot of the data obtained on the negatron distribution. It is immediately apparent that the spectra obtained with both sources show no deviation from the Fermi theory for all energies above 50 kev.[5]

Figure 2 is a plot of the positron data. Here too, it is clear that the deviation from the straight line is much less than that previously found with thicker and less uniform sources. Also, since the screening is not negligible[6] for positrons, even better agreement with the theory will be obtained when this correction is applied.

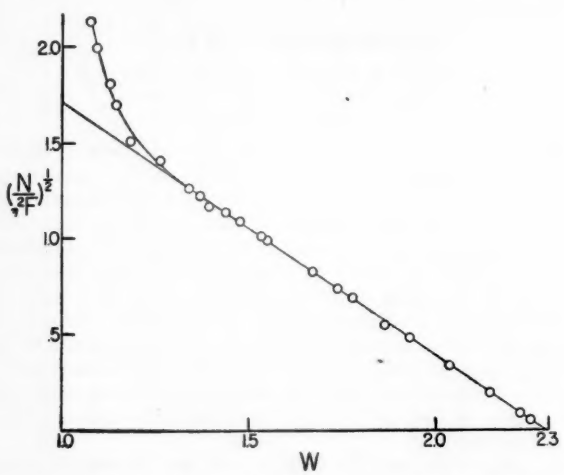

FIG. 2. Fermi plot of the positron spectrum of Cu^{64} obtained with the 75 $\mu g/cm^2$ source.

It appears, then, that there is no longer any real disagreement between the experimental spectrum shape and that predicted for an allowed transition by the Fermi theory.

This work has been assisted by a grant from the Frederick Gardner Cottrell Fund of the Research Corporation and by the Joint Program of ONR and AEC.

[1] C. Sharp Cook and Lawrence M. Langer, Phys. Rev. **73**, 601 (1949).
[2] C. S. Wu and R. D. Albert, Phys. Rev. **75**, 315, 1107 (1949).
[3] L. M. Langer and C. S. Cook, Rev. Sci. Inst. **19**, 257 (1949).
[4] Obtainable from the C. O. Jelliff Manufacturing Corporation, Southport, Connecticut.
[5] Recent measurements on the spectrum of Pm^{147} yield a Fermi plot which is straight all the way down to 8 kev. See H. C. Price, Jr., J. Motz, and L. M. Langer, Bull. Am. Phys. Soc., Chicago Meeting, November, 1949.
[6] C. Longmire and H. Brown, Phys. Rev. **75**, 264 (1949).

The Positron and Megatron Spectra of Cu^{64}

GEORGE E. OWEN AND C. SHARP COOK
Physics Department, Washington University, St. Louis, Missouri*
October 14, 1949

THE positron and negatron spectra of Cu^{64} have been studied by several groups[1] as a test of the Fermi Theory. As was described in a previous letter[2] a method has been developed which enables the preparation of very thin sources by evaporation onto a backing of 0.00025-inch aluminum foil. A source of Cu^{64} has been prepared by the process $Zn^{64}(n,p)Cu^{64}$. To insure the maximum number of fast neutrons for the reaction, the zinc was placed immediately behind a beryllium cyclotron target which was bombarded by deuterons. The copper was then electroplated onto a 0.010-inch diameter tungsten wire as previously described,[2] this wire then being used as a filament from which the active copper could be evaporated. The source thus prepared was then studied in a 6-cm radius of curvature spectrometer.[3] This source contained *only* radioactive copper atoms. The thickness as calculated from the activity is of the order of magnitude of 10^{-4} microgram/cm^2.

The $F-K$ plot of the negatrons is shown in Fig. 1, and the $F-K$ plot of the positrons is shown in Fig. 2. Both plots are con-

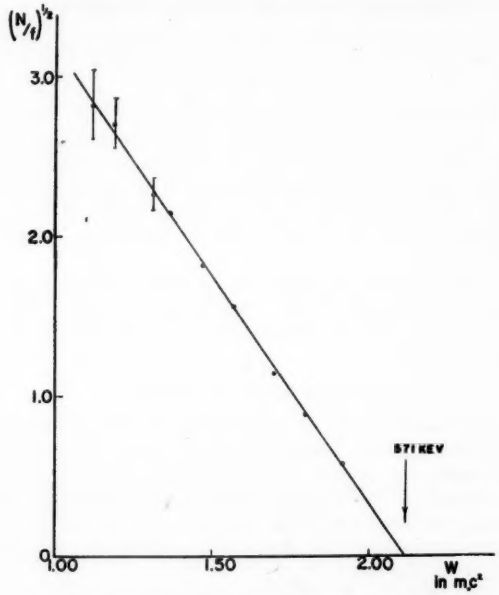

FIG. 1. $F-K$ plot of the negatrons from Cu^{64}. This source was prepared by evaporation to provide a uniform and thin source.

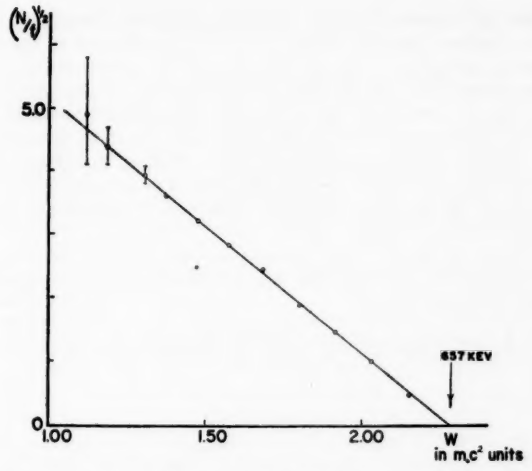

FIG. 2. $F-K$ plot of the positrons from Cu^{64} using the same source as in Fig. 1.

sistent with linearity to less than 50 kev. This strongly suggests that previous deviations found in the $F-K$ plot of this isotope were a result of finite source thickness.

* Assisted by the Joint Program of the ONR and the AEC.

[1] J. Backus, Phys. Rev. **68**, 59 (1945); C. S. Cook and L. M. Langer, Phys. Rev. **73**, 601 (1948); G. E. Owen and H. Primakoff, Phys. Rev. **74**, 1406 (1948); C. S. Wu and R. D. Albert, Phys. Rev. **75**, 1107 (1949).
[2] G. E. Owen and C. S. Cook, Phys. Rev. **76**, 1536 (1949).
[3] G. E. Owen and C. S. Cook, Rev. Sci. Inst. **20**, 768 (1949).

Magnetic Resonance Absorption of Diluted Iron Ammonium Alum*

R. T. WEIDNER, P. R. WEISS, C. A. WHITMER, AND D. R. BLOSSER**
Department of Physics, Rutgers University, New Brunswick, New Jersey

October 17, 1949

MEASUREMENTS have been made on the paramagnetic absorption spectra of iron ammonium alum at room temperatures and at 9375 mc/sec. The method used is similar to that described earlier;[1] however, the method has been modified so that the absorption is measured directly through a measurement of χ'' alone.

Bagguley *et al.*[2] have reported measurements at room temperature on undiluted single crystals of iron ammonium alum which indicate a zero-field splitting no greater than 0.10 cm^{-1}. Because of the large spin-spin interactions the individual lines to be expected were unresolved. We have been able to resolve the lines partially by using diluted single crystals in which some of the iron ions are replaced by aluminum.

TABLE I. Theoretical absorption pattern.

	$A=h\nu/g\beta$; $B=\delta c/\nu$.		
Orientation	Peak positions		
(100)	A	$A(1\pm(4/6)B)$	$A(1\pm(5/6)B)$
(111)	A	$A(1\pm(4/9)B)$	$A(1\pm(5/9)B)$
(110)	A	$A(1\pm(4/24)B)$	$A(1\pm(5/24)B)$
	Relative intensities		
All 3	9	5	8

Figures 1, 2, and 3 show measured absorption curves for the orientations of the d.c. field perpendicular to the crystalline faces (100), (111), and (110), respectively. The absorption for the undiluted salt is shown by curve 1; curves 2 and 3 apply respectively to the dilutions of 1 iron to 13 aluminum atoms and 1 iron to 38 aluminum atoms. No attempt has been made to measure absolute absorption, and the ordinate scales are not identical for the several curves; however, for all orientations the intensity decreased with dilution. The lines in the figures indicate the positions and relative intensities of the resonances as computed from the theory.

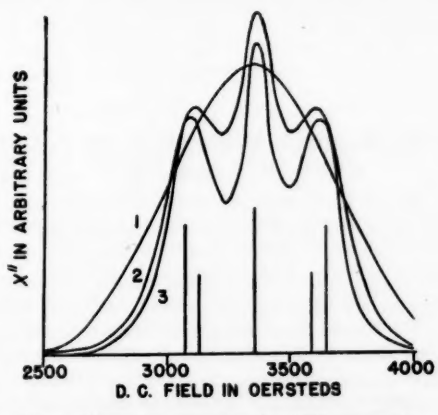

FIG. 1. Absorption curves for the (100) orientation.

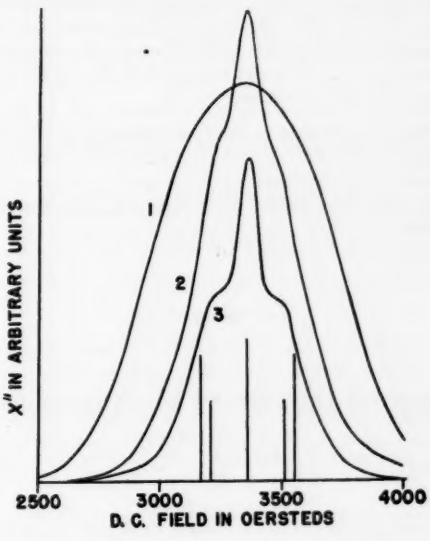

FIG. 2. Absorption curves for the (111) orientation.

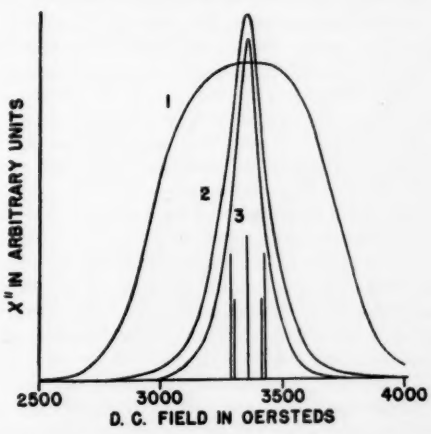

FIG. 3. Absorption curves for the (110) orientation.

The electric field acting on the iron ion is taken to be due to the octahedron of water molecules surrounding the ion and is, therefore, of predominantly cubic symmetry. The single energy level of the ^6S state of the normal ion splits,[3] under the influence of the crystalline field, into two levels, one doubly degenerate, the other quadruply degenerate. The expected relative intensities and positions in oersteds of the absorption lines are shown in Table I for the three orientations used in these measurements. δ is the level separation, or zero-field splitting in cm^{-1}, and g is the effective g value of the paramagnetic ion.

The patterns for the three orientations differ only in the separation of the side peaks from the central maximum. The side peaks are resolved from the central peak only in the (100) orientation of the diluted salts, although here, too, the overlapping of lines is appreciable. The theoretical spectra shown in the figure are those obtained with $\delta=0.032\ cm^{-1}$; this value of δ was chosen to give the best fit between the weighted mean of the side peaks in the theoretical spectrum and the observed side peaks of the (100) orientation. Because of the overlapping of the lines and their unknown shapes this value is approximate.

The curves for the (111) and (110) orientations are not inconsistent with this choice of δ. Although it is impossible to assign a value to the splitting for the undiluted salt, it appears that there is very little change in the splitting with changes in dilution.

The position of the central peak is the same for all curves and corresponds to $g=1.99\pm0.01$.

A rough graphical analysis of the observed pattern made on the assumption of a Gaussian line shape and a constant line width for all resonances in a given orientation does not yield agreement with the theoretical intensities, the intensity of the observed central peak being relatively too strong.

* This work was supported by the Joint Program of the ONR and the AEC, by the RCA Research Laboratories, and by the Rutgers University Research Council.

** Deceased October 8, 1949.

[1] Whitmer, Weidner, Hsiang, and Weiss, Phys. Rev. **74**, 1478 (1948).
[2] Bagguley, Bleaney, Griffiths, Penrose, and Plumpton, Proc. Phys. Soc. **61**, 551 (1948).
[3] H. Bethe, Ann. d. Physik **3**, 133 (1929).

Energy for Diffusion by Direct Interchange

H. B. HUNTINGTON
Physics Department, Rensselaer Polytechnic Institute, Troy, New York
AND
FREDERICK SEITZ
Physics Department, University of Illinois, Urbana, Illinois
October 17, 1949

WE are much indebted to Professor Zener for calling our attention to an error in the value given in our paper[1] for the electrostatic energy associated with the saddle-point configuration (Fig. 2A in reference 1) for direct-interchange diffusion in copper. The original value was 11 ev. On recalculation the energy for the same configuration turns out to be 4.8 ev.

Besides the electrostatic term there is an increase in the energy of this configuration associated with the closed shell repulsion of the ion cores. This has been estimated to be 6.2 ev on the basis of a repulsive potential of exponential form with parameters chosen to fit with the known elastic constants of copper. It is admittedly a severe extrapolation to use the elastic data to calculate the interaction energy of copper ions at distances of approach as close as those occurring in this configuration. We decided to re-examine also this part of the direct interchange calculation to find out to what extent the result had been prejudiced by the choice of an exponential repulsion. Recent measurements on the compressibility of copper have been reported by Bridgman[2] for pressures up to 30,000 kg/cm². They can be interpreted to give a variation of bulk modulus of 7.8×10^{10} dy/cm² for one percent change in volume. This turns out to be only about 20 percent more than the value obtained from the fourth term in the expansion of the exponential potential. While the closeness of this agreement may be some extent fortuitious, the general validity of the original approach appears to be substantiated. If one constructs a cubic expression for the potential, using the same constant term as in the expansion of the exponential and evaluating the other coefficients from the elastic constants and the high pressure data, one obtains for the energy of repulsion for the saddle-point about 5.5 ev against 6.2 as previously quoted.

Within the limits of this calculation, the results indicate that direct interchange is ruled out for the self-diffusion of copper by energetic considerations.

[1] H. B. Hungtington and Frederick Seitz, Phys. Rev. **61**, 315 (1942).
[2] P. W. Bridgman, Proc. Am. Acad. Arts Sci. **77**, 198 (1949).

Erratum: The Equation of State of Gaseous He^3

[Phys. Rev. **76**, 998 (1949)]
J. VAN KRANENDONK, K. COMPAAN, AND J. DE BOER
Institute for Theoretical Physics, University of Amsterdam, Amsterdam, Netherlands

IN consequence of an unfortunate misunderstanding this letter has been printed with the following errors:

The formula (1) for B should read:

$$\text{“}B=-\frac{N}{2\pi^2}\left(\frac{h^2}{\pi m\kappa T}\right)^{5/2}\int_0^\infty\sum_l(2l+1)\delta_l\eta_l(k)\exp\left(-\frac{h^2k^2}{m\kappa T}\right)kdk$$
$$+N\left(\frac{h^2}{\pi m\kappa T}\right)^{3/2}\sum_n\sum_l(2l+1)\delta_l(e^{-E_{nl}/\kappa T}-1)+\frac{N}{32}\left(\frac{h^2}{\pi m\kappa T}\right)^{3/2},$$

where $\delta_l=\frac{1}{2}-(-1)^l\frac{1}{4}$.”

The last sentence in the lines following the equation should read: “*The influence of the statistics*, i.e., of the symmetry character of the wave functions is reflected, firstly in the last term which is positive for F.D. statistics and negative for B.E. statistics, and secondly in the value of δ_l which transforms into $\frac{1}{2}+(-1)^l\frac{1}{4}$ in the case of B.E. statistics.”

The table should be corrected as follows:

T	He^3 $B.T^{3/2}$	He^4 $B.T^{3/2}$
0.51	−107	−388
1.02	−205	−401
2.04	−331	−477
3.07	−412	−543
4.09	−469	−592
5.11	−511	−625
6.13	−541	−644
7.15	−561	−654

“The contribution of the last term of (1) to $BT^{3/2}$ is constant and equal to 45.5 cm³ degree$^{3/2}$/mole. A detailed account of these calculations will appear shortly in *Physica*.”

On the Magnetic Moments of Sn^{115}, Cd^{111}, Cd^{113}, Pt^{195}, and Hg^{199} *

W. G. PROCTOR AND F. C. YU
Department of Physics, Stanford University, Stanford, California
October 13, 1949

USING the nuclear induction spectrometer described in an earlier letter,[1] the magnetic moments of Sn^{115}, Cd^{111}, Cd^{113}, Pt^{195}, and Hg^{199} have been measured, in good agreement with these results from hyperfine structure measurements: $\mu(Sn^{115})=-0.89\mu_N$;[2] $\mu(Cd^{111})=-0.65\mu_N$;[3] $\mu(Cd^{113})=-0.65\mu_N$;[3] $\mu(Pt^{195})=0.6\mu_N$;[4] $\mu(Hg^{199})=0.547\mu_N$.[5] Resonance amplitudes were consistent with a spin of $\frac{1}{2}$, as obtained by hyperfine structure ob-

TABLE I. Magnetic moments and diamagnetic corrections.

Nucleus	Magnetic moment in nuclear magnetons	Diamagnetic correction in percent
Sn^{115}	-0.9132 ± 0.0003	0.50
Cd^{111}	-0.5922 ± 0.0002	0.47
Cd^{113}	-0.6194 ± 0.0002	0.47
Pt^{195}	$+0.6004\pm0.0002$	0.93
Hg^{199}	$+0.4993\pm0.0002$	0.96

servations. The signs of the magnetic moments agreed in each case with those above.

The abundance of the isotope Sn^{115} being 0.4 percent,[6] its resonance was not observed with the sample which revealed the resonances of Sn^{117} and Sn^{119} reported earlier,[7] the latter nuclei having abundances near 9 percent. However, by dissolving $SnCl_2 \cdot 2H_2O$ in an aqueous solution of 2.0-molar $MnSO_4$ at 100°C it was possible to have a liquid sample in the form of a supersaturated solution that would not crystallize for many hours at room temperature. The sample finally contained tin to about a 12-molar concentration and $MnSO_4$ to about an 0.7-molar concentration. The resonance was found in the neighborhood of 6200 kc, or about 700 kc below the Sn^{117} resonance frequency for a magnetic field of 4500 gauss. The frequency of the Sn^{115} resonance was compared to that of Na^{23} from an aqueous solution of 0.2-molar NaCl with 0.2-molar $MnSO_4$. Each resonance was recorded five times with the result that

$$\nu(Sn^{115})/\nu(Na^{23}) = 1.2362 \pm 0.0001.$$

The cadmium resonances were found at a field of 6600 gauss with radiofrequencies near 6000 kc, using a saturated solution of $CdCl_2$ in 0.3-molar $MnSO_4$ as a sample. Recording each resonance four times, the frequency ratios were found to be

$$\nu(Cd^{111})/\nu(Na^{23}) = 0.8016 \pm 0.0001,$$
$$\nu(Cd^{113})/\nu(Na^{23}) = 0.8386 \pm 0.0001,$$
$$\nu(Cd^{113})/\nu(Cd^{111}) = 1.0461 \pm 0.0001.$$

The last ratio, of course, gives the ratio of the magnetic moments of Cd^{113} to Cd^{111}. The resonances were identified by using samples of cadmium enriched to about 80 percent in Cd^{111} and in Cd^{113}.[8]

The resonance of Pt^{195} was observed near 5900 kc, using a magnetic field of 6600 gauss. The sample was a 1.0-molar solution of H_2PtCl_6 with a 0.5-molar concentration of $MnCl_2$. By comparing the resonance frequency of Pt^{195} with that of Na^{23} five times, we found

$$\nu(Pt^{195})/\nu(Na^{23}) = 0.8127 \pm 0.0001.$$

The resonance of Hg^{199} was observed near 6800 kc with a magnetic field of 8900 gauss. The sample contained $HgNO_3$ in dilute nitric acid to a 7.0-molar concentration with a 0.2-molar concentration with a 0.2-molar concentration of $Mn(NO_3)_2$. By comparing the resonance frequency of Hg^{199} four times with that from D^2 from a 1.8-molar aqueous solution of $MnSO_4$ containing 25 percent D_2O, we found

$$\nu(Hg^{199})/\nu(D^2) = 1.1647 \pm 0.0001.$$

The magnetic moments resulting from the above frequency ratios are given in the second column of Table I. A correction due to the diamagnetic field of the atomic electrons has not been included in the computation for the magnetic moments but its magnitude is given in the third column. These values have been determined by linear interpolation from the values for specific atoms given by Lamb using Hartree fields,[9] and they are to be applied so as to increase the magnitudes of the magnetic moments. The magnetic moment of Na^{23} has been computed by taking

$$\mu(H^1) = (2.7928 \pm 0.0008)\mu_N$$ [10]

and

$$\nu(Na^{23})/\nu(H^1) = 0.26450 \pm 0.00003.$$ [11]

The magnetic moment of D^2 was similarly computed using

$$\mu(D_2)/\mu(H^1) = 0.307013.$$ [12]

We should like to express here our gratitude to Professor Felix Bloch for many helpful consultations during the course of this work.

* Assisted by the Joint Program of the AEC and the ONR.
[1] W. G. Proctor, Phys. Rev. **75**, 522 (1949).
[2] Properties of Atomic Nuclei, Publication BNL-I-5, Brookhaven National Laboratory, October 1, 1948.
[3] H. A. Bethe and R. F. Bacher, Rev. Mod. Phys. **8**, 82 (1936).
[4] T. Schmidt, Zeits. f. Physik **101**, 486 (1936).
[5] S. Mrozowski, Phys. Rev. **57**, 207 (1940).
[6] F. W. Aston, Nature **137**, 613 (1936).
[7] W. G. Proctor, Phys. Rev. **76**, 684 (1949).
[8] We are grateful to Dr. B. J. Moyer of the Radiation Laboratory at the University of California for lending us the enriched cadmium samples.
[9] W. E. Lamb, Jr., Phys. Rev. **60**, 817 (1941).
[10] This value differs from the value $(2.7896 \pm 0.0008)\mu_N$ given by S. Millman and P. Kusch, Phys. Rev. **60**, 91 (1941), by the correction for the magnetic moment of the electron $(1 \pm \alpha/2\pi)$ suggested by J. Schwinger, **73**, 416 (1947).
[11] F. Bitter, Phys. Rev. **75**, 1326 (1949).
[12] This figure is that given by Bloch, Levinthal, and Packard, Phys. Rev. **72**, 1125 (1947), rounded to six places.

Stopping Power of Nuclear Emulsions for Ionizing Particles

HERVASIO G. DE CARVALHO*
Laboratorio da Producao Mineral, Rio de Janeiro, Brasil
October 17, 1949

RANGE measurements in nuclear emulsions for particles of known energy are comparatively few in number. The more abundant experimental and theoretical data on range-energy relations for ionizing particles in air can be utilized in evaluating the energy of particles from track length measurements in the emulsion provided the stopping power "s" of the recording medium relative to air is known as a function of the velocity "v". We want to indicate that an empirical relation of the type:

$$S = R_0/R = A\beta^k \qquad (1)$$

holds in a wide range of velocities; R is the length of the track in the medium under consideration, R_0, in dry air at 15°C and 760 mm of pressure, A and k being constants which depend only on the nature of the medium, and $\beta = v/c$. That this is satisfactory in the range of β from 0.035 to 0.28 is exhibited in the lower part of Fig. 1 where we have plotted log "s" against β (in logarithmic

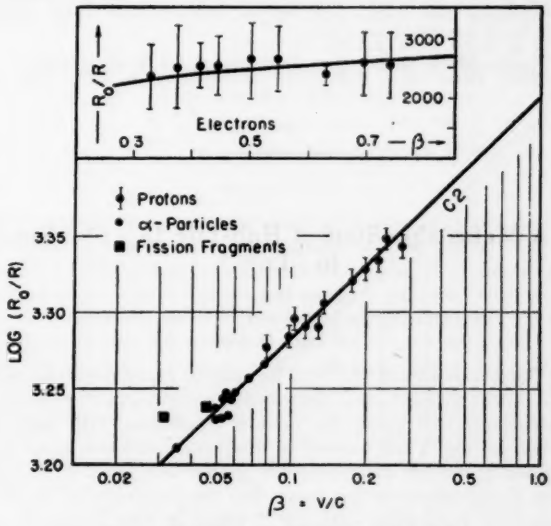

FIG. 1. Variation of R_0/R as a function of β.

scale) for the available experimental data for proton and α-particles. The values of R for the Ilford C2 emulsion in "dry conditions" were taken as follows: α-particles from Picciotto,[1] Green and Gibson[2] and Lattes, *et al.*;[3] for protons from Lattes, *et al.*[3] and Bradner, *et al.*[4]. The ranges in air for α-particles were taken from Feather;[3,5] for protons, from Smith.[6] The full line was obtained by the least square method and corresponds to the values $A=2760$ and $k=0.157$. It agrees with the experimental points within 2 percent. As pointed out by Bradner, *et al.*,[4] the moisture content has a special importance in the stopping power of the emulsions; it seems to us that this results mainly from its effect on the density of emulsion. Small deviation of the experimental points from the straight line may be attributed to this effect. It is therefore necessary to standardize the figures on the basis of dry atmosphere or vacuum conditions.

We also plotted the points for fission fragments,[7,8] the one which falls closer to the line corresponding to the lightest fragment.

Comparison with experimental data for electrons is rendered difficult by the fact that the only available data for range-energy relations in emulsions are the ones in NT4 plates.[9] However, the calculations on the basis of the chemical composition[10] using Webb-Cüer's[11] method shows that in the range of β from 0.3 to 0.8 the stopping power of C2 and NT4 agrees within 2 percent. In the upper part of Fig. 1, "s" (and the corresponding standard deviation) is plotted against β, for the experimental data of Ross and Zajac,[9] the ranges in air being taken from Tsiang *et al.*,[12] up to 100 kev and from M. Curie[13] for higher energies (in this region Curie's curve is practically an extrapolation of Tsiang's). The full line is the one previously determined. Although the discrepancy of the points with the curve goes up to 8 percent, we cannot exclude the possibility of a good agreement as the standard deviations are of the order of 20 percent.

One expects that better experimental results may decide on the general validity of relation (1) regardless of the nature of the particles up to values of β 0.8 or larger, except for very heavy particles at low velocities.

We are indebted to Mr. J. Tiomno for helpful discussions.

* Now Research Fellow at the National Institute of Health, Bethesda, Maryland.

[1] E. Picciotto, Comptes Rendus **229**, 117–119 (1949).
[2] L. L. Green and W. M. Gibson, Proc. Phys. Soc. **62**, 269 (1949).
[3] Lattes, Fowler, and Cuer, Proc. Phys. Soc. **59**, 883–900 (1947).
[4] Bradner, Bishop, and Barkas, Phys. Rev. **76**, 587 (1949); and Bradner, Smith, Barkas, and Bishop, Phys. Rev. (to be published). I am grateful to Dr. Bradner for making this paper available to me before publication.
[5] Feather, Nucleonics **5**, No. 1, 22–41 (1949).
[6] J. H. Smith, Phys. Rev. **71**, 32 (1947).
[7] Bøggild, Brostrøm, and Lauritsen, Phys. Rev. **59**, 275 (1941); and Bøggild, Minnhagen, and Nielsen, Phys. Rev. **76**, 988 (1949).
[8] P. Demers, Phys. Rev. **70**, 974 (1946) and Wollan, Moak, and Sawyer, Phys. Rev. **72**, 447 (1947).
[9] M. A. Ross and B. Zarjac, Nature **162**, 923 (1948); **164**, 311 (1949).
[10] Technical data, Kodak, Ltd., Harrow, England (April, 1949). Ilford, Ltd., Ilford, London (June, 1947).
[11] J. H. Webb, Phys. Rev. **74**, 511 (1948).
[12] Tsiang, Marty, and Dreyfuss, J. de phys. et rad. **8**, 269 (1947).
[13] Mme. Pierre Curie, *Radioactivité* (Hermann et Cie, Paris, 1935), p. 294.

A Metastable State of Half-Life 13×10^{-8} Sec. in $_{71}Lu^{177}$ *

F. K. McGowan
Oak Ridge National Laboratory, Oak Ridge, Tennessee
October 14, 1949

USING sources of Yb^{177} (1.8 hr.) and an experimental arrangement similar to that described in a previous letter,[1] delayed coincidences well above the random coincidence rate were detected. In Fig. 1 the number of delayed coincidences after subtraction of random coincidences is plotted as a function of delay time. It appears from this curve that the disintegration of Yb^{177} leads to a metastable state Lu^{177*} which in turn decays to the ground state with a half-life of $(13\pm2)\times10^{-8}$ sec.

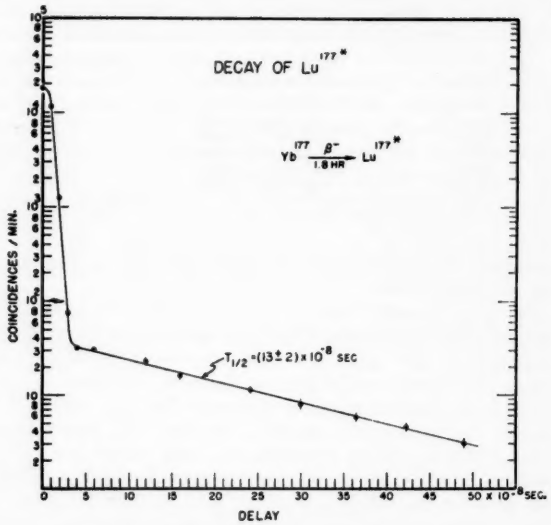

FIG. 1. Delayed coincidences as a function of delay time.

In order to reduce the variable delay introduced by a pulse height selector operating on signals of different amplitude with a finite rise time, the amplifiers were replaced by video amplifier sections with a rise time of approximately 10^{-8} sec. and maximum gain of 240. The pulses may be delayed in discontinuous steps after the first stage of amplification by inserting terminated coaxial cables (RG 7/U; characteristic impedance 100 ohms) which introduce a delay of 10^{-8} sec. per 9 feet. Pulse discrimination is performed after the coincidence stage at the input to the scalar. The resolving time of the coincidence circuit is 2.5×10^{-8} sec. The stilbene crystals and 1P21 multiplier tubes are cooled to dry-ice temperature and operated at 80 volts per stage.

A delayed coincidence scintillation spectrometer was used to investigate the radiation spectrum resulting from the isomeric transition of Lu^{177*}. For this purpose anthracene crystals and Type 5819 multiplier tubes operated at room temperature were used with the delayed coincidence unit described in the previous letter.[1] A differential pulse height selector was used in the channel

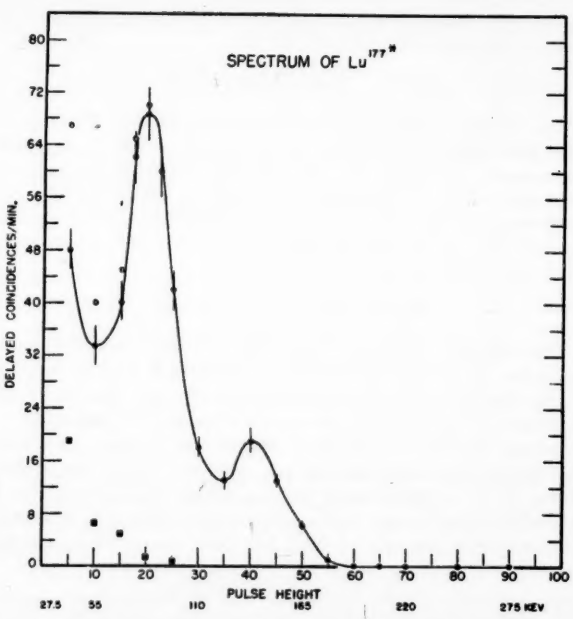

FIG. 2. Delayed coincidence counting rate as a function of pulse height.

for detection of delayed radiation. By counting delayed coincidences in a small height interval against pulse height, a measurement of the spectrum of the delayed radiation is obtained. Figure 2 shows the result of such a measurement.

The scale of the pulse height dial Bas calibrated in energy units by using the K and L internal conversion lines of the 132-kev transition from the decay of the 22μsec. metastable state in Ta^{181*} and the K internal conversion line of the 247-kev transition from the decay of the 8×10^{-8} sec. metastable state in Cd^{111*}.[2] The latter isomeric state was detected using sources of Cd^{111*} (48 min.) produced by (n,γ) reaction on a sample of enriched Cd^{110}.

The solid curve is the conversion electron spectrum obtained after subtraction of the Compton electron distribution produced by the γ-rays and x-rays. The K and L conversion lines at 87 and 140 kev correspond to a (150±10) kev transition. From the energy and half-life of this isomeric state the transition is probably electric octupole radiation or a combination of electric octupole and magnetic quadrupole radiation. It appears from this curve that no other γ-rays follow in cascade with the decay of Lu^{177*}.

The half-life of Yb^{177} as listed in the table of isotopes[3] ranges from 1.9 to 3.5 hr. A conventional half-life determination is complicated by the presence of the daughter activity Lu^{177} (6.9 day) and the Yb^{175} (100 hr.) present in the sources. By counting delayed coincidences at a fixed delay as a function of time, the coincidence rate decreases according to the decay of Yb^{177}. The decay was observed for 6 hr. and the half-life of Yb^{177} appears to be (1.8±0.1) hr.

* This document is based on work performed under Contract No. W-7405, eng. 26 for the Atomic Energy Project at Oak Ridge National Laboratory, Oak Ridge, Tennessee.

[1] McGowan, DeBenedetti, and Francis, Phys. Rev. **75**, 1761 (1949).
[2] Martin Deutsch and Donald T. Stevenson, Phys. Rev. **76**, 184 (1949).
[3] G. T. Seaborg and I. Perlman, Rev. Mod. Phys. **20**, 585 (1948).

Remarks on Non-local Spinor Field

HIDEKI YUKAWA
Columbia University, New York, New York
October 18, 1949

IN a recent letter to the editor,[1] it was shown that quantized non local fields could be so constructed as to represent assemblies of particles with the definite mass and radius. In a paper, which will appear very soon,[2] detailed account is given together with the elucidation of most of the points, on which the author was not very sure when he wrote the above letter.[1] However, there is still one point, which seems to the author to be unsatisfactory. Namely, in the case of non-local spinor field, we assumed the commutation relation

$$\beta_\mu[x^\mu,\psi]+\lambda\psi=0 \tag{1}$$

between the space-time operators x^μ and the non-local spinor operator ψ, in addition to the commutation relation

$$\gamma^\mu[p_\mu,\psi]+mc\psi=0 \tag{2}$$

between ψ and the space-time displacement operators p_μ. Further we assumed that γ^μ, β_μ, which were matrices with four rows and columns, were defined by

$$\left.\begin{array}{llll}\gamma^1=i\rho_2\sigma_1, & \gamma^2=i\rho_2\sigma_2, & \gamma^3=i\rho_2\sigma_3, & \gamma^4=\rho_3\\ \beta_1=\rho_3\sigma_1, & \beta_2=\rho_3\sigma_2, & \beta_3=\rho_3\sigma_3, & \beta_4=-i\rho_2\end{array}\right\}. \tag{3}$$

Now the difficulty was that, in contrast to (2), the relation (1) was not invariant with respect to the improper Lorentz transformation with the determinant -1, but was to change itself into the form

$$\beta_\mu[x^\mu,\psi]-\lambda\psi=0. \tag{4}$$

In the paper mentioned above,[2] a way of removing this difficulty was indicated, but was very unsatisfactory in that the number of components of the spinor ψ was to be increased from 4 to 8 without any immediate physical interpretation for the extra degree of freedom. It came to the author's notice very recently that the following alternative way was far more acceptable in that no extra components of the spinor were introduced. Namely, we take advantage of the antisymmetric tensor of the fourth rank with the components $\epsilon_{\kappa\lambda\mu\nu}$ which are $+1$ or -1 according as (κ,λ,μ,ν) are even or odd permutations of (1, 2, 3, 4) and 0 otherwise.[3] Further we take into account the relations

$$i\beta_\nu=\gamma^\kappa\gamma^\lambda\gamma^\mu, \tag{5}$$

where (κ,λ,μ,ν) are even permutations of (1, 2, 3, 4). Then (1) can be written in the form

$$\tfrac{1}{6}\sum_{\kappa\lambda\mu\nu}\epsilon_{\kappa\lambda\mu\nu}\gamma^\kappa\gamma^\lambda\gamma^\mu[x^\nu,\psi]+i\lambda\psi=0, \tag{6}$$

which is obviously invariant with respect to the whole group of Lorentz transformations. However, the invariance of (6) can be proved more explicitly by transforming ψ, while the matrices γ^μ are assumed to retain their prescribed forms as defined by (3) independent of the coordinate system. Namely, we can associate a linear transformation

$$\psi'=S\psi \tag{7}$$

with each of the Lorentz transformation

$$x_\mu'=a_{\mu\nu}x_\nu, \tag{8}$$

where S is a matrix with four rows and columns satisfying the relations

$$S\gamma^\mu S^{-1}=a_{\nu\mu}\gamma^\nu. \tag{9}$$

If we insert (7), (8) and (9) in (6) and take advantage of the fact that $\epsilon_{\kappa\lambda\mu\nu}$ are components of a tensor of the fourth rank, we obtain the commutation relation

$$\tfrac{1}{6}\sum_{\kappa\lambda\mu\nu}\epsilon'_{\kappa\lambda\mu\nu}\gamma^\kappa\gamma^\lambda\gamma^\mu[x'^\nu,\psi']+i\lambda\psi'=0, \tag{10}$$

which has the same form as (6).

It should be noticed, however, that the relation (6) is to be regarded as a unification of (1) and (4) rather than the mere reproduction of (1), because (6) must be identified with (4) in the coordinate system, which is connected with the original coordinate system by an improper Lorentz transformation with the determinant -1.

[1] H. Yukawa, Phys. Rev. **76**, 300 (1949).
[2] H. Yukawa, Phys. Rev. (to be published).
[3] The antisymmetric tensor $\epsilon_{\kappa\lambda\mu\nu}$ was useful for unifying the scalar and pseudosclar fields as well as the vector and the pseudovector fields as shown by M. Schoenberg, Phys. Rev. **60**, 468 (1941).

Detection of Radioactive Atoms in the Air with Nuclear Emulsions

Č. JECH
Department of Physics, State Radiotherapeutical Institute, Praha-Bulovka, Czechoslovakia
October 7, 1949

IT has been shown recently[1] that atoms of a radioactive deposit remaining in the air from the decay of radon can be collected together with the dust from the air on a very small surface area of a glass plate. This is done by allowing air saturated with water vapor to flow (e.g., in a Owens-Běhounek dust-counter[2]) with a considerable velocity through a small jet toward this glass. This was demonstrated by exposing the glass in contact with a nuclear emulsion and by finding many tracks of alpha-particles after development of the plate in the small region, corresponding to the position of the dust-spot on the glass. We explained this phenomenon by at least partial adsorption of atoms of active deposit on dust particles.

New experiments with low activities of the air revealed that this method of collection of radioactive atoms from the air can be

FIG. 1.

FIG. 2.

used as a sensitive indicator of radioactive contamination in the air, i.e., for air monitoring. Further simplification (which also represents a considerable increase of efficiency) was obtained by directing the stream of air toward a stripe of a nuclear plate and collecting dust together with radioactive atoms on the surface of the emulsion. By a suitable arrangement many air samples can be taken with the same stripe of the plate. Figure 1 shows a typical dust-spot on the surface of an Ilford C2 emulsion obtained by aspirating 125 cc of air containing 1.5×10^{-13} Curie/cc of radon and developed 4 hours after taking the sample. Figure 2 shows alpha-ray tracks on the same area of the plate after remova, of the dust-spot. In this area some 280 tracks were countedl which, assuming radioactive equilibrium in the air, would mean that nearly 20 percent of the atoms of active deposit were collected with the dust on the plate. This percentage may depend on the instrument used and/or on the dust-conditions in the air. The method seems capable of detecting quantities as low as 10^{-13} Curie of active deposit of radon.

Experiments have also been arranged in order to detect radioactive atoms in free atmospheric air. On dust-spots obtained by aspirating 1600 cc of free atmospheric air, on an average, 35 alpha-tracks were found. Most of them could be identified as alpha-particles of RaC. Assuming 20 percent efficiency, this would correspond to a radon concentration of 10^{-15} Curie /cc which is fairly consistent with the value found, for example, by G. Aliverti[3] by an iontometric method.

Using electron sensitive emulsions the method could be also applied for detection of artificial solid beta-emitters in the air. Low energy ends of electron tracks which would be most appropriate for counting could be found near the area of the dust-spot by energies up to 0.3 Mev.

The author would like to thank Dr. Běhounek for helpful discussions. A detailed account of the method with some applications will be published elsewhere.

[1] Č. Jech, Nature **163**, 570 (1949).
[2] F. Běhounek and E. Effenberger, Gerlands Beitr. z. Geophys. **59**, 74 (1942).
[3] G. Aliverti, Zeits. Geophysik **9**, 16 (1933).

Neutron-Proton and Proton-Proton Cross Sections at 83 Mev

L. CASTILLEJO AND H. T. RICHARDSON
University College, London, England

October 7, 1949

CAMAC and Bethe[1] have shown that with central forces only and a square-well potential it was possible to obtain the observed cross sections for n–p scattering at 80 Mev provided that the range was 2.0×10^{-13} cm. Later Blatt[2] showed that the triplet range must be reduced to about 1.5×10^{-13} cm to fit the experimental values of coherent neutron scattering by crystals and by parahydrogen.

The following calculations have been performed, using square-well potentials, to test the possibility of obtaining the correct high energy scattering results by reducing the range of the central force in the triplet interaction. The tensor force has not been neglected but this involves increasing its range.

Two sets of force constants have been used:

	r_0	r_c	r_t	V_0	V_c	V_t
A.	2.8	1.6	3.08	11.9	39.3	10.04
B.	2.8	0	3.27	11.9	$v_t=4.49\times10^{11}$ cm^{-1}	9.62

where r is the range of the force in units of 10^{-13} cm, V is the depth of the well in Mev, and the subscripts 0, c, t denote singlet, central force triplet, and tensor force triplet interaction, respectively.

The singlet constants were chosen to fit the data on p–p scattering and the zero energy n–p cross section. The triplet constants were chosen to fit the binding energy, the quadrupole moment and the magnetic moment of the deuteron. Constants A were taken from the calculations of D. Padfield.[3] These agree reasonably well with results of coherent scattering of neutrons by parahydrogen and by NaH crystals since they give a zero energy triplet scattering length $a_1=-0.533$ as compared with an experimental value of -0.51 to -0.53.[4] B was considered as the limiting case of $r_c\to0$ with $V_c=\{(I/r_c^2)\Sigma\, v_n r_c^n\}\hbar^2/M$, where from requirements of continuity $v_0=\pi^2/4$. The constants in this case were calculated by F. Ledsham.[5]

Neutron-proton cross sections have been calculated at 83 Mev for symmetric and charged meson theory type of interactions and also for the mixture suggested by R. Serber in which only the even states interact. All phase calculations were performed exactly though the $(^3D_3+^3G_3)$ and higher coupled phases were neglected. The total cross sections and the ratios of scattering at 90° and 180° are given in Table I and the differential cross sections in Fig. 1.

It would seem from these results that with the symmetric or charged theories there is no possibility of fitting the high energy data (at least with a square-well potential) by decreasing the central range r_c. This is shown in Fig. 2 where the total cross sections are plotted against r_c/r_t.[6] Though the high energy data might possibly be fitted by a Serber interaction, this has the disadvantage of introducing a new postulate, the amount of mixing of the symmetric and charged theories to account for the high energy scattering. Even then the single triplet range of 2.8×10^{-13} cm gives better results at 83 Mev though it does not, of course, fit the coherent scattering data.

Scattering of like particles.—Using the potential A, calculations have also been carried out for the p–p scattering at the same energy. To allow for the Coulomb interaction in the calculation of the nuclear phases, the equations were solved inside the well neglecting this potential and these solutions were fitted to Coulomb

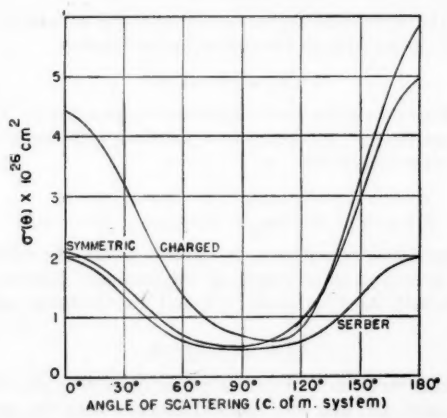

FIG. 1. Differential n–p cross section $\sigma(\theta)$ for potential A.

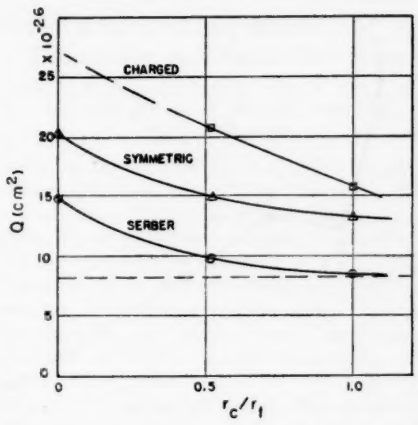

FIG. 2. Total cross section Q for symmetric, charged and Serber interactions plotted against r_c/r_t.

TABLE I. Total n–n and n–p cross sections Q in units of 10^{-26} cm² and ratio of scattering at 180° to 90° for potentials A and B.

	A				B	
	Neutron-proton		Neutron-neutron		Neutron-proton	
	Q	$\frac{\sigma(180°)}{\sigma(90°)}$	Q	$\frac{\sigma(180°)}{\sigma(90°)}$	Q	$\frac{\sigma(180°)}{\sigma(90°)}$
Symmetric	14.91	9.59	4.23	25.37	20.29	5.60
Charged	20.68	8.87	21.20	16.96	Over 22	—
Serber	9.92	4.09	—	—	14.92	4.64

wave functions as solutions outside the well. The phases were then corrected by adding a perturbation inside the well to allow for the Coulomb field there. The resulting phases differed in most cases by less than one percent from the n–p phases and the greatest difference was two percent. At this energy therefore it is reasonable to neglect the Coulomb potential in the calculation of the phases.

The angular distributions for n–n and p–p scattering are shown in Fig. 3 for the charged and symmetrical cases. The cross section at 90° (center-of-mass system) is considerably less than that given by Ashkin and Wu[7] at 100 Mev using the potential of Rarita and Schwinger[8] including the tensor forces. This could therefore be regarded as an effect arising from the double range.

At about 15° the p–p cross section falls below the n–n. The opposite is the case in the distributions described by Barker and Ravenhall[9] where the p–p cross section remains steadily above the n–n. The reason for this is that in the central force case the ^3P phase is negative and so the imaginary parts of the scattered amplitude add. For the potential used here, the $^3P_0$ phase is large and positive, and the interference between the Coulomb and the nuclear wave gives rise to the above effect. The total cross sections for n–n scattering for the charged and symmetric cases and also the ratios of the differential cross sections at 90° to those at 180° are given in Table I.

We would like to thank Dr. Hu and Dr. Burhop for their assistance and suggestions, and Professor Massey for his continued interest.

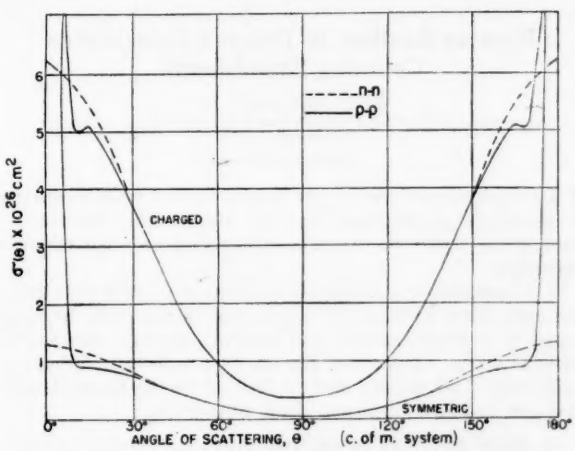

FIG. 3. Differential p–p and n–n cross sections for potential A.

[1] M. Camac and H. A. Bethe, Phys. Rev. **73**, 191 (1948).
[2] J. M. Blatt, Phys. Rev. **74**, 92 (1948).
[3] D. Padfield, Nature **163**, 22 (1949).
[4] R. B. Sutton *et al.*, Phys. Rev. **72**, 1147 (1947); C. G. Shull *et al.*, Phys. Rev. **73**, 842 (1948).
[5] F. Ledsham (to be published).
[6] Massey, Burhop, and Hu, Phys. Rev. **73**, 1403 (1948).
[7] J. Ashkin and T. Wu, Phys. Rev. **73**, 973 (1948).
[8] W. Rarita and J. Schwinger, Phys. Rev. **59**, 436 (1941); **59**, 556 (1941).
[9] Barker and Ravenhall, Nature **163**, 20 (1949).

Cosmic Rays at a Great Depth

Y. MIYAZAKI
Scientific Research Institute, Ltd., Tokyo, Japan
September 30, 1949

AFTER our experiments[1] at 1400 meter water equivalent in Shimizu Tunnel by using arrangement I in Fig. 1, we continued the same kind of measurements at 3000 m.w.e. in the same tunnel from August, 1940, to the end of 1945 with the same apparatus, and proved that intensities at the latter point were about 1/10 those at the former depth as shown in Fig. 2. The intensity *versus* depth curve is given in Fig. 3. We also measured the absorption by lead of various thickness and found that the shape of the absorption curve was almost the same as at 1400-m.w.e. depth and the existence of showers was remarkable just as at 1400 m.w.e. Therefore the cosmic-ray particles at 1400- and 3000-m.w.e. depth are concluded to have the same nature. The absorption curve is of a form similar to that on the ground and therefore the particles are presumably mu-mesons which are the decay product of pi-mesons.

The showers-to-singles under various thicknesses of lead at the two depths can be seen from Fig. 2. They are about $\frac{1}{4}$ and $\frac{1}{3}$ at 1400 m.w.e. and 3000 m.w.e., respectively.

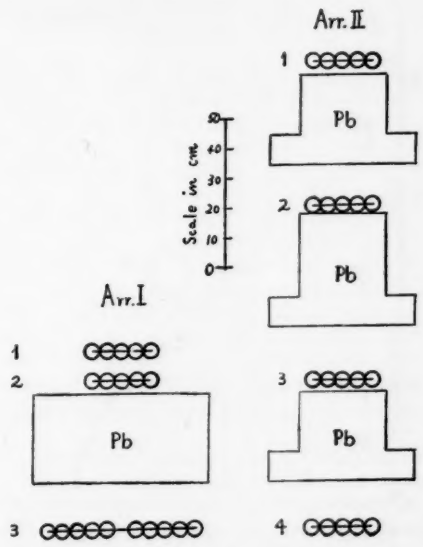

FIG. 1. Counter arrangement.

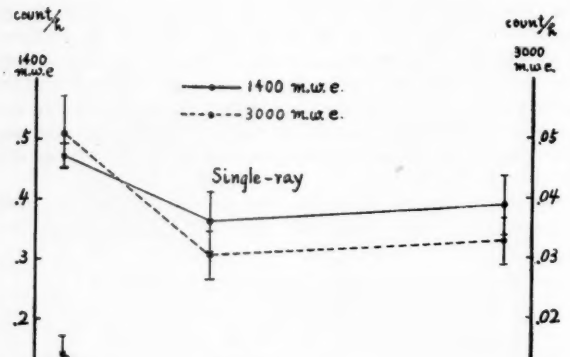

FIG. 2. Absorption curve in lead at 1400-m.w.e. and 3000-m.w.e. depth.

Barnothy and Forro[2] published their results, stating that almost all of the particles were absorbed by 90 cm of lead at a depth 1000 m.w.e. Therefore we increased the thickness of the lead up to 100 cm using arrangement II as shown in Fig. 1. Our results agree with the data published later by these authors.

The vertical incident radiation computable from $\cos^2$ distribution law yields the following value:

$$J_{\text{Arr. I}} = 0.0039\ h^{-1}\ \text{cm}^{-2}\ \text{sterad}^{-1},$$
$$J_{\text{Arr. II}} = 0.0038\ h^{-1}\ \text{cm}^{-2}\ \text{sterad}^{-1}.$$

The results of absorption obtained by arrangements I and II are plotted on one curve as shown in Fig. 4. From this, we see that a greater part of cosmic-ray particles are absorbed, but about $\frac{1}{5}$ still remained under 100 cm of lead. It is not possible to decide whether the cosmic rays which penetrate such a large amount of rocks and come to this depth are ionizing rays or non-ionizing ones.

If we assume them to be ionizing rays, at least $\frac{4}{5}$ of the particles found at this depth must be of secondary origin produced in rocks and the primary cosmic rays must be less than $\frac{1}{5}$. On the other hand, if we assume them to be non-ionizing rays, most of the particles which were measured at this depth must be hard shower particles produced by non-ionizing rays, $\frac{1}{5}$ of them having such a high energy as to enable them to penetrate one meter of lead.

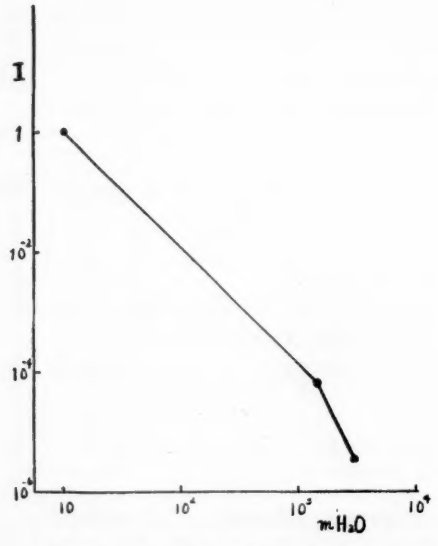

FIG. 3. Cosmic-ray intensity *vs.* depth curve.

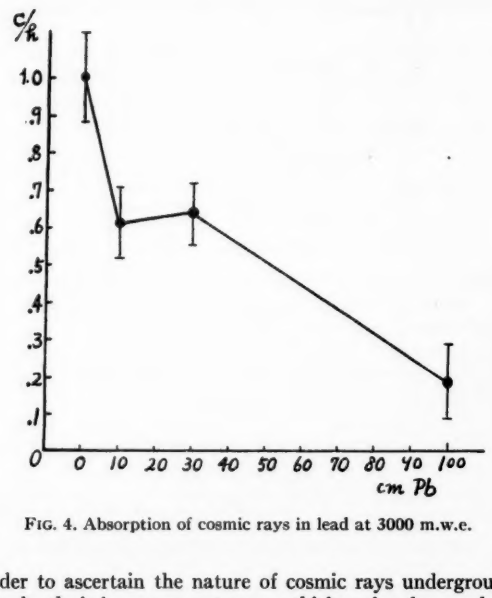

FIG. 4. Absorption of cosmic rays in lead at 3000 m.w.e.

In order to ascertain the nature of cosmic rays underground at such a depth, it is necessary to use a thicker absorber, and also a hodoscope and cloud chamber for determining the relation between various particles observed.

Unfortunately this work had not been completed when fire destroyed all instruments in February, 1946. It is very difficult to reconstruct new equipment at present but we intend to carry out the measurements in the future.

This work was done as a part of the program of the Cosmic-Ray Subcommittee of the Japan Society for the Promotion of Scientific Research. Our measurements were made possible by the help rendered by the Department of Railways and we wish to express our cordial thanks to all officials concerned. I should like to express my heartful thanks to Dr. Y. Nishina for his kind guidance and encouragement throughout this work. I also express my coridal thanks to Dr. Y. Sekido and Mr. T. Masuda who helped me in the preparation as well as in the observation throughout this work. But for their help, this work would have not been performed. We also acknowledge the kind help given by Messrs. C. Ishii, M. Iio, the late T. Ikeda, Y. Kawabata, the late H. Muromachi, and all members of Cosmic-Ray Research Group of our Institute.

[1] Nishina, Sekido, Miyazaki, and Masuda, Phys. Rev. **59**, 401 (1941).
[2] J. Barnothy and M. Forro, Phys. Rev. **58**, 844 (1940).

Note on Analysis of Delayed Coincidence Counting Experiments

F. W. VAN NAME, JR.
Department of Physics, Franklin and Marshall College, Lancaster, Pennsylvania
October 10, 1949

IN a recent note in this journal, Binder[1] has described an analysis of delayed coincidence counting experiments. Reference is made to my work[2,3] on the same subject in a way that might be misleading.

In my calculations a triangular distribution of pulse-time delays was used. Since a triangular distribution cannot easily be represented by a single, smooth and analytic function, the range of artificial delays was divided into six regions for calculation purposes only. This division had no bearing on the physical result obtained, as might be inferred from Binder's note.

[1] D. Binder, Phys. Rev. **76**, 856 (1949).
[2] F. W. Van Name, Jr., Phys. Rev. **75**, 100 (1949).
[3] F. W. Van Name, Jr., Ph.D. dissertation, Yale University (1948).

Evidence for Multiple Meson and γ-Ray Production in Cosmic-Ray Stars

M. F. KAPLON, B. PETERS, AND H. L. BRADT
University of Rochester, Rochester, New York
October 10, 1949

IN a survey of electron sensitive Kodak NTB3 plates flown at an altitude of 100,000 feet we have observed a collision of an extremely energetic primary cosmic-ray alpha-particle with a heavy nucleus (Ag or Br) of the emulsion; this collision gives rise to a very narrow penetrating shower core of some 23 relativistic singly charged particles, this core being surrounded by a more diffuse shower of 33 relativistic particles (Fig. 1). In addition, 18 non-relativistic heavy particles, carrying at least 23 units of charge and a total energy of ~3 Bev, emerge from the star at the origin of the shower.

The dense core (C) of the shower of relativistic particles, the majority of which are assumed to be mesons, has a total projected angular spread of 2.5°. The axis of this core is an exact continuation of the direction of the incident α-particle. The core is so dense that not all individual tracks are resolvable in the immediate vicinity of the star. At larger distances where resolution is possible all these tracks prove to be minimum ionization tracks. By counting over a given distance the number of grains in the core and dividing by the number of grains of a minimum ionization track we obtain $N_0^{(e)}=23\pm2$ as estimates of the number of charged relativistic particles in the narrow shower.

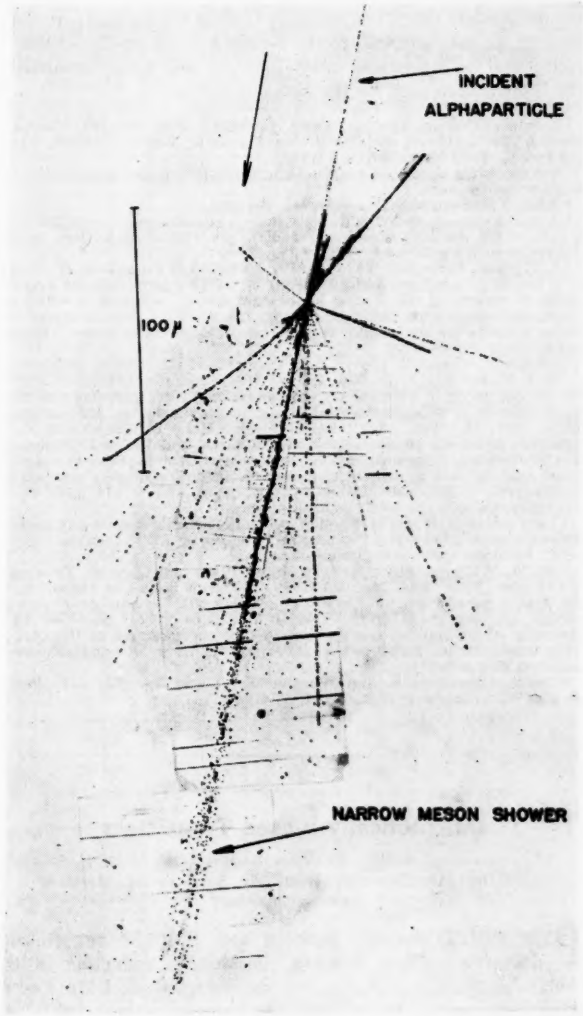

FIG. 1. Incomplete photo-micrograph (slightly retouched) of the shower. (Only a small fraction of the heavy prongs are shown.)

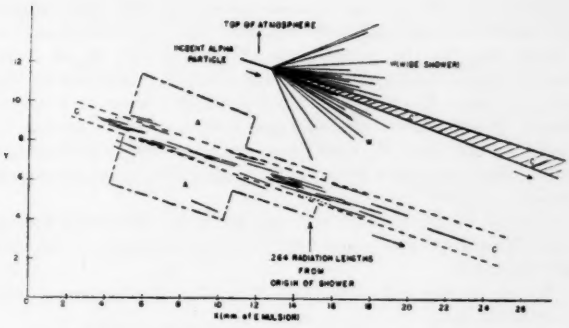

FIG. 2. Schematic diagram of the appearance of the shower in the first and second emulsions.

The region where the narrow shower C, after passage through some 2-cm glass penetrates the next plate of the stack (the dotted area C of 0.25 cm² in Fig. 2) was surveyed for tracks of such length and orientation that they can be assumed to be caused by the explosion; 44 tracks of relativistic particles were found, 38 inside and six near the edge of the dotted cone C, that is 11 more tracks than were originally contained in the narrow shower. In surveying an additional area $A=0.29$ cm² for tracks satisfying identical criteria only six more tracks were found, all but one lying very close to the core and probably also belonging to the shower. We conclude that considerable multiplication of singly charged relativistic particles (electrons) has occurred in the core. Two electron pairs of energies ~10 Bev and ~50 Bev (as estimated from the magnitude of the very small angles between the two tracks of the pair)[1,2] were created in the emulsions of both the first and the second plate. One of the pairs within the core gives rise to another pair; this fact supports the assumption that the additional charged particles appearing in the narrow core are fast electrons produced by high energy γ-rays (or possibly other neutral particles).

At least eight and probably about ten pairs are created in the core over an average path length of 0.26 radiation units of glass and emulsion; the number of γ-rays in the core must therefore at least be equal to $N_c^{(\gamma)}\sim35$.

The energy $E=4\gamma\ Mc^2$ of the primary α-particle can be estimated from the angular width of the narrow core:

$$\Delta\theta\sim\frac{1}{8}=(1-\bar{\beta}^2)^{\frac{1}{2}}=\left(\frac{2}{\gamma+1}\right)^{\frac{1}{2}}\sim\frac{1}{30},\quad \gamma=2000,\quad E_\alpha=0.8\times10^{13}\text{ ev}.$$

($\bar{\beta}$=velocity of the center of mass system of a nucleon of the incident α-particle and a nucleon of the target nucleus.)

A more detailed study shows that the value of γ obtained from the angular distribution of mesons in the core C does not vary too much if different not too extreme assumptions concerning the energy distribution of the mesons emitted isotropically in the center-of-mass system are made.* The average separation of tracks in the second plate indicates that the average γ-ray energy cannot be greatly in excess of 10 Bev. It is most probable that three or four nucleons of the incident α-particle contribute to the narrow shower. Hence, if the γ-rays result from the decay of neutral mesons, whose numbers do not exceed the number of charged mesons, the collision leading to the narrow shower should not be considered to be completely inelastic, since a completely inelastic collision (with $\gamma=2000$) would give an average γ-energy of ~50 Bev.

Unless we assume an extremely anisotropic angular distribution of mesons in the c.m. systems (emission within a double cone of opening $\vartheta\sim1/\bar{\gamma}$), the diffuse shower of ~30 relativistic particles cannot result directly from the primary encounter producing the narrow core. We thus conclude that the diffuse shower is the result of secondary and tertiary meson production in the same

nucleus by some of the nucleons emerging from the primary encounter.[3] To summarize we conclude that the event described (which may be the initial stage of development of an Auger shower) gives direct evidence for the multiple production of high energy γ-rays. If the γ-rays result from the decay of a neutral meson of rest mass $\sim$150 Mev (see following letter) we can, by assuming that the γ-rays are converted immediately into electron pairs, obtain an upper limit for the proper lifetime of the neutral meson of $\tau_0 \lesssim 10^{-13}$ sec.

A more detailed report will appear in the Helvetica Physica Acta. This work was assisted by the Joint Program of the ONR and the AEC.

We are greatly indebted to Dr. R. E. Marshak for many valuable discussions.

* The above energy estimate is reduced by a factor seven if an angular distribution $f(\vartheta) \sim \cos^4\vartheta$ is assumed in the c.m. system.

[1] M. Stearns, Phys. Rev. **76**, 836 (1949).
[2] H. S. Snyder and W. T. Scott, Phys. Rev. **76**, 220 (1949).
[3] L. Leprince-Ringuet *et al.*, Comptes Rendus **229**, 163 (1949).

Remarks on Multiple Meson and Gamma-Ray Production

R. E. Marshak
University of Rochester, Rochester, New York
October 10, 1949

Leprince-Ringuet *et al.*[1] have supplied strong evidence for the multiple production of mesons by their observation in electron-sensitive plates of a cosmic-ray star with 55 prongs of which 28 were minimum ionization tracks. Their analysis of the angular distribution of the minimum ionization tracks led to an estimate of the energy of the event ($\sim 10^{10}$ ev) and to the reasonable hypothesis that plural as well as multiple production of π-mesons had taken place. The latest star observed by Kaplon, Peters, and Bradt (see preceding letter) with its 74 prongs and 56 minimum ionization tracks is not only much more energetic (by a factor[2] of 100–1000) but supplies definitive evidence for pluro-multiple production of π-mesons (assuming that the minimum ionization tracks do not represent to any appreciable extent electrons or as yet unknown particles[3]).

The real novelty of the R(ochester) star lies not so much in its clear-cut evidence for multiple charged particle production but in its strong evidence for multiple neutral particle production in high energy nucleon-nucleon collisions. The fact that very close charged pairs (most probably electrons) are observed to originate in the emulsion within the narrow core and that appreciable charged particle multiplication takes place over a sizeable fraction of a radiation length (in the glass plate between the two emulsions) favors a gamma-ray origin for these charged particles.[4] The number of high energy gammas required to explain the observed number of electron pairs in the narrow core is very large and comparable to the number of charged particles observed initially in the narrow core. Direct nucleonic production of the gammas (bremsstrahlung) is therefore certainly excluded if the charged π-mesons possess spin zero and probably even if they possess spin one.[5]

If the analysis of the R star is combined with the results of the Berkeley experiments[6] on high energy gamma-rays, the most likely picture which emerges is as follows: the high energy gamma-rays originate in both experiments from the rapid decay of a neutral meson with a mass of about 300 electron masses. The upper limit on the lifetime ($\sim 10^{-13}$ sec.) obtained from the R star favors a spin zero neutral meson[7] as does the excellent agreement found for the gamma-ray curves in the Berkeley experiment for the forward and backward directions on the assumption of two gamma-rays arising from a neutral meson decay.[8] The rough agreement found between the gamma-ray yields and the charged meson yields[9] at Berkeley and that found between the number of charged mesons and number of gamma-rays in the R star also favor the neutral meson hypothesis. The high multiplicity of gamma-rays found in the R star ($N \sim 10$ for a nucleon energy $E_0 \sim 10^{12}$ ev) may, when extrapolated according to an $E_0^{\frac{1}{4}}$ variation and combined with the expected increase in the number and energy of the gammas towards the center of the angular aperture defined by $(2M/E_0)^{\frac{1}{2}}$ (on the basis of a neutral meson origin), explain the failure of several experimenters[10] to find multiple cores in the large Auger showers. Indeed, the analysis of the decoherence curves in the latter experiments may throw interesting light on the angular and energy distribution of the neutral mesons (and therefore of all mesons) in the original nucleon-nucleon collision responsible for the Auger shower.

Once the neutral meson hypothesis is accepted, the electron pairs supply an approximate measuring scale for the meson energies which enable one, together with the angular distribution in the laboratory system of the charged mesons, to test various theories[11] about the primary nucleonic meson-producing collision. Thus, Kaplon, Peters, and Bradt have shown that it is very difficult to reconcile all features of their star with the assumption of isotropy of the produced mesons in the c.m. system of the nucleons and total inelasticity of the collision. This conclusion does not depend sensitively on the assumed energy spectrum of the mesons in the c.m. system. While the R star is only one event, the statistics are nevertheless good and it does appear that a pseudoscalar meson theory (for both charged and neutral mesons), in which the singularities are taken less seriously than in the Low paper[11] (see, however, p. 136) will lead to the lowering of the predicted multiplicity and to deviations from isotropy and total inelasticity which seem necessary for the actual situation.

[1] LePrince-Ringuet, Bousser, Fong, Jaundeau, and Morellet, Comptes Rendus, **229**, 1 (1949); see also Brown, Camerini, Fowler, Heitler, King, and Powell, Phil. Mag. **307**, 862 (1949).
[2] See preceding letter; we shall use the value 10^{12} ev per nucleon for our rough estimates.
[3] A small fraction may be relativistic protons.
[4] A neutral meson decaying directly into an electron pair is very unlikely in view of the Berkeley experiment and the theoretical predictions on the lifetime of such a process.
[5] L. I. Schiff, Phys. Rev. **76**, 89 (1949); using Schiff's notation, $W = 0.003$ for a meson of spin zero and an energy of 1.5 Bev (approximate average energy of mesons in the R star) in the c.m. system, whereas $W = 0.05$ for a spin one meson with the same energy. The sensitive dependence of the vector formula on the energy makes the exclusion of a vector charged meson origin less decisive.
[6] Bjorkland, Crandall, Moyer, and York, Phys. Rev. (to be published).
[7] R. J. Finkelstein, Phys. Rev. **72**, 415 (1947) found a lifetime of $2 \cdot 10^{-11}$ sec. for the decay of a vector neutral meson into three gammas and 10^{-16} sec. for the decay of a pseudoscalar meson into two gammas. J. Steinberger (Phys. Rev. **76**, 1180 (1949)) has recalculated the lifetimes using Pauli regulators and finds 10^{-3} sec. for a vector meson and $10^{-14} - 10^{-10}$ sec. for spin zero mesons. If Steinberger's values are correct, the Berkeley experiment would exclude the vector neutral meson (a conclusion already reached by Steinberger); if Finkelstein were correct, the R star would have to be invoked to exclude the vector neutral meson.
[8] I am indebted to Mr. M. Kaplon for computing the gamma-ray curves; the same calculation was performed at Berkeley by Mr. T. Taylor.
[9] C. Richman (private communication).
[10] R. W. Williams, Phys. Rev. **74**, 1689 (1948) and Cocconi, Tongiorgi, and Greisen, Phys. Rev. **76**, 1020 (1949). Williams finds that the cores are less than a meter apart for $E \sim 10^{16}$ ev which would be consistent with an angular aperture of $(2M/NE_0)^{1/2} \sim 4 \cdot 10^{-5}$ in place of $(2M/E_0)^{1/2} \sim 6 \cdot 10^{-4}$, especially if the number-energy variation of the gammas in the core is taken into account. I wish to thank Professor Greisen for a useful conversation on this point.
[11] Lewis, Oppenheimer, and Wouthuysen, Phys. Rev. **73**, 127 (1948); see also W. Heisenberg, Nature **164**, 65 (1949).

Magnetically Biased Transistors

C. Bradner Brown
Naval Ordnance Laboratory, White Oak, Silver Spring, Maryland
October 21, 1949

Published data by Bardeen and Brattain[1] on semiconductor amplifiers indicate considerable reduction in the value of $\alpha(\Delta I_{\text{collector}}/\Delta I_{\text{emitter}})$ at frequencies above 4 Mc. Recent experiments at the Naval Ordnance Laboratory have led to the discovery of new physical principles which substantially extend this range. The principal cause associated with the loss of gain at

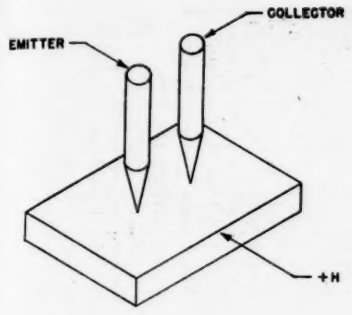

FIG. 1. Arrangement of electrodes.

high frequencies appears to be transmit time in the flow of holes from the emitter to collector. Bardeen has calculated the transit time to be $T=(2\pi s^2)/(3U_h\rho I_c)$. For typical operating conditions those that travel along the surface have a transit time of about 1.3×10^{-8} sec. For the longer important paths T may equal 2.6 to 3.9×10^{-8} sec. It is apparent that at high frequencies the effect of differences in transit angle will be an increased phase shift as well as a reduction of α since the hole current arriving at the collector will be dispersed in phase. Application of a transverse magnetic field as shown in Fig. 1 tends to compress the hole current toward the surface reducing the average path length resulting in less phase dispersion. Figure 2 shows the effect on α at frequencies from 100 kc to 10 Mc of a transverse magnetic field. This data was taken on a Bell Laboratories type "A" transistor. As can be seen most of the high frequency gain is recovered on the application of a + magnetic field bias. Negative magnetic field is substantially reduced by forcing the hole current to travel over widely varying

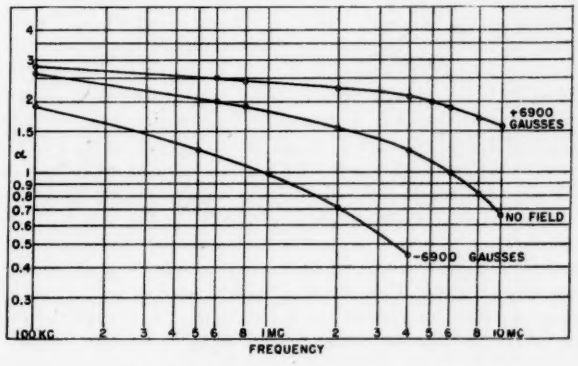

FIG. 2. Effect of frequency on the value of α.

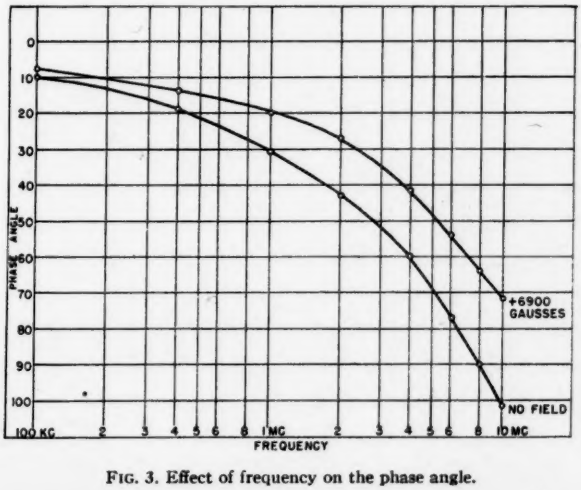

FIG. 3. Effect of frequency on the phase angle.

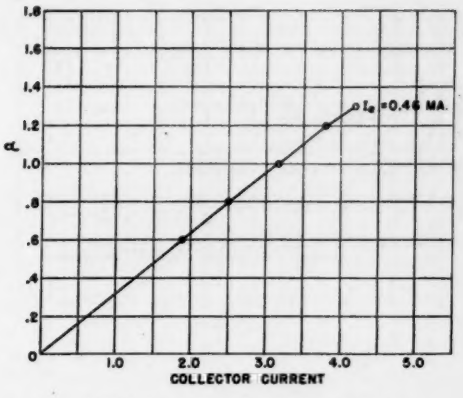

FIG. 4. Variation of α with collector current.

paths. Figure 3 shows the accompanying change in phase angle $\phi(I_{\text{collector}}/I_{\text{emitter}})$ with magnetic bias. The value of magnetic field strength was found not to be critical. In the particular unit shown here the increase in α was found to approach a saturation value at about 7000 gausses. In other units somewhat less field produced like results.

When the emitter current is small compared to the collector current the electric field strength accelerating holes from emitter to collector must be proportional to the collector current. If α is reduced by phase dispersion at high frequencies it would be expected that reducing the average transit time should increase α. Figure 4 shows the relationship between α and collector current at 10 Mc for an emitter current at 0.46 ma. As can be seen α is proportional to collector current. These results appear to be entirely consistent with the work of Shockley and Suhl.[2]

[1] J. Bardeen and W. H. Brattain, Phys. Rev. **75**, 1208 (1949).
[2] H. Suhl and W. Shockley, Phys. Rev. **75**, 1617 (1949).

Properties of Single Crystal Selenium Prepared from a Melt

HERBERT W. HENKELS
University of Pennsylvania, Philadelphia, Pennsylvania
October 21, 1949

TO data studies of the electrical conductivity of selenium have been confined to microcrystalline hexagonal selenium crystallized from the amorphous phase and polycrystalline selenium deposited in the form of hollow needles from the vapor phase. In our laboratory single crystals have been grown from a melt.

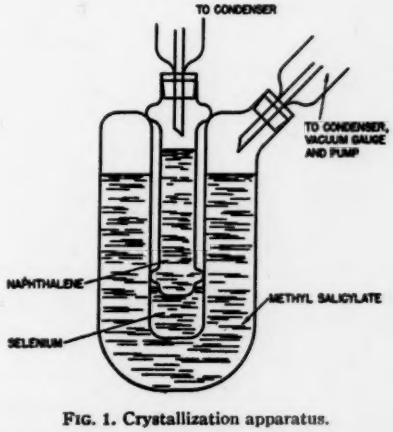

FIG. 1. Crystallization apparatus.

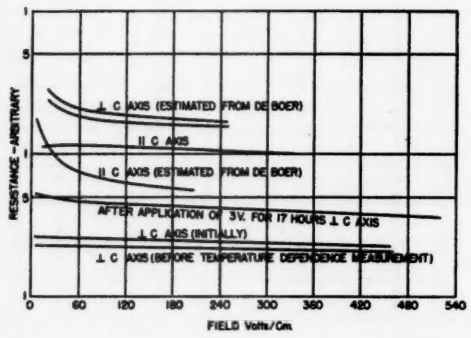

FIG. 2. Voltage dependence of resistance of selenium crystals.

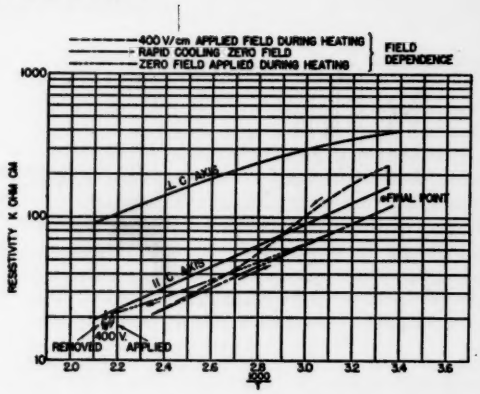

FIG. 3. Temperature dependence of resistivity of single-crystal selenium with and without high field. All measurements made at low field.

The arrangement in Fig. 1 was used. The outer container was filled with methyl salicylate boiling at atmospheric pressure at 223°C, the inner, with napthalene boiling at 218°C. Pure selenium was placed in the inner container and the entire system heated. After a length of time solid crystals of roughly cubical shape were removed from the matrix of coarse grained selenium. These were found to be hexagonal single crystals.

Electrostatic probe measurements of resistivity in vacuum were conducted. In polycrystalline material there exists the possibility that transitionary resistances at grain boundaries contribute largely to the resistance. In previous work on needle shaped crystals there has also existed the possibility of contributions of ordinary rectifier contact resistance at the ends of the crystal. The latter effect has been avoided by the method of testing. That grain boundary resistances are absent has been shown by the voltage independence of resistance. Previously tested polycrystal have shown a strong voltage dependence of resistance (especially near zero field). Figure 2 gives the data on the single crystals grown from a melt.

The resistivity of the crystals measured has been found to depend on the period of application of the field. This effect has also been observed as a function of temperature. Evidently the acceptors have a considerable mobility. The complete explanation of this effect and of the small deviations from Ohm's law at high fields will be the subject of further investigation.

The temperature dependence of resistivity is shown in Fig. 3. It is observed that the values of resistivity are about 1.6×10^5 ohm cm parallel to the c axis and, 4×10^5 ohm cm perpendicular to the c axis at room temperature. In the explanation of the observed h.f. resistivity of about 3×10^2 ohm cm for all polycrystalline samples (regardless of the d.c. resistivity which may vary from about 5×10^2 ohm cm to 10^6 ohm cm) and the correlation of that value with the resistivity of single crystals prepared from the vapor phase (10^5 ohm cm) it was postulated by Dr. Gudden that there existed a difference in the number of lattice defects in crystals from a melt and from a vapor. In a vapor the atoms of selenium are present as dimers and hexamers while in the melt and in amorphous selenium the atoms exist in long chains. On crystallization to the hexagonal lattice it was supposed that many defects would arise in the transition from the amorphous phase with a consequent increase in the number of acceptor levels and therefore in the conductivity. That this is not the case has been shown by the measurements on crystals prepared from a melt.

The activation energy of the single crystals can be calculated as about 0.25 ev parallel to the c axis and 0.24 ev perpendicular to the c axis. There appears a bend in the resistivity curve perpendicular to the c axis. Data on microcrystalline selenium shows that activation energies vary over a wide range depending on the quenching and crystallization temperatures, the impurity content (in an irregular manner) and the type of impurity, with the temperatures having the predominant effects. It has been reported from Dr. Gudden's laboratory that the activation energies decrease at higher frequencies and approach a value 0.01 ev. With new data on microcrystalline selenium and that in Fig. 3 it has been necessary to assume the presence of blocking layers at grain boundaries together with crystallite surface layers of abnormally high conductivity. The observed radical decrease of activation energy at high frequencies (to values much lower than those of single crystals) is easily understood in terms of this new model.